



Swansea University
Prifysgol Abertawe



Swansea University E-Theses

Fundamental experimental and theoretical studies on the lightfastness of azo dyes.

Guy, Owen J

How to cite:

Guy, Owen J (2001) *Fundamental experimental and theoretical studies on the lightfastness of azo dyes..* thesis, Swansea University.

<http://cronfa.swan.ac.uk/Record/cronfa42255>

Use policy:

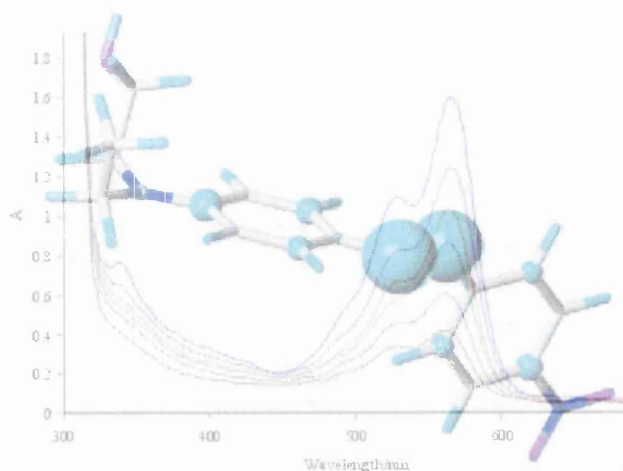
This item is brought to you by Swansea University. Any person downloading material is agreeing to abide by the terms of the repository licence: copies of full text items may be used or reproduced in any format or medium, without prior permission for personal research or study, educational or non-commercial purposes only. The copyright for any work remains with the original author unless otherwise specified. The full-text must not be sold in any format or medium without the formal permission of the copyright holder. Permission for multiple reproductions should be obtained from the original author.

Authors are personally responsible for adhering to copyright and publisher restrictions when uploading content to the repository.

Please link to the metadata record in the Swansea University repository, Cronfa (link given in the citation reference above.)

<http://www.swansea.ac.uk/library/researchsupport/ris-support/>

Fundamental Experimental and Theoretical Studies on the Lightfastness of Azo Dyes



Owen J. Guy

Thesis submitted in fulfillment of the requirements for the degree of

Doctor of Philosophy

At the

University of Wales Swansea

September 2001

ProQuest Number: 10797963

All rights reserved

INFORMATION TO ALL USERS

The quality of this reproduction is dependent upon the quality of the copy submitted.

In the unlikely event that the author did not send a complete manuscript and there are missing pages, these will be noted. Also, if material had to be removed, a note will indicate the deletion.



ProQuest 10797963

Published by ProQuest LLC (2018). Copyright of the Dissertation is held by the Author.

All rights reserved.

This work is protected against unauthorized copying under Title 17, United States Code
Microform Edition © ProQuest LLC.

ProQuest LLC.
789 East Eisenhower Parkway
P.O. Box 1346
Ann Arbor, MI 48106 – 1346



Declaration

This work described in this thesis was carried out at the university of Wales Swansea from September 1997 to September 2001 under the supervision of Professor John O. Morley. Additional work was carried out at AVECIA under the supervision of Dr. Michael Charlton.

Unless otherwise stated, this work has not previously been accepted in substance for any degree and is not being concurrently submitted in candidature for any other degree.

Signed _____ (candidate)

Date..... 27/09/01.....

This thesis is the result of my own investigations, except where otherwise stated. Other sources are acknowledged by footnotes giving explicit references. A bibliography is appended.

I hereby give consent for my thesis, if accepted to be available for photocopying and for inter-library loan, and for the title and summary to be made available to outside organisations.

Signed _____ (candidate)

Date..... 27/09/01.....

Summary

Photo-degradation reactions of donor acceptor azo dyes in methanol solution have been investigated. Irradiation of the second absorption band was confirmed to be the predominant cause of permanent photo-fading under anaerobic and oxygenated conditions. Under anaerobic conditions, 2'-nitro substituted azobenzenes and azothiophene dyes were the least lightfast, with half-lives of under one hour, whilst 4'-nitro substituted dyes had half-lives of between 1 and 1.5 hours. Photo-degradation was retarded in the presence of oxygen by between 4 and 16 times relative to fading under anaerobic conditions. The photo-fading of dyes deposited on various substrates exhibited similar behaviour to dyes in methanol solution. UV/visible spectra showed that 2'-nitro substituted dyes underwent complete loss of intensity of the visible absorption peak and a corresponding increase in the absorption in the UV region of the spectrum when irradiated under anaerobic conditions, indicating cleavage at the azo bridge and subsequent formation of mono-phenyl derivatives. In contrast, under oxygenated conditions, a gradual loss of intensity at the visible absorption maximum was observed, with no notable newly formed peaks ^{detected} are detected in the UV region suggesting that cleavage at the azo bridge is less significant. The photo-products of the reaction are suggested to include the reduced form of azo dyes containing nitro groups.

Theoretical semi-empirical AM1 and ab initio calculations using the 3-21G basis set, predicted reasonable structures for the ground states of dyes. Spectroscopic calculations using a version of the CNDO/S method gave good correlations between calculated transition energies and experimental data obtained in cyclohexane. The results of a multi electron configuration interaction treatment of AM1 structures in the gas phase were inconsistent with experimental spectral data obtained in cyclohexane but improved correlations were obtained between calculated transition energies and experimental data in methanol. The structures and energies of excited singlet and triplet states have also been calculated by the AM1 method but no apparent correlation of these energies with the lightfastness of azo dyes could be identified. A tentative relationship between calculated distributions of the unpaired electrons in the second excited triplet state and the site of reactivity in the dyes was proposed.

Acknowledgments

Special thanks to Professor J. O. Morley for his supervision over the last 3 years. Thanks also to Dr. Michael Charlton, and others at Avecia. I am very grateful to Louise Perry and Masood Yousef for all their help.

Thankyou to everyone at the chemistry department over the last seven years including all the technicians, Stan, John Lewis and Gareth Llewellyn, lecturers, rugby players, Japanese and German visitors, engineering friends Cris, Chris, Geraint, Byron, Gareth, Matt and Craig, miscellaneous people, featuring Big Dave, Gareth Thomas, Irene, Steve John Thomas and others.

Thanks also to members of my research group Tom, Ann, Simon and Richard, with a special mention for Stu, Pat, James and of course Jo.

Finally I turn to my family, who have supported me, fed me very well and let me off gardening for a long time.

Contents

| | |
|--|----|
| Chapter 1 | 2 |
| Introduction | 2 |
| Ink-jet technology | 3 |
| Dyes | 4 |
| Objectives of the research | 6 |
| Azo dyes | 10 |
| The Synthesis of Azo Dyes | 11 |
| Donor-acceptor Azo dyes | 15 |
| Position of Substituents | 19 |
| Heterocyclic Ring Systems | 23 |
| Steric factors | 25 |
| Photochemistry of azo dyes | 28 |
| Electronic transitions in azobenzenes | 35 |
| Fluorescence and Phosphorescence | 41 |
| Triplets and transient species | 49 |
| Photochemical reactions | 51 |
| Trans-Cis Photo-isomerisation | 51 |
| Mechanism of trans-cis photo-isomerisation | 51 |
| Irreversible fading | 58 |
| Photoreduction | 59 |
| Effect of the wavelength of light | 62 |
| Photo-oxidation | 64 |
| Theoretical calculations | 79 |
| Quantum mechanical models | 79 |
| Operators | 80 |
| Exact solutions | 81 |
| One electron atoms | 81 |
| Polyelectronic systems. | 82 |

| | |
|---|-----|
| The Born-Oppenheimer approximation. | 82 |
| The helium atom | 83 |
| Polyelectronic systems and Slater determinants. | 84 |
| Molecular Orbital (MO) calculations | 84 |
| The energy of a general polyatomic system | 86 |
| Hartree-Fock (H-F) equations | 87 |
| Linear combination of atomic orbitals (LCAO) in Hartree-Fock calculations | 88 |
| Roothaan-Hall equations | 89 |
| Ab initio calculations | 90 |
| Basis sets | 90 |
| Pople notation for basis sets | 90 |
| Polarisation functions | 91 |
| Open Shell systems | 92 |
| Electron Correlation. | 92 |
| Configuration interaction | 93 |
| Practical Calculations | 94 |
| Approximate MO methods. | 94 |
| Zero differential overlap (ZDO) | 95 |
| Huckel Theory | 96 |
| CNDO Complete Neglect of Differential Overlap | 97 |
| Limitations to CNDO | 99 |
| Other Semi Empirical methods | 99 |
| AM1 | 101 |
| PM3 | 101 |
| Calculating molecular properties with quantum mechanics | 102 |
| Thermodynamic and structural properties | 102 |

Chapter 2 110

| | |
|---------------------|-----|
| Experimental | 110 |
| Kinetic Experiments | 115 |
| Filters | 117 |

| | |
|---|------------|
| Laser irradiation | 117 |
| Results | 118 |
| Absorption maxima in protic and non-protic solvents | 118 |
| Hydrogen bonding solvents | 119 |
| Other absorption bands | 123 |
| Aggregation Effects | 124 |
| Identification of the absorption responsible for permanent fading | 127 |
| Kinetic experiments | 130 |
| Discussion | 153 |
| Section 2 | 157 |
| The effect of water on rates of fading | 170 |
| The effect of singlet oxygen quenchers on photofading rates under oxygenated conditions | 173 |
| The effect of the solvent medium on the rate of fading | 174 |
| Photofading of dyes on substrates | 190 |
| | |
| Chapter 3 | 197 |
| Experimental | 200 |
| Photofading reactions | 200 |
| Xenon arc lamp (1000W) | 201 |
| High performance liquid chromatography (HPLC) | 201 |
| Mass Spectrometry | 202 |
| Introduction to mass spectrometry | 203 |
| Identification of the fading products | 205 |
| Oxygenated conditions | 207 |
| Possible photo-products | 207 |
| Mass Spectrometry | 210 |
| Detection of photo-products by UV/visible spectrophotometry | 211 |
| Mass Spectrometry | 215 |
| Suggested structures | 224 |

| | |
|--|-----|
| Chapter 4 | 241 |
| Methods of calculation | 241 |
| Geometry | 243 |
| Effect of dielectric constant of the solvent on geometry | 249 |
| Results of geometry optimisations | 251 |
| Conformations | 253 |
| Summary of geometries of 4'-nitro substituted dyes | 259 |
| Dyes containing the 2'-nitro substituent | 261 |
| Rotation calculations | 272 |

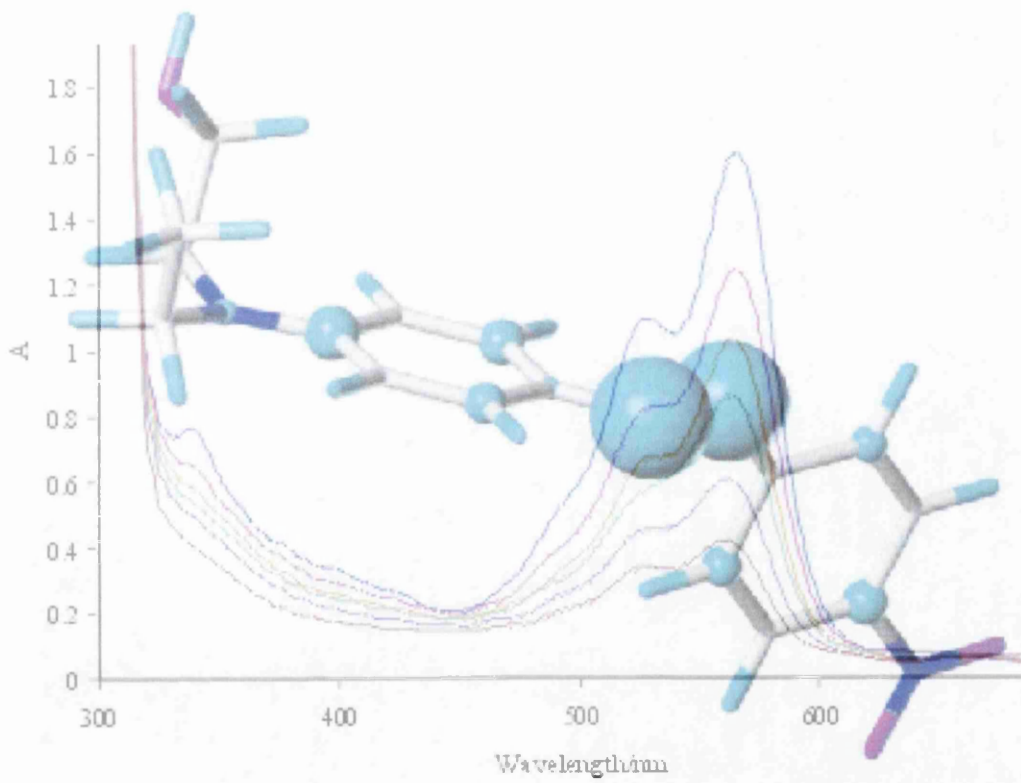
| | |
|---|-----|
| Chapter 5 | 277 |
| Cis and Trans isomers | 277 |
| Azobenzene | 277 |
| Trans azobenzene | 278 |
| Cis-azobenzene | 279 |
| Cis-trans isomers of Aminoazobenzene and a donor acceptor azobenzenes | 280 |
| Calculated electronic spectra | 283 |
| Single electron configuration interaction (C.I.) | 283 |
| Azothiophene systems | 288 |
| The effect of geometry on transition energies | 290 |
| Multi-electron configuration interaction (C.I.) | 292 |

| | |
|---|-----|
| Chapter 6 | 299 |
| The effect of solvent on the long wavelength absorption of the dyes | 300 |
| Hydrogen bonding effects of the solvent | 306 |
| Effect of dye structure on charge distribution | 308 |
| Gas phase predictions of transition energies to the second excited singlet S2 | 309 |
| Predictions of transition energies to the second excited singlet S2 in methanol | 310 |
| Excited state geometry optimisations | 313 |

| | |
|---|------------|
| Relative energies of excited states | 315 |
| Excited state structures and properties | 321 |
| The first excited states | 322 |
| The first excited singlet state | 323 |
| Optimised structures of the relaxed first triplet state | 326 |
| Spin densities | 327 |
| Second excited singlet and triplet states | 330 |
| The relaxed second excited singlet state | 330 |
| The relaxed second excited triplet state | 334 |
| | |
| Chapter 7 | 340 |
| Conclusions | 341 |

Chapter 1

Introduction



Chapter 1

Section 1.1

Introduction

Among the properties desired in a dye, lightfastness is of significant importance. Lightfastness is the stability of the dye to light. In other words, if a dye is subjected to irradiation resulting in permanent loss of colour or fading, then the rate and degree of this fading determines the lightfastness of the dye. Lightfastness is very important in the dyestuff industry, as manufacturers require fade resistant dyes for materials, textiles, inks etc. and it is desirable to produce dyes with high lightfastness. It is common experience that dyed fabrics fade or change colour to commercially unacceptable shades on exposure to sunlight. Dyes in polymer and paper substrates may also experience photofading. Much research has therefore, been devoted towards producing dyes with higher lightfastness than dyes which are currently used in industry.^{1,2,3,4,5,6}

The lightfastness of a dye is influenced by a number of factors including the physical structure of the substrate and its chemical nature, the relative humidity and the presence of moisture in the substrate, the chemical constitution of the dye, the wavelength and intensity of the light used for fading, the presence or absence of oxygen and its concentration, the physical state of the adsorbed dye and the dyeing method.

Dye lightfastness can differ depending on the application for the dye. For example, in textile dyeing, the photofading mechanism of a dye may be different on non-protein materials like cellulose, to protein substrates such as wool.⁷ This means that the same dye could have different lightfastness ratings on different materials. Another example of this is that dyes which exhibit good lightfastness in textiles frequently display poor lightfastness in printing applications. This is attributed to the different distribution of the dye in printing, where the dye layer is at the surface and only a few microns thick, while in the textile fibre, the dye is distributed homogeneously through a much thicker fibre. Thus, whilst fading of the top few microns of dye in a print can be catastrophic, the same degree of fading within a textile fibre may not be noticeable.⁸

Ink-jet technology⁹

Ink jet dyes with improved lightfastness properties are of considerable interest to industry, including the sponsors of this project, Avecia (formally Zeneca Specialities). Ink jet printing combines low cost, full colour and high quality and is becoming the dominant technology for low to medium speed printing. It is therefore highly suitable for use in the home in combination with personal computers.

The first successful ink-jet technology products were developed by Enquist in 1951¹⁰. Many large companies such as Hewlet Packard and Dataproducts (formally Exxon), Cannon, Seiko Epson, BASF and Avecia are involved in this technology. The majority of new developments in this technology are centred around dyes, dye synthesis, dye mixtures and dye purification.¹¹

The system used to apply the ink to the substrate, usually paper, is called drop-on-demand technology. Here the ink droplets are ejected onto the substrate (paper) at the desired position to form the image. The drop on demand system can be divided into 2 further classes; piezo and thermal (bubble jet). In the bubble jet system, thousands of temperature rises per second in a heater at the tip of the printer nozzle produce tiny bubbles. The bubbles cause a pressure increase which results in the ejection of a fine ink droplet onto the paper. In piezo systems, a piezo electric crystal is deformed by an electric signal. This deformation produces a pressure wave in the ink causing a droplet to be ejected onto the paper. Piezo systems may be classified further according to the type of ink used in the system.

Piezo systems can use three types of ink:

1. Aqueous based inks.
2. Solvent based inks.
3. Hot melts (solid inks which form a fluid ink on heating which cools and solidifies on the substrate).

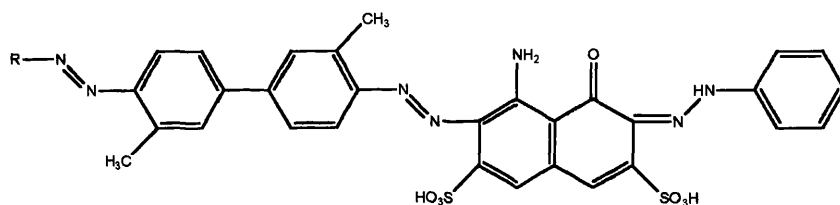
Good ink-jet dyes must have good solubility either in water for aqueous inks, or in solvents such as ethanol, for solvent based inks. This prevents crystallisation of the dye which blocks the nozzles of the ink jet printer.¹²

In addition to this, ink-jet dyes must have good wet fastness, smear fastness and lightfastness. This can be a particular problem for aqueous dyes, as these dyes must be sufficiently soluble for compatibility with the printer, but should also be reasonably resistant to smearing or smudging. Solvent based dyes do not suffer from this problem as they are insoluble in water.

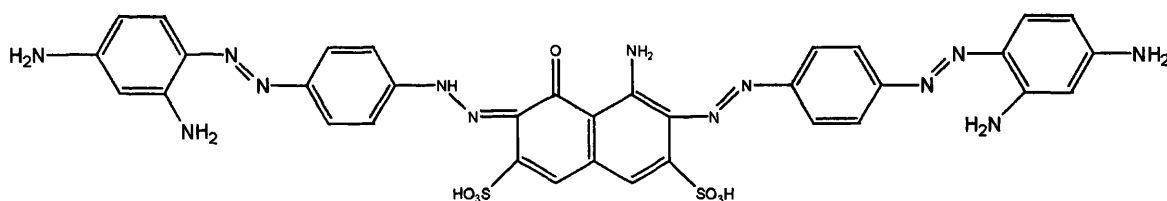
Dyes

Black, yellow, cyan and magenta dyes are used in ink-jet printing, with the three secondary colours required to create full colour printing. Dyes which have narrow absorption bands and no secondary visible absorptions are preferred, as these have a brighter colour. Unfortunately bright dyes often have poor lightfastness.⁹ Ink-jet dyes should have good colour or tinctoral strength, in other words, the dye should have an intense visible absorption giving it a strong colour. Dyes also need to have the same shade of colour on different substrates, for example on papers with different pH, different additives and different adsorption and texture properties. They should also be stable to temperatures of up to about 300 °C, which might be encountered in printing.

Black dyes used in ink jet printing are usually polyazo dyes such as the trisazo dye CI Direct Black 154 (1-1) and the tetrakisazo dye CI Direct Black 19 (1-2).

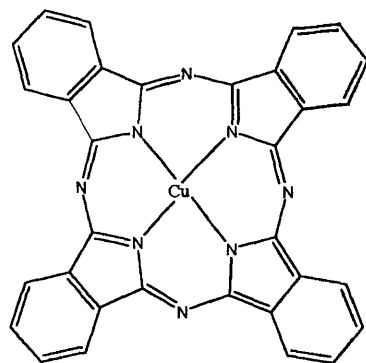


(1-1)



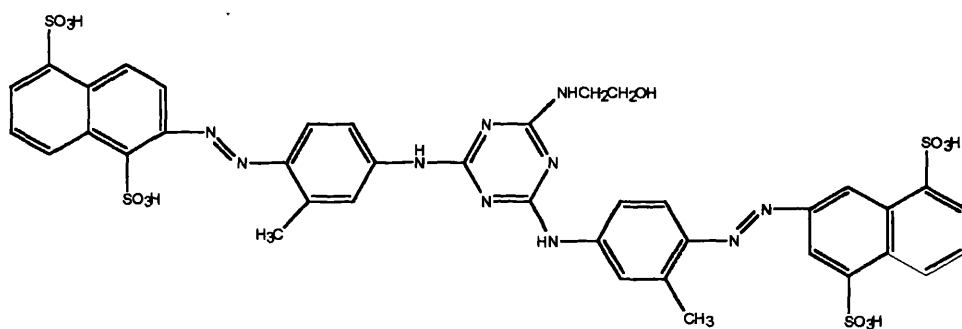
(1-2)

The dyes used for cyan are copper phthalocyanines such as CI Direct Blue 199. This has the molecular formula $\text{CuPc}(\text{SO}_3\text{H})_2\text{SO}_2\text{NH}_2$, where CuPc = Copper phthalocyanine (1-3).



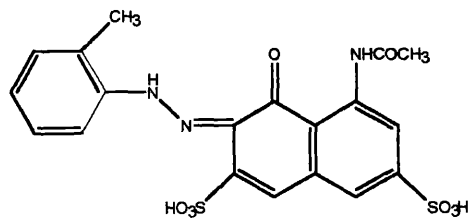
(1-3)

The yellow dye used as standard in industry is Direct Yellow 86 (1-4).



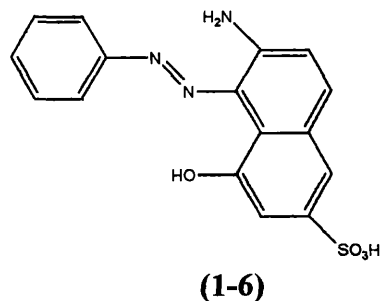
(1-4)

An example of a magenta dye used in ink-jet printing is CI Acid Red (1-5). These acid type dyes exist predominantly in the hydrazone tautomeric form rather than the azo form.



(1-5)

Other dyes such as the aminoazo dye (1-6) exist in the azo tautomeric form but these tend to be duller in shade than the acid dyes.



The above mentioned dyes have been used in aqueous based inks and contain sulphonic acid (SO₃H) groups to increase their solubility in water.

Solvent soluble inks are currently new to the market and the products are less well established, but it is likely that the dyes will be of the solvent or disperse type and will probably include azo and anthraquinone dyes.

Black dyes often suffer from problems with toxicology, lightfastness, wet fastness and smear fastness. In contrast cyan dyes have a very strong bright colour and have good wet fastness and lightfastness properties making them excellent for use in inj-jet printing. The yellow dye, Direct Yellow 86 (1-4) has quite good wet and smear fastness properties and also has reasonable lightfastness. Finding a magenta dye with good lightfastness has proved much more difficult and the magenta dye, CI Acid Red (1-5) suffers from poor lightfastness. This may be due to the hydrazone tautomeric form, in which (1-5) predominantly exists, being unstable towards light.⁹ Other dyes such as the aminoazo dye (1-6) exist in the azo tautomeric form and have better lightfastness but are duller in shade than the acid dyes. A fully satisfactory magenta dye which is both bright in colour and has good lightfastness properties has not been produced yet. The yellow dyes and particularly the magenta dyes fade much more quickly than the highly stable cyan dyes, causing an unequal and undesirable fading.

Objectives of the research

Because of the problems with the lightfastness of magenta dyes outlined above, Avecia, are interested in understanding the mechanism of photofading of azo dyes, which would help in the design of better dyes than those currently in use.

The aim of this work is to look initially at a series of substituted donor-acceptor azobenzenes like the one shown in Figure 1.1, and examine their stability towards light by both experimental and theoretical methods.

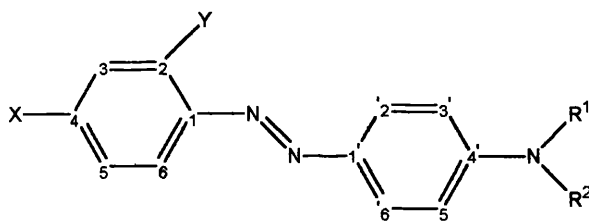


Figure 1.1 A donor-acceptor azobenzene containing an 4-dialkylamino group as the donor group and electron acceptor groups X or Y, for example NO₂, at the 2 or 4 position.

Several papers have proposed mechanisms for the photofading reactions of azo dyes on polyamide substrates^{19,13,14} but the reaction on non protein substrates is less well understood and the fading products are not well established.¹⁵

By studying the dyes fading behaviour and identifying some of the fading products of their photo-reactions it was hoped to suggest possible mechanisms for these photo-reactions.

Since the principle interest of this research is in dyes for application in ink-jet printing, it would be preferable to study the fading behaviour of azo dyes on paper. However, following the photo-reaction involving the dye on paper and identifying the fading products is a complicated process. It was therefore decided to use a simpler model solvent system to mimic the fading on paper. The solvent chosen when modelling the system is very important, and the solvent should imitate the chemical nature of the paper substrate as far as possible.

Paper is a form of cellulose which is a plant material consisting of macromolecules varying in molecular weight from several hundred to several thousand glucose units,¹⁶e.g. Figure 1.2

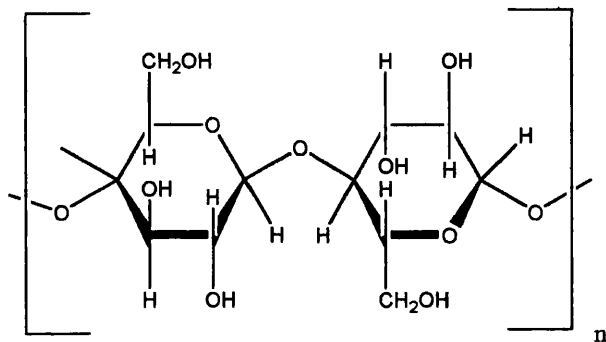


Figure 1.2 The structure of cellulose

Cellulose contains multiple OH groups and a CH₂OH group. Methanol also contains an OH group joined to an alkyl group, and should therefore have a some correlation with the properties of cellulose. A better choice for a model solvent might have been ethylene glycol as it contains two hydroxy groups, but unfortunately the dyes to be studied have poor solubility in ethylene glycol. The solubility of these dyes in methanol is comparatively good. It is also much easier to follow any fading behaviour in the solvent phase than on substrates. Thus methanol was chosen as a first approximation for the cellulose model system.

The irradiation source chosen to fade the dyes was a 1000 W xenon arc lamp. It has a similar irradiation profile to the sun in the 200 to 900 nm range, unlike the spiked output of an alternative mercury lamp, and should therefore imitate conditions under which natural solar fading would occur (see Figure 1.3 and Figure 1.4).¹⁷

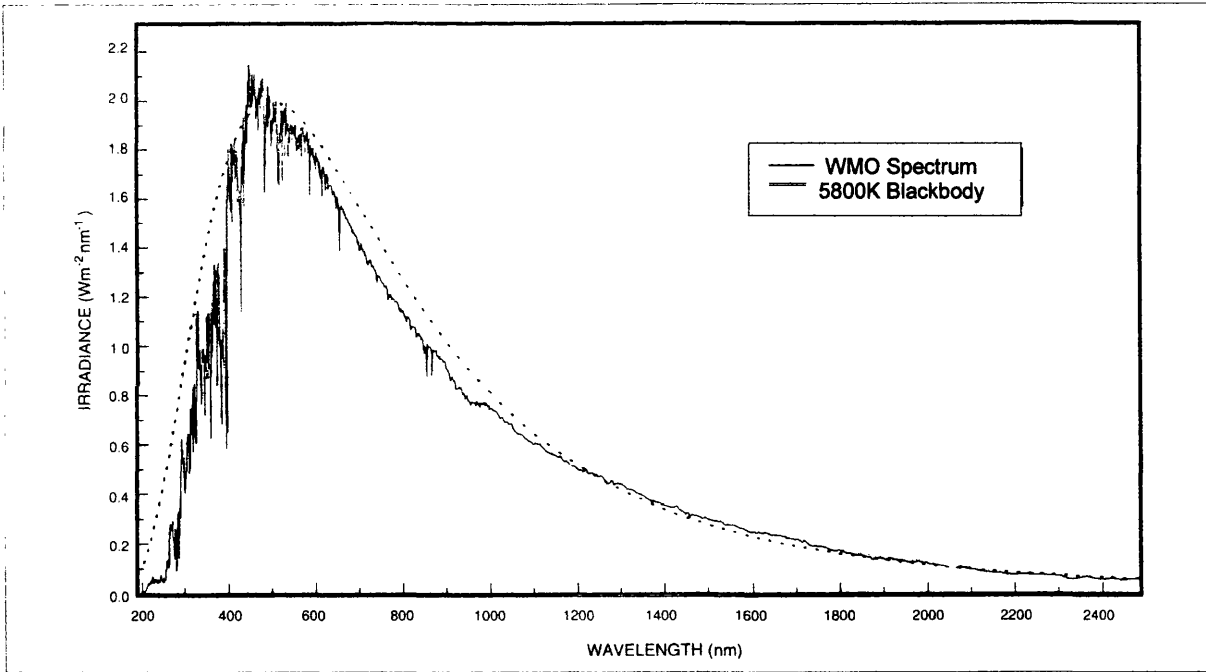


Figure 1.3 Spectrum of the solar radiation outside the earth's atmosphere compared to the spectrum of a 5800 K blackbody. The surface temperature of the sun is 5800 K, so the spectrum of the radiation from the blackbody is similar.

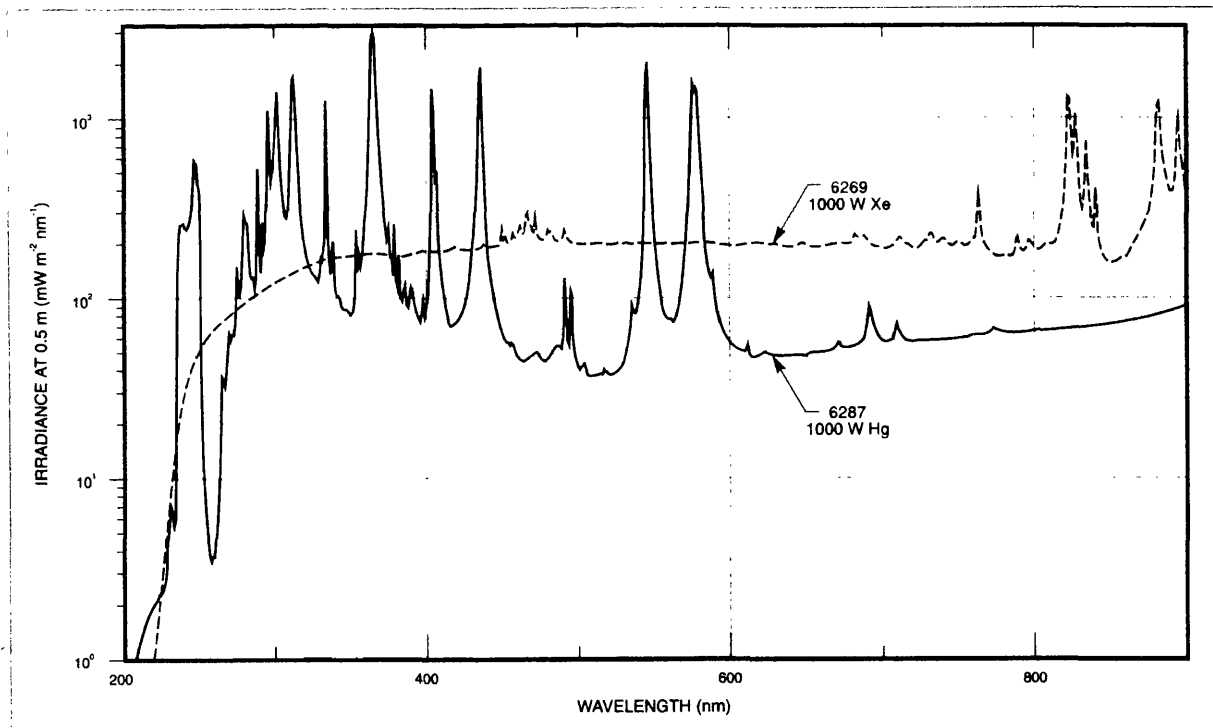


Figure 1.4 Spectral irradiance curves from 200 to 900 nm for 1000 W Xenon and Mercury arc lamps.

There are a vast number of publications on the relationship of colour and constitution of organic dyes,^{18,19,20,21} some of which have described theoretical methods for spectroscopic predictions of the visible absorption band.^{22,23} Relatively few of these papers have focused on the relationship between lightfastness and structure²⁴ and unlike spectroscopic properties there is no theoretical or semi empirical method for the prediction of lightfastness.

The objective of this work therefore, was to explore the computational modelling techniques to examine possible excited state species which might be involved in the photo-reactions of the dyes and to try and establish if there is a correlation between physical properties of the excited states of azo dyes, such as their relative energies, geometries, charge distribution etc., and lightfastness.

Section 1.2

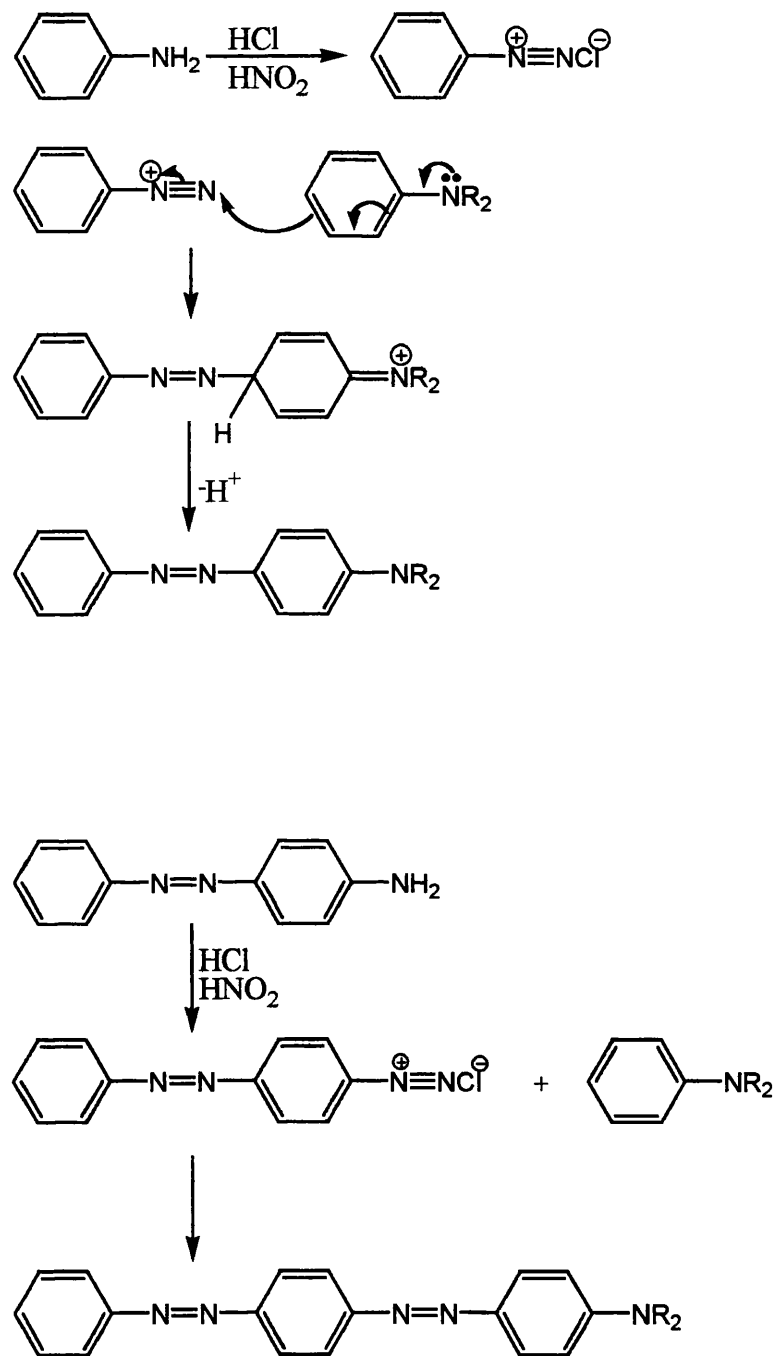
Azo dyes²⁵

Azo dyes are by far the most important class of colouring matters. They are used in the coloration of all types of fibres, they provide many useful pigments and analytical colorimetric reagents. The versatility of these dyes stems from the ease with which they can be manufactured; almost any diazotized aromatic amine can be coupled with a wide variety of stable nucleophilic unsaturated systems to give a coloured azo product.²⁵

The synthesis is outlined in Scheme 1.1. The initial step shown in Scheme 1.1 is the formation of a diazonium compound from an aromatic amine, using hydrochloric and nitric acids at a temperature below 5°C. Above this temperature the diazonium compound formed can break down losing nitrogen. The diazonium salt is an electrophile which can attack a nucleophilic aromatic substrate known as the coupling component. The coupling component is usually a phenol, in the presence of sodium hydroxide or an amine in the presence of sodium acetate.

If the azo dye itself contains a primary amino group it too can form a diazonium salt which is then able to couple with another coupling component to give a bis azo dye.

The Synthesis of Azo Dyes

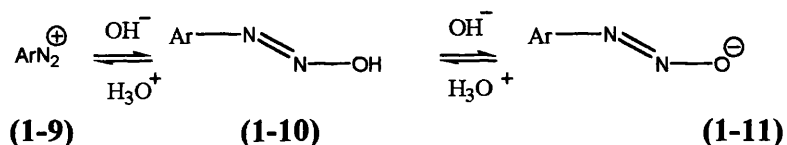


Scheme 1.1 Synthesis of mono and bis azo dyes.²⁶

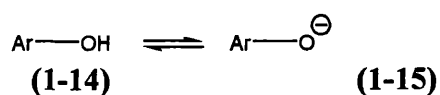
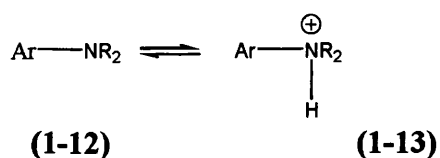
The diazotisation reaction involves the nitrosation of a primary amine, followed by its deprotonation and dehydration as in Scheme 1.2.

Here the rate determining step is a function of the nitrosating species, which reacts with the amine as soon as it is formed. With non basic amines such as para-nitroaniline, Equation (1-2) is never adopted, even at low acidities, because of the poor nucleophilicity of the amine nitrogen. At higher acidities, the acidity of the medium and the basicity of the amine have an effect on the rate of reaction. Diazotisations are preferably carried out in dilute mineral acids (approximately 2.5 molar) at 0-5°C with concentrated sodium nitrite (NaNO₂) solution. Concentrated acid, usually sulphuric acid, is used for non basic amines like poly-nitroanilines and heteroaromatic amines like aminodinitrothiophenes.

Diazotisations in organic solvents with organic nitrites such as pentyl nitrite are usually only used for the preparation of solid diazonium salts in the laboratory. These are explosive, and hence the diazonium salt is usually used without isolation in industry. The diazonium salt is thus reacted in situ with the coupling component. Depending on the pH of the medium, the diazonium exists in equilibrium with the possible species (1-9), (1-10) and (1-11).²⁷



The common coupling components, amines (1-12) and phenols (1-14) also exist in equilibrium with the ammonium salt (1-13) and the phenolate (1-15) respectively.

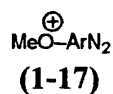
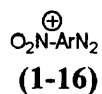


It is actually the species (1-12) and (1-15) that react with the diazonium salt. The pH of the reaction is obviously very important. A pH of 4-10 is chosen for reaction of the diazonium salt with phenols. The pH must not be too high, or the diazonium salt will decompose. For amines a pH range of between 4 and 7 is chosen as again the stability of the diazonium salt is poor above pH 7 and there is enough free amine to act in this range.

The rate of reaction then satisfies Equation (1-3):



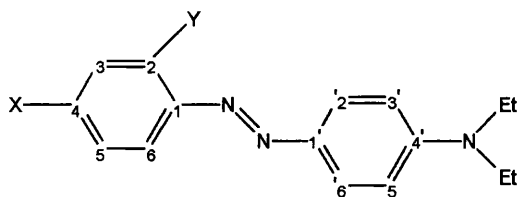
The position on the coupling component at which electrophilic attack by the diazonium ion takes place may be related to the position of highest electron density. This is at the para position for amines and phenols but steric factors may influence the position of attack. The reaction is also dependent on the reactivity of the diazonium salt and the coupling component. The best diazonium salts are those that contain electron withdrawing groups, as these groups make the diazonium ion more electrophilic. For example the diazonium salt (1-16) reacts 10^5 times faster than (17).²⁷



The best coupling components contain one or more donor substituent such as an amino group. These donor substituents increase the rate of reaction by increasing the electron density of the aromatic ring, making it more vulnerable to electrophilic attack.

Donor-acceptor Azo dyes

Donor-acceptor dyes such as (1-18) are made up of a donor group, often an amino or dialkyl amino group, that readily releases electrons, linked by an unsaturated bridge to an acceptor group.



(1-18)

The lone pair of the amino nitrogen, is aligned with the adjacent conjugated π system. The acceptor group is the phenyl ring (labelled C¹-C⁶) which may contain a substituent X and/or Y, where X and Y are electron withdrawing groups, for example a nitro or cyano groups. The -N=N- bridge serves to extend the conjugation of the system moving the principle absorption band further into the visible region of the spectrum.

The π electron system of donor acceptor azo dyes can be described by the three models illustrated in Figure 1.5.

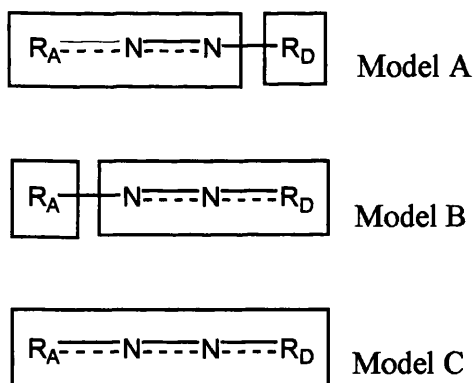
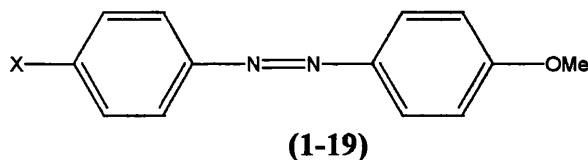


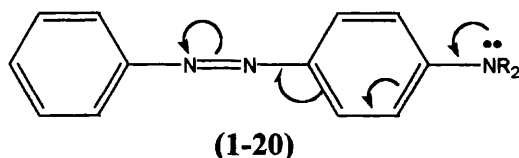
Figure 1.5 The representation of the π electron system of donor acceptor azo dyes by 3 models.⁴⁹

The system of the substituted acceptor phenyl ring and the azo bridge can be regarded as a complex acceptor group, as there is a significant amount of electron density going to the azo

group from the donor. This situation is described by Model A in Figure 1.5. This type of delocalisation might be seen in azo compounds such as (1-19) where the X-Ph-N=N- acts as a complex acceptor group.

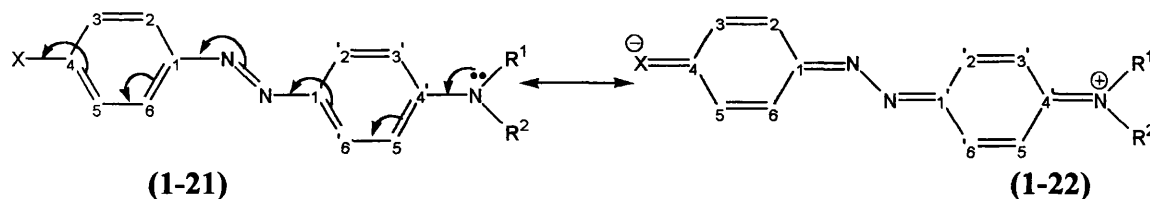


If there is no strongly electron withdrawing substituent present on the acceptor phenyl ring, then the π electron system may be described as Model B in Figure 1.5, where the azo moiety acts as the electron acceptor group. This situation might occur for compound (1-20), where there is no electron withdrawing group and delocalisation may be partially restricted to the movement of charge to the azo moiety and build up on the azo nitrogen attached to the acceptor phenyl ring.



If however, a strong electron donor substituent is present on the donor phenyl ring and a strong electron acceptor substituent is present in the acceptor phenyl ring, then the azo group can be thought of as losing its individuality and the azo dye π electron system may be considered as a whole, according to Figure 1.5 Model C. This type of model describes the donor-acceptor dyes such as compound (1-21), in which X is a strong electron withdrawing substituent such as a nitro group. The migration of electron density from the donor to acceptor group, that occurs during an electronic transition, can be represented by the canonical structures (1-21) and (1-22). This migration of electron density is often referred to as a charge transfer configuration, and charge transfer configurations contribute strongly to the lowest excited state of donor acceptor azobenzenes. This charge transfer configuration results from mixing between the donor p_π orbitals and the π -system of azobenzene. Donors of low ionisation potential, such as amino and mercapto substituents, produce shifts of the long wavelength absorption band to lower energies. Thus the energy of the transition from the ground state to the excited state of the dye will depend on the strength of both donor and acceptor groups and on the nature of the bridging group of the molecule. The colour of the dye generally deepens with the strength of the acceptor substituent.

In the ground state π electrons in the molecule are polarized from the donor to the acceptor groups. The polarity of the molecule and thus its wavelength are increased by attaching electron withdrawing substituents to the acceptor phenyl ring (C₁-C₆).



A shift to longer wavelength on substitution of electron withdrawing groups, such as X = NO₂ or X = CN into azo dyes like (1-21) can be described as a *Bathochromic* or *Red shift*, implying a displacement of the absorption band to longer wavelength or the red end of the spectrum. Generally, the stronger the electron withdrawing substituent, X, the larger the bathochromic effect and the better the lightfastness.^{4,102} Some examples of the effect of substituents with different electron acceptor strength on the wavelength and lightfastness of the amino azo derivatives of (1-23) are given in Table 1.1.

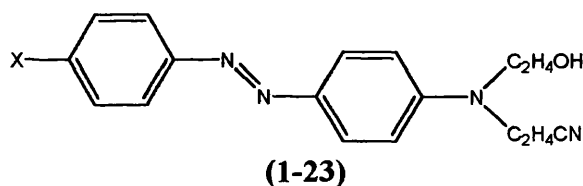


Table 1.1 Absorption maxima and lightfastness ratings of para-substituted derivatives of structure (1-23).⁴

| X | λ_{\max} (ethanol) | Lightfastness Rating (polyester) |
|----------------------------------|----------------------------|----------------------------------|
| H | 397 | 4 |
| Cl | 408 | 5 |
| COOC ₂ H ₅ | 422 | 4 |
| CN | 433 | 4-5 |
| NO ₂ | 451 | 4-5 |

From the values in Table 1.1, there is an obvious bathochromic shift with substituents of increasing electron acceptor strength, while lightfastness ratings on polyester do not seem to differ greatly.

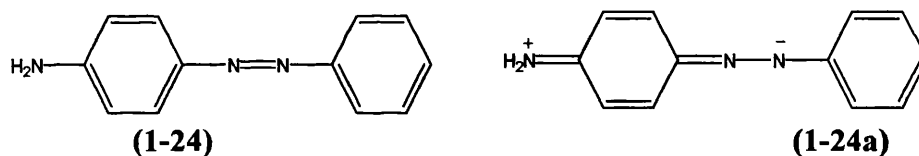
The nitro group is a strong acceptor group and dyes containing a para-nitro group are usually the most bathochromic and lightfast of their series. However, the position of the nitro group is all important, as shall be seen below. Correlations between Hammett σ constants and electron acceptor strength are reasonable,^{4,25,41,120,28} as σ constants are based on ground state properties, which may have little relevance to the excited state. Hammett σ constants are a measure of the electronic effects of substituents on a ring system. The magnitude of the σ constant is related to the electron donating or withdrawing strength of the substituents and their position on the ring i.e. ortho, meta or para. Some Hammett σ constants for substituents on azobenzenes are given in Table 1.2. Hydrogen has a σ -constant of zero and electron withdrawing substituents have positive and electron donating substituents negative σ -constants, respectively.

Table 1.2 Hammett σ -constants for meta and para substituents²⁹

| Substituent | σ_{meta} | σ_{para} |
|--------------------|------------------------|------------------------|
| NH ₂ | -0.16 | -0.66 |
| OH | 0.12 | -0.37 |
| CH ₃ | -0.07 | -0.17 |
| H | 0.00 | 0.00 |
| Cl | 0.37 | 0.23 |
| CH ₃ CO | 0.38 | 0.50 |
| CN | 0.56 | 0.66 |
| NO ₂ | 0.71 | 0.78 |

Note the influence of the position of the substituent (meta or para) on the magnitude of the σ -constant. In general para substituents have a larger σ -constants, particularly for electron donors. For compound (1-21), correlation between λ_{max} and Hammett σ constants for different substituents X show an expected red shift as electron withdrawing strength increases.¹⁹ Better correlations may be found with σ constants that take into account the inductive and resonance components, σ_i and σ_r respectively of the substituent.^{19,41}

For X= F, Ph, CF₃, CN, NH₂, NHAc, NO₂, CO₂Et, CO₂⁻, and SO₃⁻ correlations are good, but for other electron donors i.e. X= Me, Et, MeO, PhO etc the correlation is worse. This implies that the resonance effect has a much greater influence on colour than the inductive effects. Resonance theory states that if an organic molecule can be represented as a hybrid of 2 extreme canonical structures then the closer these are in energy, the smaller will be the gap between the ground and excited states, i.e. the more bathochromic the absorption will be. When several low energy resonance forms are available, it is assumed that the greater the number of these, the more bathochromic the molecule. Examination of the spectra of compound **(1-24)** and its meta and ortho isomers showed that the meta and ortho aminoazobenzenes were the most bathochromic, and the para the least. This is in direct contradiction with the predictions of resonance theory. Resonance theory suggests that charge separated structures such as **(1-24a)** help to describe the first excited state, but PPP²⁵ calculations show that in fact, electron density build up is greater at the α azo nitrogen, and is much less significant at the β nitrogen atom than suggested by structure **(1-24a)**. Therefore, resonance interpretations of colour and colour change phenomena in azo dyes must be treated with suspicion²⁵. PPP calculations on **(1-24)** also give better agreement with experimental spectra than resonance predictions.



Position of Substituents

The effect of placing more than one acceptor substituent into the acceptor ring and the position of these substituents in the rings is exemplified by considering structure **(1-25)**. The absorption maxima of the di-cyano aminoazobenzene derivatives³⁰ of **(1-25)** are listed in Table 1.3.

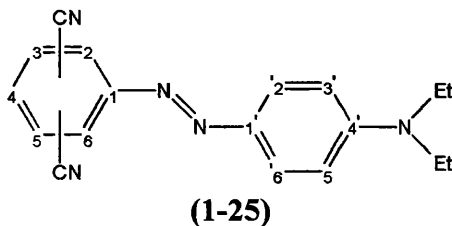
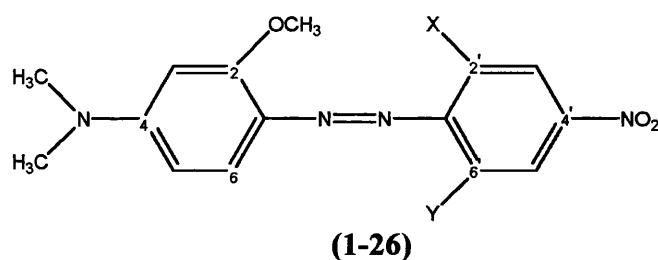


Table 1.3 Absorption wavelengths of cyano substituted aminoazobenzene dyes

| Position of cyano-group (s) | λ_{\max} /nm (ethanol) |
|-----------------------------|--------------------------------|
| 2 | 462 |
| 3 | 446 |
| 4 | 466 |
| 2,3 | 490 |
| 2,4 | 514 |
| 2,5 | 495 |
| 2,6 | 503 |
| 3,4 | 500 |
| 3,5 | 478 |
| 2,4,6 | 562 |

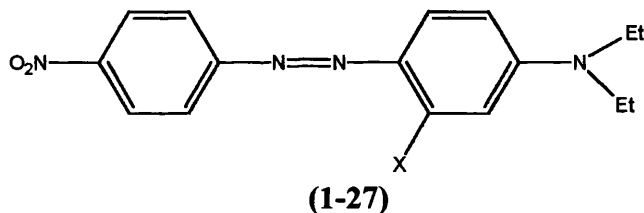
These values show that electron withdrawing groups are most favorable in the ortho and para positions and that the effects are additive, with more substituents producing larger bathochromic shifts. The λ_{\max} of the derivatives increases in the order 3'5' < 2'3' < 2'5' < 3'4' < 2'6' < 2'4'. The above evidence suggests that electron withdrawing substituents in ortho and para positions on the acceptor ring produce the most bathochromic dyes. Indeed, electron withdrawing groups at the 2' and 6' positions on the acceptor ring of **(1-26)** may cause large bathochromic shifts - which are not expected for Dewar's rules (see PMO theory).¹⁹



Certain substituents may have an inductive or mesomeric effect depending on their position. The MeO for example, is an electron donor in the para position, but in the meta position it is a weak electron acceptor.

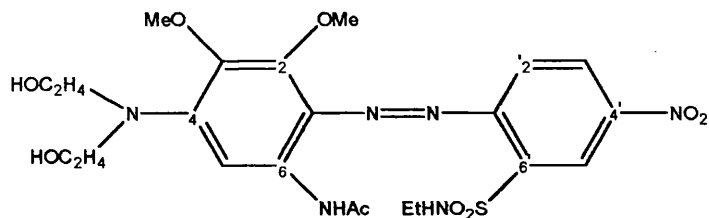
Electron withdrawing groups in the ortho and para positions of the acceptor ring enhance light fastness, whereas electron donors reduce it. The exception is the ortho nitro group which has poor lightfastness and a smaller bathochromic shift and a lower intensity, which may be due to its steric interactions with the azo nitrogen.⁴ It has been suggested¹⁰² that the ortho nitro substituent may inhibit trans-cis isomerisation, which is a possible process for energy loss, thus increasing the likelihood of rupture of the β C-N bond. The ortho nitro group also inhibits delocalisation of electrons between the azo nitrogen atoms according to Freeman and McIntosh,¹⁰² rendering the C-N bond on the coupler side more susceptible to photolytic cleavage. Alternatively, it may be able to cause an intramolecular oxidation.

So far, we have only mentioned the effect of substituents on the acceptor ring. Increasing the number of substituents on the donor ring also affects the absorption wavelength, and possibly the lightfastness. Attachment of electron withdrawing substituents to the donor residue usually results in a small shift to higher energies (shorter wavelengths) of the absorption band. For example the azo dye (1-27), where X = H has an absorption wavelength of 486 nm in ethanol³¹ whereas, when X is the electron withdrawing group NO₂, (1-27) has a wavelength of 470 nm in ethanol. This shift to shorter wavelengths is termed a *Hypsochromic* or *Blue shift* and implies the displacement of the absorption band to shorter wavelengths or the blue end of the spectrum.²⁵



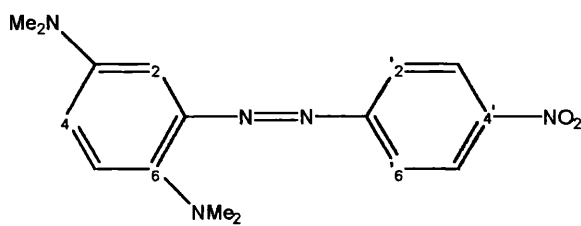
The effect of placing more than one donor group in the donor ring results in a shift of the low energy absorption band to longer wavelengths. This is exemplified by considering the wavelength of structure (1-27) when substituted by different X. The wavelength of structure (1-27) when X = NEt₂ is 542 nm in ethanol, compared with 486 nm when X = H.¹⁹

The most bathochromic dyes, i.e. dyes absorbing at *ca* 600 nm, should be heavily substituted with donor groups and preferably have at least 2 strong acceptors²⁵, such as the blue mono azo dye (1-28), which absorbs at 600 nm in methanol.



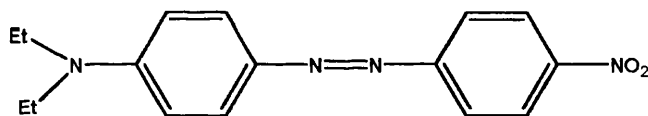
(1-28)

Dyes with more than one electron donating substituent such as (1-29), are predicted to absorb at even longer wavelengths. The λ_{max} of (1-29) is predicted to be near 700 nm.¹⁹



(1-29)

In comparison, (1-30), with only one donor amino group, has λ_{max} at 457 nm in cyclohexane,¹⁹ illustrating how the number of amino and alkoxy groups and their placement at resonating positions affect the position of absorption maxima.



(1-30)

With respect to lightfastness, electron acceptor substituents generally enhance dye lightfastness.¹⁴ On polyamide fabrics, like nylon, however, ortho and meta electron acceptor groups appear to reduce lightfastness but para acceptor groups enhance it.¹⁰⁸ This behaviour may also be seen in certain selected solvents.

The above evidence suggests that electron withdrawing substituents in ortho and para positions on the acceptor ring (with the exception of the 2'-nitro group) produce the most bathochromic and lightfast dyes. However, too many electron withdrawing groups can reduce lightfastness by distortion and weakening of the azo link.

In summary, any factor which lowers the ionization energy of the donor unit generally causes a bathochromic shift.

Factors include:

1. Increasing donor strength.
2. Increasing the strength of the acceptor.
3. Varying the position of the donor.
4. Replacement of the benzene ring by a heterocyclic ring

Donor amino group

Aminoazobenzenes, where the donor amino substituent is at the 2 or 3 position absorb at longer wavelengths than 4 aminoazobenzenes ($\lambda_{\text{max}} = 415\text{nm}$ for 2-aminoazobenzene in ethanol and $\lambda_{\text{max}} = 450\text{nm}$ for 3-aminoazobenzene in methanol, compared to $\lambda_{\text{max}} = 386\text{nm}$ for 4-aminoazobenzenes in methanol)³², but have a high degree of bond equalization and alternation. The groups on the amino nitrogen also have a big effect on the photofading rate, which may be related to the change in electron density on azo nitrogen, as migration of electron density to the azo bridge will affect the rate of degradation.

Ashutosh *et al.*¹ reports that an electron withdrawing group on an amino nitrogen reduces basicity and improves lightfastness, and studies by Seu¹⁰⁷ show a linear relationship between the inductive effect of substituents, attached to the amino nitrogen, and the λ_{max} and fading rate of a series of aminoazo dyes. More electron withdrawing substituents give a greater the shift to shorter wavelength and a higher the rate of fading.

It is also reported that increased branching on at least one of the N-alkyl chains at the a position on the amino group gives better lighthfastness compared to unbranched isomers and homologues.³³

Heterocyclic Ring Systems

Further variations in wavelength of azo dyes can be achieved replacing one of the phenyl rings of azobenzene by a heterocyclic ring such as thiophene. This produces a large bathochromic effect and examples of the wavelengths of some azothiophene derivatives of (1-31) are given in Table 1.4.

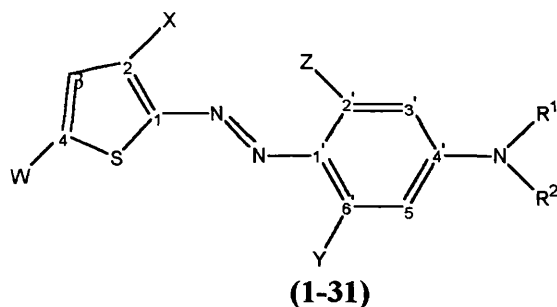


Table 1.4 Absorption maxima of some substituted aminoazothiophenes in methanol.[†]

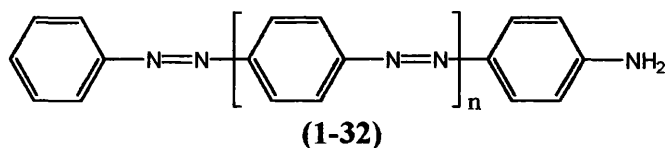
| W | X | Y | Z | R ¹ | R ² | λ_{\max}/nm |
|-----------------|----------------------------------|-------|---------------------|--|--|----------------------------|
| NO ₂ | NO ₂ | _____ | NHCOCH ₃ | C ₂ H ₅ | C ₂ H ₅ | 613 |
| NO ₂ | COCH ₃ | _____ | CH ₃ | (C ₂ H ₅) | C ₂ H ₄ COOCH ₃ | 609 |
| NO ₂ | COOC ₂ H ₅ | _____ | CH ₃ | C ₂ H ₄ COOCH ₃ | C ₂ H ₄ COOCH ₃ | 615 |
| NO ₂ | NO ₂ | None | _____ | C ₂ H ₄ OCOCH ₃ | C ₂ H ₄ OCOCH ₃ | 627 |

[†] Experimental results obtained in this work.

In addition to changes in wavelength, substitutions may also result in a change in the intensity of the absorption band. These changes are described in terms of the *Hyperchromic effect*, implying an increase in the absorption band intensity and the *Hypochromic effect*, defined as a decrease in absorption band intensity. The intensity of the absorption band is at a maximum when the donor is in the para position; ortho and meta donors give a weaker intensity band. For more examples of substituted azo dyes absorption maxima data, refer to M. Okawara et al. *Organic Colourants*.³²

Bisazo/ Polykisazo

By extending conjugation by incorporating different electron donor and acceptor groups into the azo dye, or by including additional azo groups as in the disazo dye **(1-32)**, a large range of spectral colours can be produced. The position of the first intense absorption of **(1-32)** is shifted to longer wavelengths with the extension of the π system. For example when for **(1-32)**; $n = 0$, $\lambda_{\max} = 490$ nm compared to 585 nm when $n = 1$ and 610 when $n = 2$.



Further variations in colour can be achieved by replacing the phenyl acceptor ring in the azo dye with a heterocyclic ring such as thiophene.

Section 1.3

Steric factors²⁵

The twisting of a conjugated molecule can greatly affect its physical properties. When a molecule is crowded to disrupt the coplanarity of its conjugated atoms, changes in its electronic spectra may be observed when compared to the planar model. There are three types of spectral effect³⁴:

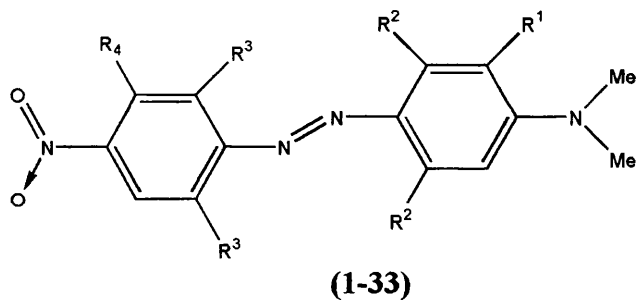
1. Slight twisting about a bond gives a hyperchromic effect only.
2. Moderate twisting giving both hyperchromic and hypsochromic effects.
3. Severe twisting giving steric inhibition of resonance and resulting in the cumulative spectra of the molecules isolated chromophores.

The extent of twisting may be calculated by the Braude and Sondheimer³⁵ equation:

$$\cos^2 \theta = (\mu_{\text{observed}} - \mu_{90^\circ}) / (\mu_{0^\circ} - \mu_{90^\circ})$$

This equation relates the interplanar angle θ between the aryl and carbonyl chromophores of benzaldehyde and acetophenone derivatives to the dipole moment. μ_{90° and μ_{0° are the dipole moments for the completely deconjugated molecule and completely conjugated molecule respectively. Azobenzene and its para derivatives have a π conjugated planar structure but as we shall see below, substituents in the ortho position may cause varying degrees of steric hindrance. The effect of steric hindrance on the visible spectrum is best exemplified by considering the structure of the mono azo dye (1-33). There are three possible sources of steric hindrance, each of which can cause a subsequent hypsochromic shift of the visible absorption band. If R^1 , is large then it causes the rotation out of the plane of the donor amino group, thus giving a hypsochromic shift. A large R^4 will cause a similar rotation out of conjugation of the acceptor nitro group, again leading to a hypsochromic shift. Bulky R^2 and R^3 groups can interact with the lone pair on the azo nitrogens, giving rise to a loss of planarity and a hypsochromic shift of the visible absorption band.

Of these types of hindrance, the first 2 are well known but the third is more complex. It is only significant when either both R^2 or both R^3 groups are present on the same ring, as is illustrated in (1-33).



When only one ortho substituent is present, its steric interaction is greatest with the lone pair of the more remote azo nitrogen.

This crowding can be relieved by rotation into the conformation shown in Figure 1.6b, so a single substituent has little effect on the spectrum. Similarly when there is one ortho substituent on each ring there are three possible conformations (see Figure 1.7), of which the least strained will be adopted.

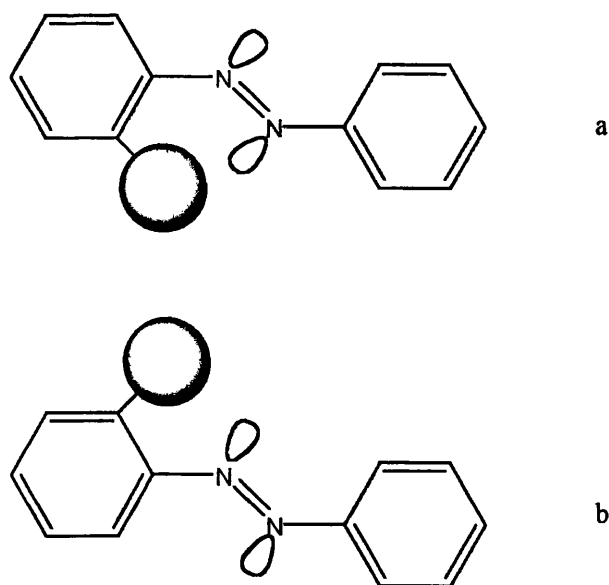


Figure 1.6 Two possible conformations for an ortho substituted azobenzene

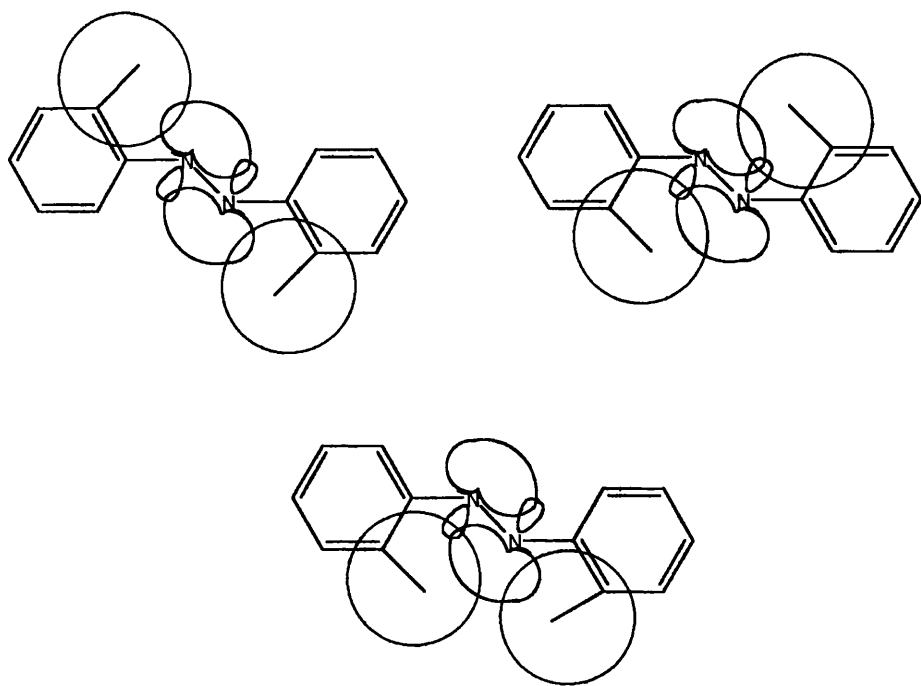
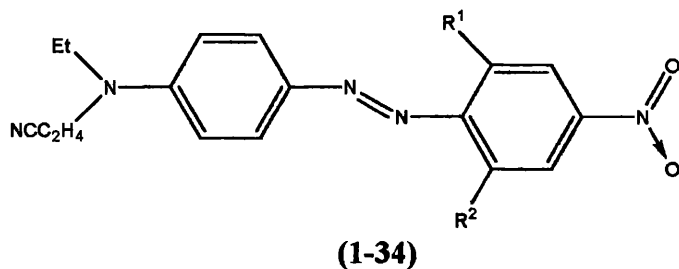


Figure 1.7 The three possible conformations for an ortho disubstituted azobenzene. *The mushroom shaped orbital is the sp^2 density function where there is a 95% probability of finding a lone pair.³⁴

When two substituents are present e.g. both R^2 groups, both conformations are sterically strained, and the molecule is trapped in a non planar geometry resulting in a marked hypsochromic shift.

This is demonstrated by structure (1-34), when $R^1 = R^2 = H$ ($\lambda_{max} = 453$ nm), compared to (1-34) when $R^1 = Me$ and $R^2 = H$ ($\lambda_{max} = 454$) which is virtually unaffected by replacement of H by Me.

Whereas when $R^1 = R^2 = Me$, (1-34) suffers a large hypsochromic shift, to $\lambda_{max} = 383$ nm.



The more bulky the group, the greater the effect; rod like cyano groups have only a small effect. Planar substituents, like the ortho nitro group will relinquish their planarity with the phenyl rings in order to avoid interaction with the azo bridge³⁶. This is supported by the longer wavelength of the para nitro isomer compared to the ortho nitro compound. If there are four ortho substituents present, for example four methyl groups, the $n-\pi^*$ absorption band shifts to longer wavelength and higher intensity due to greater conjugation of the phenyl rings and the lone pair.

The placement of multiple donor and acceptor groups in both ortho positions should therefore be avoided to produce the most bathochromic dyes.

Section 1.4

Photochemistry of azo dyes

Several papers have examined the electronic spectra and physical properties of the azo dyes,^{19,30,37,38,39,40,41} particularly the long wavelength visible transition. However, for lightfastness studies, it is necessary to consider the other transitions of the molecule as these may be involved in the photo-fading reaction. This section reviews the photochemical transitions and reactions of mono azo dyes discussed in the literature.⁴²

Before considering the photochemical transitions of azo dyes the changes in electronic structure that can occur on the absorption of a photon of light into a molecule will be reviewed.

The concepts of basic molecular orbital theory will be introduced by considering the types of bonding that can occur between two atoms. The motion of an electron in an atom or molecule can be described by a wave function, Ψ . The square of the wave function, Ψ^2 , can be used to find the probability of an electron occupying a certain region in space. The regions where there is a high probability of finding an electron are called orbitals. The orbitals for s electrons are symmetrical and spherical in shape whereas p orbitals have a dumbbell shape. The wave function also indicates that orbitals have phase represented as + or - regions. In phase overlap of atomic orbitals (+ with + or - with -) leads to constructive overlap and a bonding molecular orbital, while out of phase overlap (+ with -) leads to cancellation of the wave function and a high energy anti-bonding orbital.

Symmetrical or in phase overlap of s orbitals gives a σ bond, and anti-symmetrical or out of phase s orbital overlap, gives the high energy anti-bonding σ^* molecular orbital. The situation for p orbitals is more complicated as they are dumbbelled in shape with regions of + and - phase. They

can therefore overlap in two possible ways, the first of which is end on overlap which again results in the formation of σ and σ^* bonds. Both types of σ bonding orbitals are shown in Figure 1.8.

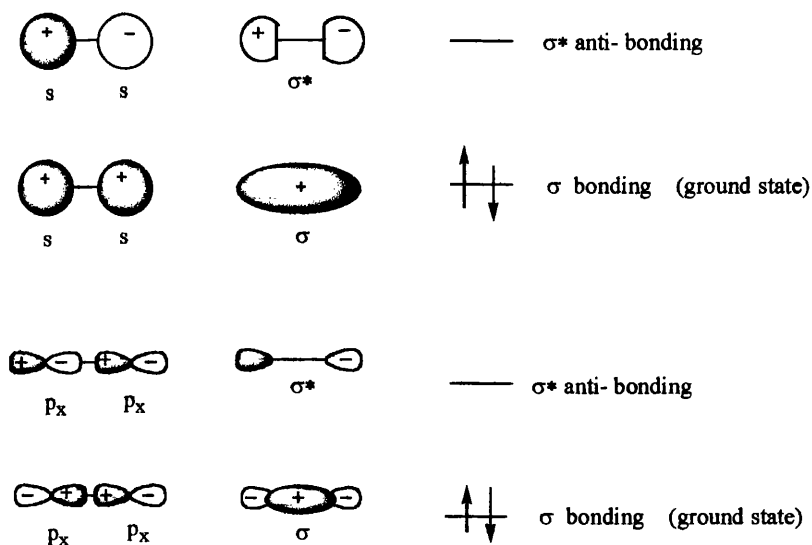


Figure 1.8 The σ and σ^* molecular orbitals formed from overlap of s orbitals and overlap of p_x orbitals along the inter-nuclear axis.

The second possibility is sideways overlap of the p_z orbitals, which results in π and π^* molecular orbitals, from in phase and out of phase overlap respectively, as shown in Figure 1.9. The π molecular orbital has two regions of electron density, one above and one below the plane of the molecule along the inter-nuclear axis.

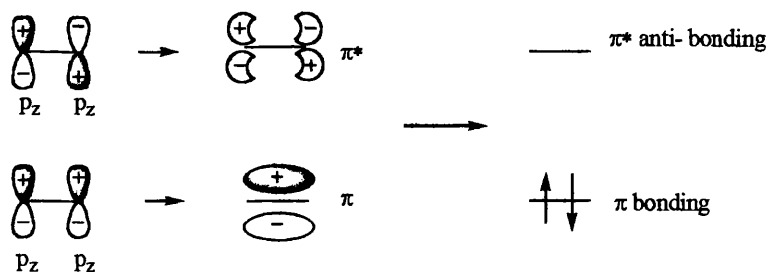


Figure 1.9 In phase and out of phase overlap of p_z orbitals.

This type of π bonding is encountered in unsaturated hydrocarbon systems, such as, ethylene, butadiene and benzene. Both end on (σ) and sideways (π) overlap contribute to the bonding between the two carbon atoms in ethylene. The σ bonding orbital is much lower in energy than either the π or the π^* orbitals in ethylene and the σ^* orbital is higher than both the π and π^* orbitals in ethylene.

The $2p_z$ orbitals in butadiene can overlap in a similar way to the $2p_z$ orbitals in ethylene to give a large π bonding molecular orbital. There are however several ways in which the butadiene $2p_z$ orbitals of the same and opposite phase can combine to produce bonding and anti-bonding molecular orbitals of different energies. These orbital combinations are shown in Figure 1.10.

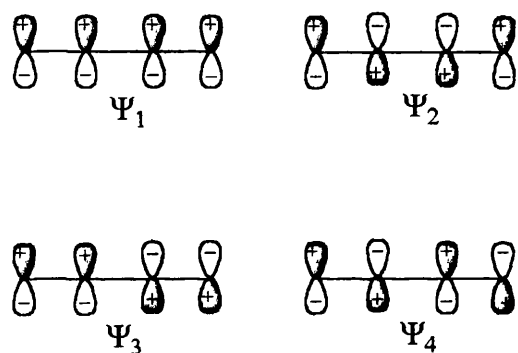


Figure 1.10 The lowest energy bonding orbital Ψ_1 produced by symmetric (in phase) overlap of all the p-orbitals in butadiene. The highest energy orbital Ψ_4 from out of phase overlap of all the p-orbitals and two degenerate bonding molecular orbitals Ψ_2 and Ψ_3 from intermediate symmetric overlap of some of the butadiene p-orbitals.

The intermediate bonding orbital Ψ_2 is of higher energy than orbital Ψ_1 but lower in energy than the intermediate anti-bonding orbital Ψ_3 , which is in turn lower in energy than the anti-bonding orbital Ψ_4 . Butadiene's four π electrons are placed in the two bonding orbitals with the anti-bonding orbitals unfilled as in Figure 1.11..

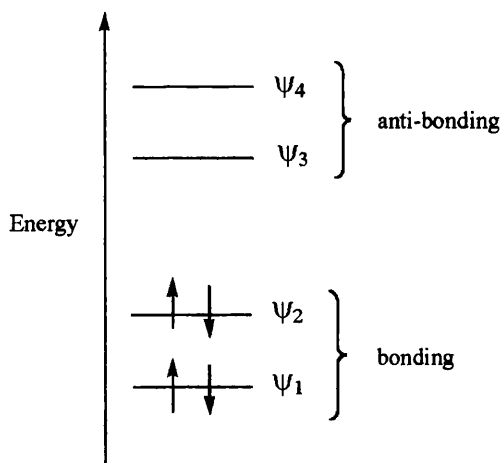


Figure 1.11 Energy diagram for the π molecular orbitals in butadiene

A diagram for a general system of molecular orbitals is given in Figure 1.12. The highest energy bonding orbital is called the HOMO (Highest Occupied Molecular Orbital) and the lowest energy anti-bonding orbital is called the LUMO (Lowest Unoccupied Molecular Orbital). The HOMO and LUMO in ethylene would correspond to the filled π bonding and unfilled π^* anti-bonding molecular orbitals respectively, shown in Figure 1.11. The orbital energy diagram in Figure 1.12 shows what happens after the absorption of a photon of radiation, with energy $h\nu$, into a molecule. This photon absorption causes an electron to be excited from the HOMO to the LUMO. There is no change of electron spin and this transition corresponds to the first excited singlet state S_1 . Also shown are the possible transitions for the second and third excited singlets S_2 and S_3 , resulting either from excitation of an electron from the HOMO to the LUMO+1 or from the HOMO-1 to the LUMO. Which of these transitions is lower in energy depends on the energies of the molecular orbitals involved. It may be the case that the transition energy from $S_0 \rightarrow S_3$ is lower than that for $S_0 \rightarrow S_2$, and thus the second excited singlet would be S_3 and the third would be S_2 . The singlet states should then be relabeled according to the order of increasing energy. Transitions to the S_2 and S_3 states require photons of different energy obviously both of higher energy than photons for excitation to S_1 .

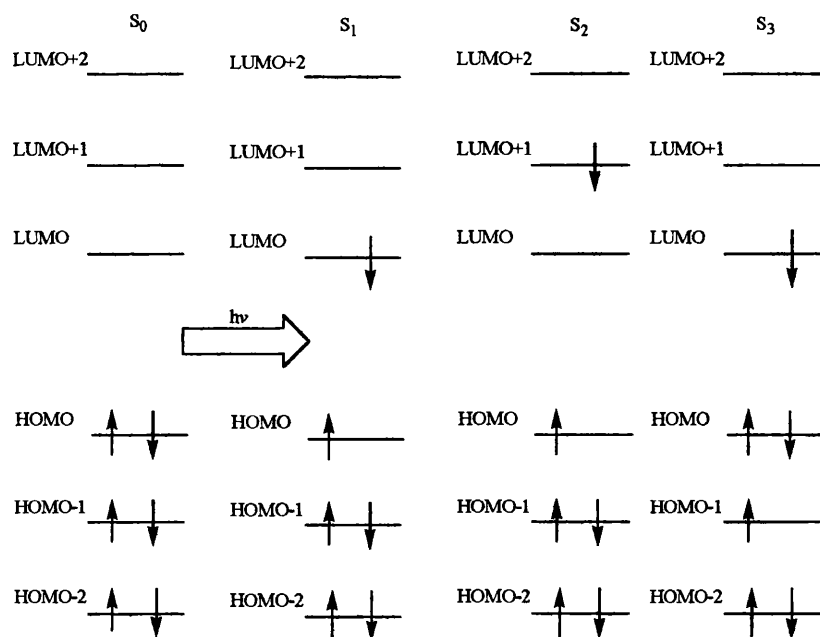


Figure 1.12 The excitation of an electron from a bonding molecular orbital to an unfilled anti-bonding molecular orbital caused by the absorption of a photon.

If there is a change in the spin of the excited electron then this corresponds to a triplet state.

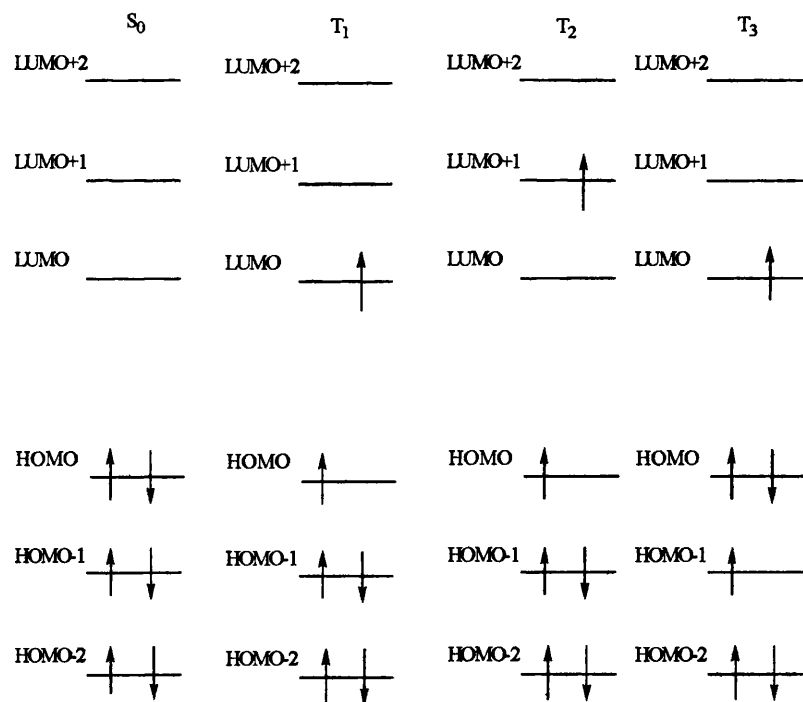


Figure 1.13 The electronic occupation of molecular orbitals in the triplet state.

Figure 1.13 compares the three lowest possible triplet states, T_1 , T_2 and T_3 with the ground state S_0 . The triplet states have two unpaired electrons. In addition to singlet and triplet states there is the possibility of doublet states. Doublets occur for systems with an odd number of electrons, or in other words, one unpaired electron.

Electronic transitions⁴³

The behaviour of a molecule, after an electronic transition can be explained by the Franck-Condon Principle, which states that because the nuclei of a molecule are much more massive than its electrons, an electronic transition takes place much faster than the movement of the nuclei. The electron density of the molecule can therefore move rapidly from one region to another, resulting from the electronic transition, whilst the nuclei remain stationary. After the transition from the ground electronic state to some excited electronic state, via the absorption of a photon $h\nu$, the nuclei will adjust their position from their original geometry (with the nuclei positioned at their equilibrium distances, R_e , from each other) to a new geometry in response to the change in electron density encountered in the excited state. This adjustment of nuclear positions takes the form of vibrations.

The Franck-Condon Principle is illustrated in Figure 1.14, which represents the constant nuclear geometry during the electronic excitation as a vertical line.

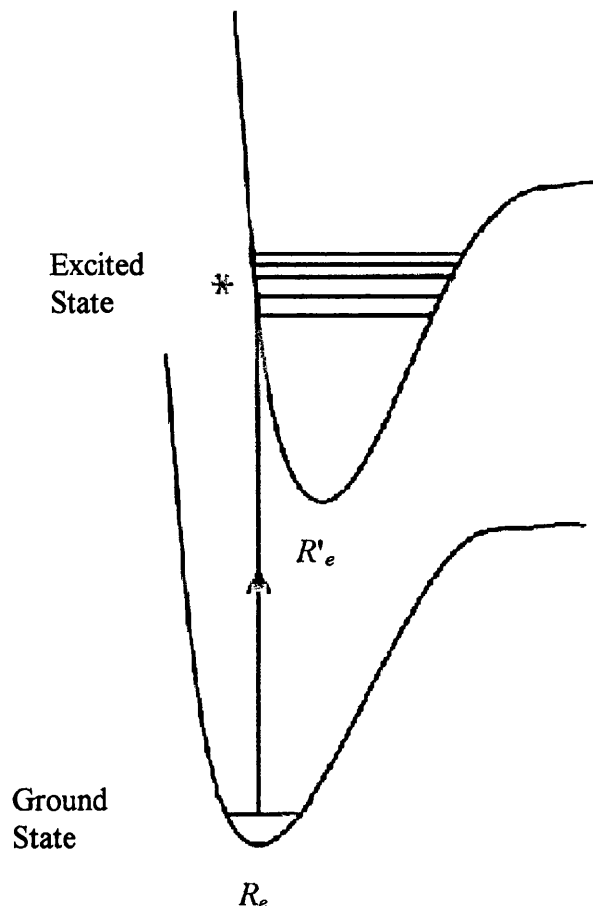


Figure 1.14⁴⁴ The representation of an electronic transition, from the lowest vibrational level in the ground state to a vibrational level lying vertically above it in the excited state, according to the Franck-Condon principle. R_e and R'_e are the equilibrium bond separations of nuclei in the ground and excited states respectively.

This instantaneous electronic transition from the equilibrium ground state geometry to an identical geometry in the excited state has the highest probability of taking place and is therefore intense. There is, of course, a smaller probability of transitions to other vibrational levels in the excited state, which are close to the equilibrium separation of the nuclei, R_e , and therefore in the same region as the most probable transition. There is a lower probability of these transitions occurring and they are therefore less intense.

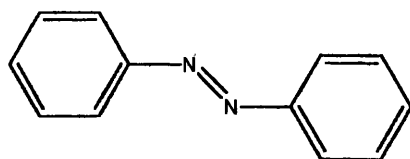
As shown in **Figure 1.14**, the upper potential energy curve of the excited state is usually displaced to the right of the lower potential energy ground state curve, signifying the greater equilibrium bond length, R'_e , in the excited state. This is because electronically excited states usually contain electrons in anti-bonding orbitals and therefore have a greater degree of anti-bonding character than ground electronic states.

The vibrational structure of the absorption spectrum is dependent on the displacement of the two potential energy curves. If the ground and excited state potential energy curves have a considerable displacement from each other, this results in a lot of vibrational structure. Vibrational structure can be observed for molecules in the gas phase, but in solution, this structure merges together resulting in a broad, almost featureless band.

Section 1.5

Electronic transitions in azobenzenes

Before considering the electronic transitions of the donor-acceptor azo dyes, the transitions involved in the absorption spectra for the more simple case of azobenzene (1-35), will be examined.



(1-35)

In trans-azobenzene there are two types of electronic transitions, namely $\pi-\pi^*$ and $n-\pi^*$. The π and π^* orbitals are formed from overlap of some of the p orbitals on the benzene rings and on the two azo nitrogen atoms, which are perpendicular to the plane of the molecule. The π orbital is a doubly occupied molecular orbital whilst the π^* orbital is an unoccupied anti-bonding molecular orbital. The transition of an electron, resulting from the absorption of a photon, between these π and π^* molecular orbitals is known as a $\pi-\pi^*$ transition and corresponds to the UV absorption band at wavelength 314 nm⁴² in the spectrum of azobenzene. This transition is allowed by symmetry selection rules and is therefore quite intense.

However, this is not the lowest energy electronic transition in trans azobenzene. The lowest energy transition is attributed to an $n-\pi^*$ transition⁴². To understand the origin of this $n-\pi^*$ transition we must consider the interaction between the non-bonding lone pair orbitals of the azo nitrogen atoms. This interaction is illustrated in Figure 1.16 for trans-azobenzene. Here, the nitrogen lone pairs are approximately sp^2 hybrid orbitals and are considered to interact to give two filled orbitals.^{25,42} The lone pair orbitals can interact symmetrically (out of phase overlap) to give a high energy doubly occupied orbital designated n_s . They can also interact anti-

symmetrically (in phase overlap) to give a lower energy doubly occupied orbital designated n_a . Both orbitals are shown in Figure 1.16.

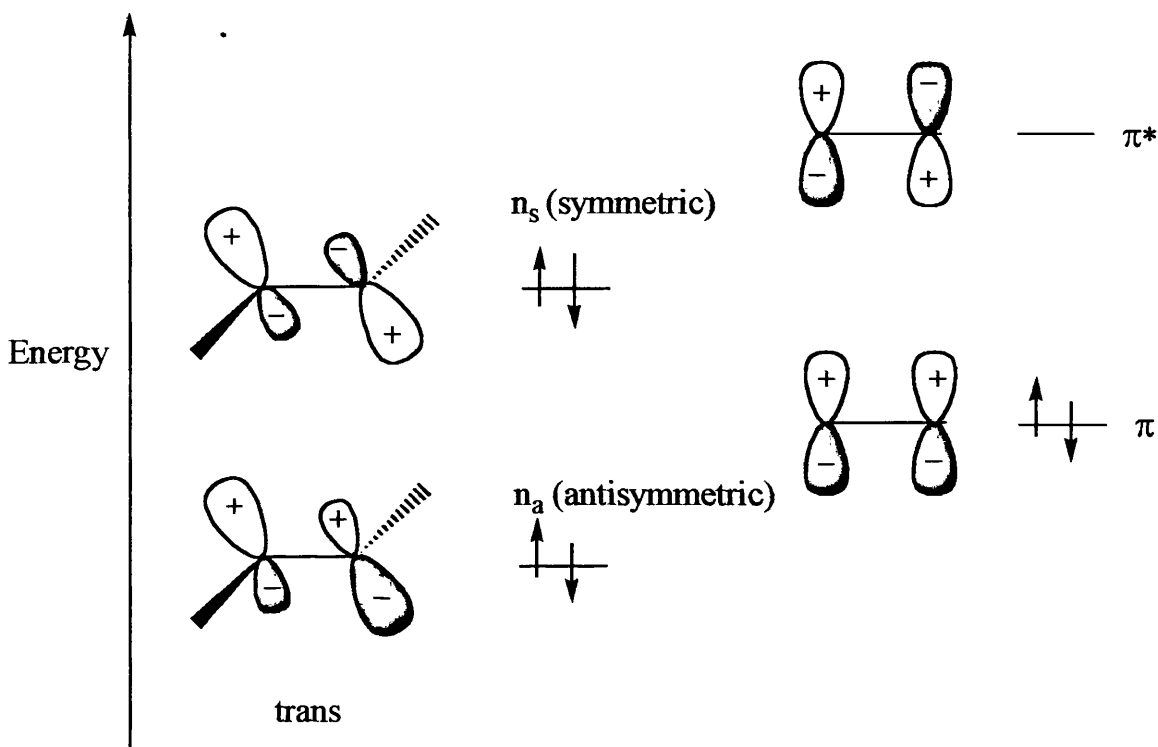


Figure 1.15 Figure 1.16 Overlap of the nitrogen lone pair orbitals in the $-N=N-$ bond in trans-azobenzene.⁴⁵

The orbital sequence in order of increasing energy shown in Figure 1.16 is n , π , n , π^* , which has been confirmed experimentally by Houk et al.⁴⁶

It is the electronic transition between the higher energy n_s orbital and the empty π^* orbital, previously discussed, that is responsible for the lowest energy $n-\pi^*$ transition in azobenzene^{38,42} and corresponds to the $n-\pi^*$ absorption band at 444 nm ($\epsilon = 450$) in the UV/Visible absorption spectrum of trans-azobenzene. Both the $n-\pi^*$ and $\pi-\pi^*$ absorption bands in the UV/Visible absorption spectrum of azobenzene are shown in Figure 1.17 and the molecular orbitals involved in these transitions are shown in Figure 1.7. Because of the symmetry of n_s orbital, the $n-\pi^*$ transition is symmetry forbidden. The intensity of this absorption is unusually high for a forbidden transition and this intensity can be explained in terms of coupling between the $n-\pi^*$ and $\pi-\pi^*$ singlet states, which results in an effective borrowing of intensity by the $n-\pi^*$ state from the

allowed π - π^* band. Intensity borrowing is particularly significant when the molecule is non-planar as in cis-azobenzene. In the cis isomer, the n - π^* state is symmetry allowed and has an extinction coefficient of 1260.²⁵ This transition is consequently much more intense than the n - π^* transition in trans azobenzene which has an extinction coefficient value of about 450.

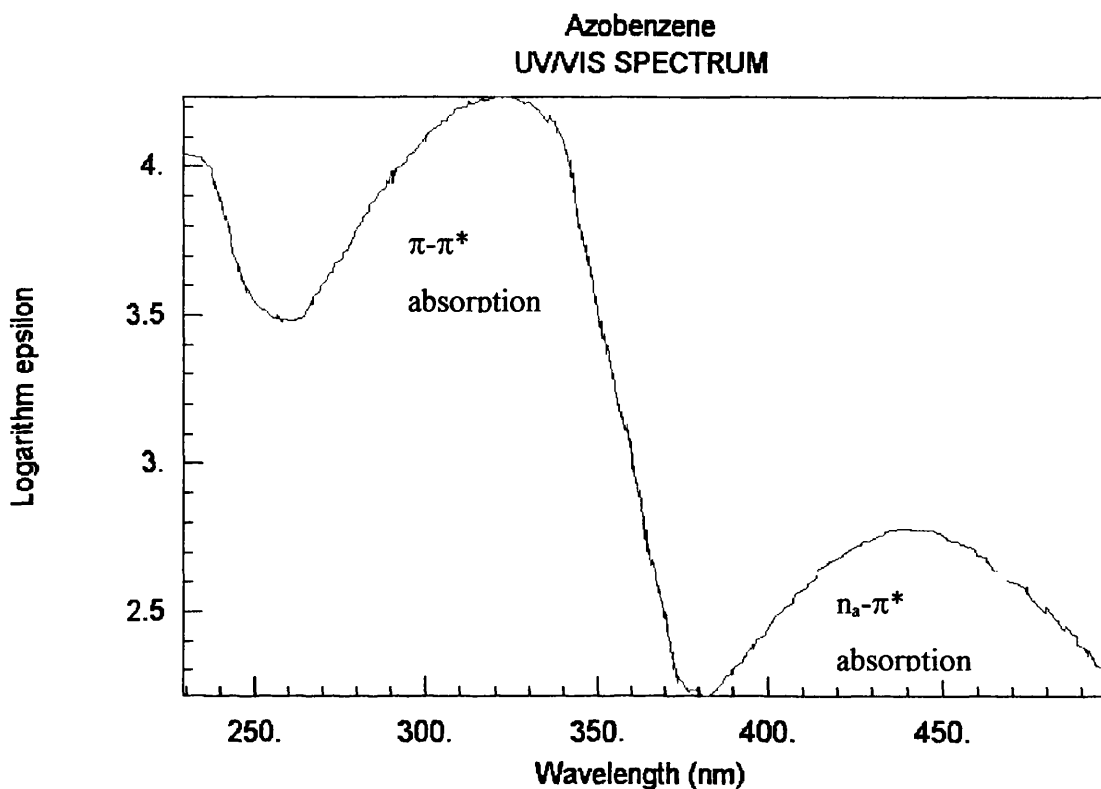


Figure 1.17 The uv/visible spectrum of azobenzene.⁴⁷

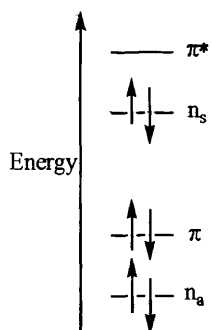


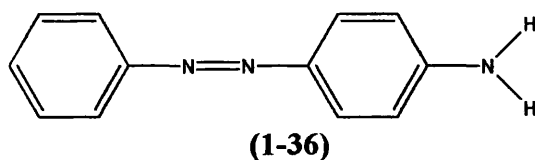
Figure 1.18 Energy levels of molecular orbitals involved in n - π^* and π - π^* transitions of azobenzene.

The geometry of the azobenzene can have an important effect on the transition energies and intensities of its absorption bands. Trans-azobenzene has been reported by (270,271) to be planar in the solid state but twisted in the gas phase (272). Crystallographic structures on the Cambridge database have rings twisted out of the plane by between 5° and 21°. ⁴⁸ By comparison cis-azobenzene is much more twisted, by 36° and 57° in crystal structures. ⁴⁸ The deviation from planarity in the cis-isomer results in the π - π^* absorption band shifting to shorter wavelengths and lower intensities than the corresponding band for the trans isomer. The loss of planarity has a smaller effect on the n - π^* band. ⁴² The degree of twisting of the phenyl rings therefore has an effect on the energy and intensity of the π - π^* band and to a lesser extent, the n - π^* band.

Transitions have thus far been described as either n - π^* or π - π^* . In fact molecular orbitals may not be exclusively n or π in character and there may be some mixing contribution of n and π orbitals involved in the composition of molecular orbitals.

Only for a few azobenzenes is there a well resolved n - π^* band. ⁴⁹ In most azo dyes, the n - π^* band is buried beneath the π - π^* band and in these cases, nothing is known about its exact location. The n - π^* band undergoes a blue shift from non-polar to polar solvents and mostly disappears in acids. HMO and PPP calculations of the n - π^* band also predict another n - π^* band. ⁴⁹ A more detailed discussion of the electronic transitions of azobenzene and some other azobenzenes is given in Chapter 5.

The spectra of donor acceptor dyes are quite different to the spectra of simple azobenzenes. This is due to the introduction of an electron donor group into the azobenzene system. Considering the simplest example of a donor acceptor azobenzene (1-36), which contains a donor amino group, which is predicted by PMO theory to introduce a new π orbital into the electronic system.



This new π orbital results from mixing between the lone pair of the donor amino group and the HOMO of azobenzene to form the new π orbital, which is delocalised over the whole molecule. The amino nitrogen atom is most likely to be sp^2 hybridised, with the amino group in the plane of the azobenzene moiety allowing greater orbital overlap. This assumption is made from consideration of the HOMO of (1-36) predicted by CNDOVS and AM1 calculations. The results

of these calculations are discussed fully in Chapter 5. Because the electrons of the amino nitrogen orbital originate from the non-bonding lone pair of the amino group nitrogen atom, this new π orbital is often referred to as a non-bonding molecular orbital (NBMO)⁴², but here it will be designated as the π_N orbital, where the suffix N refers to the N-amino nitrogen atom.

This π_N orbital is higher in energy relative to the n_s and n_a orbitals in **(1-36)** and thus the lowest energy electronic transition in **(1-36)** is due to the transition between the π_N orbital and the empty π^* anti-bonding orbital formed from the overlap of the azo nitrogen p electrons. The relative energies of these molecular orbitals are displayed in Figure 1.19. This $\pi_N - \pi^*$ transition is responsible for the long wavelength absorption band in the UV/visible spectrum of **(1-36)** shown in Figure 1.20 together with the relative energies of the molecular orbitals.

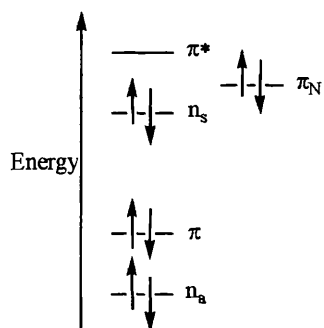


Figure 1.19 Relative energies of molecular orbitals in 4-aminoazobenzene.

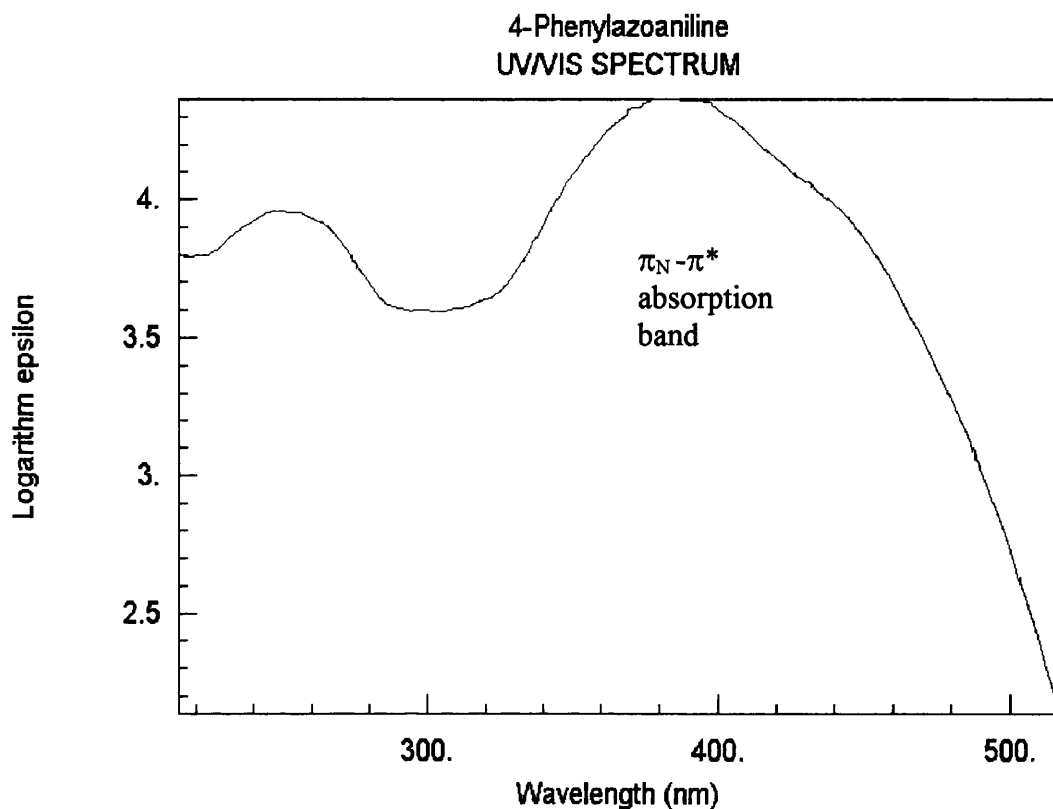


Figure 1.20 The UV/Visible spectrum of 4-phenylazoaniline (**1-36**) together with its molecular orbital levels.

The $\pi_N-\pi^*$ band is at 386 nm in methanol and the extension of this broad band into the visible region of the spectrum is responsible for the yellow colour of (**1-36**). The $\pi_N-\pi^*$ transition is allowed by symmetry selection rules and is much more intense than the shorter wavelength $n-\pi^*$ band, often completely obscuring it.

The electronic excitation process causes a general migration of electron density from the donor group into the rest of the chromophore and such a transition is often described as a charge transfer transition. As such, the $\pi_N-\pi^*$ transition is greatly affected by the substituents on the donor and acceptor phenyl rings of the amino azobenzene, as these substituents will affect the degree of electron density migration from the donor to the acceptor regions of the molecule. Obviously the transition energy of such a process depends critically on the relative strengths of the donor and acceptor groups. The effect of different substituents on the wavelengths of azo compounds was discussed on pages 18-24.

This is not the case for the $n-\pi^*$ transition however, which is relatively insensitive to substituent

effects⁴² as it involves the excitation of electrons from the n_x orbital formed by interaction of the azo nitrogen lone pairs.

Excitation to the first excited singlet state S_1 from the ground state, is responsible for the colour of the molecule and this state and higher singlet states may be involved in the photochemical reactions of these donor-acceptor azobenzenes. The associated triplet states may be even more important in photoreactions and these states are discussed in Section 1.7.

Section 1.6

Fluorescence and Phosphorescence⁴³

When a molecule is electronically excited by a photon, it then contains a large amount of stored energy. This electronic energy must then be released from the molecule to its surroundings or else it may be converted into excess vibrational energy resulting in the break up of the molecule. There are several ways in which the electronic energy can be dissipated. *Internal conversion* (IC) involves the loss of vibrational energy via collisions of the excited state molecule with the surrounding solvent molecules. Rapid transfer of vibrational energy to the solvent results in energy being lost as heat.

The molecule thus decays to the lowest vibrational level of the first excited singlet state S_1 in approximately 10^{-12} seconds. From here internal conversion to the ground state occurs in about 10^{-8} seconds. There is also a small probability of vibrational energy loss between excited singlet and triplet states. Though this inter-conversion process between singlet and triplet states, involving a change of electron spin is quantum mechanically forbidden, it may occur under favourable conditions and is called *intersystem crossing* (ISC). There is also the possibility of loss of the electronic excitation energy as radiation. This energy loss via the emission of radiation occurs as fluorescence. Fluorescence is the emission of light from the lowest vibrational level of the first excited singlet state S_1 , leaving the molecule in the ground state S_0 . The steps involved in the fluorescence process are shown in Figure 1.21.

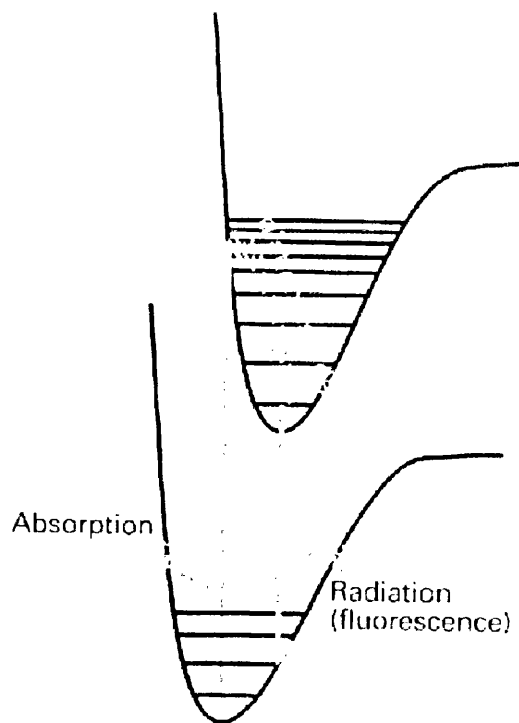


Figure 1.21⁵⁰ The sequence of steps leading to fluorescence. Absorption is followed by radiationless decay to the lowest vibrational level of the first excited singlet state. There then follows a radiative transition from the lowest vibrational level of the excited state to a vibrational level in the ground state.

After the initial Franck-Condon type absorption, the resulting excited state of the molecule is subjected to collisions with the surrounding solvent molecules, with each collision giving up energy, as the molecule steps down the vibrational states to the lowest vibrational energy level of the excited state. If the energy difference between the excited state and the ground state is too great for the solvent molecules to accept, the non-radiative decay to the lowest vibrational level of the excited state may be followed by spontaneous emission of radiation and leave the molecule in some vibrational level of the ground state. The fluorescence spectrum thus has vibrational structure characteristic of the ground electronic state. The fluorescence spectrum also occurs at longer wavelengths than the absorption spectrum, as some vibrational energy has already been lost from the excited state to the surrounding solvent. The ability of the solvent to accept the vibrational and electronic energy is thought to affect the intensity of fluorescence, as solvent molecules which have widely spaced vibrational levels, such as water, can accept large quantities of electronic energy and effectively quench the fluorescence.

Fluorescence is an allowed process taking around 10^{-8} seconds, which is much slower than internal conversion from the higher singlet states e.g. from S_2 to S_1 , and thus fluorescence normally occurs only from S_1 .

The other possibility for the emission of radiation is phosphorescence. The sequence of events leading to the phosphorescence of molecules is shown in Figure 1.22.

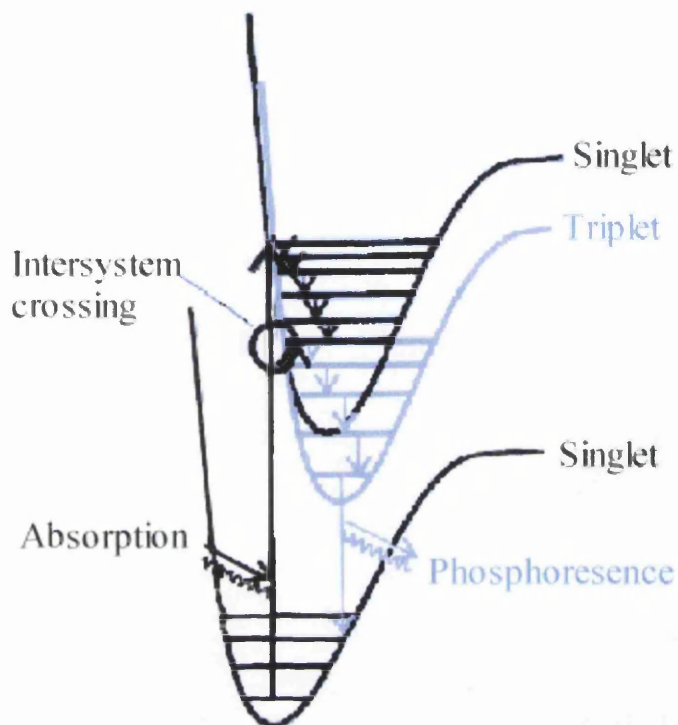


Figure 1.22⁵¹ The sequence of steps leading to phosphorescence. Absorption is followed by vibrational relaxation in the excited singlet state until a vibrational state is reached where the singlet and triplet excited states share a common geometry. A singlet to triplet switch may be brought about by spin-orbit coupling and the triplet state may then undergo vibrational relaxation to the lowest level of the excited triplet. The radiative transition to a vibrational level in the ground state which follows, constitutes phosphorescence.

The first steps of the process are similar to those in the fluorescence process; absorption followed by loss of vibrational energy by stepping down the vibrational ladder. However, phosphorescence involves the excited triplet state of the molecule, which shares a common geometry with the molecule's excited singlet state at the point where their potential energy curves intersect.

If there is an accompanying change of spin of one of the molecules spin paired electrons $\downarrow\uparrow$, to give two unpaired spins $\uparrow\uparrow$, then the molecule may undergo intersystem crossing to the triplet state.

This change of spin is forbidden by spectroscopic selection rules, but the selection rule may be broken in the presence of spin-orbit coupling. If a moderately heavy atom, such as sulphur, is present in the molecule, there is increased spin-orbit coupling and hence a greater probability of intersystem crossing.

Spin-orbit coupling arises from the generation of magnetic fields from the movement the charged electron. The electron has a magnetic moment associated with the spin of the electron, known as its spin angular momentum. The electron also has a magnetic moment arising from the charged electrons orbital angular momentum. Spin-orbit coupling is the result of the interaction of these two magnetic moments.

After intersystem crossing to the excited triplet state, the molecule may continue to step down the vibrational levels of the triplet state, until it reaches the lowest vibrational level of the triplet excited state. It remains effectively trapped here, as it is of lower energy than the excited singlet state, and cannot return to the singlet ground state, as this involves another forbidden change of spin. However, spin-orbit coupling allows some contravention of the spin selection rule and emission of radiation from the lowest vibrational level of the excited state to a vibrational level in the ground state may occur. Because the triplet to ground state transition is forbidden and the probability of the transition occurring is low, the emission of radiation from the lowest vibrational level of the triplet state is akin to a slow leaking of radiation and phosphorescence may continue long after the initial absorption of light. The rate of phosphorescence is therefore much lower than for fluorescence, anywhere between 10^{-3} to 10 seconds, and phosphorescence emission is weak. The above processes are summarised in the Jablonski diagram in Figure 1.23.

Like the fluorescence spectrum, the phosphorescence emission spectra are mirror images of the absorption spectrum of the molecule but they occur at longer wavelength than the absorption spectrum, as some vibrational energy has already been lost from the excited state to the surrounding solvent.

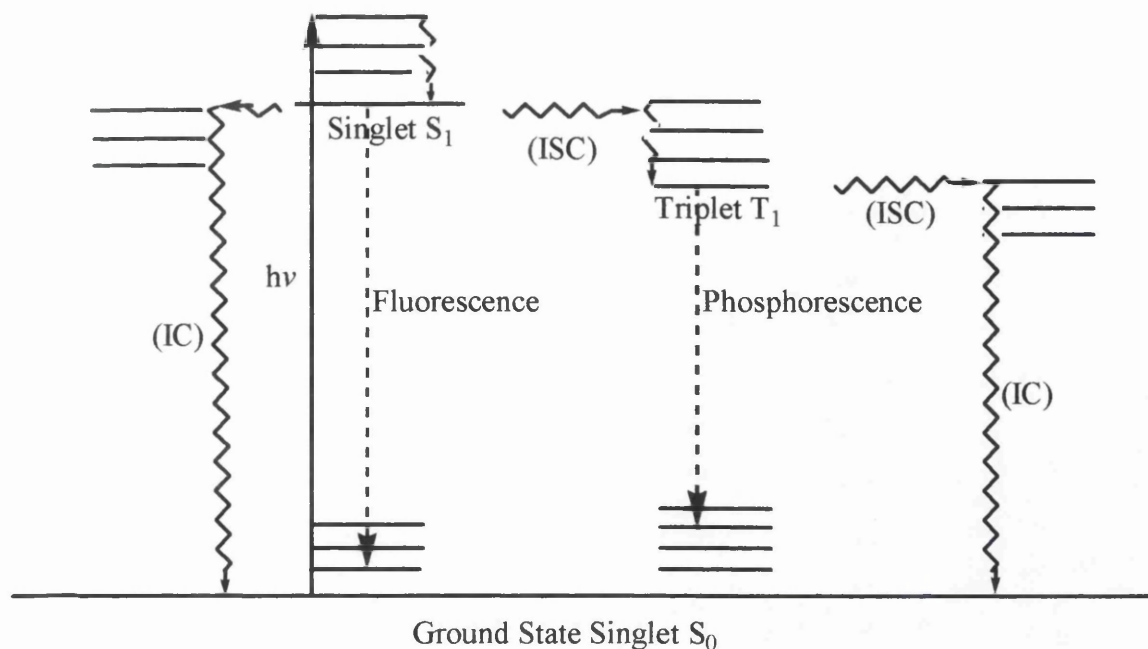


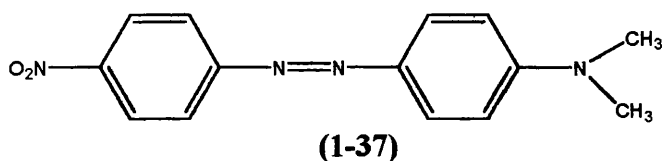
Figure 1.23⁵² A Jablonski diagram showing the possible modes of energy dissipation from electronically excited states following the absorption of a photon of energy $h\nu$; **(IC)** internal conversion, **(ISC)** intersystem crossing, fluorescence and phosphorescence.

Most azo dyes show no phosphorescence. Indeed the first evidence of phosphorescence for azo dyes was not detected until 1989 by Nepras et al⁵³. Given that phosphorescence is rarely detected, the quantum yield of intersystem crossing must therefore be very low and population of T₁ by direct optical excitation from the first singlet S₁ has a low probability. Alternatively, the lowest triplet state could have very favorable ways for the internal conversion to the ground state.

In addition to phosphorescence, fluorescence is also rare in azobenzenes, although some fluorescence has been reported for azobenzene derivatives, which comply with certain conditions. For example, the ability of an azobenzene molecule to fluoresce depends on the position of the n-π* and π-π* absorption bands. If the n-π* singlet transition is lower in energy than the π-π* singlet transition then fluorescence may be observed. The above condition holds for some sterically hindered substituted mono azobenzenes, where very weak luminescence of these mono azo dyes observed at 77k was interpreted as fluorescence from the S₁ n-π* state.^{54,55} However, if the n-π* transition is higher in energy than the π-π* transition then no fluorescence is seen.

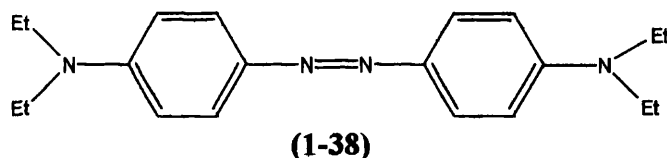
Fluorescence may also occur if there is coupling of the n-π* and π-π* states as in the case of the

azo dye 4-dimethylamino-4'-nitroazobenzene (1-37).⁴² Here, the luminescence of dye (1-37), observed at 77K was interpreted as fluorescence.



Whether or not fluorescence occurs, may also depend on the character of the triplet states of the molecule and their energies.

For example, the disubstituted dye, 4-N,N-diethylamino-4'-methoxyazobenzene, has a lowest triplet with $n-\pi^*$ character but the lowest triplet of 4-N,N-diethylamino-4' nitroazobenzene has $\pi-\pi^*$ character.⁵³ As there is an additional $n-\pi^*$ state localised on the nitro group of 4-N,N-diethylamino-4' nitro azobenzene, there are two $n-\pi^*$ triplet states below the lowest excited singlet $\pi-\pi^*$ state S_1 and the S_1 state may therefore be deactivated by intersystem crossing to these $n-\pi^*$ triplets. All of the dyes mentioned above exhibit only weak fluorescence. The only azobenzenes that show strong fluorescence are those which are di-4, 4'-substituted with N-dialkyl amino groups such as bis-4,4'diethylaminoazobenzene (1-38)

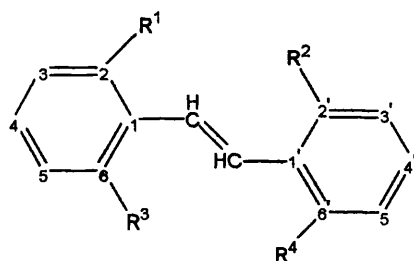


These types of molecules fluoresce strongly in glassy MTHF solution.⁵³ The reasons for the exceptional fluorescence properties of di-4, 4' amino substituted dyes are thought to be due to the rigidity and planarity of these types of molecules. For most mono and di-substituted azobenzenes, neither cis-trans isomerisation or intersystem crossing (except for 4-N,N-diethylamino-4' nitroazobenzene), is thought to be important in the deactivation of the S_1 state in glassy solution. The main deactivation of S_1 is believed to be by internal conversion caused by changes in the geometry of the S_1 state, bringing the S_1 and ground state S_0 potential energy surfaces closer together.

In contrast di-4,4' amino substituted dyes such as (1-38) have an S_1 state which is rigid and planar in glassy MTHF solution at low temperatures. This planarity is caused by the two electron donor groups and the high viscosity of the MTHF solvent preventing the rotation of the phenyl rings of

(1-38) out of the plane of the molecule.

Evidence for this planar rigid geometry was produced by Nepras *et. al.*⁵³ who considered the absorption spectra of (1-38) in MTHF at different temperatures. At low temperatures there are remarkable changes in the vibronic structure of the spectrum. The long wavelength absorption band of (1-38) at 477 nm is assigned to an $S_1 - S_0$ $\pi-\pi^*$ transition on the basis of this low temperature vibronic structure of the long wavelength absorption band, and the fact that an increase in the ${}^1(n-\pi^*) - {}^1(\pi-\pi^*)$ vibronic interaction with decreasing temperature is not expected. The presence of the vibronic fine structure indicates that there is no twisting of the phenyl rings via rotation about the C-N bonds in (1-38), resulting in a planar conformation for the molecule. This was concluded from the analogy with stilbene (1-39), for which it has been shown that twisting around the C-Ph bond in trans stilbene causes “blurring” of the vibronic structure in fluid solution while at low temperatures in glassy solution the vibronic structure becomes clear, as twisting is prohibited by the high solvent viscosity and the stilbene approaches a nearly planar conformation.



(1-39) $R^1 = R^2 = R^3 = R^4 = H$

(1-40) $R^1 = R^2 = R^3 = R^4 = \text{Alkyl}$

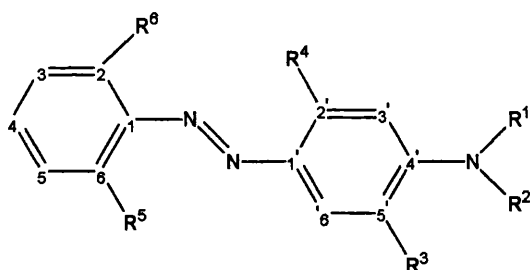
However, stilbenes which have bulky alkyl groups at positions ortho to the carbon bridge e.g. (1-40) are sterically hindered, and show no vibronic structure, which is explained by a non planar equilibrium geometry, with torsional vibrations giving strong blurring of vibronic structure. In contrast to trans stilbenes, azobenzenes have the possibility of electronic interactions between the lone pair electrons of the azo group and π -electrons of the phenyl rings⁵⁶ and repulsion between these n-electrons and any substituents ortho to the azo group. The degree of these interactions may influence the distortion of the phenyl rings around the N-Ph bonds.

In mono-substituted trans azobenzenes the $\pi-\pi^*$ conjugation band is strongly blurred due to rotation about the N-Ph bonds even at low temperature. This explanation agrees with theoretical results where a distorted geometry is favoured,⁵⁷ in accordance with the crystal structure.⁵²

In contrast to all para-monosubstituted and many disubstituted azobenzenes, the π - π^* conjugation band of **(1-38)** shows a hint of fine structure even at room temperature and the vibronic structure becomes clear at low temperature. It was concluded by Nepras⁵³ that two strong electron donating groups, such as amino or alkylamino groups, give a molecule which is nearly planar in glassy solution and exhibits only stretching vibrations. The bathochromic shift of vibronic bands on cooling also implies a planar structure in glassy solution and a distorted structure in fluid solution. The twisting or torsional vibrations of the phenyl groups are a means of dissipating electronic excitation energy in azobenzenes. In **(1-38)** the absence of these vibrations at low temperatures in MTHF means that the electronic excitation energy is emitted as fluorescence as an alternative way of releasing the energy. The strong fluorescence of **(1-38)** at 77K is therefore attributed to emission from the S_1 (π - π^*) excited state of the molecule. The fluorescence spectrum is mirror symmetrical to the absorption spectrum but is shifted 400 cm^{-1} to longer wavelength.

In flash spectroscopic experiments undertaken by Gorner⁵⁸ *et al.* on trans-azobenzene, fluorescence lifetimes of 25 and ≤ 5 ps have been detected for the first and second excited singlets S_1 and S_2 respectively in cyclohexane. Also examined were the fluorescence emission spectra of for several substituted azobenzenes including some 4-dialkylamino-4'-nitroazobenzenes with bulky ortho substituents **(1-41)**-**(1-43)**.^{54,59,60,61}

Unlike trans-azobenzene, no fluorescence was observed at room temperature for the substituted 4-dialkylamino-4'-nitroazobenzenes **(1-41)**, **(1-42)**, **(1-43)**, implying a time of picoseconds rather than nanoseconds for S_1 .



(1-41) $R^1 = \text{CH}_2\text{CH}_2\text{OH}$, $R^2 = \text{CH}_2\text{CH}_2\text{CN}$, $R^3 = \text{OCH}_3$, $R^4 = \text{NHCOCH}_3$, $R^5 = \text{Br}$, $R^6 = \text{NO}_2$

(1-42) $R^1 = \text{CH}_2\text{CH}_2\text{OH}$, $R^2 = \text{CH}_2\text{CH}_2\text{CN}$, $R^3 = \text{OCH}_3$, $R^4 = \text{NHCOCH}_3$, $R^5 = \text{Br}$, $R^6 = \text{CN}$

(1-43) $R^1 = \text{CH}_2\text{CH}_2\text{OH}$, $R^2 = \text{CH}_2\text{CH}_2\text{CN}$, $R^3 = \text{OCH}_3$, $R^4 = \text{NHCOCH}_3$, $R^5 = \text{Cl}$, $R^6 = \text{NO}_2$

Some fluorescence was however detected at low temperatures and had a lifetime of 10 ns.

As it has been mentioned for **(1-38)**, strong fluorescence indicates the absence of fast energy

dissipation processes competing effectively with emission. Consequently, dyes which fluoresce remain in the excited state longer and thus have an increased probability of undergoing a photochemical reaction. Fluorescent dyes often have poor lightfastness.⁶² Vibration or fast trans-cis isomerisation (another means of dissipating energy from the excited states) bring about fast deactivation of the excited state of the azo dyes⁴² such as (1-37). These dyes often have high lightfastness.⁶²

Section 1.7

Triplets and transient species⁶³

The excited singlet states of azobenzene have been studied extensively by steady state spectroscopic and photochemical methods including UV/Visible^{64,65,66,67}, and Raman^{68,69,70} spectroscopy and also theoretical modeling.^{86,71,72,73,74} Several studies have looked at the excited state species of azobenzene and some of its derivatives. Much interest has centered on species that may be involved in the mechanism for the trans-cis photoisomerisation reaction (see Section 1.9). This has been of interest recently because of its use in optical switching and image storage devices.^{75,76,77}

The excited states of azobenzene have been considered Nepras *et al.*⁵³. As it was mentioned previously, in azobenzene the first excited singlet is of $n-\pi^*$ type and found at 22500 cm^{-1} (444 nm). Its high intensity is explained by the vibronic interaction or coupling with the second excited singlet $\pi-\pi^*$ state.

Para substituents on azobenzene shift the $\pi-\pi^*$ band to longer wavelength but the $n-\pi^*$ band remains unchanged. This implies both bands may be similar in energy with the more intense $\pi-\pi^*$ band overlapping the $n-\pi^*$ band.

Little is known about the properties of the lowest triplet state of azobenzenes as experimental techniques commonly used for triplet detection are unsuccessful. For example, direct observation of the first or lowest triplet state T_1 of azobenzene by Monti,^{78,79} was not successful as no phosphorescence was detected at 77K ⁸⁰, and short lived transients were not detected for azobenzene and some substituted azobenzenes. The energy of T_1 was therefore estimated from flash kinetic spectroscopy. This technique involves energy transfer from the triplet states of aromatic hydrocarbons to the triplet state of the dye.^{78,79} Such energy transfer experiments have assigned an upper limit of 45 kcal/mol for the first triplet state of azobenzene.^{78,81,82,83} Other

estimates for the triplet energy of trans azobenzene have been hypothesized at 48 kcal/mol from a magneto optical rotary dispersion experiment,⁸⁴ and 44.5 kcal/mol from PPP calculations.⁸⁵

However ab initio SCF CI calculations indicate that both the cis and trans isomers of T_1 have $n-\pi^*$ character and have energies of 28kcal/mol and 31.5 kcal/mol respectively.⁸⁶

It was suggested by Monti⁸⁶ that further information from energy transfer from aromatic hydrocarbons to azobenzenes needs to be performed by flash kinetic spectrophotometry for a further understanding of these states.

The lowest triplet state T_1 of some donor acceptor azobenzenes, including (1-41)-(1-43) was identified by Gerner *et al.* Using laser flash spectroscopy and absorption and emission spectroscopy they detected a transient species at 700 nm, which had a lifetime of 10 –30 ns at room temperature. They assigned this transient species to a triplet – triplet absorption specifically, the lowest triplet T_1 of the trans isomer. This assignment was supported by experiments with sensitizers and quenchers and heavy atom effects (which increased the 700 nm transient yield when H was substituted by Cl or Br). Also, the lifetime of T_1 was quenched by both oxygen and ferrocene at a diffusion controlled rate. The triplet yield increased with viscosity, which was suggested to be related to the elevated barrier to radiationless decay by geometry changes in excited states resulting from increased viscosity. This barrier increases the lifetime of the lowest excited singlet and thus increases the chance of intersystem crossing to the triplet. The presence of fluorescence even at low temperatures supports this observation. There is also the possibility of higher excited triplets from the excited singlet.

Section 1.8

Photochemical reactions

Azo compounds undergo several photochemical reactions e.g. photolysis, photocyclisation, photoreduction, photo-oxidation and photo-isomerisation. The most important of these processes relating to the lightfastness of dyes are the photoreduction and photo-oxidation reactions. However trans-cis photo-isomerisation is indirectly involved in the stability of the dye and will be considered in detail here.

Section 1.9

Trans-Cis Photo-isomerisation

Trans azobenzene can be converted to cis azobenzene on absorption of light, as shown in Figure 1.24. However, the cis isomer is thermally unstable and therefore the trans form predominates.⁴²

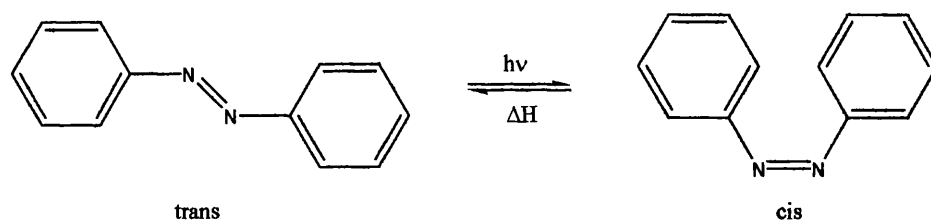


Figure 1.24 Trans-cis photo-isomerisation

The inter-conversion (photo-isomerisation) can occur by 2 possible routes, inversion^{64,87} and rotation^{64,87,88,89} with inversion thought to be the principle process. Rotation involves a simple rotation about the azo bond whereas, inversion consists of a bending of one of the N=N-C bond angles from approximately 120° in the trans isomer to around 240° in the cis isomer. The arguments as to which mechanism takes place are discussed in the following section.

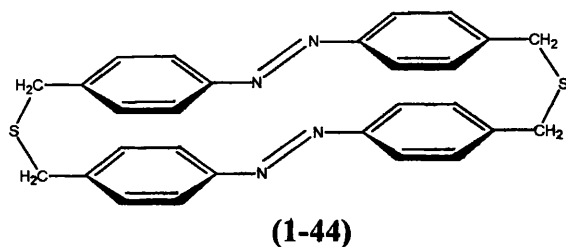
Mechanism of trans-cis photo-isomerisation

There has been much controversy surrounding the mechanism by which trans-cis isomerisation occurs in azobenzenes and substituted azobenzene derivatives. Numerous papers have examined photo-isomerisation experimentally (see Section 1.9) and more recently theoretical studies have provided further insight into the subject. Since photo-isomerisation may be important when considering lightfastness – dyes which are more photochromic tend to be more lightfast¹⁰² – a

review of the literature would be helpful in understanding this relationship. Before looking at the substituted donor acceptor azobenzene derivatives the photo-isomerisation of azobenzenes will be considered.

There are thought to be two possible mechanisms by which photo-isomerisation of azobenzenes can occur; rotation about the $-N=N-$ bond, or inversion, where one of the C-N bond angles is inverted to give the cis isomer.

Rau provided evidence of such an inversion process by considering azobenzeneophanes^{64,90} such as (1-44).



In these compounds, an inversion should be possible, but rotation about the $-N=N-$ bond would be inhibited by the physically restricted phane structure. Rau observed that these compounds generally have typical trans azobenzene spectra, with the two azobenzene units absorbing independently. There are also distinct features of the cyclophane structure in the spectra; the oscillator strength of the structureless $n-\pi^*$ transitions decrease relative to the $\pi-\pi^*$ bands the more the azobenzene units are force into planarity. Compound (1-44) can be isomerised to the cis conformer reversibly, by successive isomerisation of the two azobenzene units in photoreactions and dark reactions. On direct excitation to the $n-\pi^*$ state, quantum yields for trans – cis isomerisation of the trans, trans molecule to the trans, cis conformation have the same value as the $n-\pi^*$ state isomerisation of azobenzene. However, in (1-44) the $n-\pi^*$ and $\pi-\pi^*$ state isomerisation quantum yields are equal, which differs significantly from the azobezene case whose quantum yield of isomerisation is greater for $n-\pi^*$ than for $\pi-\pi^*$ isomerisation. The quantum yield of a photochemical process, such as isomerisation, is defined as the probability of a molecule undergoing that process on the absorption of a photon. The quantum yield of photo isomerisation is therefore equal to the number of molecules that undergo isomerisation divided by the total number of photons absorbed.

The trans, cis conformation of molecule (1-44) is thermally unstable i.e. its activation energy for cis-trans isomerisation is lower than that for azobenzene presumably because of steric strain. The cis,cis isomer on the other hand is kinetically much more stable than cis-azobenzene.

The reversible photo-isomerisation of (1-44) provides proof that trans-cis isomerisation of azo compounds can proceed via inversion, but does not rule out the possibility of rotation occurring in other azo compounds. In azobenzene itself, excitation to either the first excited singlet S_1 $n-\pi^*$ state at 447 nm⁶³ in hexane reached by visible irradiation, or the high energy second excited singlet S_2 ($\pi-\pi^*$ state) at 316 nm in hexane, reached by UV irradiation, is said to give photo-isomerisation, though excitation to S_2 results in a lower quantum yield of isomerisation, suggesting that trans-cis isomerisation may proceed by a different mechanism for S_2 state to the S_1 state and a rotation mechanism via the S_2 state. By comparison, in the cyclophane (1-44) the $n-\pi^*$ and $\pi-\pi^*$ quantum yields of isomerisation are equal indicating that $\pi-\pi^*$ excited molecules end up in the same $n-\pi^*$ state that is populated by direct $n-\pi^*$ excitation. This behaviour stems from the reluctance of (1-44) to undergo rotation. Also the $n-\pi^*$ state photo-isomerisation quantum yield is equal for (1-44) and for azobenzene suggesting that isomerisation proceeds by the same mechanism in both molecules. In addition the absorption spectra for (1-44) and azobenzene are similar for the $n-\pi^*$ absorption band but different in the $\pi-\pi^*$ band, suggesting that normal azobenzenes isomerise by inversion, but on $\pi-\pi^*$ excitation a rotational mechanism may become important.⁹¹

Photo-isomerisation from the second excited singlet was investigated by Lednev⁶³ *et al.*, who observed several excited transient species. The results of Lednev's⁶³ study showed that on photolysis of azobenzene, transient absorptions are seen at 370-450 nm and transient bleaching occurs at 303nm. The transient species which absorbed in the 370-450 nm range, with a lifetime of 1 ps was assigned to the first formed S_2 $\pi-\pi^*$ state, which decays via the processes shown in Figure 1.25. The probable decay of the S_2 species is by isomerisation via a conformational change on the S_2 surface and internal conversion to the trans S_1 and S_0 (ground state) states. The trans S_2 to trans S_1 transition was indicated by trans S_1 to trans S_0 fluorescence after excitation to the S_2 state. The longer lived transient species, which absorbed at 303 nm and had a lifetime of 13 ps in alkaline solution, was attributed to the decay of a bottleneck S^\ddagger transition state to S_0 , where S^\ddagger was assigned as a twisted conformer found on the S_1 or S_2 potential energy surface (see Figure 1.25). This scheme includes the possibility of isomerisation by inversion via the trans- S_1 state,

either from direct excitation to S_1 or indirectly from initial excitation to S_2 and then internal conversion to S_1 , as well as isomerisation by a rotation mechanism via the $S^\#$ species following excitation to the S_2 state.

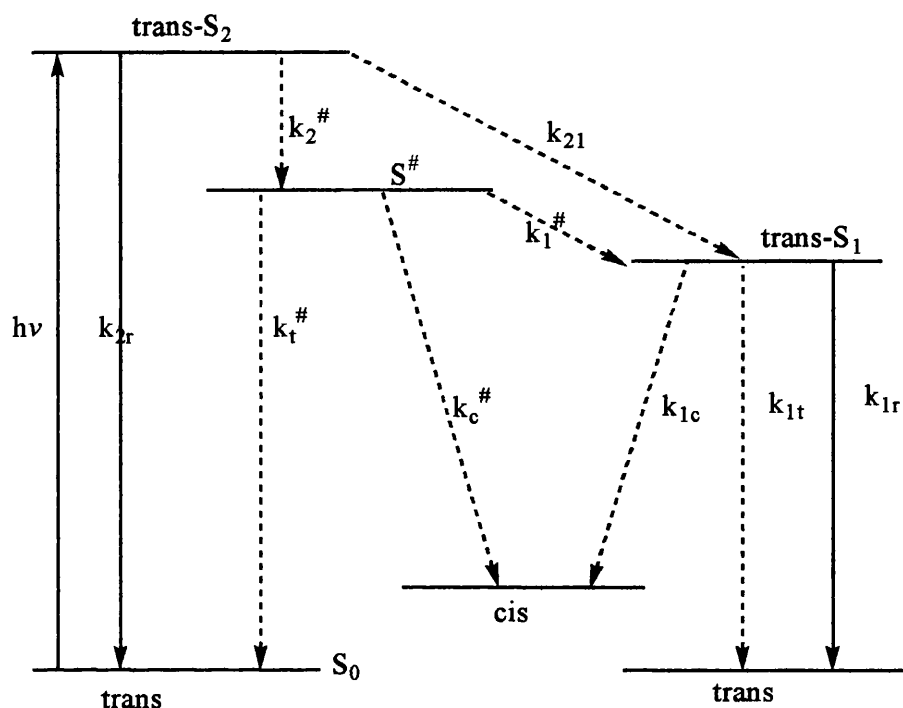


Figure 1.25 Excited states involved in trans-cis photo-isomerisation. Vibrational levels are omitted from this diagram for clarity.

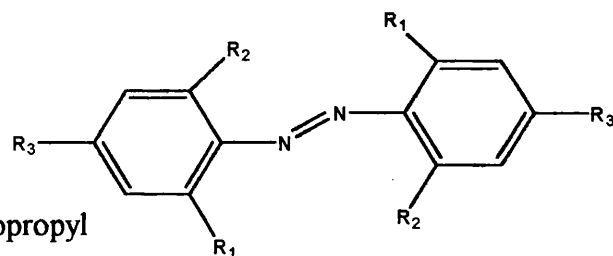
Calculated potential energy curves,⁷⁰ have suggested that the bottleneck state may be assigned to a twisted form of trans-azobenzene with the S_1 or S_2 surface on either side.

For trans-azobenzene, rapid decay of the 1st π - π^* state and existence of a bottleneck state $S^\#$ indicate that changes in electronic structure produced by the nitrogen heteroatoms exert a strong influence on excited state structures and ultra-fast dynamics.

Rau and Luddecke⁶⁴ inferred that both rotation and inversion occur in azobenzenes; inversion for the n - π^* state and rotation for the π - π^* state.

Evidence for the inversion path includes the rapid isomerisation of imines, for which an inversion path is possible, in comparison with olefins, which cannot follow this path but have reasonable activation energies for a rotational path. The inversion mechanism for azobenzenes is also supported by the lack of solvent effect on the rate of isomerisation, cited as evidence against rotation.⁹² Also, azobenzenes with bulky groups, which would be expected to hinder rotation, have a similar rate of isomerisation to unsubstituted azobenzenes.⁹³ It has been suggested that

inversion may proceed through a semi linear (sp hybridized) transition state, in which the azo double bond is retained.^{94,95} Although azobenzenes are essentially planar,^{96,97,98} calculations by Bunce⁹⁹ indicate that they can twist around the C-N bond when they have substituents ortho to the azo group. Bunce showed that a combination of phenyl rotation and opening of the C-N=N bond angles is required to rationalize spectral $n-\pi^*$ and $\pi-\pi^*$ band shifts. In addition to this, despite molecules having bulky substituents, trans-cis isomerisation still occurs, inferring that some twisting of the phenyl rings may take place.



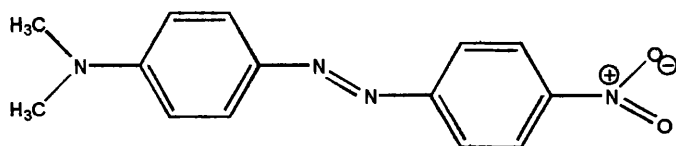
$R_1 = R_2 = R_3 = \text{isopropyl}$

(1-45)

Bunce *et al*⁹⁹ isolated the cis isomer of one such substituted azobenzene (1-45). They determined its structure by X-ray analysis and investigated the cis-trans thermal reaction, proving that the photoreaction is really a geometric isomerisation. The assumption made in a calculation for the cis isomer, a parallel structure formed by the 90° rotation of the phenyl groups about the C-N bond leaving the azo group planar, explains the phenomenon of equal oscillator strengths of the $n-\pi^*$ bands in both cis and trans forms. These structures are also the least strained configurations in cis,cis azobenzeneophanes.⁶⁴

Rau concludes that the quantum yields of trans-cis isomerisation for both $n-\pi^*$ and $\pi-\pi^*$ excitation become equal in azobenzenes with increasingly large substituents in the ortho positions. Very big groups – such as phenyl groups – however, lock the azobenzene in the trans form, and there is a clear trend to smaller trans-cis isomerisation yields for very bulky groups. A singlet mechanism is suggested for the isomerisation, as yields for triplet sensitized experiments in unsubstituted azobenzenes are only a few percent.^{83,100}

In contrast to simple azobenzenes, donor acceptor azobenzenes such as the (1-46) have only been isolated as trans isomers.^{92,79}

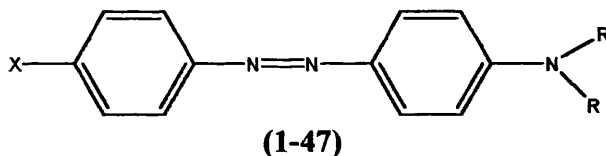


(1-46)

Here it is assumed that the equilibrium in favour of the trans isomer is greater than 99%, or alternatively, there is a very low barrier to isomerisation and it occurs very rapidly. When (1-46) is irradiated in benzene with visible light ($\lambda > 400$ nm), short term temporary bleaching, or loss of intensity of the long wavelength absorption band is observed.⁹² The photo-bleached solution then returns to the original intensity. In more polar solvents, the bleaching effect is much shorter lived. Low temperature spectra following flash excitation indicate that the product short lived product formed on photo-bleaching is the cis isomer, which has a much lower absorption than the trans isomer. Rapid thermal isomerisation of the cis isomer back to the original trans isomer then occurs.

The rate of photo-isomerisation in azobenzenes depends strongly on the substituents on the azobenzene. The cis isomers of donor-acceptor type azo dyes have very short lifetimes, 4-5 seconds in poly methyl methacrylate (PMMA), and therefore revert very quickly back to the trans form. This contrasts with cis isomer of azobenzenes, which have much longer lifetimes of hours in polymeric films.

In donor acceptor aminoazobenzenes, such as derivatives of (1-47), the less electron withdrawing the substituent group X is, the greater the amount of photo-isomerisation occurs from both $n-\pi^*$ and $\pi-\pi^*$ excitation.^{1,87}



For example, when $X = \text{NO}_2$ there is very fast thermal reversion to the ground state, giving almost none of the cis isomer, but with $X = \text{Cl}$ and $X = \text{OMe}$, there is slower thermal reversion and so an increase in the percentage of the cis isomer is present.

Experimentally it is seen by spectroscopic investigations⁹² that cis-trans thermal isomerisation is generally faster in more polar solvents and has first order kinetics, for example in hexane the cis to trans rate constant is 0.007 sec^{-1} , while in propan-2-ol the rate constant is 17 sec^{-1} . The rate increases sharply for polar solvents such as DMSO, where the rate constant is 440 sec^{-1} . By comparison, the rate constant for cis-trans isomerisation of 4-amino-4'-diethylaminoazobenzene is 0.003 sec^{-1} in benzene and does not increase in polar solvents. Addition of water to solutions of acetone or DMSO also increases relaxation rates. The activation energy for isomerisation is 14 kcal mol^{-1} in benzene and 10 kcal mol^{-1} in acetone. These activation energies are considerably

lower than those reported for monosubstituted azobenzenes. The observed solvent effect implies a polar or dipolar transition state.

To understand the mechanism of cis – trans isomerisation of donor acceptor azobenzenes better, Kikuchi¹⁰¹ carried out an *ab initio* study of the solvent effect on the cis-trans isomerisation of a donor-acceptor (push-pull) azobenzene (1-46), using the Generalised Born (GB) method. This is a continuum model with the solvent property reflected by its dielectric constant. This paper examines the energies of the possible transition states involved in cis-trans isomerisation in relation to various changes in the angles of orientation of the phenyl rings with respect to the azo bond for both inversion and rotation mechanisms.

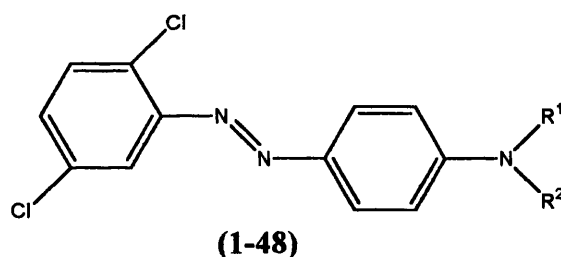
While it is generally accepted that azobenzenes undergo inversion¹⁰¹ – where sp^2 - sp hybridization of the azo nitrogen gives a semi linear transition state, push pull or donor-acceptor azobenzenes, in which the N=N bond is weakened by the para substituents, favour isomerisation via a rotation around the double bond. The reaction rate depends largely on solvent – it is faster in polar solvents.¹⁰¹ This implies a change in mechanism from inversion in non polar to rotation in polar solvents. Azobenzenes have been found to favor an inversion route via a transition state with a perpendicular orientation of the phenyl ring to the azo bond.¹⁰¹ The relation between two reaction paths on the basis of two dimensional energy surfaces defined by rotation and linear inversion motions and secondly, the effect of solvent polarity on the transition state structures and reaction mechanism are considered.

Kikuchi calculated that a pull-group inversion was more favourable than push-group inversion in the gas phase and in solvent and calculated activation energies compared well with experimental values. Analysis of the electronic configurations revealed that the rotation transition state clearly resembles the inversion transition state and the two states were found to be comparable in energy for the pull-group inversion. Calculations were performed using *ab initio* RHF methods on closed shell electronic structures and for the diradical state expected for the rotational mechanism transition state and ROHF calculations with the general SCF formulation applied to the excited singlet state were used. The polar solvent was represented by $\epsilon = 79$ (dielectric constant of water). The STO-3G basis set was used for geometry optimization and the 6-31G basis set used for energetic calculations with optimized structures. Transition state structures were determined by minimizing the norm of the energy gradients.

The trans-cis photoisomerisation process may be involved in the dissipation of electronic

excitation energy from excited states of the molecule, and according to Rau,^{64,65} the mechanism of energy dissipation from the excited state is dependent on whether $n-\pi^*$ or $\pi-\pi^*$ excited singlet state is lowest. At an intermediate geometry between the trans and cis isomers, corresponding to 135° inversion angle, the energy gap between the ground state and the $n-\pi^*$ singlet excited state becomes smaller and the rate of radiationless decay increases⁶⁴ resulting in loss of energy from the excited state of the molecule. However, if the $\pi-\pi^*$ state is the lowest singlet excited state, then trans-cis isomerisation proceeds by rotation and the lifetime of the excited state is longer, even giving the possibility of fluorescence.⁶² It has been found that the more photo stable dyes are those having a higher rate of cis trans reversion, which are less likely to rupture at the beta nitrogen-carbon link.¹⁰² Absence of isomerisation, which is one possible mechanism for the dissipation of energy, may reduce light stability.⁶²

The photoisomerisation reaction, may result in the dye undergoing a colour change if the cis form is reasonably stable, as the cis isomer absorbs longer wavelength than the trans. As a consequence there will be a bathochromic shift in the wavelength attributable to the absorption of the cis isomer, giving a deeper hue to the dye⁴². The shift may be attributed to the cis isomer having a broad $n-\pi^*$ band extending to slightly longer wavelengths than the intense $\pi-\pi^*$ band of the trans compound. The cis isomer of 2',5'-dichloro aminoazobenzene, **(1-48)**, exists as the cis form long enough for such a colour change to be observed.¹



This colour change may be undesirable in fabrics etc. Dyes with fast interconversion are therefore usually chosen. The reaction is of course totally reversible. Reversion to the original colour will eventually result after storing in the dark. This reversible colour change on photoisomerisation may be useful in other applications e.g. light filters and photoimaging.¹⁹

Section 1.10

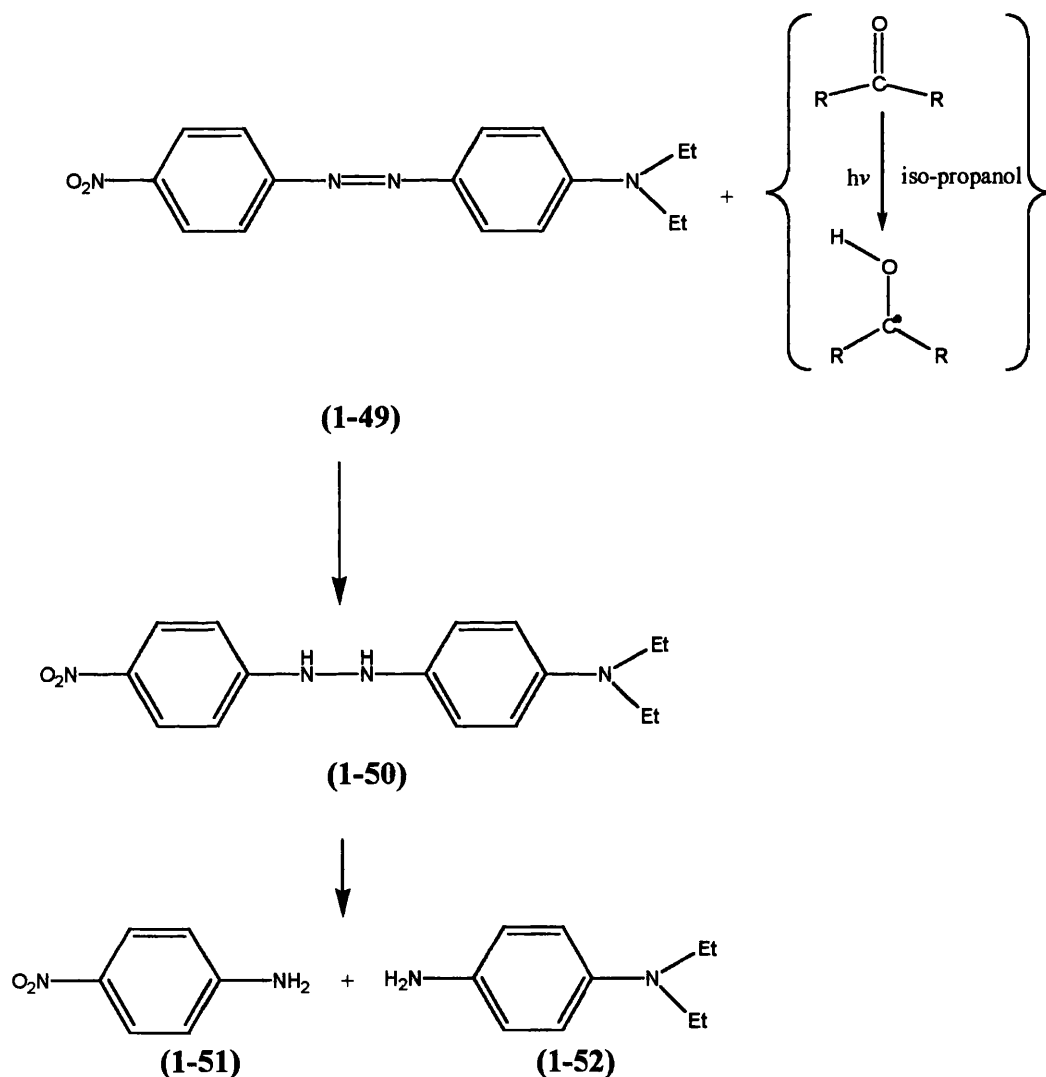
Irreversible fading

As explained earlier, photoisomerisation is a totally reversible process. The most important fading

processes are however irreversible and involve the destruction of the azo group in most cases. The azo dyes can also undergo photoreduction and photo-oxidation reactions^{103,104}, whilst the amino group may also be oxidised. If a nitro group is present in the dye then it is possible that this may undergo a reduction.⁴² These reactions are discussed below.

Photoreduction

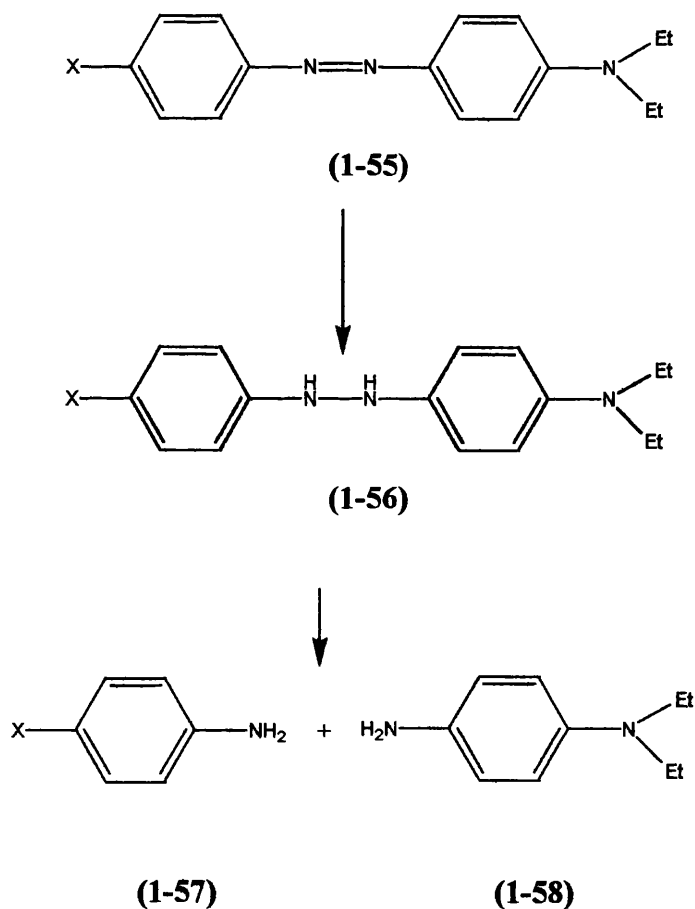
There are two types of photoreduction reaction possible for the azo group in azo dyes.^{2,14} The first is indirect reduction which either involves energy transfer from a sensitizer, for example, a carbonyl compound¹⁰⁵, or the sensitizers may abstract hydrogen from the solvent and form a radical (Scheme 1.3).¹⁴



Scheme 1.3 Reaction mechanism for the indirect photoreduction of an azo dye

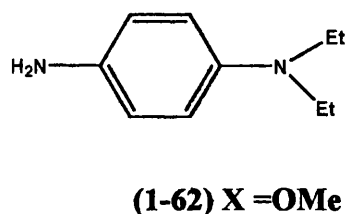
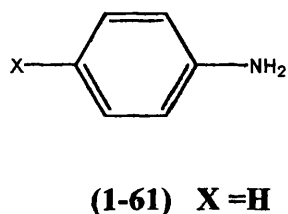
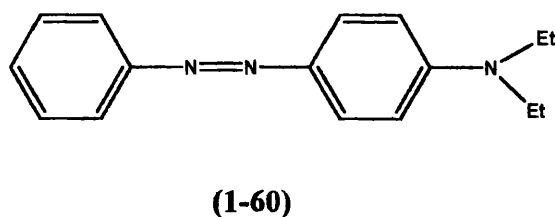
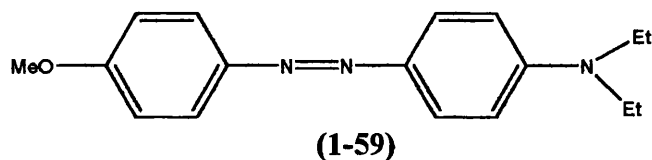
In Scheme 1.3 the excited ketone sensitizer abstracts hydrogen from the solvent and forms a ketyl radical, which then attacks the azo bond. Intramolecular hydrogen transfer gives a hydrazo radical which may itself abstract hydrogen from the solvent and reduce the azo dye to a hydrazine compound (1-50).

The second way is by direct photoreduction, which was investigated first by Irick and Pacifici,¹⁰⁶ who faded solutions of compound (1-49) at 254 nm in several solvents, including iso-propanol at 310 nm and 366 nm. They found that compound (1-49) was completely and rapidly regenerated on readmission of air into the sample. They therefore assumed that the photoproduct was the hydrazo derivative (1-50). The results of Irick and Pacifici and a separate study by Albini, showed that (1-49) was regenerated in air in iso-propanol solution implying compound (1-50) as the photoproduct. However, in methanol or cyclohexane, the main products, found by TLC and GC-MS analysis, were the anilines as in the reaction Scheme 1.4. Here hydrogen is abstracted from the solvent by a photo-excited state of the dye itself, which breaks down further to give anilines as shown in the reaction scheme below.^{14,87,90,109,107,108}



Scheme 1.4 Direct photoreduction of an azo dye

In propan-2-ol, which is more viscous and has an easily abstractable hydrogen, photo reduction leads to (1-50) whereas in methanol, a stepwise pathway gives anilines. However, a subsequent paper by Albini⁸⁷ states that although (1-49) is suspected to form the hydrazo derivative, the methoxy and hydrogen analogues (1-59) and (1-60) are reduced to the amines (1-61), and (1-62), these products arising from the further reaction of the hydrazyl radical formed in the primary hydrogen abstraction. The same products are assumed from the acetone sensitized experiments.^{106,109}



It was presumed that the hydrazo derivatives for these dyes are unstable and undergo quick disproportionation to the starting material and the amines. An alternative possibility is that the amines arise from direct cleavage of the hydrazyl radical. The efficient oxygen quenching is thought to be due to the reaction of oxygen with the hydrazo radicals rather than with some excited state of the azo dyes which would be too short lived to be intercepted by oxygen⁵⁸ The products of the indirect photoreduction, with chemically sensitized photobleaching in acetone methanol solutions, gives partly compound (1-49) and partly anilines.

Besides chemical sensitization through radical initiation,⁵⁸ energy transfer is also effective in promoting the reaction. The energy of the sensitizer is very important, for example, anthracene is ineffective in promoting the reaction, although its triplet is higher in energy than that of (1-49) (40kcal/mol).⁵⁸ Sensitizers with triplet energy greater than 67 kcal/mol are more effective.

Effect of the wavelength of light

Datyner et al.¹²⁶ have shown using a glass plate which absorbs all energy below 300 nm that most of the fading occurs due to light below this wavelength while Accoria *et al.*¹³ say that dyed films exposed to 254 nm fade much faster than those exposed to 350 nm.

Albini *et al.* showed¹⁰⁹ the rate of reaction was much greater when using quartz filtered rather than pyrex filtered light. Therefore the reaction is strongly wavelength dependent and irradiation of the first absorption band had no effect on fading, while photoreduction began to occur at 313nm, and thus some higher lying state is involved. They found that compound (1-49) was not completely regenerated in air and suggested that the reduction of compound (1-50) proceeds via reaction with radicals in solution. Albini suggests that photoreduction of the cis isomer of (1-49), which has accumulated in cyclohexane and is more efficiently reduced than the trans form, may occur. The rate of cis→trans thermal reversion is $7 \times 10^{-3} \text{ s}^{-1}$ in cyclohexane and 17 s^{-1} in iso-propanol.¹⁰⁹ The build up of the cis isomer is therefore higher in cyclohexane than in the better hydrogen donors iso-propanol and methanol.¹⁰⁶ However, the lifetime of the cis isomer is immeasurably short in alcohols and therefore, photoreduction is proposed to occur from the trans isomer.¹⁰⁹

Albini reiterates that to understand the photochemistry of these dyes, not only the lowest singlet and triplet states, but also high lying states must be considered. The lowest excited singlet undergoes highly efficient geometric isomerisation and thus only minimal intersystem crossing and no trace of hydrogen abstraction is detected. As opposed to the low lying charge transfer state, the π - π^* singlet states corresponding to weak benzenoid absorptions at shorter wavelengths undergo efficient intersystem crossing to high lying triplets. Analogously to the lowest singlet, the lowest triplet state undergoes only geometric isomerisation (see Section 1.9). The high lying triplets have some, although low probability of abstracting hydrogen from the solvent¹⁰⁹, but the overwhelming process is conversion to T_1 . The photoreduction occurs only for the π - π^* excitation and only in low quantum yield.^{14, 109} In view of the predicted weak hydrogen abstracting ability¹¹⁰ of π - π^* triplet state of azobenzenes, and the high reactivity of the high lying triplet state of (1-49) and very short lifetime of its singlets (S_1 has a lifetime of picoseconds), high lying triplets are assumed to be involved in the photoreduction. These triplets can be reached by energy transfer or by intersystem crossing from high lying singlet states. The low quantum yield for the photoreduction reaction is not surprising in view of the short lifetime of the states involved ($\tau_{Tn} \leq$

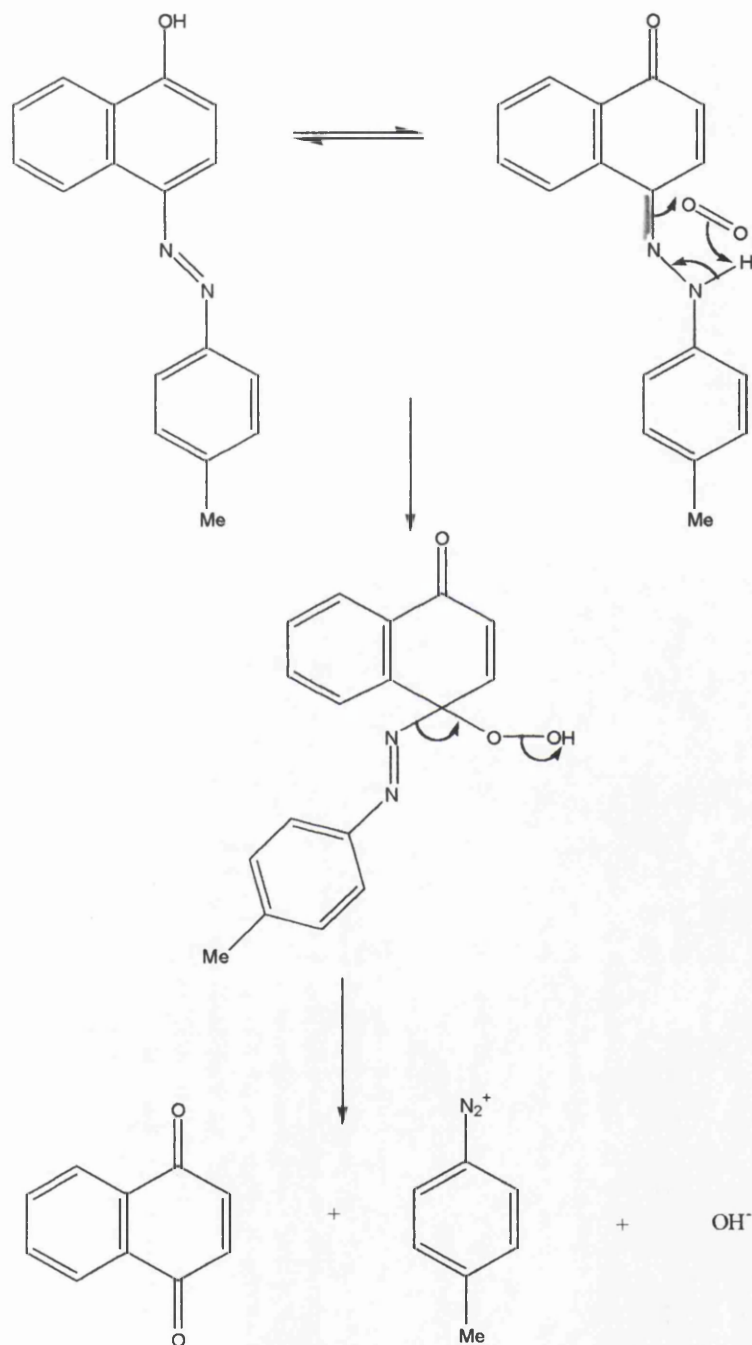
$\tau_{T1} < 10^{-9}$ s).⁵⁸ The involvement of high lying triplets is again confirmed by the fact that high energy sensitizers promote both reduction and isomerisation, while the low energy ones promote isomerisation only. For azobenzene, only high lying triplets of the cis form have been reported to undergo hydrogen abstraction.¹¹¹

The experiments are extremely sensitive to O₂ and it is hard to get reproducible results.¹⁰⁹ The presence of oxygen is an important factor in this reaction. A small amount of O₂ may increase the rate of the process^{14,110} - implying that this induces the excited singlet- triplet (S₀*-T_n) transition, whereas large amounts of O₂ quench the reduction. This implies the involvement of ³(π - π *) in the reaction. The reaction is quenched by quenchers acting as radical traps. The same effect is seen with di-tertiary butyl phenol, but at high concentrations.

Section 1.11

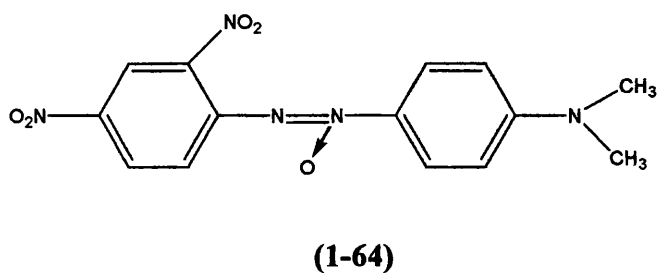
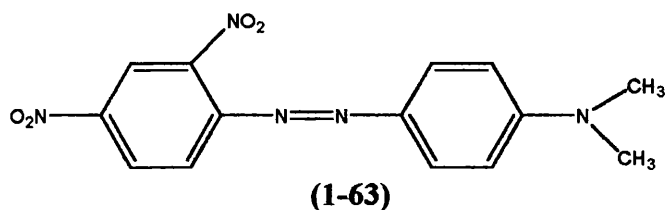
Photo-oxidation

The photo-oxidation of azonaphthols, which exhibit azo-hydrazone tautomerism (**Scheme 1.5**) is well established.^{42,112} Here, oxidation is of the hydrazone tautomer, and may involve an "ene" reaction with singlet oxygen, and it has also been shown that arylazonaphthols photosensitize oxygen.



Scheme 1.5 Mechanism of the photo-oxidation of azonaphthols

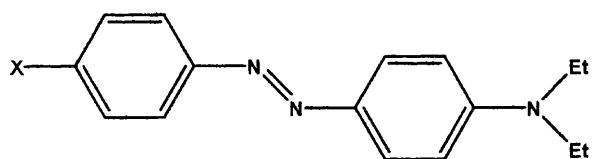
The only evidence for oxidation of a non tautomerising dye is for compound **(1-63)**⁴², which gives the azoxy compound **(1-64)**



Singlet oxygen

Singlet oxygen has been suggested to be involved in the photodegradation but research by Albini¹⁴ et al., states that azo dyes show only a slight activity with singlet oxygen and only slow fading takes place in the presence of singlet oxygen sensitizers such as methylene blue.¹⁴ This is discussed further in the following section.

Self sensitized singlet oxygen oxidation has been considered by Albini et al.¹¹³, who examined fading of simple mono azo dyes **(1-65)**, **(1-66)** and **(1-67)** in aerated solutions.



(1-65) X = H

(1-66) X = OMe

(1-67) X = NO₂

These azo dyes show only slight reactivity with singlet oxygen. Practically no reaction is observed when singlet oxygen is generated by thermal decomposition of 9,10-dimethyl-anthracene endoperoxide and only slow fading takes place by irradiation in the presence of oxygen sensitizers such as Methylene Blue (MB) or Rose Bengal (RB).

In the presence of singlet oxygen acceptors, the azo dyes showed no oxygen sensitization within the limits of the Albini experiment.

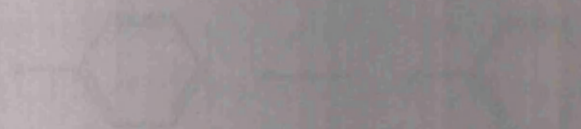
A very small quantum yield of oxygen sensitization has however, been found for some derivatives of (1-67) in viscous solvent.

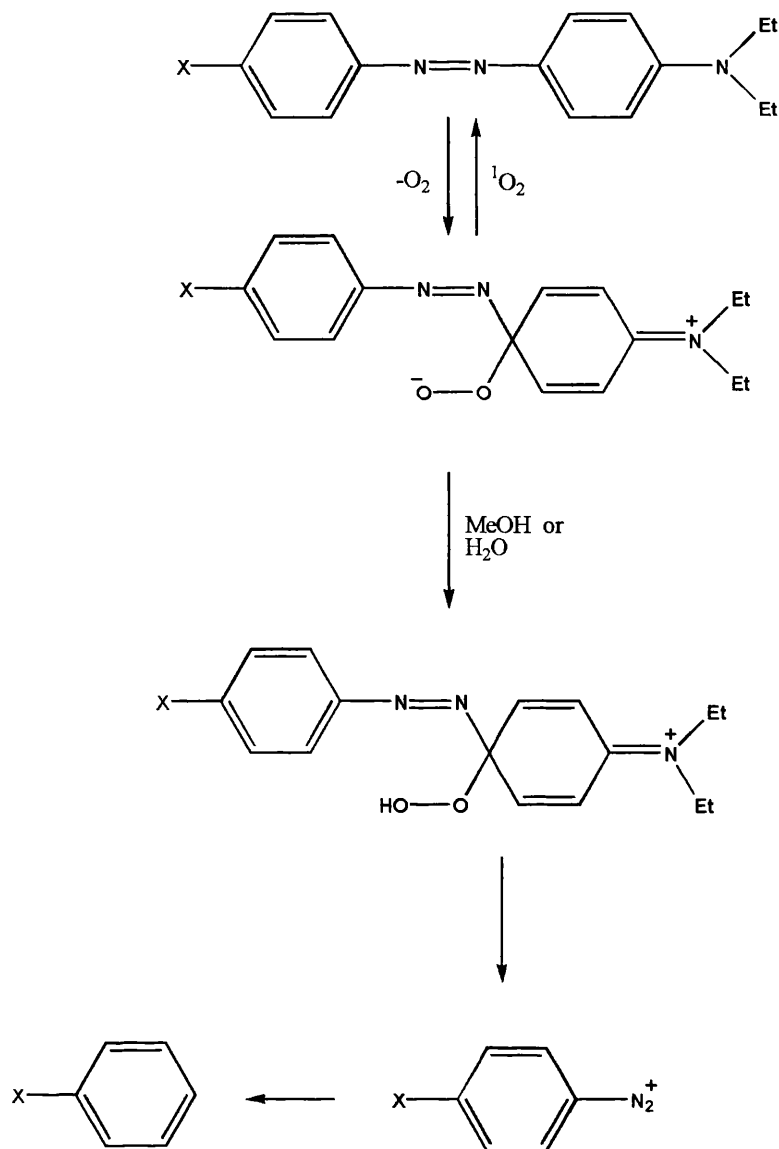
Fading rates of dyes (1-65)-(1-67) were found to be much slower when compared to azo naphthol dyes under a standard set of conditions, but both sets of dyes showed increased fading rates in going from methanol to methanol - water mixtures, and also in deuteriated solvents, while the reaction was quenched by the known singlet oxygen quencher, diaza bicyclo-[2.2.2]octane (DABCO) and by nickel salts.

The photo-oxidation products of (1-66) and (1-67) were found to be anisole and nitrobenzene respectively, with benzene formed from (1-65).

The involvement of singlet oxygen is deduced from the increase in fading rate of about an order of magnitude in going from methanol to methanol-water mixtures reflected by the increased singlet oxygen lifetime in methanol-water solutions. From this evidence Albini proposed the following possible mechanism for singlet oxygen oxidation (see Scheme 1.6).

This scheme involves electrophilic attack by singlet oxygen on the aromatic ring at the position para to the dimethylamino group.

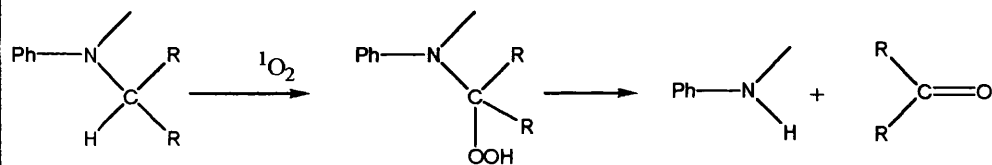




Scheme 1.6 Possible singlet oxygen mechanism for the oxidation of azo dyes

Cleavage of the C-N bond on the donor side yields the diazonium ion which loses N₂ to give a benzene derivative as the final product.

There is another possibility for an oxidative fading reaction, this time involving a dealkylation proposed by Griffiths⁴² (Scheme 1.7) by analogy with similar processes that have been found for aliphatic amines.



Scheme 1.7 Oxidation of the N-alkylamino group by singlet oxygen

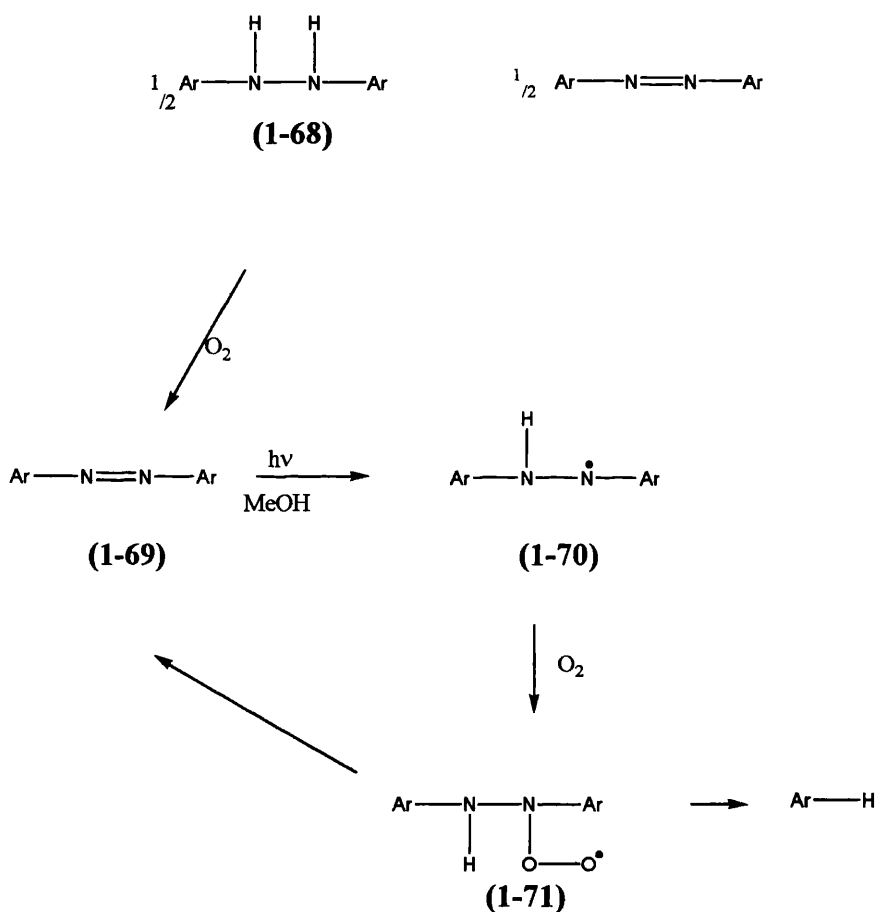
Here the photo-oxidation product is the dealkylated monomethyl derivative. Only a small amount of the dealkylated monomethyl derivative c.a. 2% of dyes **(1-65)** and **(1-66)** were found by Albini, who states that this low yield is not due to the decomposition of this derivative, as it is more stable to photo-oxidation than the dimethyl derivative. He concludes therefore that the main photofading reaction does not involve chemical attack on the amino group.

For dyes **(1-65)**-**(1-67)** the main process in the fading of degassed solutions is reductive cleavage of the azo bond to give anilines⁸⁷This process is quenched by oxygen. Analysis of the fading products, for fading under aerated conditions, showed that in addition to anilines, benzene and anisole were also produced. This process only occurs with UV light. The fading is initially slow until about 10-20% conversion after which fading accelerates rapidly. The fading is not linearly dependent on the photon flux. Albini concludes that fading under aerated conditions is very slow and not a significant component of the observed photofading - not unexpected considering the well known quenching of singlet oxygen by tertiary anilines.¹¹⁴

Dyes **(1-65)** and **(1-66)** fade at a faster rate than expected for a singlet oxygen, process giving anilines as products in addition to anisole and nitrobenzene from dyes **(1-66)** and **(1-67)** and benzene from **(1-65)**.

Possible mechanism involving oxygen

A possible mechanism, suggested by Albini¹⁴, for the photofading of azo dyes involving oxygen is shown in reaction Scheme 1.8. He proposed that the initial step of the reaction is a reduction, giving the hydrazyl radical (1-70). It is thought that high lying triplets reached by short wavelength irradiation and intersystem crossing abstract hydrogen from the solvent in the initial reduction process. In the absence of O₂, the hydrazyl radicals formed, disproportionate to the starting material and a hydrazobenzene (1-68), which is further cleaved to the aniline. If O₂ is present, it may react with the hydrazyl radical at the nitrogen, yielding a peroxy radical (1-71) which either reverts to the starting material or undergoes further decomposition to the end products.

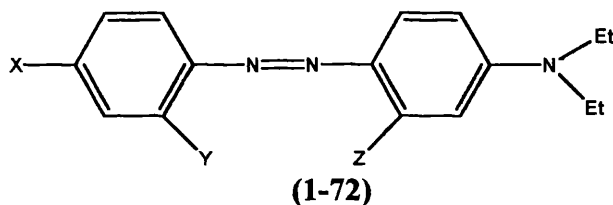


Scheme 1.8 Probable photo-oxidation mechanism for azo dyes

The substrate

The chemical structure of the substrate may be important in determining the mechanism by which the dye fades and the rate of photofading. On non proteins, it is believed that photo-oxidation occurs.¹¹⁵ It is thought that fibers like cellulose don't take part in the reaction and are in fact protected by the dye from degradation.¹¹⁶ NS Allen's experiments¹⁰⁸ showed that rate of fading on cellulose was greater in aerated conditions than under deoxygenated conditions, providing further evidence of an oxidative process.

On proteins e.g. wool, silk and polyamide, fading occurs via a reductive pathway^{108,116} implied by the formation of amines from reduction of the azo group. The presence of oxygen makes little difference here, as the oxygen interacts preferentially with the polyamide film¹³ There is a slight difference in the rates in air due to competition between the dye and oxygen for the initial reducing species. Fading may be first or zero order depending on which ring of the dye is substituted.



For example, Arcoria *et al.*¹³ reports that this aminoazobenzene fades with first order kinetics when Z is an NH₂, NHC(=O)CH₃ or NHC(=O)CH₂CN substituent but has zero order kinetics when Z is H, in (1-72), on nylon film.

For first order dyes, light is preferentially absorbed by the film¹³. Dyes may fade with zero order kinetics in solution¹¹⁷ and in dyed materials, with large particles of dye e.g. disperse dyes or pigments, the fading may also be zero order.¹¹⁸ Fading may also occur only on the surface of the dye particle; the layers underneath being protected from exposure to light.

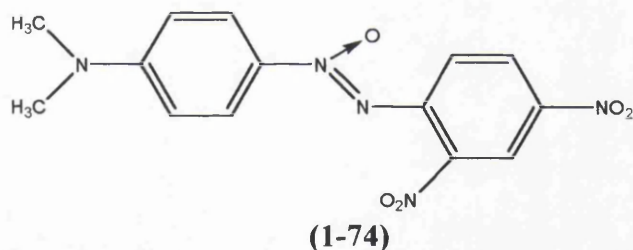
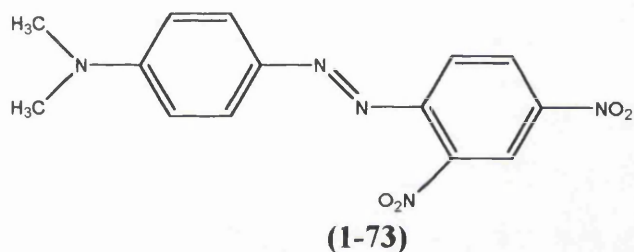
Photoreduction may be direct or indirect, as in solution, and may be sensitized by the carbonyl group in the polyamide film.^{13,119} This has been suggested by studies using sensitizers^{14,90,120} such as biacetal, methylene blue and ketones. It is suggested that the sensitizer may undergo energy transfer with the dye to give a reactive triplet state of the dye. Alternatively, a ketyl radical (formed by abstraction of hydrogen from the solvent by a ketone triplet) may transfer a hydrogen atom to the azo linkage.¹⁰⁵

Involvement of the substrate in photo-oxidation

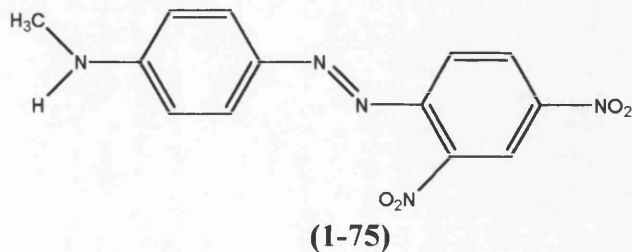
Since the substrate, or radicals from it, may be a primary cause of photofading for certain systems, investigations by Albini¹²¹ showed that self sensitized photo-oxidation was not significant in the photofading of azo dyes, which quench rather than react with singlet oxygen,¹¹³ when a solution model system was used.

The model system for this was photofading in the presence of carbonyl compounds. Carbonyls sensitize fading in degassed solution through radical initiation (acetone enhances fading rates by 1 to 2 orders of magnitude.⁸⁷ Also COOH radicals from the decomposition of mandelic acid cause fading of certain azo hydrazone structures even in aerated solution.¹²²

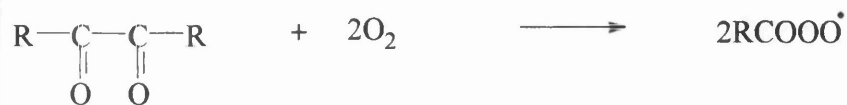
Albini used Acetone, benzophenone, anthraquinone, benzil and 2,2-dimethoxy-2-phenylacetophenone (DMPA) - which undergoes efficient Norrish I cleavage to radicals¹²³ - in high enough concentration to ensure they absorbed a large part of the light used and produced radical species. The dye used was (1-73), which was quite fade resistant and has been reported to give the azoxy derivative on irradiation in aerated iso-propanol.¹²⁴



However, irradiation of (1-73) in benzene in the presence of carbonyl sensitizers, resulted in the isolation of the monomethyl derivative of the dye (1-75) in 30 to 40 % yield.

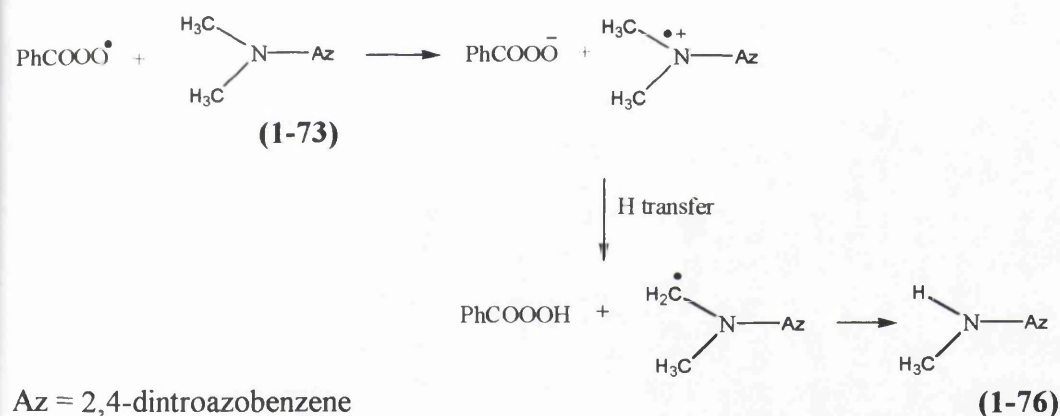


Other processes giving more decomposition were also present but di-nitroaniline and di-nitrobenzene were not formed. It was assumed that peroxy radicals formed from carbonyls in the presence of oxygen (Scheme 1.9) are involved in the demethylation (1-73).



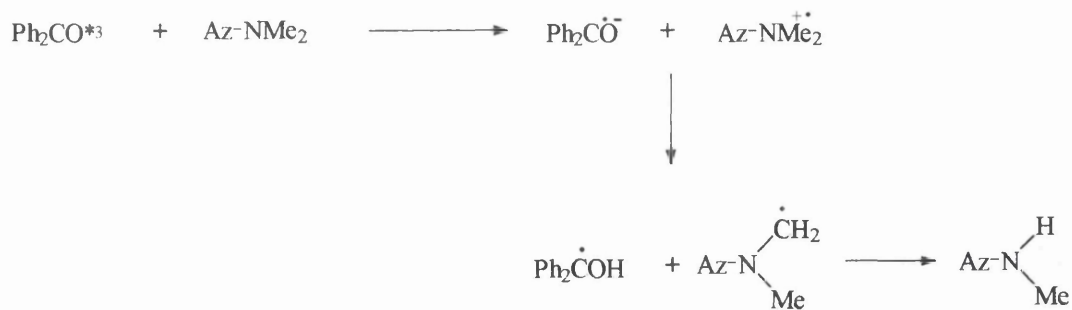
Scheme 1.9 Reaction of a diketone with oxygen to yield a peroxy radical.

Reaction of the diketone triplet precedes cleavage of the C-O bond. The peroxy radicals produced are strong electrophiles and can abstract an electron from the aminoalkyl group of (1-73) to give a peroxy anion and the radical cation of (1-73). The peroxy anion and radical cation of (1-73) formed, can then undergo a proton transfer. The radical species formed loses CH₃, ultimately giving the monomethyl derivative (1-76) (see Scheme 1.10).



Scheme 1.10 Reaction of peroxy radical species with an aminoazo dye.

DMB (dimethyl benzene) is found to quench the reaction as it is oxidised by the peroxy radical. The reaction of the amino azo dye (1-73) with benzophenone also produces the monomethyl derivative (1-76), but may involve a different mechanism to that for the peroxy radicals. Unlike benzil and DMPA, benzophenone does not decompose itself and its triplet state may interact directly with the dye as in Scheme 1.11.

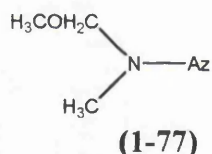


Scheme 1.11 Reaction of benzophenone with the azo dye

The radical cation of the azo dye (**1-73**) is formed along with the radical anion of benzophenone, and proton is transferred to the anion from the cation. The final product is again the monomethyl derivative whilst benzophenone regenerated.

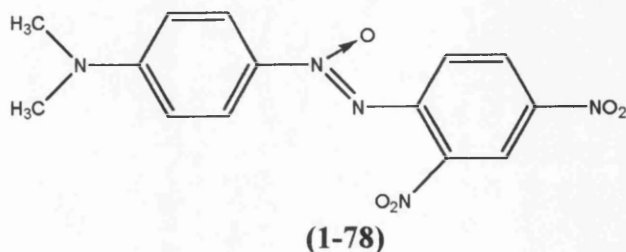
In the polar solvent methanol, the photo-decomposition was dependent on the presence or absence and the nature of carbonyl sensitizers.

Direct radiation with no sensitizer yielded no coloured product and fading was very slow. Irradiation in the presence of benzil, DMPA or benzophenone gives a much faster photoreaction and yielded an orange product (**1-77**), identified from its chemical behaviour and too labile to be isolated. This in turn gives the monomethyl derivative (**1-76**).

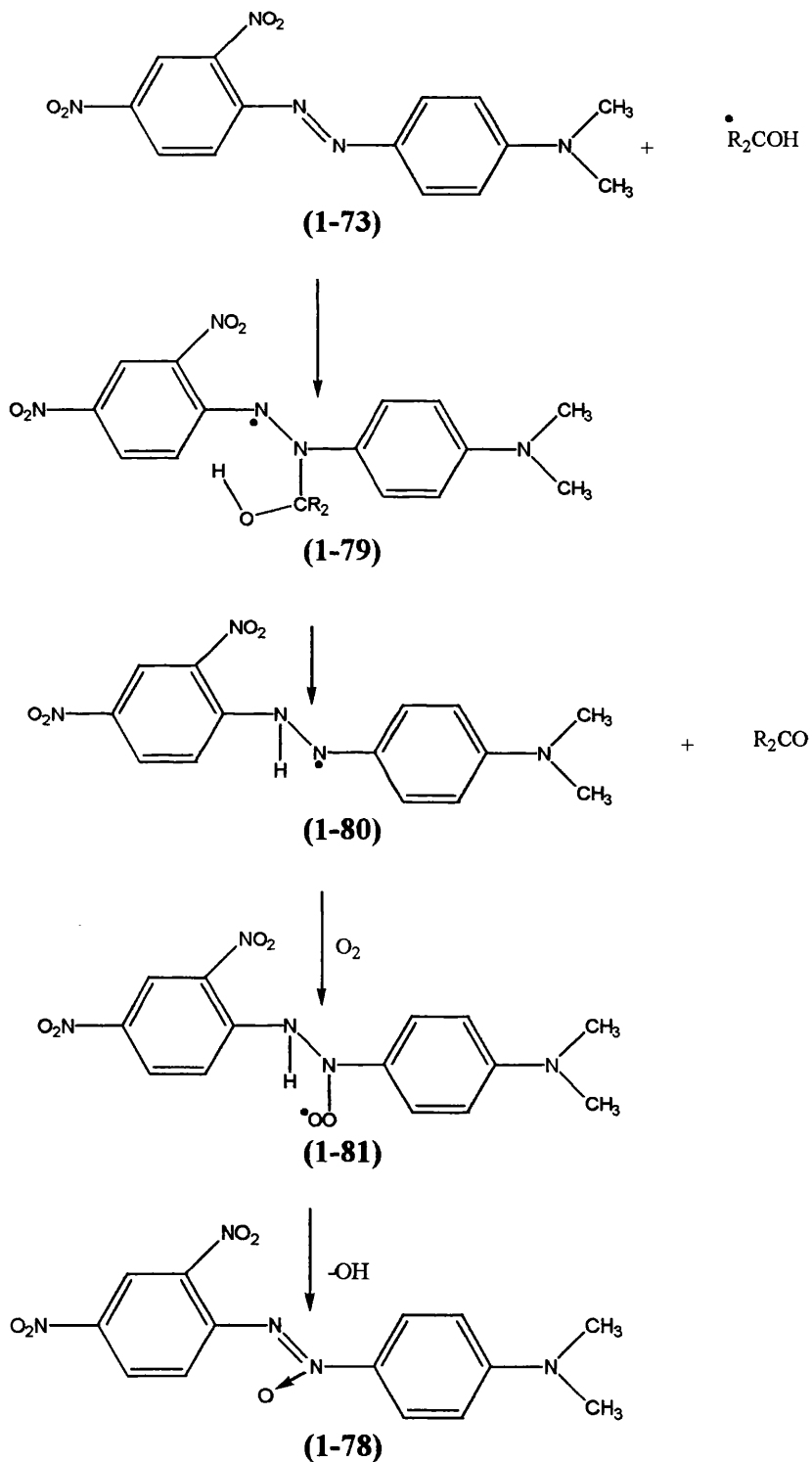


The initial hydrogen abstraction step is the same as in benzene solvent and the benzoylperoxyl radical is the reactive species.

For acetone and anthraquinone however, a completely different reaction is observed, with the only coloured product observed being (**1-78**) and dealkylation being a minor process.



As it has been seen in Scheme 1.11, the inert triplet state of benzophenone reacts with the amino group of compound (1-73) in benzene, but in methanol, hydrogen donating solvents give ketyl radicals which attack the azo dye (1-78) as shown in Scheme 1.12.



Scheme 1.12 Mechanism of indirect photo-oxidation in methanol.¹²⁴

Here the ketyl radical adds to the double bond, an intramolecular hydrogen shift accompanied by loss of the ketone, gives a hydrazo radical (1-80) which reacts with oxygen to give (1-78). However, direct irradiation in propan-2-ol,¹²⁴ gives (1-78) in a 9:1 ratio with the monomethyl derivative of (1-73), implying that propan-2-ol, being a better hydrogen donor competes for the dilute dye with the ketone triplet, forming ketone radicals which attack the dye.

The conclusion drawn is that (1-73) is an efficient and selective radical trap. Strongly electrophilic radicals such as peroxy radicals are reduced by the amino group giving the demethylated derivative (1-75), whereas ketyl radicals attack the azo chromophore and in the presence of oxygen, give an azoxy compound (1-78). This work suggests that radicals at the oxygen atom of carbonyls attack the amino group whilst radicals at the carbon of carbonyls attack the azo bridge.

Effect of wet substrate systems

The importance of humidity in dye photofading is closely related to the influence of oxygen and the role of singlet oxygen.

In general, moisture content of dyed fibers reduces lightfastness¹⁰⁸. Moisture apparently swells the fibres thus enabling air to penetrate into the substrate more efficiently. By this reasoning, dyes which undergo photo-oxidation reactions will have an increased rate of photofading with increasing humidity, while dyes that degrade by photoreductive processes should fade more slowly, as oxygen diffuses into the substrate and quenches the excited triplet states of the dye.

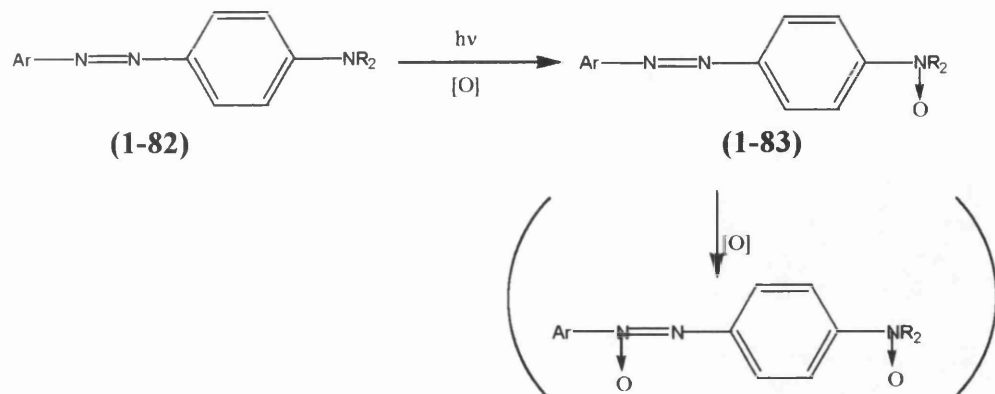
Nichols and co-workers¹²⁵ found that a reactive azo dye faded by a mechanism involving the photoejection of an electron



The presence of moisture was found to greatly enhance the rate of a photoejection of an electron by solvating it as in equation Equation (1-4).¹²⁶ The radical species produced by the photoejection may then undergo subsequent reactions involving H₂O and oxygen.^{13,105}

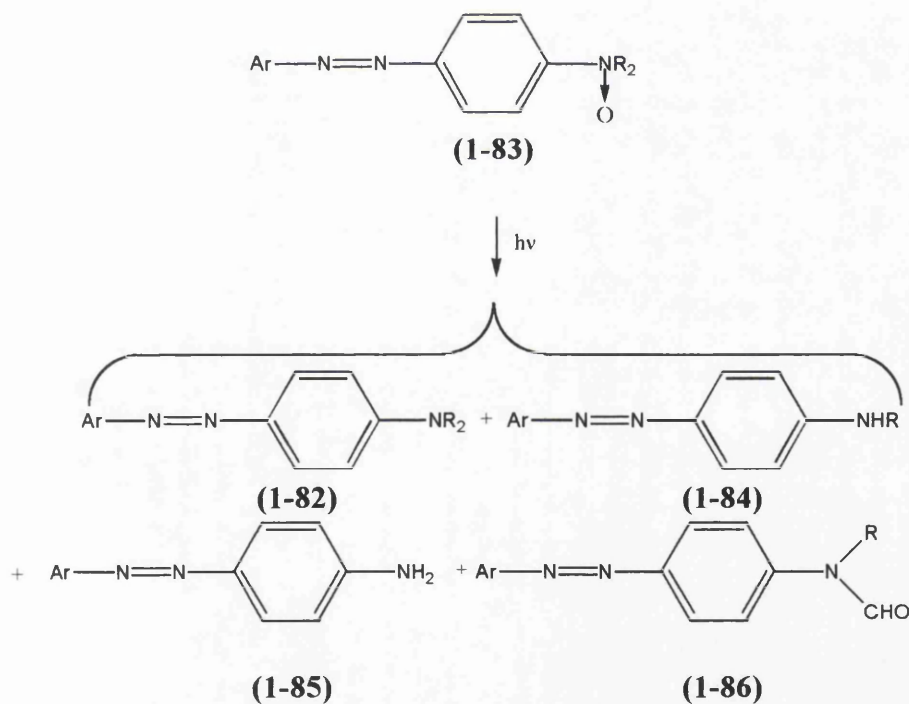
N-oxidation¹²⁷

The amino nitrogen is far more electron rich than the azo linkage and therefore N-oxide derivatives are expected to be formed during oxidation. No such product has yet been isolated, but this could be due to its fast secondary composition.



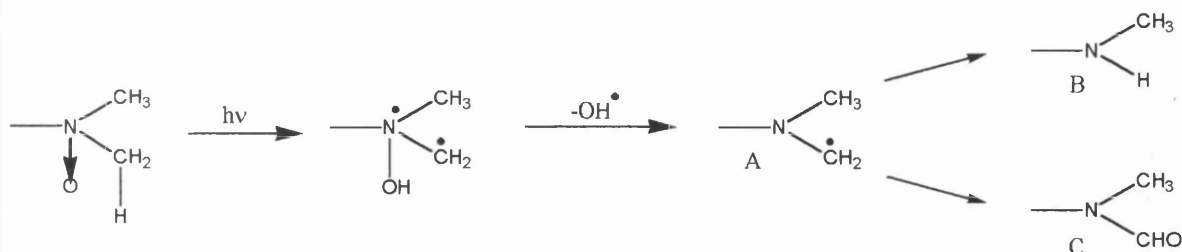
Scheme 1.13 N-oxidation of the amino nitrogen. Ar = Ph or $\text{CH}_3\text{O}-\text{Ph}$, R = CH_3 or C_2H_5 .

The photochemical decomposition of azo N-oxides is known. Compound (1-83) can be produced by oxidation with perbenzoic acid. Photofading of (1-83) gives (1-82), (1-84), (1-85), and (1-86) as products.



Scheme 1.14 Photo-products of N-amino oxidised azo dye

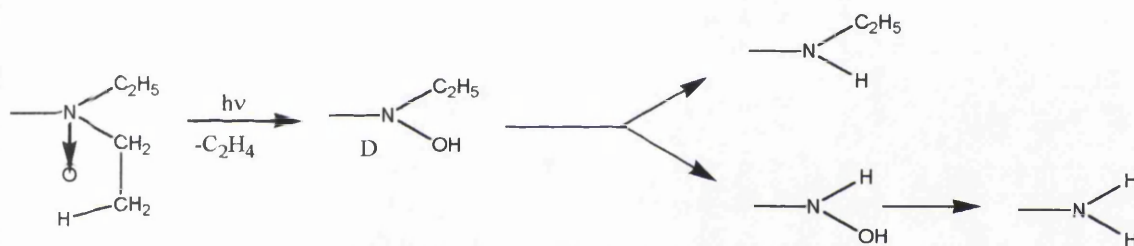
In the dimethyl derivative of (1-83), the photochemistry apparently involves oxygen transfer to the solvent and intramolecular hydrogen abstraction as shown in **Scheme 1.15**.



Scheme 1.15 Mechanism of N-amino group photo-oxidation

The major and minor end products, B and C, correspond to those observed when the radical species A is formed by the photosensitised reaction of an azo dye, as in Scheme 1.15.

For the diethyl derivative, there is easy abstraction from the β position giving the elimination of ethylene (Scheme 1.16). The mechanism of formation of the dealkylated amino group is similar to that in Scheme 1.15.



Scheme 1.16 Mechanism of N-amino photo-oxidation of a diethyl aminoazo dye

The hydroxylamine D found, undergoes further photochemical fragmentation to the observed products in Scheme 1.9.

Oxidation of the N amino nitrogen makes its lone pair unavailable for conjugation and negates its bathochromic effect on the spectra of the dye (by 70 to 100 nm). The electronic spectra of the N-oxides are almost identical with those of azobenzenes. These type of oxidations are reversible. On excitation to the π - π^* state of the N-oxide, charge is transferred from the phenyl ring to the azo bridge, making the N-oxygen atom electrophilic and radical in character and thus giving the oxygen transfer and hydrogen atom abstraction seen in Scheme 1.16.

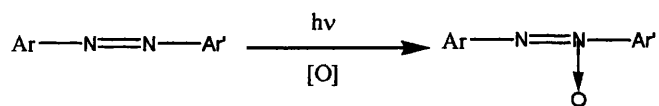
Further oxidation yields a azoxy N-oxide. These can be prepared by oxidation by peracetic acid of the corresponding azo derivatives. Recent evidence¹²⁷ confirms that the second oxygen atom is at

the azo nitrogen atom attached to the acceptor phenyl ring. Both N-oxides and azoxy N-oxides were found to be stable in alcoholic solvents, but reactive in benzene when irradiated.

Photodecomposition of these N-oxides in aprotic solvents is more efficient than for azo dyes with similar structure.

In summary there are four types of oxidation reactions for the azo dyes:¹²⁷ Oxidative cleavage of the Ar-N=N bond,^{128,129,130,131}

1. Oxidation of the azo bridge (Scheme 1.5 and Scheme 1.6).
2. Oxidation of the amino group following interaction with a sensitizer.
3. Oxidation of the azo bridge to give azoxy derivatives (Scheme 1.17) which, are known to undergo further photoreduction to o-hydroxy azo derivatives.¹²⁷ Note that this reaction has only actually been demonstrated for dye (1-64).



Scheme 1.17 Oxidation of the azo bridge.

4. N-oxidation of the amino nitrogen (Scheme 1.13).

Section 1.12

Theoretical calculations

There are several theories for the colour/structure relationships including empirical rules based on experiment or quantitative relationships based more or less on theoretical reasoning. These include resonance theory (see p82), Dewar's rules and PPP theory.^{19,25} Molecular orbital (MO) methods of various levels of sophistication are available for computing light absorption characteristics of a molecule starting with a knowledge of the main structural features of the molecule and a small number of parameters. The following text gives an brief description of the theory of some of molecular orbital methods used in this work.

Quantum mechanical models

There are a number of quantum mechanical theories for modelling molecular systems. The one we shall consider is molecular orbital theory, which is the theory behind the computational calculations carried out for this thesis. It is very useful to have some idea of the theoretical background behind these calculations and a description of some of the relevant details of quantum theory will be attempted. Much of this chapter is based on chapters of Andrew R. Leach's excellent book "Molecular Modelling : Principles and applications"¹³²

The starting point of the discussion must be the Schrödinger Wave Equation.

$$\left\{ \frac{\hbar^2}{2m} \left(\frac{\partial^2}{\partial x^2} + \frac{\partial^2}{\partial y^2} + \frac{\partial^2}{\partial z^2} \right) + V \right\} \Psi(r, t) = i\hbar \frac{\partial \Psi(r, t)}{\partial t} \quad \text{Equation (1-5)}$$

Equation (1-5) is the full time dependent form of the Schrödinger Equation, referring to a single particle of mass m (e.g. an electron), moving through space with a position $\mathbf{r} = x\mathbf{i} + y\mathbf{j} + z\mathbf{k}$ (where \mathbf{i}, \mathbf{j} and \mathbf{k} are vectors) at time t , under the influence of an external field V (for example, due to the electrostatic potential of the nuclei in an atom). Plank's constant divided by 2π is denoted by \hbar , i is the complex number equal to the square root of -1 and Ψ is the wave function, which characterises the particle's motion. When V is time independent, the wave function can be written as the product of a time part and a spatial part:

$$\Psi(r, t) = \Psi(r) \Psi(t) \quad \text{Equation (1-6)}$$

In the remainder of this discussion, only the simplified time independent form shown in Equation (1-7) will be considered.

$$\left\{ -\frac{\hbar^2 \nabla^2}{2m} + V \right\} \Psi(r) = E\Psi(r) \quad \text{Equation (1-7)}$$

Here E is the energy of the particle and:

$$\nabla^2 = \frac{\partial^2}{\partial x^2} + \frac{\partial^2}{\partial y^2} + \frac{\partial^2}{\partial z^2} \quad \text{Equation (1-8)}$$

The left hand side of Equation (1-7) can be written as $H\Psi$ where H is called the Hamiltonian operator:

$$H = -\frac{\hbar^2 \nabla^2}{2m} + V \quad \text{Equation (1-9)}$$

and Equation (1-9) can be rewritten in the abbreviated form of Equation (1-10)

$$H\Psi = E\Psi \quad \text{Equation (1-10)}$$

To solve the Schrödinger equation values of E and functions Ψ must be found, such that when the wave function is operated on by the Hamiltonian, it returns the wave function multiplied by the energy. The Schrödinger equation is a partial differential eigenvalue equation, in which an operator acts on a function (called the eigenfunction) and gives the function multiplied by a scalar (called the eigenvalue).

An example of this is: $\frac{dy}{dx} = ry$. Here the operator $\frac{dy}{dx}$ acts on an eigenfunction e.g. $y = e^{rx}$

giving the result re^{rx} where r is a scalar. The Schrödinger equation is a second order differential equation like $\frac{d^2 y}{dx^2} = ry$, which has solutions of the form: $y = A\cos kx + B\sin kx$

Operators

The most commonly used operator is the Hamiltonian, which is used to obtain the energy of the system by evaluating the integral in Equation (1-11):

$$E = \frac{\int \Psi^* H \Psi d\tau}{\int \Psi^* \Psi d\tau} \quad \text{Equation (1-11)}$$

Equation (1-11) is obtained by multiplying Equation (1-10) by Ψ^* (the complex conjugate of the wave function) and then integrating both sides over all space (i.e. from $+\infty$ to $-\infty$), giving $\int \Psi^* H \Psi d\tau = \int \Psi^* E \Psi d\tau$. As E is a scalar it can be taken out side the integral leading to Equation

(1-11). The Hamiltonian operator is made up of two parts; the kinetic energy operator $-\frac{\hbar^2 \nabla^2}{2m}$, and the potential energy operator $V = \frac{Ze^2}{4\pi\epsilon_0 r}$ for an electron and a nucleus with Z protons.

Exact solutions

The Schrödinger equation can only be solved exactly for a few systems. For example, the particle in a box or on a ring, the harmonic oscillator, the particle on a sphere and the hydrogen atom. In addition, certain boundary conditions may be necessary for exact solutions to the Schrödinger equation e.g. the box must have infinitely high walls in the particle in the box case, which is equivalent to the wavefunction being zero at the boundaries.

The square of the electronic wavefunction gives the probability of finding an electron at a point in space. The probability of finding the electron over all space is 1 and hence $\int \Psi^* \Psi d\tau = 1$. Wavefunctions that satisfy this condition are said to be normalised. Solutions of the Schrödinger equation are usually required to be orthogonal, which means that the product of any pair of orbitals integrated over all space, is zero, unless the two orbitals are the same. This condition can be expressed as: $\int \Psi_m^* \Psi_n d\tau = 0$ ($m \neq n$). Orthogonality and normalisation can be defined in one neat expression as: $\int \Psi_m^* \Psi_n d\tau = \delta_{nm}$ using the Kronecker delta; $\delta_{nm} = 1$ if $m = n$ and 0 if $m \neq n$. Wave functions that are both orthogonal and normalised are said to be orthonormal. Solutions of Schrödinger equation are either real or occur in degenerate complex conjugate pairs, that can be combined to give real energetically equivalent solutions. For example solutions of the 2p orbitals comprise of one real and two complex functions and linear combinations of solutions are used to obtain real 2p solutions.

One electron atoms

The potential energy of a system consisting of an electron orbiting a nucleus, depends on the distance between the electron and the nucleus; as given by the Coulomb equation. The Hamiltonian then takes the form of Equation (1-12) as expressed in atomic units[†].

[†] Atomic units avoid the use of large constant in the equation by replacing constants such as the mass of an electron by m_e or nuclear charge by Z.

$$H = -\frac{\hbar}{2m} \nabla^2 - \frac{Ze^2}{4\pi\epsilon_0 r} = -\frac{1}{2} \nabla^2 - \frac{Z}{r}$$

Equation (1-12)

Here, Z is the nuclear charge and r is the distance of the electron from the nucleus. The Hydrogen atom is a one electron atom where $Z = 1$. The He^+ cation is also a one electron atom, but with nuclear charge $Z = 2$.

Polyelectronic systems.

The wave function for many atom systems may adopt more than one functional form and is complicated by electron spin¹³³, characterised by the quantum number s ($s = \frac{1}{2}$). Electron spin is incorporated into the wavefunction by writing it as a product of spin and spatial parts. The spin orbitals are denoted by χ and the spatial orbitals by ϕ for atomic orbitals, and Ψ for molecular orbitals. The spatial orbitals describe the distribution or density of the electrons in space, while the spin orbitals define electron spin and are labelled α or β (which can be thought visualised as spin up and spin down states respectively). The spin functions have a value of 1 or 0 depending on the value of the magnetic quantum number m_s , i.e. $\alpha(\frac{1}{2}) = 1$, $\alpha(-\frac{1}{2}) = 0$, $\beta(\frac{1}{2}) = 0$ and $\beta(-\frac{1}{2}) = 1$.

Each spatial orbital can have two electrons with paired spins. The electronic structure of a system is dictated by the Aufbau principle whereby two electrons are assigned per orbital. When there are degenerate states, Hund's rule states that electrons occupy these states with a maximum number of unpaired electrons. As electrons are indistinguishable, it follows that if any pair of electrons are exchanged, the electron density of the system remains the same. The electron density is given by the square of the wave function and from the above statement, the wavefunction must either remain unchanged or change sign. The latter condition, being required for electrons, is called the antisymmetry principle.

The Born-Oppenheimer approximation.

As the mass of the nuclei is far greater than the mass of an electron, the nuclei can be regarded as being stationary and the Born Oppenheimer approximation treats the nuclei as being fixed in space. The total wavefunction can then be split into nuclear and electronic parts. e.g.

$$\Psi_{\text{Total}}(\text{nuclei, electrons}) = \Psi(\text{nuclei})\Psi(\text{electrons})$$

The total energy, is then equal to the sum of nuclear energy (the repulsion between the nuclei) and the electronic energy (comprising of the kinetic and potential energy of the electrons moving in

the electrostatic field of the nuclei and the electron-electron interaction), i.e. $E_{\text{total}} = E(\text{nuclei}) + E(\text{electrons})$.

The helium atom

The helium atom system is approached by finding a simpler related problem, and considering the differences between this and the more complicated problem. This approach is called perturbation theory.

A simplified model of the helium atom is a pseudo atom with no electron-electron interaction, which can be solved using the separation of variables method. This method can be applied whenever the Hamiltonian can be divided into parts dependent solely on subsets of the coordinates. The equation to be solved (Equation (1-13)) is given in atomic units and can be written in the abbreviated form of Equation (1-14):

$$\left\{ -\frac{1}{2}\nabla_1^2 - \frac{Z}{r_1} - \frac{1}{2}\nabla_2^2 - \frac{Z}{r_2} \right\} \Psi(r_1, r_2) = E\Psi(r_1, r_2) \quad \text{Equation (1-13)}$$

$$\{H_1 + H_2\} \Psi(r_1, r_2) = E\Psi(r_1, r_2) \quad \text{Equation (1-14)}$$

where H_1 and H_2 are the individual Hamiltonians for electrons 1 and 2.

If we assume that the wavefunction can be written as a product of individual one electron wavefunctions, $\phi_1(r_1)$ and $\phi_2(r_2)$ with $\Psi(r_1, r_2) = \phi_1(r_1)\phi_2(r_2)$, then equation Equation (1-14) becomes:

$$[H_1 + H_2] \phi_1(r_1)\phi_2(r_2) = E\phi_1(r_1)\phi_2(r_2) \quad \text{Equation (1-15)}$$

Premultiplying by $\phi_1(r_1)\phi_2(r_2)$ and integrating over all space then gives:

$$\int d\tau_1 \phi_1(r_1) H_1 \phi_1(r_1) \int d\tau_2 \phi_2(r_2) \phi_2(r_2) + \int d\tau_1 \phi_1(r_1) \phi_1(r_1) \int d\tau_2 \phi_2(r_2) H_2 \phi_2(r_2) \\ = E \int d\tau_1 \phi_1(r_1) \phi_1(r_1) \int d\tau_2 \phi_2(r_2) \phi_2(r_2) \quad \text{Equation (1-16)}$$

The separation of variables method can then be used to give a hydrogen atom solution for each electron, but with nuclear charge, $Z = 2$.

This wavefunction satisfies the indistinguishability criterion $-1s(1)1s(2) = 1s(2)1s(1)$ but must also obey the antisymmetry principle. Therefore the spin and space functions must be combined to give an overall wavefunction which is antisymmetric; a symmetric space function therefore must be combined with an antisymmetric spin function or vice versa, giving wavefunctions of the form of Equation (1-17)

$$(1/\sqrt{2})[1s(1)2s(2) + 1s(2)2s(1)][\alpha(1)\beta(2) - \alpha(2)\beta(1)]$$

Equation (1-17)

Polyelectronic systems and Slater determinants.

$\Psi(1,2,3,\dots,N) = \chi_1(1) \chi_2(2) \chi_3(3)\dots \chi_N(N)$ is not an appropriate form for the wavefunction of a many electron atom as the product of the spin orbitals is unacceptable because of the antisymmetry principle - exchanging pairs of electrons does not give the negative of the wavefunction. The energy of this expression, known as the Hartree product is equal to the sum of the energy of the one electron spin orbitals.

An acceptable form for the wavefunction is like that in equation (14) for a 2 electron atom.

e.g. $1s(1)1s(2)\alpha(1)\beta(2) - 1s(1)1s(2)\alpha(2)\beta(1)$

This can be written as a 2 x 2 determinant:

$$\begin{vmatrix} 1s(1)\alpha(1) & 1s(1)\beta(1) \\ 1s(2)\alpha(2) & 1s(2)\beta(2) \end{vmatrix}$$

The spin and space functions, for each electron can be written as a combined function called a spin orbital denoted by $\chi_1(1) = 1s(1)\alpha(1)$ and $\chi_2(1) = 1s(1)\beta(1)$ for the electron labelled 1, and $\chi_1(2) = 1s(2)\alpha(2)$ and $\chi_2(2) = 1s(2)\beta(2)$ for the electron labelled 2 etc.

Similarly the wavefunction for polyelectronic system of N electrons, can be represented concisely as a Slater determinant (Equation (1-18)).

$$\Psi = \frac{1}{\sqrt{N!}} \begin{vmatrix} \chi_1(1) & \chi_2(1) & \dots & \chi_N(1) \\ \chi_1(2) & \chi_2(2) & \dots & \chi_N(2) \\ \vdots & \vdots & & \vdots \\ \vdots & \vdots & & \vdots \\ \chi_1(N) & \chi_2(N) & \dots & \chi_N(N) \end{vmatrix}$$

Equation (1-18)

Exchange of 2 electrons corresponds to the exchange of 2 rows in the determinant and results in a change of sign of the determinant, thus obeying the antisymmetry principle. Also, if any 2 rows of the determinant are equal - equivalent to 2 electrons occupying the same spin orbital, then the determinant vanishes. The normalisation constant $1/\sqrt{N!}$ is needed as expansion of the determinant gives N! terms because of the N! different permutations of N electrons.

Molecular Orbital (MO) calculations

In the most popular type of quantum mechanical calculations, each molecular spin orbital is expressed as a linear combination of atomic orbitals (LCAO)

$$\text{e.g. } \Psi_i = \sum_{\mu=1}^k c_{\mu} \phi_{\mu}$$

Each molecular (spatial) orbital Ψ_i can be written as the sum of k atomic orbitals ϕ_{μ} multiplied by various constants c_{μ} .

Hydrogen gas H_2 is considered as an example of the LCAO method. The Hamiltonian for H_2 is made up of the kinetic energy operator for each electron plus the potential energy operator arising from the Coulomb attraction between the electrons and the nuclei, plus an inter-electronic repulsion term. i.e.

$$H = -\frac{1}{2}\nabla_1^2 - \frac{1}{2}\nabla_2^2 - \frac{Z_A}{r_{1A}} - \frac{Z_B}{r_{1B}} - \frac{Z_A}{r_{2A}} - \frac{Z_B}{r_{2B}} + \frac{1}{r_{12}} \quad \text{Equation (1-19)}$$

The energy of the H_2 molecule is found using Equation (1-20)

$$E = \frac{\int \Psi H \Psi d\tau}{\int \Psi \Psi d\tau} \quad \text{Equation (1-20)}$$

with $\Psi = \chi_1(1)\chi_2(2) - \chi_1(2)\chi_2(1)$ where:

$$\chi_1(1) = 1\sigma_g(1)\alpha(1)$$

$$\chi_2(1) = 1\sigma_g(1)\beta(1)$$

$$\chi_1(2) = 1\sigma_g(2)\alpha(2)$$

$$\chi_2(2) = 1\sigma_g(2)\beta(2)$$

and the spatial orbital $1\sigma_g = A(1s_A + 1s_B)$ is a linear combination of two hydrogen atom $1s$ orbitals.

This gives:

$$E = \frac{1}{2} \iint d\tau_1 d\tau_2 \{ [\chi_1(1)\chi_2(2) - \chi_2(1)\chi_1(2)] \times [H_1 + H_2 + (1/r_{12})] \times [\chi_1(1)\chi_2(2) - \chi_2(1)\chi_1(2)] \}$$

Equation (1-21)

Here the Hamiltonian in Equation (1-21) has been split into two H_2^+ Hamiltonians plus the inter-electronic repulsion term. i.e. $H = H_1 + H_2 + 1/r_{12}$

Once these integrals have been expanded out and separated into spin and space parts, many of the terms can be simplified or cancelled using the Kronecker delta relation. The remaining terms from integrals containing the $1/r_{12}$ repulsion term correspond to the Coulombic repulsion between the two orbitals. Many of these terms again cancel due to the orthogonality of the α and β spin states. Note that, this is not always the case in excited states of atoms. For example in the triplet state,

both spin states are the same (both α), so these terms do not disappear and they contribute a negative term to the repulsion term thus stabilising the total energy of the triplet state. This contribution is called the exchange interaction.

The energy of a general polyatomic system

The general Hamiltonian for an N-electron system is:

$$H = \left(-\frac{1}{2} \sum_{i=1}^N \nabla_i^2 - \frac{1}{r_{1A}} - \frac{1}{r_{1B}} \dots + \frac{1}{r_{12}} + \frac{1}{r_{13}} + \dots \right) \quad \text{Equation (1-22)}$$

To find the energy for each molecular orbital χ_i it is more convenient to write the energy as a sum of the three types of interaction making up the electronic energy of the system.

$$H_{ii}^{core} = \int d\tau_1 \chi_i(1) \left(-\frac{1}{2} \nabla_i^2 - \sum_{A=1}^M \frac{Z_A}{r_{iA}} \right) \chi_i(1) \quad \text{Equation (1-23)}$$

Equation (1-23) is the kinetic and potential energy term for each electron moving in the field of the M nuclei, which for N electrons in N molecular orbitals gives the total core energy as:

$$E_{total}^{core} = \sum_{i=1}^N \int d\tau_1 \chi_i(1) \left(-\frac{1}{2} \nabla_i^2 - \sum_{A=1}^M \frac{Z_A}{r_{iA}} \right) \chi_i(1) = \sum_{i=1}^N H_{ii}^{core} \quad \text{Equation (1-24)}$$

The second term (Equation (1-25)), is due to the electrostatic repulsion between electrons, and is dependent on the inter-electronic distance. The energy of this Coulomb interaction between an electron in an orbital χ_i and the other (N-1) electrons, is a sum of the Coulombic integrals:

$$E_i^{coulomb} = \sum_{j \neq i}^N \int d\tau_1 d\tau_2 \chi_i(1) \chi_j(2) \frac{1}{r_{12}} \chi_j(2) \chi_i(1) \quad \text{Equation (1-25)}$$

$$\equiv \sum_{j \neq i}^N \int d\tau_1 d\tau_2 \chi_i(1) \chi_i(1) \frac{1}{r_{12}} \chi_j(2) \chi_j(2)$$

the total Coulomb energy being:

$$E_{total}^{coulomb} = \sum_{i=1}^N \sum_{j=i+1}^N \int d\tau_1 d\tau_2 \chi_i(1) \chi_i(1) \frac{1}{r_{12}} \chi_j(2) \chi_j(2) = \sum_{i=1}^N \sum_{j=i+1}^N J_{ij} \quad \text{Equation (1-26)}$$

Here J_{ij} represents the Coulomb integral.

The third contribution is the exchange interaction, which is only non zero if the spins of the electrons in spin orbitals χ_i and χ_j are the same. The exchange energy between the electron in spin orbital χ_i and the other (N-1) electrons is given by:

$$E_i^{exchange} = \sum_{j \neq i}^N \iint d\tau_1 d\tau_2 \chi_i(1) \chi_j(2) \left(\frac{1}{r_{12}} \right) \chi_i(2) \chi_j(1) \quad \text{Equation (1-27)}$$

with the total energy :

$$E_{total}^{exchange} = \sum_{i=1}^N \sum_{j'=i+1}^N \iint d\tau_1 d\tau_2 \chi_i(1) \chi_{j'}(2) \left(\frac{1}{r_{12}} \right) \chi_i(2) \chi_{j'}(1) = \sum_{i=1}^N \sum_{j'=i+1}^N K_{ij} \quad \text{Equation (1-28)}$$

where K_{ij} represents the exchange integral.

The three terms above constitute the electronic energy of the system. To complete the total energy for the whole system the inter-nuclear repulsion term $\sum_{A=1}^M \sum_{B=A+1}^M \frac{Z_A Z_B}{R_{AB}}$ must be added.

Hartree-Fock (H-F) equations

In electronic structure calculations, calculation of the molecular orbitals is attempted. This can be done using the *variation theorem*, which states that the energy of the approximate wave function proposed is always greater than the true wave function. This implies that the better the wavefunction, the lower the energy. The best wavefunction occurs when the energy is a minimum e.g. at $\delta E = 0$.

The H-F equations are obtained by imposing this condition on the energy expression. The molecular orbitals must remain orthonormal, this condition being written in terms of the overlap integral S_{ij} between orbitals i and j :

$$S_{ij} = \int \chi_i \chi_j d\tau = \delta_{ij} \quad (\delta_{ij} \text{ is the Kronecker delta})$$

The main difference between single and polyelectronic systems is the presence of electron-electron interactions, expressed as Coulomb and exchange integrals.

For a polyelectronic system, a solution simulating all the electronic motions must be found. To do this, a single electron in spin orbital χ_i in the field of the nuclei and the other electrons in fixed spin orbitals χ_j is considered. The Hamiltonian for the single electron contains the three terms identified above; Core, Coulomb and Exchange.

Their contribution to the energy can be written as

$$\text{Core} + \text{Coulomb} - \text{Exchange} = \text{Energy} \quad \text{Equation (1-29)}$$

$$H^{core}(1)\chi_i(1) + \sum_{j \neq i}^N J_j(1)\chi_i(1) - \sum_{j \neq i}^N K_j(1)\chi_i(1) = \sum_j \epsilon_{ij} \chi_j(1)$$

and using $[J_j(1) - K_j(1)]\chi_i(1) = 0$, equation Equation (1-29) becomes:

$$\left[H^{core}(\mathbf{1}) + \sum_{j=1}^N \{J_j(\mathbf{1}) - K_j(\mathbf{1})\} \right] \chi_i(\mathbf{1}) = \sum_{j=1}^N \epsilon_{ij} \chi_j(\mathbf{1}) \quad \text{Equation (1-30)}$$

or

$$F_i \chi_i = \sum_j \epsilon_{ij} \chi_j(\mathbf{1}) \quad \text{Equation (1-31)}$$

where F_i is called the Fock operator.

For a closed shell system with N electrons in $N/2$ orbitals, the Fock operator is:

$$F_i(\mathbf{1}) = H^{core}(\mathbf{1}) + \sum_{j=1}^{N/2} [2J_j(\mathbf{1}) - K_j(\mathbf{1})] \quad \text{Equation (1-32)}$$

Equation (1-32) is written as such to avoid counting each inter-electronic repulsion twice.¹³³

Recall that in these equations, each electron moves in field comprising of the nuclei and the other electrons. Any solution we find affects the other solutions for the other electrons in the system. This is called the self consistent field (SCF) approach. To solve this a set of trial solutions χ_i to the H-F eigenvalue equations must be obtained. These are used to calculate the Coulomb and Exchange operators. The H-F equations are solved giving a second set of solutions χ_i which are then used in a second iteration. The SCF method gradually refines individual electronic solutions corresponding to lower energies for each iteration, until a point is reached where the results for all electrons are unchanged, which is the self consistent point.

Linear combination of atomic orbitals (LCAO) in Hartree-Fock calculations

Each spin orbital is written as a LCAO of single electron orbitals:

$$\Psi_i = \sum_{v=1}^k c_{vi} \phi_v \quad \text{Equation (1-33)}$$

The single electron orbitals ϕ_v are commonly called basis functions and correspond to atomic orbitals. The minimum number of basis functions are the number required to just accommodate all the electrons in the molecule.

More sophisticated calculations use more basis functions until a H-F limit is reached, where the energy is not reduced by further addition of basis functions.

The best wavefunction and coefficients are found when $\frac{\partial E}{\partial c_{vi}} = 0$ for all the coefficients c_{vi} , giving the minimum energy.

Roothaan-Hall equations

Unlike the H-F equations, the R-H equations are written in matrix format. The H-F equation $f_i(1)\chi_i(1) = \varepsilon_i\chi_i$ may be rewritten as the matrix Equation (1-34), by substituting for the spin orbitals χ_i with the corresponding atomic orbital expansions (Equation (1-33)) followed by multiplication of an additional basis function $\phi_\mu(1)$ and subsequent integration.

$$\sum c_{vi} \int d\nu_1 \phi_\mu(1) f_i(1) \phi_\nu(1) = \varepsilon_i \sum c_{vi} \int d\nu_1 \phi_\mu(1) \phi_\nu(1) \quad \text{Equation (1-34)}$$

$$\text{or } \sum_{\mu=1}^k (F_{\mu\nu} - \varepsilon_i S_{\mu\nu}) = 0 \quad \text{Equation (1-35)}$$

The integral on the right hand side of equation Equation (1-34) is the overlap integral, $S_{\mu\nu} = \int d\nu_1 \phi_\mu(1) \phi_\nu(1)$, between two basis functions μ and ν . Unlike molecular orbitals, which are required to be orthonormal, μ and ν may not be zero if, for example, two basis functions are located on different atoms. The integral on the left-hand side of equation Equation (1-34), $F_{\mu\nu} = \int d\nu_1 \phi_\mu(1) f_i(1) \phi_\nu(1)$, gives the elements of the Fock matrix, which may be expanded by substitution of the Fock operator (Equation (1-30)) and replacement of spin orbitals by the corresponding atomic orbital expansions. This equation can be tidied up by introducing the density matrix P, $P_{\mu\nu} = 2 \sum c_{\mu i} c_{\nu i}$ and $P_{\lambda\sigma} = 2 \sum c_{\lambda i} c_{\sigma i}$ giving the standard expression for the

Fock matrix in the Roothaan-Hall equations (Equation (1-36)).

$$F_{\mu\nu} = H_{\mu\nu}^{core} + \sum_{\lambda=1}^k \sum_{\sigma=1}^k P_{\lambda\sigma} [\langle \mu\nu | \lambda\sigma \rangle - \frac{1}{2} \langle \mu\lambda | \nu\sigma \rangle] \quad \text{Equation (1-36)}$$

If k basis functions are used to represent the molecular orbitals, then a set of k simultaneous equations in terms of the unknown coefficients c_{vi} are obtained. For non trivial solutions to these equations, the determinant of equation Equation (1-35) must equal zero i.e.

$$|F_{\mu\nu} - \varepsilon_i S_{\mu\nu}| = 0$$

This is called the secular equation and its roots are the orbital energies ε_i . The Hartree-Fock - Roothaan equations are solved by an iterative process as the Fock integral or elements depend on the orbitals χ_i which in turn are dependent on the unknown coefficients c_{vi} . A guess for the molecular orbitals (from a linear combination of basis functions) is used to calculate the Fock

operator and the elements of the Fock matrix initially. The secular equation is then solved giving an initial set of orbital energies ϵ_i . These ϵ_i values are then used in equation Equation (1-35) to solve for an improved set of coefficients. These improved coefficients in turn give better molecular orbitals which are used to compute a new Fock operator and so on until there is no further improvement in the energies for the next cycle. This is the point of convergence. Convergence may be monitored by comparing the energy and basis coefficients after each iteration. Roothaan equations are best solved using matrix algebra.

Ab initio calculations

Ab initio means “from first principles” and implies the input of physical constants only e.g. Plank’s constant h , the speed of light c , mass of electron m_e etc. In fact, Ab initio calculations refer to calculations using the full Hartree-Fock Roothaan-Hall equations, not ignoring or approximating any integrals of the Hamiltonian. They do not rely on any calibration methods.

The difference between ab initio and semi empirical calculations is the simplification of the semi-empirical calculations by using parameters in place of some integrals, and ignoring some terms in the Hamiltonian.

Basis sets

Basis sets are commonly composed of atomic functions often approximated by Slater type orbitals (STO). However, STOs are complex expressions which are difficult to evaluate and are therefore replaced with Gaussian functions of the form $f = e^{-\alpha r^2}$, multiplied by powers of x , y and z to give a basis function $f = x^a y^b z^c e^{-\alpha r^2}$ to be used in ab-initio calculations. In this function, the term α determines the radial spread of the Gaussian function. Replacing the STO by one Gaussian function however, leads to unacceptable errors such as the underestimation of long range overlap and charge and spin density at the nucleus when using Gaussian functions. An advantage of using Gaussian-type functions is that the product of 2 Gaussians can be expressed as a single Gaussian. Much better approximations can be obtained by using linear combinations of Gaussians.

Pople notation for basis sets

Pople and his co-workers developed a shorthand notation to describe the basis sets used in ab-initio calculations. A minimal basis set contains just enough functions required to accommodate all

the filled orbitals in each atom. Thus a minimal basis set normally includes all the atomic orbitals in the shell. For hydrogen and helium, a single 1s type function is required, and for the lithium to neon elements 1s, 2s and 2p functions are needed. The STO-3G, STO-4G...STO-nG are all minimal basis sets with n Gaussian functions used to represent the Slater type orbital. In practice, it is found there is little difference between results using the STO-3G and larger minimal basis sets, though some do perform better for certain calculations. Increasing the size of the basis set increases the computational effort.

Minimal basis sets have several drawbacks. These include problems with atoms at the end of a series e.g. oxygen or fluorine. Such atoms are described by the same number of basis functions as those earlier in the series, even though they have more electrons. A minimal basis set cannot describe non spherical electron distribution either, and is thus insufficient for the 2p orbitals.

These problems can be overcome by using more than one function for each orbital. For example, doubling the number of functions in the minimal basis set – called a double zeta basis. Using a linear combination of a ‘contracted’ function and a ‘diffuse’ function gives an intermediate effect. The SCF procedure then determines whether a more contracted or diffuse function is required. Alternatively, the number of functions for the valence electrons can be doubled whilst keeping a single function for the inner electrons; as the core electrons don’t affect the chemical properties very much. The notation for one such split valence double zeta basis sets is 3-21G i.e. the core electrons are represented by 3 Gaussians as are the valence electrons of which the contracted part is represented by 2 and the diffuse part by 1 Gaussian function. Other common split valence basis sets are 4-31G and 6-31G.

Polarisation functions

Electron distribution of an atom in a molecule is distorted when compared with the isolated atom e.g. the electrons of a hydrogen atom in a hydrogen molecule are attracted towards the other nuclei. This distortion can be considered as mixing p-type character into the 1s orbital creating a sort of sp hybrid. Also, unoccupied d-orbitals introduce asymmetry into p-orbitals. The solution to both these problems is to introduce polarisation functions which have a higher angular quantum number corresponding to p-orbitals for hydrogen and d orbitals for 1st and 2nd row elements. These polarisation functions are denoted by a * as in 6-31G* which refers to the 6-31G basis set with polarisation functions on the heavy atoms, and 6-31G**, which indicates additional polarisation functions on hydrogen and helium atoms also. Partial polarisation basis sets can also

be used e.g. 3-21G^(*) has the same basis set as 3-21G, but is supplemented by 6 d-type Gaussians for 2nd row atoms. A deficiency of the basis sets mentioned is their inability in dealing with species which have large degrees of electron density away from the nuclear centres, as found in anions and lone pairs, for example. This arises due to the low amplitude of the Gaussian basis functions far from the nuclei. To compensate for this, highly diffuse functions can be added to the basis set, and are denoted by a + e.g. 3-21+G has an additional set of diffuse s and p-type Gaussian functions.

Open Shell systems

The Roothaan-Hall equations are not applicable to open-shell systems, which contain one or more unpaired electrons e.g. radicals or some ground states like O₂.

For these type of systems we can use spin restricted Hartree-Fock (RHF) theory, which uses combinations of singly and doubly occupied orbitals. Or we can use Unrestricted Hartree-Fock (UHF) theory, which uses one set of orbitals for α spin and one set for β spin. These approaches are illustrated in Figure 1.26

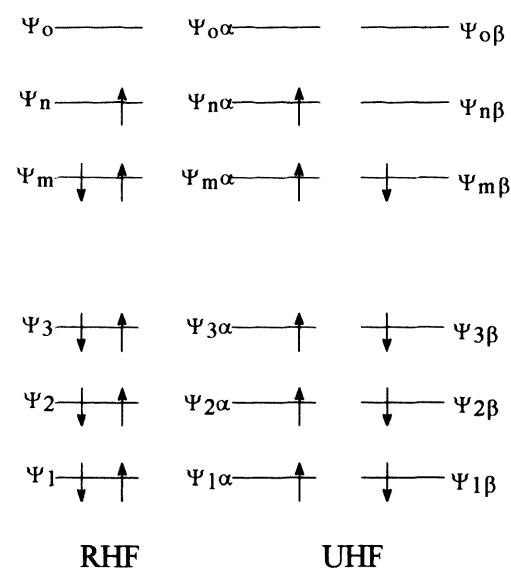


Figure 1.26 Representation of the treatment of unpaired electrons in RHF and UHF theory.

Electron Correlation.

In SCF methods, electrons are assumed to move in an average potential field of the other electrons, so the instantaneous position of one electron is not affected by its neighbouring electrons. Actual motion is correlated; electrons tend to avoid each other in their motions.

Hartree-Fock theory fails to represent electron correlation adequately but the error in the H-F calculated energy can be reduced by accounting for the electronic repulsion interaction. This correlation energy is equal to the difference between the exact energy and the H-F energy. Ignoring electron correlation can sometimes lead to anomalous results, especially at dissociation limits.

Configuration interaction

There are several possible ways to incorporate electron correlation effects into ab-initio calculations. One way of introducing electron correlation into the wave function is to include the inter-electronic distances r_{ij} , but this is only practical for systems with a few electrons. An alternative approach is configuration interaction (CI).

CI involves mixing in contributions from excited state configurations with that of the ground state to produce an improved wave function. For example, the wave function of lithium, which has a $1s^2 2s^1$ configuration in the ground state and $1s^2 3s^1$ on excitation, would be produced from a combination of these states. A better description of the wave function is a linear combination of ground and excited state wave functions. The atomic or molecular orbitals are first written as linear combination of basis functions. For example, if a H-F calculation is performed with k basis functions then $2k$ spin orbitals are obtained. If the $2k$ spin orbitals are then filled with N electrons, where $N < 2k$, this will give $2k - N$ unoccupied virtual orbitals. Excited states are generated by replacing one or more of the occupied spin orbitals with a virtual spin orbital. The C.I. wavefunction is represented as:

$$\Psi = c_0 \psi_0 + c_1 \psi_1 + c_2 \psi_2 + \dots$$

where ψ_0 is the single determinant obtained by solving the H-F equations and ψ_1, ψ_2 etc. are wavefunctions that represent configurations derived by replacing one or more of the occupied spin orbitals by a virtual spin orbital. The variational method is then used to minimise the energy for the system and determine the coefficients c_0, c_1 etc. A huge number of configurations are needed for an accurate wave function and thus for systems of more than a few electrons CI calculations are difficult. To scale down the size of the calculation, only the configurations with the same symmetry properties as the state being calculated are used. The number of excited states considered in the calculation can be limited by using only wavefunctions that differ from the H-F wavefunction by a single spin orbital – called configuration interaction singles (CIS) – or by

double substitutions (CID), or both singles and doubles (CISD). The number of configurations can be reduced further by using only excitations involving the valence shell electrons. Including all the configuration functions is called full CI. However, if full CI is not used, this can lead to substantial errors. The more excited state configurations involved, the bigger the calculation.

In a MCSCF – multi configuration SCF approach the basis functions as well as the coefficients of the determinants are allowed to vary unlike in H-F theory, where only the determinant coefficients vary. Thus MCSCF theory is much more complicated than the R-H equations.

Practical Calculations

Ab initio calculations can take a long time to complete. To save time, there are some ‘shortcuts’ which can be used. Lower levels of theory, such as semi empirical theory, can be used to provide the initial estimate for the density matrix used in the first SCF iteration, or for a geometry optimisation, before using a high level to consider the electron correlation.

In an SCF calculation the wavefunction is gradually refined until self consistency is achieved. In some cases, the energy may oscillate from one iteration to the next. To correct this, an average set of orbital coefficients can be used to weed out coefficients giving higher energies.

Approximate MO methods.

Ab initio calculations are slow and require much computational power. Approximate quantum mechanical or semi-empirical methods have been developed to treat medium and large molecules and can be much quicker computationally. Indeed Huckel theory was developed in the 1930s, before computers. Some approximate methods can be better for calculating certain properties than the highest level ab initio calculations. Earlier theories such as the Huckel and Pariser-Parr-Pople (PPP),^{134,135} take in to account only π electron orbitals.

Semi empirical methods are again based on the R-H equations Equation (1-37) to Equation (1-40):

$$FC = SCE$$

$$\text{Equation (1-37)}$$

$$F_{\mu\nu} = H_{\mu\nu}^{core} + \sum_{\lambda=1}^K \sum_{\sigma=1}^K P_{\lambda\sigma} [\langle \mu\nu | \lambda\sigma \rangle - \frac{1}{2} \langle \mu\lambda | \nu\sigma \rangle] \quad \text{Equation (1-38)}^\dagger$$

$$P_{\lambda\sigma} = 2 \sum_{i=1}^{N/2} c_{\lambda i} c_{\sigma i} \quad \text{Equation (1-39)}$$

$$H_{\mu\nu} = \int dv_1 \phi_\mu(1) \left[-\frac{1}{2} \nabla^2 - \sum_{A=1}^M \frac{Z_A}{|r_1 - R_A|} \right] \phi_\nu \quad \text{Equation (1-40)}$$

The elements for the Fock matrix for ab initio calculations are calculated using Equation (1-38). For semi empirical methods, it is useful to consider the Fock matrix in three groups; $F_{\mu\mu}$ (the diagonal elements), $F_{\mu\nu}$ (where ϕ_μ and ϕ_ν are on the same atom) and $F_{\mu\nu}$ (where ϕ_μ and ϕ_ν are on different atoms). Semi empirical methods neglect or approximate some of these integrals, considering only the valence electrons explicitly and treat the core electrons as part of the nuclear core. The justification for separate treatment of σ and π electrons was the different symmetry and the greater polarisability of π electrons, which makes them more susceptible to perturbations such as in a chemical reaction. Semi empirical calculations use basis sets comprising of Slater type s,p and sometimes d-orbitals. The orthogonality of such orbitals enables further simplifications to be made to the equations. Commonly the overlap matrix S is set equal to the identity matrix I, thus giving all diagonal elements equal to one and all off diagonals are zero. Some would naturally be zero due to the orthogonality of basis sets on each atom. But in addition, elements corresponding to overlap between two atomic orbitals on different atoms are also set to zero. The Roothaan-Hall equations can thus be simplified so that the matrix equation $FC = SCE$ becomes $FC = CE$. It must be noted that setting $S = I$ does not mean that all overlap integrals in the calculation of the Fock matrix are set to zero. Indeed it is important to include some overlap integrals even in simple semi empirical models.

Zero differential overlap (ZDO)

Many semi empirical theories are based on the ZDO approximation, where overlap between pairs of different orbitals is set to zero for all volume elements dv ; $\int \phi_\mu \phi_\nu dv = 0$, leading to $S_{\mu\nu} = \delta_{\mu\nu}$ for

[†] The $[\mu\mu|\nu\nu]$ is shorthand for the electron repulsion integral $[\phi_\mu\phi_\nu(1/r_{12})\phi_\lambda\phi_\sigma] = \int \phi_\mu\phi_\nu(1/r_{12})\phi_\lambda\phi_\sigma dv_1 dv_2$

the overlap integrals. If ϕ_μ and ϕ_ν are atomic orbitals located on different atoms then differential overlap is referred to as diatomic differential overlap but if ϕ_μ and ϕ_ν are on the same atom then it is called monatomic differential overlap. If ZDO is applied to two electron repulsion integrals $\langle \mu\nu | \lambda\sigma \rangle$ then the integral is zero if $\mu \neq \nu$ and/or $\lambda \neq \sigma$ written in terms of the Kronecker delta as: $\langle \mu\nu | \lambda\sigma \rangle = \langle \mu\mu | \lambda\lambda \rangle \delta_{\mu\nu} \delta_{\lambda\sigma}$ and therefore all three and four centre integrals are set to zero. If ZDO is applied to all orbital pairs, the R-H Equation (1-38) for a closed shell molecule with $\mu = \nu$ becomes:

$$F_{\mu\mu} = H_{\mu\mu}^{core} + \sum_{\lambda=1}^K [P_{\lambda\lambda} \langle \mu\mu | \lambda\lambda \rangle - \frac{1}{2} P \langle \mu\mu | \mu\mu \rangle] \quad \text{for } \mu = \nu \quad \text{Equation (1-41)}$$

Summation over all λ includes $\lambda = \mu$ and terms in $\langle \mu\mu | \mu\mu \rangle$ can be separated to give:

$$F_{\mu\mu} = H_{\mu\mu}^{core} + \frac{1}{2} P_{\mu\mu} \langle \mu\mu | \mu\mu \rangle + \sum_{\lambda=1; \lambda \neq \mu}^K P_{\mu\mu} \langle \mu\mu | \lambda\lambda \rangle \quad \text{Equation (1-42)}$$

For $\nu \neq \mu$ equation Equation (1-38) reduces to:

$$F_{\mu\nu} = H_{\mu\nu}^{core} - \frac{1}{2} P_{\mu\nu} \langle \mu\mu | \nu\nu \rangle \quad \text{Equation (1-43)}$$

Huckel Theory

This method is limited to conjugated π -systems and was devised to explain the aromatic nature of compounds such as benzene. It separates the π electrons and constructs molecular orbitals into which these electrons are put according to the Aufbau principle. The π electrons are considered in a field of the fixed nuclei and core electrons. Molecular orbitals are constructed from the LCAO method. Huckel theory ignores overlap integrals, using the approximation in Equation (1-44), where $\delta_{\mu\nu}$ is the Kronecker delta. If $\delta_{\mu\nu} = 0$, for $\mu \neq \nu$, then this amounts to the Zero Differential Overlap (ZDO) approximation discussed above.

$$S_{\mu\nu} = \int \phi_\mu(1) \phi_\nu(1) d\nu = \delta_{\mu\nu} \quad \text{Equation (1-44)}$$

Huckel theory is a ZDO method and can be considered in terms of a CNDO approximation. In a neutral species the net charge is approximately zero, and if penetration effects are eliminated, the Fock matrix elements are:

$$F_{\mu\mu} = U_{\mu\mu} + (P_{AA} - \frac{1}{2} P_{\mu\mu}) \gamma_{AA} \quad \text{Equation (1-45)}$$

If each nucleus in the π -system is the same then this expression is approximately constant for all the nuclei being considered. The $F_{\mu\mu}$ matrix elements are assigned the symbol α called the

Coulomb integral. All off diagonal elements are assumed to be zero except $F_{\mu\nu}$, where μ and ν are π orbitals on two bonded atoms- assigned the symbol β and known as resonance integrals.

The Huckel Fock matrix has $n \times n$ elements where n is the number of atoms. All diagonal elements are α and all off diagonals are 0 unless atoms i and j are bonded, in which case the element is β .

The Fock matrix for benzene is given in Equation (1-46).

$$\begin{pmatrix} \alpha & \beta & 0 & 0 & 0 & \beta \\ \beta & \alpha & \beta & 0 & 0 & 0 \\ 0 & \beta & \alpha & \beta & 0 & 0 \\ 0 & 0 & \beta & \alpha & \beta & 0 \\ 0 & 0 & 0 & \beta & \alpha & \beta \\ \beta & 0 & 0 & 0 & \beta & \alpha \end{pmatrix} \quad \text{Equation (1-46)}$$

If the overlap matrix = the identity matrix, the matrix equation $FC = CE$ can then be solved to give the basis set coefficients and molecular orbital energies E .

Orbital energies for benzene are $E_1 = \alpha + 2\beta$; $E_2, E_3 = \alpha + \beta$; $E_4, E_5 = \alpha - \beta$; $E_6 = \alpha - 2\beta$, so the ground state has two electrons in Ψ_1 and two each in the degenerate Ψ_2 and Ψ_3 respectively.

Unlike Huckel theory, the PPP method includes electron repulsion effects. Huckel theory can be used to predict the longest wavelength bands for aromatic hydrocarbons for example and PPP can predict π electron transitions. These methods are not used to determine equilibrium geometries.

As in Huckel theory the PPP method neglects orbital overlap and makes the approximation of zero differential overlap ZDO:

CNDO Complete Neglect of Differential Overlap

The Huckel and PPP methods apply only to planar molecules. For non-planar molecules the simplifying approximation of treating the σ and π electrons separately is not available, and all the valence electrons must be considered together.¹³³

In the CNDO method the two electron integrals $\langle \mu\mu | \lambda\lambda \rangle$, where μ and λ are on different atoms A and B, are set equal to the parameter γ_{AB} , dependent only on the nature of A and B and the inter-nuclear distance and not on the type of orbital. γ_{AB} can be considered to be the average electrostatic repulsion between an electron on atom A and an electron on atom B. When both atomic orbitals are on the same atom, γ_{AA} represents the average electron-electron repulsion between two electrons on atom A. The elements of the CNDO Fock matrix can be split into the

diagonal elements $F_{\mu\mu}$, $F_{\nu\nu}$ for basis functions μ and ν on different atoms, and $F_{\mu\nu}$ with μ and ν on the same atom. Substituting the two electron integrals $\langle \mu\mu | \lambda\lambda \rangle$ for γ_{AB} and γ_{AA} for the cases outlined above, gives the following equations for the Fock matrix:

$$F_{\mu\mu} = H_{\mu\mu}^{core} + \sum_{\lambda=1; \lambda \text{ on } A}^k P_{\lambda\lambda} \gamma_{AA} - \frac{1}{2} P_{\mu\mu} \gamma_{AA} + \sum_{\lambda=1; \text{not on } A}^k P_{\lambda\lambda} \gamma_{AB} \quad \text{Equation (1-47)}$$

$$F_{\mu\nu} = H_{\mu\nu}^{core} - \frac{1}{2} P_{\mu\nu} \gamma_{AA} ; \mu \text{ and } \nu \text{ both on atom A} \quad \text{Equation (1-48)}$$

$$F_{\mu\nu} = H_{\mu\nu}^{core} - \frac{1}{2} P_{\mu\nu} \gamma_{AA} ; \mu \text{ and } \nu \text{ on different atoms A and B.} \quad \text{Equation (1-49)}$$

In the CNDO method, the core components of the above Fock equations are considered for the following 3 cases:

1. $H_{\mu\mu}^{core}$ involving integrals with the atom on which ϕ_μ is situated (atom A) and all the other atoms (labelled B). Here, $H_{\mu\mu}^{core}$ is given by Equation (1-50).

$$H_{\mu\mu}^{core} = U_{\mu\mu} - \sum_{A \neq B} V_{AB} \quad \text{Equation (1-50)}$$

where $U_{\mu\mu}$ is the energy of the orbital ϕ_μ in the field of its own nucleus(A) and V_{AB} is the energy of the electron in the field of the other nuclei(B).

2. In the case where orbitals ϕ_μ and ϕ_ν are both on the same atom (A), due to the orthogonality of atomic orbitals and using the ZDO approximation, $H_{\mu\mu}^{core} = 0$ in CNDO.

3. When ϕ_μ and ϕ_ν are on different atoms A and B then:

$$H_{\mu\nu}^{core} = \beta_{AB}^0 S_{\mu\nu} \quad \text{Equation (1-51)}$$

where, β_{AB}^0 is the resonance integral (written $\beta_{\mu\nu}$) and is the main cause of bonding and therefore not subject to the ZDO approximation. In CNDO the resonance integral is made proportional to the overlap integral e.g. $H_{\mu\nu}^{core} = \beta_{AB}^0 S_{\mu\nu}$ where β_{AB}^0 is a parameter depending on A and B. The CNDO elements for the Fock matrix then become:

$$F_{\mu\mu} = U_{\mu\mu} + \sum_{A \neq B} v_{AB} + (P_{AA} - \frac{1}{2} P_{\mu\mu}) \gamma_{AA} + \sum_{A \neq B} P_{BB} \gamma_{AB} \quad \text{Equation (1-52)}$$

$$F_{\mu\nu} = -\frac{1}{2} P_{\mu\nu} \gamma_{AB} \quad \mu \text{ and } \nu \text{ on the same atom} \quad \text{Equation (1-53)}$$

$$F_{\mu\nu} = \beta_{AB}^0 - \frac{1}{2} P_{\mu\nu} \gamma_{AB} \quad \mu \text{ on atom A and } \nu \text{ on atom B} \quad \text{Equation (1-54)}$$

To perform CNDO calculations the integrals required are; $S_{\mu\nu}$ the overlap integral, $H_{\mu\mu}^{core}$ the core integral, the electron-core interactions V_{AB} , γ_{AB} and γ_{AA} the electron repulsion integrals and β_{AB}^0 the bonding parameter. The CNDO basis set uses STOs for the valence shell. The electron repulsion integral γ_{AB} is given in equation Equation (1-55):

$$\gamma_{AB} = \iint d\nu_1 d\nu_2 \phi_{S,A}(1) \phi_{S,A}(1) \left(\frac{1}{r_{12}} \right) \phi_{S,B}(2) \phi_{S,B}(2) \quad \text{Equation (1-55)}$$

The Core Hamiltonians $U_{\mu\mu}$ are not calculated, but are obtained from experimental data from ionisation energies. The electron-core interaction (equation) is the interaction between valence s orbital on A with the nuclear core of B.

$$V_{AB} = \int d\nu_1 \phi_{S,A}(1) \left(\frac{Z_B}{r_1 - R_B} \right) \phi_{S,A}(1) \quad \text{Equation (1-56)}$$

The resonance integral β_{AB}^0 is written in terms of empirical single atom values, as in Equation (1-57), with β^0 values chosen to fit the results of a minimal basis set ab initio calculation on diatomic molecules.

$$\beta_{AB}^0 = \frac{1}{2}(\beta_{AB}^0 + \beta_{AB}^0) \quad \text{Equation (1-57)}$$

Limitations to CNDO

For the CNDO method, two neutral atoms have an incorrect significant attraction even when separated by several Angströms. Also, the predicted equilibrium distances for diatomics are too short and dissociation energies too large, due to electrons on one atom penetrating the volume shell of another, implying nuclear attraction. An improved version of the method ,CNDO/2 eliminated the penetration integral and defined the core Hamiltonian $U_{\mu\mu}$ differently, using ionisation energies and electron affinities.

Other Semi Empirical methods

Huckel theory is a basic approximation of the CNDO method. Improvements to the CNDO method are the INDO and NDDO methods. The CNDO, INDO and NDDO methods developed further by Pople and Dewar into the popular MINDO/3, MNDO and AM1 methods. A brief description of these methods, with comments on some of their limitations is given below.

INDO

CNDO ignores electrons relative spin interaction, which can be severe for electrons on the same atom. The intermediate neglect of differential overlap (INDO) includes monatomic differential overlap for one centre integrals i.e. integrals involving basis functions on the same atom. This enables interaction between two electrons on the same atom with parallel spins to have lower energy than two electrons with paired spins. Some one centre two electron integrals in INDO are obtained by fitting to atomic spectra data. INDO requires little additional computational effort and includes different multiplicities i.e. singlets and triplets.

NDDO

Neglect of diatomic differential overlap, neglects only differential overlap between atomic orbitals on different atoms. This means that all two-electron, two centre integrals $\langle \mu\nu | \lambda\sigma \rangle$ with μ and ν and also λ and σ on the same atom are included. The number of two electron two centre integrals is increased by approximately 100 times for every pair of heavy atoms in the system and thus NDDO requires greater computational effort.

MINDO/3

The problem with CNDO,INDO and NDDO is the fact that they are parameterised on low levels of ab initio theory – which itself has poor correlation with experiment and is limited to small classes of molecules and requires good input geometries as the optimisation algorithms are not very sophisticated. Modified INDO is parameterised using experimental data and also incorporates a geometry routine so crude input geometries can be accepted and minimum energy structures derived.

MNDO Modified neglect of diatomic overlap

Problems with MINDO/3 included errors in heats of formation of unsaturated molecules, bond angles which were too large and the inability to deal with molecules with lone pairs due to the limitations of the INDO approximation. The MNDO method, which is based on NDDO, was then introduced. It uses different core-core repulsion terms to MINDO/3 and OH and NH bonds are treated separately. MNDO can be applied to a much wider range of elements. However, the sp basis set is not applicable to transition elements, which require d-orbitals, and sulphur and

phosphorous are also not well modelled. More recent MNDO includes d orbitals for heavy elements. Another serious limitation is the inability of MNDO to accurately model intermolecular hydrogen bonding. For example, the heat of formation for the water dimer predicted by MNDO, is far too low, because of the tendency to overestimate the repulsion between atoms separated by distances approximately equal to the sum of their Van der Waals radii. Conjugated systems can also present problems, as in the case of nitrobenzene, where the nitro group is predicted to be orthogonal to the aromatic ring rather than conjugated with it. In addition, MNDO energies are too positive for sterically crowded molecules and too negative for molecules containing four membered rings.

AM1

The Austin Model 1 method was developed by Dewar and was designed to eliminate the MNDO problems of over repulsion between atoms separated by the sum of their Van Der Waals radii. This correction was achieved by modifying the core-core term using Gaussian functions. Both attractive and repulsive Gaussians were used and centred in the region where repulsions were too large. AM1 is significantly better than MNDO.

PM3 Parametric method 3

This method is also based on MNDO theory. PM3 uses essentially the same elements as AM1 by is parameterised by a different method. Problems specific to PM3 are an underestimation of the rotational barrier of the amide bond. There is still some debate over the relative merits of AM1 and PM3.

SAM1

The most recent development is Semi ab initio Model 1 (Dewar 1993). This uses a standard STO-3G Gaussians basis set to evaluate the electronic repulsion integrals. AM1 overestimates steric effects because of the way it calculates its electronic repulsion integrals.

MNDO, PM3 and AM1 are included in the programs MOPAC and AMPAC. Other programs like Zerner's ZINDO program have been used for transition metal and lanthanide compounds as well as for predicting electronic spectra.



Calculating molecular properties with quantum mechanics

Quantum mechanics can be used to predict thermodynamic and structural values, electronic distribution properties, the location of transition state structures and for deriving force field parameters.

Thermodynamic and structural properties

The total energy of a system is equal to the sum of its electronic energy plus the Coulombic

nuclear repulsion energy.
$$E_{Total} = E_{electronic} + \sum_{A=1}^M \sum_{B=A+1}^M \frac{Z_A Z_B}{R_{AB}}$$

A more useful comparison with experimental results is with the heat of formation ΔH_f , defined as the enthalpy change when one mole of compound is formed from its constituent elements in their standard states. ΔH_f can be calculated by subtracting, heats of atomisation of the elements and the atomic ionisation energies, from the total energy. Ab initio calculations not including any electron correlation give poor ΔH_f estimates. Including electron correlation gives much better results, but is computationally expensive. When combined with an energy minimisation algorithm, quantum mechanics can be used to calculate equilibrium geometries of molecules. The results of such geometry optimisations can be compared with X ray structures and with spectroscopic results. The agreement between theory and experiment improves with the size of the basis set. Some errors are systematic e.g. STO-3G calculations give bond lengths which are too long and 6-31G* gives bond lengths which are too short. One can then calculate the relative energy of conformers and predict the most stable geometry. Semi empirical methods can also be used to calculate these properties.

References

- ¹ Ashutosh, N.D. Pandey and J.K. Mehrotra, *Textile Industry and Trade Journal.*, **17**, (1979) 18.
- ² R. Capignano, *J. Chem. Tech. Biotechnol.*, **48**, (1990) 303.
- ³ J. Griffiths, *J. of China Textile University., (Eng. Ed.)* **8**, no.4 (1991) 24.
- ⁴ Himanshu Mehta and A. Peters, , *Dyes and Pigments.*, **2**, (1981) 259.
- ⁵ Himanshu Mehta and A. Peters, *Dyes and Pigments.*, **3**, (1981) 71.
- ⁶ Z. Csepregi, P. Aranyosi, I. Rusznak, L. Lore, J. Frankl and A. Vig., *Dyes and Pigments.*, **37**, No.1 (1998) 1.
- ⁷ J.G. Neevel, H.C.A. van Beek, H.H.I. den Ouden and B van de Graaf, *JSDC* **106**, (1990) 176
- ⁸ R. Bradbury, *Zeneca Specialties confidential reports*, Zeneca Specialties, Hexagon house, Blackley, Manchester, U.K.
- ⁹ P. Gregory, *Chemistry in Britain.*, No. **8**, Aug (2000) 39.
- ¹⁰ J. Heinzl, C.H. Hertz, *Advances in Electronics and Electron Physics.*, **65**, (1985) 91.
- ¹¹ P.L. Gendler, *SPSE Third International Congress on Advances in Non-Impact Printing Technologies San Francisco.*, (1986) 148
- ¹² P. Gregory, *Topics in Applied chemistry: High technology applications of organic colorants*, Plenum Press, New York (1991) Chapter. 9.
- ¹³ A. Arcoria, M. Longo, G. Parisi, *JSDC.*, **100**, (1984) 339.
- ¹⁴ A. Albin, E. Fasani, S. Pietra, A. Sulpizio, *J. Chem. Soc., Perkin Trans. 2.*, **11** (1984) 1689.
- ¹⁵ R. Steiger, *International conference on digital printing technologies*. 1988.
- ¹⁶ R.W. Phillips, *Photodegradation studies of azo dyes and sunscreens in solution and on cotton textiles, PhD thesis*, University of Wales, Swansea., (1996).
- ¹⁷ Oriol Corporation, Light sources catalogue Vol. **2**, 39-43.
- ¹⁸ O. Annen, R. Egli, R. Hasler, B. Henzi, H. Jakob, P. Matzinger *Rev. Prog. Coloration* **17** (1987) 72.
- ¹⁹ J Griffiths, *Rev. Prog. Coloration.*, **11**, (1981) 37.
- ²⁰ G. Hallas, A. Towns, *Dyes and Pigments.*, **33**, no. 3 (1997) 205.
- ²¹ G. Hallas, A. D. Towns, *Dyes and Pigments.*, **34**, no. 2 (1997) 133.
- ²² H. Mustroph, J. Epperlein, *J.f. prakt Chemie.*, **322** (1980) 305.
- ²³ M.H. Charlton, R. Docherty, D. J. McGeein and J.O. Morley, *J. Chem. Soc. Faraday Trans.* **89** (11) (1993) 1671.

-
- ²⁴ R.H. Kineale, E. Stearns, P. van der Meulen *J. Phys. Chem.*, **50** (1946) 363.
- ²⁵ J. Griffiths, *Color and Constitution of Organic Molecules*, Academic Press (1976) 180.
- ²⁶ Jerry March, *Advanced Organic Chemistry: Reaction, Mechanisms and structure*, 4th edition (1992) John Wiley and Sons
- ²⁷ P.F. Gordon and P. Gregory; *Organic Chemistry in Colour*, Springer + Verlag (1983)
- ²⁸ See reference 22.
- ²⁹ Reproduced from J. Griffiths, *Color and Constitution of Organic Molecules*, Academic Press (1976) 102.
- ³⁰ J Griffiths, B Roozpeikar, *J. Chem. Soc., Perkin I*(1976) 42.
- ³¹ P. Gregory and D. Thorp, *J. Chem. Soc., Perkin I* (1979)1990.
- ³² M. Okawara. T. Kitao, T. Hirashima and M. Matsuoka; *Organic Colourants: A Handbook of Data of Selected Dyes for Electro-Optical Applications*: Tokyo, Amsterdam, New York: Elsevier (1988).
- ³³ R. Bradbury, *Zeneca Specialities confidential reports*, Zeneca Specialties, Hexagon house, Blackley, Manchester.
- ³⁴ S. Yamamoto, N. Nishimura, S. Hasegawa, *Bulletin of the Chem. Soc. Of Japan.*, **44** (1971) 2018.
- ³⁵ E. A. Braude and F. Sondheimer; *J. Chem. Soc.*, (1955) 3754
- ³⁶ E. Hoyer, R. Schickfluss and W. Steckelberg, *Angew. Chem. Internat. Edit.* **12** (1973) 926.
- ³⁷ E. Sawaki, *J. Org. Chem.*, (1957) 915.
- ³⁸ J. Griffiths, *Chem. Soc. Revs.*, **1** (1972) 481.
- ³⁹ S. Millefiori and A. Millefiori, *J. Chem. Soc. Faraday Trans 2.*, **77** (1981) 259.
- ⁴⁰ R.W. Castelino, G. Hallas, *J. Chem. Soc (B) Phys. Org.*, (1971) 793.
- ⁴¹ H. Mustroph, *Zeitschrift für Chemie.*, **25** (1985) 385-392.
- ⁴² J. Griffiths, *Developments in polymer Photochemistry-1* (Allen) Applied Science Publ. Ltd. London (1980)145 and references therein.
- ⁴³ P.W. Atkins; *Physical Chemistry*, 5th edition, Oxford University Press 1994.
- ⁴⁴ Reproduced from reference 43.
- ⁴⁵ J. Griffiths, *Colour and constitution of organic molecules*, publ. Academic press, (1976) and references therein.
- ⁴⁶ K.N. Houk, Y.M. Chang and P.S. Engel; *J. Am Chem. Soc.*, **97** (1975) 1824.

- ⁴⁷ Reproduced from NIST Chemistry Webbook <http://webbook.nist.gov>
- ⁴⁸ Cambridge Structural Database, Cambridge Crystallographic Data centre, University chemical laboratory, Lensfield Road, Cambridge, CB2 2EW, U.K.
- ⁴⁹ J. Fabian, H. Hartmann; *Light Absorption of Organic Colourants*: Publ. Springer-Verlag (1980) Chapter 7 and references therein.
- ⁵⁰ Reproduced from reference 43.
- ⁵¹ Reproduced from reference 43.
- ⁵² Reproduced from reference 43.
- ⁵³ M. Nepras, S. Lunak Jr., R. Hrdina and J. Fabian. *Chem. Phys. Letters.*, **159**, (1989) 366.
- ⁵⁴ H. Bisle, M. Romer and H. Rau, *Ber. Bunsenges. Physik. Chem.*, **80** (1976) 301.
- ⁵⁵ W.S. Struve, *Chem. Phys Letters.*, **46** (1977) 15.
- ⁵⁶ H. Suzuki, *Electronic Absorption spectra and geometry of organic molecules* (Academic press, New York, 1967) Chapter 23.
- ⁵⁷ Ch. L. Forber, E.C. Kelusky, N.J. Bunce and M.C. Zerner, *J. Am. Chem. Soc.*, **107** (1985) 5884.
- ⁵⁸ H. Gerner, H. Gruen and D. Schulte-Frohlinde, *J. Phys. Chem.*, **84** (1980) 3031.
- ⁵⁹ H. Rau, *Angew. Chem.*, **85** (1973) 248.
- ⁶⁰ H. Rau, B. Bunsenges, *Physik. Chem.*, **71** (1968) 48.
- ⁶¹ H. Bisle, H. Rau; *Ber. Chem. Phys Letters.*, **31** (1975) 264
- ⁶² E.A. Kramer, *CHIMIA.*, **40** (1986) 160 and references therein.
- ⁶³ I.K. Lednev, Tian-Quing Ye, R.E. Hester, and J.N. Moore, *J. Phys. Chem.*, **100** (1996) 13338.
- ⁶⁴ H. Rau, E. Luddecke *J. Am. Chem. Soc.*, **54** (1982) 1616
- ⁶⁵ H. Rau; *J. Photochem.*, **26** (1984) 221
- ⁶⁶ N. Siampiringue; G. Guyot; S. Monti; P. Bortolus, *J. Photochem.*, **37** (1987) 185
- ⁶⁷ A. P. Prikhotko, V.A. Pavloshchuk; A.G. Tereschenko, L.I. Shanaskii, *Ukrainskii. Fizicheskii Zhurnal*, **37** (1982) 1822.
- ⁶⁸ H. Okamoto, H. Hamaguchi; M. Tasumi; *Chem. Phys. Lett.*, **130** (1986) 185.
- ⁶⁹ A. Biancalana; E. Campani; G. Gorini; G. Masetti, M. Quaglia, *J. Raman Spectroscopy* **23** (1992) 155.
- ⁷⁰ R. D. Curtis; J.W. Hiborn; G. Wu; M.D. Lumsden; R.E. Wasylshen; J. A. Pincock; *J. Phys. Chem.* **97** (1993) 1856 and references therein

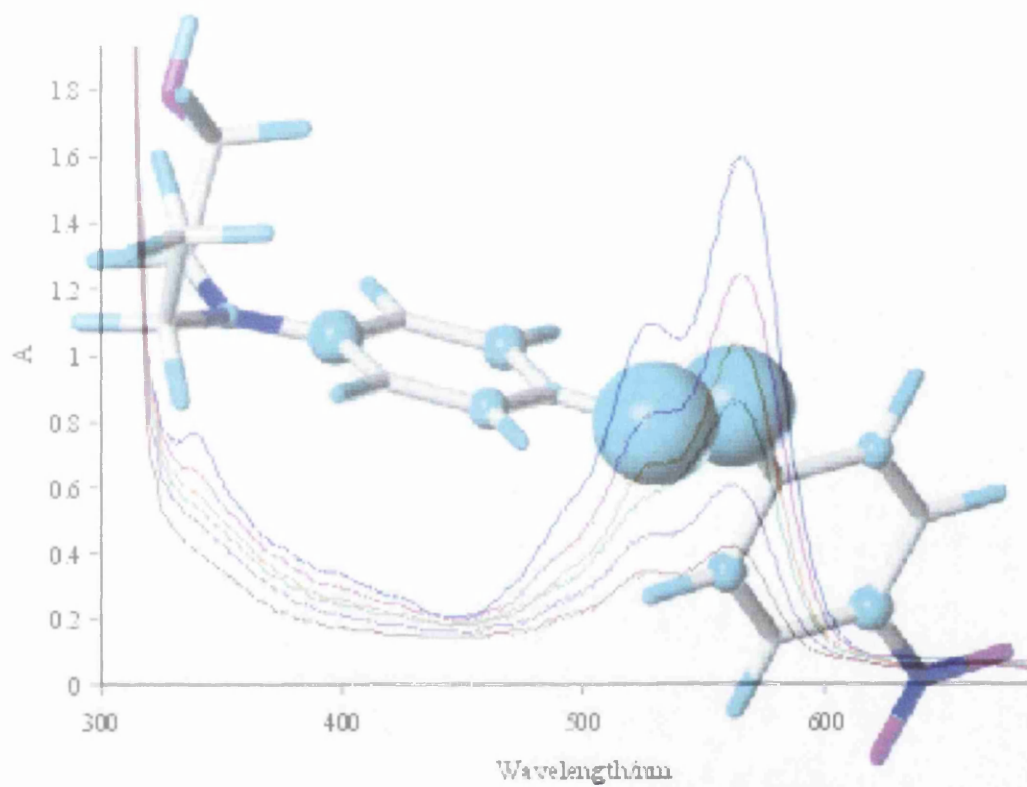
- ⁷¹ H. Rau, *Angew. Chem. Int. Ed. Engl.*, **12** (1973) 224.
- ⁷² R. Cimiraglia, H. Hofmann, *J. Chem. Phys. Lett.*, **217** (1994) 430.
- ⁷³ D. R. Armstrong; J. Clarkson; W.E. Smith, *J. Phys. Chem.*, **99** (1995) 17825.
- ⁷⁴ N. Biswas; S. Umapathy, *Chem. Phys. Lett.*, **234** (1995) 24.
- ⁷⁵ T. Ikeada, O Tsutsumi, *Science* **268** (1995) 1873.
- ⁷⁶ Z. Sekkat, M Dumont, *Appl. Phys. B* **54** (1992) 486.
- ⁷⁷ Z. F. Lui; K. Hashimoto, A. Fujishima, *Nature* **347** (1990) 658.
- ⁷⁸ S. Monti ; E. Gardini; P. Bortolus and E. Amouyal, *Chem. Phys. Letters.*, **77** (1981)115.
- ⁷⁹ S. Monti; S. Dellonte; P. Bortolus, *J. Photochem.*, **23** (1983) 249.
- ⁸⁰ H. Rau; *Agnew. Chem. Intern Ed.*, **12** (1973) 224.
- ⁸¹ V. E. Shashoua, *J. Am. Chem. Soc.*, **82** (1960) 5505.
- ⁸² D.Bontschev and E. Ratschin, *Monatsh. Chem.*, **101** (1970) 1454.
- ⁸³ P. Bortolus and S. Monti, *J. Phys. Chem.*, **83** (1979) 648.
- ⁸⁴ V. E. Shashoua; *J. Am. Chem. Soc.* **82** (1960) 5505.
- ⁸⁵ D.Bontschev and E. Ratschin; *Monatsh. Chem.* **101** (1970) 1454.
- ⁸⁶ S. Monti, G. Orlandi and P. Palmieri, *Chem. Phys.* **71** (1982) 87
- ⁸⁷ A. Albini, E. Fasani and S. Pietra, *J. Chem. Soc. Perkin Trans. 2.*, (1983) 1021.
- ⁸⁸ Z. Sekkat, J. Wood, W. Knoll, *J. Phys. Chem.*, **99** (1995)17226.
- ⁸⁹ M. Schonhofi, M Mertesdorf, *J. Phys. Chem.*, **100** (1996) 7558.
- ⁹⁰ S.Hashimoto, K. Kano, *Bulletin of the Chem. Soc. of Japan*, **45** (1972) 852.
- ⁹¹ H. Rau, *J. Photochem and Photobiol A : Chemistry*, **42** (1988) 321.
- ⁹² P. D. Wildes, J.G. Pacifici , G. Irick, *J. Am. Chem. Soc.* **93** 1971 2004-2008.
- ⁹³ D. Gegiou, K. A. Muszkat and E. Fischer, *J. Am. Chem. Soc.*, **90** (1968) 3907.
- ⁹⁴ E. R. Talaty and J. C. Fargo; *Chem. Commun.*, (1967) 65
- ⁹⁵ J. Binenboym, A. Burcat, A. Lifshitz and J. Shamir, *J. Am. Chem. Soc.*, **88** (1966) 5039.
- ⁹⁶ G. Zimmerman, L. Y. Chow and U. I. Paik, *J. Am. Chem. Soc.*, **80** (1959) 3528.
- ⁹⁷ J. M. Robertson, *J. Chem. Soc.*, (1939) 232.
- ⁹⁸ C. J. Brown, *Acta Crystallogr.*, **21** (1966) 146
- ⁹⁹ Ch. L. Forber, E. C. Kelusky, N. J. Bunce and M. C. Zerner, *J. Am. Chem. Soc.*, **107** (1985) 5884.
- ¹⁰⁰ L. B. Jones and G. S. Hammon, *J. Am. Chem. Soc.*, **87** (1965) 4219

-
- ¹⁰¹ O. Kikuchi, M. Azuki, Y Inadomi, K. Morihashi; *J. Molecular Structure (Theochem)* 468 (1999) 95-134 and references therein.
- ¹⁰² H.S. Freeman, S~A. McIntosh, *Textile Research Journal.*, **59** (1989) 343.
- ¹⁰³ V. Rehak, F. Novak and J. Cejeiansky, *Collect. Czech. Chem. Commun.* **38** (1973) 697.
- ¹⁰⁴ A. M. J. Ali and Z. Y. Al-Saigh, *Indian J. Chem.*, **16B** (1978) 910.
- ¹⁰⁵ J.C. Pacifici and G. Irick, *Tetrahedron Lett.*, No.27 (1969) 2207.
- ¹⁰⁶ G. Irick and J. C. Pacifici; *Tetrahedron Lett.*, 1969, 1303
- ¹⁰⁷ G. Seu, *American. Dyestuff Reporter.*, March (1985) 29-30.
- ¹⁰⁸ N.S. Allen, *Rev. Prog. Coloration.*, **17** (1987) 61-71.
- ¹⁰⁹ A. Albini, E. Fasani and S. Pietra, *J. Chem. Soc., Perkin Trans. 2* (1982), 1393 and references therein.
- ¹¹⁰ S.J. Formosinho, *J. Chem. Soc. Faraday Trans. 2.*, **72** (1976) 1332
- ¹¹¹ J. Ronayette, R. Arnaud, J. Lemaire; *Compt. Rend.* **52** (1976) 1858
- ¹¹² J. Griffiths, *J. Chem. Soc., Perkin Trans. 2.*, (1976) 747.
- ¹¹³ A. Albini, E. Fasani and S. Pietra., *J.Chem. Soc. Perkin Trans. 2* (1984)1689-1692
- ¹¹⁴ D. Bellus, in "Singlet oxygen," eds. B. Ranby and J. F. Rabek, Wiley. Chichester, (1978) 61.
- ¹¹⁵ E.N. Abrahart, *Dyes and their intermediates*, 2nd Ed. Edward Arnold, London (1977).
- ¹¹⁶ D. Shah; R. Srinivasan; *J. Appl. Chem. Biotechnol.* **27** (1997) 429-436.
- ¹¹⁷ Alberghina, A. Arcodia, *American. Dyestuff reporter.*, March (1983) 21-22.
- ¹¹⁸ E. Dubini-Paglia, P. L. Beltrame, A. Seves and G. Prati, *J.S.D.C.*, **105** March (1989)109-111.
- ¹¹⁹ S.C. Neevel, H.C.A. van Beek, H.H.I. den Ourden and B. van de Graaf, *J.S.D.C.*, **106** May (1990) 176.
- ¹²⁰ E. Sawaki, F. Ray, *J. Org. Chem.*, (1954) 1686.
- ¹²¹ A. Albini, E. Fasani and S. Pietra; *J. Chem. Soc. Perkin Trans. 2* (1986) 681.
- ¹²² H. C. A. Van Beek, P.M. Heertjes and K. Schaafsma; *Rect. Trav. Chim. Pays-Bas.* **92** (1973) 1189.
- ¹²³ M. Sander and C. L. Osborn; *Tetrahedron Lett.*, 1974, 415.
- ¹²⁴ H. Gruen and B. Shulte-Frohlinde, *J. Chem. Soc. Chem. Commun.*,1974, 923
- ¹²⁵ N.S. Allen, *Rev. Prog. Coloration.*, **17** (1987) 61 and references therein.
- ¹²⁶ A. Daytner *et al*, *J.S.D.C.*, June (1977) 213.

-
- ¹²⁷ A. Albini, E. Fasani, M. Moroni, *J. Chem. Soc. Perkin Trans. 2.*, (1986) 1439 and references therein.
- ¹²⁸ J. Griffiths and C. Hawkins, *J. Chem. Soc., Chem. Commun.* 1972, 463; *J. Chem. Soc. Perkin Trans. 2*, 1977, 747
- ¹²⁹ N. Kuramoto and T. Kitao, *Nippon Kagaku Kaishi*, (1977) 258, (*Chem. Abstracts*), (1977) 86, 141 593h
- ¹³⁰ P. B. Merkel and D. R. Kearns, *J. Am. Chem. Soc.*, **94**, 1972, 7244
- ¹³¹ R. Haessner, H. Mustroph and J. Epperlein; *J. Prakt. Chem.* **325** (1983) 943.
- ¹³² Andrew R. Leach, *Molecular Modelling: Principles and Applications*, Longman (1999)
- ¹³³ Ira N. Levine, *Quantum Chemistry*, 4th Edition, Prentice Hall (1991)
- ¹³⁴ R. Pariser and R. Parr, *S. Chem. Phys.* **21** (1953) 466,767.
- ¹³⁵ J.A. Pople, *Trans. Faraday Soc.*, **49** (1953) 1375.

Chapter 2

Experimental Studies on Azo Dyes



Chapter 2

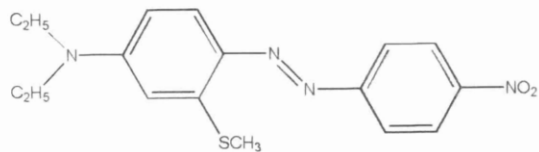
Experimental

The azo dyes investigated in this study are shown as [I] -[XIX] in Scheme 2.1 Dyes [I]-[VII] and [XIV]-[XIX] were supplied by Zeneca Fine Chemicals Service.¹ Dyes [VIII], [IX], [XII] and [XIII] were supplied by Aldrich² and dyes [XI] and [X] were synthesised by S. Whittaker³ and K. Mort⁴ respectively. All the dyes were purified by recrystallisation from ethanol and air dried. Each dye was found to have only one spot on silica thin layer chromatography plates which absorbed in the visible region, and under 254 nm and 366 nm ultraviolet light, no fluorescence was observed

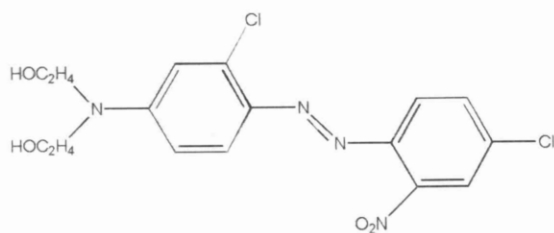
Melting points were determined for all 19 dyes using standard melting point apparatus. The melting point range for each dye is listed in Table 2.1 along with literature values, where available.

Table 2.1 Melting point data for azobenzene and azothiophene dyes

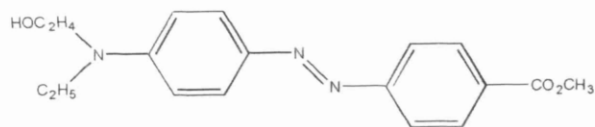
| Dye | Melting Point/°C | | Dye | Melting Point/°C | |
|--------|------------------|-------------------------|---------|------------------|------------|
| | Experimental | Literature ² | | Experimental | Literature |
| [I] | 160-162 | | [XI] | 158-160 | |
| [II] | 168-170 | | [XII] | 129-135 | 122-129 |
| [III] | 120-125 | | [XIII] | 170-175 | 170 |
| [IV] | 99-100 | | [XIV] | | |
| [V] | 134-137 | | [XV] | 138-141 | |
| [VI] | | | [XVI] | 205-209 | |
| [VII] | 152-153 | | [XVII] | 237-241 | |
| [VIII] | 200-201 | 200 | [XVIII] | 150-155 | |
| [IX] | 162-165 | 160-162 | [XIX] | 130-132 | |
| [X] | | | | | |



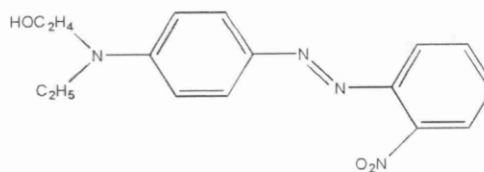
[I]



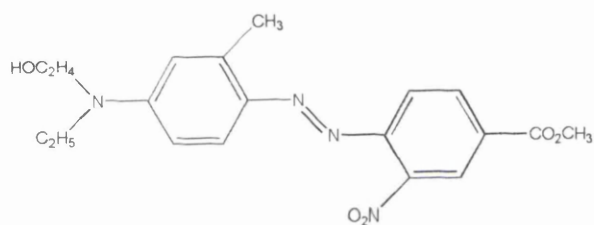
[III]



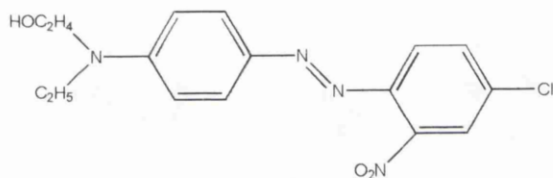
[IIII]



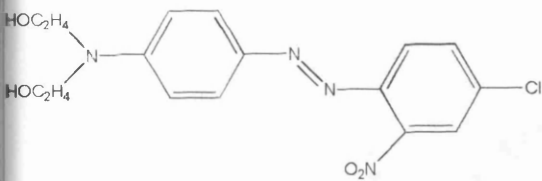
[IV]



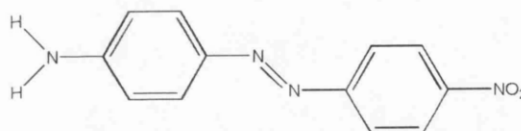
[V]



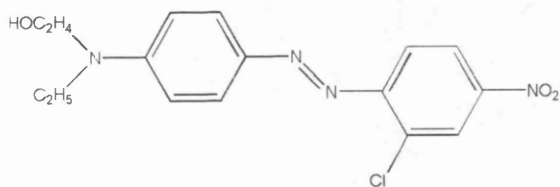
[VI]



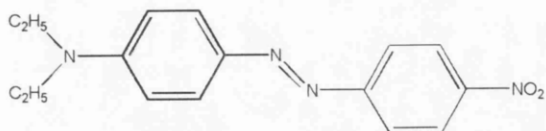
[VII]



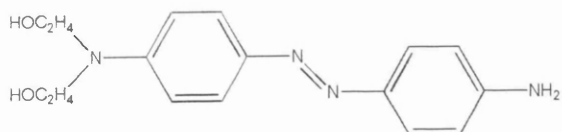
[VIII]



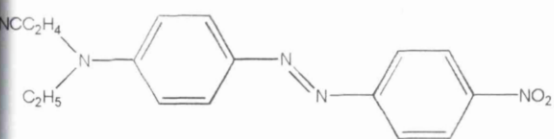
[IX]



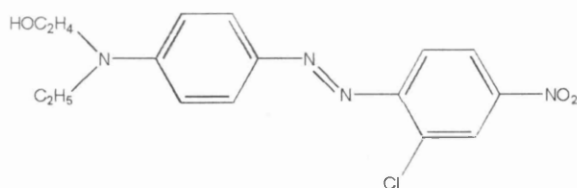
[X]



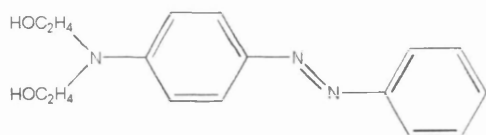
[XI]



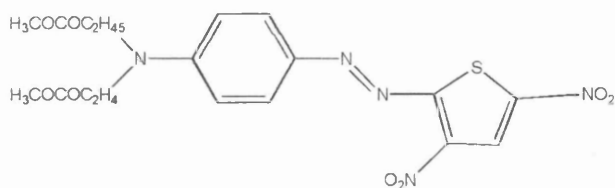
[XII]



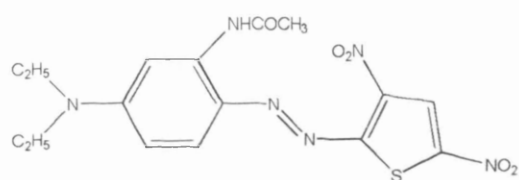
[XIII]



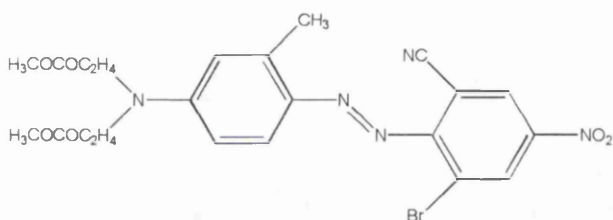
[XIV]



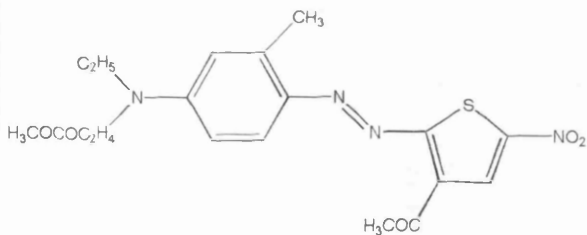
[XV]



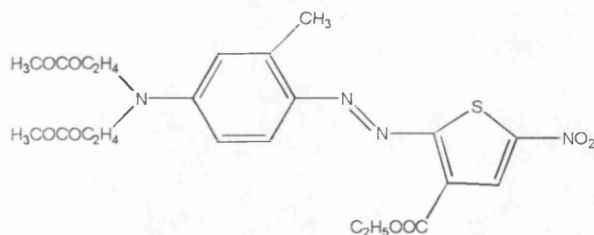
[XVI]



[XVII]



[XVIII]



[XIX]

Scheme 2.1 The azobenzene and azothiophene dyes examined

Both proton and carbon-13 nmr spectra were consistent with the structures for the dyes shown in Scheme 2.1. Mass spectra show molecular ion peaks consistent with the relative molecular masses of the dye structures in Scheme 2.1 and accurate mass spectra confirmed the molecular formulas of the dyes

Absorption spectra

The UV/visible spectra of dyes [I] -[XIX] were recorded in cyclohexane and methanol on a Perkin Elmer Lambda 19 spectrophotometer in quartz cuvettes with a 1 cm path-length at room temperature. UV/visible diffuse reflectance spectra were recorded using the Perkin Elmer Lambda 19 spectrophotometer, with a diffuse reflectance integrator attachment (B130-9941).

The spectra of dyes [I]-[XIX] were recorded in cyclohexane and methanol. The absorption spectrum of [IX] in methanol shows (Figure 2.1) a strongly absorbing coloured band at 482 nm and a second lower intensity band at 286 nm. The spectra of dyes [I]-[VIII] are similar to that of [IX].

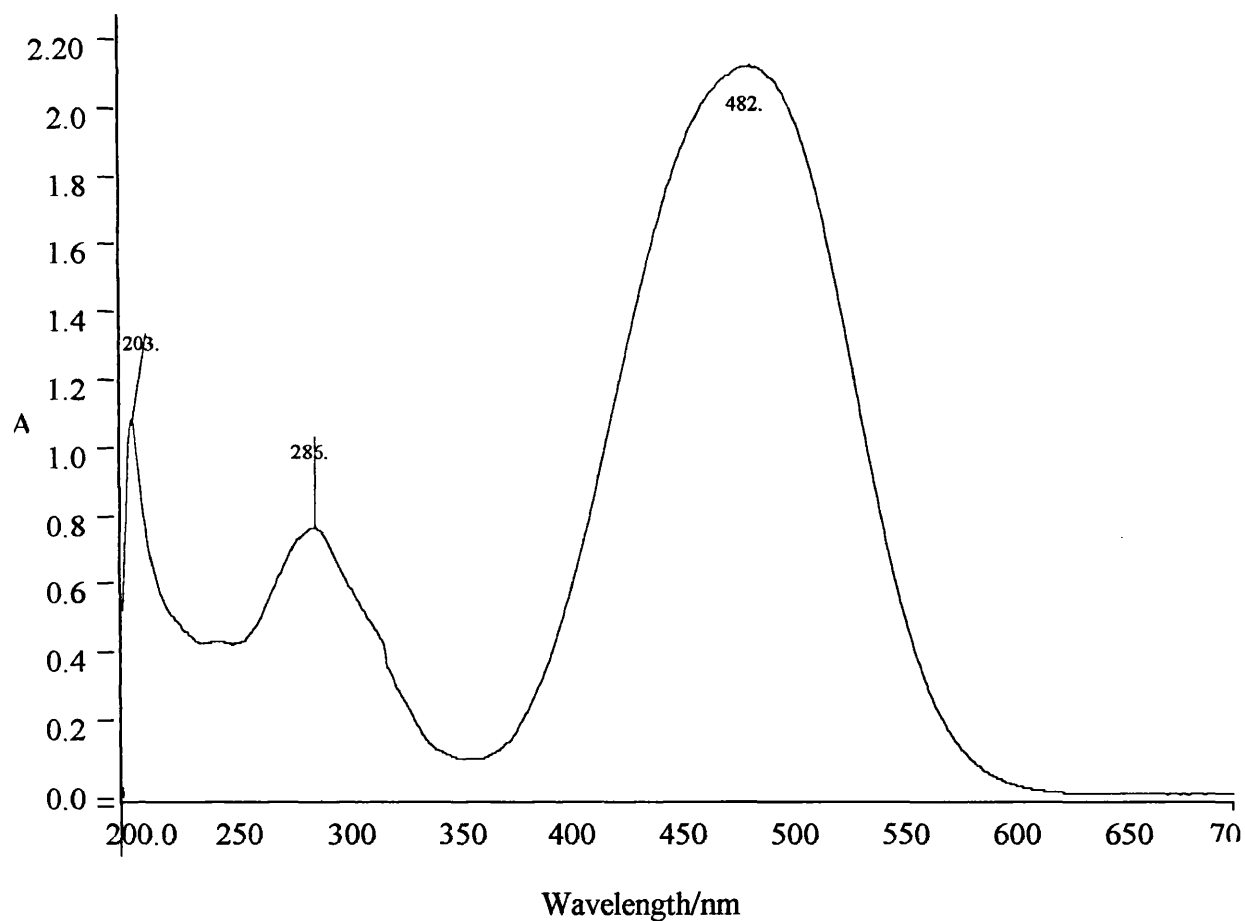


Figure 2.1 The UV/visible absorption spectrum of [IX] in methanol. *A is the absorbance.

The spectra of dyes [II]-[IX] were also recorded in a number of other solvents chosen to span a large range of dielectric constants, to examine the effects of dielectric constant on the spectra. The solvents used together with their dielectric constants are given in Table 2.2.

Table 2.2 Dielectric constants of some solvents⁵

| Solvent | Dielectric constant ϵ |
|---------------------------|--------------------------------|
| Cyclohexane | 2.02 |
| 1,4-Dioxane | 2.21 |
| Chloroform | 4.8 |
| Tetrahydrofuran (THF) | 7.6 |
| Acetone | 20.7 |
| Ethanol | 24.6 |
| Methanol | 32.7 |
| Dimethyl Sulfoxide (DMSO) | 46.7 |
| Ethylene Carbonate | 89.6 |
| Formamide | 111.0 |

The solvents used were of spectroscopic grade or the highest purity grade available and methanol was dried by refluxing with magnesium and iodine. Due to the low solubility of the dyes in some solvents, some dyes gave very weak absorption spectra and only the long wavelength absorption band could be determined. For some dyes, the solubility in cyclohexane was so low that mixed solvent solutions of hexane and dioxane were used to extrapolate for the wavelength of the dye in pure cyclohexane. For example, [V] was almost insoluble in pure cyclohexane, so dyes solutions of 5%, 10%, 20%, 33% and 50% dioxane in hexane, were made up. The wavelength of the dye in each solution was plotted against the percentage of cyclohexane in the solution, as in Figure 2.2. A curve can be fitted to the experimental data points and the wavelength for 100% cyclohexane solution can then be extrapolated from this curve. The wavelength given at the point where the curve intersects the y-axis, which corresponds to the wavelength in 100% cyclohexane solution, is 463.6 nm.

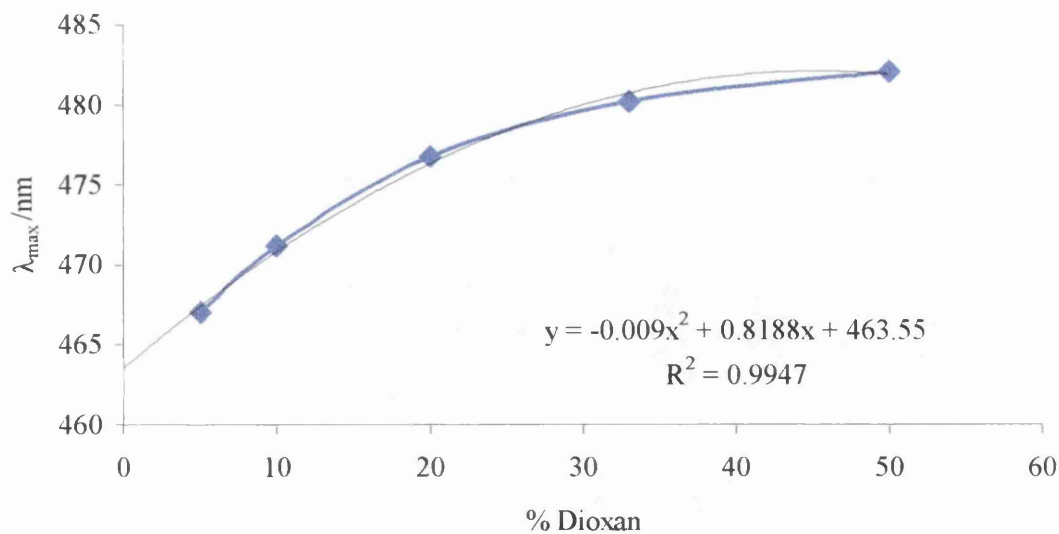


Figure 2.2 The visible absorption maxima (λ_{max}) of [V] in cyclohexane solutions containing varying amounts of dioxane.

The equation for the curve fitted polynomial is given in Figure 2.2. R^2 is the correlation coefficient.

Kinetic Experiments

Kinetic experiments were carried out at room temperature (25°) in a spectrophotometer quartz cuvette (50 mm by 5 mm) with a 10 mm path length and an internal cell volume of 2 ml. The cuvette was made air tight with a teflon stopper.

Methanol solutions of dyes of concentration $1 \times 10^{-4} \text{ mol dm}^{-3}$ in the stoppered quartz cuvette were photo-faded using a 1000W Xenon arc lamp, as in the arrangement shown in Figure 2.3.

The Xenon Arc lamp consisted of a 1000W bulb obtained from Oriel,⁶ housed in a steel casing with the lamp fan cooled. To maximize the output of the lamp, a concave rear reflector mirror was used to focus the light through an opening, which was 30 mm, by 20 mm in size. The bulb was aligned to allow a maximum output of light through the opening. A shutter, which is either open or shut, controlled the light allowed out of the lamp housing. This shutter was linked to timer so the exposure time of the sample to irradiation was controlled. The minimum exposure time allowed by the timer is 1 second.

A water filter was placed in front of the opening so that infrared emission from the Xe lamp was absorbed to avoid excessive heating of the sample. The sample, contained in the quartz cell was then placed directly in line with the opening to allow maximum exposure to irradiation.

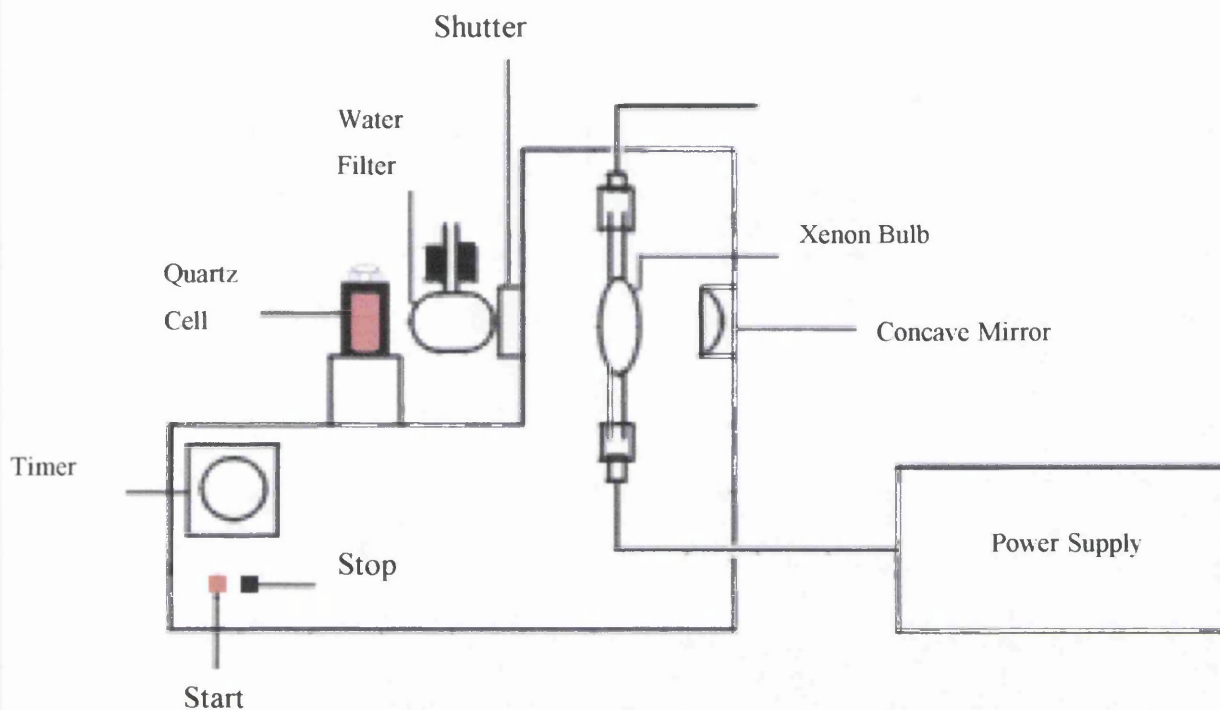


Figure 2.3 Diagrammatic representation of the 1000W Xenon Arc Lamp apparatus for the photofading of dye solutions in a quartz spectrophotometric cuvette.

The reasons for the choice of the Xenon arc lamp have been outlined in Chapter 1 page 9. The lamp produces an intense output of both UV and visible light capable of simulating hours of sunlight in a few minutes. The output power of the lamp at a single wavelength was estimated according to Oriel's data,⁶ from the spectral irradiance curve of the 1000 W Xenon arc lamp. The total power output at 280 nm is used as an example. The value from the irradiance curve at 280 nm is $100 \text{ mWm}^{-2} \text{ nm}^{-1}$. This is multiplied by a conversion factor of 0.12 originating from the lamp housing and condenser type. The value obtained must be further multiplied by a factor of 1.5 to take into account the use of the rear reflector. Therefore the total power output at 280 nm = $100 \times 0.12 \times 1.5$

$$= 18 \text{ mW nm}^{-1}$$

The total power output over a range of wavelengths is given by the area under the irradiance curve for the wavelength range and substituting this value for the single wavelength value.

Experiments were carried out under degassed conditions, by bubbling argon through a solution of the dye in the cuvette, with the top of the cuvette partially sealed from the atmosphere by the stopper, to prevent any atmospheric oxygen diffusing into the solution. Prevention of the infusion of oxygen into the solution is critical, as oxygen has an enormous effect on the rate of photofading.

Photo-fading experiments carried out under oxygenated conditions, were prepared by bubbling oxygen through solutions of the dye in methanol for five minutes.

Filters

A glass microscope slide, Pyrex glass filter or an Oriel heat and UV reflecting mirror, was placed between the lamp opening and the sample to limit the ultraviolet wavelength range that irradiates sample. Unless otherwise stated, experimental data refers to samples irradiated without filters present.

Laser irradiation

Laser irradiation of samples were performed using a Coherent air-cooled continuous wave argon ion laser with a photon bag attachment port for simple light refueling from BS Industries, Columbus, Ohio at 514.5nm with an operating power of 15mW and 1mm beam width.

Results

Absorption maxima in protic and non-protic solvents

If the variation in wavelength with respect to the dielectric constant of the solvent for each of the dyes [I]-[IX] is plotted, it can be seen from Figure 2.4, that the relationship between the visible absorption maximum, λ_{max} , and the dielectric constant, ϵ , is not readily identifiable. There seems to be a very general shift to longer wavelength in solvents of higher dielectric constant, but the relationship is somewhat erratic. It is well known that there are two effects of the solvent: a dielectric effect and a hydrogen bonding effect.⁷ If the solvents are separated into those that have the capacity to hydrogen bond, and those that do not, a clearer pattern emerges. Figure 2.5 shows that there is a general increase in the wavelength of the dye with increasing dielectric constant of the solvent in so called non-protic solvents, which have little capacity for hydrogen bonding.

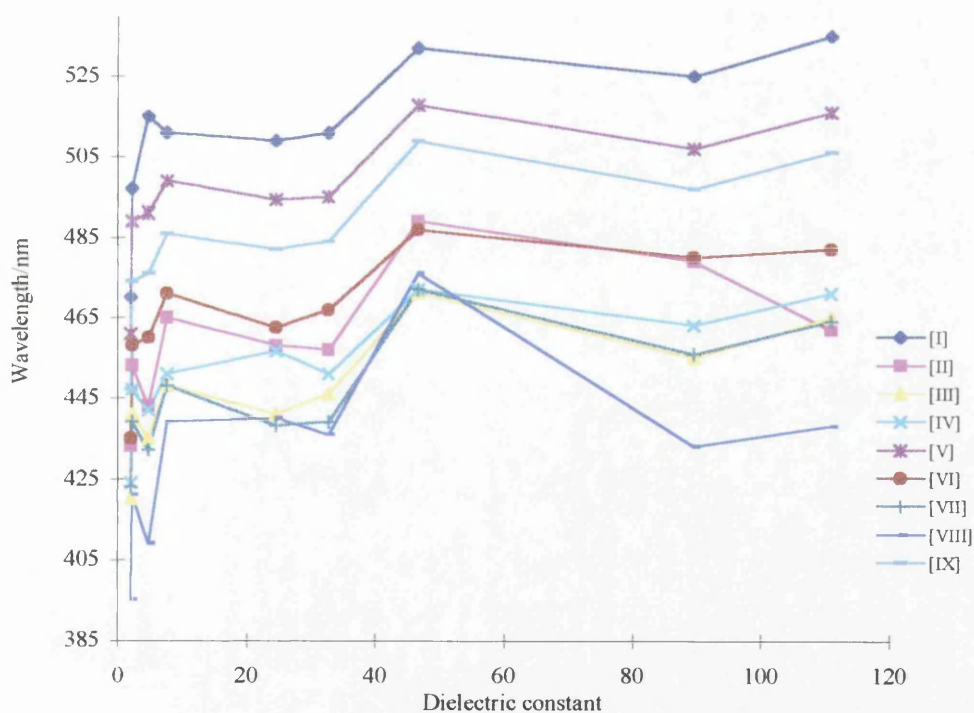


Figure 2.4 The variation of visible absorption maxima of dyes [I]-[IX] in solvents of different dielectric constant.

The non-protic solvents used in this work were cyclohexane, dioxane, THF, acetone, DMSO and ethylene carbonate. The wavelengths of the dyes are shortest in cyclohexane, ranging from 390

nm for [VIII], to 467 nm for [I]. When considering the wavelengths of these dyes in non-protic solvents, the largest bathochromic shift occurs in DMSO, with values ranging from 471 nm for [III] to 532 nm for [I]. Even though ethylene carbonate has a higher dielectric constant than DMSO, the wavelengths of most of the dyes in ethylene carbonate and DMSO are similar. The anomalous appearance of results for DMSO, particularly noticeable for [VIII], which has a far shorter wavelength in ethylene carbonate (433 nm) than in DMSO (476 nm), possibly arises because of the presence of small amounts of water, which are difficult to remove completely. If water is present, it may hydrogen bond with dyes causing a bathochromic shift. This bathochromic shift may be more pronounced for [VIII] due to the possibility of strong hydrogen bonding interactions between the amino group hydrogen atoms in [VIII] and water molecules.

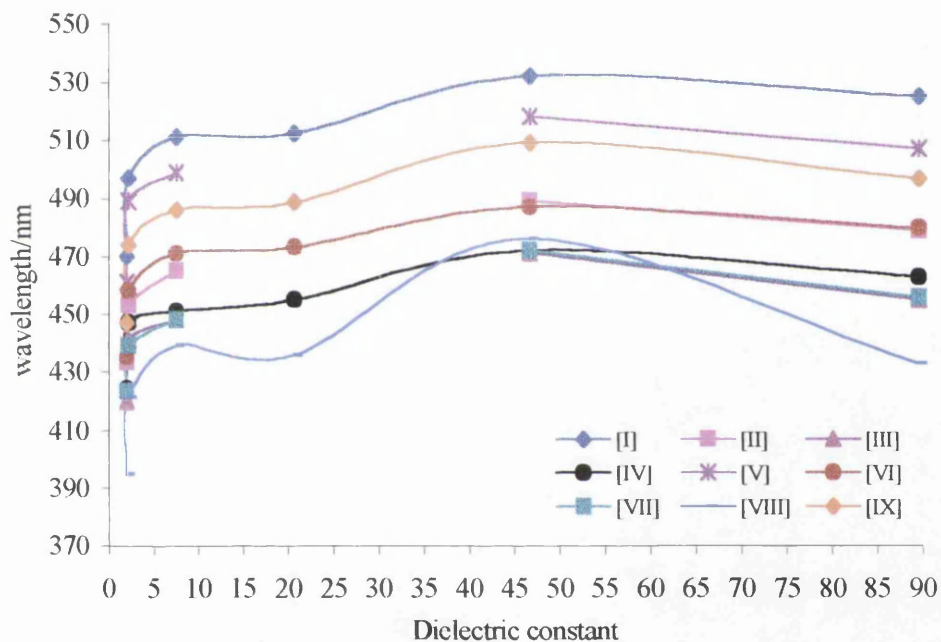


Figure 2.5 The variation of visible absorption maxima with dielectric constant of dyes [I]-[IX] in the non-protic solvents, cyclohexane, dioxan, THF, acetone, DMSO and ethylene carbonate.

Hydrogen bonding solvents

Figure 2.6 shows the behaviour of the dyes in protic solvents, which do have a capacity for hydrogen bonding. The protic solvents considered are chloroform, ethanol, methanol and formamide. Again there is a general shift to longer wavelength with increasing dielectric constant of the solvent. The wavelengths of the dyes in methanol range from 436 nm for [VIII] to 513 nm for [I]. Morley and Fitton⁷ have separated shifts in protic solvents into a distinct dielectric component, and a hydrogen bonding component in their study of indoaniline dyes.

They suggest that the dielectric effect saturates fairly quickly, as there is no further shift observed in moving from ethylene carbonate ($\epsilon = 89.6$) to N-methylacetamide ($\epsilon = 179$). It seems this saturation effect also applies to these azo dyes, as the shift from acetone ($\epsilon = 20.7$) to ethylene carbonate is relatively small compared to the difference in dielectric constant. They also estimate the size of the hydrogen bonding and dielectric component to the total shift of indoanilines. Ethanol for example, has a larger hydrogen bonding component but smaller dielectric component than formamide. The total shift of the absorption maxima in azo dyes seems to have a similar dependence on dielectric and hydrogen bonding components.

Hydrogen bonding is therefore very significant when considering the effect of solvent polarity on the wavelength of these donor-acceptor azo dyes. The effect of hydrogen bonding solvents is particularly noticeable for [VIII]. This is due to the capacity of its amino group's hydrogen atoms to form strong hydrogen bonds with protic solvents. In addition, the amino groups involvement in hydrogen bonding interactions may affect its electron density and thus the electronic interaction of the amino nitrogen atom with the rest of the dye chromophore.

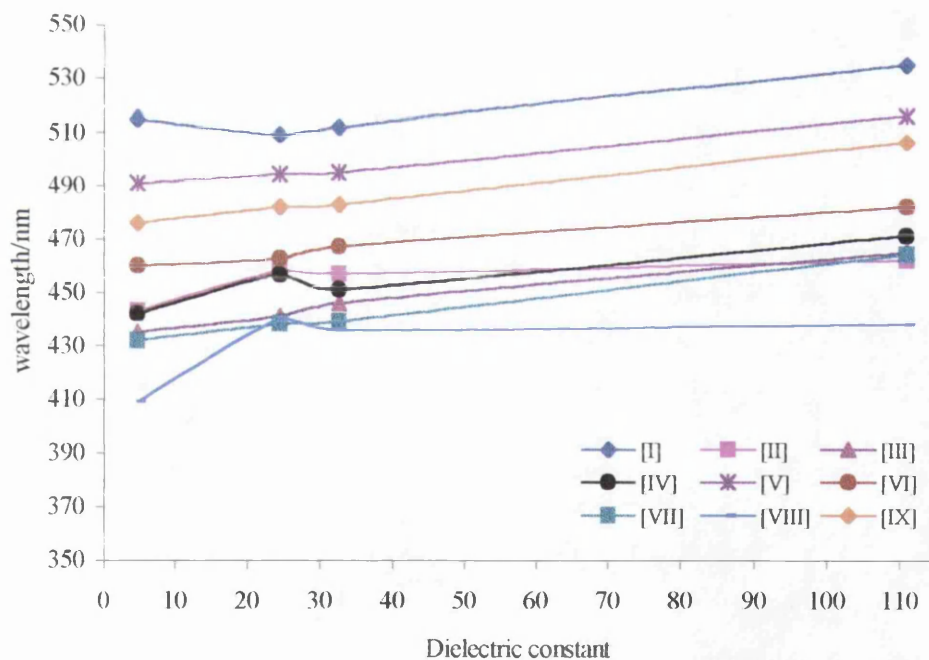


Figure 2.6 The variation of visible absorption maxima with dielectric constant, of dyes [I]-[IX] in the protic solvents, chloroform, ethanol, methanol and formamide.

This situation is different from [IX] for example, which has a hydroxy group, which would be involved in hydrogen bonding. However, the hydroxy group of [IX] is attached to the ethyl

group on the amino nitrogen and its effect on the electron density of the amino nitrogen atom is likely to be small. Therefore hydrogen bonding in [IX] is less likely to have such a profound effect on the chromophoric system, compared to [VIII].

The range of data was extended by examining all 19 dyes in methanol solution. The wavelengths of the long wavelength absorption bands for the 19 dyes in methanol are reported in Table 2.3. The long wavelength absorption band of each dye has an ϵ_{\max} in the region of 40000 mol⁻¹ dm³ cm⁻¹ and undergoes bathochromic shifts of up to 60 nm when moving from non-polar to polar solvents. The donor acceptor azo dyes [II]-[IX] range in colour from yellow to red (absorption maxima from 436 nm to 513 nm in methanol) while dye [XVII] is violet (λ_{\max} = 580nm). The acceptor substituent strongly influences the position of this band, as is exemplified by the much shorter wavelength of [XIV] in methanol (409 nm), which has no acceptor substituent. The long wavelength absorption band of the azothiophene dyes in methanol occurs at longer wavelengths than in the azobenzene dyes, at around 600-630 nm compared to 450 – 580 for the azobenzene dyes. This bathochromic shift may be attributed to the increased capacity of the sulphur atom in the thiophene ring to accept electron density because of the vacant d-orbitals. Also given in Table 2.3, are the wavelengths of the second absorption band and any additional absorption bands seen in the spectra of some of the dyes in methanol. For example, the spectrum of [IX] in methanol, (Figure 2.1) shows a second absorption band in the vicinity of 286 nm. This band is present in the spectra of most of the azo dyes in the region of 270 to 310 nm. There are a few exceptions, and these are discussed below.

Table 2.3 The wavelengths of the main absorption bands present in the absorption spectra of dyes [I] -[XIX] in methanol.

| Dye | Wavelength /nm | | | |
|---------|----------------|-------------|-------------|-------------|
| | λ_1 | λ_2 | λ_3 | λ_4 |
| [I] | 513.4 | 307.0 | 245.8 | |
| [II] | 455.9 | 291.4 | | |
| [III] | 444.7 | 276.8 | | |
| [IV] | 447.8 | 274.4 | 240.8 | |
| [V] | 495.2 | 288.6 | | |
| [VI] | 464.7 | 278.8 | | |
| [VII] | 438.1 | 286.9 | | |
| [VIII] | 435.9 | 275.0 | | |
| [IX] | 481.9 | 285.9 | | |
| [X] | 487.8 | 285.3 | | |
| [XI] | 445.2 | 412.3 | 317.7 | 253.0 |
| [XII] | 455.8 | 281.2 | | |
| [XIII] | 500.3 | 285.8 | | |
| [XIV] | 408.6 | 258.7 | | |
| [XV] | 618.8 | 286.8 | | |
| [XVI] | 613.12 | 459.0 | 275.6 | |
| [XVII] | 580.2 | 306.7 | | |
| [XVIII] | 612.1 | 280.3 | | |
| [XIX] | 615.2 | 286.7 | | |

The position of the second absorption band is influenced less by substituents than the long wavelength absorption band and occurs in the region of 275 nm to 307 nm for all of the dyes in methanolic solution.

Table 2.4 The wavelengths of the second absorption band of dyes [I]-[IX] in cyclohexane, methanol, THF and some values in formamide.

| Dye | Wavelength in solvent/nm | | | | | |
|--------|--------------------------|-------|---------|----------|------|-----------|
| | Cyclohexane | THF | Ethanol | Methanol | DMSO | Formamide |
| [I] | 301.8 | 309.7 | 307.9 | 307.0 | 313 | 308 |
| [II] | Not Soluble | 293.3 | 290.5 | 291.4 | 300 | - |
| [III] | 270.9 | 277.5 | 275.5 | 276.8 | 276 | - |
| [IV] | 270.7 | 276.8 | 286 | 274.4 | - | 283 |
| [V] | 278.0 | 289.7 | 287 | 288.6 | 275 | 288.2 |
| [VI] | 274.2 | 280.8 | 275.9 | 278.8 | 281 | 284 |
| [VII] | Not Soluble | 289.7 | 286.8 | 286.9 | 293 | 287.1 |
| [VIII] | 264.0 | 276.7 | 274.4 | 275.0 | 277 | 281.0 |
| [IX] | 280.0 | 285.9 | 279.9 | 285.9 | 275 | 275.1 |

Data for this second absorption band in the spectra of dyes [I]-[IX] in methanol, cyclohexane, THF, and formamide, are reported in Table 2.4. From these values it can be seen that the effect of solvent on the wavelength of this second band is less pronounced than for the long wavelength band. There is a relatively small bathochromic shift of between 5 and 10 nm for most of the dye on going from cyclohexane to methanol, and the largest shift for the dyes and solvents examined is 12 nm, which corresponds to the difference in the wavelength of the second absorption band of [V] in cyclohexane and THF respectively. There does seem to be some wavelength dependence in solvents of different dielectric constant, with wavelengths in cyclohexane consistently shorter than those in THF and methanol, though the difference between wavelengths in THF and methanol is minimal, echoing the results for the long wavelength absorption band.

Other absorption bands

Griffiths reports⁸ that higher energy π - π^* bands are readily discernable in the near UV absorption spectra of diarylazo compounds, and these are generally associated with local excitations in the aromatic residues.

Some of the dyes examined in this work have additional absorption bands also at around 245 nm. An example of these bands is given in Figure 2.7 for [I] which has the additional band at 246 nm

in methanol. It should be noted that not all the azobenzene dyes have these additional absorption bands.

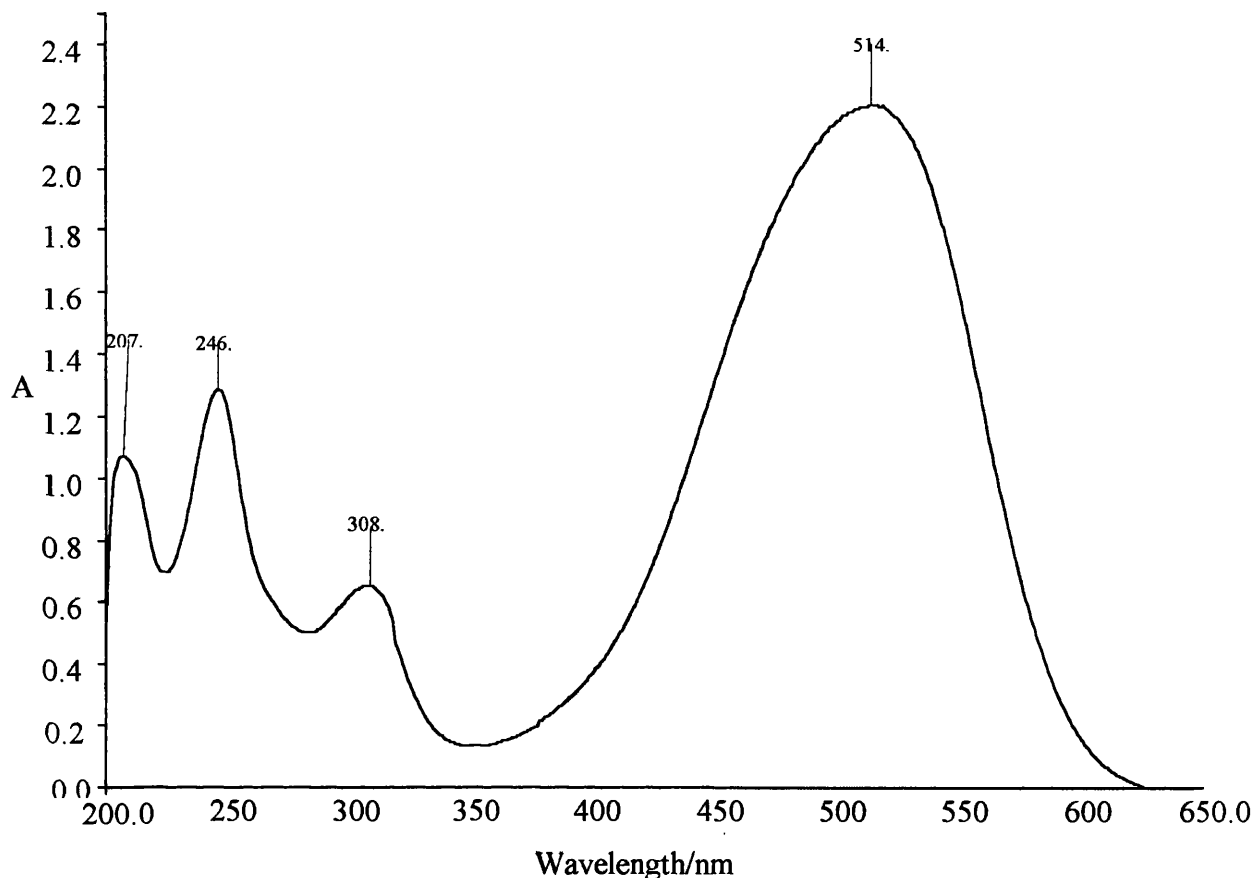


Figure 2.7 The UV/visible spectrum of [I] in methanol, illustrating the additional absorption bands present.

Dyes [XV], [XVIII] and [XIX] show an absorption band in the region of 280 nm, which is of much lower intensity than the long wavelength band. [XVI] also has a low intensity absorption band at 276 nm but unlike the other azothiophene dyes, it has an additional absorption band at 459 nm. The wavelengths of all the other absorption bands, recorded for the dyes in methanol solution, are reported in Table 2.3.

Aggregation Effects

According to Beer's law, Equation (2-1), the absorbance of the dye varies linearly with the concentration of the dye [C],

$$A = \epsilon \cdot [C] \cdot l$$

Equation (2-1)

where A is the absorbance, ϵ is the molar extinction coefficient of the dye and l is the path length of the cell, which is 1 cm for all the experiments in this study.

However, at high concentrations, the dye molecules may aggregate together and the aggregated molecules may absorb light less efficiently. This leads to a deviation from Beer's law, where the absorption is no longer related linearly to the concentration of the dye. The effect of aggregation is exhibited in the spectra of **[IX]** (Figure 2.8). Considering these spectra we can see that as the concentration rises above $5 \times 10^{-7} \text{ mol dm}^{-3}$ the absorbance begins to plateau and no longer varies linearly with concentration. If Beer's law was obeyed, the absorbance of the solution of concentration $1 \times 10^{-4} \text{ mol dm}^{-3}$ should be twice that of the solution of concentration $5 \times 10^{-5} \text{ mol dm}^{-3}$.

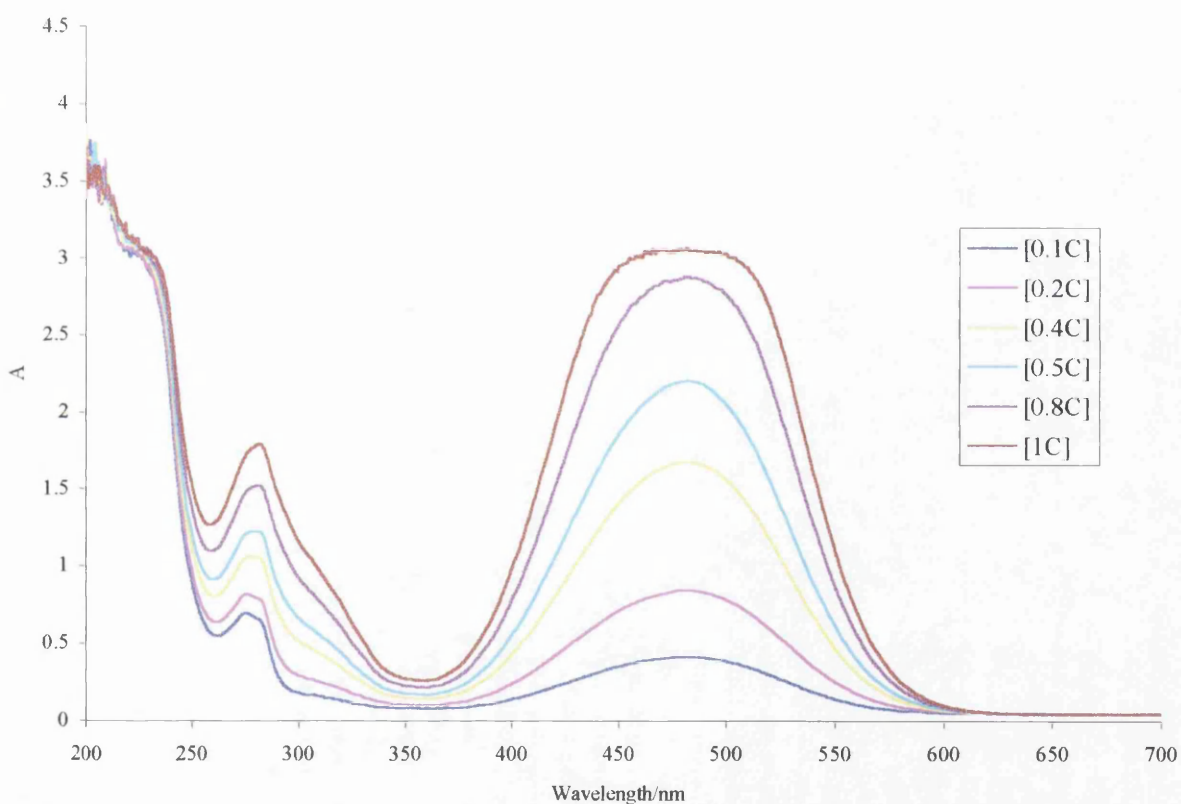


Figure 2.8 The effect of increasing the concentration of **[IX]** on the absorbance of solutions in methanol. The concentrations vary from 0.1C to 1C, where $C = 1 \times 10^{-4} \text{ mol dm}^{-3}$.

The actual absorbance values are 2.197 and 3.063 respectively for the two solutions. The absorbance at λ_{max} of various strength methanolic solutions of **[IX]** is plotted against the concentration of the solutions in Figure 2.9.

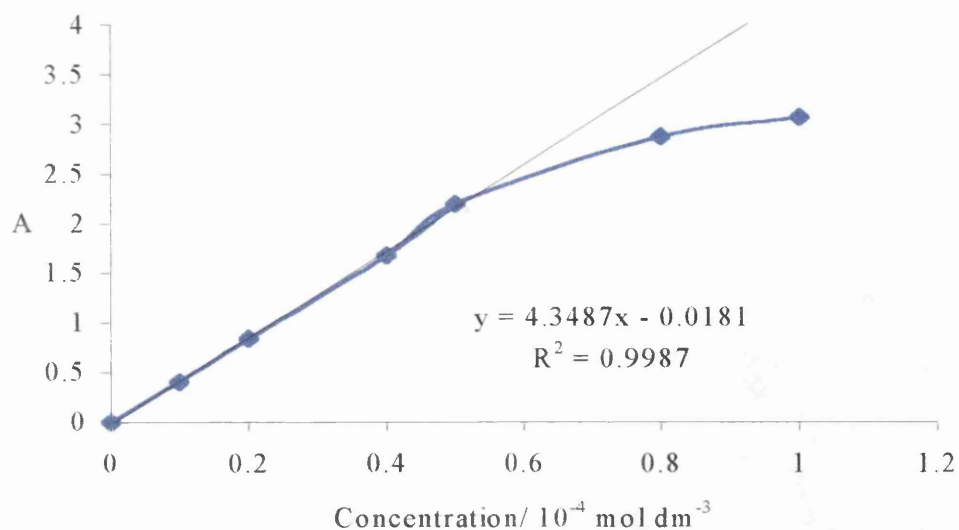


Figure 2.9 Absorbance versus concentration plot for [IX] in methanol.

At concentrations below $5 \times 10^{-5} \text{ mol}^{-1} \text{ dm}^{-3}$ Beer's law is seen to be obeyed, as the relationship between absorbance and concentration is linear. Above this concentration though, the absorbance begins to deviate from the straight line in , and Beer's law is no longer valid. In fact the absorbance hardly increases at all when the concentration rises above $1 \times 10^{-4} \text{ mol dm}^{-3}$, with changes in the spectrum limited to broadening of the peak. This could be attributed to aggregation effects. However, it is much more probable that this effect is due to the limited light being transmitted at these concentrations. For example, when the solution has an absorbance of 3, the transmitted light is 0.1% of the incident light and it is doubtful whether the instrument used will give reliable results with absorbancies this high. These limitations could be overcome by reducing the path length l by using a thinner spectrophotometer cell.

Since we know the concentrations of the dye solutions used, the molar extinction coefficient, ϵ , can be calculated by rearranging Beer's Law as follows:

$$\epsilon = A / [C]l = 2.3 / 0.5 \times 10^{-4} = 46000 \text{ mol}^{-1} \text{ dm}^3 \text{ cm}^{-1}$$

Identification of the absorption responsible for permanent fading

Degassed solutions of the dyes in a quartz cell faded quickly, with complete loss of colour in less than two hours for [IV]. However, according to the Albini,⁹ irradiation of the long wavelength absorption band of donor acceptor azo dyes has no permanent effect and photofading begins to occur only with ultraviolet light at 312 nm and shorter wavelengths. To confirm this, a glass filter was placed in front of the cell containing the dye solution. The transmittance of light through the glass filters can be seen in Figure 2.10 along with transmittances of some UV filters.

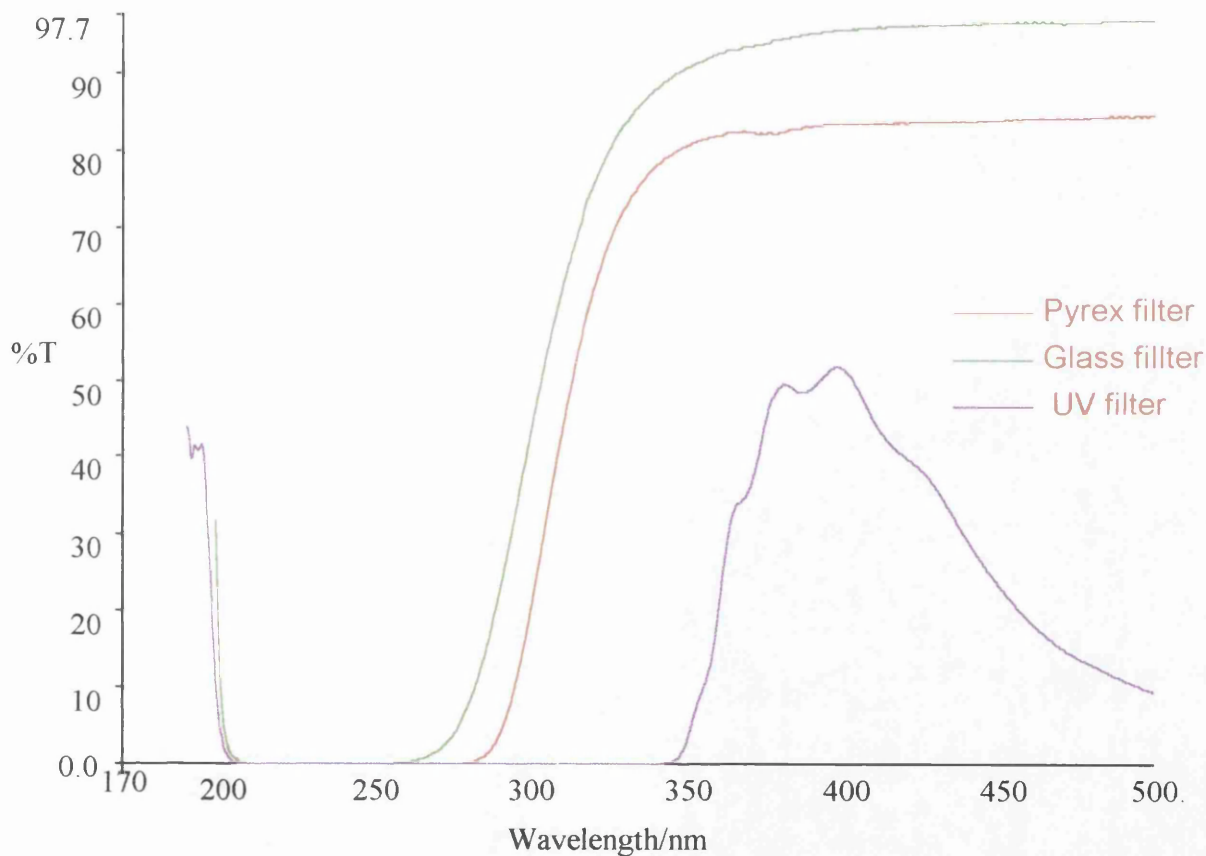


Figure 2.10 The transmittance of ultraviolet light through UV filters.

The glass microscope slide filter had 0 % transmittance of light below 250 nm. The second absorption band of the azobenzene dyes have wavelengths, which range from 276 nm for dyes [III], [IV], [VI] and [VIII] to 307 for [I]. The light transmitted through the glass filter at 276 nm is 3.3% and rises to 70% at 307 nm. Since this filter allows limited irradiation of the second absorption band, a Pyrex filter was used to decrease the radiation allowed through to the sample

solution. The Pyrex filter has 0.01% transmittance at 276 nm, but still 33% transmittance at 307 nm. However the Oriel UV filter, cuts out all light between 200 nm and 335 nm and transmittance does not rise above 1% until 350 nm. As a result, only the long wavelength absorption band was irradiated when a UV filter was employed. As would be expected from Albini's work,⁹ there is little if any permanent photofading under these conditions.

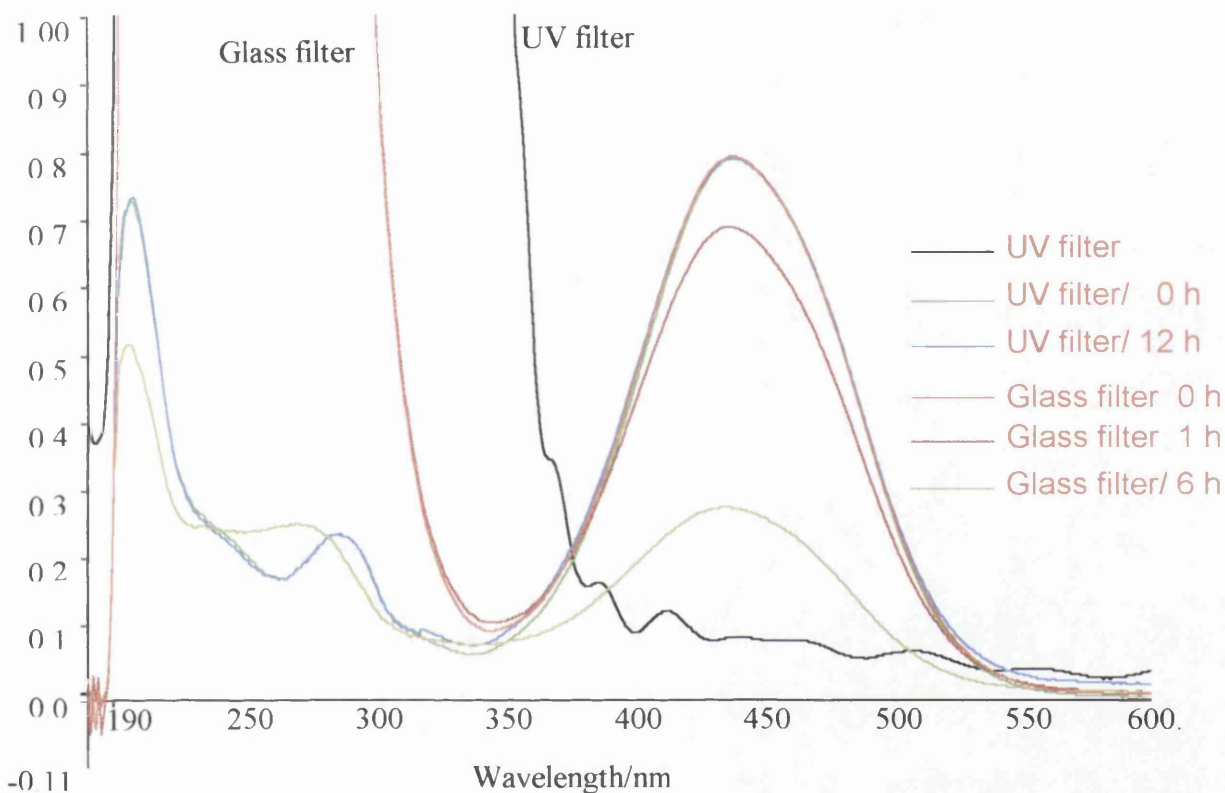


Figure 2.11 Comparison of photofading behaviour of [VII] in degassed methanol when irradiated through glass and UV filters using a Xe lamp.

Figure 2.11 shows the changes in the absorption spectra of [VII] when irradiated through glass and UV filters. Using a UV filter, the absorbance of [VII] after an irradiation time of 12 hours, is exactly the same as before start of irradiation. Irradiation through a glass filter produces permanent loss of colour for [VII] but at a much slower rate than when no filter is present. The rate of photofading of [IX], through a glass filter is too low to measure. The half-lives for the dyes in methanol for photofading with various filters are given in Table 2.5.

Table 2.5 The half-lives of azobenzene dyes in de-oxygenated methanol at room temperature irradiated through UV filters.

| Filter | None | Glass | Pyrex | UV |
|--------|----------------------------|-----------|-------|-----------|
| Dye | Half-life $\tau_{1/2}$ / h | | | |
| [I] | 1.11 | 14.7 | | No fading |
| [IV] | 0.87 | 7.7 | 18.2 | 42.4 |
| [VII] | 0.86 | 5.8 | | No fading |
| [IX] | 1.12 | No fading | | No fading |

For [I] though, some permanent loss of colour does occur. This is probably due to some transmittance of light at around 300 nm, which is therefore able to irradiate both the long wavelength and second absorption bands. An experiment where a quartz cuvette containing a methanol solution of [I] was irradiated with an argon laser at 514 nm for 8 hours produced no change in the absorbance value of the dye at λ_{max} , as can be seen from Figure 2.12.

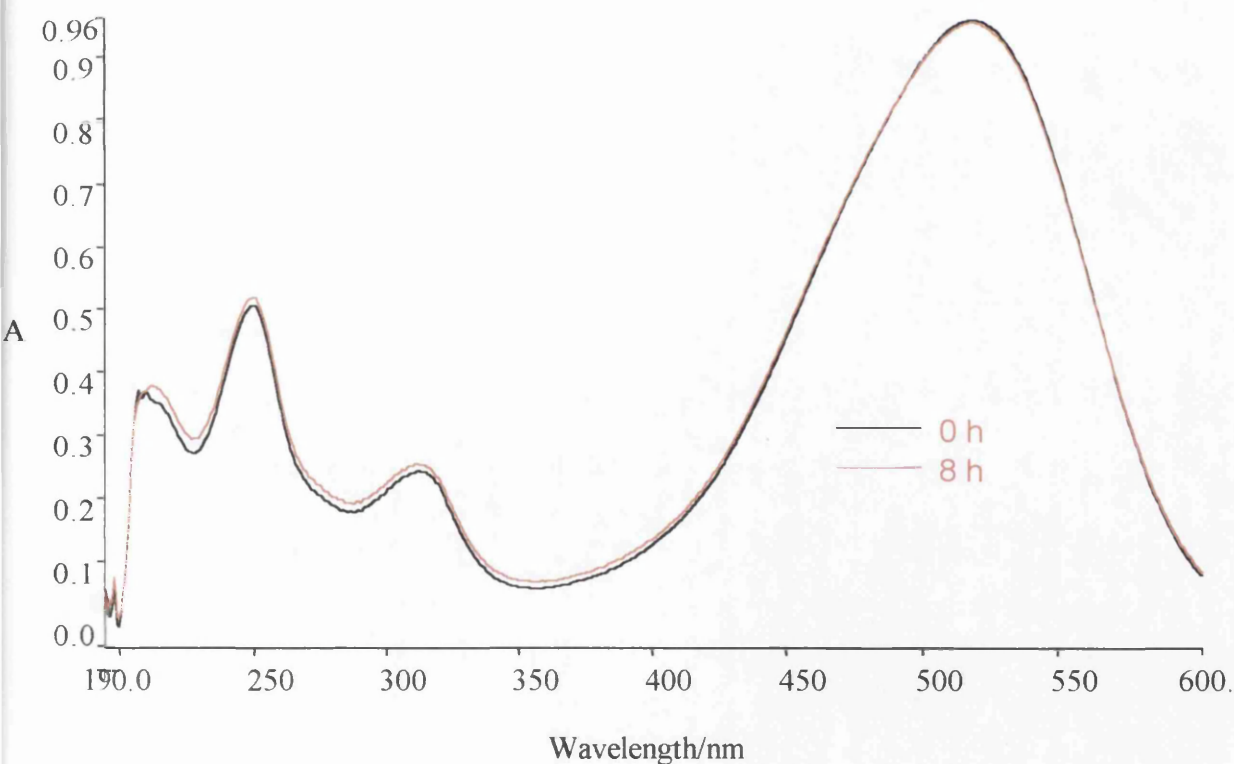


Figure 2.12 Absorption spectra of [I] before and after 8 hours laser irradiation at 512 nm

The advantage of using the laser for irradiation is that a very narrow spectral range, the long wavelength band at its λ_{max} , is selectively irradiated. Since irradiation of the 1st absorption band at 512 nm gave no permanent fading, it can be concluded that it is irradiation of the second absorption band which is responsible for causing permanent fading in the case of [I]. A methanol solution of [VII] does exhibit a permanent loss of colour despite the presence of the glass slide filter, though the half-life is an order of magnitude longer than when no filter is present. Irradiating through a UV filter however, causes a cessation of photofading which suggests that some light penetrates the glass filter to irradiate the second absorption band and cause fading, but this is not possible when the UV filter is used. Photofading of [IV] still occurs with both glass and UV filtration of the light, with the half-life of the dye similar when filtered by the Pyrex and UV filters. This suggests that irradiation of the second absorption band is important in the photofading mechanism, but that permanent photofading is also caused by irradiation of light at above 350 nm in the case of [IV].

A methanol solution of [I] fades very slowly when the glass filter is used and there is no detectable fading of dye 9 in the 12 hour duration of the experiment with a glass filter.

Therefore dyes [I] and [IX] and [VII] undergo permanent photofading only with UV irradiation, and the rate of photofading is much greater when the irradiation wavelength is shorter than 315 nm. Photofading of [IV] is also predominantly caused by irradiation at wavelengths shorter than 315, but some photofading does occur at longer wavelengths, albeit at a reduced rate.

Kinetic experiments

Results using nitrogen as a degassing agent proved inconsistent and nitrogen was replaced by argon gas. Argon has the advantage of being heavier than air and should therefore form a layer of argon gas between the dye solution and the atmosphere, preventing oxygen from the air infusing into the solution. Initial experiments with most dyes produced linear fading curves, for example for [IV] in Figure 2.13.

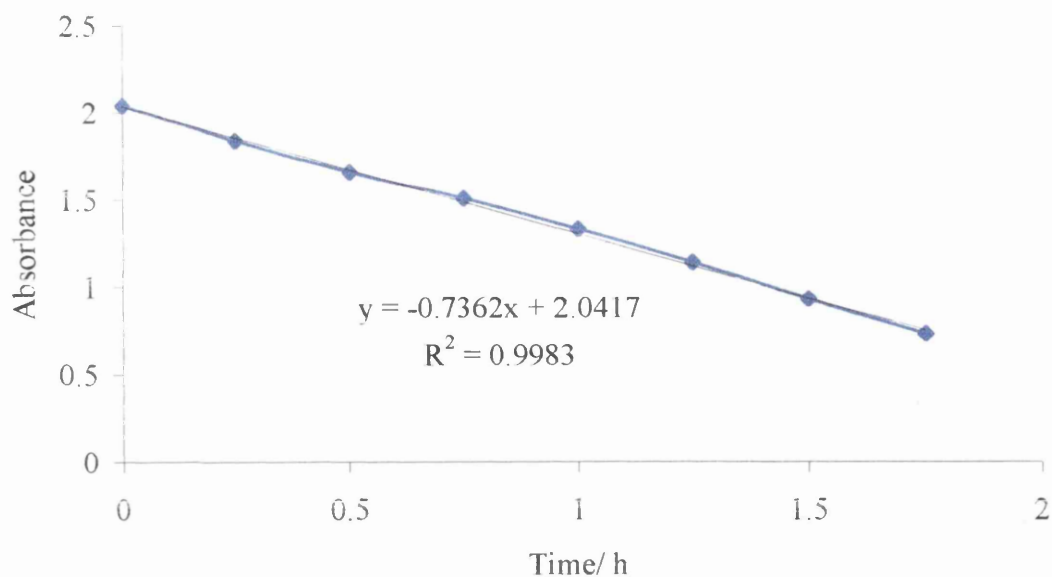


Figure 2.13 The variation of the absorbance with irradiation time of a partially degassed solution of [IV] in methanol at 25°.

A straight line is fitted to the experimental data points using a curve fitting package¹⁰ and the equation for this line and its correlation coefficient R^2 are displayed in Figure 2.13.

This linear relationship between the absorbance of the dye solution at its λ_{\max} and the time of irradiation indicates zero order kinetics for the photoreaction, where the absorbance varies linearly with time. This implies the following expression for the rate law.

$$\text{Rate} = d[A]/dt = -k \quad \text{Equation (2-2)}$$

Where $[A]$ is the absorbance at λ_{\max} of the dye and k is the rate constant for the reaction. This expression can be then be integrated according to Equation (2-3),

$$\int d[A] = -\int k dt \quad \text{Equation (2-3)}$$

to give the solution in Equation (2-4)

$$[A] = -kt + C \quad \text{Equation (2-4)}$$

where C is also a constant.

Equation (2-4) has the same form as the general straight line equation $y = mx + C$, where m is the gradient of the line and C is the y-axis intercept. Hence a plot of $[A]$ against time, as in Figure 2.13, yields the constants k and C . The rate constant k , is generated by calculating the gradient of

the straight line in Figure 2.13, and the constant C , is equal to the absorbance where the line intercepts the y axis, that is, at time $t = 0$. At this time, C is equal to the absorbance of the dye before irradiation, or the initial absorbance A_0 . Thus for the above case of [IV], the straight line has an equation of the same format as Equation (2-4), with $k = 0.7362$ and $C = 2.0417$.

It is notoriously difficult to obtain consistent results for degassed solutions, as even a tiny amount of oxygen significantly affects rates of photofading⁹. The degassing conditions therefore had to be optimised to exclude oxygen. These conditions included the flow rate of argon through the solution, (too little results in some oxygen remaining in solution), and the degassing time. The fading curve in Figure 2.13 were found to be invalid for fully degassed solutions and must have contained some dissolved oxygen. These assertions were made after further experiments with [IV] gave photofading profiles such as that shown in Figure 2.14.

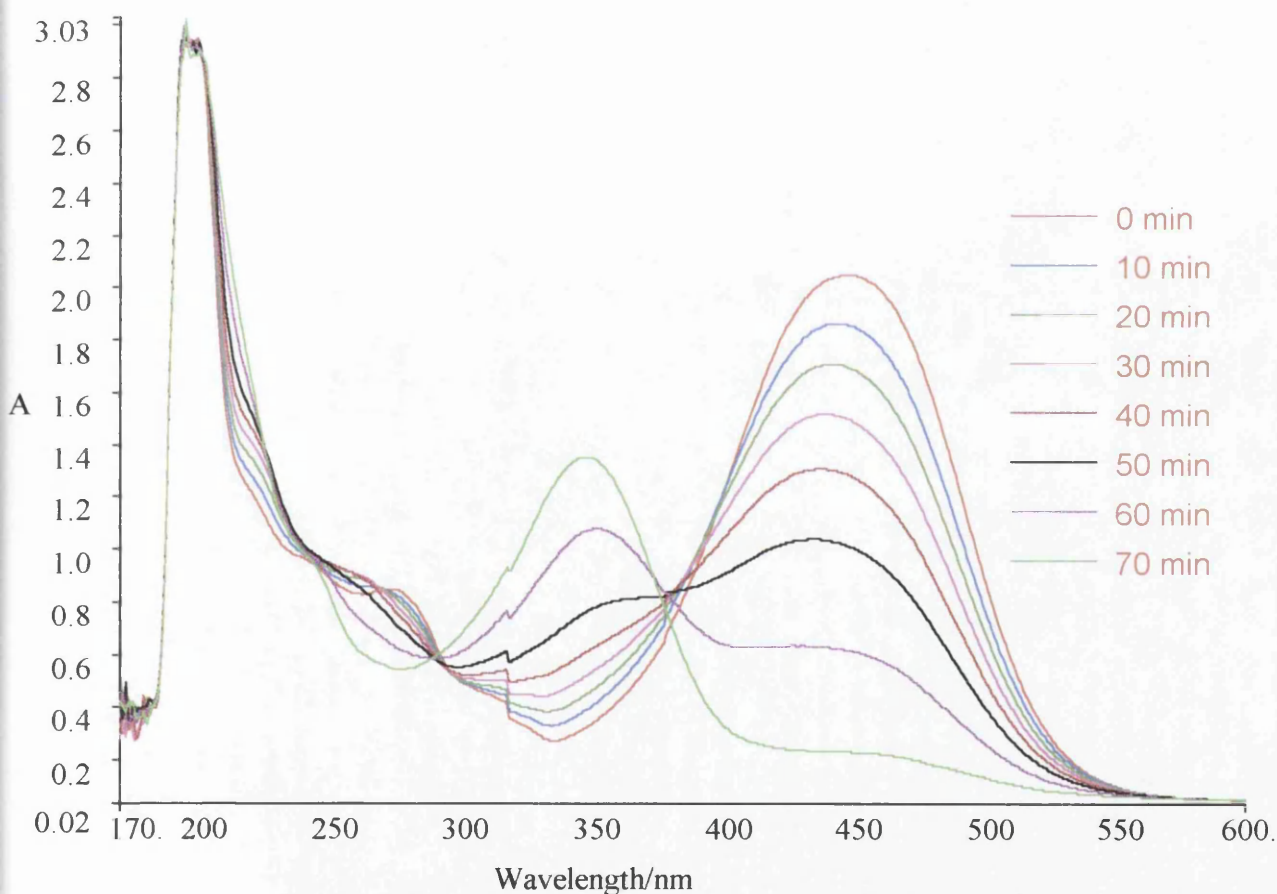


Figure 2.14 The changes in the absorption spectrum with irradiation time of a degassed methanolic solution of [IV].

A plot of the Absorbance at λ_{max} against irradiation time for this experiment gave the photofading curve shown in Figure 2.15. Here, in contrast to the linear plot previously obtained, the variation in absorbance with irradiation time produces a photofading curve. The rate of photofading increases as the irradiation time increases, resulting in far quicker rates of fading than had been observed in previous experiments. A curve fitting program¹⁰ was used to generate a curve to fit the data points of the photofading curve of [IV] in Figure 2.15. This curve is given by the polynomial equation displayed in Figure 2.15.

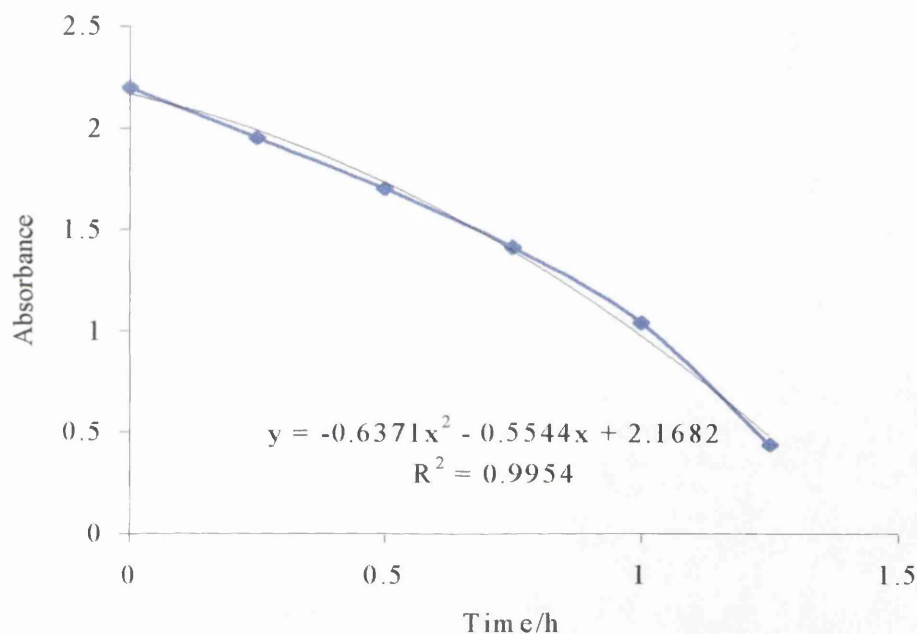


Figure 2.15 The variation in absorbance with irradiation time of a methanol solution of [IV] under anaerobic conditions.

Since it is not possible to directly compare the rates of reaction for linear and polynomial photofading curves, it is necessary to define some measure of the relative photo-stability of the dyes. The parameter used will therefore be the half-lives and lifetimes of the dyes defined as follows.

The **lifetime** of the dye (given the symbol τ), is the time at which the absorbance of the dye solution becomes zero.

The **half-life** of the dye (given the symbol $\tau_{1/2}$), is the time taken for the **absorbance** A of the dye to reduce to half its initial value.

For a linear fading curve, the lifetime can be determined by calculating from the graph the irradiation time at which the absorbance (A) is equal to zero. Substituting $A = 0$ and $C = A_0$ into Equation (2-4) we obtain,

$$0 = kt + A_0 \quad \text{Equation (2-5)}$$

which rearranges to

$$t = -A_0/k = \tau \quad \text{Equation (2-6)}$$

Considering the absorption/irradiation time plot in Figure 2.13, as an example, the values $k = -0.7362$ and $A_0 = 2.0417$ can be substituted into Equation (2-6) for the lifetime of [IV] in this experiment.

$$\tau = -2.0417/-0.7362 = 2.77 \text{ hours.} \quad \text{Equation (2-7)}$$

The half-life is the time t , where the absorbance A is half the experimentally measured initial absorbance A_0 . The half-life can be determined therefore, by calculating from the graph the irradiation time at which the absorbance (A) is equal to $(A_0/2)$.

The half-life can be calculated by substituting $A_0/2$ for A and A_0 for C in Equation (2-4), and rearranging to give the general solution in Equation (2-8)

$$t = \tau_{1/2} = (A_0/2 - A_0)/k \quad \text{Equation (2-8)}$$

Again considering the absorbance versus irradiation time in Figure 2.13, the experimental value of A at time $t = 0$ is $A_0 = 2.04$ and therefore $A_0/2 = 1.02$, which can then be substituted for A into Equation (2-8) to find $t = \tau_{1/2}$.

$$t = \tau_{1/2} = (1.02 - 2.0417)/-0.7362 = 1.387 \text{ hours} \quad \text{Equation (2-9)}$$

As can be seen from Figure 2.15, the photofading curve of dye 4 with more rigorous degassing can be approximated by a polynomial. The general form of a polynomial is given in Equation (2-10)

$$y = ax^2 + bx + c \quad \text{Equation (2-10)}$$

Which can be rewritten in terms of absorbance, A and time, t as,

$$A = at^2 + bt + c \quad \text{Equation (2-11)}$$

The lifetime of the dye is again found by substituting $A = 0$ in Equation (2-11). The resulting quadratic equation can then be solved for t using Equation (2-12)

$$t = [-b \pm \sqrt{(b^2 - 4ac)}/2a \quad \text{Equation (2-12)}$$

The half-life is calculated in a similar way, except here A is substituted by $A_0/2$ in Equation (2-11) before rearranging to give Equation (2-13),

$$0 = at^2 + bt + (c - A_0/2) \quad \text{Equation (2-13)}$$

which can then be solved for t using Equation (2-12).

To exemplify these calculations consider the quadratic equation for the photofading curve of dye [IV], in Figure 2.15.

$$y = -0.6371x^2 - 0.5544x + 2.1682 \quad \text{Equation (2-14)}$$

which in terms of A and t can be rewritten as

$$A = -0.6371t^2 - 0.5544t + 2.1682 \quad \text{Equation (2-15)}$$

To find the lifetime of the dye, $A = 0$ is substituted in Equation (2-15) and then this quadratic can be solved for t using Equation (2-16) e.g.

$$t = -(-0.5544) \pm [\sqrt{(0.5544^2 - 4(-0.6371)(2.1682))}] / 2(-0.6371) \quad \text{Equation (2-16)}$$

which gives solutions of t to be,

$$t = -2.33 \text{ or } t = 1.46$$

Since the irradiation time must be a positive quantity, then the only real solution for the half-life of the dye is $t = \tau = 1.46$ hours.

The half-life is calculated by substituting A_0 for A in Equation (2-15) and rearranging to give Equation (2-17).

$$0 = -0.6371t^2 - 0.5544t + (2.1682 - A_0/2) \quad \text{Equation (2-17)}$$

The value of A_0 is 2.2 and therefore, $A_0/2 = 1.1$ and the constant term c becomes 1.0682. The quadratic Equation (2-17) can thus be solved for t using Equation (2-18).

$$t = -(-0.5544) \pm [\sqrt{(0.5544^2 - 4(-0.6371)(1.0682))}] / 2(-0.6371) \quad \text{Equation (2-18)}$$

This yields the solutions $t = -1.80$ and $t = 0.93$ of which only the later can be a real solution, and therefore $\tau_{1/2} = 0.93$ hours.

The pattern of fading seen for dyes [VI] and [VII] is very similar to the photofading behaviour observed for [IV], and this similarity is illustrated in Figure 2.16. Both dyes produce a photofading curve where the initial rate of fading is relatively slow, compared to the rate of fading as the irradiation proceeds.

The non-linear relationship between the absorbance of the long wavelength absorption peak at its λ_{max} and the time of irradiation of the sample dye solution implies that the kinetics is not zero order for these dyes. The similarities in the photofading curves of these dye are perhaps not surprising, as all three of these dyes contain the 2'-nitro substituent and as such, might be expected to undergo similar fading patterns and have similar kinetic behaviour.

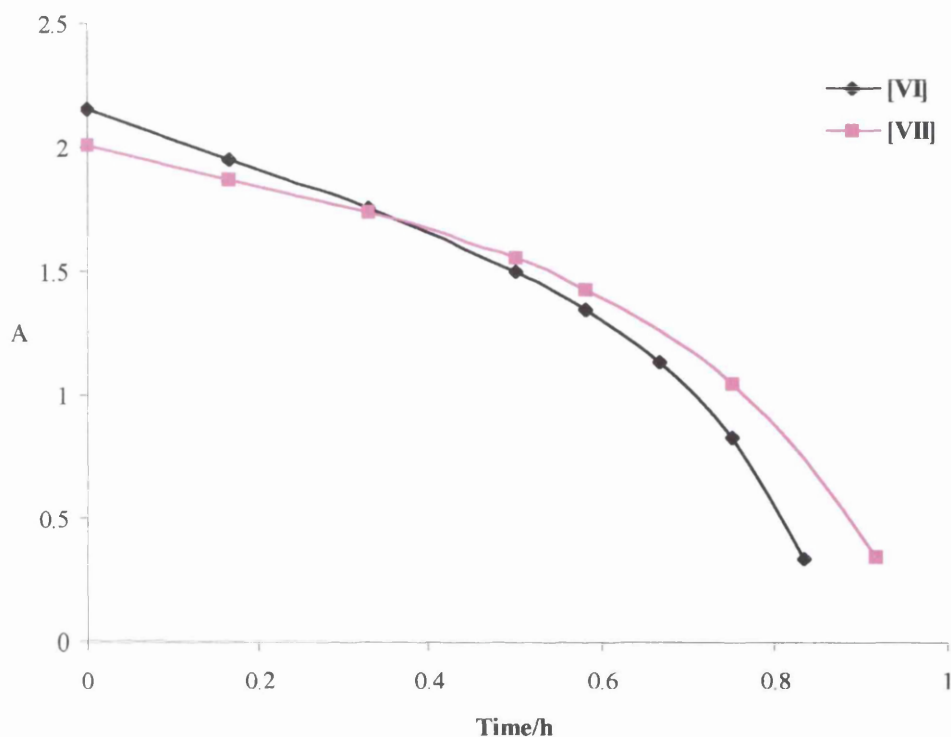


Figure 2.16 The variation in absorbance with irradiation time for dyes [VI] and [VII] in methanol under anaerobic conditions.

Structure [II] also contains the 2'-nitro group and has a similar photofading curve to the three other 2'-nitro substituted dyes.

The quadratic equations generated to fit the data points of the photofading curves of dye [III], [IV], [VI] and [VII] are given in Table 2.6. These quadratic equations are then used to calculate the lifetimes and half-lives of the dyes as in the above example for [IV].

| Dye | Expression | Equation | τ / h | $\tau_{1/2} / h$ |
|-------|-------------------------------------|------------------------|------------|------------------|
| [III] | $A = -3.426t^2 + 1.0965t + 1.8689$ | Equation (2-19) | 0.92 | 0.69 |
| [IV] | $A = -0.6371t^2 - 0.6189t + 2.0163$ | Equation (2-20) | 1.27 | 0.80 |
| [VI] | $A = -2.3657t^2 - 0.0411t + 2.0929$ | Equation (2-21) | 0.93 | 0.65 |
| [VII] | $A = -1.2514t^2 + 0.1386t + 1.9925$ | Equation (2-22) | 1.31 | 0.95 |

^a τ is the lifetime and $\tau_{1/2}$ is the half-life

In reality, the absorbance of the irradiated solution at λ_{\max} will rarely degrade to zero, as photofading products may have a small absorbance at this wavelength. Thus the lifetimes reported for the dyes above, which are extrapolated from the photofading curves, are somewhat artificial. However, they do give a more accurate assessment of the rapid fading towards the end of the photoreaction. Thus for dyes with non-linear photofading curves, it is beneficial to consider both the half-life and lifetime.

Considering the changes in the uv/visible spectrum that occur as fading proceeds, it was seen that for some dyes, there was a decrease in the intensity of the long wavelength absorption band, but the wavelength of this band remained essentially the same. But for other dyes, a hypsochromic shift of the band accompanied its decrease in intensity. After sufficient fading time the appearance of new absorption peaks, which absorbed in different regions to the original dye, were detected. These peaks indicate the presence of breakdown products of the original dye. The three dyes that contain the 2'-nitro substituent undergo very similar changes in their absorption spectra, with an initial decrease in the intensity of the long wavelength absorption peak, followed by a relatively rapid loss in colour to give a product absorption peak in the uv region of the spectrum at around 360-400 nm. These changes can be seen in Figure 2.14, for [IV] and in Figure 2.17 for [VI].

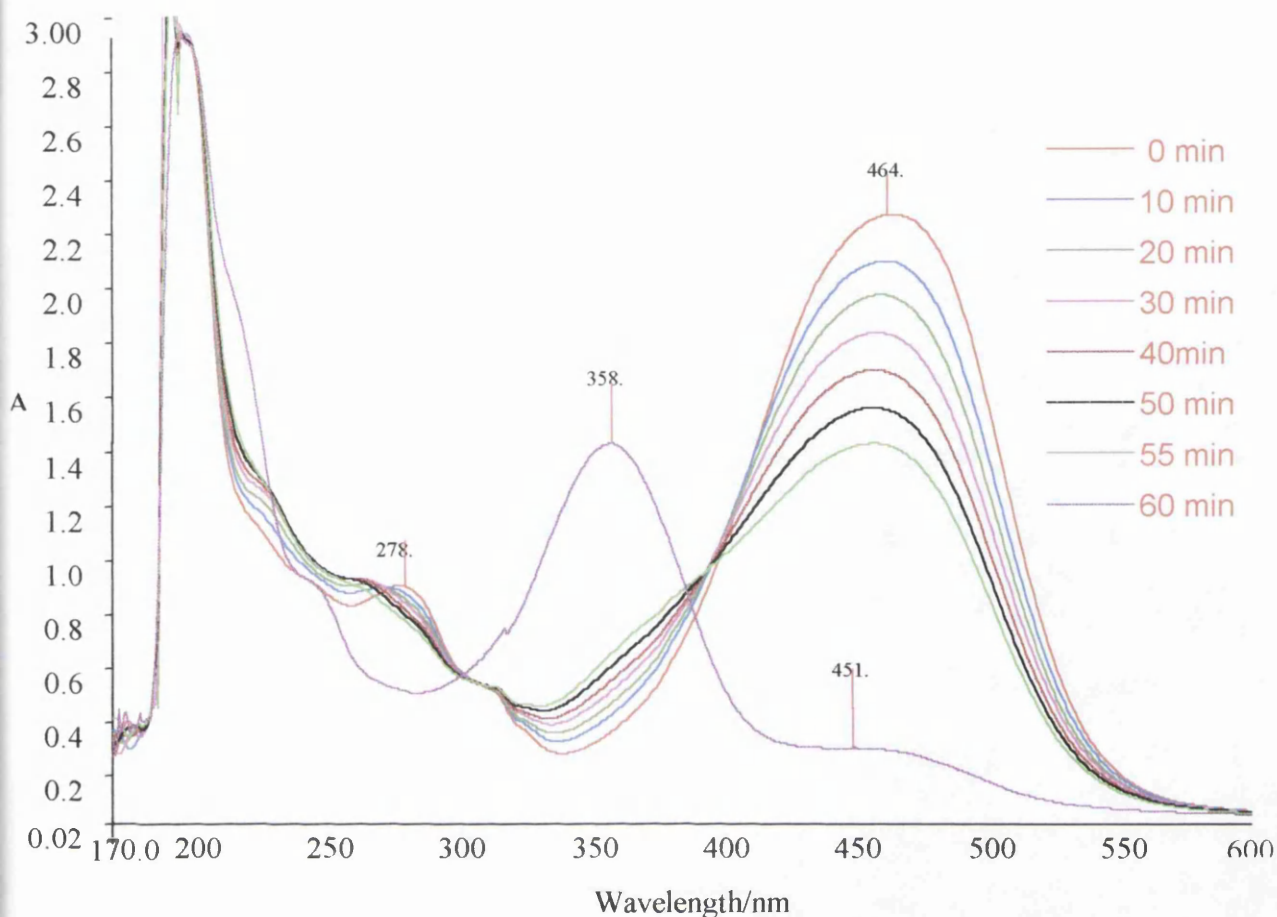


Figure 2.17 The changes in the absorption spectrum of a methanol solution [VI] on irradiation of the solution under degassed conditions.

In view of the similarities in the photofading behaviour of the dyes containing the 2'-nitro substituent, it might be reasonable to expect some of the other azo dyes that have the same substituent groups, for example dyes that contain the 4'-nitro substituent, to have some similarities in their photofading behaviour. The variation in absorbance with irradiation time for dyes containing 4'-nitro substituents is shown in Figure 2.18.

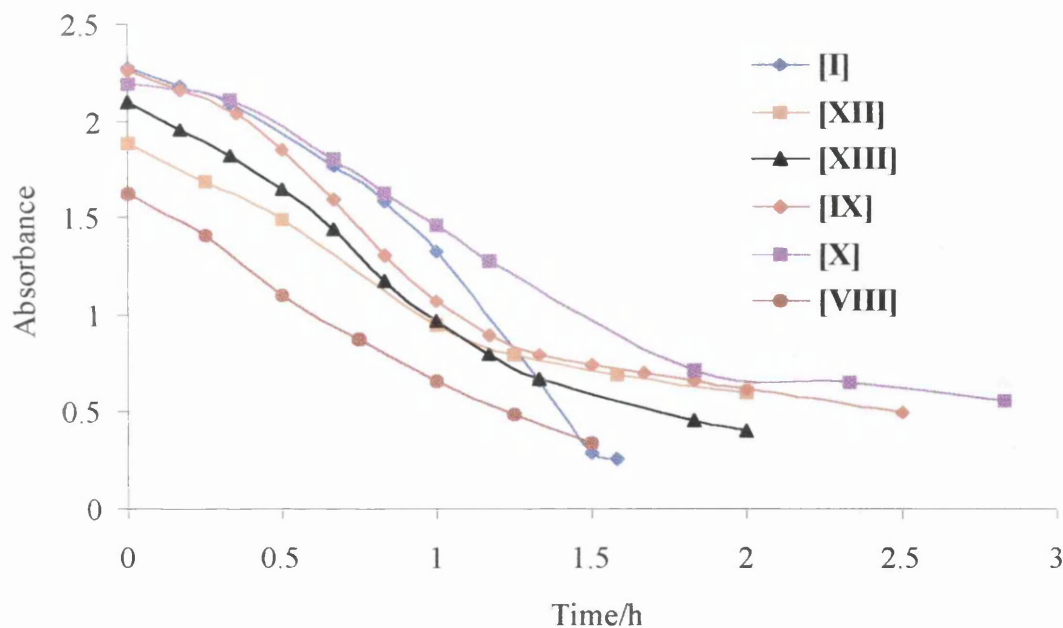


Figure 2.18 The variation in absorbance with irradiation time of 4'-nitro substituted dyes [VIII], [IX], [XII], [XIII], and [X], photo-faded under anaerobic conditions in methanol.

The dyes, [VIII], [IX], [XII], [XIII], and [X], which contain the 4'-nitro substituent on the acceptor phenyl ring, display similar fading behaviour to one another. In each case, an initial slow start to fading is followed by a period of relatively quick fading, before the photofading rate becomes very slow. The photo-fading curve for [I], which also contains the 4'-nitro substituent has a slightly different shape when compared to the other dyes. Solutions of [I] fade considerably quicker than the other dyes containing the 4'-nitro group. This is perhaps not entirely surprising, as [I] also has an SMe substituent on the donor phenyl ring. This donor ring substituent may affect the order of the reaction¹¹, and the heavy atom sulphur may increase the rate of photochemical transitions such as intersystem crossing, because of the large spin orbit coupling,¹² which may be involved in the fading of the dye. The changes in the spectra, on photo fading of the 4'-nitro dyes, are also quite different to those for dyes [II], [IV], [VI] and [VII]. The 4'-nitro dyes undergo a hypsochromic shift initially, before a double absorption peak is formed, which then undergoes a slow decrease in its intensity but remains at the same wavelength. This is illustrated for [IX] in Figure 2.19.

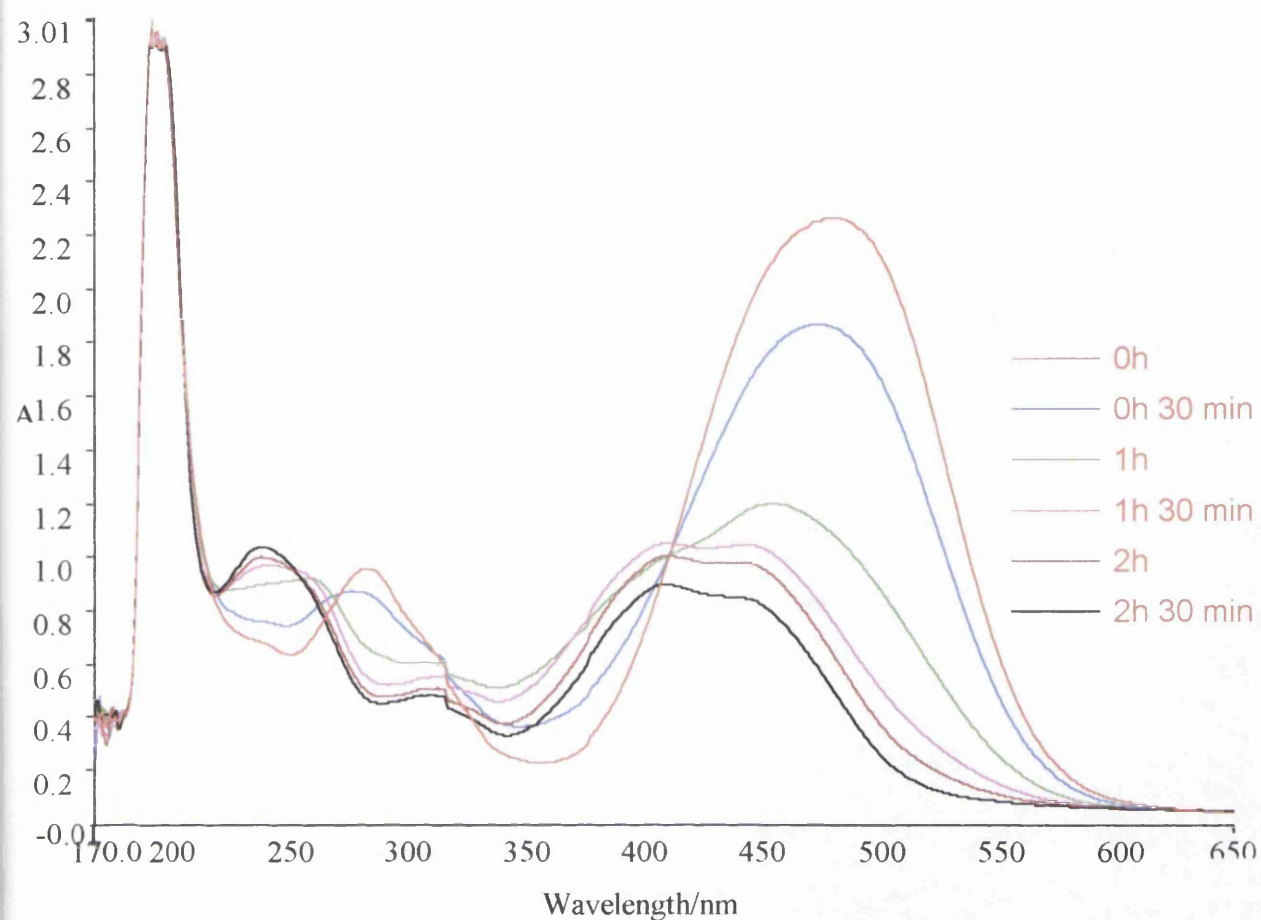


Figure 2.19 The variation in the uv/visible absorption spectrum with irradiation time of a methanolic solution of **[IX]** under degassed conditions.

The equations fitted to the photofading curves of the 4'-nitro containing dyes are given below, along with the half-lives and lifetimes for each dye calculated from these equations.

The first dye in the series is **[VIII]**, which has a linear photofading curve,

$$A = -0.8814t + 1.5882 \quad \text{Equation (2-23)}$$

From which the lifetime and half-life are calculated to be:

$$\tau = 1.80 \text{ hours and } \tau_{1/2} = 0.88 \text{ hours}$$

For dyes **[VIII]**, **[IX]**, **[XII]**, **[XIII]**, and **[X]**, there are no solutions for the curve fitted quadratic equations for $A = 0$. Therefore, the linear portion at the end of the recorded photofading curve, (see Figure 2.18), is used to obtain a straight linear equation, from which the lifetime τ can be

found from the point at which this line intercepts the x axis. As an example of this method, consider the plot shown in Figure 2.20.

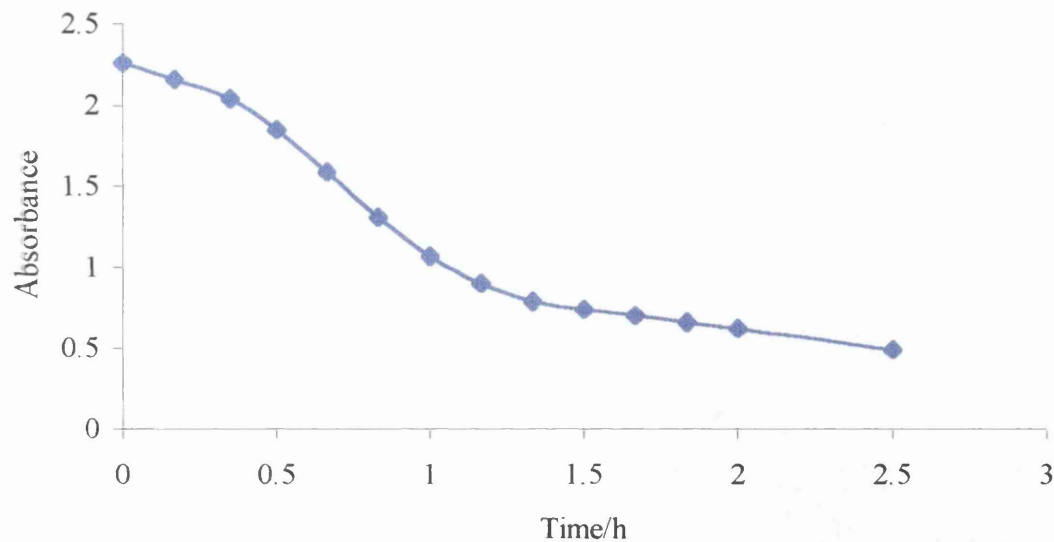


Figure 2.20 The variation in absorbance of a methanolic solution of [IX] at its λ_{\max} with irradiation time under anaerobic conditions.

Taking the linear portion of the curve as the last six data points, the liner fading plot in Figure 2.21 is produced, and the equation of this straight line can then be used to calculate the lifetime of the dye. The equation shown in Figure 2.21 can then be written in terms of A and t as:

$$A = -0.2536t + 1.1246$$

Equation (2-24)

Which gives the lifetime of [IX] as:

$$\tau = 4.46 \text{ hours}$$

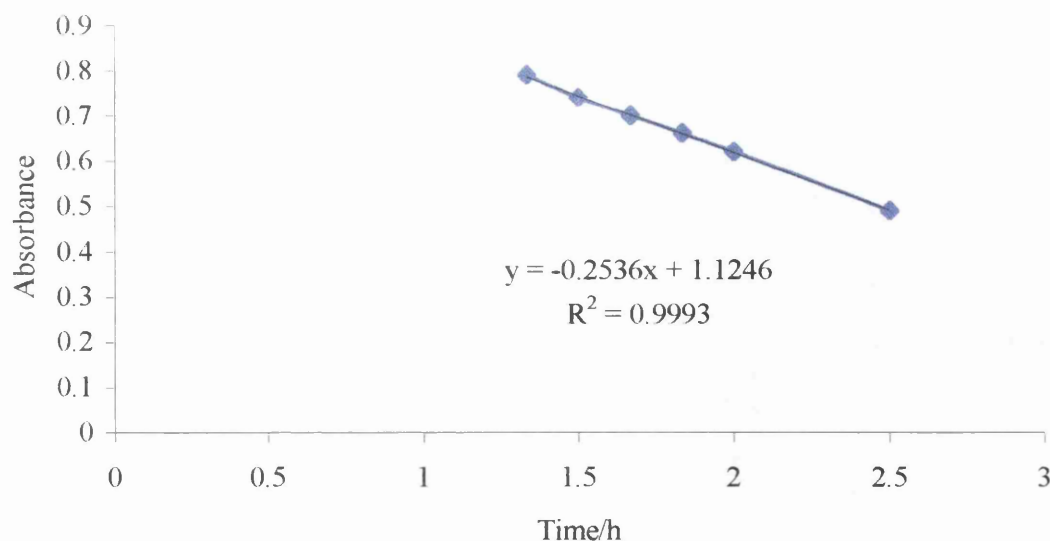


Figure 2.21 The linear portion of the photofading curve of [IX] in methanol under anaerobic conditions, taken from the last six data points of the full fading curve of [IX] (see Figure 2.20).

The half-life of the dye is calculated in the same way as for the previous dyes, using the quadratic equation fitted to the data points in Figure 2.20, and given in Equation (2-25).

$$A = 0.331t^2 - 1.593t + 2.4178$$

Equation (2-25)

From which, the half-life is calculated to be:

$$\tau_{1/2} = 1.03 \text{ hours}$$

The other dyes in the series can be treated in a similar way. For dyes [XII], [XIII], and [X] the quadratic equations and half-lives calculated from them are given in Table 2.7. Algebraic expressions for the linear end part of the fading curve, and lifetimes calculated from them are also given in Table 2.7.

Table 2.7 Polynomial and linear equations used to calculate half-lives and lifetime of dyes [X], [XII] and [XIII], under anaerobic conditions in methanol.

| Dye | Expression | Equation | τ / h | $\tau_{1/2}$ / h |
|--------|------------------------------------|------------------------|------------|------------------|
| [X] | $A = -0.9949t + 2.4519$ | Equation (2-26) | 6.6 | - |
| [X] | $A = 0.1397t^2 - 1.0478t + 2.34$ | Equation (2-27) | - | 1.48 |
| [XII] | $A = -0.2518t + 1.099$ | Equation (2-28) | 4.36 | - |
| [XII] | $A = 0.2692t^2 - 1.2195t + 1.9418$ | Equation (2-29) | - | 1.08 |
| [XIII] | $A = -0.4131t + 1.2184$ | Equation (2-30) | 2.95 | - |
| [XIII] | $A = 0.2617t^2 - 1.4431t + 2.1992$ | Equation (2-31) | - | 1.08 |

^a τ is the lifetime and $\tau_{1/2}$ is the half-life

There are two other dyes that contain the 4'-nitro group; [I] and [XVII]. As these dyes contain another substituent on the donor ring, in addition to the donor 4-amino group present in all the dyes, [I] and [X] are considered separately from the other 4'-nitro dyes. [XVII] also contains substituents at the 2' and 4 positions of the acceptor ring which may influence its kinetic behaviour.

The curve fitted quadratics, Equation (2-32) and Equation (2-33), derived from kinetic plots for [I] (Figure 2.22) and [XVII] (Figure 2.23) were used to calculate the lifetime and half-life of [I] and of [XVII] (see Table 2.8).

Table 2.8 Polynomial and linear equations used to calculate half-lives and lifetime of dyes [I] and of [XVII] under anaerobic conditions in methanol.

| Dye | Expression | Equation | τ / h | $\tau_{1/2}$ / h |
|--------|------------------------------------|------------------------|------------|------------------|
| [I] | $A = -0.7278t^2 - 0.2155t + 2.252$ | Equation (2-32) | 1.61 | 1.11 |
| [XVII] | $A = -3.0857t + 2.6457$ | Equation (2-33) | 0.86 | 0.44 |

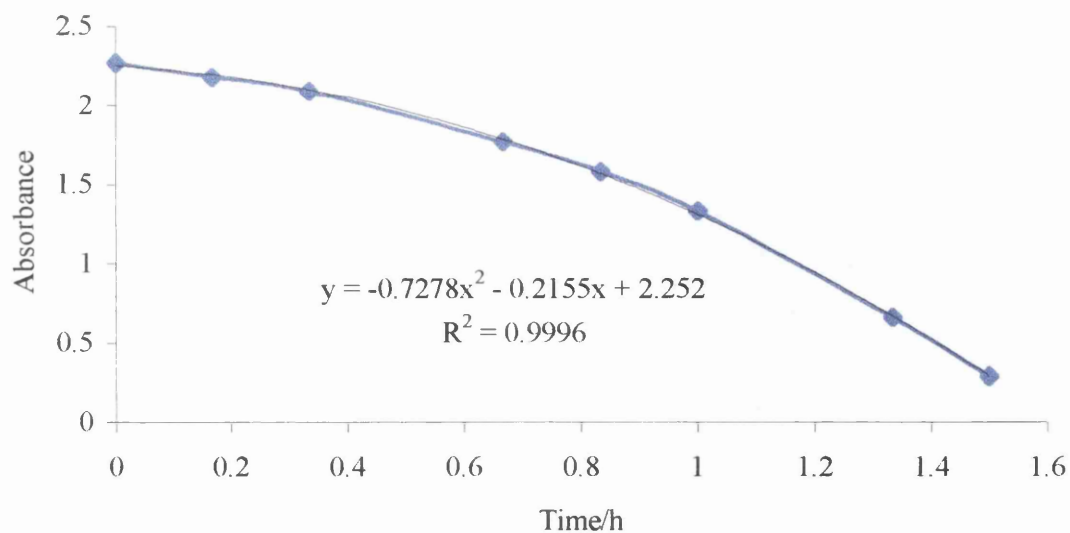


Figure 2.22 The variation in the absorbance at λ_{\max} of a methanol solution of dye **[II]** with irradiation time under anaerobic conditions.

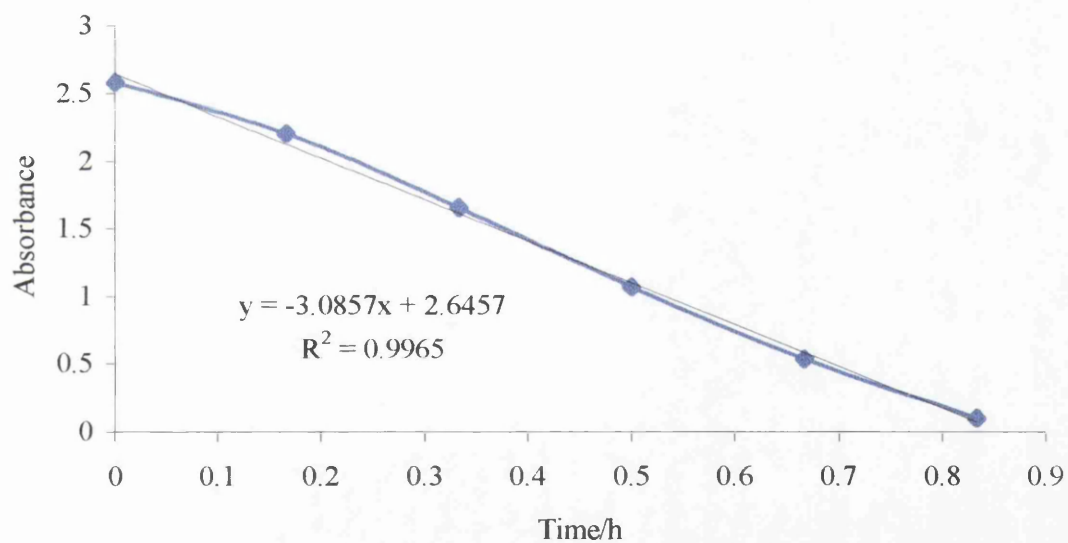


Figure 2.23 The variation in the absorbance at λ_{\max} of a methanol solution of dye **[XVII]** with irradiation time under anaerobic conditions.

It might be expected that **[III]** and **[V]** will exhibit a different pattern of photofading and kinetics than for the dyes with 4'-nitro or 2'-nitro substituents, and this is certainly the case. These dyes both contain the 4'-ester substituent, though the absorbance/ irradiation time plot of **[III]** (Figure

2.24) is virtually linear suggesting that the photofading of [III] obeys zero order kinetics, while the absorbance/ irradiation time plot of [V] (Figure 2.25) is non-linear.

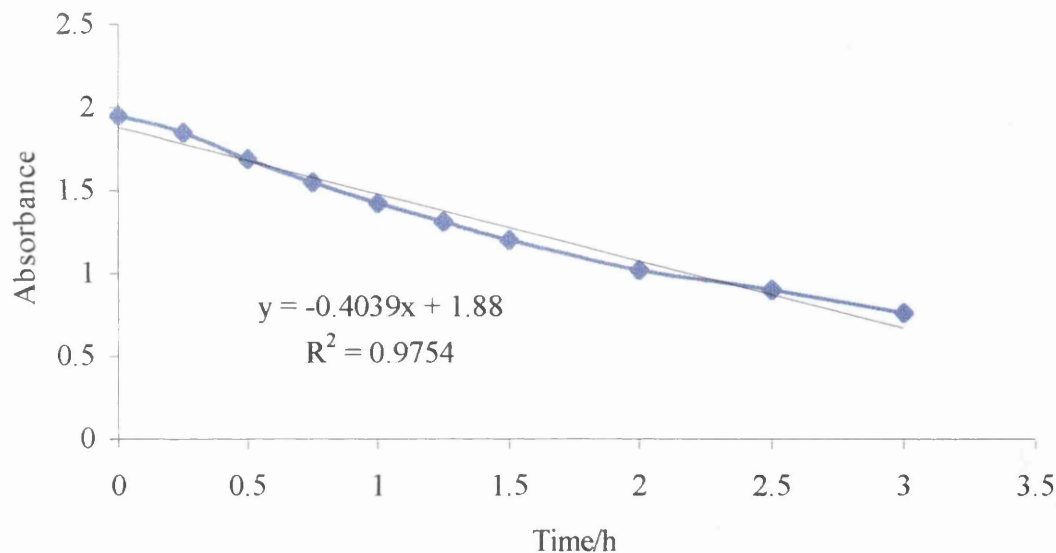


Figure 2.24 The variation in absorbance with irradiation time in hours of a methanolic solution of [III] under anaerobic conditions.

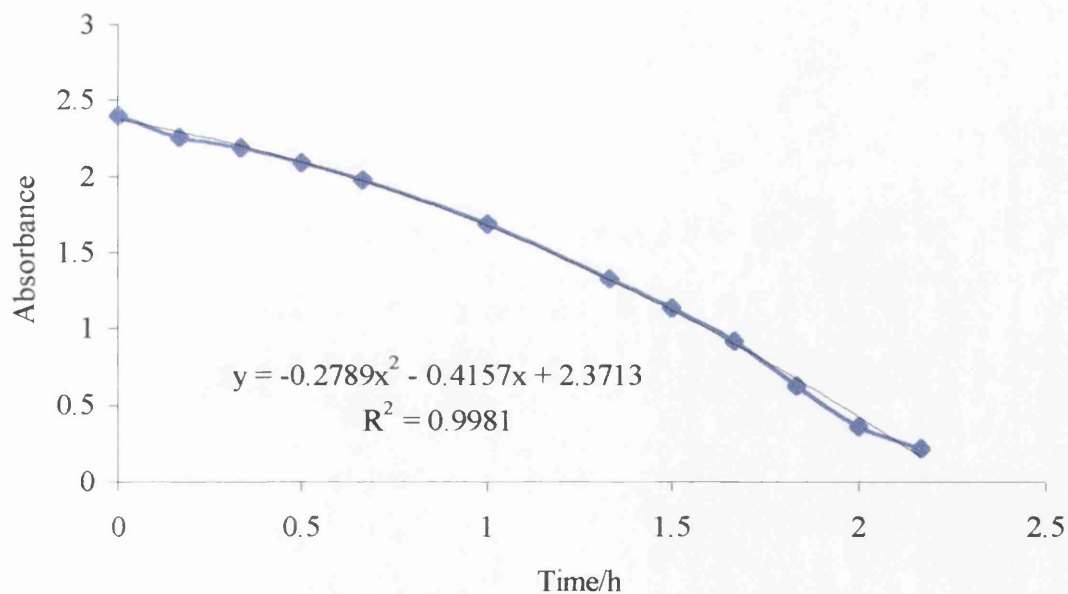


Figure 2.25 The variation in absorbance with irradiation time of a methanolic solution of [V] under anaerobic conditions.

A possible explanation for this is that, although [III] and [V] contain the same 4'-ester and 4-diethylamino groups, the presence of the 2-methyl and more importantly the 2'-nitro substituent may have a major influence on the photofading behaviour of these dyes.

Equation (2-34) and Equation (2-35) from the absorbance/ irradiation time plots of [III] and [V] were used to calculate their lifetimes and half-lives

Table 2.9 Polynomial and linear equations used to calculate half-lives and lifetime of [III] and [V] under anaerobic conditions in methanol.

| Dye | Expression | Equation | τ / h | $\tau_{1/2}$ / h |
|-------|-------------------------------------|-------------------------|------------|------------------|
| [III] | $A = -0.5514t + 1.992$ | Equation (2-34) | 3.61 | 1.8 |
| [V] | $A = -0.2789t^2 - 0.4157t + 2.3713$ | Equation (2-35) | 2.26 | 1.44 |

The changes in these spectra on photofading will be discussed further in Chapter 3, when considering the photo fading products of the dyes.

The remaining azobenzene type dyes are [XI] and [XIV]. The aminoazobenzene [XIV] differs from the dyes previously considered, as it contains only the 4-alkylamino substituent and no substituents on the acceptor ring. [XI] is unusual as in place of the electron acceptor substituent at the 4 position of the acceptor ring, encountered in many of the other dyes, it has an electron donating amino group. This gives [XI] the unusual distinction of having 2 donor groups. [XIV] fades slowly and there is no major shift observed in the wavelength of the long wavelength absorption band - only 6 nm (408.9 nm to 402.9 nm) after a fading time of 2 hours 40 minutes.

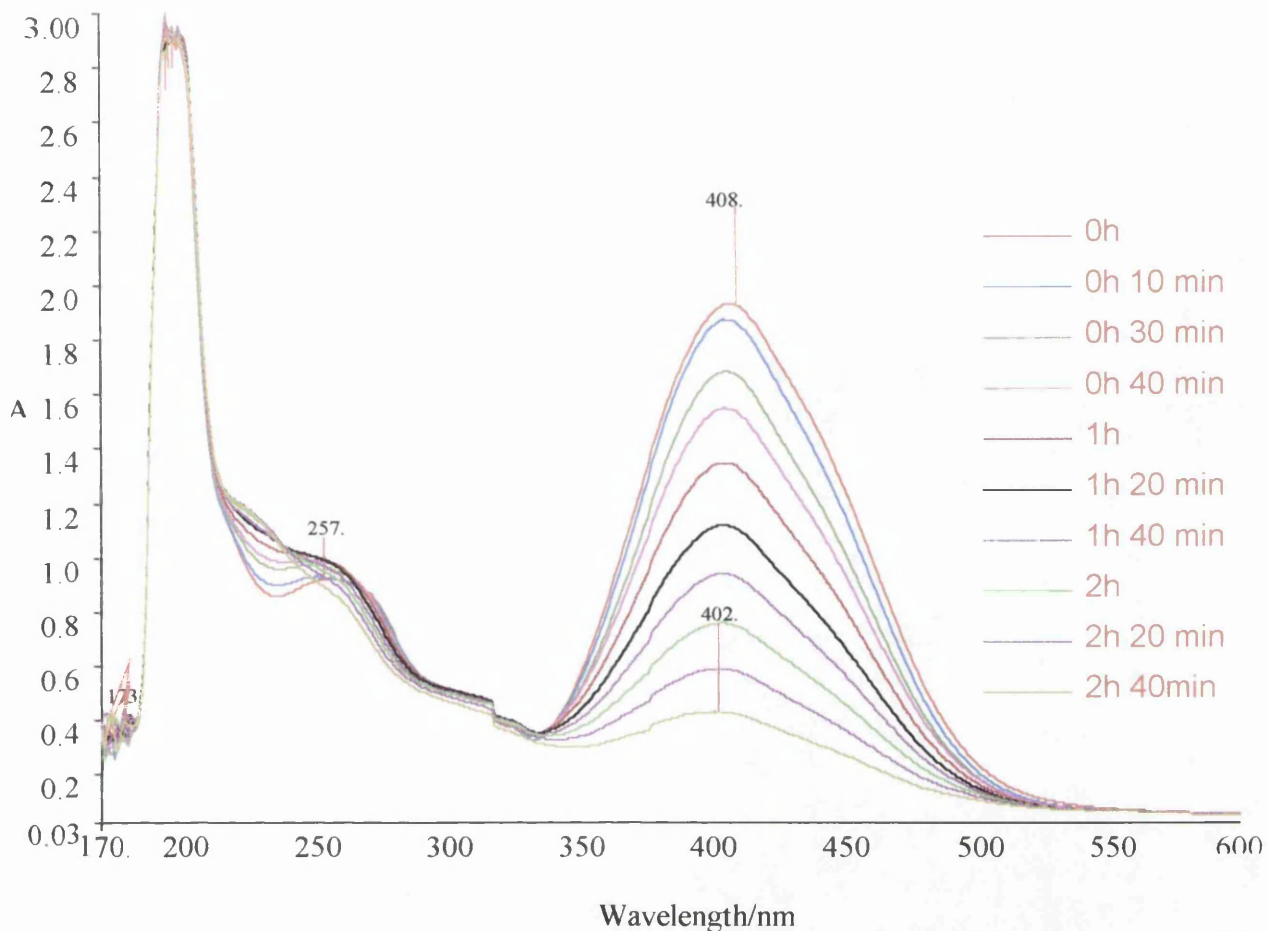


Figure 2.26 The variation in the uv/visible absorption spectrum with irradiation time of a methanol solution of [XIV] under anaerobic conditions.

A similar pattern of fading is seen for [XI] (Figure 2.27) with an almost negligible hypsochromic shift in wavelength from the spectrum of the original dye to the spectrum after 2 hours irradiation time. Note the presence of the two absorption peaks in the visible region of the spectrum occurring at 445 nm and 415 nm. This unusual phenomenon is probably due to the presence of the two donor amino groups. The electronic effects of the two donor groups will be discussed further in Chapter 3.

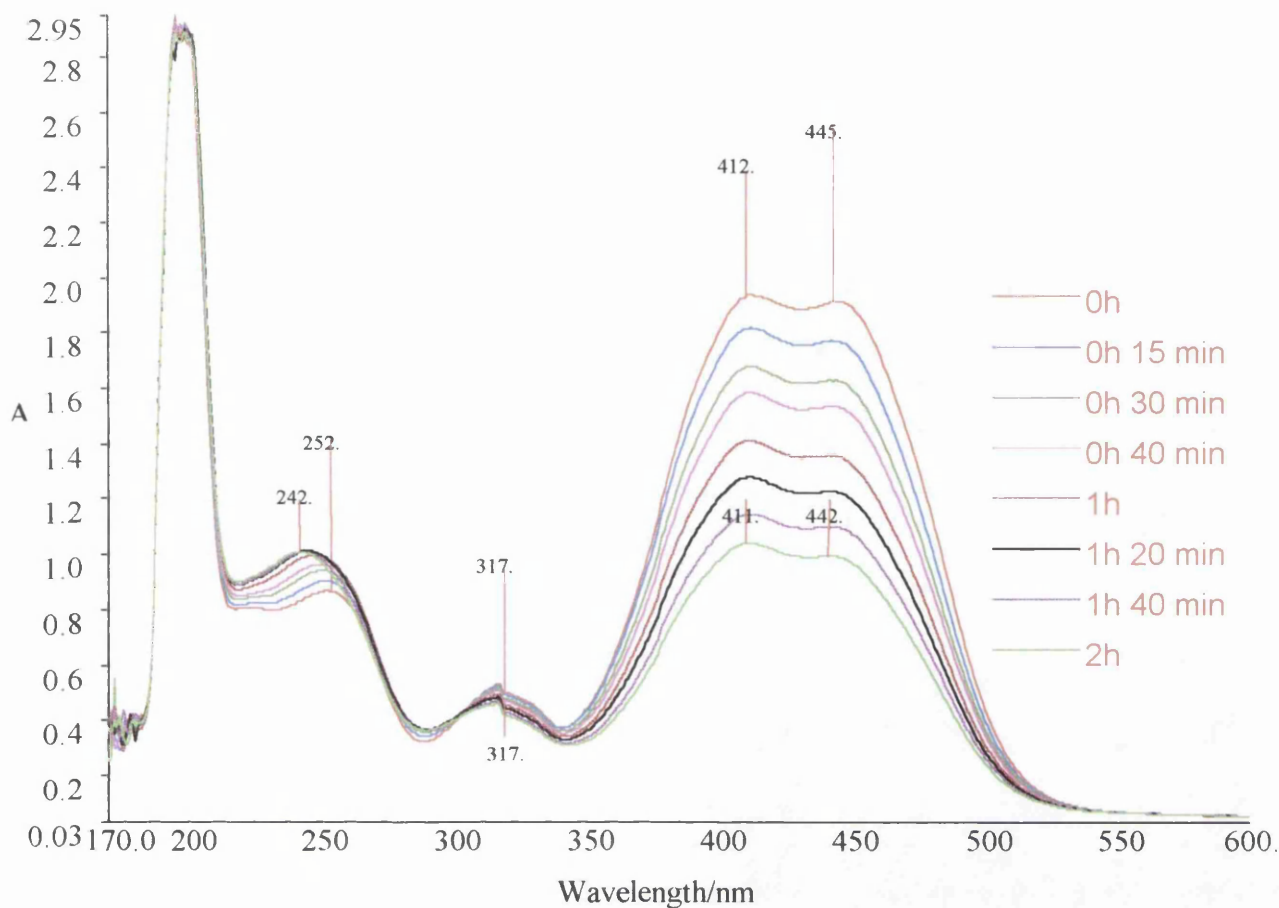


Figure 2.27 The variation in the uv/visible absorption spectrum with irradiation time of a solution of a methanol solution of [XI], under degassed conditions.

From Figure 2.26 and Figure 2.27 it appears that the change in the absorbance at λ_{\max} for [XIV] and [XI] is directly proportional to the irradiation time of the sample solution. A plot of the absorption at λ_{\max} of [XIV] against irradiation time (Figure 2.28) shows [XIV] to have a linear relationship between its absorbance at λ_{\max} and the time of irradiation. This linear relationship implies zero order kinetics, with a rate law expression defined by **Equation (2-36)**. The relationship between irradiation time and the absorbance of [XI] at its λ_{\max} is also linear (see Figure 2.29), again implying zero order kinetics according to **Equation (2-37)**.

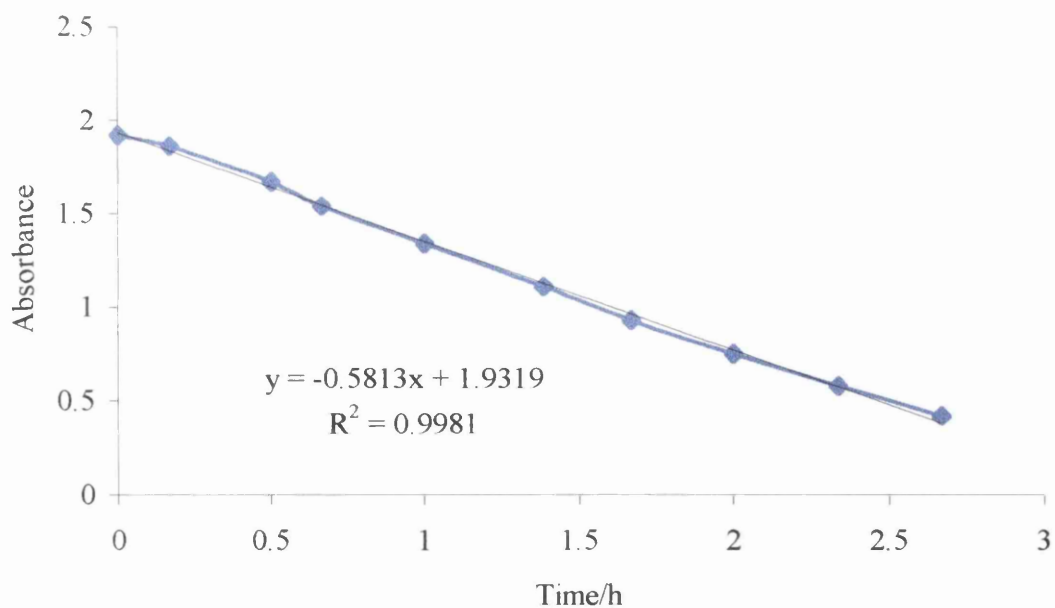


Figure 2.28 The variation in absorbance at λ_{\max} with irradiation time of a methanolic solution of [XIV] under anaerobic conditions.

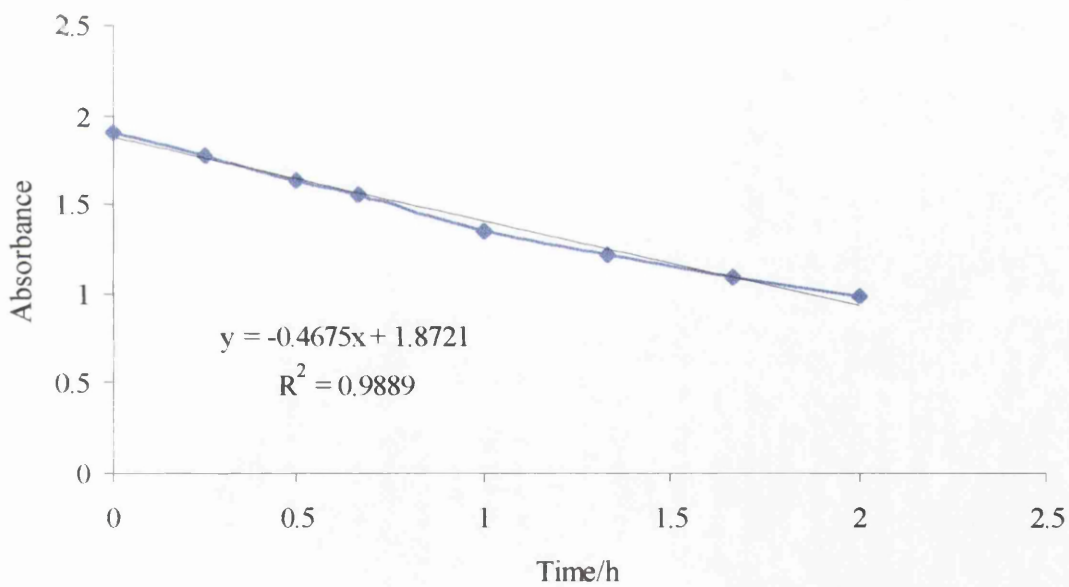


Figure 2.29 The variation in absorbance at $\lambda_{\max} = 445 \text{ nm}$ with irradiation time of a methanolic solution of [XI] under degassed conditions.

Table 2.10 Linear equations used to calculate half-lives and lifetime of dyes [XIV] and [XI] under anaerobic conditions in methanol.

| Dye | Expression | Equation | τ / h | $\tau_{1/2}$ / h |
|-------|-------------------------|------------------------|------------|------------------|
| [XIV] | $A = -0.5813t + 1.9319$ | Equation (2-36) | 3.32 | 1.67 |
| [XI] | $A = -0.4675t + 1.8721$ | Equation (2-37) | 4.00 | 1.96 |

As well as donor-acceptor type azobenzene dyes and the aminoazobenzenes, the kinetics of some donor-acceptor azothiophenes have been studied. The azothiophenes tend to fade quite quickly compared to their azobenzene counterparts. Here there is a decrease in the size of the coloured absorption band and the appearance of some smaller absorption bands at shorter wavelengths. An example of the spectral changes on irradiation of an azothiophene dye are shown in Figure 2.30 for [XV]. There is extensive loss of intensity of the long wavelength absorption peak after an hour of fading, with a slight hypsochromic shift of the absorption peak.

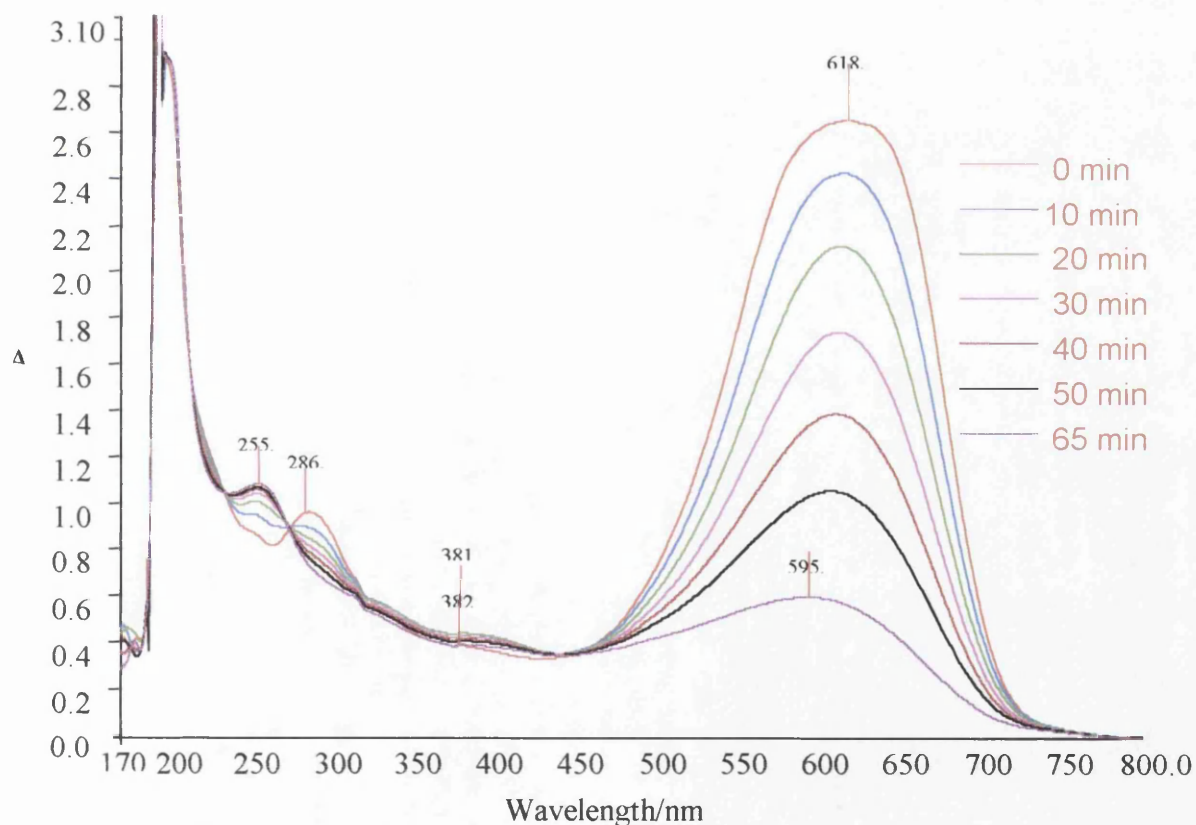


Figure 2.30 The changes in the absorption spectrum of [XV] in methanol under anaerobic conditions with increasing irradiation time.

The rates of fading, measured as a function of the change in absorbance of the dye at its λ_{\max} with respect to the fading time. The absorbance/ irradiation time plots of [XV], [XVI] and [XVIII] (Figure 2.31, Figure 2.33, and Figure 2.33 respectively) show a linear relationship between the absorbance and the irradiation time. The equations for these straight lines were used to calculate the lifetimes and half-lives of these dyes (see Table 2.11).

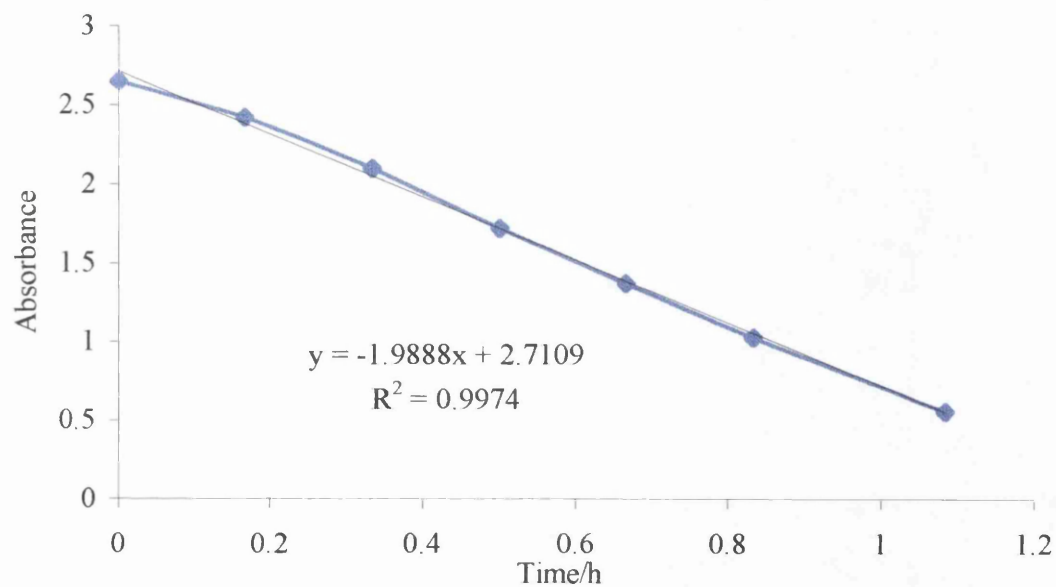


Figure 2.31 The variation in the absorbance at λ_{\max} of a methanol solution of [XV] with irradiation time.

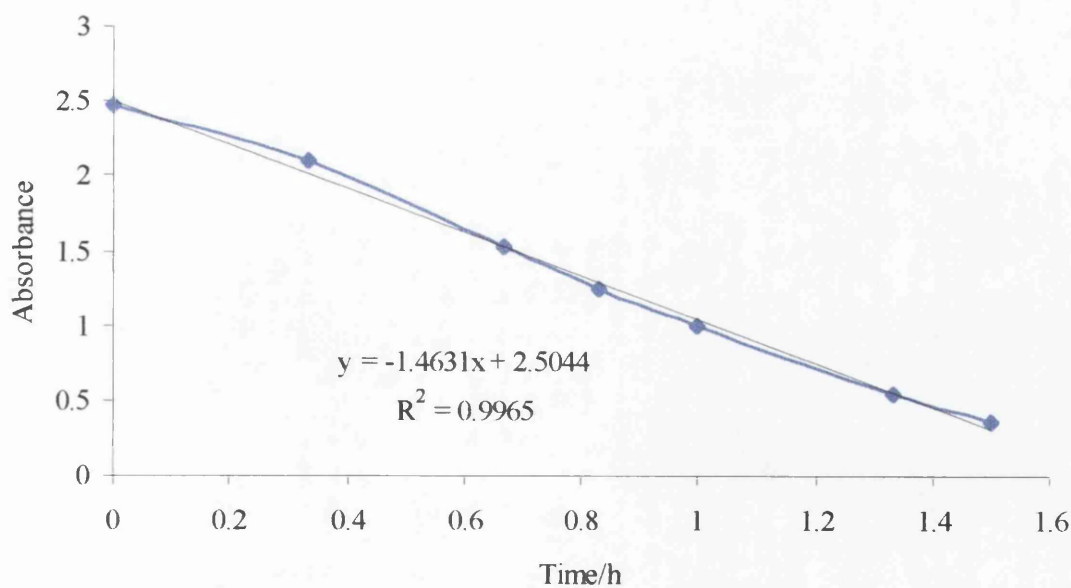


Figure 2.32 The variation in absorbance at λ_{\max} of a methanol solution of [XVI] with irradiation time under anaerobic conditions.

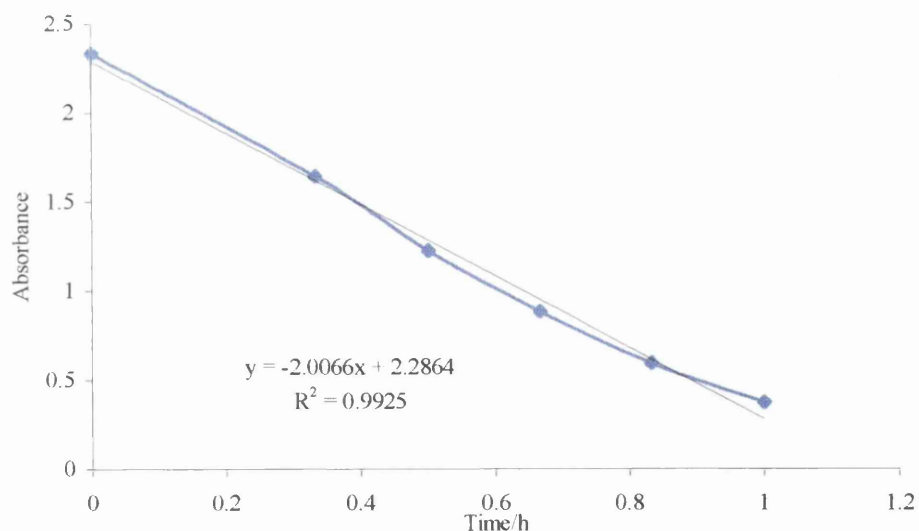


Figure 2.33 The variation in absorbance at λ_{\max} of a methanol solution of [XVIII] with irradiation time under anaerobic conditions.

Table 2.11 Polynomial and linear equations used to calculate half-lives and lifetime of [XV] dyes [XVI] and [XVIII] under anaerobic conditions in methanol.

| Dye | Expression | Equation | τ / h | $\tau_{1/2}$ / h |
|---------|--------------------------|------------------------|------------|------------------|
| [XV] | $A = -1.9888t + 2.7109$ | Equation (2-38) | 1.36 | 0.70 |
| [XVI] | $A = -1.543 t + 2.6224$ | Equation (2-39) | 1.69 | 0.87 |
| [XVIII] | $A = -1.4631 t + 2.5044$ | Equation (2-40) | | |

For the azothiophene dyes there seems to be is a similar pattern to their photofading curves, with all three dyes obeying zero order kinetics and having similar lifetimes and half-lives.

Discussion

The lifetimes and half-lives of all the dyes are summarized in Table 2.12 and are displayed graphically in Figure 2.34. The different series of dyes are colour coded for easy comparison of the data.

Table 2.12 The lifetimes and half-lives of all the azo dyes in methanol solution, under anaerobic conditions.*

| Dye | τ / h | $\tau_{1/2}$ / h | Dye | τ / h | $\tau_{1/2}$ / h |
|--------|------------|------------------|---------|------------|------------------|
| [II] | 0.92 | 0.69 | [X] | 6.6 | 1.48 |
| [IV] | 1.37 | 0.87 | [I] | 1.61 | 1.11 |
| [VI] | 0.93 | 0.65 | [XVII] | 0.89 | 0.44 |
| [VII] | 1.18 | 0.86 | [III] | 3.61 | 1.8 |
| [XIV] | 2.76 | 1.38 | [V] | 2.26 | 1.44 |
| [XI] | 4 | 1.96 | [XV] | 1.36 | 0.7 |
| [VIII] | 2.07 | 1.06 | [XVI] | 1.42 | 0.72 |
| [IX] | 4.46 | 1.12 | [XVIII] | 1.71 | 0.84 |
| [XII] | 4.36 | 1.08 | [XIX] | 1.15 | 0.34 |
| [XIII] | 2.95 | 1.08 | | | |

* τ is the lifetime and $\tau_{1/2}$ is the half-life. * Averaged data from several experiments.

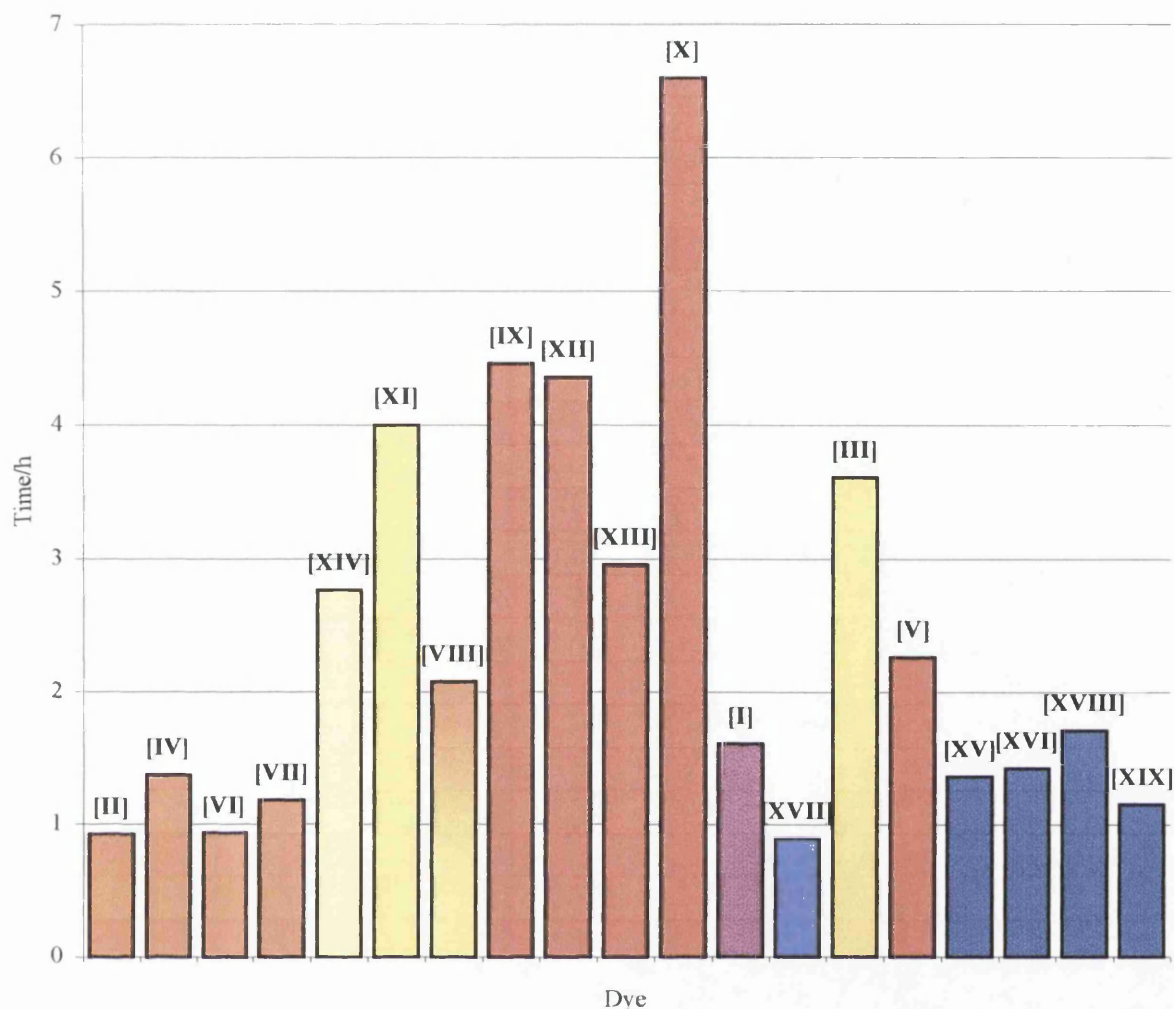


Figure 2.34 The lifetimes in methanol of all the dyes examined under anaerobic conditions.

As can be seen from the bar chart representation of the lifetimes of the dyes, the 2'-nitro dyes have similar lifetimes, which are relatively short compared to the 4'-nitro dyes. The anomalous dye in this series is [VIII], which has a much shorter lifetime than the other 4'-nitro dyes. This is probably due to the absence of any alkyl groups on the amino nitrogen.

The most stable dye is [X]. [I] and [XVII], which contain additional substituents on the donor phenyl ring have comparatively short lifetimes.

The azothiophene dyes all have similar lifetimes, which are in general slightly longer than for the 2'-nitro dyes.

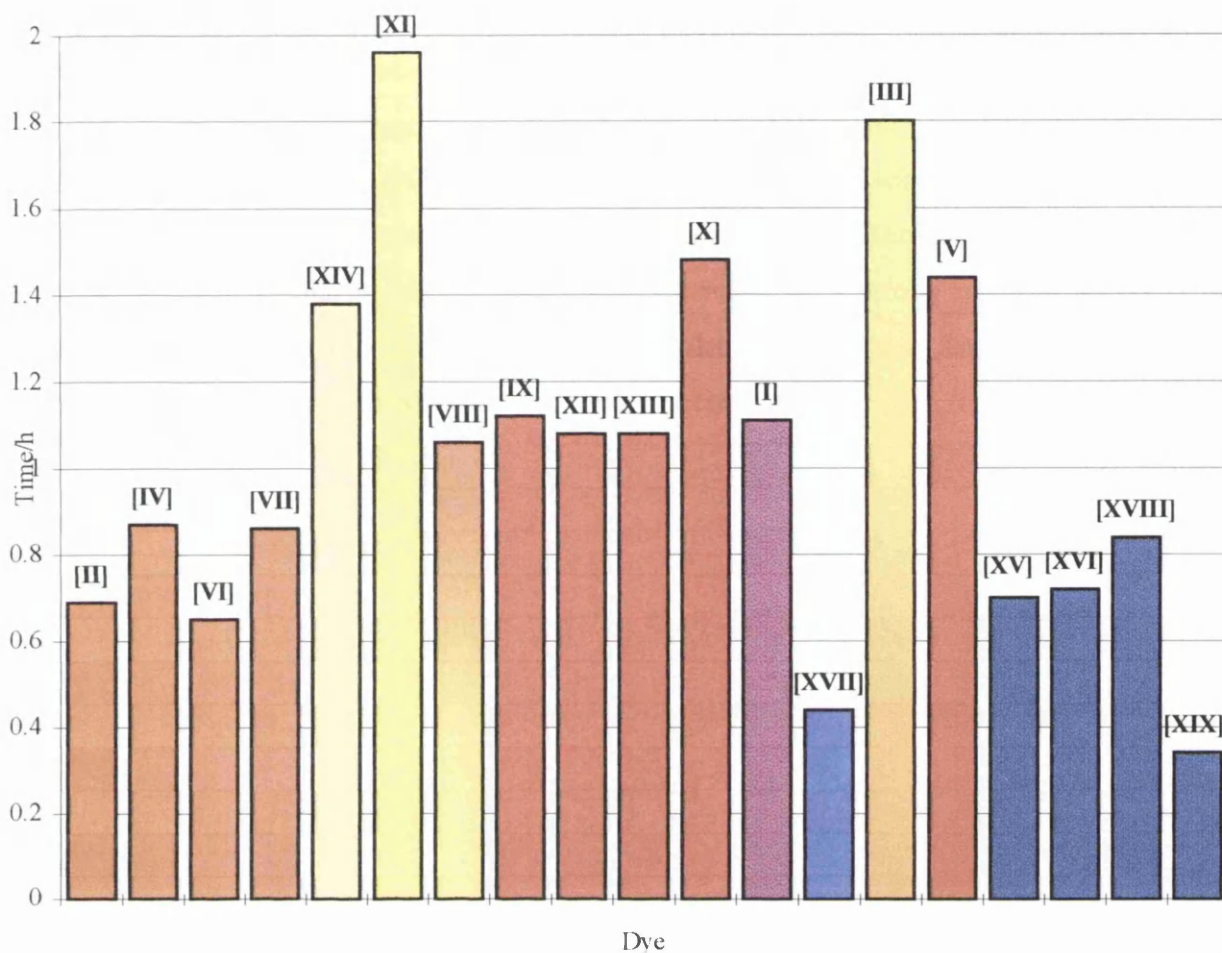


Figure 2.35 The half-lives of the dyes examined under anaerobic conditions in methanol.

With respect to the half-life of the dyes, the azothiophenes are the series with the shortest half-lives, followed by the 2'-nitro substituted dyes. The 4'-nitro substituted dyes have similar half-lives all of just over an hour. [III] and [V] both have relatively long half-lives. The most surprising results are for [XI] and [XIV], which have, quite long half-lives.

The 4'-nitro substituted dyes are also quite stable, and more stable than the 2'-nitro substituted counterparts, though not as much as is expected from light fastness values reported in the literature. There is a much more significant difference in the lifetimes of the dyes than the half-lives, as dyes which have the 2'-nitro substituent tend to fade faster near the end of the fading reaction, while the 4'-nitro substituted dyes fade much more slowly toward the end of the reaction.

The azothiophenes are relatively unstable compared to the azobenzene type dyes. Possible reasons for these differences in rates may be affected by the strength of the azo bond. The

weaker the bond, the more easily it may be broken down and degradation products formed. One factor that may affect the strength of this bond is the electron density in this region of the molecule. Any factor which causes a decrease or disruption of electron density may cause the bond to be weakened and consequently cleaved. Thus strong electron withdrawing groups may weaken the azo bond compared to [XI] and [XIV], and the 2'-nitro substituent may also disrupt the electron density between the azo nitrogens causing additional weakening.

The azothiophenes contain a sulphur atom, which can act as a strong electron acceptor by accepting electrons into its vacant d-orbitals. This also may cause a major decrease in the electron density around the azo bond making it more liable to cleave.

Section 2

The effect of Oxygen on the rate of photofading

Oxygen greatly retards the rate of photofading of all of the dyes studied. Solutions of dye [IX] were oxygenated by bubbling pure oxygen gas through the solution for a time period of between 1 and 10 minutes. The amount of oxygen dissolved in solution is critical when considering the lifetime of the dye in oxygenated methanol solution. This is illustrated in Figure 2.36, which gives the plots of absorbance against fading time for solutions [IX] in methanol, which have been oxygenated for 0, 5 and 10 minutes respectively. Note that the solution oxygenated for 0 minutes is in fact degassed with argon as for the experiments where no oxygen is present.

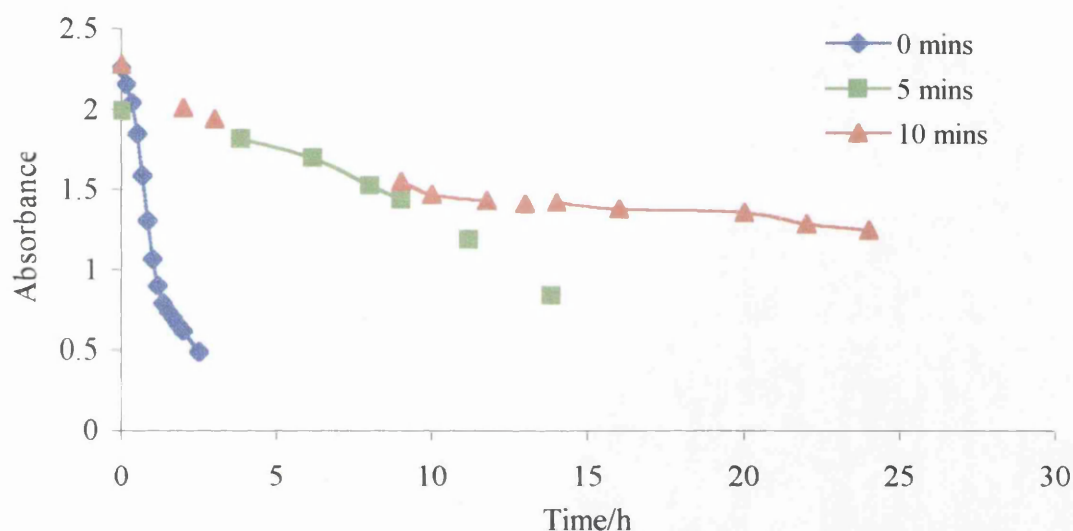


Figure 2.36 The changes in the absorption at λ_{\max} with irradiation time, of three methanol solutions of [IX] subjected to 0, 5 and 10 minutes oxygenation respectively.

The longer oxygenation time results in an increase in the half-life and the lifetime of the dye. For all the different oxygenation times, there is an initial period where the rate of fading is very slow. This period is followed by an increase in the rate of fading for the solution that had been oxygenated for 5 minutes. The rate of fading of the oxygenated solutions is much slower than the rate of fading for the solution where no oxygen is present. The initial rates for the two oxygenated solutions are quite similar, but whereas, after approximately 9 hours, there is an increase in the fading rate of the solution oxygenated for 5 minutes, there is a corresponding

retardation of the fading rate of the solution that had been oxygenated for 10 minutes. The rate of fading of the dye solutions therefore seems to be determined by the amount of oxygen present in the solution. For example, the solution that had been oxygenated for 10 minutes obviously has more oxygen present in solution than the solution oxygenated for 5 minutes and consequently fades more slowly.

Although the rate of photofading is greatly retarded in the presence of oxygen, a decrease in the intensity of the long wavelength absorption band is still observed. If the dye solution is faded for long enough, a total loss of colour is seen. This result is shown in Figure 2.37.

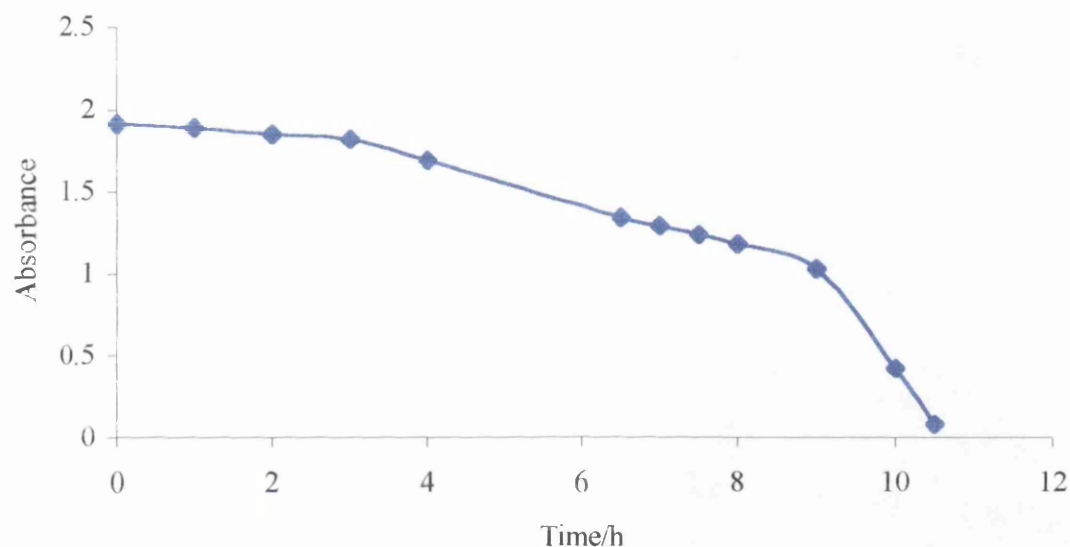


Figure 2.37 The variation in the absorbance at the λ_{\max} of a methanol solution of [IX] that had been oxygenated for 10 seconds, with irradiation.

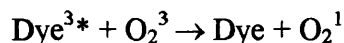
Here a methanol solution of dye [IX], which had been oxygenated for 10 seconds only, was irradiated. Initially, the rate of fading is very slow. After around 3.5 hours, there is an increase in the rate of fading which remains constant until an irradiation time of 9 hours. From this point in time there is a dramatic increase in the rate of fading, and the intensity of the absorption peak at λ_{\max} , degrades to zero. The rate of each stage of the fading reaction can be calculated from the gradient of the three straight line sections of the fading plot. The time intervals for each stage and the corresponding rate are given in Table 2.13.

Table 2.13 The rates of reaction of the three fading stages observed for the irradiation of a methanol solution of [IX] oxygenated for 10 minutes.

| Stage | Time interval | Rate |
|-------|-----------------------|--------|
| 1 | 0 to 3 hours | 0.031 |
| 2 | 3 to 9 hours | 0.1297 |
| 3 | 9 to 10 hours 30 mins | 0.63 |

From Table 2.13, it can be seen that the rate of fading for stage 2 is 4.18 times faster than the rate in stage 1 and that stage 3 has a fading rate 4.8 times faster than for stage 2 and thus 20.3 time faster than for stage 1.

A possible explanation for the initial very slow rate of fading, is that oxygen quenches the photoreaction. The oxygen may be acting as a quencher of some excited state species of the dye, possibly a triplet, which would otherwise undergo further processes leading to degradation of the dye. Oxygen is a triplet in its ground state and thus has the ability to interact with other triplet species, according to Equation (2-41).



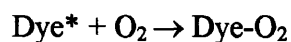
Equation (2-41)

In this instance, the excited triplet state of the dye interacts with ground state triplet oxygen and yields the dye in its ground state, plus singlet oxygen. It is quite likely that in the initial stages of the reaction oxygen quenches most of the excited state species and therefore little if any photofading occurs.

The change in the rate of photofading suggests that the oxygen may be used up in some way or converted to some inactive species so that its quenching action is reduced, and photofading may proceed.

There is the possibility that fading may then occur in the same way as if no oxygen were present.

There is also the possibility of some excited state of the dye reacting with oxygen, according to Equation (2-42), until all the oxygen is consumed, after which reductive fading may occur.



Equation (2-42)

The oxygen could also be deactivated in some way. This could result perhaps, from the interaction with the triplet state of the dye converting ground state triplet oxygen into singlet oxygen. This process would prevent further quenching of a reactive triplet state of the dye by triplet oxygen. The singlet oxygen may also interact with the dye in some way, causing fading.

The changes in the absorption spectra of the dyes faded under oxygenated conditions are also markedly different to changes observed under degassed conditions. These differences are discussed in the discussion of the photo-products in Chapter 3. Not all of the dyes have the same pattern of fading under oxygenated conditions. The rates of fading under oxygenated conditions affect some dyes much more than others. For example Figure 2.38, shows [IV] to have a linear relationship between the irradiation time and the absorbance of the dye at its λ_{max} . In contrast to [IX], [IV] has a constant rate of fading, and obeys zero order kinetics. There is no initial induction period, where fading is slow and no sudden changes in the rate of fading. These factors suggest that even though oxygen slows down the photofading reaction in some way, some photoreaction still occurs at a constant rate resulting in the constant loss of intensity of the long wavelength absorption peak. [IV] thus has a definite lifetime in the presence of oxygen. This lifetime is calculated from the straight line equation in Figure 2.38 to be $\tau = 7.11$ hours with the half-life calculated to be $\tau_{1/2} = 3.52$ hours. Even though, the half-life is approximately 4 times longer and the lifetime 5 times longer than in the presence of oxygen than under deoxygenated conditions, the half-life and lifetime of [IV] are much shorter than for [IX] under the same conditions.

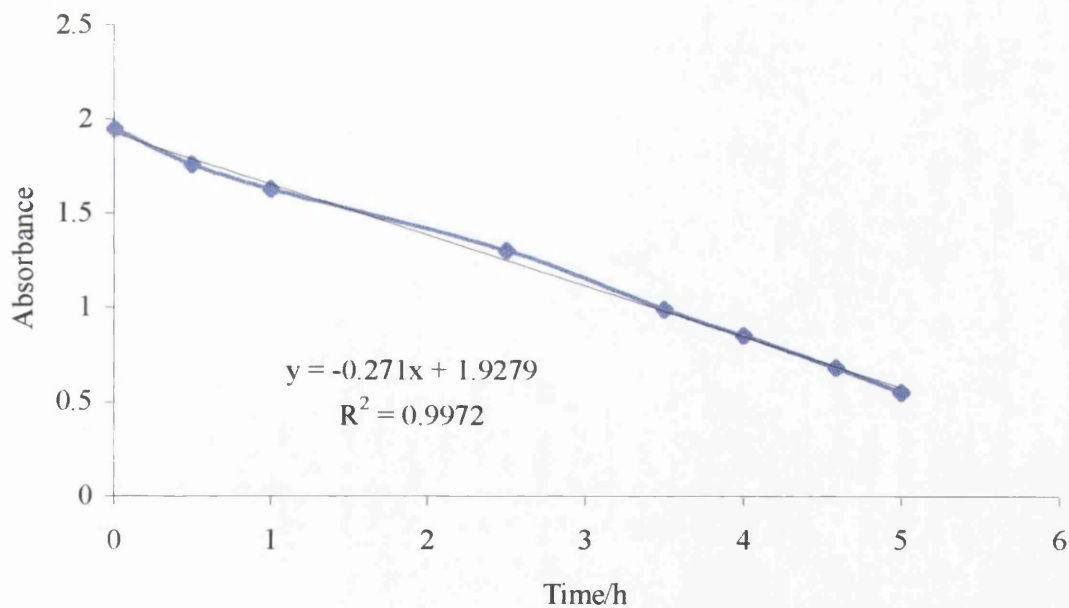


Figure 2.38 The change in the absorbance of a methanol solution of [IV] with irradiation time under oxygenated conditions.

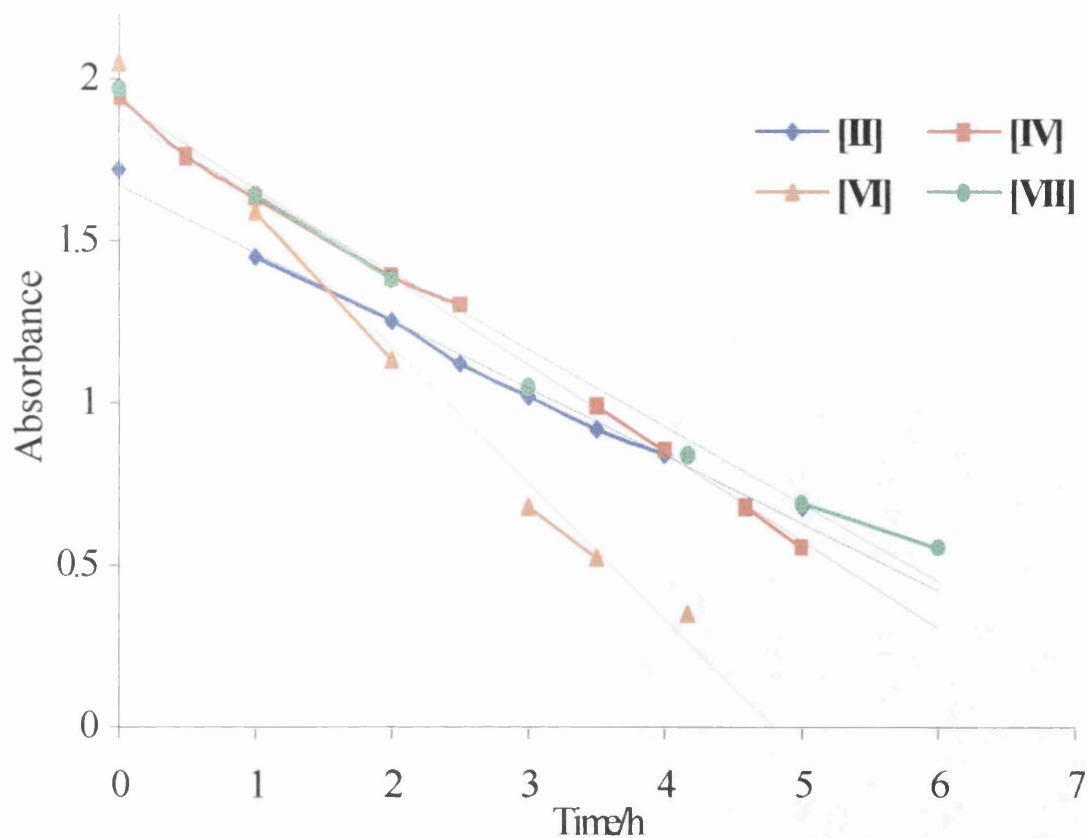


Figure 2.39 The changes in the absorbance at the λ_{\max} of a methanol solutions of dyes [III], [IV], [VI] and [VII] with irradiation time under oxygenated conditions.

Similar results are seen for the other dyes containing the 2'-nitro substituent (Figure 2.39) suggesting that dyes that contain the 2'-nitro substituent, may have similar photofading behaviour in the presence of oxygen.

In view of the similar results obtained for the photofading of the series of 2'-nitro substituted dyes, it might be expected that other series of dyes with similar structure may have similar kinetic behavior to one another. From Figure 2.40, it can be seen that this assumption seems to hold for [IX], [XII] and [XIII] of the series of dyes containing the 4'-nitro substituent. (Figure 2.40).

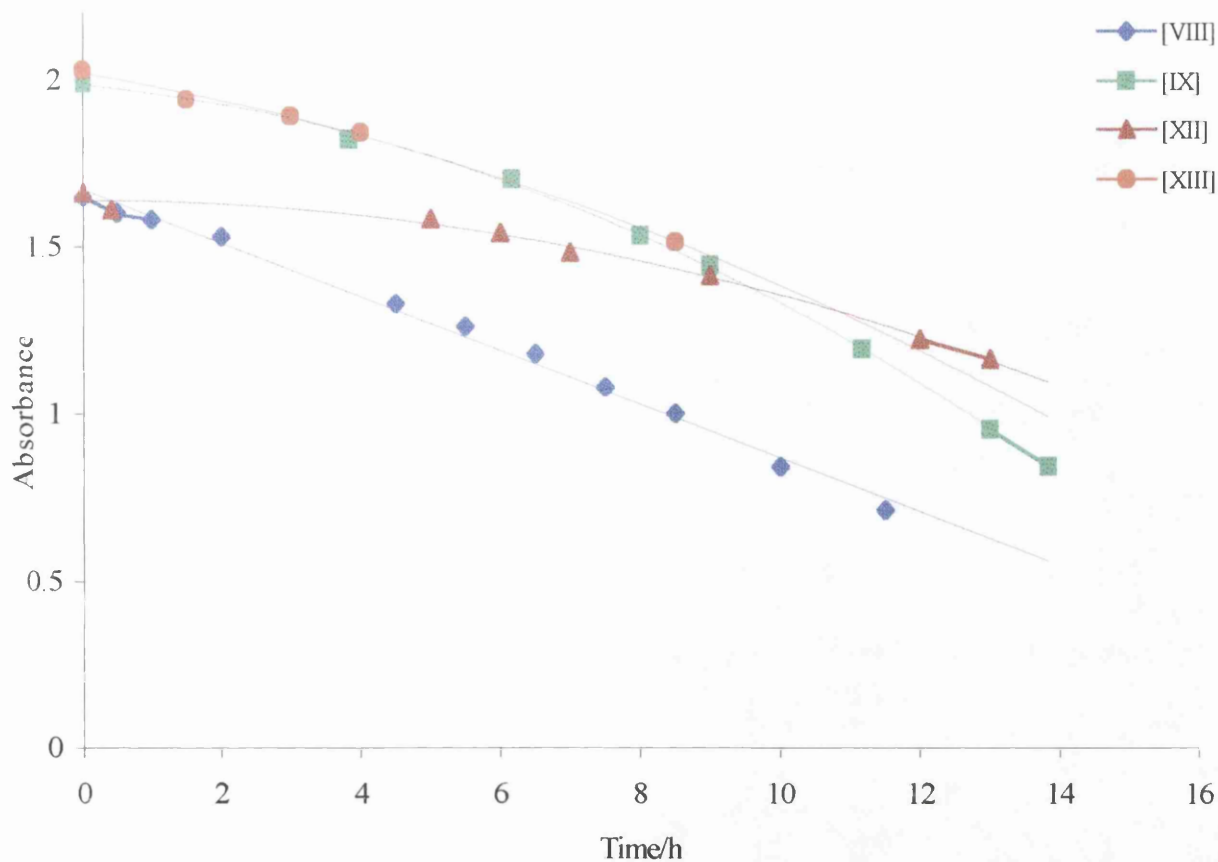


Figure 2.40 The changes in the absorbance at the λ_{\max} of a methanol solutions of dyes [VIII], [IX], [XII] and [XIII] with irradiation time under oxygenated conditions.

However, the other dyes in the series do not seem to conform to this general pattern of photofading behaviour. [VIII], for example has a linear relationship between its absorbance at λ_{\max} and the irradiation time, and thus has zero order kinetics. [I] has similar fading times in oxygenated solution as [IX], [XII] and [XIII], but the fading curve is linear. Both the fading times and the appearance of the fading curve are very different for [XVII]. The photofading curves for [I] and [XVII] are compared to that for [IX] in Figure 2.41. The Microsoft excel package does not provide an adequate curve fitted trendline to correlate with the data points of [XVII] but it can be seen that the lifetime and half-life of this dye are far shorter than those for the other dyes in the 4-nitro series.

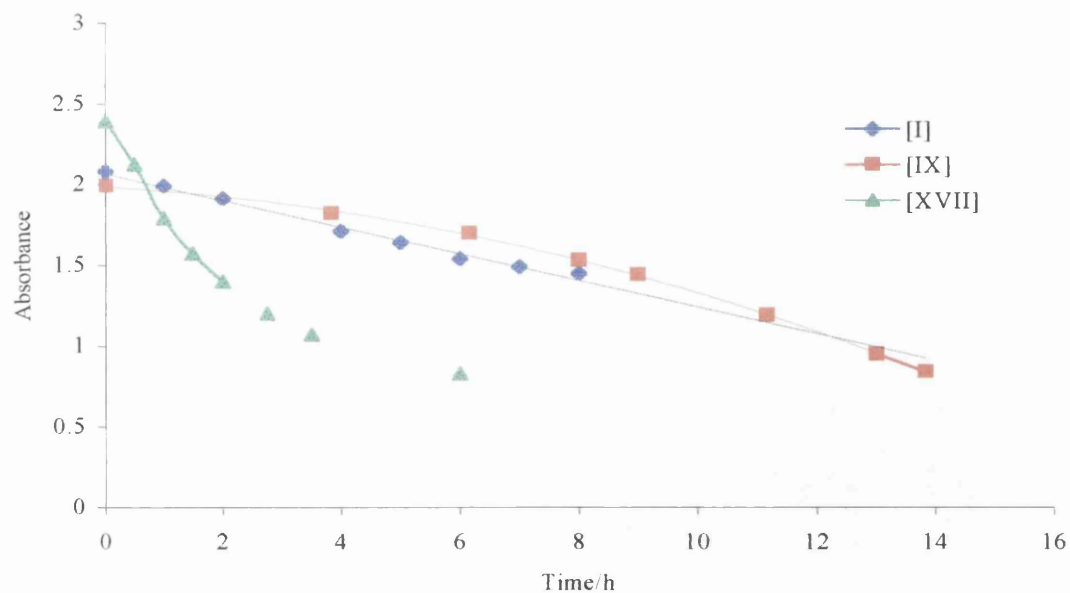


Figure 2.41 The changes in the absorbance at the λ_{\max} of a methanol solutions of [I], [IX], and [XVII] with irradiation time under oxygenated conditions

Both dye [XI] and [XIV] produce straight line fading curves under oxygenated conditions (see Figure 2.42).

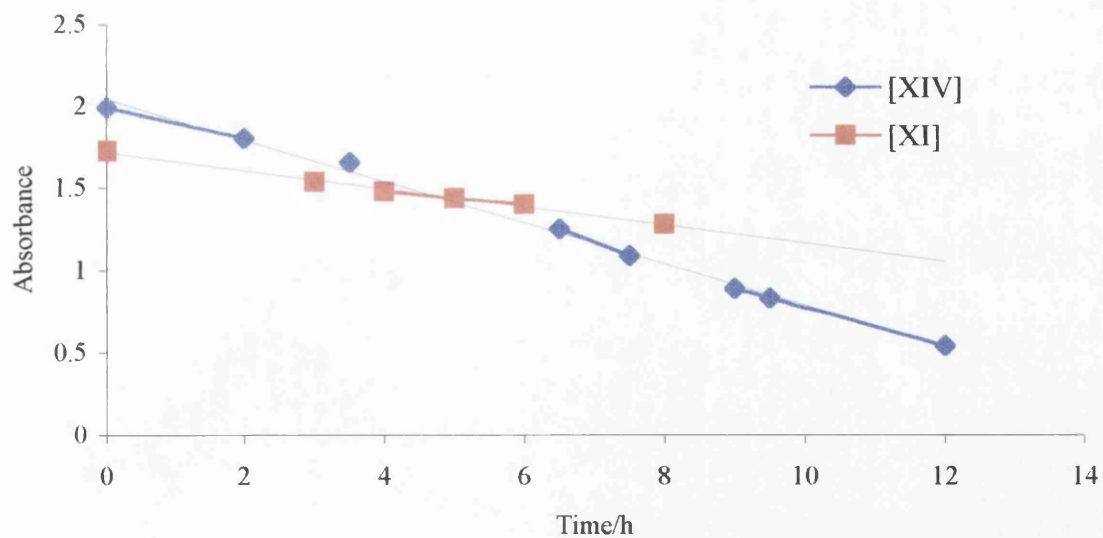


Figure 2.42 The changes in the absorbance at the λ_{\max} of methanol solutions of [XIV] and [XI] with irradiation time under oxygenated conditions.

Both dyes are quite photo-stable in oxygenated solution. [XI], which contains two donor amino groups perhaps surprisingly, has one of the longest lifetimes of all the dyes examined.

Dyes curves for [III] and [V] showed a linear relationship between the irradiation time and the variation in absorbance (Figure 2.42) and [III] in particular was very photo-stable in oxygenated solution, with respect to the other dyes.

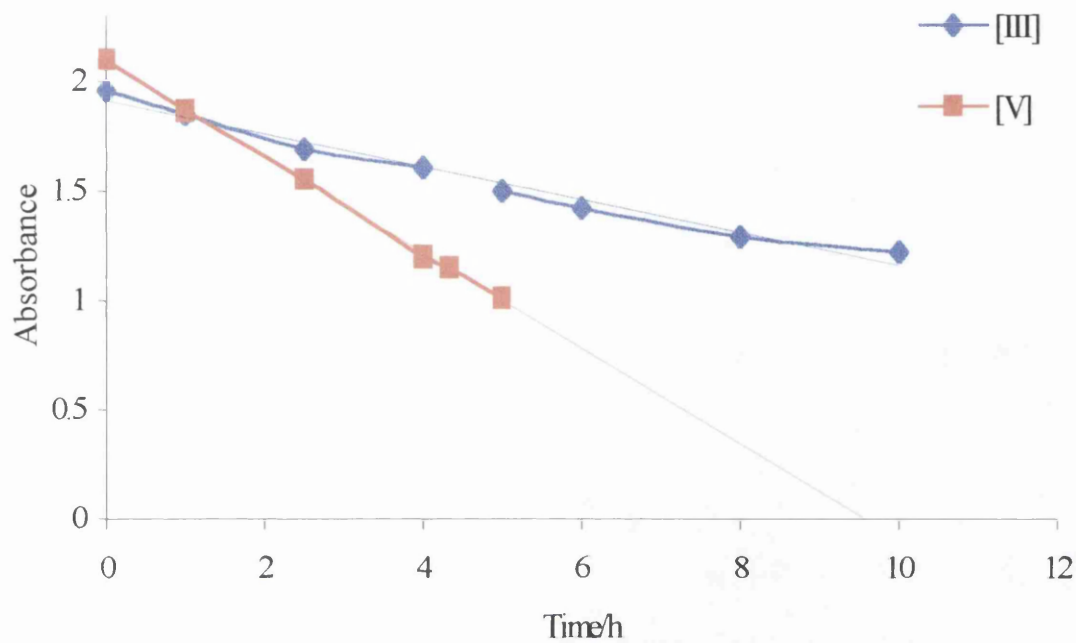


Figure 2.43 The changes in the absorbance at the λ_{\max} of methanol solutions of [III] and [V] with irradiation time under oxygenated conditions

Finally, the photofading curves for the series of azothiophene dyes (Figure 2.44) show considerable variation in the half-lives and lifetimes of the azothiophene dyes, with [XV] having a very short lifetime in oxygenated solution, whilst [XVI] and [XVIII] have much longer lifetimes under the same conditions. The lifetimes and half-lives of 18 of the dyes examined under oxygenated conditions are calculated from graphical plots of the irradiation time versus the absorbance of the dye at its λ_{\max} . These results are given in Table 2.14.

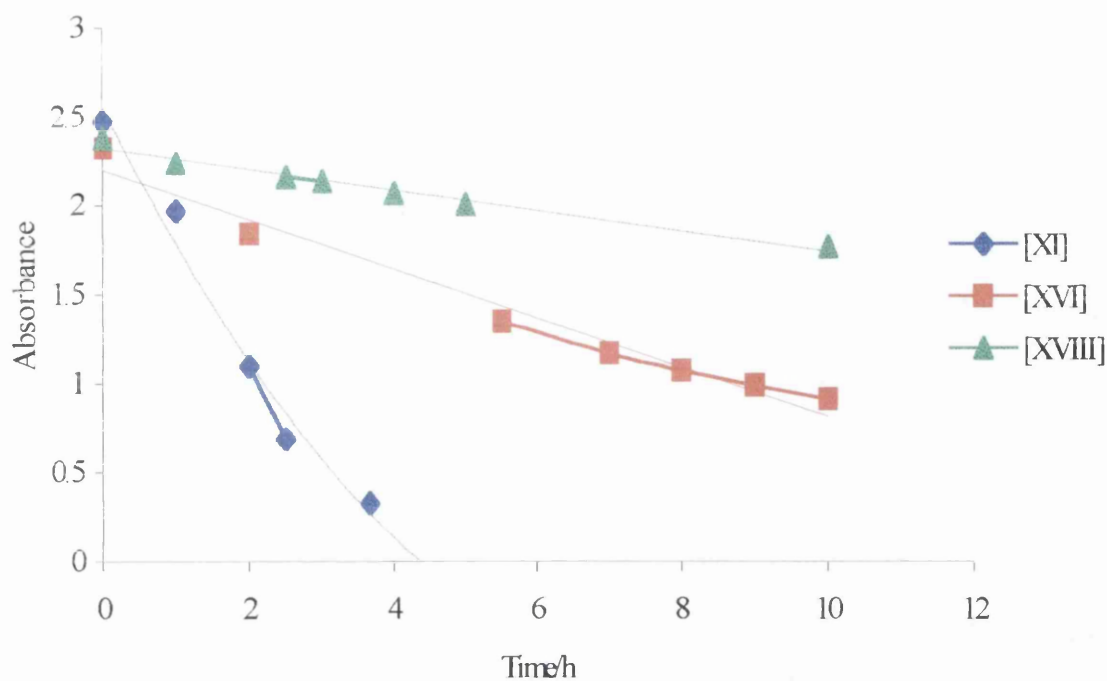


Figure 2.44 The changes in the absorbance at the λ_{\max} of methanol solutions of [XV], [XVI], [XVIII] with irradiation time under oxygenated conditions.

Table 2.14 The lifetimes and half-lives of all the dyes examined in methanol under oxygenated conditions.

| Dye | Lifetime/h | Half-life/h | Dye | Lifetime/h | Half-life/h |
|--------|------------|-------------|--------|------------|-------------|
| [II] | 7.91 | 3.83 | [XIII] | 21.18 | 13.57 |
| [IV] | 7.11 | 3.52 | [I] | 23.13 | 11.57 |
| [VI] | 9.55 | 4.77 | [XVII] | 14.65 | 2.72 |
| [VII] | 7.97 | 3.84 | [III] | 25.30 | 12.42 |
| [XIV] | 16.27 | 8.33 | [V] | 9.55 | 4.77 |
| [XI] | 31.16 | 15.46 | [XV] | 4.37 | 1.82 |
| [VIII] | 20.77 | 10.52 | [XVI] | 6.00 | 3.47 |
| [IX] | 18.83 | 12.71 | | | |
| [XII] | 23.50 | 16.54 | | | |

The results in Table 2.14 can be displayed as the bar charts in Figure 2.45 and Figure 2.46.

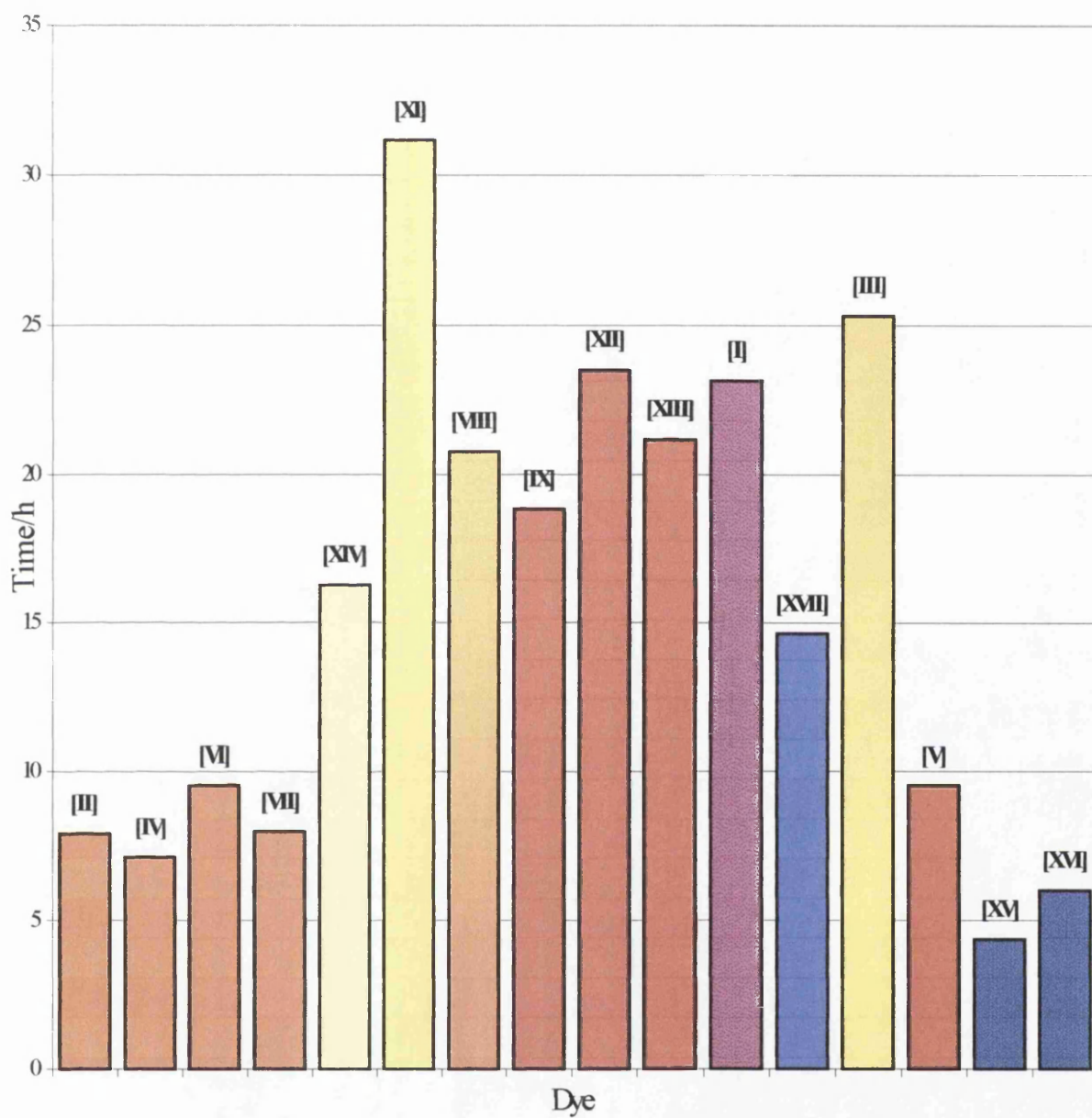


Figure 2.45 The lifetimes of the dyes examined in oxygenated methanol solution.

From the bar chart, the series of dyes containing the 2'-nitro substituent all have relatively short lifetimes compared to the other azobenzene dyes. The shortest lifetimes however, belong to the two azothiophene dyes examined.

The dyes containing the 4'-nitro substituent, including [VIII] and [I], also have similar lifetimes to one another, of around 20 hours. The odd one out in this series is [XVII], which has a shorter lifetime of 14.65 hours. This difference is not that surprising though, as the structure of [XVII] is quite different to the other dyes in the series. [III] has a long lifetime, with [V] having quite a short lifetime, perhaps being indicative of its greater similarity to the 2-nitro dyes than to [III]. The data for the half-lives of the dyes under oxygenated conditions is displayed in the bar chart in Figure 2.46.

Again the half-lives of the 2'-nitro dyes are relatively short compared to the other azobenzene based dyes, as are the half-lives of the two azothiophene dyes. Dye [XVII] has a surprisingly short half-life, which is disproportionate to its lifetime.

The 4'-nitro dyes are again amongst the most stable along with [III] and [XI]. Dyes [VIII], [XIV] and [XI] have half-lives that are shorter than would be expected due to the linear nature of their photofading curves. [V] again has a half-life more akin to that of the 2-nitro series of dyes than to [III]. The relative photo-stability of the dyes can be measured in terms of the lifetime or the half-life. Both of these give similar orders for the relative stability of the dye in oxygenated and deoxygenated conditions. The half-life is perhaps the more reliable measure of light fastness, as it measures half the time taken for the intensity of the long wavelength coloured absorption band to halve. The lifetime is the time taken for the total loss of intensity of this peak, and since photo-degradation products may also absorb to some extent at the λ_{\max} of the original peak, the lifetime may be misleading. In addition, the lifetime is calculated in most cases, from the extrapolation of curves from actual data points, and therefore, there exists the possibility that the error margin for the lifetime is far greater than that for the half-life of the dye.

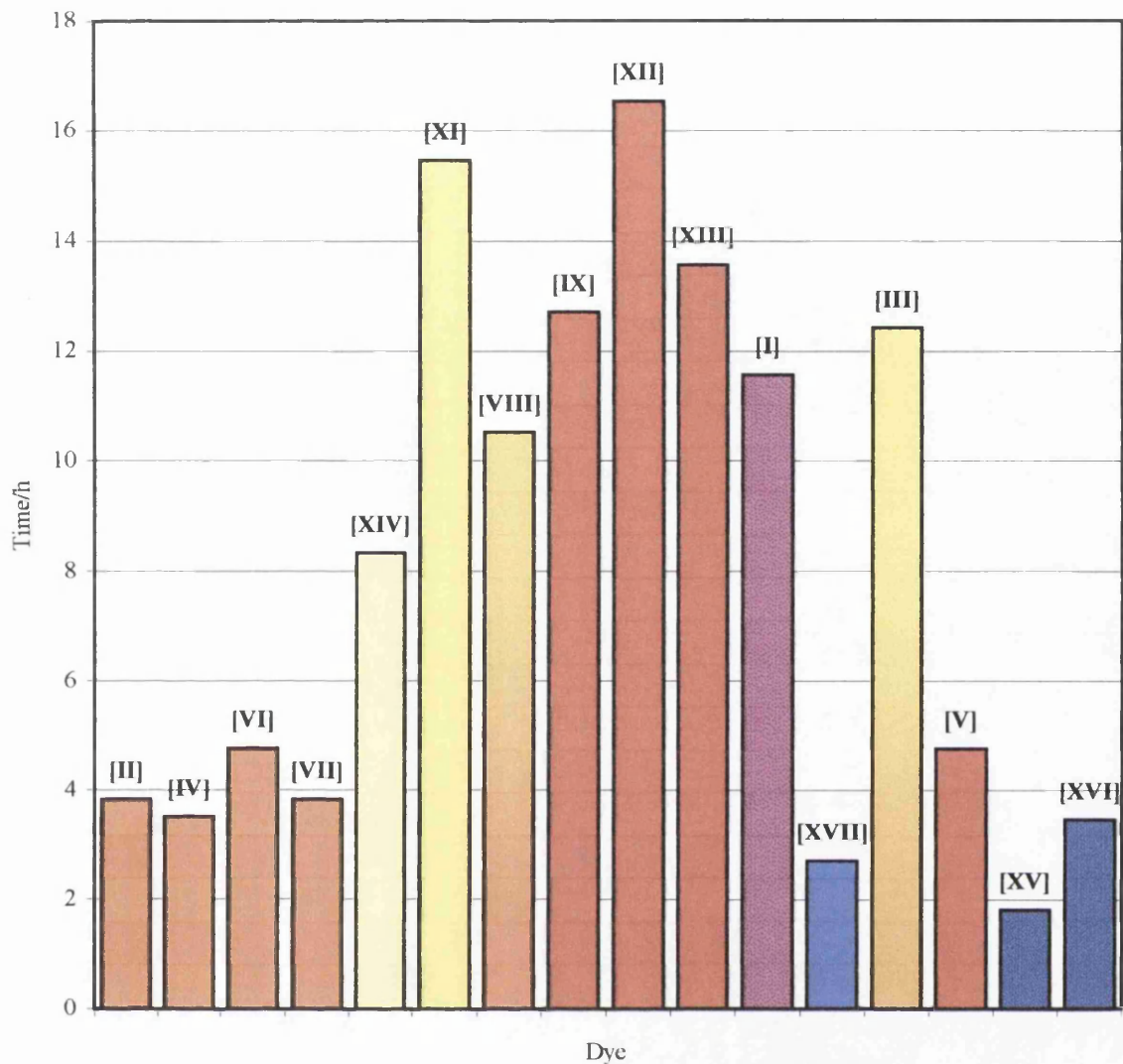


Figure 2.46 The half-lives of the dyes examined in oxygenated methanol solution.

The order of lightfastness for the 19 dyes in oxygenated methanol is similar to the order under degassed conditions, with dyes that contain the 2'-nitro substituent on the acceptor ring having half-lives and lifetimes, of approximately three to four times shorter than the more stable dyes [III] and [XI] and the 4'-nitro substituted dyes. The aminoazobenzene [XIV] has a half-life approximately twice as long as the 2'-nitro dyes, while dye [V] has a half-life similar to the most stable 2'-nitro dyes. The azothiophenes [XV] and [XVI] along with the heavily substituted 2-acetylamino-4-diethylamino-2'-cyano-4'-nitro-6'-bromoazobenzene [XVII] have the shortest half-lives of all the dyes, though the lifetime of [XVII] is deceptively long.

Oxygen greatly retards the rate of photofading of all the dyes examined in this work, though some dyes are stabilised to a greater extent than others. The stabilization factor of oxygen on fading rates, can be defined as the lifetime of a dye in oxygenated methanol divided by the lifetime of that dye when no oxygen is present i.e. $S = \tau^{\circ}/\tau$. This stabilisation factor along with a similar expression in terms of the half-lives of the dyes $S_{1/2} = \tau_{1/2}^{\circ}/\tau$, gives an indication of the degree to which oxygen retards the rate of fading for each dye. The lifetimes and half-lives of the dyes under oxygenated and deoxygenated conditions, together with the stabilization factors S and $S_{1/2}$ are reported in Table 2.15. The stabilization factor of the half-lives throws up the expected anomalous results for [XVII], and significantly different stabilization factors between the lifetimes and the half-lives of the 4'-nitro dyes.

Table 2.15 The lifetimes and half-lives in deoxygenated^a and oxygenated^b methanol solution, and the stabilization factors of oxygen on the lifetime^c and half-life^d of [I]-[XIX].

| Dye | τ / h | $\tau_{1/2}$ / h | τ° / h | $\tau_{1/2}^{\circ}$ / h | S | $S_{1/2}$ |
|---------|------------|------------------|--------------------|--------------------------|------|-----------|
| [II] | 0.92 | 0.69 | 7.91 | 3.83 | 8.6 | 5.6 |
| [IV] | 1.37 | 0.87 | 7.11 | 3.52 | 5.2 | 4.0 |
| [VI] | 0.93 | 0.65 | 9.55 | 4.77 | 10.3 | 7.3 |
| [VII] | 1.18 | 0.86 | 7.97 | 3.84 | 6.8 | 4.5 |
| [XIV] | 2.76 | 1.38 | 16.27 | 8.33 | 5.9 | 6.0 |
| [XI] | 4 | 1.96 | 31.16 | 15.46 | 7.8 | 7.9 |
| [VIII] | 2.07 | 1.06 | 20.77 | 10.52 | 10.0 | 9.9 |
| [IX] | 4.46 | 1.12 | 18.83 | 12.71 | 4.2 | 11.3 |
| [XII] | 4.36 | 1.08 | 23.50 | 16.54 | 5.4 | 15.3 |
| [XVIII] | 2.95 | 1.08 | 21.18 | 13.57 | 7.2 | 12.56 |
| [X] | 6.6 | 1.48 | NA | NA | NA | NA |
| [I] | 1.61 | 1.11 | 23.13 | 11.57 | 14.4 | 10.42 |
| [XVII] | 0.89 | 0.44 | 14.65 | 2.72 | 16.5 | 6.2 |
| [III] | 3.61 | 1.8 | 25.30 | 12.42 | 7 | 6.9 |
| [V] | 2.26 | 1.44 | 9.55 | 4.77 | 4.2 | 3.3 |
| [XV] | 1.36 | 0.7 | 4.37 | 1.82 | 3.2 | 2.5 |
| [XVI] | 1.42 | 0.72 | 6.00 | 3.47 | 4.2 | 4.8 |
| [XVIII] | 1.71 | 0.84 | NA | NA | NA | NA |
| [XIX] | 1.15 | 0.34 | NA | NA | NA | NA |

^a τ and $\tau_{1/2}$ are the lifetimes and half-lives of dyes in methanol under anaerobic conditions. ^b τ° and $\tau_{1/2}^{\circ}$ are the lifetimes and half-lives of dyes in oxygenated methanol. ^c The stabilisation factors in terms of the lifetimes of each dye is $S = \tau^{\circ}/\tau$. ^d The stabilisation factors in terms of the half-lives of each dye of the dyes $S_{1/2} = \tau_{1/2}^{\circ}/\tau$.

The half-life and lifetime of [I] are greatly stabilized by the presence of oxygen, as are the half-life and lifetime of [VIII]. The 2-nitro series of dyes are stabilized to varying degrees, with [VI] particularly well stabilized by oxygen, but [IV] much less so. Dye [II] and [VII] are intermediate between [VI] and [IV]. The stabilization of the lifetimes of the 4-nitro dyes is average, but their half-lives are the most stabilized by oxygen of all the dyes. [III] is average with respect to both the lifetime and the half-life. The least stabilized dyes are the azothiophenes and [V].

The effect of water on rates of fading under anaerobic conditions

Factors that may affect the lightfastness of azo dyes on paper include the relative humidity. The effect of humidity on the rate of photofading was examined for [IX] and [IV] by conducting photo-fading experiments in methanol/water solutions. Figure 2.47, shows the fading curves for 100 % methanol solutions to 60/40-methanol/water ratio.

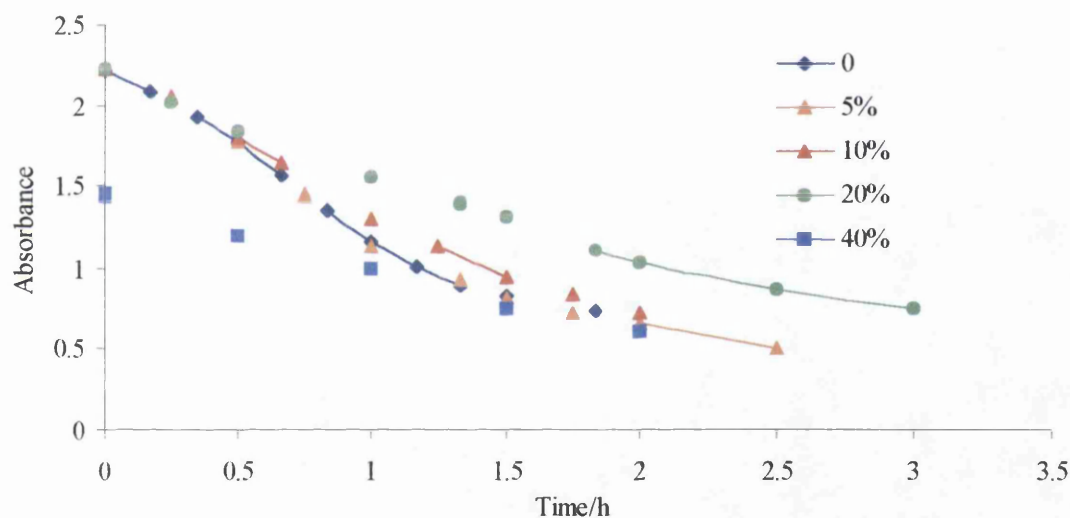


Figure 2.47 The changes in the absorbance at the λ_{\max} of methanol/water solutions of [IX]. The percentage content of the solutions varies from 0% water and 100% methanol to 40% water and 60% methanol.

Increasing the amount of water in the solution further than 40 % leads to problems with the solubility of the dye. Even at 40% water content, the solubility of the dye is significantly less than in the other solutions, resulting in the lower absorbance values for the same concentration of dye in the 40% water solution. The rate of fading of degassed solutions of [IX] does not seem to

be greatly affected by the amount of water, with the rates of fading similar in all the solutions (see Table 2.16). If anything there is a slight decrease in the rate of fading with increasing water content. The effect of water on oxygenated solutions of [IX] is negligible, and the difference in the rate of fading is attributable to experimental error. [IV] also shows a decrease in the rate of fading with increasing water content (Figure 2.48), and this decrease is slightly more noticeable than for [IX]. The rates of fading for the [IV] methanol/water solutions are also given in Table 2.16.

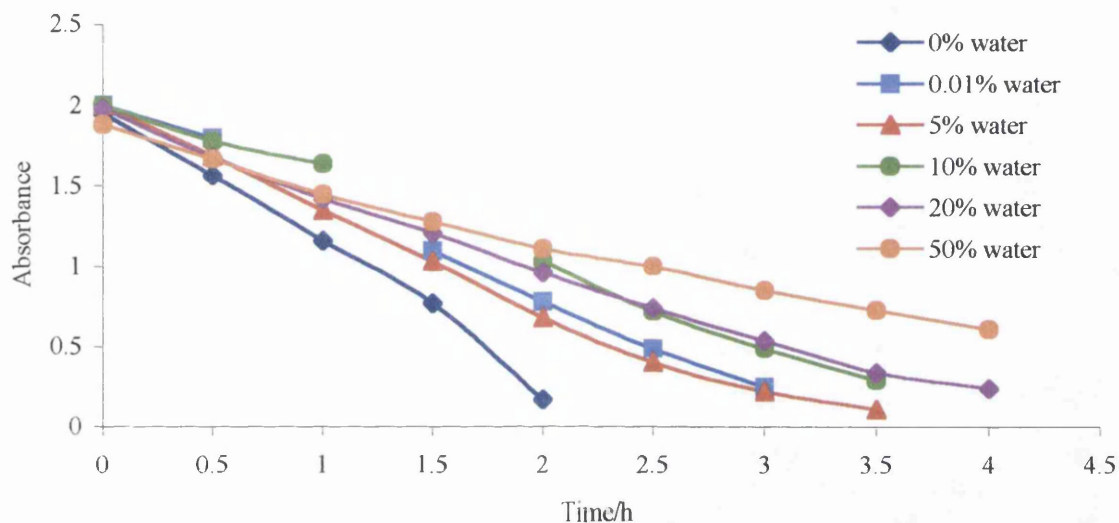


Figure 2.48 The changes in the absorbance at the λ_{max} of methanol/water solutions of [IV]. The percentage content of the solutions varies from 0% water and 100% methanol to 50% water and 50% methanol

Rates of fading in methanol/water solutions were inconsistent with the results of experiments by Albini, who attributed increases in rates of fading to increased protonation by water of an initially formed intermediate in the photodegradation process.¹³

Table 2.16 The results of the effect of different amounts of water in water/methanol solutions for [IV], [IX]. The rate constant k is given in $\text{mol dm}^{-3}\text{s}^{-1}$.

| Dye | | | [IV] | [IV] | [IX] | [IX] |
|---------------|--------|-----------|-------------------------------------|-------------|-------------------------------------|-------------|
| Solution | %water | %methanol | $k/\text{mol dm}^{-3}\text{s}^{-1}$ | Half-life/h | $k/\text{mol dm}^{-3}\text{s}^{-1}$ | Half-life/h |
| Dry methanol* | 0 | 100 | 0.87 | 1.14 | 0.90 | 1.21 |
| HPLC methanol | 0.01 | 99.99 | 0.61 | 1.67 | | |
| 5% water | 5 | 95 | 0.57 | 1.70 | 0.74 | 1.41 |
| 10% water | 10 | 90 | 0.51 | 1.73 | 0.79 | 1.39 |
| 20% water | 20 | 80 | 0.44 | 2.14 | 0.50 | 2.11 |
| 40% water | 40 | 60 | | | 0.43 | 1.68 |
| 50% water | 50 | 50 | 0.31 | 2.88 | | |

*Methanol dried by refluxing and distilling over magnesium and iodine.

The amount of water that is present in HPLC methanol can be determined by a Karl Fisher titration experiment.¹⁴ This uses a reagent, which undergoes a colour change from dark brown to clear when it reacts with water in the methanol. The amount of the reagent added to consume all of the water is proportional to the amount of water present.

The amount of water present in HPLC grade methanol was determined by experiment to be approximately 0.01% in a freshly opened bottle.

Since a small amount of water has a negligible effect on the rates of fading of both [IV] and [IX], HPLC methanol is suitable for use in place of dry methanol.

The presence of water seems to have a minor effect on the fading rate of [IX] under anaerobic conditions, and a slightly more pronounced effect on the fading rate of [IV]. Increasing the percentage of water in the methanol/water solutions has a retarding effect on the rate of photofading for both dyes.

The effect of singlet oxygen quenchers on photofading rates of [IV] under oxygenated conditions

Evidence for the involvement of singlet oxygen in the fading reaction could be provided by experiments involving singlet oxygen quenchers. If singlet oxygen were involved in the photofading reaction, then a singlet oxygen quencher, such as diaza-bicyclo-2,2,2-octane (DABCO), would be expected to reduce the rate of photofading. Since [IV] has a relatively fast rate of fading in the presence of oxygen compared with some of the other dyes, this was chosen for experiments involving the singlet oxygen quencher DABCO.

Solutions of [IV] in methanol with various concentrations of DABCO were oxygenated for five minutes and then irradiated. The rates of fading and half-lives for these solutions are given in Table 2.17.

Table 2.17 The rate constants and lifetimes half-lives methanol solutions of [IV], oxygenated for five minutes and containing specified quantities of DABCO.

| Mass of DABCO in 10 ml of dye solution/g | Concentration of DABCO / mol dm ⁻³ | k/ mol dm ⁻³ s ⁻¹ | $\tau_{1/2}$ / h |
|---|--|--|------------------|
| 0 | 0 | 0.271 | 3.52 |
| 0.25 | 0.222 | 0.1973 | 4.85 |
| 0.275 | 0.244 | 0.2743 | 3.64 |
| 0.58 | 0.515 | 0.2701 | 3.71 |

The results in Table 2.17, show that the presence of DABCO does not affect the rate of fading of oxygenated solutions of [IV], as the rate of photofading and the half-life and lifetime of [IV] is almost the same in the presence or absence of DABCO. Increasing the concentration of DABCO has no effect on the rate of fading of the solution either. These results are in agreement with Albini's results, which showed that azo dyes are efficient quenchers of singlet oxygen, but show very little chemical reactivity with oxygen.¹³

The effect of the solvent medium on the rate of fading

Referring back to Chapter 1, the expected mechanism for the photoreduction of dyes is thought to involve the photo excited state of the dye abstracting hydrogen from the solvent to give a hydrazobenzene. The hydrazobenzene formed may then revert back to the original dye, or undergo further degradation. The experiments of Hashimoto and Kano¹⁵ were carried out in propan-2-ol. An initial decrease in the intensity of the long wavelength absorption peak was followed by complete recovery of the absorption peak on letting oxygen into the solution. The results of their study are confirmed by inspection of Figure 2.49.

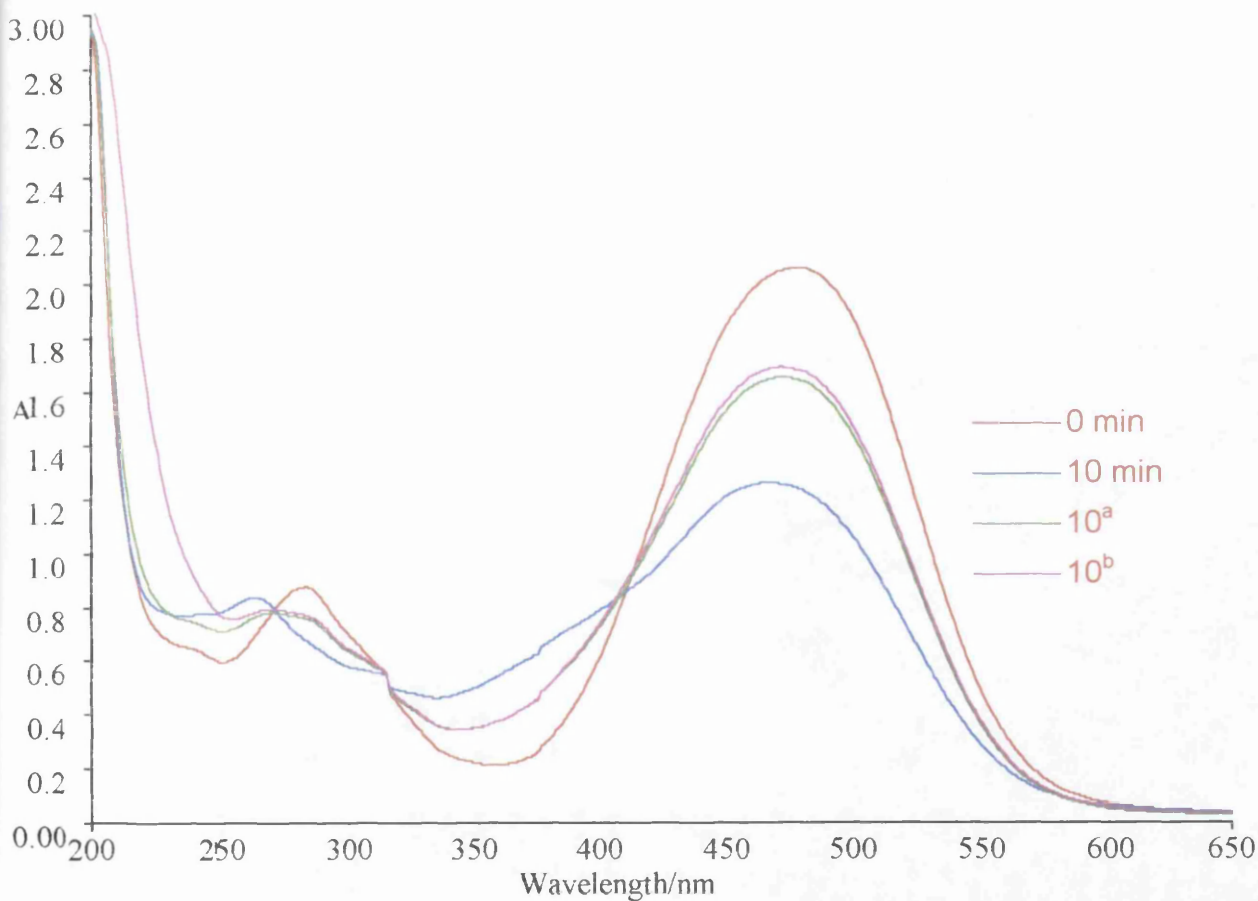


Figure 2.49 The changes in the absorption spectrum of [IX] in deoxygenated propan-2-ol with irradiation of 10 minutes. 10^a is the spectrum taken after storing the solution that had been irradiated for 10 minutes in the dark for 24 hours. 10^b is the spectrum taken after exposing the solution 10^a to oxygen.

Figure 2.49 shows that after irradiation, in contrast to Hashimoto and Kano's results, a full recovery of the original intensity of the long wavelength absorption peak did not occur. The absorbance intensities at λ_{\max} for the spectra in Figure 2.49 are given in Table 2.18.

Table 2.18 The absorption intensities at λ_{\max} of a degassed propan-2-ol solution of [IX], before irradiation, after 10 minutes irradiation, after storing the irradiated solution in the dark for 24 hours and after admitting oxygen into the stored solution.

| Spectrum | Irradiation time/ mins | Absorbance |
|-----------------|------------------------|------------|
| 0 | 0 | 2.06 |
| 10 | 10 | 1.24 |
| 10 ^a | 10 | 1.64 |
| 10 ^b | 10 | 1.68 |

10^a is the spectrum taken after storing the solution that had been irradiated for 10 minutes in the dark for 24 hours.

10^b is the spectrum taken after exposing the solution 10^a to oxygen.

It is also apparent from Figure 2.49 and Table 2.18, that recovery of peak intensity occurs with or without the introduction of oxygen into solution, as storing for a time period in the dark, produced a recovery of intensity from an absorbance of 1.24 to 1.64. The addition of oxygen into the solution had a minor effect on recovery of intensity. The introduction of oxygen into the solution immediately after irradiation did not produce the immediate recovery of intensity either. The recovery time is reached essentially within 30 minutes of the end of the irradiation. After this time, any further recovery of intensity is small. This recovery time is found to be independent of the presence of oxygen.

The rate of fading of [IX] in propan-2-ol solution is much quicker than in a methanol solution of the dye. The recovery of intensity exhibited by the dye in propan-2-ol is not seen in methanol. Experiments with [IV] in propan-2-ol solutions, showed similar recovery behaviour and again, much faster rates of fading than for methanol solutions of [IV].

Photofading of [IX] in other alcohols

Experiments in different alcohols were carried out to examine the effect of the length of the alkyl chain and also the effect of branching on rates of fading of solutions of [IX] in order to

investigate the process of hydrogen abstraction from the solvent in the photoreduction mechanism proposed by Hashimoto and Kano.¹⁵

A methanol solution of concentration $5 \times 10^{-5} \text{ mol dm}^{-3}$ was placed into the quartz cell and the methanol evaporated off, leaving a known quantity of the dye in the cell. The required dry solvent was then added to the dye in the cell and this solution was then degassed under argon for 10 minutes. All these experiments were carried out under the same conditions. The lifetimes of [IX] in different alcohol solutions are displayed as the bar chart in Figure 2.50.

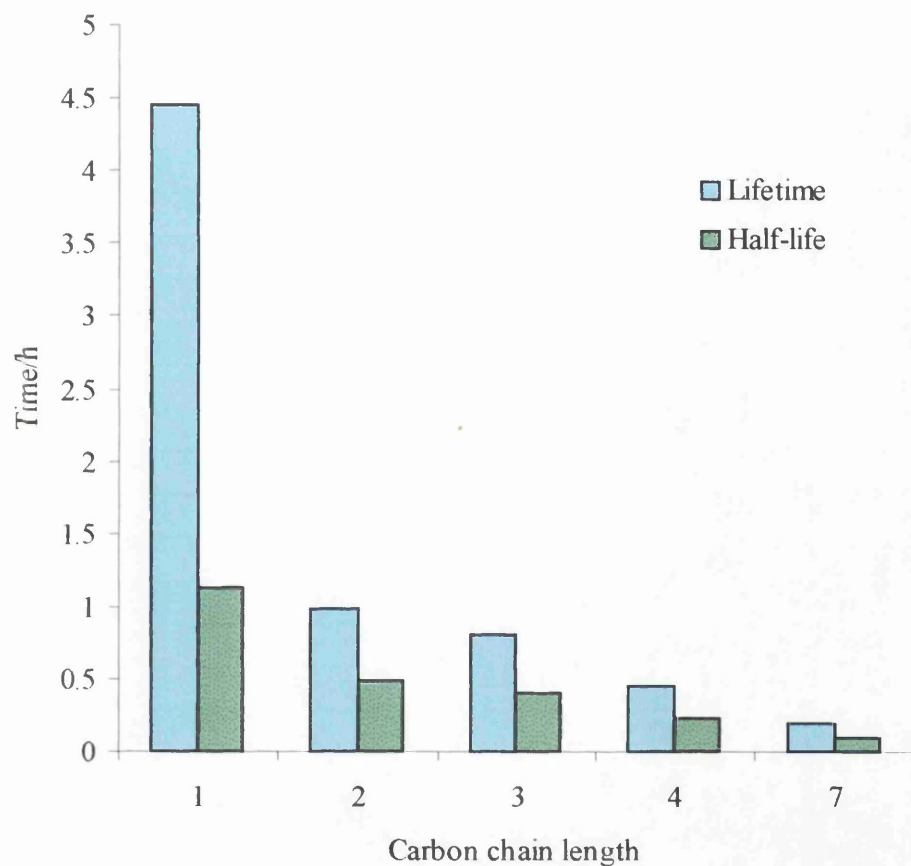


Figure 2.50 A comparison of Lifetimes and half-lives of [IX] in alcohols of increasing Carbon chain length.

The alcohols used were methanol, ethanol, propan-1-ol, butan-1-ol and heptan-1-ol, for carbon chain lengths 1, 2, 3, 4 and 7 respectively. These are all straight chain primary alcohols which shows a dramatic increase in the rate of fading of [IX] with increasing alkyl chain length of the solvent (Figure 2.50). The rate of fading of [IX] is slow in methanol, but is over two times faster in ethanol and propanol and five times faster in butanol, while in heptanol the rate of fading is over ten times faster than in methanol.

The rate of photofading in branched alcohol solutions

The effect of branching is pronounced by the difference in rates between n-propanol and propan-2-ol and between n-butanol and t-butyl alcohol. These results are illustrated in Figure 2.51.

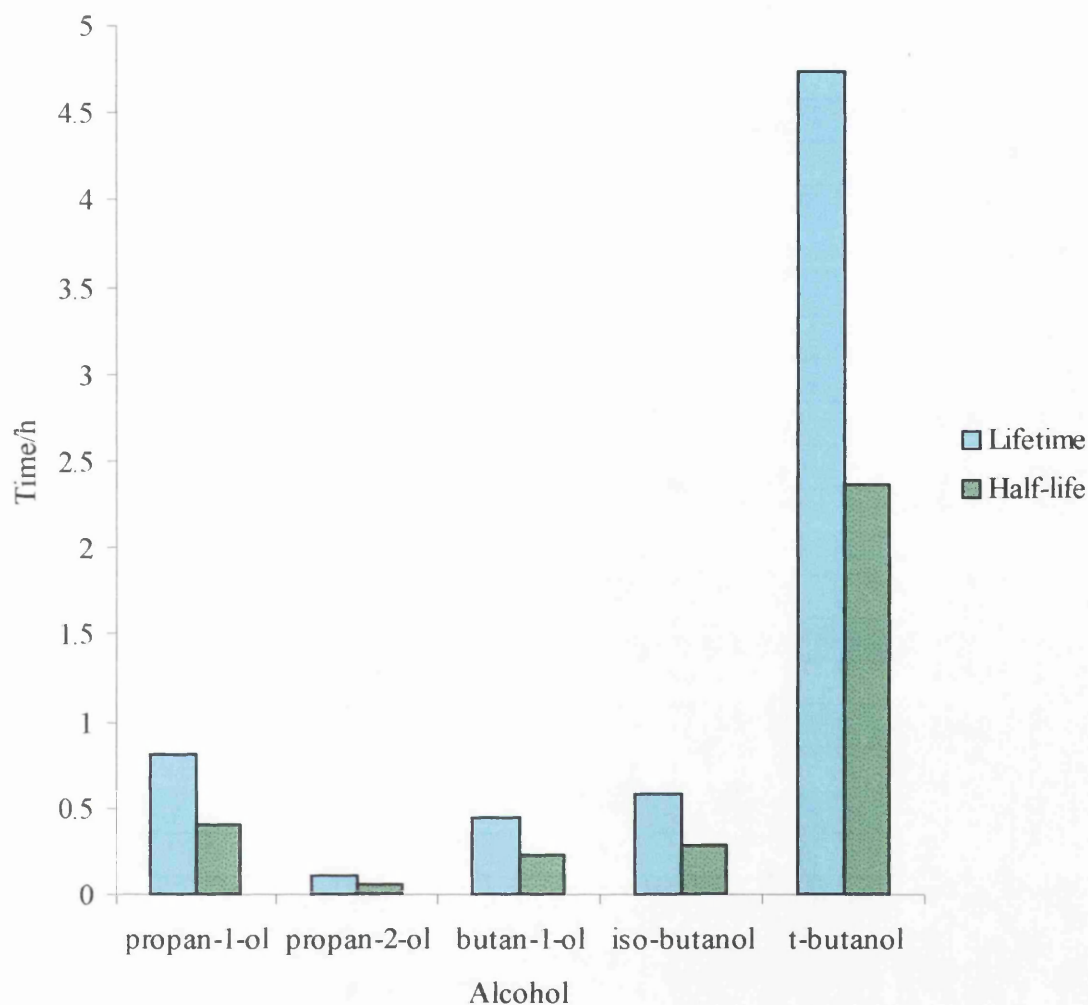


Figure 2.51 A comparison of the lifetimes and half-lives of [IX] in linear and branched alcohol solutions under anaerobic conditions.

The difference between the lifetimes of the dye in primary and secondary alcohols can be seen by comparing propan-1-ol and propan-2-ol. The lifetime of [IX] in the secondary alcohol, propan-2-ol is approximately seven times shorter than in the primary alcohol, propan-1-ol. This suggests that branching in alcohols has a dramatic effect on the rate of fading of the dye.

The effects of further branching can be seen by considering the differences in the lifetimes and half-lives of the primary alcohols, butan-1-ol and iso-butanol and t-butanol, which is a tertiary

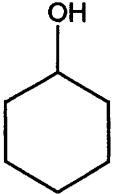
alcohol. The lifetimes and half-lives of the two primary butanols are very similar, but t-butanol has a lifetime and half-life which is eight to ten times longer than the two primary butanols. In fact [IX] has a longer lifetime and half-life in t-butanol than in methanol.

The lifetimes and half-lives of the alcohols are summarized in Table 2.19, the structure of each alcohol is also shown and is designated as primary, secondary or tertiary. From Table 2.19, it can be seen that dye [IX] is very photo-stable in methanol. [IX] is less photo-stable in the other primary alcohols, with a decrease in photo-stability accompanying an increase in chain length. Branching of the alkyl chain seems to have little effect at positions other than α to the hydroxy group, as the rate of fading of iso-butanol and the unbranched butan-1-ol are similar. In contrast, branching at the carbon α to the hydroxy group has a dramatic effect on the rate of photofading of the dye. The photo-stability [IX] in the secondary alcohol, propan-2-ol is much less than in propan-1-ol, its unbranched isomer. Another example of a secondary alcohol is cyclohexanol, in which [IX] also has a short lifetime and half-life.

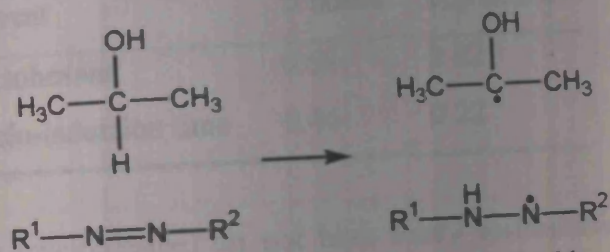
Since branching at the α -hydroxy carbon atom causes such a large increase in the rate of fading, it might be surprising that further branching at this carbon has the opposite effect.

In fact in tertiary-butyl-alcohol, [IX] has an even longer lifetime and half-life than in methanol.

Table 2.19 The lifetimes and half-lives of [IX] in solutions of some different alcohols under anaerobic conditions.

| Solvent | Solvent Structure | Alcohol type | Lifetime/h | Half-life/h |
|-----------------|--|--------------|------------|-------------|
| Methanol | $\begin{array}{c} \text{H} \\ \\ \text{H}-\text{C}-\text{OH} \\ \\ \text{H} \end{array}$ | Primary | 4.46 | 1.12 |
| Ethanol | $\begin{array}{c} \text{H} \\ \\ \text{H}_3\text{C}-\text{C}-\text{OH} \\ \\ \text{H} \end{array}$ | Primary | 0.98 | 0.49 |
| Propan-1-ol | $\begin{array}{c} \text{H} \quad \text{H} \\ \quad \\ \text{H}_3\text{C}-\text{C}-\text{C}-\text{OH} \\ \quad \\ \text{H} \quad \text{H} \end{array}$ | Primary | 0.80 | 0.40 |
| Propan-2-ol | $\begin{array}{c} \text{CH}_3 \\ \\ \text{H}-\text{C}-\text{OH} \\ \\ \text{CH}_3 \end{array}$ | Secondary | 0.11 | 0.06 |
| Butan-1-ol | $\begin{array}{c} \text{H} \quad \text{H} \quad \text{H} \\ \quad \quad \\ \text{H}_3\text{C}-\text{C}-\text{C}-\text{C}-\text{OH} \\ \quad \quad \\ \text{H} \quad \text{H} \quad \text{H} \end{array}$ | Primary | 0.44 | 0.22 |
| Iso-butanol | $\begin{array}{c} \text{CH}_3 \quad \text{H} \\ \quad \\ \text{H}-\text{C}-\text{C}-\text{OH} \\ \quad \\ \text{H} \quad \text{H} \end{array}$ | Primary | 0.58 | 0.29 |
| T-butyl-alcohol | $\begin{array}{c} \text{CH}_3 \\ \\ \text{H}_3\text{C}-\text{C}-\text{OH} \\ \\ \text{CH}_3 \end{array}$ | Tertiary | 4.73 | 2.36 |
| Cyclohexanol |  | Secondary | 0.22 | 0.11 |

The probable reasons for these differences in the photostability of [IX] in the different alcohols can be explained by considering the hydrogen abstraction process shown in Scheme 2.2. This hydrogen abstraction is the initial step in the photoreduction reaction of azo dyes proposed by Albini.¹⁶



Scheme 2.2 The abstraction of hydrogen from propan-2-ol by an azo dye.

Here, hydrogen is abstracted from propan-2-ol by the azo dye giving a hydrazo intermediate and a propan-2-ol radical species.

The reason for these differences in rates of reaction in the various alcohols may be explained by considering the ease of abstraction of hydrogen from the solvent by the dye. The ease of abstraction will be affected by the strength of the C-H bond and also the stability of the radical formed after abstraction of hydrogen. A radical is stabilized by a greater number of alkyl groups attached to the radical centre. A greater the number of alkyl groups gives increased stabilisation due to hyperconjugation. Propan-2-ol has two alkyl groups to stabilize the radical at its central carbon atom, whereas, methanol has no alkyl groups to stabilize the CH_3^\bullet radical. Thus, hydrogen should be more easily abstracted from a secondary alcohol like propan-2-ol than a primary alcohol, such as methanol because of the greater stability of the radical formed from propan-2-ol compared to the CH_3^\bullet radical that would be formed from methanol. This would explain the much faster rate of fading in propan-2-ol than in methanol, as the dye would abstract hydrogen more easily and therefore undergo faster colour loss. Longer alkyl chains would presumably increase radical stability slightly further and thus increase the rate of fading. Fading is accordingly slightly faster in butan-2-ol than in propan-2-ol.

In contrast to the other alcohols studied, the rate of fading of the dye in t-butyl alcohol was very slow. This may be attributed to the fact that t-butyl alcohol has no readily abstractable hydrogens and the probability of hydrogen abstraction by the dye is low, consequently the rate of fading will also be low.

Rates of photofading in other solvents

The results of fading of some other solvent solutions of [IX] that were photofaded are summarized in Table 2.20.

Table 2.20 The lifetimes and half-lives of [IX] in cyclohexane.

| Dye | Solvent | τ / hours | $\tau_{1/2}$ / hours |
|------|----------------------|----------------|----------------------|
| [IX] | Cyclohexane | 0.66 | 0.42 |
| [IX] | Cyclo-induction time | 0.46 | 0.22 |

These solvents (cyclohexane) do not have easily abstractable hydrogen atoms and the rate of photofading of [IX] in cyclohexane is thus slower than for propan-2-ol and cyclohexanol, which have relatively fast rates of photofading. The faster rate of fading of the dye in cyclohexane than in methanol might be due to the existence of an alternative reactive pathway. It has been suggested that photo-reduction of the cis isomers of azo dyes occurs in cyclohexane. The lifetimes of cis isomers is longer in cyclohexane than in methanol and this could explain the faster rate of fading in cyclohexane relative to the rate in methanol, as the cis isomer persists longer and therefore has a greater probability of undergoing some reaction.

Experiments with sensitizers

The rate of photo reaction of [IX] in methanol solution is increased dramatically by up to 100 times in the presence of sensitizers such as acetone (see Chapter 1 pages 65-70).

Table 2.21 The lifetimes (τ) and half-lives ($\tau_{1/2}$) of [IX] in the presence of some sensitizers.

| Solvent | Sensitizer | [Sensitizer] ^a | τ / h | $\tau_{1/2}$ / h |
|---------------|--------------|---------------------------|------------|------------------|
| Methanol | None | 0 | 4.46 | 1.12 |
| Methanol | Acetone | 3.4×10^{-3} | 0.0041 | 0.0020 |
| Methanol | Acetone | 6.8×10^{-4} | 0.0067 | 0.0032 |
| Methanol | Acetone | 1.7×10^{-4} | 0.0106 | 0.0053 |
| Methanol | Benzophenone | 1.0×10^{-4} | 0.0018 | 0.0009 |
| Acetone | - | - | 0.0293 | 0.0146 |
| Cyclohexanone | - | - | 0.0118 | 0.0059 |

^a[Sensitizer] is the concentration of sensitizer in mol dm⁻³.

The results of these experiments reveal that the rate of fading is up to 550 times faster when acetone is present in a methanol solution of the dye than when no acetone is present. There is a similar rapid increase in the rate of fading when benzophenone is present as the sensitizer. The amount of acetone present also has an effect on the rate of fading. For example, when 10 μ l of acetone is present, the rate is approximately 1.6 times faster than when only 2 μ l of acetone is present and around seven times faster than when only 0.25 μ l of acetone is used. Even so, only a small volume of sensitizer is needed and in pure acetone, there is no increase in the rate of reaction.

To examine how the other azo dyes are affected by the presence of sensitizers, one representative dye was taken from each of the series of dyes and irradiated in the presence of acetone. Table 2.22 shows the lifetimes of some of these other azo dyes in methanol solution and in the presence of acetone.

Table 2.22 The half-lives ($\tau_{1/2}$) of some azo dyes in methanol solution and the presence of acetone.

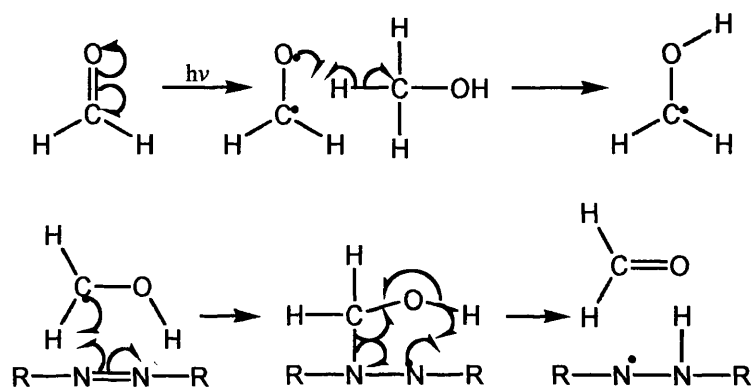
| Dye | Acetone concentration/ mol dm ⁻³ | $\tau_{1/2}$ / mins | $\tau_{1/2}$ / h |
|-------|--|---------------------|------------------|
| [IV] | 0.9×10^{-4} | 1.323 | 0.0118 |
| [IV] | 1.7×10^{-4} | 0.707 | 0.022 |
| [IX] | 1.7×10^{-4} | 0.437 | 0.00730 |
| [XI] | 1.7×10^{-4} | 0.59 | 0.0099 |
| [XIV] | 1.7×10^{-4} | 0.71 | 0.012 |
| [XV] | 1.7×10^{-4} | 0.86 | 0.0144 |

As can be seen from the above results, the rate of photofading is increased dramatically for all of the azo dyes and the lifetimes and half-lives of the dyes are reduced to the same order of magnitude. It would be unwise to draw any conclusions from the relative rates of the dyes in the presence of acetone, as these experiments have quite a high margin of error associated with them. This error margin results from the difficulty in reproducing the exact same conditions for each experiment, such as complete deoxygenation and using the same volume of sensitizer. Because of the rapid nature of the sensitised experiments, these slight differences in experimental conditions, may cause a relatively large variation in lifetimes and half-lives of dyes.

As can be seen from the above results, the rate of photofading is increased dramatically for all of the azo dyes and the lifetimes and half-lives of the dyes are reduced to the same order of magnitude. It would be unwise to draw any conclusions from the relative rates of the dyes in the presence of acetone, as these experiments have quite a high margin of error associated with them. This error margin results from the difficulty in reproducing the exact same conditions for each experiment, such as complete deoxygenation and using the same volume of sensitizer. Because of the rapid nature of the sensitised experiments, these slight differences in experimental conditions, may cause a relatively large variation in lifetimes and half-lives of dyes.

The reason for the rapid increases in the rate of photofading may be attributed to the two different mechanisms possible for photoreduction. When no sensitizer is present, direct photoreduction takes place, where an excited state of the dye itself abstracts hydrogen from the solvent, as shown in Scheme 2.2. However, when sensitizer such as acetone is present in the dye solution, indirect photoreduction (Scheme 2.3) can occur.¹⁷ A possible curly arrow mechanism

for the initial stages of this indirect photoreduction are given in Scheme 2.3. Here, the sensitizer is acetone and the solvent is methanol. The first step is the excitation of the acetone by irradiation to yield a diradical type species. This diradical species then abstracts hydrogen from the solvent yielding a free radical species. The free radical may then interact with the azo dye and an intramolecular hydrogen abstraction in the resulting intermediate gives a hydrazo radical species. The hydrazo radical may then itself abstract another hydrogen from the solvent to form a hydrazo compound (see Chapter 1, Section 1.10).



Scheme 2.3 Possible curly arrow mechanism for the indirect photoreduction of azo dyes.

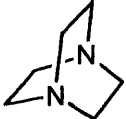
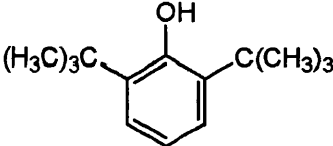
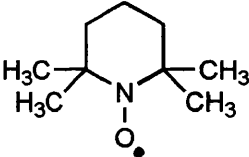
Since the sensitizer has a high probability of being converted to a radical species, the probability of hydrogen abstraction from the solvent and subsequent transfer to the azo dye is also high, resulting in a very fast rate of reaction. Conversely, the probability of the azo dye itself being excited to a triplet diradical state and abstracting hydrogen from the solvent is very low, and the rate of photoreaction is therefore much slower.

It is also interesting to note the changes in the absorption spectra of the dye solution that occur when acetone is present and compare these changes to the fading profile when no acetone is present. These differences are considered in the discussion of the photofading products in Chapter 3.

The effect of quenchers on anaerobic fading

The sensitized photoreaction probably involves a radical type mechanism. To investigate this, some well known radical traps were added to methanol solutions of the dyes, which also contained 10 μl of acetone acting as a sensitizer. Table 2.23 contains the structures of the reagents and the lifetimes of the dye in sensitized dye solutions containing the reagent.

Table 2.23 The effect of various quenchers on the half-life ($\tau_{1/2}$) of [IX] in acetone sensitized photoreactions in methanol and on the unsensitized photoreaction.

| Vol. of Acetone/ μl^a | Reagent | Structure of Reagent | $\tau_{1/2}$ / min | $\tau_{1/2}$ / h |
|----------------------------------|--------------------------|---|--------------------|------------------|
| 0 | none | — | 67.2 | 1.12 |
| 10 | none | — | 0.437 | 0.0073 |
| 10 | DABCO ^b 98 % |  | 2.5 | 0.0417 |
| 10 | Di-tertiary-butyl phenol |  | 13 | 0.217 |
| 10 | TEMPO ^b |  | 213 | 3.55 |
| 0 | TEMPO | As above | 247 | 4.12 |

^a Acetone was added to increase the rate of the radical reaction. ^bTEMPO free radical is 2,2,6,6-tetramethyl-1-piperidinyloxy free radical. ^b DABCO is 1,4,-Diazabicyclo [2,2,2] octane.

Modes of action

These reagents have different and sometimes multiple modes of action. DABCO is principally known as a singlet oxygen quencher, but can act in other ways as a radical quencher. 2-6-di-tert-

butyl phenol is a radical trap or radical quencher and TEMPO free radical exists as a stable free radical, and can thus act as a very efficient radical trap or quencher.

There was little effect on rates of photo fading with the addition of DABCO to degassed methanol solutions of [IX] This is perhaps unsurprising, as DABCO is principally a singlet oxygen quencher and would therefore not be expected to have much effect on fading rates in the absence of oxygen.

There is a slight reduction in the rate of fading, indicating that DABCO may also act in some quenching capacity.

The structure of 2-6-di-tert-butyl phenol has a delocalised system substituted by electron withdrawing substituents, which enables it to exist as a relatively stable free radical in comparison to other radical species. Thus 2-6-di-tert-butyl phenol may interact with an unstable radical species and the free radical may transfer from this species onto the 2-6-di-tert-butyl phenol. In this 2-6-di-tert-butyl phenol therefore acts as a radical trap or quencher. Di-tertiary butyl phenol has a retarding effect on the rate of photofading of a methanol solution of [IX] in the presence of acetone. This could be due to its behaviour as a radical trap whereby, it may interact with a radical formed from the acetone sensitizer and thus prevent the acetone radical species from interacting with the dye, or alternatively, it may trap a radical species of the dye and inhibit degradation of the dye. The photoreaction is slowed substantially by the presence of 2-6-di-tert-butyl phenol. Hexachlorobenzene also had a minor effect on the rate of fading of the sensitized dye solution. The half-life of the dye was only marginally longer (x mins) in the presence of hexachlorobenzene than when no hexachlorobenzene is present (y mins).

Different concentrations of TEMPO were used in degassed solutions of [IV] and [IX]. After degassing the solutions, 10 μ l of acetone was added to the solution to act as a sensitizer for the reaction. The effect on the rate of fading is dramatic, with the rate of the sensitised photoreaction being retarded by almost five hundred times. The rate of fading of the sensitized photoreaction in the presence of TEMPO is only slightly faster than the unsensitized reaction in the presence of TEMPO. Both photoreactions involving TEMPO have a slightly longer half-life than the unsensitized reaction with no TEMPO present. TEMPO has a similar retarding effect on the sensitized photoreactions of some of the other dyes and the results are summarized in Table 2.24. The structure of TEMPO free radical is shown in Table 2.23. TEMPO is a stable free radical at room temperature and might therefore be expected to trap any radicals formed in the photoreaction.

Table 2.24 The half-lives for the TEMPO quenched acetone sensitized photoreaction of [IV], [IX] and [XV].

| Dye | Concentration of acetone / mol dm ⁻³ | Concentration of TEMPO / mol dm ⁻³ | Half-life / h |
|------|---|---|---------------|
| [IV] | 0.0034 | 0.1 | 0.83 |
| [IX] | 0 | 0.1 | 3.55 |
| [IX] | 0.0034 | 0.1 | 0.65 |
| [XV] | 0.0034 | 0.1 | 0.40 |

The half-lives of all the dyes tested were greatly increased by the presence of TEMPO in the sensitized photoreaction and stabilized to the same order of magnitude. The concentration of TEMPO in solution is critical, the greater the concentration, the longer the lifetime of the dye in solution. The fading profile of [IX] in a methanol solution containing TEMPO and acetone are shown in Figure 2.52.

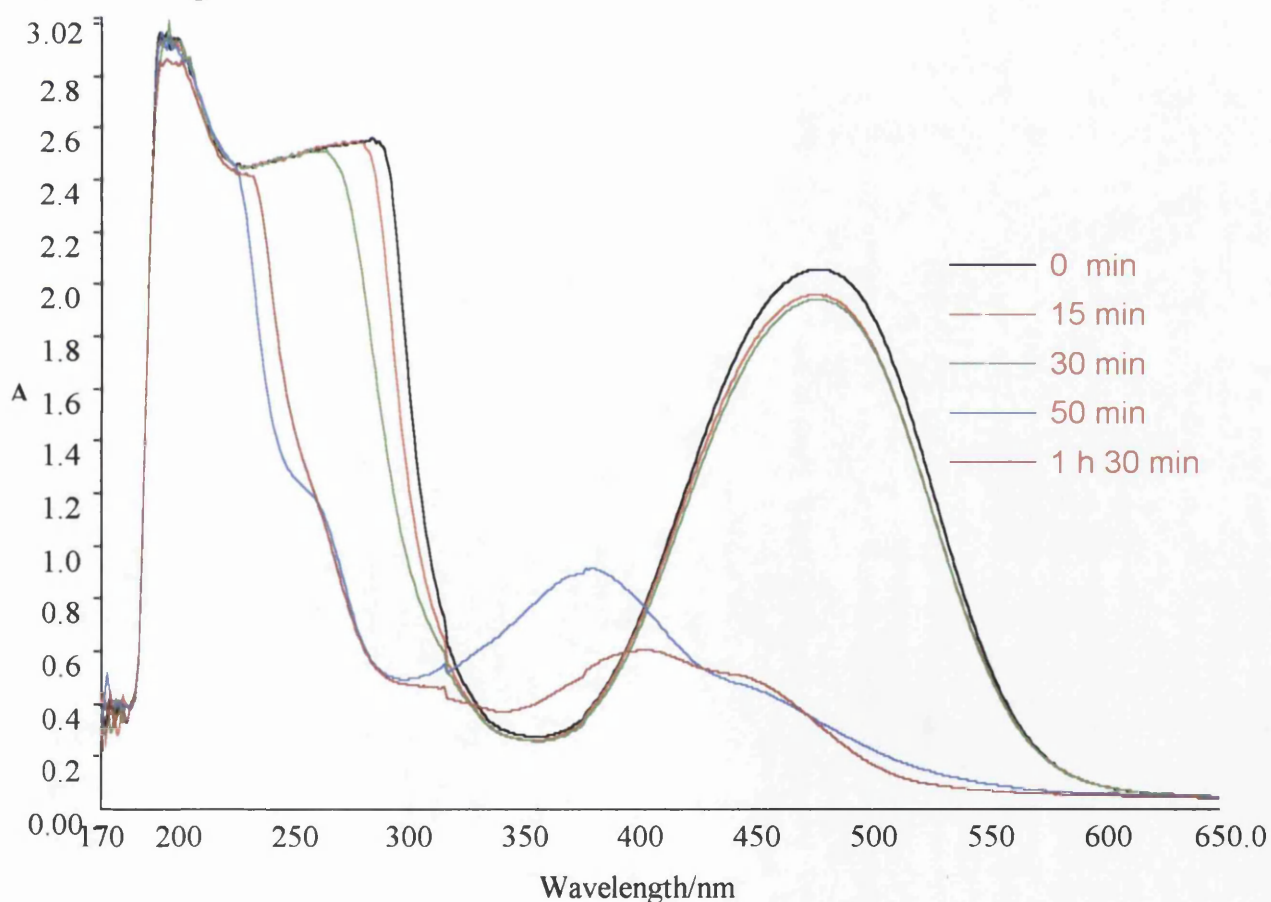


Figure 2.52 The changes in the spectrum of [IX], in the presence of acetone sensitizer and TEMPO quencher in methanol solution under anaerobic conditions, on irradiation.

It is interesting to note the changes in the spectra of the dye system in these reactions. The changes in the absorbance at λ_{max} of **[IX]** in methanol and in the presence of acetone and 0.1 mol dm^{-3} TEMPO (Figure 2.53), show the initial rate of fading of the solution is very slow, but at an irradiation time of between 30 minutes and 50 minutes, there is a rapid increase in the rate of fading. Also shown in Figure 2.53, are the changes in the absorbance at λ_{max} of a methanol solution of 0.1 g of TEMPO only. From Figure 2.52 and Figure 2.53 there appears to be a relationship between the length of the slow induction period and the quantity of TEMPO present in solution. The rate of fading of the dye seems to be similar to the rate of fading of TEMPO itself. This suggests that fading proceeds slowly while TEMPO is present, but increases, as TEMPO is used up.

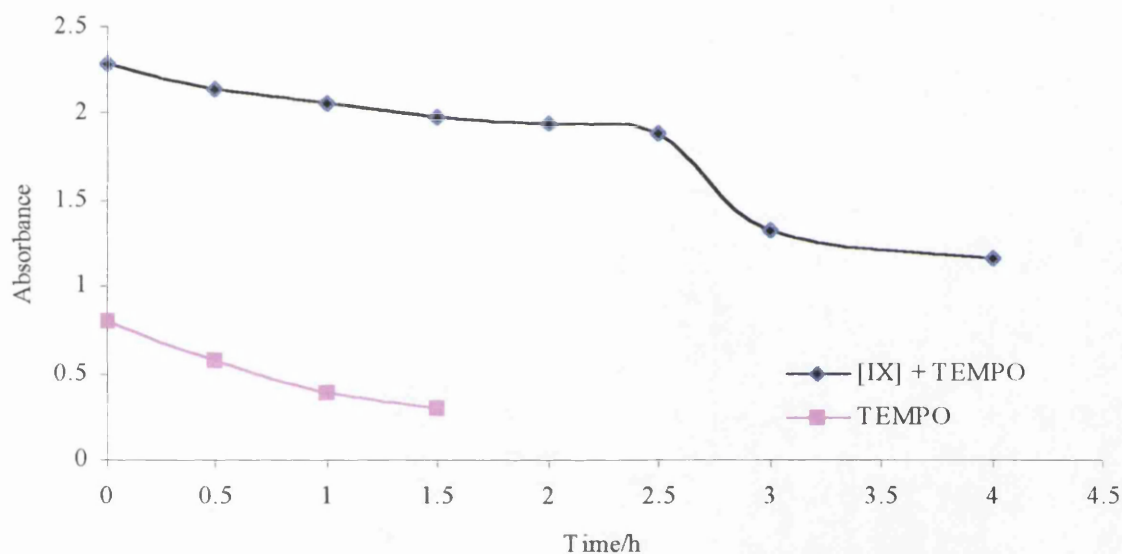


Figure 2.53 The changes in the absorbance of **[IX]** in a methanol solution in the presence of $10 \mu\text{l}$ acetone and 0.1 mol dm^{-3} TEMPO, and the changes in the absorbance of TEMPO in methanol solution at their respective λ_{max} values.

This rapid increase in the fading rate corresponds to the complete degradation of the TEMPO free radical. After the TEMPO is consumed or destroyed, the fading reaction proceeds at a relatively fast rate. Thus the rapid increase in the rate of photofading is almost certainly due to the degradation of TEMPO itself under the photo fading conditions.

The 2'-nitro substituted dye **[IV]** also exhibits an inhibition of fading when TEMPO is present, though rather than an initial slow period of fading, there is a gradual and constant retardation of

the fading rate. This rate of fading is much slower (*ca.* 70 times) than when no TEMPO is present. The photofading profile of the TEMPO quenched and acetone-sensitized photoreaction of [IV] is shown in Figure 2.54.

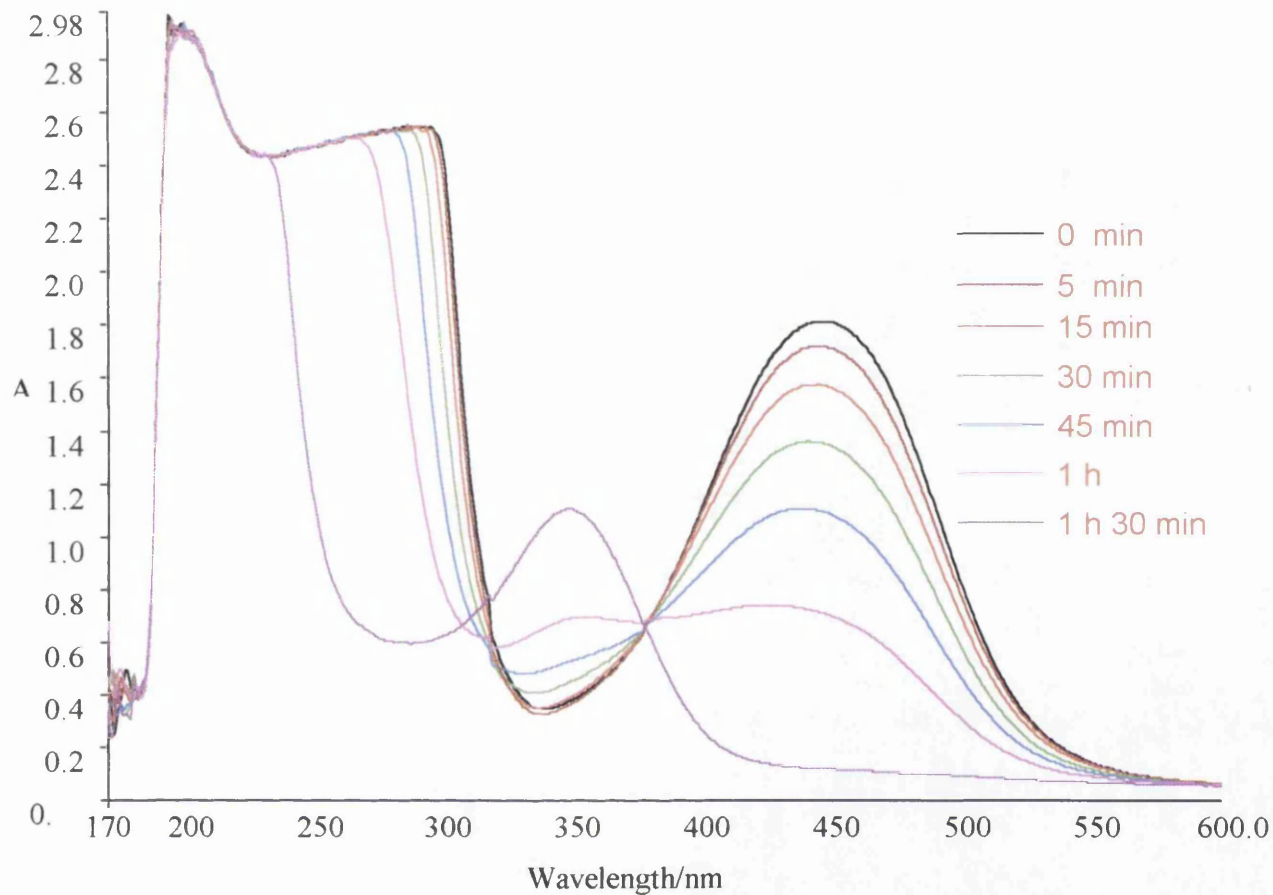


Figure 2.54 The changes in the spectrum of [IV], in the presence of acetone sensitizer and TEMPO quencher in methanol solution, on irradiation

Photofading of dyes on substrates

All of the experiments discussed so far have centered on the photoreactions of dyes in solution. Many of these experiments were conducted in methanol, which was chosen as a mimic system for the photofading behaviour of dyes on paper. The following experiments involve dyes on substrates, including paper and some other substrates intended to mimic paper.

The first of these experiments involved [IX], with the substrates standard printing paper and filter paper. Samples were prepared by dipping the substrate in to a methanolic solution of the dye. This method produced a poor take up of the dye from the solution, and the paper was only weakly coloured. To enhance the color of the paper, these samples were dried and a strong methanolic solution of the dye was dripped onto them. The samples were spun simultaneously, to try and provide a more even distribution of the dye and also to speed up the evaporation of the solvent. The uptake of the dye however was still limited. The dyes have poor solubility in water, and since cellulose is a polymer with multiple hydroxy groups, it is not surprising that the adhesion of the dye to the cellulose substrate (paper) is poor. Indeed the dye does not interact at all with microcrystalline cellulose. This is presumably the reason for the poor uptake of the dye by the paper substrate.

Two types of paper were used, a standard white printing paper, and filter paper. These two different types of paper were used to examine how the substrate might affect the fading behaviour of the dye. For example, the dye may penetrate the different papers to different degrees, or may chemically or physically bond with some papers. Other important factors, when considering the photofading behaviour on substrates, include the ability of oxygen to diffuse into the substrate and hence interact with the dye, and also any additives in the paper, which may interact with the dye.

It is not possible to record the UV/visible absorption spectra of dyes on an opaque substrate such as paper. Therefore, these spectra were recorded using the diffuse reflectance technique. This technique has the advantage of being able to record the spectra of dyes on opaque substrates. The spectrum is produced as light of various wavelengths is directed at the sample. Some of this light is then reflected, but at certain wavelengths, some light will have been absorbed by the dye. There are 2 parallel sample slots in the diffuse reflectance apparatus, one for the sample and one for the reference, which in this case is un-dyed paper. The fading profile of [IX] on paper is shown in Figure 2.55.

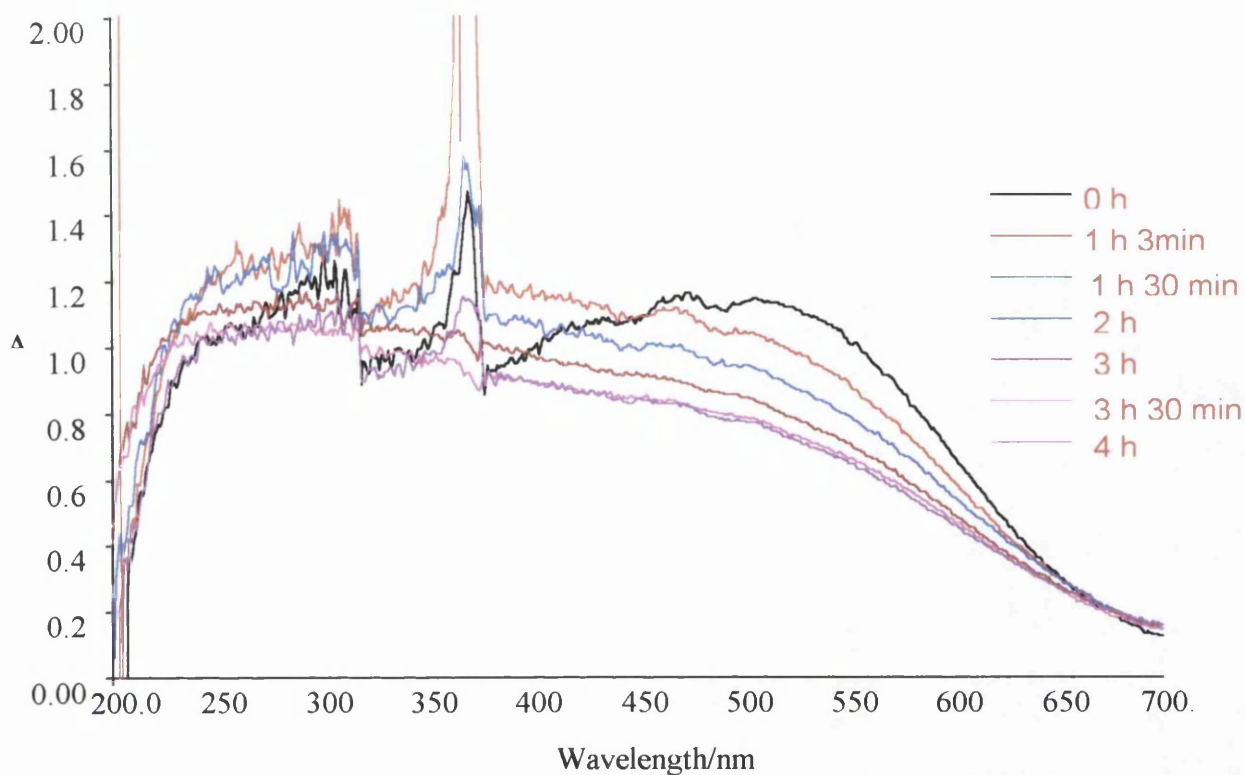


Figure 2.55 The changes in the diffuse reflectance spectrum of dye [IX] on paper with irradiation time.

Figure 2.55 shows that the uptake of the dye on the paper is poor, resulting in the paper being faintly coloured with a weak absorption spectrum. The dye can still be seen to degrade quite slowly on the paper up to a time of 4 hours, after which most of the colour has disappeared and further fading is slow. The fading profile of [IX] on filter paper, displayed in Figure 2.56, shows similar photofading behaviour, with fading becoming slower with increasing irradiation time.

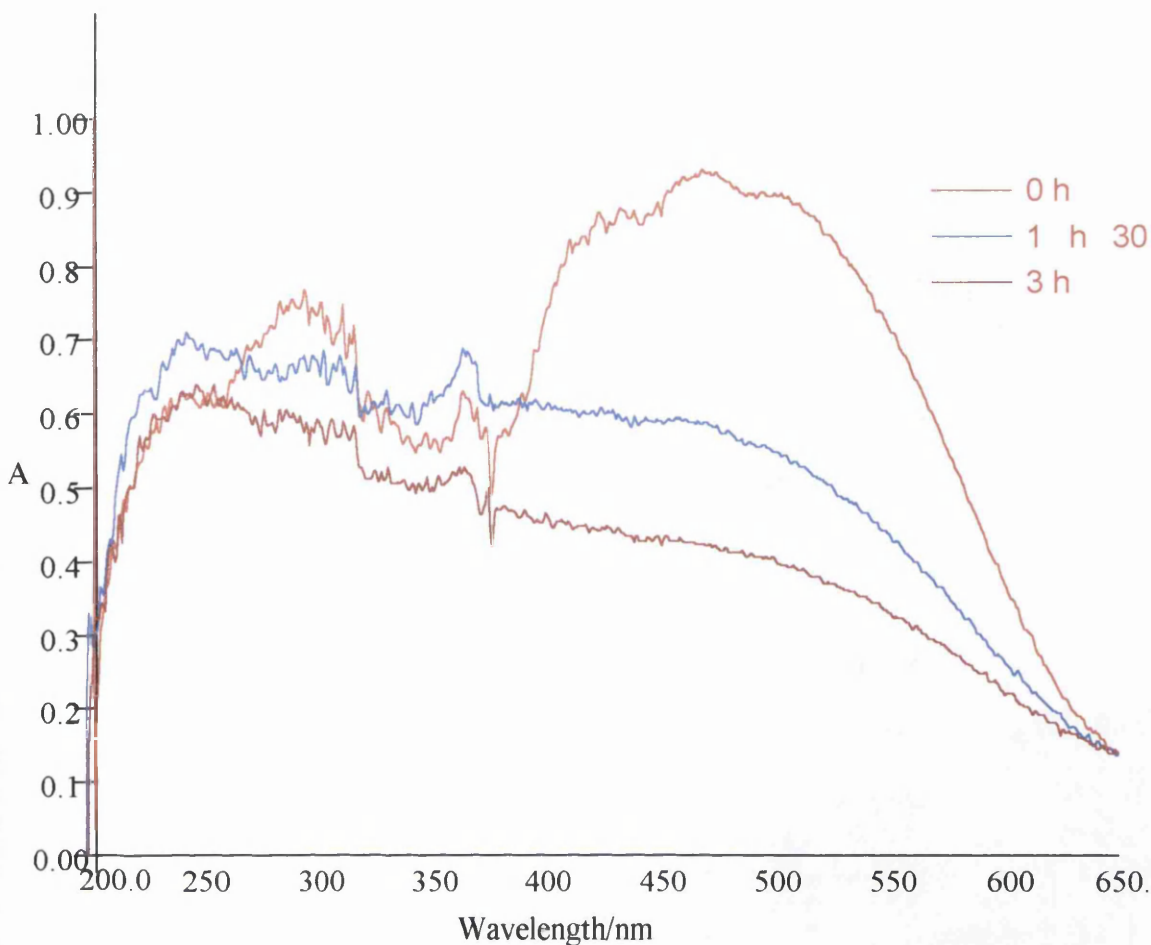


Figure 2.56 The changes in the diffuse reflectance spectrum of [IX] on filter paper, with irradiation time.

These spectra are not as clear or informative as UV/visible spectra, as the spectrum is low resolution and it is difficult to detect any possible fading products that are produced. It was thus decided to try to find a substrate, which was similar to cellulose, but was also transparent.

Experiments on ink-jet transparencies films, could be followed using UV/Visible absorption spectroscopy as they transmit light above 300 nm . A 10mm by 20mm piece of the film was coated with a concentrated solution of [IX]. This gave a reasonably good absorption spectrum and the photo-degradation of the dye on the film, with time can be easily followed. Below 300nm the film absorbs strongly, therefore this part of the spectrum is not shown. One of the reasons that the ink-jet transparent film was used, was that the photofading profile of a commercial magenta dye used in ink-jet printing, could be compared with that of [IX] (Figure

2.57). The magenta ink-jet dye was from the coloured ink used in the Hewlet-Packard Desk-jet 840 ink cartridge, and was printed directly onto the ink-jet transparency film.

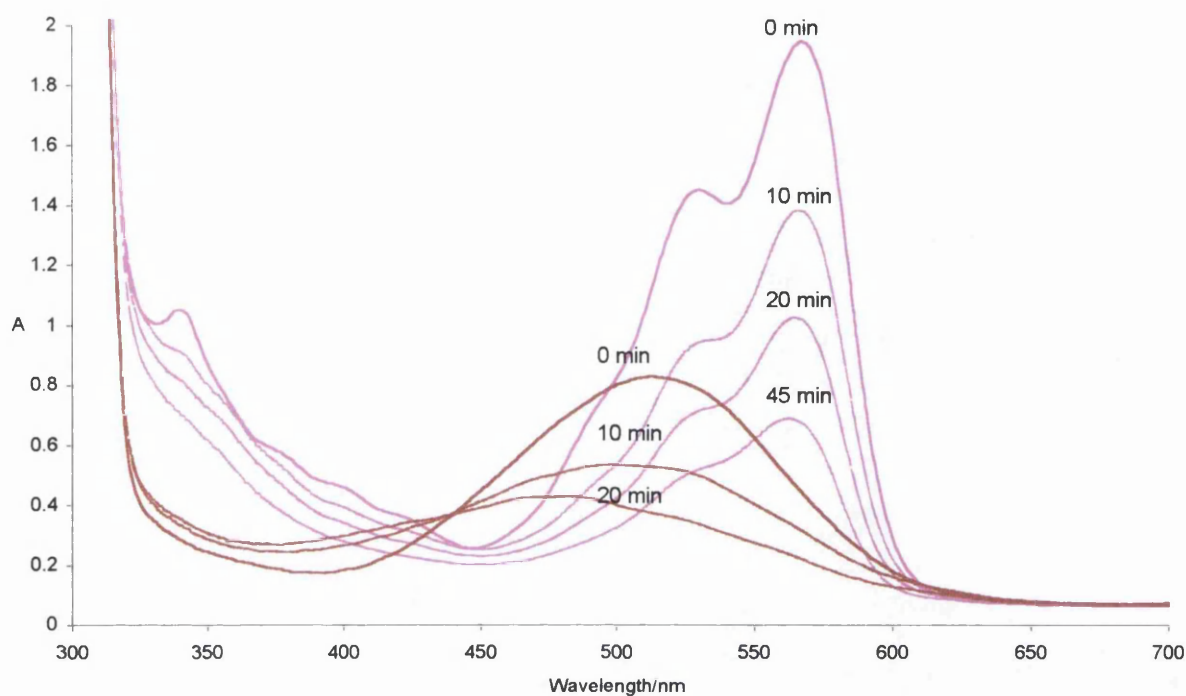


Figure 2.57 Photo-degradation of Hewlet Packard magenta ink jet dye and [IX] on ink-jet transparency film.

The initial loss of colour is quite fast resulting in a change in absorbance from 1.95 to 1.02 at $\lambda_{\text{max}} = 567$ nm after 20 minutes irradiation for the HP-magenta dye. This equates to a 48% loss in absorbance. After 20 minutes, fading is much slower. For the same time period, [IX] undergoes a change in absorbance from 0.83 to 0.38 at $\lambda_{\text{max}} = 513$ nm on irradiation, which is a 55% loss of absorbance. The rates of fading of the magenta ink jet dye and [IX] on ink-jet transparencies are similar with the HP-magenta dye slightly more lightfast than [IX] under these conditions. Note that while the magenta dye does not undergo any shifts in its absorption spectrum to shorter wavelength on irradiation, the absorption band of [IX] undergoes a bathochromic shift. This means that though [IX] loses intensity of colour at its λ_{max} , some colour is still present, but at shorter wavelengths.

One side of the ink-jet film is coated with a hydrophilic surface treatment, to which the magenta ink-jet dye preferentially adheres to, as the dye does not adhere well to the film itself. However dye [IX] does not adhere preferentially to the surface treatment, but forms an evenly distributed

coloured covering of the film. This difference in the adhesion to the substrate of the two dyes is elucidated further on irradiation of the films. Photofading of the HP-magenta dye leaves tiny dots of magenta colour surrounded by much less intensely coloured regions ((2a) Figure 2.58). In contrast, the region of [IX]-coated film that has been exposed to irradiation is evenly distributed with a yellow/brown colour ((1a) Figure 2.58), which is less intense than the original red colour of the unfaded dye ((1b) Figure 2.58). No densely coloured regions or dots are seen for the faded [IX] film. This suggests that the two dyes interact quite differently with the film with the HP-magenta dye probably aggregating at the sites where the surface treatment is concentrated. The initial relatively fast fading of the HP-magenta dyed film is probably due to the fading of the dye at sites of lower aggregation. The dye remaining at sites of higher aggregation fades more slowly. [IX] does not tend to aggregate, and thus fading is more even.

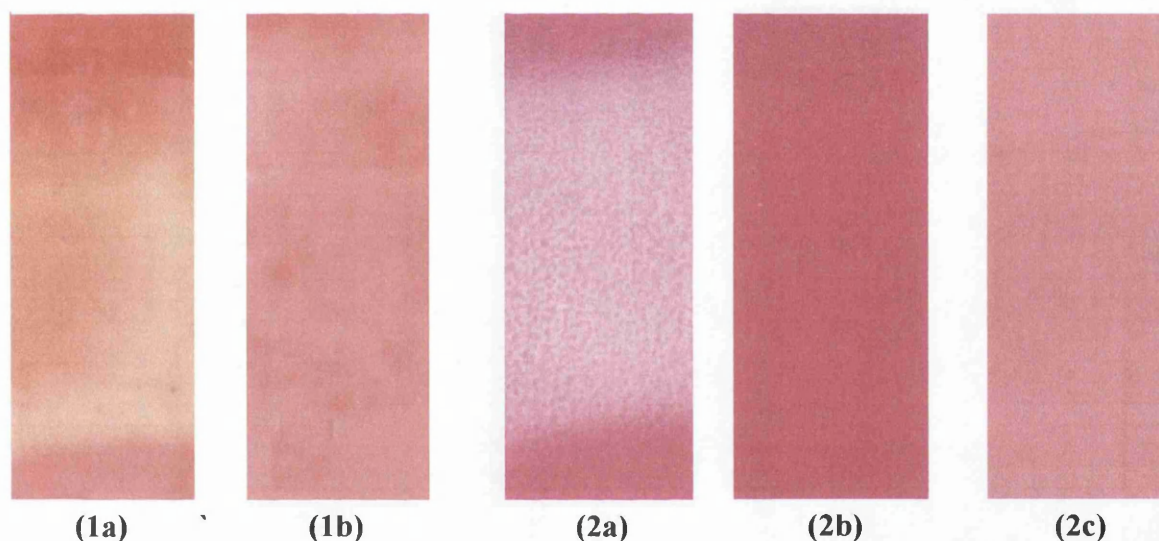


Figure 2.58 Examples of dyed ink-jet transparency film. Samples (1a) and (1b) show the film coated with dye [IX] which have been faded and unfaded respectively. Samples (2a) and (2b) show the film printed with the HP-magenta ink-jet dye which have also been faded and unfaded respectively. Sample (2c) shows the unfaded HP-magenta ink-jet dye printed onto paper.

When the samples are irradiated through a glass filter, there is a noticeable difference in the photofading rates. The fading profiles of the magenta ink-jet dye and [IX], irradiated through a glass filter are shown in Figure 2.59 and Figure 2.60 respectively. The rates of fading of both dyes through a glass filter and with no filter present are given in Table 2.25.

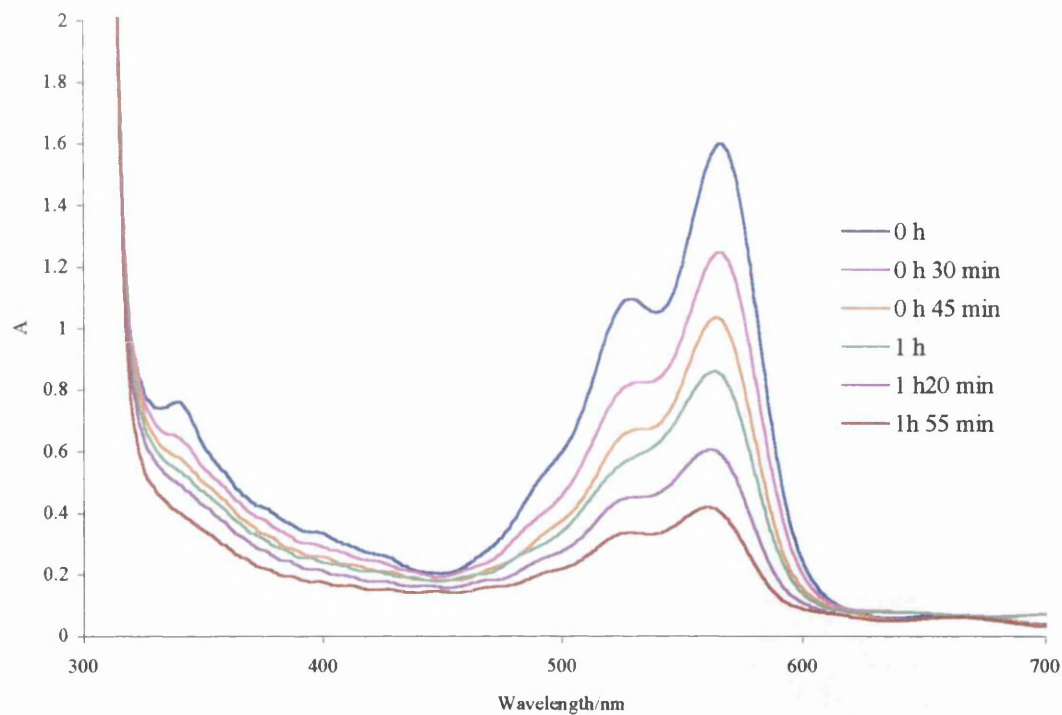


Figure 2.59 Photofading profile of magenta ink-jet dye printed onto an ink-jet transparency and irradiated through a glass filter.

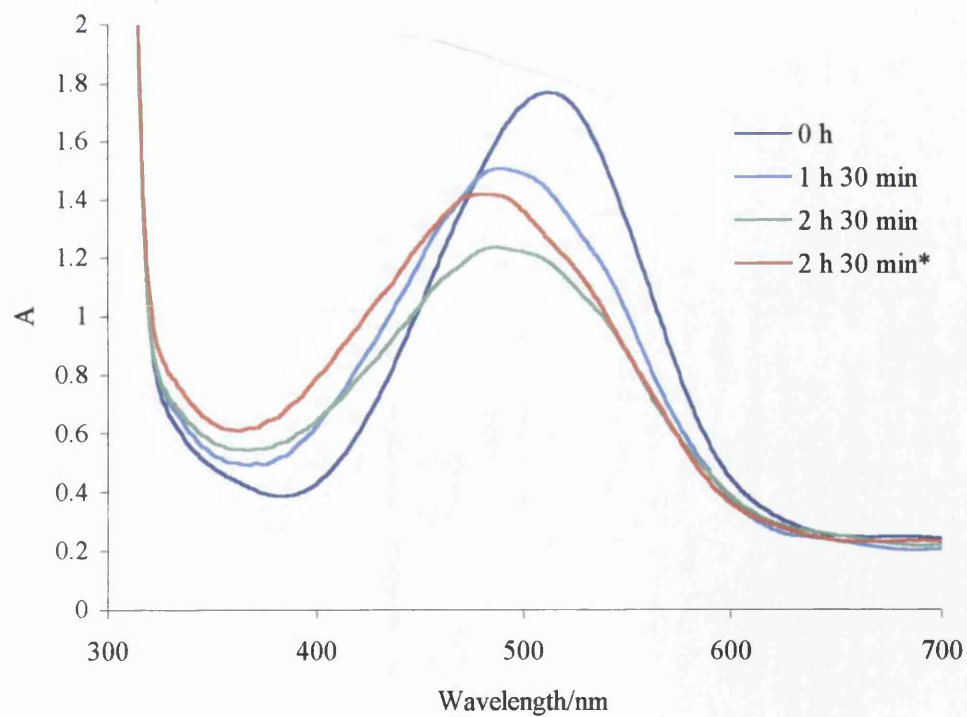


Figure 2.60 Photofading profile of [IX] on an ink-jet transparency and irradiated through a glass filter.

Table 2.25 Rates of fading of HP-magenta and [IX] on ink jet film with and without a glass filter.

| Dye | Filter | Rate constant k | % Absorbance loss after 20 mins |
|------------|-------------|-----------------|---------------------------------|
| HP-magenta | None | -1.58 | 48 |
| [IX] | None | -1.36 | 55 |
| HP-magenta | Glass slide | -0.65 | 4 |
| [IX] | Glass slide | -0.23 | 17 |

When the dyed films are irradiated through a glass slide filter, the rate of fading of the magenta ink jet dye is approximately 3 times faster than for [IX] is present. These ink-jet transparency films are quite good models for paper substrates, and the photofading reaction can be clearly monitored. The nature of the film is not known but it may be manufactured from cellulose acetate and consequently it may be chemically different to paper, especially if it contains carbonyl groups which may act as sensitizers.

Ethyl cellulose was therefore used as another model substrate substitute system for paper. Ethyl cellulose is a crystalline white powder, which is soluble in a toluene/methanol mixed solvent system. When 0.5g of ethyl cellulose is dissolved in 5ml of 80:20 ratio of toluene: methanol solution, a clear viscous solution is formed. 0.1g of [IX] can then be dissolved in this solution and the resulting coloured viscous solution can then be used to coat one side of a quartz spectrophotometer cell. A quartz cell was used so that the whole UV/visible spectrum could be observed. When the solvent has evaporated, a thin transparent film coloured with the azo dye is left attached to the quartz cell. The changes in the spectrum of the dyed film on irradiation can be seen for [IV] in Figure 2.61.

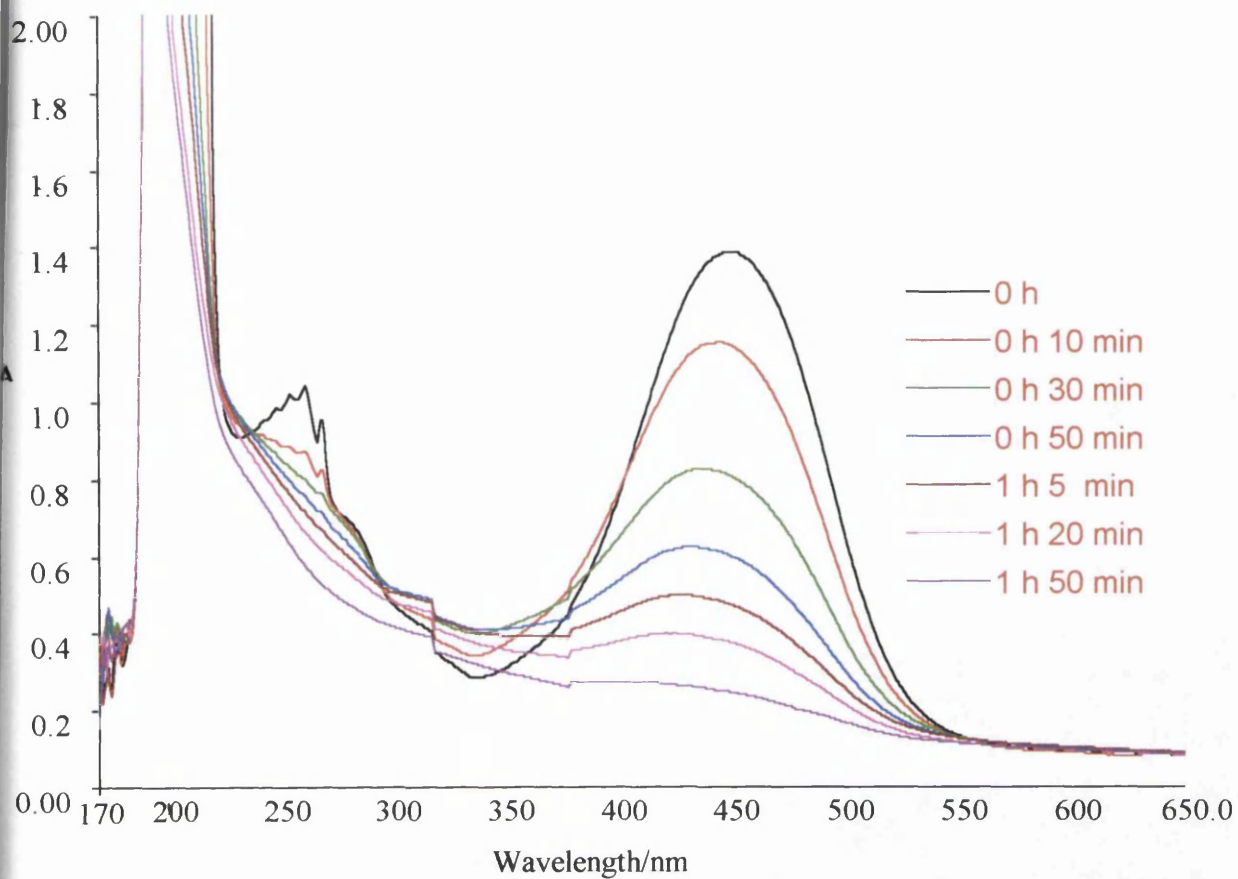


Figure 2.61 Fading profile of [IV] in an ethyl cellulose film.

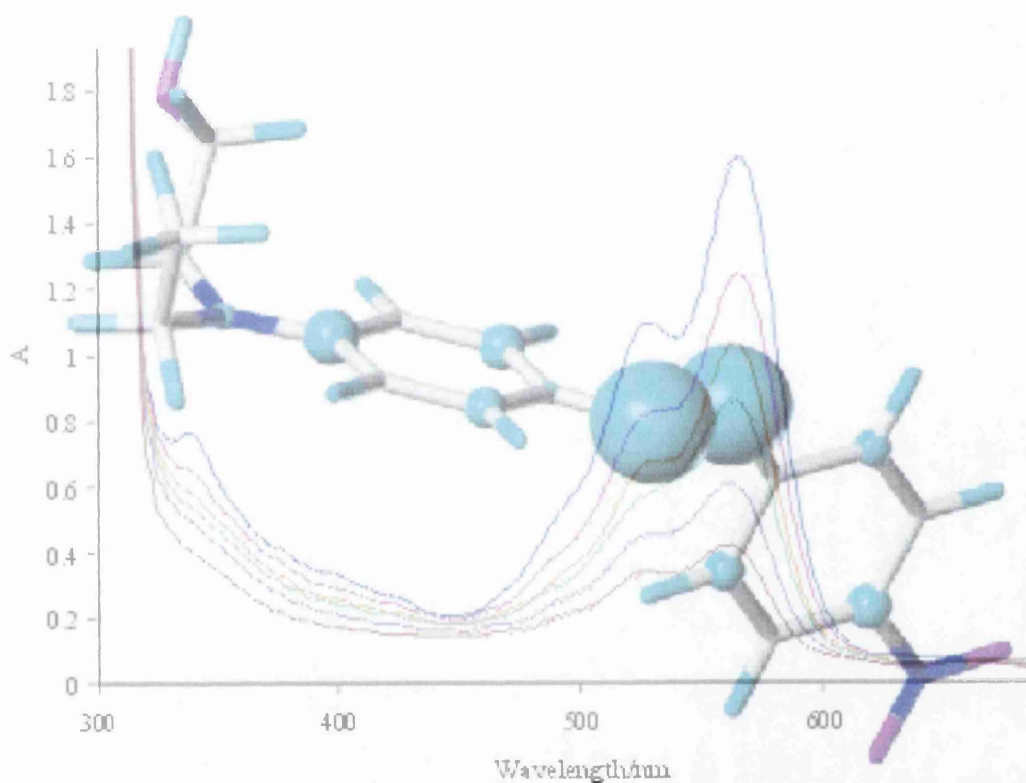
The photo-fading rate constants of [IV] and [IX] ethyl cellulose films are -0.61 and -0.31 respectively corresponding to half-lives of 0.86 hours and 1.77 hours, which are comparable to the half-lives of [IV] and [IX] in methanol.

References

- ¹ Zeneca Specialities, Hexagon house, Blackley, Manchester, U.K.
- ² Aldrich Chemical Company.
- ³ Stuart Whitaker, Chemistry Dept., University of Wales Swansea.
- ⁴ Catherine Mort, Chemistry Dept., University of Wales Swansea.
- ⁵ Klick, E.W., Ed. *Industrial Solvents Handbook*; Noyes Data Corporation; Park Ridge, NJ, 1985.
Organic Solvents 3rd edition; Riddick and Bunger, *Techniques of chemistry* volume II; Wiley-Interscience: New York, 1970.
- ⁶ Oriel Corporation: L.O.T. –Oriel Ltd. 1 Mole busines park, Leatherhead, Surrey KT22 7AU.
- ⁷ J.O. Morley and Ann L. Fitton, *J. Am. Chem. Soc.*, (1999) 11442.
- ⁸ J. Griffiths, *Developments in Polymer Photochemistry-1* (Allen) Applied Science Publishers Ltd. London (1980) Chapter 6.
- ⁹ A. Albini, E. Fasani and S. Pietra, *J. Chem. Soc., Perkin Trans 2* (1982) 1393.
- ¹⁰ Microsoft Excel
- ¹¹ A. Arcoria, M. L. Longo and G. Parisi, *J.S.D.C .*, **100** (1984) 339.
- ¹² P. W. Atkins *Physical Chemistry*, 5th edition, Oxford University Press (1994).
- ¹³ A. Albini, E. Fasani and S. Pietra, *J.Chem. Soc. Perkin Trans. 2.*, (1984) 1689.
- ¹⁴ *Water Determination by Karl Fischer Titration*, G. Wieland, GIT Verlag, (1985)
- ¹⁵ S.Hashimoto, K. Kano, *Bulletin of the Chem. Soc. of Japan*, 45 (1972) 852.
- ¹⁶ A. Albini, E. Fasani and S. Pietra, *J. Chem. Soc. Perkin Trans. 2.*, (1983) 1021; G. Irick and J. C. Pacifici; *Tetrahedron Lett.*, (1969) 1303.
- ¹⁷ J.C. Pacifici and G. Irick, *Tetrahedron Lett.*, No.27 (1969) 2207.

Chapter 3

Experimental Study of the Photo-degradation Products of Azo Dyes



Experimental

Photofading reactions

Large scale photofading reactions were carried out using a 250 W Hanovia high pressure quartz mercury vapour immersion lamp. The arrangement of this apparatus is given in Figure 3.1.

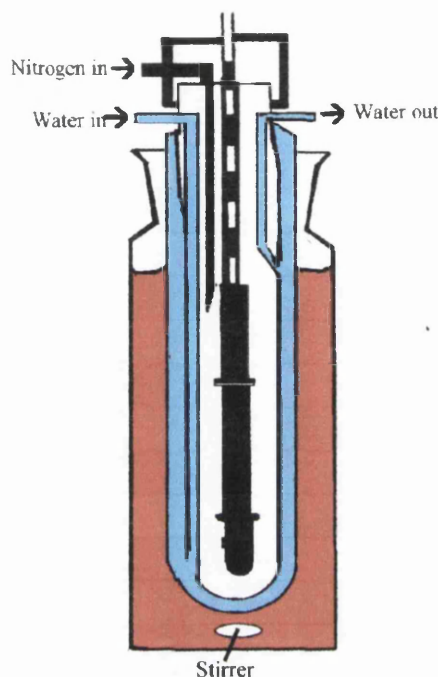


Figure 3.1 Hanovia high pressure mercury lamp and reactor vessel set up.

The lamp is inserted into an inner quartz jacket around which is placed an outer quartz jacket. This unit is then surrounded by a pyrex glass tube with a ground glass joint to form a sealed air tight unit. A methanolic solution of the dyes is placed in this air tight pocket so it surrounds the lamp. The brightest part of the lamp then irradiates the dye solution. The lamp produces a lot of heat energy and the apparatus must be cooled by a constant supply of tap water to prevent the methanol dye solution from boiling. The tube containing the dye solution is thus surrounded by another glass tube through which the water can flow constantly. The dye solution can be degassed with nitrogen first, or may alternatively be continuously degassed. Similarly, if oxygenated conditions are required, the solution can be initially or continuously oxygenated by bubbling through with oxygen.

The power of the mercury lamp was 250 W and the photon flux was reported by Hanovia to be 4.18×10^{18} photon s^{-1} cm^{-1} at 0.5 cm distance from the lamp. The distribution output of radiation per 100 W for the mercury lamp at different wavelengths is shown in Figure 3.2.

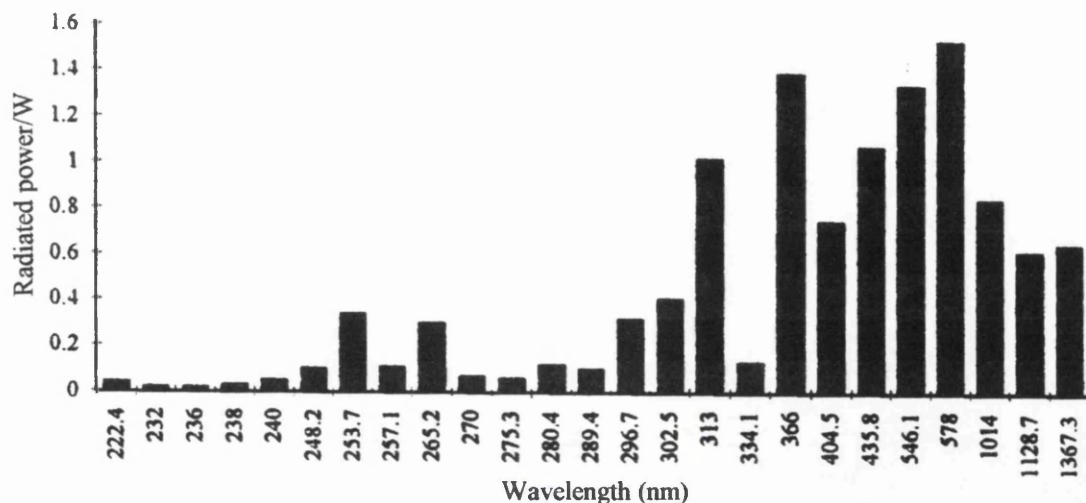


Figure 3.2 Absolute output of a high pressure mercury lamp at different wavelengths, for each 100 W of power.

Dye solutions of concentration $2.5 \times 10^{-3} \text{ mol dm}^{-3}$ contained in the reactor vessel were irradiated until the colour of the solution had essentially disappeared.

Concentration of photo-fading products

The colourless solution formed after irradiation was then concentrated by evacuating off most of the excess solvent, leaving a concentrated brown mixture of photo-fading products. This concentrated mixture was then analysed using high performance liquid chromatography (see below).

Xenon arc lamp (1000W)

Methanolic dye solutions of concentration $5 \times 10^{-5} \text{ mol dm}^{-3}$ were irradiated in a quartz spectrophotometer cuvette by a xenon arc lamp, under degassed conditions, as in the kinetic experiments previously discussed (See chapter 2). Photo-faded solutions were analysed using HPLC and mass spectrometry

High performance liquid chromatography (HPLC)

Initial HPLC separations were carried out on a Milton Roy LDC Constametric model III pump with a a spectromonitor variable wavelength detector set at 450nm or 254nm for single

wavelength monitoring. Separations were carried out on a reverse phase APEXII ODS 5 μ m 150 x 4.6mm column. The mobile phase was 40% water / 60% acetonitrile at a flow rate of 1ml min⁻¹. HPLC grade solvents from Fisher scientific were used.

Separations were also carried out at Zeneca Specialities on a Hewlet Packard, (Bracknell, Berks.,UK) 1100 autosampler and pumping system, connected to an Applied biosystems 757 Absorbance detector and a HP3396 Series II Integrator. The same ODS column was used. The solvent composition was acetonitrile/water run on a gradient from 10/90 to 90/10 at a flow rate of 1ml min⁻¹ and injection volume of 2 μ l. The absorbance detector was set to detect at 254 and 450nm.

Further HPLC analysis was carried out by Louise Perry¹ on a Hewlet Packard 1100 autosampler and pumping system with an ODS2-Ik.5-23956, 150 x 4.6mm column from Capital HPLC Ltd. A gradient elution method was developed using acetonitrile and a 10mM solution of ammonium acetate in water at a flow rate of 1ml/min. The ammonium acetate buffer was added to aid ionization in the mass spectrometer. Injection volumes of 20 μ l were used. The detection wavelength was at 254nm.

HPLC separations and analysis of peaks in the chromatogram were also performed by Massood Yousef² on a Hewlet Packard 1100 autosampler and pumping system with a LUNA C18 (2) 3 μ m 100 x 4.6mm column. A gradient elution method was again developed, using acetonitrile and a 10mM solution of ammonium acetate in water at a flow rate of 1ml/min. Sample injections of 20 μ l were performed. The detector used was a diode array detector (DAD) and detection wavelengths were set at 254, 350 and 450nm.

Mass Spectrometry

To identify some of the separated component peaks in the HPLC chromatogram, a mass spectrometer was interfaced with the HPLC instrument to analyse the masses of components of the mixture separated by HPLC.

LC-MS work was carried out at Zeneca using a Hewlett Packard 1050 HPLC system with autosampler and online degasser connected to a SCIEX API-3 triple quadrupole mass spectrometer. The quadrupole mass spectrometer is capable of multiple fragmentation of ions i.e. a component of the mixture may be ionised and this M+H⁺ ion may then itself be fragmented to give a fragment ion pattern.

Data analysis of mass spectrometry data was carried out on an Apple Macintosh Quadra 900 computer for data acquisition using "Tune" software for single runs and "RAD" software for an

automated series of runs. Data processing was carried out on an Apple Macintosh Quadra 700 computer using the software package MacSpec 3.1

Mass spectrometry analysis of photo-degradation products was performed by Louise Perry¹ was performed on a Bruker Esquire LC ion trap. Infusion was performed using a Cole Palmer 74900 series syringe pump and a Hamilton-Microfilter (Nevada USA) 250µl syringe with a 2.3mm diameter.

Mass spectrometry was also performed by Masood Yousef² using a LCQ Ion Trap instrument with an electrospray source in positive ionisation mode.

Samples for accurate mass measurements were submitted to the EPSRC mass spectrometry centre in Swansea. Accurate mass spectra were performed on a Finnigan MAT 900XLT double focusing magnetic sector trap.

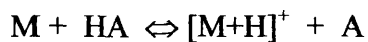
Introduction to mass spectrometry

HPLC is capable of detecting these dyes at concentrations of $5 \times 10^{-6} \text{ mol dm}^{-3}$. Concentrations of $5 \times 10^{-6} \text{ mol dm}^{-3}$ were used for mass spectrometry, thus concentrations of products detected by HPLC are within the detection range of the mass spectrometer. A mass spectrometer consists of three main components; a sample inlet, a mass analyser and a detector.

Ions generated by an electrospray interface enter through a slit, and are separated according to their mass to charge ratio in the mass analyser, which in this case was an ion trap. The ions are then released into an ion detector which generates the mass spectrum. An electrospray interface was used to generate the ions, as it is a relatively gentle technique for fragmentation. This is important, to avoid confusion of mass peaks produced by fragmentation with mass peaks for actual fading products.

The sample is introduced into the electrospray chamber as fine droplets. The electrostatic field in the chamber causes ions of opposite polarity to the electric field to move to the surface of the droplet, creating a fine mist of charged droplets. The solvent in the droplet evaporates as heated drying gas passes through the chamber. This causes a reduction in the size of the droplet and the charges at the surface of the droplet are forced closer together. Strong repulsive Coulombic forces cause the droplet to explode, producing more smaller charged droplets. Further evaporation of solvent from these droplets takes place until bare ions are emitted from the droplet.³

Acid solution (HA) is added to the samples in order to create positive ions by protonating the sample as shown in Equation 3-1.



Equation 3-1

The sample molecule is represented by M. Basic molecules have a greater affinity for protons and are therefore suited to positive ion analysis. The positive ions then pass into the ion trap, where they may be fragmented.

High performance liquid chromatography (HPLC)

It is possible that some of the products of the fading reaction are non volatile and may therefore go undetected by GC analysis. On this basis, HPLC was chosen as a method for the separation and detection of photo-products. Both visible and ultraviolet absorbance detectors were used, as the original dye absorbs in the visible region, but some of the photo-products were thought to contain aromatic residues which, may be detected by an ultraviolet detector.

Separations using HPLC are dependent on the degree of interaction between molecules of differing size or polarity and the column packing or stationary phase. In reverse phases HPLC, the mobile phase is usually more polar than the column packing, thus in general more polar compounds will elute faster than non-polar compounds since the non-polar compounds will have a greater affinity for the relatively non-polar column packing. The time taken for a component to pass through the column is called its retention time, t_R . The other factor affecting the retention time of a component is its size. Generally, larger molecules have longer retention times. A mixture of components can therefore be separated on the column so that its constituent components elute at different times. The separated components then pass through a detector – usually a UV or visible detector. The degree of separation of the components of course will depend on the solvent system and the similarity of the components in terms of size and polarity as well as hydrogen bonding strength.

Initial HPLC analysis was performed on a Milton Roy (see HPLC experimental details) instrument with a reverse phase ODS column. The solvent system used for this work was a mixture of acetonitrile and water. It was found after trying several solvent ratios that better separations were obtained with a 60% acetonitrile / 40% water system. As the fading reaction proceeded, a 10 μ l sample of the solution was removed at time intervals and injected into the HPLC machine. Figure 3.3 shows the chromatograms of [III] at the various time intervals during photofading. At time zero ($t = 0$ hours), the dye solution had not yet been irradiated, and the only species detected at 450 nm was dye [III] itself. This corresponds to the single large peak with

retention time of 11.44 minutes on the HPLC chromatogram. There are no other species detected at this wavelength or at 254 nm, indicating that the dye was present in high purity.

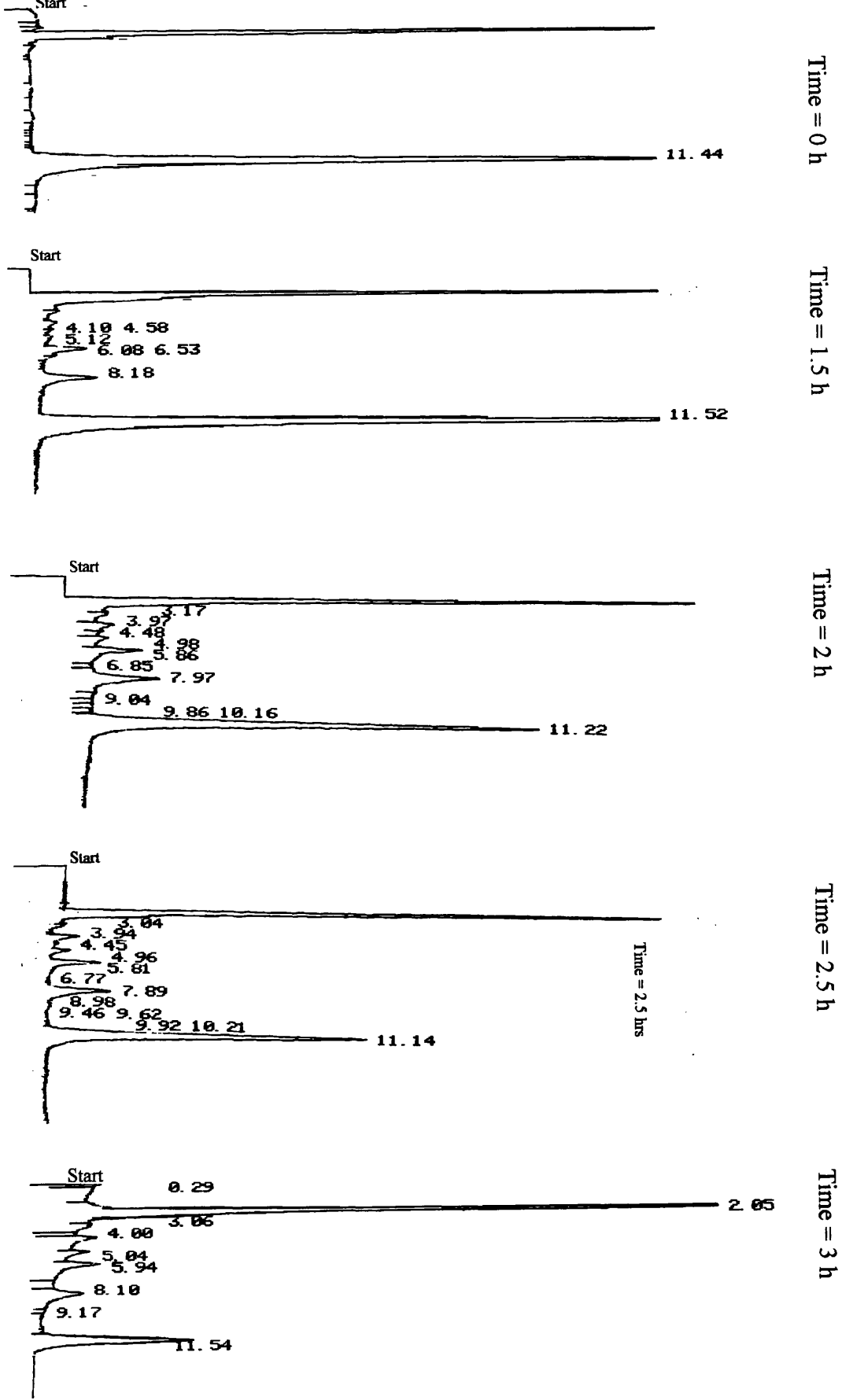
As the fading reaction proceeds, the intensity of the peak representing the dye begins to decrease and is accompanied by the appearance of several new peaks. These are assumed to be product peaks of the photo reaction, formed from the breakdown of the original dye under irradiation. As fading proceeds further, the intensity of these product peaks increase and the original peak continues to decrease in size presumably as the dye degrades to form more of the breakdown products.

As the photo reaction progresses the product peaks increase in size until they reach a maximum intensity at time t_A after which these peaks also begin to decrease in size. The reason for this is thought to be due to the photodegradation of the products initially produced and this is supported by the diminishing size of these peaks and their eventual disappearance.

Identification of the fading products

As it is likely that the products initially formed from the breakdown of the azo dyes also degrade upon further irradiation of the solution, it was necessary to abort fading after a time t_A , where t_A was the time at which enough of the original dye had photo-degraded to give sufficient amount of products, but before there is any substantial degradation of these initially formed products. Once the dye solutions had been faded for this optimum time, the photo-degraded solution was placed in a round bottomed flask to evacuate most of the excess methanol solvent. The small amount of solution that remained contained concentrated fading products and the original dye.

Figure 3.3 HPLC chromatograms at photo-fading times 0 h, 1.5 h, 2 h, 2.5 h and 3 h for a degassed methanol solution of dye [II].



Analysis of the concentrated fading products by HPLC

A 2.5×10^{-3} mol dm⁻³ solution of 4-[N,N di(β -hydroxyethyl)amino]-2-chloro-2'-nitro-4'-chloroazobenzene, [II], in methanol was degassed with nitrogen and irradiated for 18 hours until decolourised. A 2 μ l volume of the concentrated photo-product solution was injected onto the column using a 60/40 ratio of acetonitrile/water as the mobile phase. The chromatogram of the concentrated solution of [II] faded under degassed conditions showed a large number of peaks detected at 254 nm, in addition to the peak originating from the pure dye itself. The retention time of [II] was found from its chromatogram, performed under the same HPLC conditions. Most of the other components detected in the mixture had retention times which are shorter than the original dye. This implies that the species are either more polar, or more probably, smaller in size than the original dye molecule, as both these situations would result in shorter retention times.

Oxygenated conditions

A 2.5×10^{-3} mol dm⁻³ solution [II] in methanol was irradiated for 36 hours under oxygenated conditions until decolourised, by continuously bubbling oxygen through the solution. (It took twice as long for the colour of this solution to fade than the corresponding degassed solution). The chromatogram for a 2 μ l injection of the concentrated mixture formed in this photoreaction also showed a number of photo-product peaks, though fewer than under anaerobic photo-fading conditions and with different retention times. This suggested that different products were formed under degassed and oxygenated conditions and that there may be different mechanisms associated with these two fading reactions.

Possible photo-products

Irick and Pacifici reported that some of the products of the anaerobic photo reaction of azo dyes are anilines, formed from cleavage of the azo bridge of the parent azo dye.^{4,5,6,7,8}

Photo-products for the photo-oxidation reaction are said to include benzene derivatives from cleavage of the donor C-N bond⁵ and possibly dealkylated derivatives of the azo dyes⁹ (see Chapter 1 p65-69) for a detailed explanation and proposed mechanisms for these reactions). One of the two possible anilines that would be formed from photo-cleavage of the N=N bond was 4-chloro-2-nitroaniline and irradiation of dye 2 under anaerobic conditions might therefore, be expected to give this compound as one of the fading products. This hypothesis was investigated

by HPLC analysis of 4-chloro-2-nitroaniline and also a photo-faded solution of 4-chloro-2-nitroaniline, under the same conditions. The chromatogram of the solution of [III] irradiated under oxygenated conditions contained a peak with the same retention time to that of 4-chloro-2-nitro aniline and two other peaks which had similar retention times to photo-products of 4-chloro-2-nitroaniline. Peaks with these retention times were not clearly apparent in the solution of [III] faded under anaerobic conditions. It is of course possible that the other aniline component of the azo dye may be present, but this was not available to test.

These results were inconclusive as the HPLC method used was inadequate for a meaningful comparison of retention times of photo-products and further examination of these products was necessary.

In order to identify these fading products, it would be helpful to separate them in order to examine them by NMR spectroscopy or mass spectrometry. Separations were attempted on a silica preparatory cartridge, but provided poor separation and many of them failed to elute. A HPLC prep column enables a slightly improved separation, with 14 fractions collected. However, these fractions still contained a number of components. As the amount of each component was small and fractions were impure, it was not possible to study them by NMR or mass spectrometry. The next course of action was thus to try to separate the products by HPLC and then analyse each component by mass spectrometry.

HPLC work was carried out at Zeneca laboratories on the same ODS column, but with a Hewlett Packard 1100 system. This instrument has the advantage of being able to perform gradient elution chromatography. The solvent gradient started at 10/90 acetonitrile/water and ended at 90/10 acetonitrile/water after 30 minutes. The hp 1100 also has the capacity to detect components at several different wavelengths using a diode array detector, and can even produce a full UV/visible absorption spectrum of an isolated peak in the chromatogram.

Concentrated solutions of photo-products that had been previously prepared at Swansea University were injected onto the column and detected at 254 and 480 nm detection wavelengths. The chromatograms of solutions of [III] which had been irradiated under anaerobic conditions (Figure 3.4) and oxygenated conditions (Figure 3.5) show a peak from the dye itself at around 18.3 minutes and another common peak at 14.8 minutes. There are however several peaks which are not common to both chromatograms.

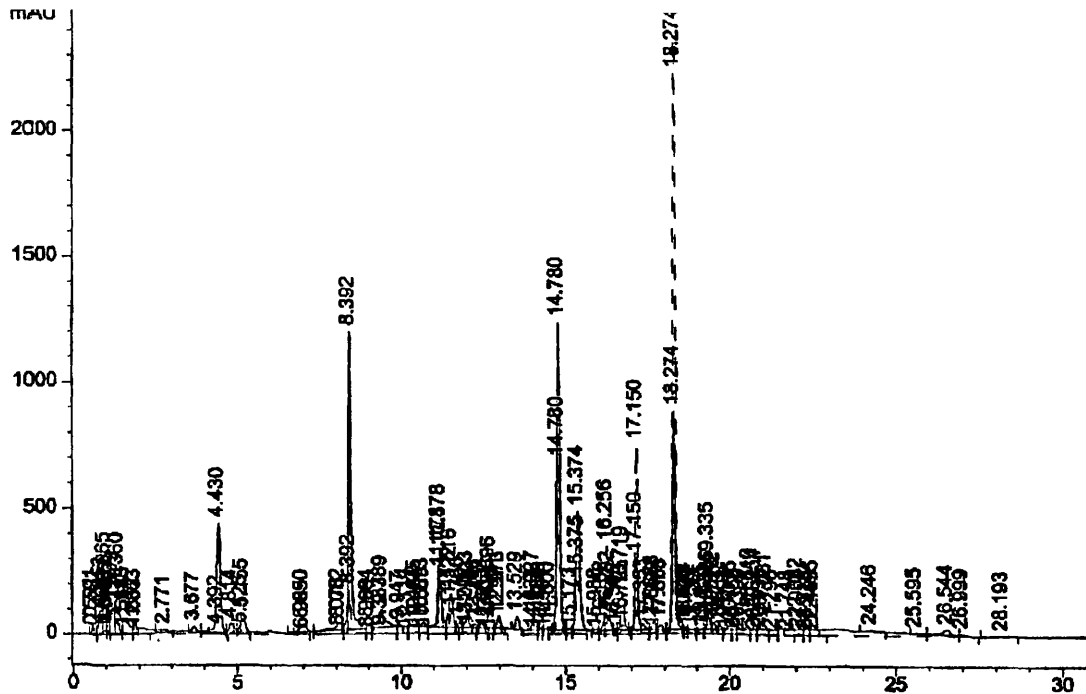


Figure 3.4 HPLC chromatogram of a photo-degraded methanol solution of [II] irradiated under anaerobic conditions for 18 hours.

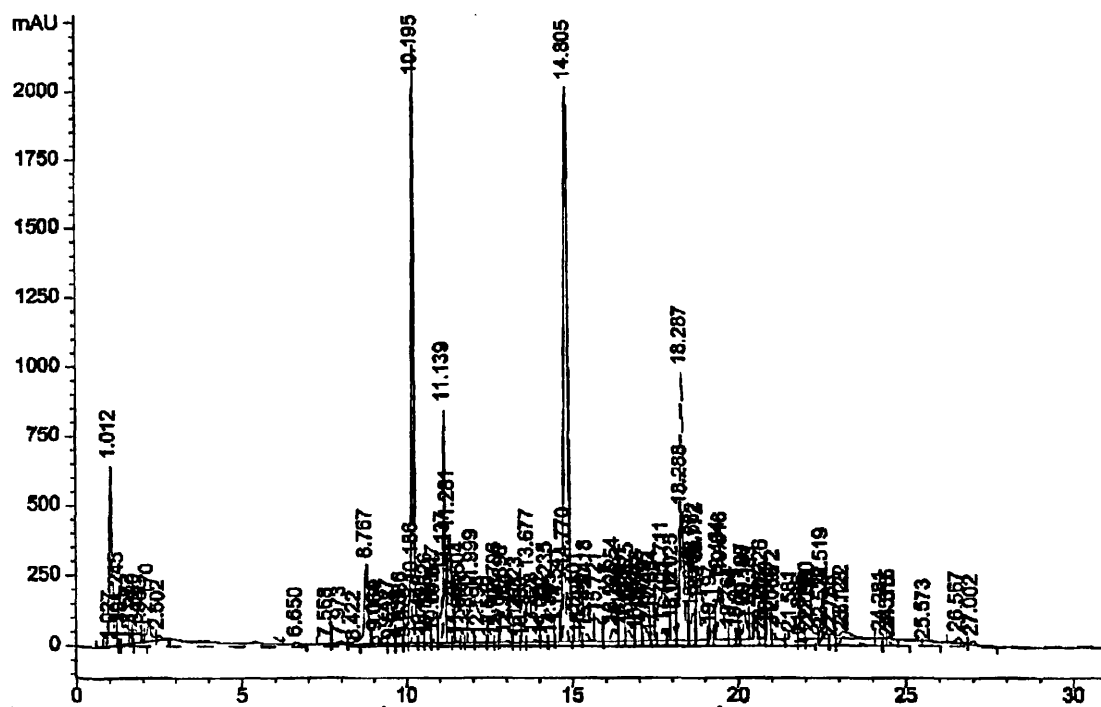


Figure 3.5 HPLC chromatogram of a photo-degraded methanol solution of [II] irradiated under oxygenated conditions for 18 hours.

The DAD detector allows the determination of a UV/VIS absorption spectrum for peaks in the chromatogram. Some of these spectra, at similar retention times to [III] were identical to that of the pure dye. However there were numerous other peaks that could not be identified from their spectra. Better separations were not obtainable at this point in time, but it was again clear that many of the species obtained under anaerobic and aerobic conditions are different, and that more photo-products are produced than are described in the literature.⁴⁻⁹

Mass Spectrometry

Mass spectrometry analysis was performed on photo-degradation products at the retention times of separated component peaks in the HPLC chromatogram. There was a short delay time between detection by the UV/visible detector and detection of ions in the mass spectrometer and therefore, the retention times of the mass peaks in the total ion chromatogram were slightly longer than the retention times of the peaks in the HPLC chromatogram. Of the several peaks detected by HPLC of the solution of photo-products from anaerobic irradiation of [III] only those at 18.3 and 19.8 and 22.1 minutes, correspond to mass peaks in the total ion chromatogram (TIC) with similar retention times. Several of the peaks in the LC chromatogram of the solution of [III] faded under oxygenated conditions, have similar retention times to mass peaks in the TIC (see Table 3-1).

Table 3-1 Retention times of LC peaks and corresponding masses of an irradiated oxygenated solution of [III].

| Peak No. | Retention Time/mins | Masses (M+H) ⁺ |
|----------|---------------------|---------------------------|
| 1 | 2.905 | 106, 178, 180 |
| 2 | 4.510 | 150, 170, 180 |
| 3 | 14.220 | NA |
| 4 | 15.865 | NA |
| 5 | 19.724 | NA |
| 6 | 22.424 | 399 |
| 7 | 23.750 | 355, 358 |
| 8 | 27.619 | 326, 328 |

An ion peak at a mass of 399 (the mass of the protonated dye), was clearly detected in the TIC of the solution of products from irradiation in the presence of oxygen, together with some other

relatively intense peaks, though the intensity of these peaks was not necessarily related to the intensity of the peaks in the LC chromatogram, the intensity of ion peaks of course being dependent also on the degree of ionisation of the molecule. Some of the peaks in the LC chromatogram do not have any significant mass peaks associated with them. Mass peaks corresponding to the masses of the nitro aniline products expected were not detected above background noise in the TIC. This raises the possibility that the anilines may not have ionised sufficiently to be detected by the mass spectrometer. Further studies are required to try and resolve these problems and uncertainties.

Detection of photo-products by UV/visible spectrophotometry

Conditions for the large scale photofading experiments conducted in the immersion lamp apparatus, could not be controlled precisely and there was also the possibility that some oxygen remained in solution despite attempts to degas solutions. It was also difficult to monitor the extent of the photoreaction, without introducing oxygen into the system. Because of these difficulties, further fading reactions were carried out in a 1cm path length quartz cuvette, irradiated by a xenon arc lamp, as in the kinetic experiments. The photo-fading was then monitored over time by UV/visible absorption spectrophotometry.

Changes in the absorption spectrum of 4-(N- β -hydroxyethyl, N-ethyl)amino]-4'-nitroazobenzene, [IX], with irradiation time under anaerobic conditions (Figure 3.6), show a relatively fast degradation of the main absorption peak at 482 nm, and a new "double absorption peak" at 412 nm and 441 nm. Also shown in Figure 3.6 are the absorption spectra of 4-nitroaniline and nitrobenzene. These compounds are possible products of the photo-reaction. Comparison of spectrum of irradiated dye 9 with the spectra of 4-nitroaniline and nitrobenzene, indicates that neither of these compounds were present in the irradiated solution in significant quantities.

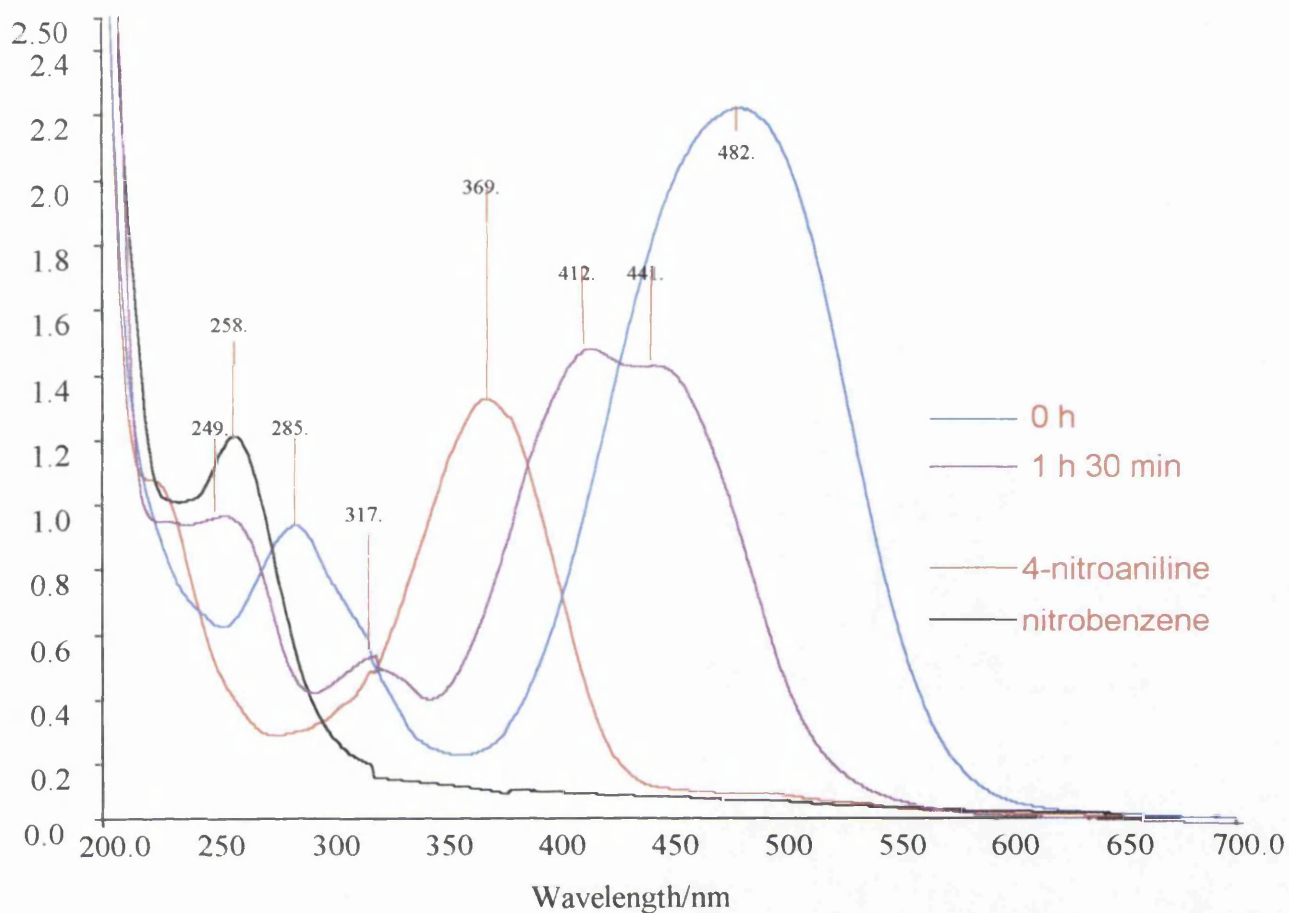


Figure 3.6 Comparison of the spectra of [IX] at time zero and after 1½ hours irradiation time with the spectra of 4-nitroaniline and nitrobenzene.

Under oxygenated conditions there are no clearly visible absorption peaks from possible fading products. However, there is a slow decrease in the size of the long wavelength absorption band. This is in contrast to absorption spectra of [IX] under degassed conditions, and suggests the formation of different photo-products in each reaction.

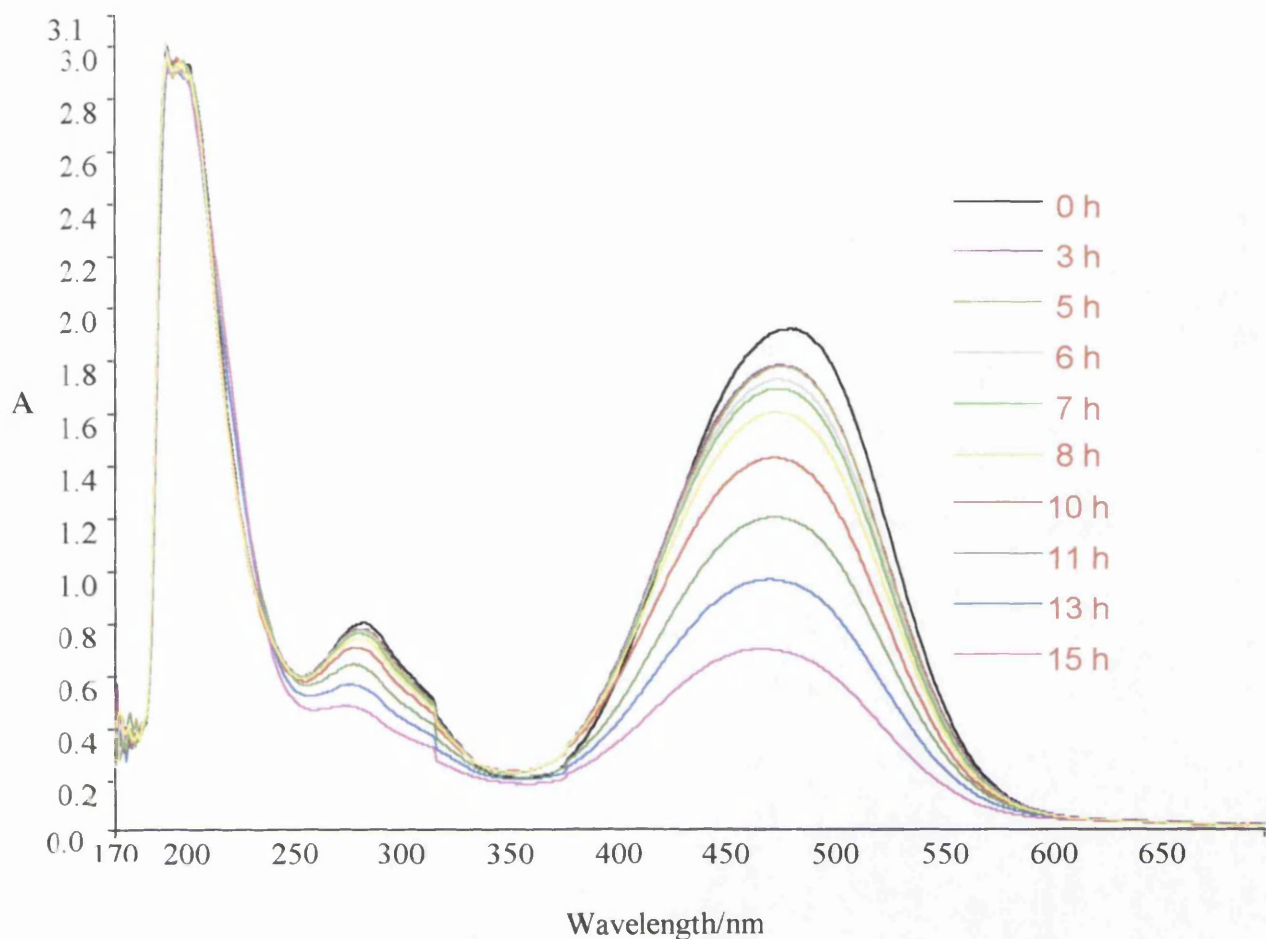


Figure 3.7 Changes in the spectrum of [IX] in oxygenated methanol solution with irradiation time.

Despite irradiation the oxygenated solution of [IX] remains coloured. In contrast, 2'-nitro substituted dyes, [IV], [VI] and [VII] all undergo complete loss of colour. This colour loss results from the complete degradation of species absorbing in the visible region of the spectrum, as can be seen in Figure 3.8, which also shows the absorption spectra of suspected photo-products, 4-chloro-2-nitroaniline, 2-nitroaniline and nitrobenzene. The irradiated dye solution showed no absorptions at the absorption maxima wavelengths of these suspected photo-products.

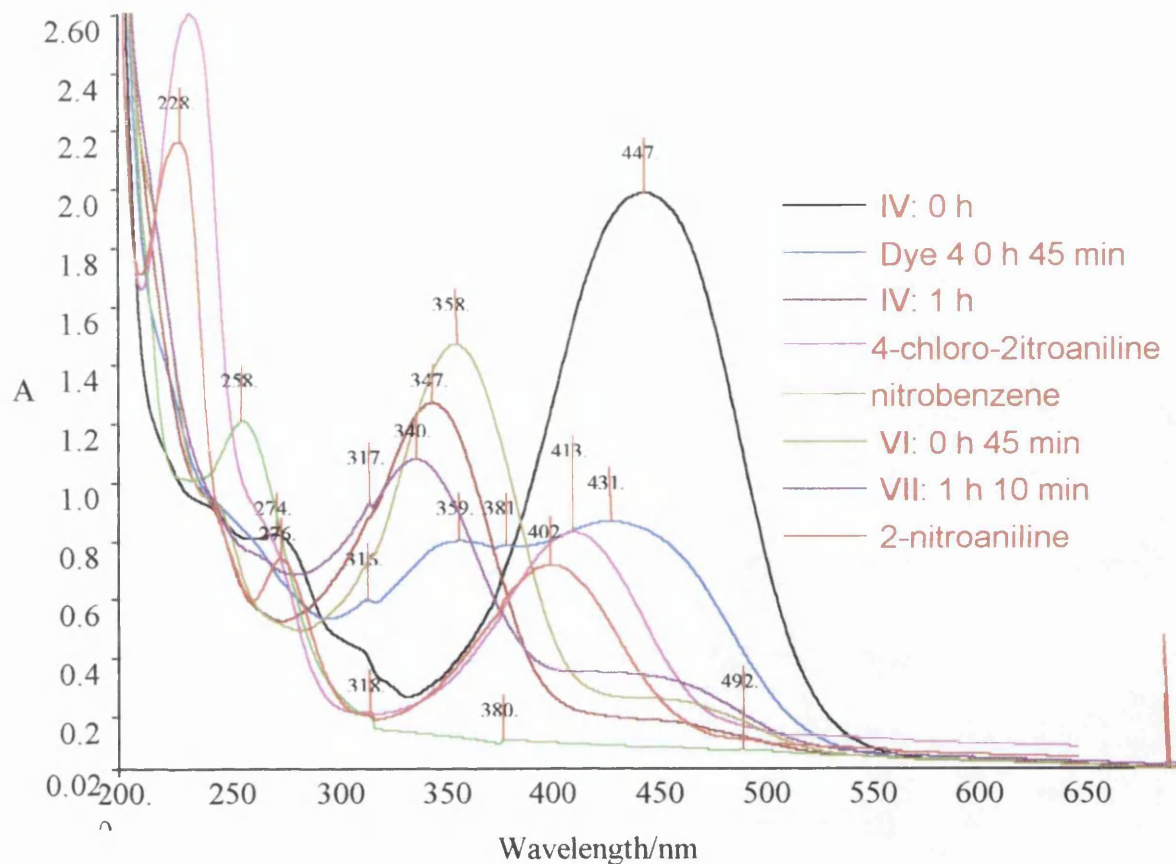


Figure 3.8 Comparison of [IV], [VI] and [VII] fading products with 2-nitroaniline, 4-chloro-2-nitroaniline and nitrobenzene.

Following these interesting results, work was undertaken with Louise Perry¹ to try and identify some of the products of the photo-reduction and photo-oxidation reactions of the azo dyes using HPLC and mass spectrometry.

Mass Spectrometry[†]

Initial experiments involved infusion of samples of photo-faded solutions into the mass spectrometer where positive ion electrospray was performed.

The mass spectra of all dyes [II]-[IX] in solution in methanol were recorded. The mass spectrum of 2-methyl-4-[N- β -hydroxyethyl, N-ethyl]amino]-2'-nitro-4'-acetylazobenzene, [V], is shown in Figure 3.9. The peak with the highest intensity has mass 387.2. This corresponds to the protonated molecular ion of [V], $[M+H]^+$. The mass peaks at 218.9 and 159.0 are probably due to fragment ions of the original dye produced by breakdown of the dye in the mass spectrometer. The peak at 413.3 was found to be characteristic of a well known phthalate. This peak was found in the mass spectra of all of the dyes and its intensity remains constant. Thus it has nothing to do with the azo dyes or their fading products and can be ignored.

MS/MS fragmentation of the dyes was then performed in order to determine the fragmentation patterns for the dyes. Fragments are produced by collision of the protonated dyes with helium gas present in the ion trap. The fragmentation pattern of dye [V] is shown in Figure 3.10.

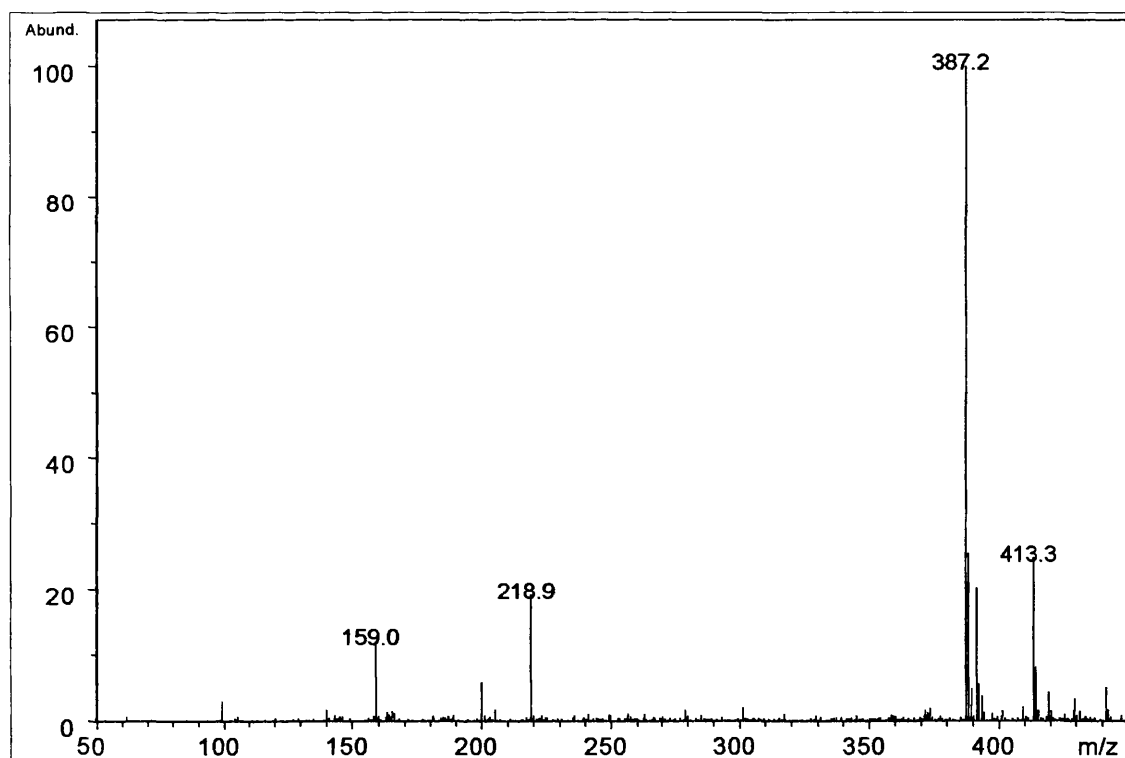


Figure 3.9 Full scan spectrum for [V] (1ppm).¹⁰

[†] Mass Spectrometry performed by Louise Perry.¹

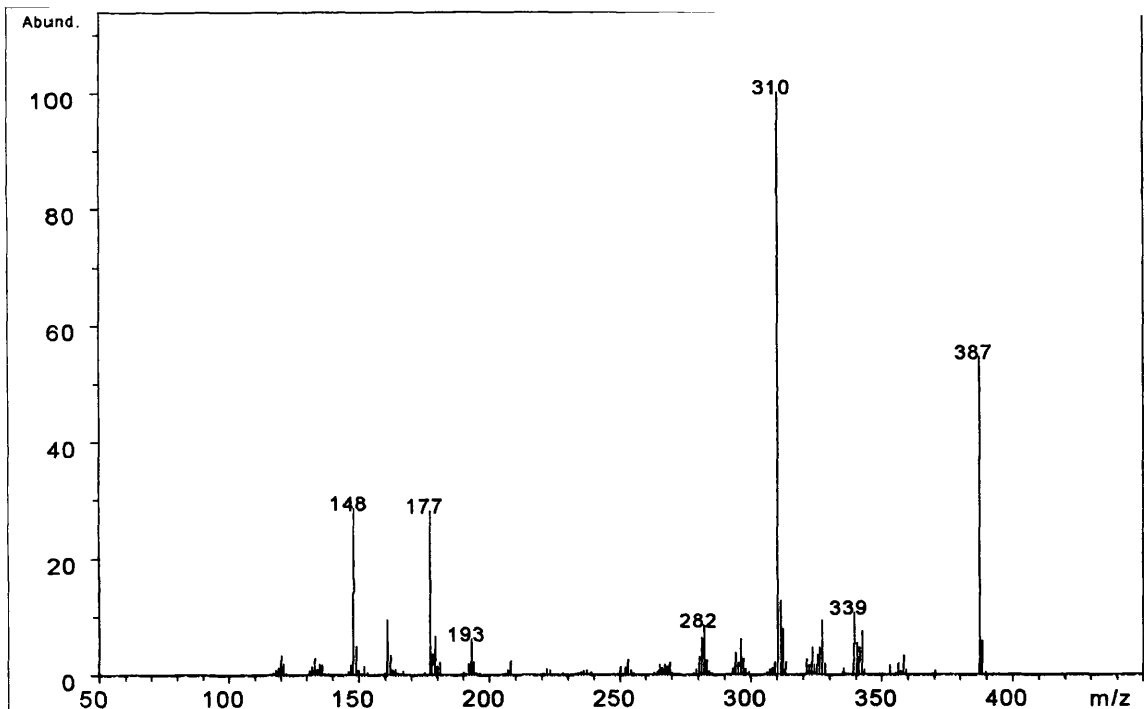


Figure 3.10 MS/MS Spectra for [V]. Isolation of $[M+H]^+ = 387$, and fragmentation amplitude of 0.70.¹⁰

MS/MS produced several fragment ion mass peaks which are listed in Table 3-2. The fragment ion peak with the highest intensity has a mass of 310. This peak was isolated and fragmented. This technique is referred to as MS/MS/MS and the fragment ions of peak 310 are also listed in Table 3-2.

Table 3-2 Fragments masses from fragmentation of isolated ions 387 and 310.

| Isolated ion | M/z of ions present (Relative intensity) |
|--------------|---|
| 387 | 339, 310, 282, 193, 177, 159, 148 |
| 310 | 310, 281, 222, 147 |

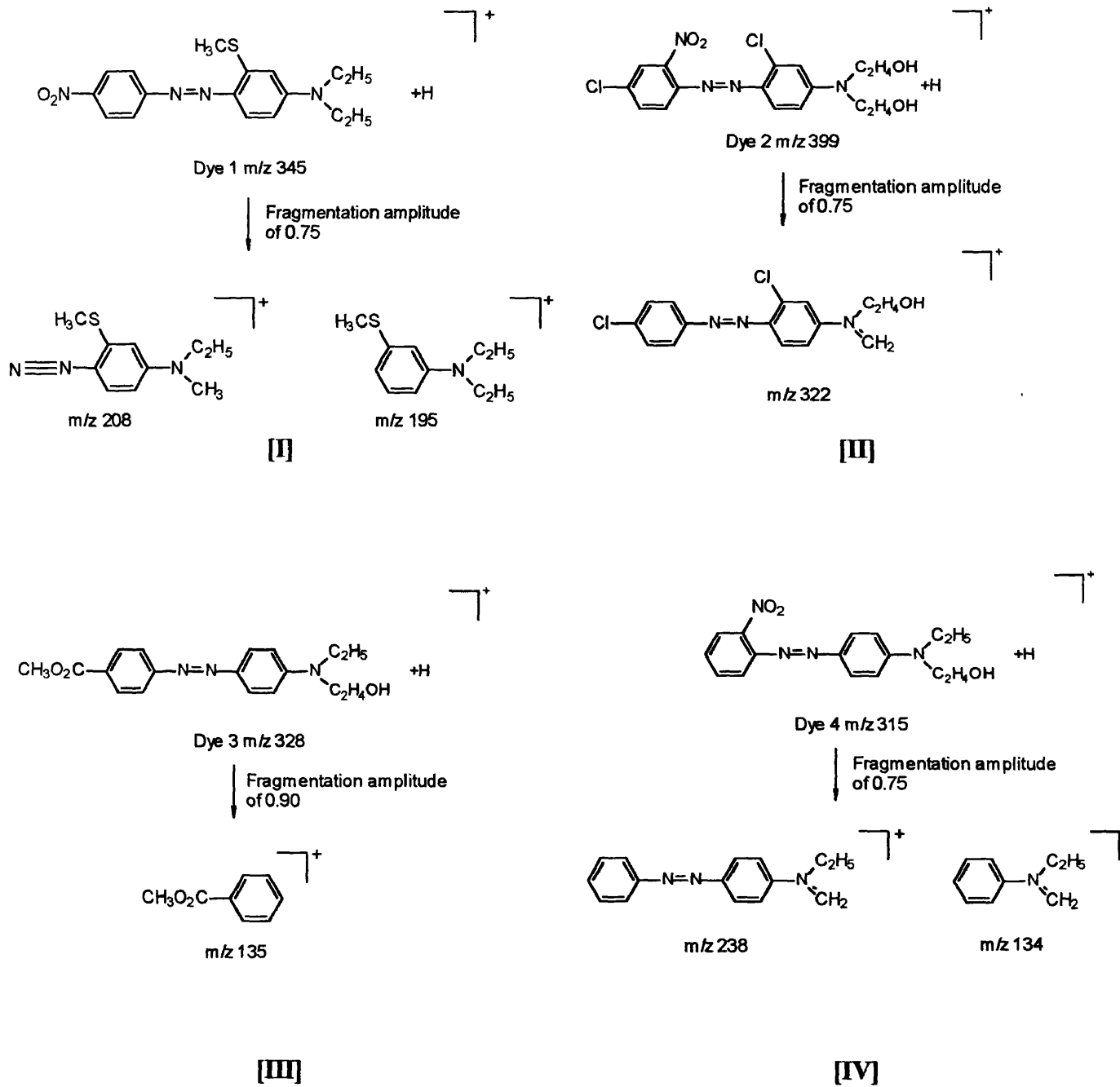
MS/MS was performed on the $[M+H]^+$ peak followed by MS/MS/MS on the most intense fragment for dyes [I]-[IX]. The fragment masses for these experiments are reported in Table 3-3. The mass spectrometer is such a sensitive instrument that many low intensity peaks are observed just above the baseline. Note that only masses with intensities above a certain threshold are reported to avoid recording a vast number of low intensity peaks.

Table 3-3 MS/MS and MS/MS/MS fragment ion masses for dyes[I]-[IX].¹⁰

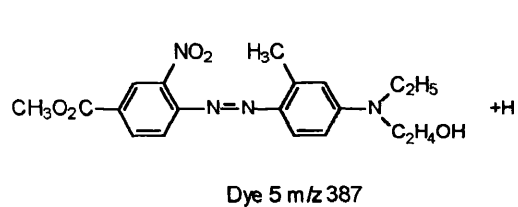
| Dye | Fragment ions isolated | Fragmentation amplitude | m/z of ions present (relative abundance) |
|------------|-------------------------------|--------------------------------|--|
| 1 | <u>345</u> | <u>0.75</u> | <u>345, 208, 195, 193, 180, 151</u> |
| | 208 | 0.55 | 208(4),193(5) |
| | 195 | 0.52 | 195(100),193(49), 180(82), 166(12), 151(17). |
| | 180 | 0.53 | 180(78),152(50), 151(100). |
| 2 | <u>399</u> | <u>0.75</u> | <u>399, 381, 351, 322, 304, 278, 229, 184, 166</u> |
| | 322 | 0.65 | 322(55), 278(100). |
| 3 | <u>328</u> | <u>0.90</u> | <u>328, 299, 283, 268, 153, 135, 119, 103</u> |
| | 283 | 0.57 | 283(84), 148(100), 120(94). |
| | 153 | 0.45 | 153(27), 121(48), 109(100). |
| 4 | <u>315</u> | <u>0.75</u> | <u>315, 284, 267, 238, 194, 179, 134, 106</u> |
| | 238 | 0.80 | 238(50), 210(93), 133(100), 105(19), 77(29). |
| | 267 | 0.70 | 267(49), 236(57), 222(90), 208(34). |
| | 179 | 0.57 | 179(80), 148(100), 135(28). |
| | 134 | 0.66 | 134(100), 106(53) |
| 5 | <u>387</u> | <u>0.70</u> | <u>387, 339, 310, 282, 193, 177, 148</u> |
| | 310 | 0.80 | 310(64), 281(100), 222(23), 147(22). |
| 6 | <u>349</u> | <u>0.85</u> | <u>349, 318, 301, 272, 179, 134, 106</u> |
| | 301 | 0.70 | 301(62), 207(78), 256(100), 242(31). |
| | 272 | 0.85 | 272(53), 244(100), 133(65), 111(31). |
| 7 | <u>365</u> | <u>0.90</u> | <u>365, 347, 317, 288, 244, 229, 166</u> |
| | 288 | 0.80 | 288(10), 244(100) |
| 8 | <u>243</u> | <u>0.70</u> | <u>243, 226, 212, 197, 150, 122, 94</u> |
| | 226 | 0.60 | 226(11), 120(100), 92(43). |
| 9 | <u>315</u> | <u>0.80</u> | <u>315, 284, 270, 255, 165, 134, 106, 94</u> |
| | 284 | 0.55 | 284(100), 255(87). |
| | 165 | 0.35 | 165(70), 134(100). |

All of the dyes fragmented well under the electrospray conditions. Possible structures for the main fragment ion masses for each dye are suggested in Scheme 3-2. Structures corresponding to masses of fragment ions are likely to arise from cleavage of the C-N bond between the

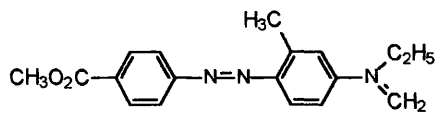
acceptor phenyl ring and the azo group, yielding a benzene derivative and a diazonium compound, which loses nitrogen to give an aniline derivative. Cleavage of the C-N bond between the donor phenyl ring and the azo group is also likely to occur. Many of the dyes have fragment ion masses corresponding to loss of the nitro group and to cleavage at the alkyl amino groups.



Scheme 3-2 Principal fragment ions by direct infusion.

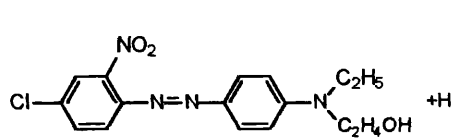


Fragmentation amplitude of 0.70



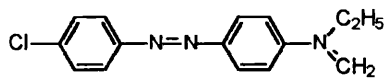
m/z 310

[V]



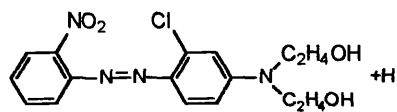
Dye 6 m/z 349

Fragmentation amplitude of 0.85



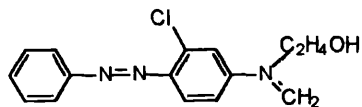
m/z 272

[VI]



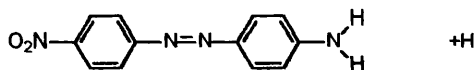
Dye 7 m/z 365

Fragmentation amplitude of 0.90



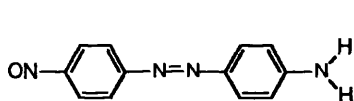
m/z 288

[VII]

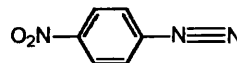


Dye 8 m/z 243

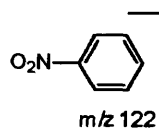
Fragmentation amplitude of 0.70



m/z 226

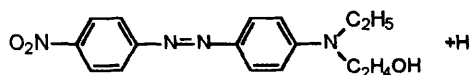


m/z 150



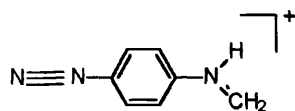
m/z 122

[VIII]



Dye 9 m/z 315

Fragmentation amplitude of 0.80



m/z 134

[IX]

Scheme 3-2 (continued)

Mass spectrometry and MS/MS was next performed on photo-faded eye solutions. The mass spectra of the infused [V] solutions that had been photo-faded for 1 hour (Figure 3.11) and 1½ (Figure 3.12) can be compared with the spectrum of the unfaded solution in Figure 3.9.

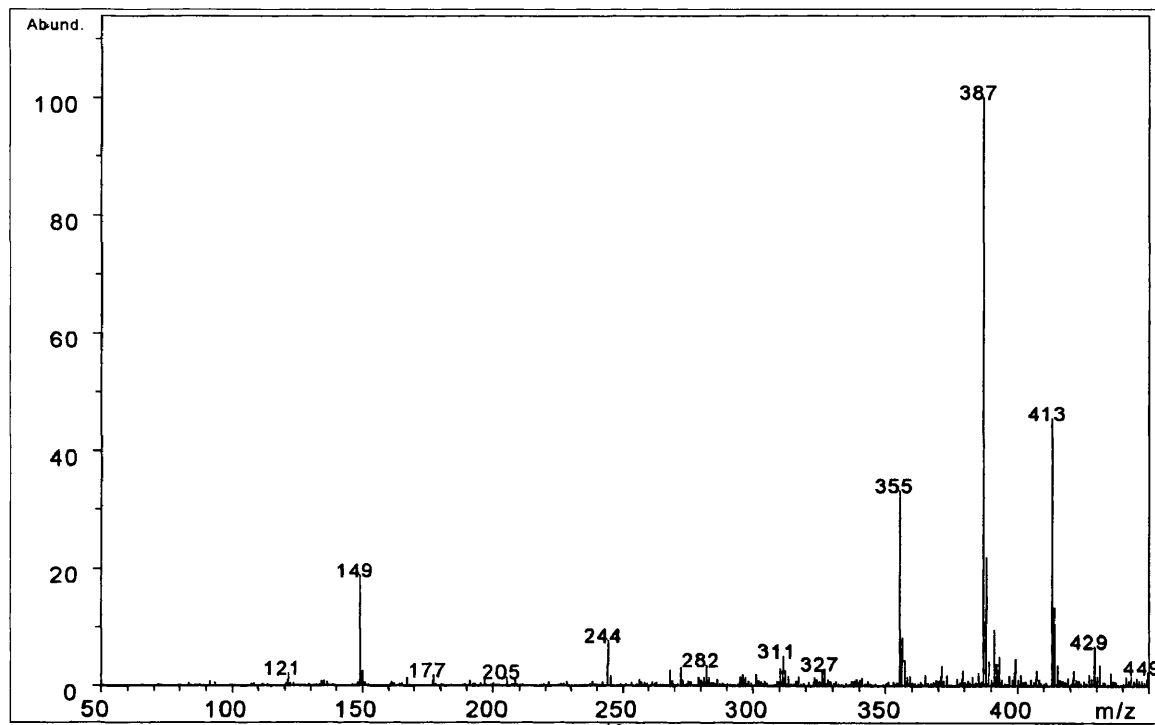


Figure 3.11: Infusion of [V] faded for 1 hour.¹⁰

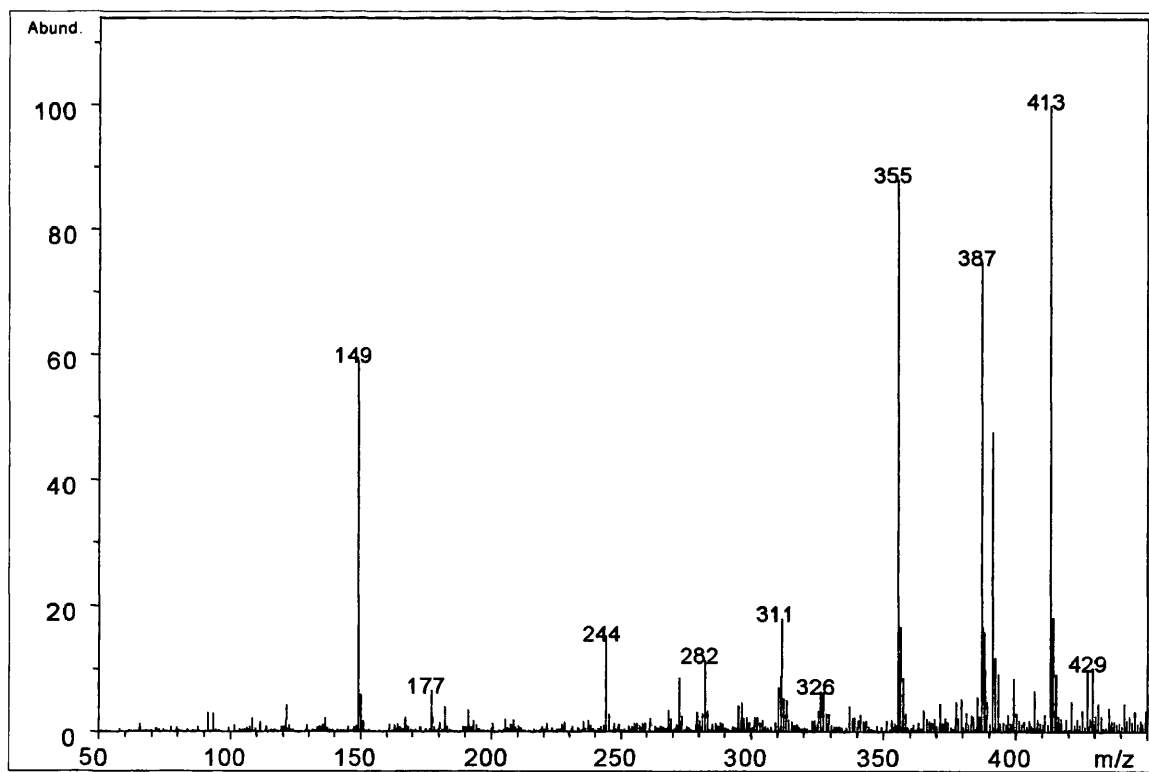
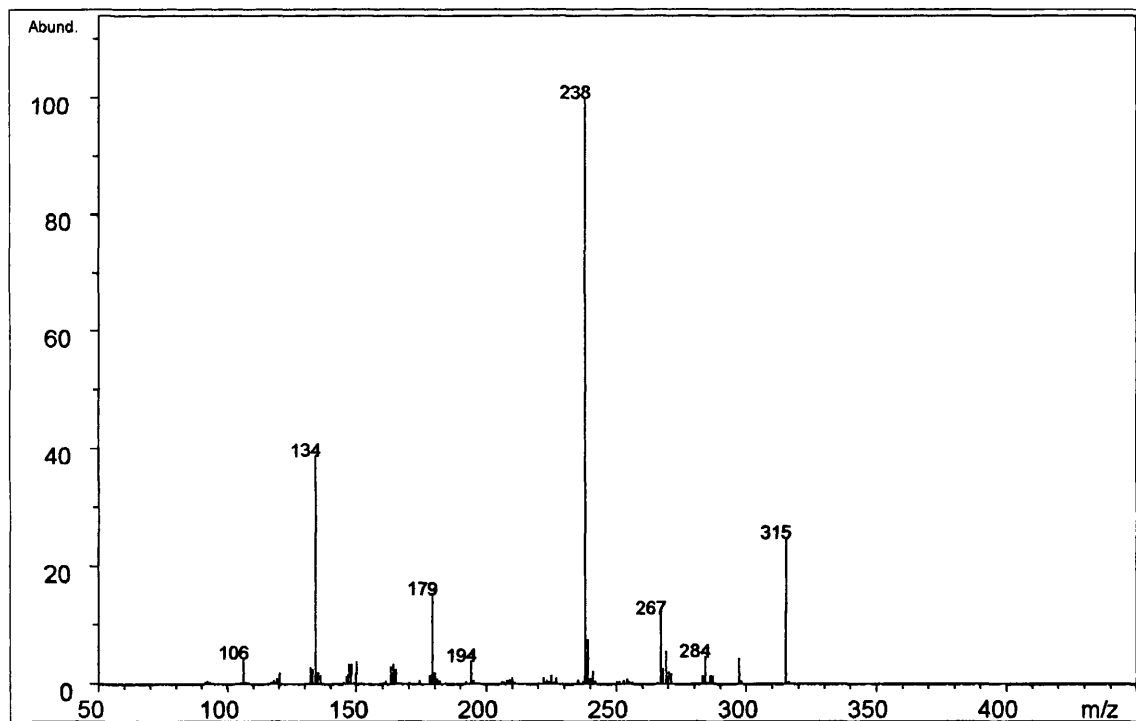


Figure 3.12: Infusion of [V] faded for 1 hour 30 minutes.¹⁰

A number of ions are seen in the spectrum of the photo-faded solution that were not present in the spectrum of the original dye. These peaks also have different masses to the MS/MS fragment ions of [V] and it is therefore suggested, that these new peaks originate from fading products of the dye. It is of course possible that some of these peaks are due to fragments of the fading products themselves. In order to elucidate the structure of some of these ions, MS/MS was performed on each major peak of the infusion mass spectrum. It is also interesting to note the changes in the relative intensity of the 387 and 355 peaks with irradiation time. As irradiation time proceeds, the intensity of the $[M+H]^+$ peak at 387 decreases while the intensity of the peak at 355 increases.

Other interesting examples are 4-(N- β -hydroxyethyl, N-ethyl)amino]-2'-nitroazobenzene [IV] and 4-(N- β -hydroxyethyl, N-ethyl)amino]-4'-nitroazobenzene [IX], which have the same molecular formula, but differ with respect to the position of the nitro substituent on the acceptor phenyl ring. The MS/MS spectrum of the unfaded [IV] solution in Figure 3.13 can be compared



with the mass spectrum of the photo-faded solution, shown in Figure 3.14.¹⁰

Figure 3.13 MS/MS spectra for [IV]. Isolation of $[M+H]^+=315$, and fragmentation amplitude of 0.75.

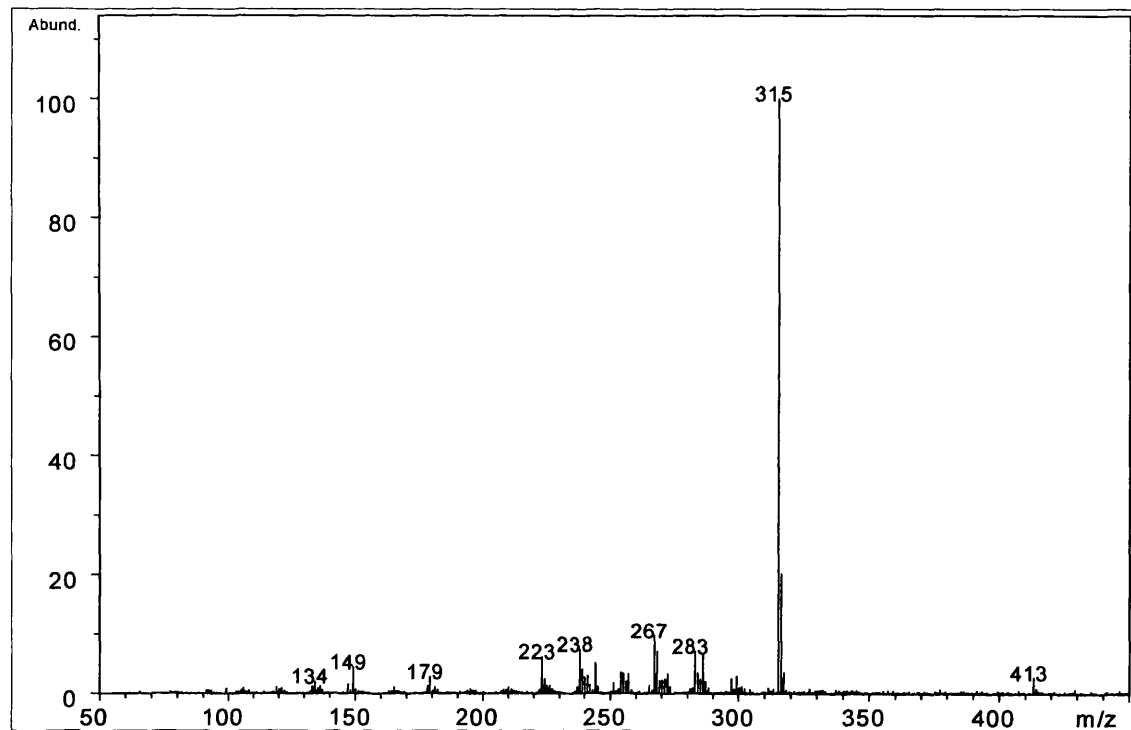


Figure 3.14 Infusion of [IV] faded for 1 hour.¹⁰

Even though [IV] and [IX] have the same molecular formula, the mass spectra of both the unfaded and photo-faded solutions for each dye are quite different. The mass spectra for dye [IX] can be seen in Figure 3.15 and Figure 3.16. It is clear that the mass peaks observed in the spectrum of the infused photo-faded solution do not correspond to fragments of the original dye. It is also interesting to note that the ions produced by fragmentation of dyes [IV] and [IX] are not all the same, and ions that are present in the spectra of both dyes have different intensities. The photo-faded solutions of [IV] and [IX] also produce mass spectra containing different mass peaks.

A number of ions that appeared in the mass spectra of all the dyes. These ions have masses 149, 244, 272, and 413 and their intensities remain constant with varying irradiation times. These ions are assigned as being contaminants present in the mass spectrometer and as such they will be overlooked in the consideration of the dye photofading products. The masses of ions suspected to be photo-products of the dyes are listed in Table 3-4.

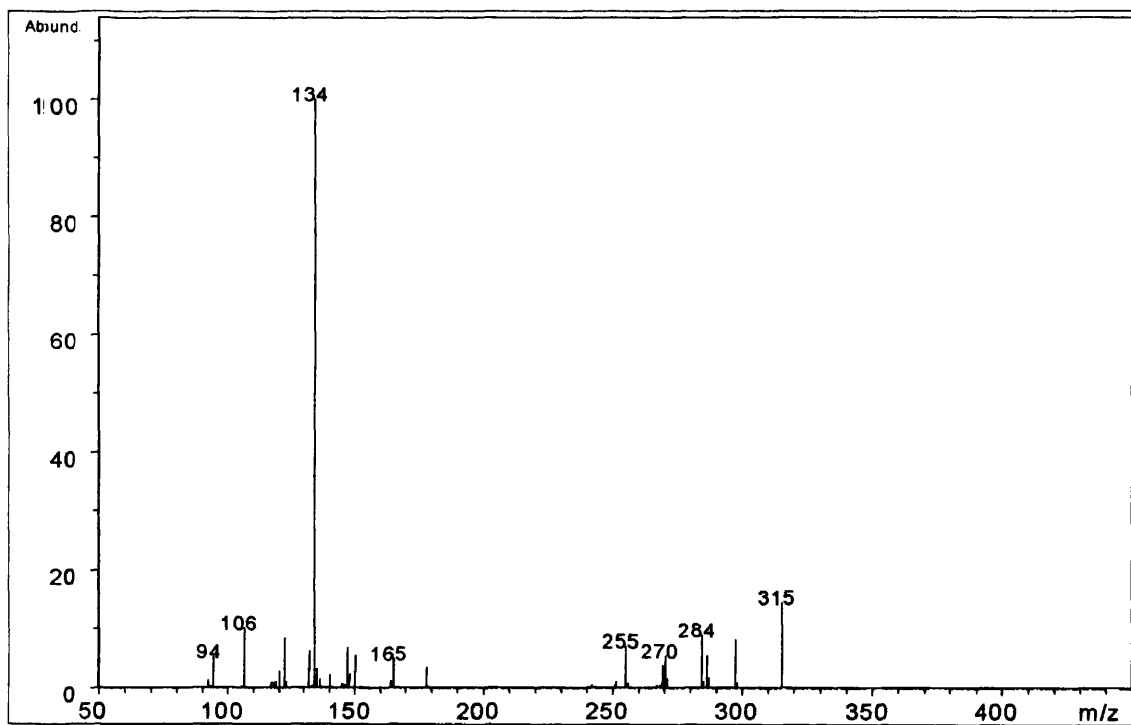


Figure 3.15 MS/MS spectra for [IX]. Isolation of $[M+H]^+=315$, and fragmentation amplitude of 0.80.¹⁰

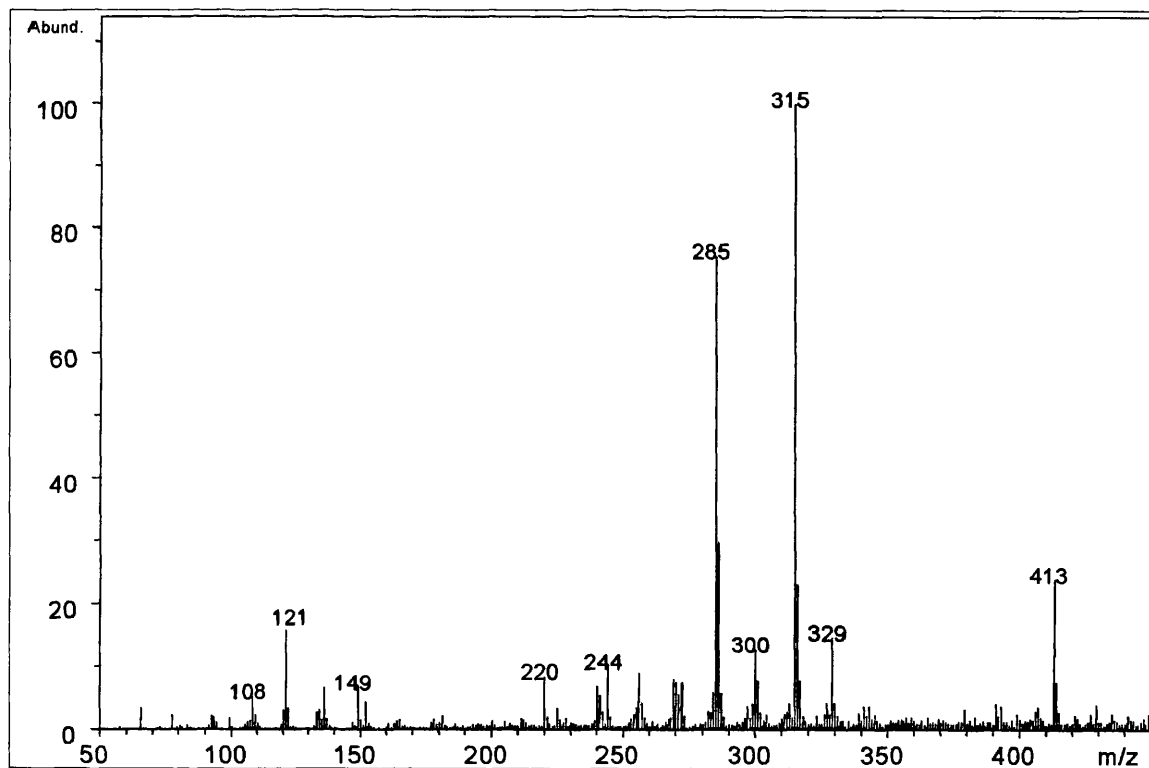


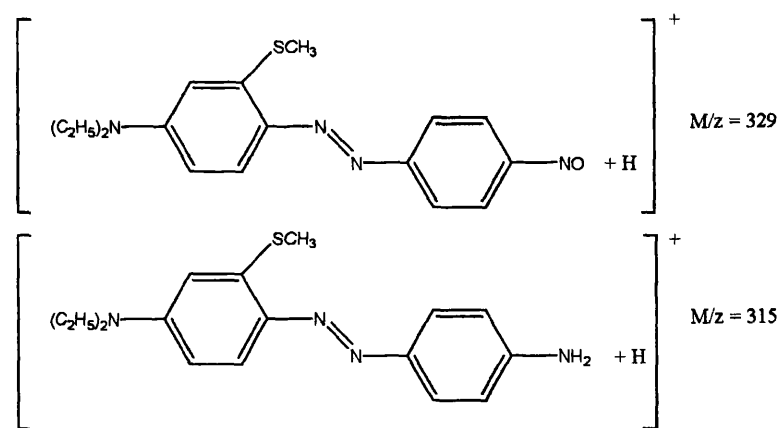
Figure 3.16 Infusion of [IX] faded for 2 hours 15 minutes.¹⁰

Table 3-4 The masses of possible photo-products in the infusion mass spectra of dyes [I]-[IX].

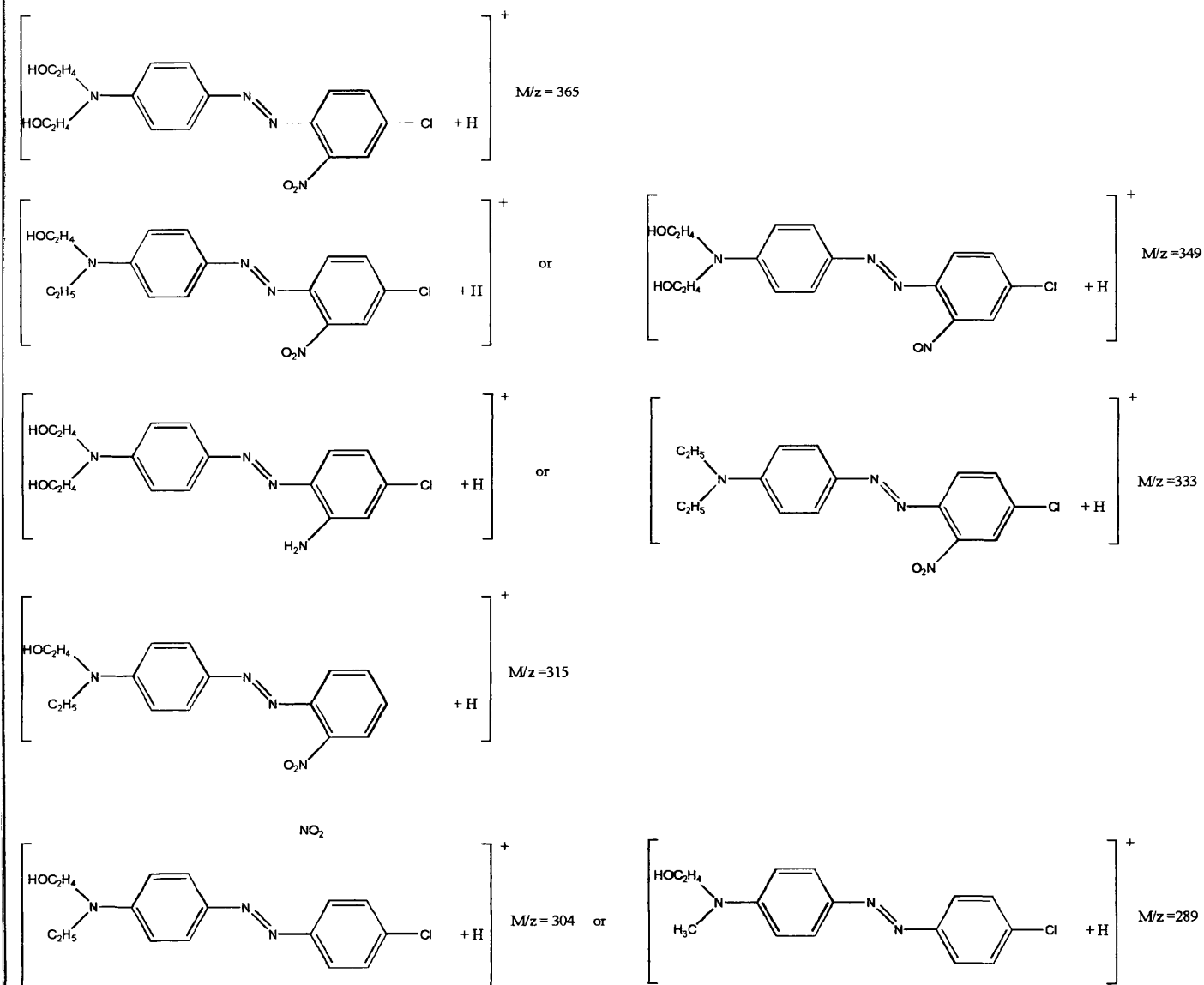
| Faded Dye | [M+H] ⁺ | M/z value of possible fading products |
|-----------|--------------------|---------------------------------------|
| 1 | 345 | 329, 315, 299, 207, 178, 163 |
| 2 | 399 | 365, 333, 304, 289, 200, 119 |
| 3 | 328 | 288 |
| 4 | 315 | 283, 267, 238, 223, 179, 134 |
| 5 | 387 | 355, 311, 282, 177 |
| 6 | 349 | 317, 288, 257, 228, 165, 134, 119 |
| 7 | 365 | 351, 336, 317, 299 |
| 8 | 243 | — |
| 9 | 315 | 300, 285 |

Suggested structures

This infusion data gives us the masses of possible photo-products present in the faded dye solutions. MS/MS spectra of these ions may also give us a clue as to the identity of their structures. From the MS/MS fragment ion data, it is possible to suggest some likely structures for the photo-products. The main product mass peak initially observed for the thiol substituted dye, [I], was at 315, with 329 also prominent. Possible structures for these masses are:

**Scheme 3-3** Possible structures for product mass peaks 329 and 315.

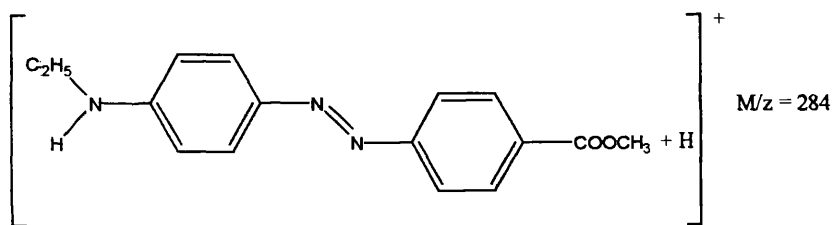
Possible structures for product mass peaks of [II]-[IX], (Scheme 3-4)-(Scheme 3-6) are discussed below.



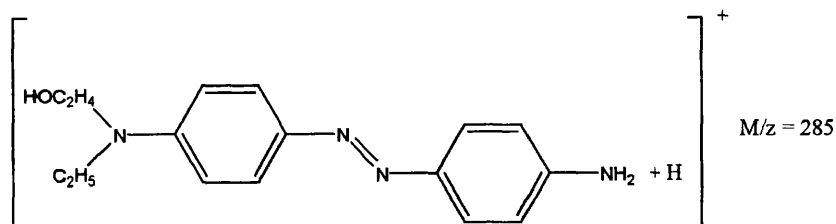
Scheme 3-4 Possible structures of photo-products of [III].

The main product of [III] initially formed had a mass to charge ratio m/z of 333 corresponding to loss of Cl and reduction of the nitro group to NH_2 . These structures were consistent with MS-MS fragmentation patterns. The structures shown refer to photo-products in which the 2-chloro substituent has been removed. It is of course possible that the 4'-chloro, and not the 2-chloro substituent, is removed and structures amended to include the 2-chloro group may be equally viable.

A reduction in mass of 44, suggests the loss of the $\text{C}_2\text{H}_4\text{OH}$ group in [III], while a mass reduction of 30 for [IX] is likely to correspond to a reduction of the nitro group to an amino group. This reduction



Scheme 3-5 Possible structure of photo-products of [III].



Scheme 3-6 Possible structure of photo-products of [IX].

Note that though fragmentation patterns had certain similarities for several dyes, such as loss of 44 or 28, it was not possible to assign sensible structures, that were consistent with fragmentation patterns, for photo-products of all the dyes examined.

The information from infusion of photo-products into the mass spectrometer, is insufficient to determine the relative quantity of photo-products produced, as the intensity of the ion peaks is strongly dependent on the ease of ionisation of the species. Thus for example, a molecule that ionises well may have a peak of much higher intensity than a molecule that does not ionize as readily, even though the concentration of the easily ionised species may actually be lower. It is also possible that peaks assigned as being photo-products may in fact be fragment ions of the original dye, or indeed, fragments of the photo-products themselves.

To assist in the determination of the photo-products LC-MS was performed. The LC chromatograms of photo-faded samples of dyes [I]-[IX] (Figure 3.17 to Figure 3.24) showed numerous product peaks in addition to the peak for the original azo dye. Dyes [IX] and [I], which are substituted with a 4-nitro group, had one major product peak and a few much smaller peaks in the chromatograph at 254 nm detection wavelength. At these irradiation times, there was still a large amount of the original dyes present, as the peaks at retention times 22.360 minutes and 29.015 minutes, which correspond to [IX] and [I] respectively were still the largest peaks detected. Note that these peaks are detected at 254 nm where the original dyes absorb only weakly compared to their absorption in the visible region between 450 and 510 nm.

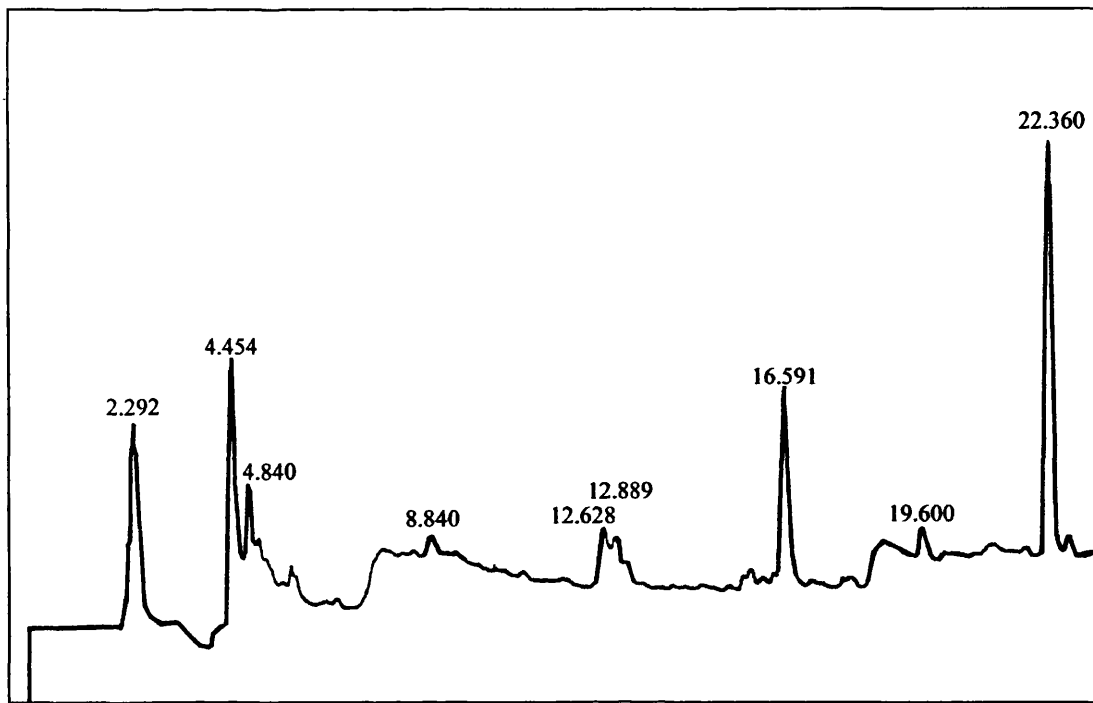


Figure 3.17 LC chromatogram of [IX] at detection wavelength 254 nm after 2 hours irradiation time.¹⁰

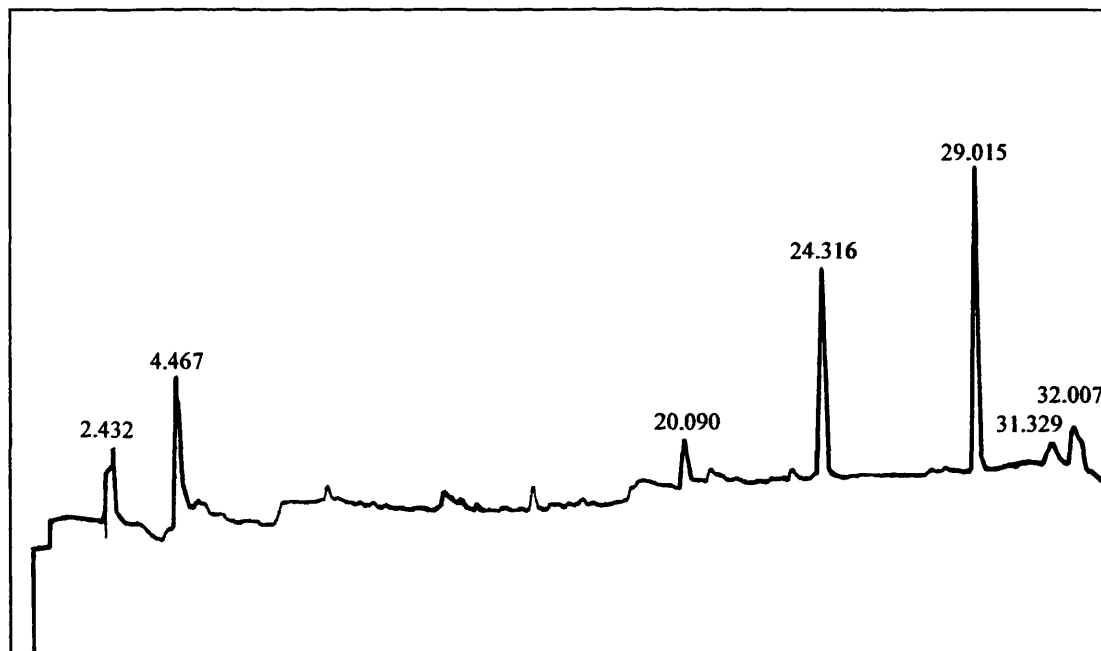


Figure 3.18 LC chromatogram of [I] at detection wavelength 254 nm after 20 minutes irradiation time.¹⁰

The chromatographs of dyes [III] and [V] show a significant degradation of the original dye, as the peaks at 17.488 and 18.902 minutes, which correspond to the retention times of dyes 3 and 5 respectively, are greatly reduced in intensity. Figure 3.19 shows one large peak and a few smaller peaks, at shorter retention times than for dye [III], which may be attributed to photo-products. [V] has two major product peaks a few of intermediate size, and a number of smaller peaks present in its chromatograph (Figure 3.20).

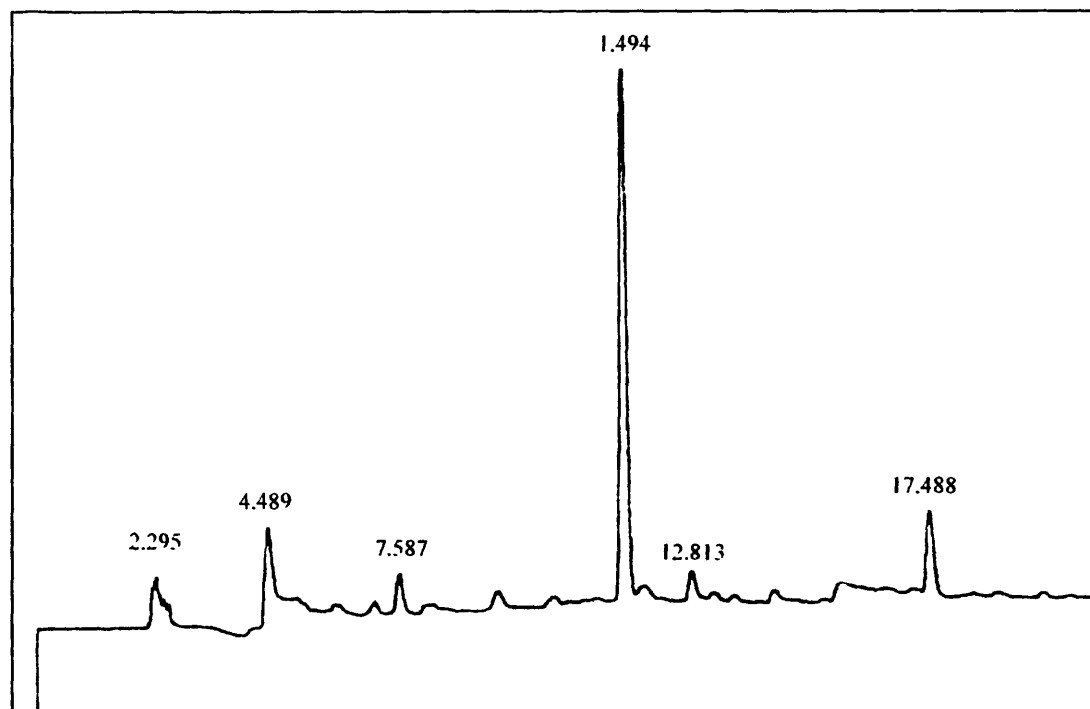


Figure 3.19 LC chromatograph of [III] at detection wavelength 254 nm after 3 hours irradiation time.¹⁰

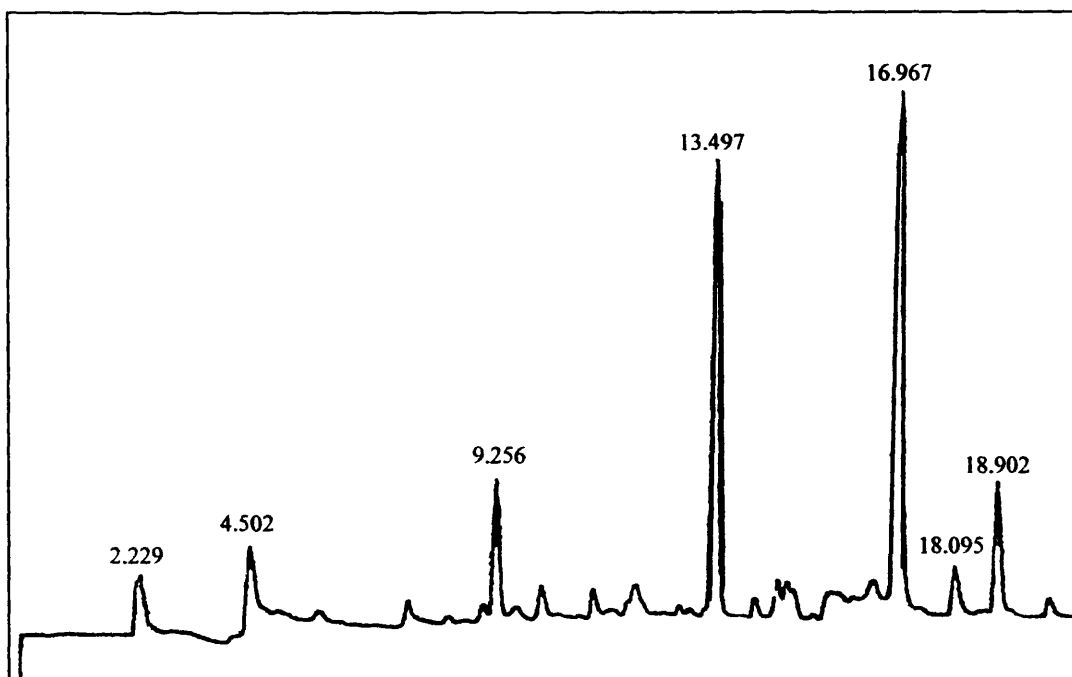


Figure 3.20 LC chromatograph of [V] at detection wavelength 254 nm after 1 hour 30 minutes irradiation time.¹⁰

The four dyes that contain a 2-nitro substituted acceptor phenyl ring show some similarities in their chromatographs. The original dye peaks were significantly degraded and there were between three and six major product peaks at slightly shorter retention times (between 0 and 6 minutes shorter than the retention time of the original dye). In addition to these peaks, there were several much smaller peaks with retention times in the region of 4 to 20 minutes.

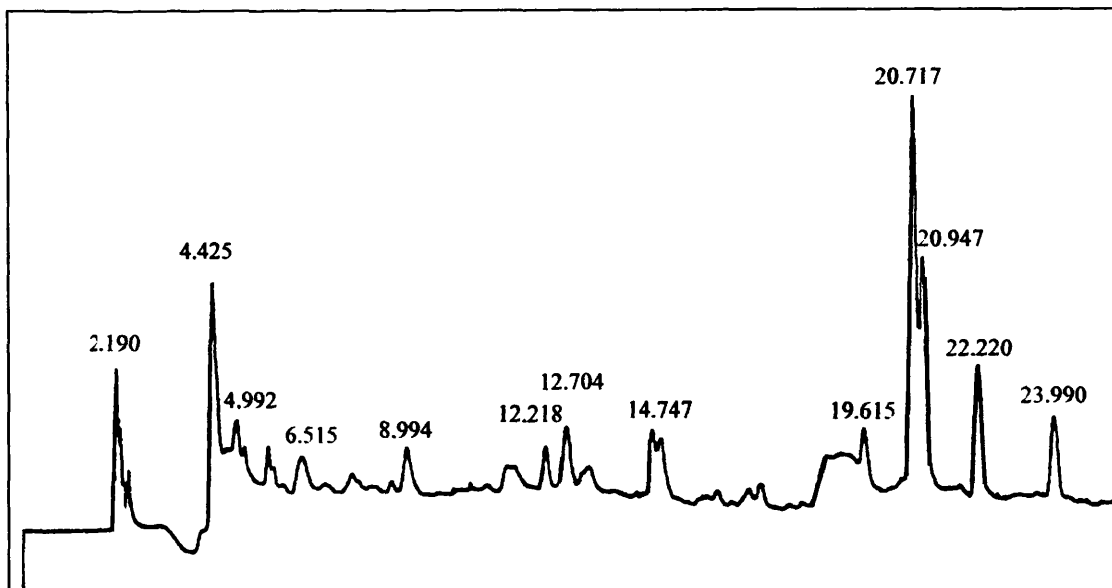


Figure 3.21 LC chromatograph of [IV] at detection wavelength 254 nm after 2 hours irradiation time.¹⁰

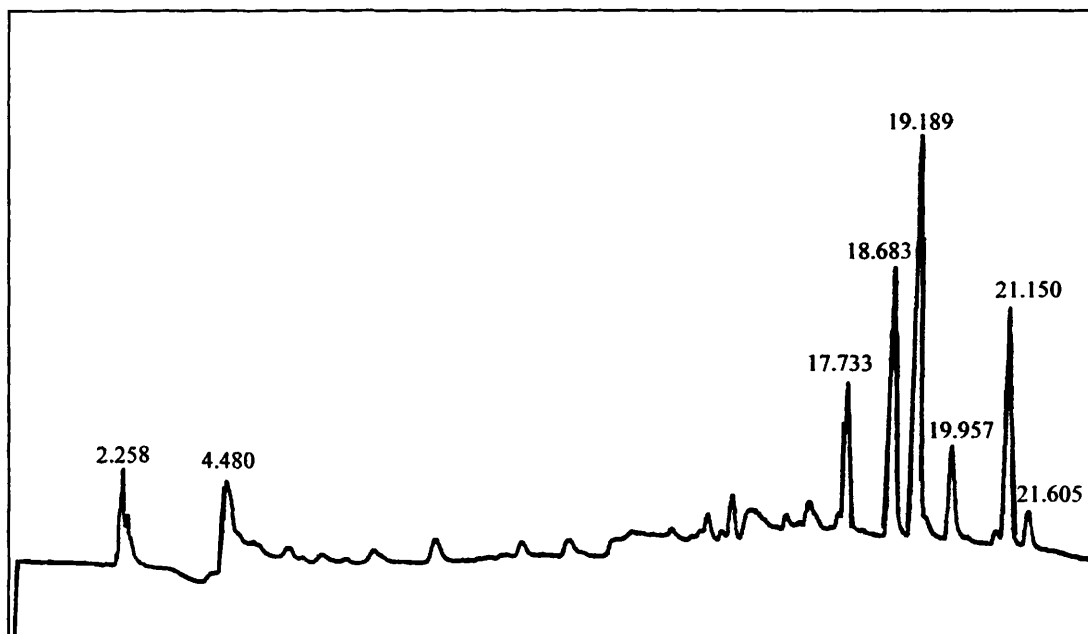


Figure 3.22 LC chromatograph of [VI] at detection wavelength 254 nm after 1 hour 30 minutes irradiation time.¹⁰

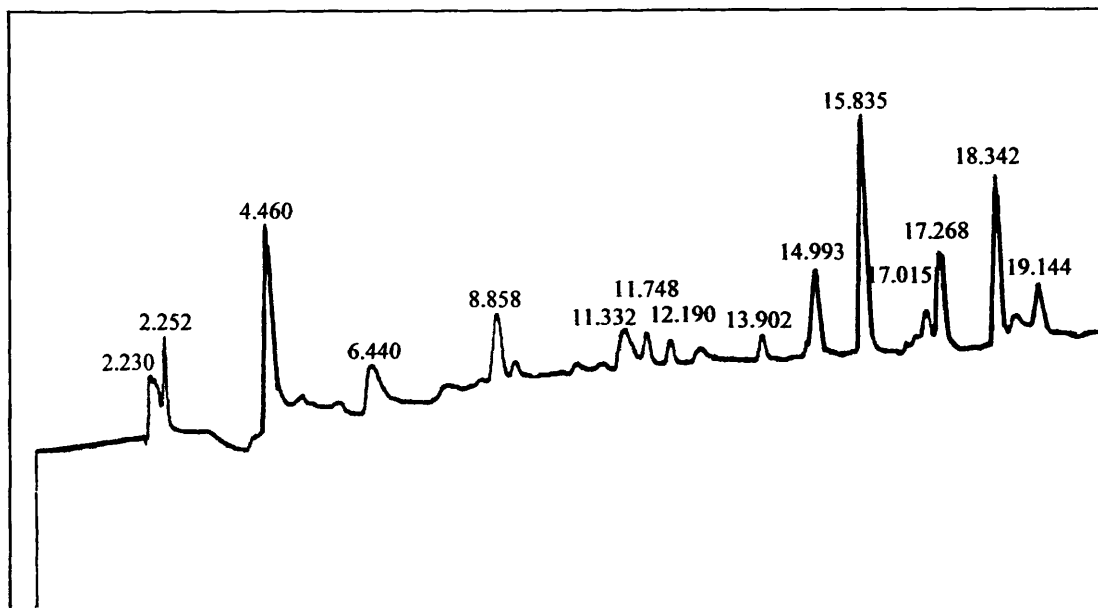


Figure 3.23 LC chromatograph of [VII] at detection wavelength 254 nm after 1 hour 15 minutes irradiation time.¹⁰

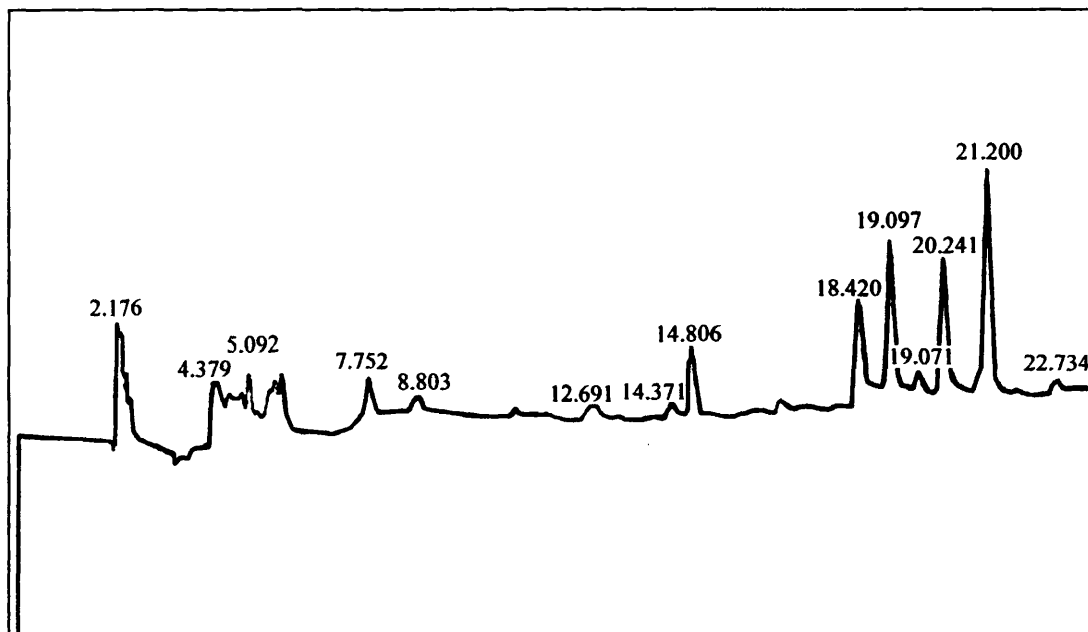


Figure 3.24 LC chromatograph of [III] at detection wavelength 254 nm after 1 hour 30 minutes irradiation time.¹⁰

Due to the low concentration of the fading products, few of the peaks in the LC chromatogram could be directly detected. Therefore, single ion monitoring (SIM) ions thought to be present in the solution was performed. This technique gives elution time of the ion being monitored. An

example of the SIM trace ions 315 and 285 for [IX] is shown in Figure 3.25.

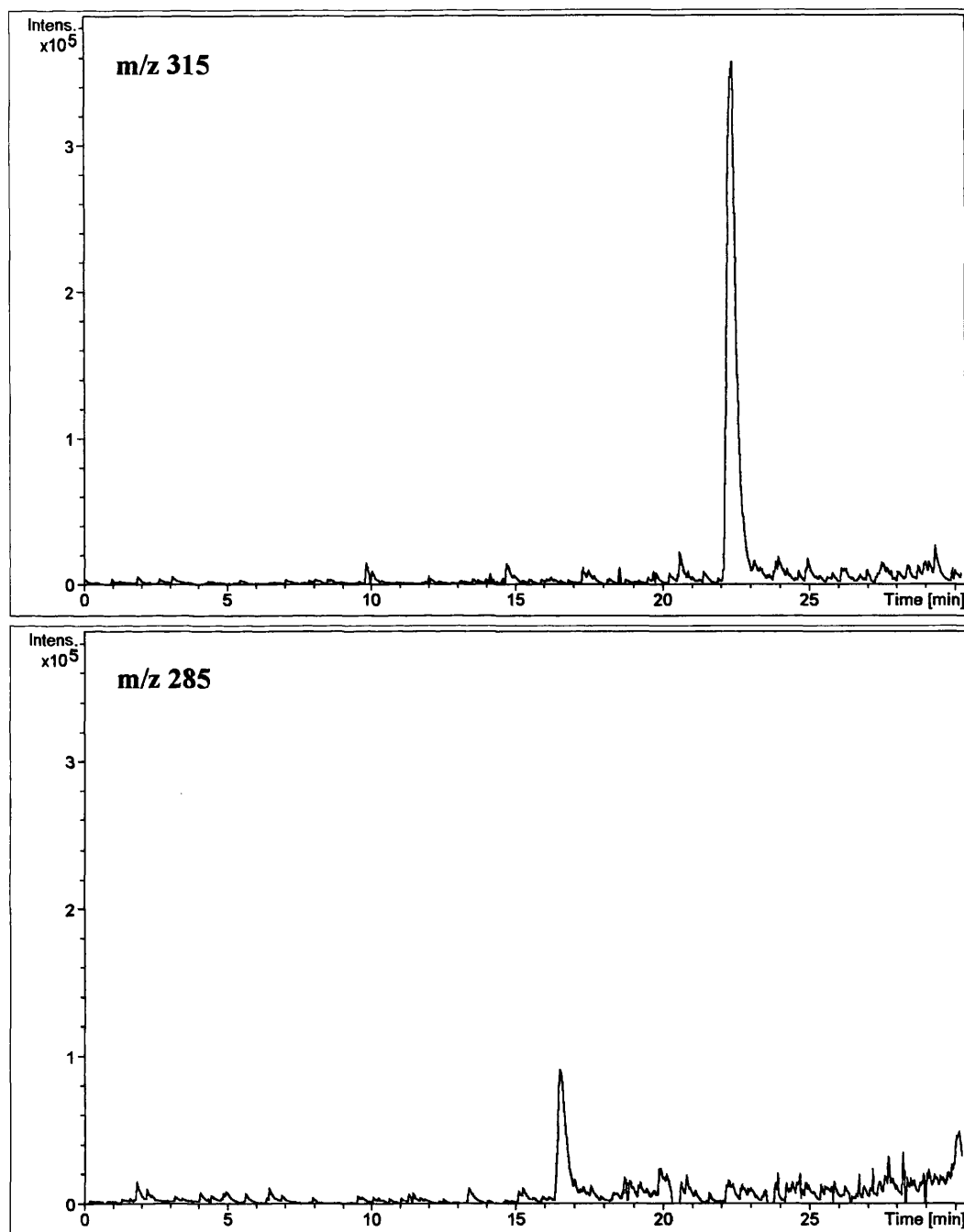


Figure 3.25 Mass chromatograms of m/z 315 and 285 for faded solution of [IX].¹⁰

The elution time of the 315 ion was 22.5 minutes which was very close to the LC elution time. This peak is of course the $[M+H]^+$ molecular ion. The 285 ion had an elution time of 16.6 minutes which had the same elution time as the largest product peak in the LC chromatogram. It

can therefore be concluded with some confidence that the main photoproduct ion had a mass of 285. Unfortunately it was not possible to obtain SIM traces for all of the dyes, or for all of the ions of the dyes examined. Similar SIM analysis identified the masses for the main products of dyes [I], [III], [V] and [VI]. Table 3-5 gives the masses of the isolated fading products and the fragment ions of these mass peaks obtained by MS/MS.

Table 3-5 MS/MS spectra of suspected photo-products of azo dyes [I], [III], [V] and [VI] and [IX].¹⁰

| Dye | Isolated fading product | Fragmentation amplitude | M/z of fragment ions (relative abundance) |
|-------|-------------------------|-------------------------|--|
| [I] | 315 | 0.70 | 315(100), 296(6), 271(20), 268(21), 207(24), 195(81), 180(24), 150(14), 120(19), 92(23) |
| [III] | 333 | 0.73 | 333(77), 315(100), 297(45), 287(40), 270(80), 257(16) |
| [V] | 355 | 0.70 | 355(100), 337(67), 326(61), 310(96), 295(65), 178(27), 160(38), 145(11), 132(13), 117(5) |
| [VI] | 317 | 0.70 | 317(82), 299(74), 288(71), 272(100), 257(38), 221(12), 147(11), 132(7) |
| [IX] | 285 | 0.75 | 285(89), 256(74), 240(34), 164(41), 133(62), 120(154), 92(100) |

Although LC-MS and MS/MS on selected ions give some idea of possible structures for the photoproduct, this information is not sufficient to designate these structures as definite photoproducts. Confirmation of molecular formulas is given by accurate mass spectra of the main photoproduct peaks in the LC chromatogram. Accurate mass measurements produce a mass number which is accurate to four decimal places. Only a certain number of molecular formulas correspond to the accurate mass and only a few of these can possibly be fading products. For example, accurate mass measurements on the main product peak of [IX] yield an accurate mass of 285.1717. There are 10 possible molecular formulae that correspond to this mass of which all but one can be effectively ruled out.

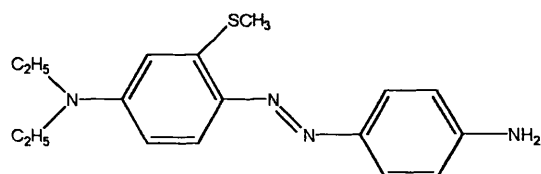
The molecular formula of the photo-product with mass 285.1717 is therefore formula 1, $C_{16}H_{21}N_4O$ which almost certainly corresponds to structure (3-4).

The accurate masses, and the most probable molecular formulae of the main photo-product for each dye examined are given in Table 3-6. Probable structures corresponding to these formulas are also referred to in the table.

Table 3-6 Formulae from accurate mass data for the main photo-products of dyes.

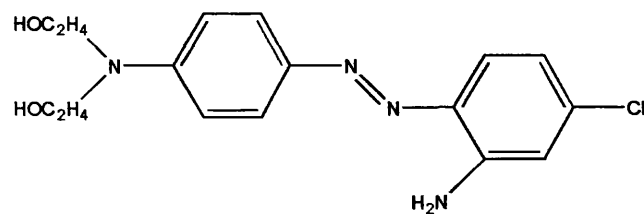
| Dye | Mass of original dye | Accurate Mass of [P+H] ⁺ | Molecular formula of original dye | Molecular formula of product | Probable structure |
|-------|----------------------|-------------------------------------|-----------------------------------|--|--------------------|
| [II] | 344.431 | 315.1629 | $C_{17}H_{20}N_4O_2S$ | $C_{17}H_{23}N_4S$ | (3-1) |
| [III] | 399.233 | 333.1105 | $C_{16}H_{16}N_3O_4Cl_2$ | $C_{13}H_{21}Cl_2N_5O$ $C_{13}H_{20}ClN_3O_5$ $C_{16}H_{18}ClN_4O_2$ | (3-2) or (3-3) |
| [V] | 386.407 | 355.1769 | $C_{19}H_{22}N_4O_5$ | $C_{19}H_{23}N_4O_3$ | |
| [VI] | 348.788 | 317.1165 | $C_{16}H_{17}N_4O_3Cl$ | $C_{15}H_{16}N_4O_4$ | |
| [IX] | 314.343 | 285.1717 | $C_{16}H_{18}N_4O_3$ | $C_{16}H_{21}N_4O_2$ | (3-4) |

Reduction in mass of 29 for [II]. Loss of 2 oxygen atoms and gain of three hydrogen atoms

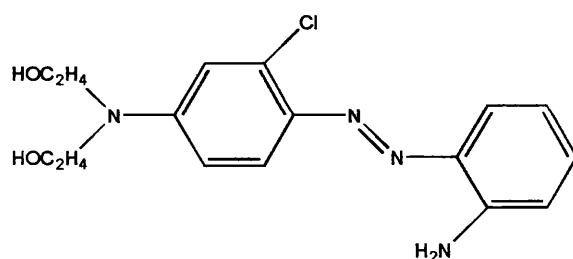


(3-1)

The mass of the product of [III] indicates a similar reduction of the nitro group to an amino group, with an additional loss of one of the chlorine atoms, giving two structures possible for this mass, (3-2) or (3-3).



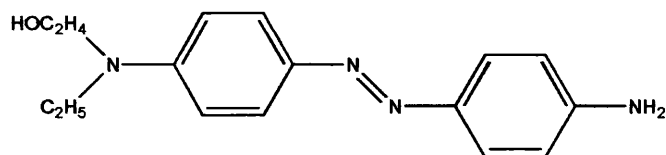
(3-2)



(3-3)

The mass reduction for [V] is 31 – loss of 2 oxygen atoms. There are several possible sites for the loss of these oxygen atoms including loss from the nitro group, from the ester group and from the alcohol group. Combinations of loss of oxygen from these sites are also possible. The 2'-nitro-4-chloro substituted dye, [VI], has its m/z reduced by 31, corresponding to a loss of Cl and CH and addition of oxygen.

Finally, [IX] loses 29 corresponding to the reduction of the nitro group to an amino group.



(3-4)

The structures of many of the photo-products of azo dyes, detected by HPLC remain unresolved. This is either because no clear ion peak could be detected in the total ion chromatogram at retention times corresponding to peaks in the HPLC chromatogram or because not enough data was generated to suggest reasonable structures for ion mass peaks. Further LC-MS analysis on photo-products was carried out in collaboration with M. Yousef² and is still in progress. This work focused on improved separation of photo-products by HPLC and MS-MS analysis on ion peaks in the total ion chromatogram corresponding to peaks detected by HPLC. HPLC was performed at three detection wavelengths, 254nm, 350nm and 450nm.

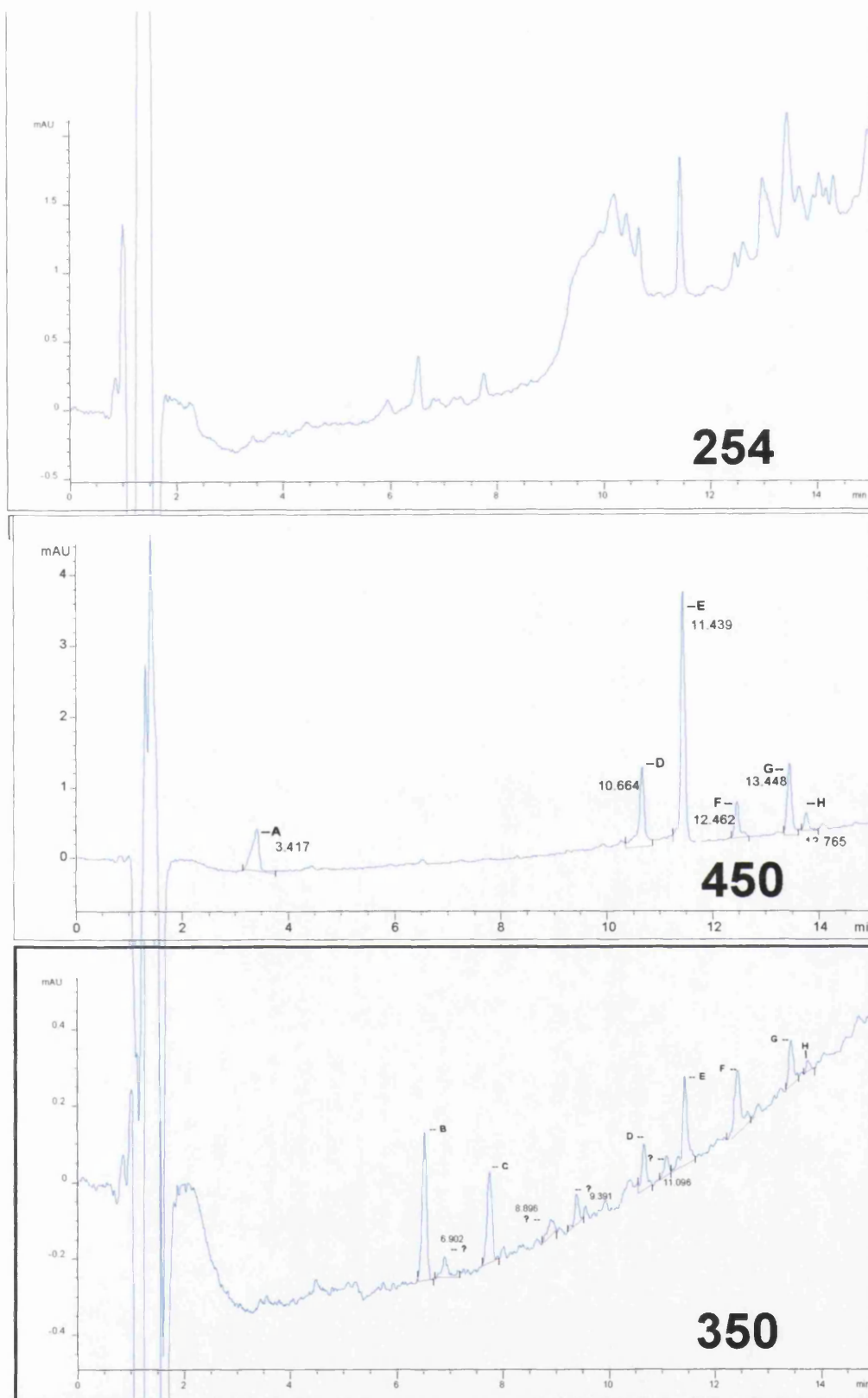


Figure 3.26 HPLC chromatograms of photo-products of [IV] under oxygenated conditions at detection wavelengths 254, 350 and 450nm.

Figure 3.26 shows that several products are detected at 350nm and also at 450nm. The chromatogram at 254nm contains several broad peaks and it was difficult to distinguish photo-degradation products from impurities present in the dye solution before irradiation. Mass spectrometry analysis was therefore restricted to peaks detected at 350nm and 450nm. Total ion chromatograms corresponding to retention times of some of these peaks are shown in Figure 3.27.

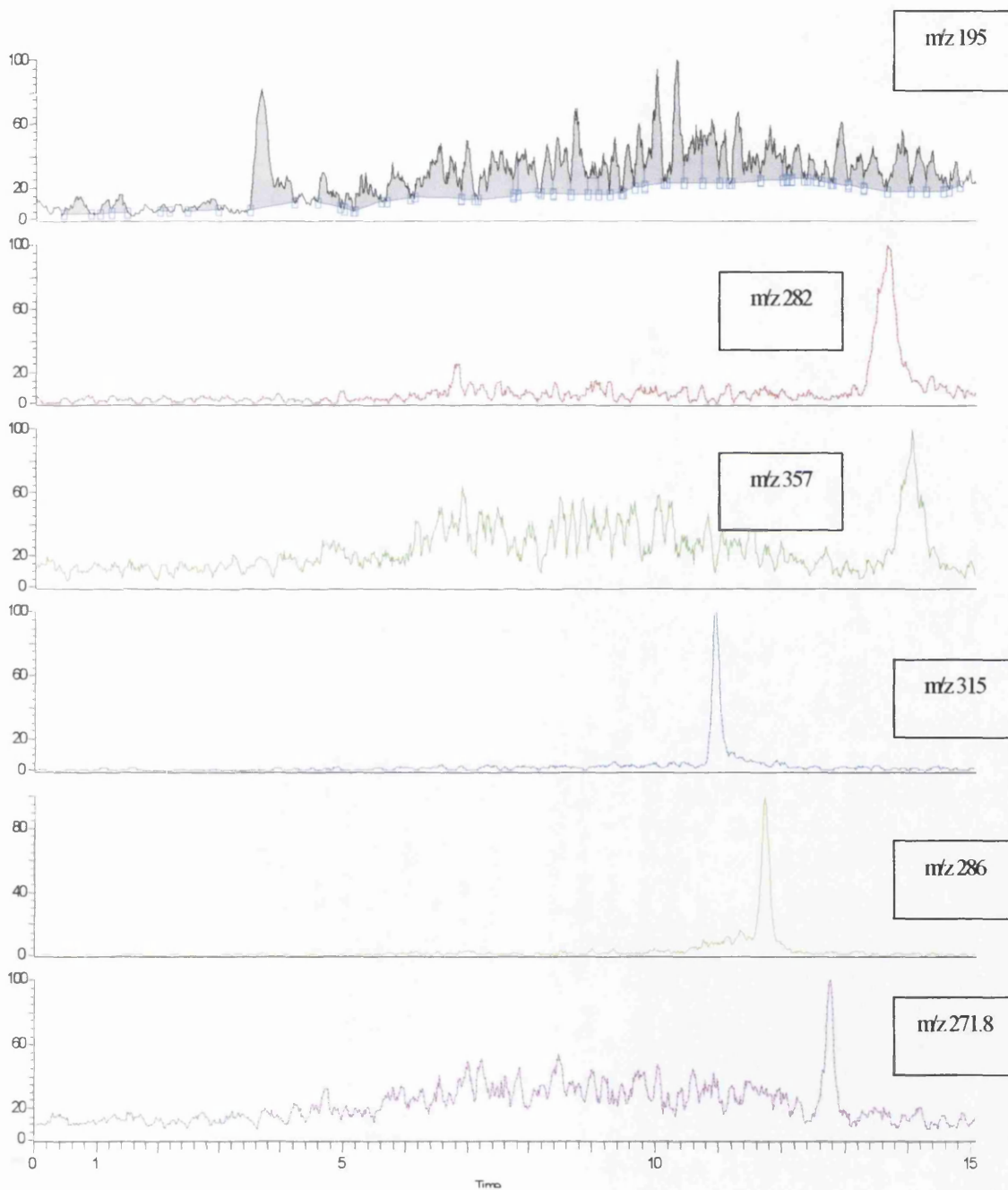
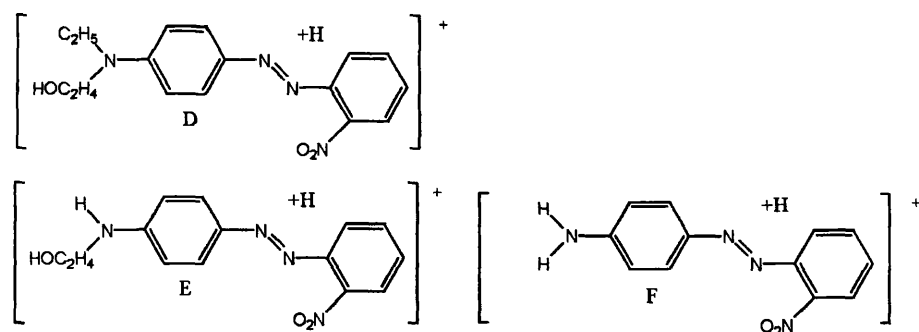


Figure 3.27 Total ion chromatograms of photo-products of 4 faded under oxygenated conditions.

MS-MS analysis was then performed on the ion peaks detected at retention times corresponding to HPLC peaks. From these results Table 3-7, the structures in Scheme 3-7 were proposed for photo-products labeled A-H, in order of their elution. Compounds B and C could not be detected in the mass spectrometer and MS/MS analysis was achieved only for compounds A, D, E and F of which compound D is the original dye. From MS/MS fragment patterns, compounds D, E and F were assigned to the structures in Scheme 3-7.

Table 3-7 Retention times, masses and fragment masses of photoproducts.

| Compounds | LC RT (min) | MS RT (min) | Parent ion | %CE | MS/MS Major Fragments |
|-----------|-------------|-------------|------------|-------|------------------------------|
| A | 3.42 | 3.71 | 195 | 16.00 | 164, 147, 84 |
| B | 6.52 | - | - | - | - |
| C | 7.75 | - | - | - | - |
| D | 10.66 | 10.97 | 315 | 20.50 | 284, 269, 238, 194, 179, 134 |
| E | 11.44 | 11.75 | 287 | 16.80 | 287, 179, 149 |
| F | 12.46 | 12.77 | 271 | 18.00 | 225, 209, 197, 148, 135, 120 |
| G | 13.45 | 13.71 | 282 | - | - |
| H | 13.76 | 14.04 | 356 | - | - |



Scheme 3-7 Probable structures for photo-products A-H.

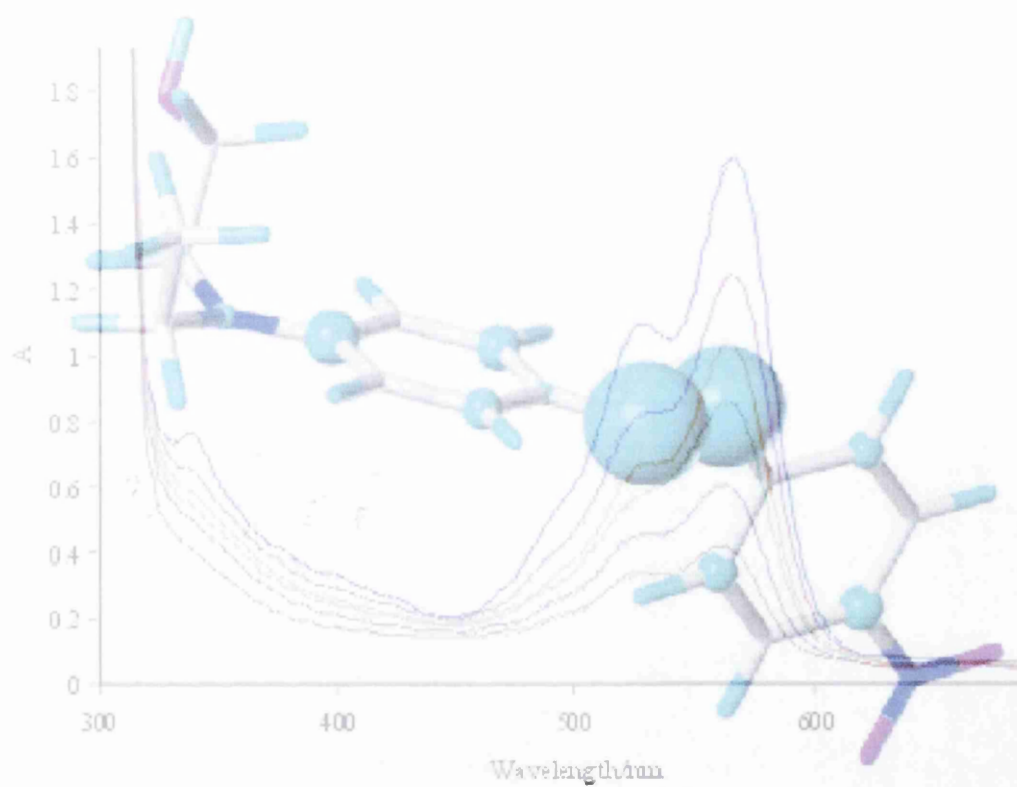
Further investigations are required to confirm the structures of photo-degradation products and to assess product peaks observed in HPLC chromatography, which were not detected by mass spectrometry.

References

- ¹ Louise Perry, Chemistry Dept., University of Wales, Swansea, U.K.
- ² Masood Yousef, Chemistry dept. University of Wales Swansea, U.K.
- ³ J. V. Iribaine, B. A. Thompson, *J. Chem. Phys.*, **64** (1976) 2237
- ⁴ G. Irick and J. C. Pacifici, *Tetrahedron Lett.*, (1969) 1303
- ⁵ A. Albin, E. Fasani, S. Pietra, A. Sulpizio, *J. Chem. Soc., Perkin Trans. 2.*, (1984) 1689.
- ⁶ A. Albin, E. Fasani and S. Pietra, *J. Chem. Soc. Perkin Trans. 2.*, (1983) 1021.
- ⁷ S. Hashimoto, K. Kano, *Bulletin of the Chem. Soc. of Japan*, **45** (1972) 852.
- ⁸ N.S. Allen, *Rev. Prog. Coloration.*, **17** (1987) 61-71.
- ⁹ J. Griffiths in “*Developments in Polymer photochemistry*” ed. N. S. Allen, Applied Science, London, 1980, vol. 1 Chapter 6.
- ¹⁰ Reproduced from Louise Perry, *Mass spectral and separation techniques for the characterisation of natural products and degradation products of dyes*, M. Phil. Thesis, (2000), University of Wales Swansea.

Chapter 4

Theoretical Studies on Azo Dyes



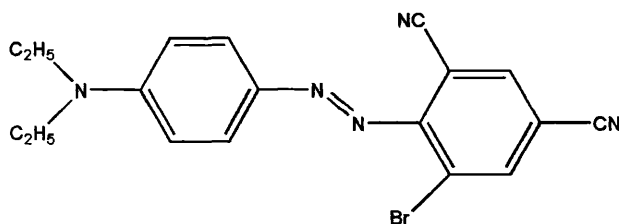
Chapter 4 Theoretical results

Theoretical work was performed on Silicon Graphics¹ workstations, primarily using the molecular modeling package SYBYL². Crystal Structures for the construction of starting structures and for comparative purposes, were obtained from the Cambridge Structural Database (CSD) of crystallographic compounds,³ which contains details of key bond lengths, angles and torsions of organic compounds.

Methods of calculation

To calculate the spectroscopic properties of the azo dyes described here reasonable theoretical geometric structures for each dye molecule were required initially. Geometry optimisation calculations were performed starting structures constructed by modifying existing crystal structures obtained from the CSD or from empirical structures. These involve iterative calculations with the variation of bond lengths and angles, to achieve a minimum energy structure. Each iterative cycle produces a point on a potential energy curve, and the minimum energy structure is reached when the gradient of this curve approaches zero. There is however a possibility that the energy minimum calculated is a local minimum, and not the lowest energy minimum corresponding to the most energetically stable structure. The energy and geometry of the optimised structures depends on the starting structures, with dramatic deviations from the starting geometry unlikely. It is therefore important, when interpreting the results of these calculations, to make sure that the energy minimum calculated is the lowest energy possible.

Geometry optimisations were carried out on all 19 dyes in the gas phase using both the AM1⁴ (Austin Model 1) and PM3⁵ (Parametric Method 3) semi empirical methods⁶ of the MOPAC 93⁷ program, which is a semi-empirical molecular orbital package (see Introduction). Starting structures for geometry optimisations were constructed from crystal structures of azo dyes obtained from the Cambridge Structural Database. These crystal structures were imported into SYBYL, and their structures modified to obtain structures for [I]-[IX]. For example the crystal structure BEDSEI³, 4-N,N-diethylamino-2',4'cyano-6'-bromoazobenzene (4.1), was adapted by deleting the Br and CN substituents and adding a 4'-nitro substituent to obtain structure [X].



(4.1)

The other azobenzene dyes were constructed in a similar way. Unfortunately, there are no azothiophene crystallographic structures available on the Cambridge Structural Database, so the azothiophene dyes were created by replacing one of the phenyl rings of an azo dye with a thiophene ring. Full optimisations were performed using the keywords AM1 or PM3 with the additional keywords PREC, NOLOG, NOINTER, EF, GEO-OK and XYZ. NOLOG and NOINTER prevent the printing of the inter-atomic distances in the output file, the XYZ keyword forces the calculation to run in Cartesian co-ordinates, GEO-OK is a keyword overriding the inter-atomic distance checks and EF is an optimisation method.⁸⁸ Geometry optimizations were also performed on structures in which, the co-ordinates of the heavy atoms (atoms other than hydrogen) were adjusted so that the azobenzene or azothiophene section of the molecule was constrained to be planar. Both gas phase calculations and calculations incorporating solvent effects were performed. The latter used the dielectric continuum method COSMO^{9,10,11} (conductor-like screening model) incorporated in MOPAC 93. COSMO is a method which uses a dielectric field to imitate the effect of the solvent on the molecule. The COSMO calculation is invoked by the keyword EPS = ϵ , where ϵ is the dielectric constant of the solvent being modeled. Thus each particular solvent is specified by inputting the value of its dielectric constant into the calculation. For example if the solvent is methanol, then the keyword EPS = 32.7 is added to the input file for the calculation (32.7 being the dielectric constant of methanol).

In addition to semi-empirical calculations, ab initio optimizations on dyes [I] -[IX] were carried out using the 3-21G basis set. Further ab initio calculations on selected dyes were performed using 4-31G, 4-31G* and 6-31G* basis sets to evaluate the differences in the geometry resulting from the use of different basis sets. Optimized AM1 structures were used as the input geometries.

Calculations involving a 360° rotation of either the donor phenyl ring, the acceptor phenyl ring or the nitro group in the molecule were performed on ground state structures using the additional keywords: 1SCF STEP = 2 and POINT = 180. This specifies a single point calculation at every 2° step of a 360° rotation.

Spectroscopic calculations were carried out on ground state structures using multi-electron configuration interaction¹² (MECI) and various levels of configuration interaction specified by the keyword C.I. = n (see Chapter 5). The C.I. = n keyword, where n is an integer between 2 and 8, controls the number of orbitals treated in the calculation. For example, C.I. = 2 involves only two orbitals; the HOMO and the LUMO while C.I. = 4 involves four orbitals; the HOMO, HOMO-1, LUMO and the LUMO+1. The maximum C.I. that was possible was C.I. = 8. Additional keywords used are 1SCF, VECTORS, SINGLET, ROOT = n and OPEN(2,2). The 1SCF keyword signifies a single point calculation, SINGLET specifies the multiplicity of the state to be calculated, ROOT = n indicates the excited state i.e. ROOT = 1 is the ground state and ROOT = 2 is the first excited state and OPEN(2,2) specifies two unpaired electrons in two unoccupied orbitals.

Analysis of configuration interaction calculations was performed on the ground state of the molecule using the supplementary keywords LET and LARGE. These keywords produce an output file which contains singlet and triplet states, the number of which is specified by the level of the C.I. calculation. For example, C.I. = 4 produces the 36 excited states from all possible from excitations involving the 2 HOMO and 2 LUMO orbitals, whereas C.I. = 6 generates the first 400 possible excited states from transitions involving the 3 HOMO and 3 LUMO orbitals. These excited states are ordered in terms of their energy relative to the ground state S_0 .

An alternative CNDOVS method¹³ was also used to evaluate the spectroscopic properties. This method uses single excitation of electrons and a large number of occupied and unoccupied orbitals, and has been specifically developed for dyes and pigments. The spectroscopic constant K was set at 0.65 or 0.58.

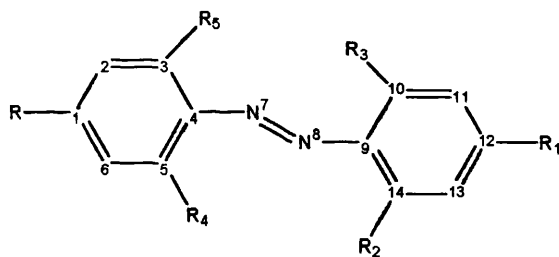
Full geometry optimisations of the excited singlet states of structures were performed using the same keywords as for ground state optimisations and the additional keywords SINGLET, ROOT = n (where n is greater than 1) and OPEN(2,2). Optimisations of triplet states were performed by replacing SINGLET by TRIPLET and using ROOT = n (where n is the n th triplet state). Configuration interaction treatment of the excited states used the additional keywords MECI, VECTORS, C.I. = n and 1SCF. The distribution of the two unpaired electrons in a molecule, in a triplet state calculation, can be specified using the keyword ESR.

Geometry

The geometry of some similar donor-acceptor type azo dyes have been determined at various levels of theory in previous studies¹². Crystal structural data on donor acceptor type azobenzenes (Table 4.1) show these molecules to be essentially planar, with torsion angles between the aromatic rings

and the -N=N- bond ranging from 1.2 to 4.8°. AM1 calculations on 4-dimethylamino-4'-nitroazobenzene (**4.2a**) gave a non planar conformation, with the nitrophenyl ring twisted by 37.3° to the plane formed between the azo group and the donor phenyl ring. However, calculations where the heavy atoms of the dye were constrained to lie in the same plane, produced very similar heats of formation to the twisted conformations.

The azo -N=N-, Ar-N(CH₃)₂ and Ar-NO₂ bond lengths of (**4.2a**) were calculated to be 1.232, 1.396 and 1.485 Å respectively. Ab initio calculations by the same authors, using an extended basis set at the 3-21G level gave a planar structure, with a -N=N- bond length of 1.244 Å. In comparison, crystal structures of azobenzenes (**4.2b-h**) have -N=N-, bond lengths of between 1.254 and 1.294 and an average of 1.273 Å (refer to Table 4.1), which is considerably longer than in calculated structures. The average C-NR₂ and C-NO₂ bond lengths were 1.370 and 1.462 Å respectively, which are shorter than in calculated structures.



(4.2)

- a** R = N(CH₃)₂; R¹ = NO₂; R² = R³ = R⁴ = R⁵ = H
- b** R = N(C₂H₅)₂; R¹ = CN; R² = Br; R³ = R⁴ = R⁵ = H
- c** R = N(C₂H₅)₂; R¹ = NO₂; R² = Br; R³ = CN; R⁴ = H; R⁵ = NHCOCH₃
- d** R = N(C₂H₅)₂; R¹ = SO₂CH₃; R² = Cl; R⁴ = NHCOCH₃; R³ = R⁵ = H;
- e** R = N(C₂H₅)₂; R¹ = NO₂; R² = Br; R³ = CN; R⁴ = H; R⁵ = NHCOC₂H₅
- f** R = N(C₂H₅)₂; R¹ = SO₂CH₃; R² = Cl; R⁴ = NHCOC₂H₅; R³ = R⁵ = H;
- g** R = N(CH₃)₂; R¹ = R² = R³ = R⁴ = H; R⁵ = COOH
- h** R = N(C₂H₅)₂; R¹ = NO₂; R² = R³ = R⁴ = H; R⁵ = CH₃
- i** R = N(C₂H₅)₂; R¹ = NO₂; R² = CN; R³ = R⁴ = R⁵ = H
- j** R = N(C₂H₄OH)₂; R² = NO₂; R¹ = R³ = R⁴ = R⁵ = H

Previous authors¹⁴ have also reported on AM1 and PM3 calculations on the geometry of the azothiophene, 4-[N,N-bis(2acetoxylethyl)amino]phenyl-1-azo-2'-(3',5'-dinitrothiophene) [XV], which

produced a twisted structure, where the thiophene ring is approximately orthogonal to the plane of the phenylazo group for full optimisations. Calculations where the heavy atoms were constrained to lie in the same plane gave heats of formation only slightly higher in energy than the twisted structures. The calculated –N=N- bond length (1.25 Å) was longer than that for the azobenzene.

Ab initio calculations¹⁵ at the STO-3G level¹⁶ on the azothiophene dye 2-(2-acetamido-4-diethylaminophenylazo)-3', 5'-dinitrothiophene, gave a planar structure with an azo bond length of 1.291 Å, which compares with 1.278 Å in donor acceptor azobenzenes at the same level of calculation.¹²

Table 4.1 Experimental crystal structure data for donor-acceptor azobenzenes (4.2b-i)³.

| Structure | CSD ^a | bond length/ Å | | | bond angles/ degrees | | | Torsion angles / degrees | | | |
|-----------|----------------------|--------------------------------|---------------------------------|----------------------------------|--|--|---|--|--|--|----------------|
| | | N ⁷ -N ⁸ | C ¹ -NR ₂ | C ¹² -NO ₂ | C ⁴ N ⁷ N ⁸ | N ⁷ N ⁸ C ⁹ | C ⁵ C ⁴ N ⁷ N ⁸ | N ⁷ N ⁸ C ⁹ C ¹⁰ | ^b CNC ¹ C ² | ^b CNC ¹ C ⁶ | R ^c |
| b | BEDSEI | 1.254 | 1.364 | | 115.7 | 113.0 | 4.8 | -2.6 | -2.0 | -6.7 | 5.3 |
| c | CEMSOC10 | 1.281 | 1.353 | 1.472 | 114.2 | 114.0 | -1.3 | -1.2 | 3.3 | 3.2 | 6.5 |
| d | ACLMSA | 1.278 | 1.373 | | 117.6 | 112.6 | 0.5 | -4.2 | 5.3 | 3.5 | 7.7 |
| e | BCNPPC10 | 1.294 | 1.354 | 1.464 | 114.6 | 113.3 | 1.3 | 5.7 | -0.5 | 1.9 | 6.5 |
| f | MAAZCZ | 1.276 | 1.375 | | 118.9 | 111.9 | 0.0 | 8.0 | 11.8 | 12.8 | 4.8 |
| g | CEMSPB10 | 1.268 | 1.361 | | 116.8 | 114.5 | 6.0 | 5.6 | 2.2 | -3.9 | 9.3 |
| h | STRUCT01 | 1.260 | 1.415 | 1.446 | 113.0 | 111.0 | 1.5 | 0.6 | 6.6 | 8.3 | 8.0 |
| i | STRUCT02 | 1.271 | 1.362 | 1.464 | 115.3 | 112.7 | 3.0 | -1.5 | -8.0 | -8.5 | 5.4 |
| | Average ^d | 1.273 | 1.370 | 1.462 | 115.8 | 112.9 | 2.0 | 1.3 | 2.3 | 1.3 | |

^a The codenames for structures (4.2b-i) are taken from reference 3. ^b Carbon of the NR₂ group relative to the donor phenyl ring. ^c The R factor is a measure of the agreement between the structure as postulated relative to the diffractometer data as collected (as %). ^d Average data from structures (4.2b-i).

Geometry optimisations

Full geometry optimisations, and optimisations where some of the heavy atoms were constrained to lie in the same plane were performed on [I] -[XIX] using the AM1 method and on a selected number of dyes using the PM3 method. The atoms constrained to lie in the same plane, were the heavy atoms of both phenyl rings in the azobenzene dyes or the phenyl and thiophene rings in the azothiophene dyes, the amino nitrogen and in certain cases, the carbon or hydrogen atoms attached directly to the amino nitrogen. Constrained optimisations were performed, as full optimisations often produce structures in which the acceptor phenyl ring is twisted with respect to the phenyl azo plane, whereas

spectroscopic evidence suggests that in solution molecules are less twisted.¹² This procedure was carried out by removing the optimisation flags for the z-coordinate of atoms to be constrained to lie in the same plane, after first placing these atoms at a fixed z-coordinate 0.0. Only optimisations in the x and y directions are then permitted. Both rings are thus completely planar. The nature of the constrained atoms will be specified in the discussion of each dye.

Calculations were carried out in the gas phase and using the COSMO method to incorporate dielectric field effects. All 19 dyes were optimised with COSMO at dielectric 32.7 (the dielectric constant of methanol) by specifying the keyword EPS = 32.7. In addition, [I]-[IX] have also been optimised using the dielectric constants of the following solvents listed in Table 4.2.

Table 4.2 The dielectric constants (ϵ) of solvents¹⁷ used in the calculations.

| Solvent | ϵ | Solvent | ϵ |
|-----------------------|------------|----------------------------|------------|
| Hexane | 2 | Acetone | 20.7 |
| Cyclohexane | 2.1 | Ethanol | 24.6 |
| Dioxan | 2.2 | Methanol | 32.7 |
| Chloroform | 4.8 | DMSO (dimethyl-sulphoxide) | 46.7 |
| THF (tetrahydrofuran) | 7.6 | Ethylene carbonate | 89.6 |
| Pyridine | 12.3 | Formamide | 111 |

These solvents were chosen to cover a large range of dielectric constants so that the effect of increasing the dielectric constant of the medium on the geometries, heats of formation and transition energies of [I]-[IX], could be assessed.

Structures [I]-[IX] were optimised at the ab initio level using the 3-21G basis set, and also the 4-31G and 6-31G basis set for [VIII]. The bond lengths, bond angles and torsion angles along with the heat of formation and dipole moment for each dye, calculated by AM1, PM3 and ab initio methods, are reported in the following discussion and results for gas phase calculations and calculations including the solvent are also compared. The bond lengths, angles and torsions are reported along with the heat of formation and dipole moment. for each dye.

The simplest structure is [VIII], which contains only an amino donor and nitro acceptor groups. The atom numbering system for [VIII] is given in Figure 4.1, where hydrogen atoms are omitted for clarity. This convention has been adopted for all the azo dyes discussed in this work. The bond lengths, bond angles and torsions for each optimization method are reported in Table 4.3. Planar

structures have all of the heavy atoms, except for the N¹⁶, O¹⁷ and O¹⁸ atoms of the nitro group, constrained to lie in the same plane. The hydrogen atoms of the amino group, H¹⁹ and H²⁰ are also constrained to lie in the same plane in planar optimisations.

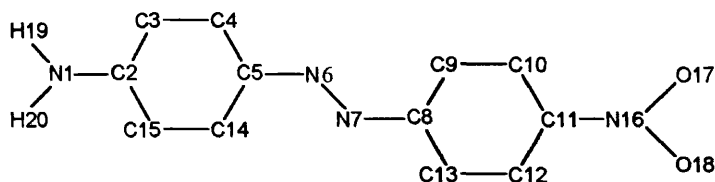


Figure 4.1 Atom numbering convention for [VIII].

Table 4.3 Calculated structural data^a, heats of formation and dipole moments for [VIII] optimised by the AM1 and PM3 methods in the gas phase and solution (EPS=32.7) and by ab initio methods using the 3-21G and 6-31G basis sets.

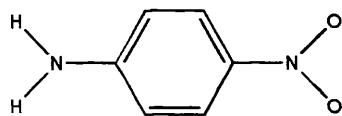
| | AM1 ^b | AM1/ COSMO ^b | AM1 ^c | AM1/ COSMO ^c | PM3 ^b | PM3/ COSMO ^b | PM3 ^c | PM3/ COSMO ^c | Ab-initio 3-21G | 6-31G |
|---|------------------|----------------------------|------------------|----------------------------|------------------|----------------------------|------------------|----------------------------|--------------------|--------|
| Bond lengths | | | | | | | | | | |
| N ¹ -C ² | 1.372 | 1.358 | 1.386 | 1.389 | 1.393 | 1.369 | 1.423 | 1.425 | 1.365 | 1.364 |
| C ² -C ³ | 1.421 | 1.427 | 1.418 | 1.419 | 1.409 | 1.418 | 1.404 | 1.405 | | |
| C ³ -C ⁴ | 1.383 | 1.379 | 1.384 | 1.383 | 1.383 | 1.378 | 1.386 | 1.386 | | |
| C ⁴ -C ⁵ | 1.415 | 1.418 | 1.414 | 1.415 | 1.404 | 1.408 | 1.403 | 1.403 | | |
| C ⁵ -C ¹⁴ | 1.411 | 1.145 | 1.411 | 1.412 | 1.402 | 1.406 | 1.401 | 1.401 | | |
| C ¹⁴ -C ¹⁵ | 1.384 | 1.380 | 1.385 | 1.384 | 1.384 | 1.378 | 1.386 | 1.386 | | |
| C ² -C ¹⁵ | 1.420 | 1.427 | 1.417 | 1.419 | 1.408 | 1.418 | 1.404 | 1.404 | | |
| C ⁵ -N ⁶ | 1.426 | 1.419 | 1.427 | 1.426 | 1.436 | 1.427 | 1.440 | 1.441 | 1.408 | 1.405 |
| N ⁶ -N ⁷ | 1.233 | 1.235 | 1.233 | 1.231 | 1.234 | 1.237 | 1.233 | 1.230 | 1.277 | 1.223 |
| N ⁷ -C ⁸ | 1.438 | 1.436 | 1.438 | 1.439 | 1.449 | 1.449 | 1.449 | 1.451 | 1.419 | 1.419 |
| C ⁸ -C ⁹ | 1.410 | 1.410 | 1.409 | 1.401 | 1.399 | 1.399 | 1.399 | 1.398 | | |
| C ⁹ -C ¹⁰ | 1.391 | 1.391 | 1.391 | 1.391 | 1.389 | 1.388 | 1.389 | 1.388 | | |
| C ¹⁰ -C ¹¹ | 1.403 | 1.405 | 1.403 | 1.405 | 1.400 | 1.403 | 1.399 | 1.404 | | |
| C ¹¹ -C ¹² | 1.404 | 1.406 | 1.404 | 1.407 | 1.401 | 1.404 | 1.400 | 1.404 | | |
| C ¹² -C ¹³ | 1.389 | 1.389 | 1.389 | 1.389 | 1.388 | 1.387 | 1.388 | 1.388 | | |
| C ¹³ -C ⁸ | 1.413 | 1.414 | 1.413 | 1.411 | 1.401 | 1.402 | 1.401 | 1.398 | | |
| C ¹¹ -N ¹⁶ | 1.486 | 1.475 | 1.486 | 1.475 | 1.496 | 1.469 | 1.497 | 1.469 | 1.446 | 1.456 |
| N ¹⁶ -O ¹⁷ | 1.202 | 1.207 | 1.202 | 1.207 | 1.216 | 1.224 | 1.215 | 1.224 | 1.245 | 1.194 |
| N ¹⁶ -O ¹⁸ | 1.202 | 1.207 | 1.202 | 1.207 | 1.216 | 1.224 | 1.215 | 1.223 | | |
| N ¹ -H ¹⁹ | 0.986 | 0.992 | 0.993 | 1.000 | 0.988 | 0.987 | 0.995 | 0.997 | | |
| N ¹ -H ²⁰ | 0.986 | 0.992 | 0.993 | 1.000 | 0.988 | 0.987 | 0.995 | 0.997 | | |
| Bond Angle | | | | | | | | | | |
| H ¹⁹ N ¹ C ² | 120.18 | 120.42 | 116.48 | 114.55 | 120.12 | 120.19 | 112.31 | 111.48 | | |
| H ²⁰ N ¹ C ² | 120.16 | 120.42 | 116.46 | 114.55 | 120.12 | 120.21 | 112.32 | 111.46 | | |
| N ¹ C ² C ³ | 120.94 | 121.18 | 120.88 | 120.90 | 120.09 | 120.44 | 120.02 | 119.97 | | |
| N ¹ C ² C ¹⁵ | 120.98 | 121.19 | 120.92 | 120.90 | 120.10 | 120.45 | 120.04 | 120.01 | | |
| C ⁴ C ⁵ N ⁶ | 116.11 | 116.16 | 116.07 | 116.03 | 115.48 | 115.49 | 115.44 | 115.32 | | |
| C ¹⁴ C ⁵ N ⁶ | 125.59 | 125.62 | 125.56 | 125.43 | 124.45 | 124.63 | 124.43 | 124.36 | | |
| C ⁵ N ⁶ N ⁷ | 120.24 | 120.60 | 120.18 | 120.74 | 120.46 | 120.46 | 120.37 | 120.83 | 117.23 | 116.64 |
| N ⁶ N ⁷ C ⁸ | 119.22 | 119.50 | 119.26 | 118.85 | 119.36 | 119.36 | 119.48 | 118.93 | 115.46 | 114.93 |
| N ⁷ C ⁸ C ⁹ | 125.42 | 125.32 | 125.40 | 122.55 | 124.62 | 124.62 | 124.56 | 119.39 | | |

Table 4.3 (continued)

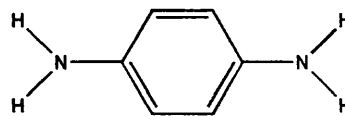
| Bond angles | | | | | | | | | | |
|---|--------|--------|--------|--------|--------|--------|--------|--------|---|---|
| N ⁷ C ⁸ C ¹³ | 115.66 | 115.54 | 115.65 | 117.56 | 115.28 | 115.28 | 115.29 | 119.43 | | |
| C ¹⁰ C ¹¹ N ¹⁶ | 119.70 | 119.55 | 119.70 | 119.49 | 120.12 | 120.12 | 120.11 | 120.06 | | |
| C ¹² C ¹¹ N ¹⁶ | 119.65 | 119.49 | 119.64 | 119.46 | 120.09 | 120.09 | 120.07 | 120.08 | | |
| C ¹¹ N ¹⁶ O ¹⁷ | 118.99 | 120.08 | 118.98 | 120.08 | 119.50 | 119.50 | 119.46 | 121.11 | | |
| C ¹¹ N ¹⁶ O ¹⁸ | 118.99 | 120.07 | 118.98 | 120.07 | 119.51 | 119.51 | 119.47 | 121.20 | | |
| Torsional Angle | | | | | | | | | | |
| H ¹⁹ N ¹ C ² C ³ | 0 | 0 | 20.9 | 26.1 | 0 | 0 | 29.1 | 30.3 | 0 | 0 |
| H ¹⁹ N ¹ C ² C ¹⁵ | 0 | 0 | -20.9 | -25.5 | 0 | 0 | -28.7 | -29.9 | 0 | 0 |
| C ⁴ C ⁵ N ⁶ N ⁷ | 180 | 180 | -180 | -179.8 | 180 | 180 | -179.7 | -179.3 | 0 | 0 |
| C ¹⁴ C ⁵ N ⁶ N ⁷ | 0 | 0 | 0 | -0.1 | 0 | 0 | 0.3 | 0.5 | 0 | 0 |
| N ⁶ N ⁷ C ⁸ C ⁹ | 0 | 0 | 0.4 | 51.3 | 0 | 0 | 0.1 | -92.5 | 0 | 0 |
| N ⁶ N ⁷ C ⁸ C ¹³ | 180 | 180 | -179.7 | -133.8 | 180 | 180 | -180 | 92.9 | 0 | 0 |
| C ¹⁰ C ¹¹ N ¹⁶ O ¹⁷ | 0 | 0 | 0 | 0.9 | 0 | 0 | 0 | -15.6 | 0 | 0 |
| C ¹² C ¹¹ N ¹⁶ O ¹⁸ | 0 | 0 | 0 | 0.8 | 0 | 0 | 0 | -15.4 | 0 | 0 |
| C ⁵ N ⁶ N ⁷ C ⁸ | 180 | 180 | -180 | -179.2 | 180 | 180 | -179.9 | 180 | 0 | 0 |
| ΔH _f ^d | 101.45 | 80.99 | 101.15 | 79.23 | 82.94 | 56.42 | 79.45 | 51.82 | 0 | 0 |
| μ ^e | 9.12 | | 8.40 | 8.90 | 8.89 | 13.23 | 7.41 | 9.60 | 0 | 0 |

^a Bond lengths in angstroms and angles in degrees. ^b Structures with heavy atoms of the azobenzene moiety and hydrogen atoms 19 and 20 constrained to lie in the same plane. ^c Fully optimised structures. ^d ΔH_f is the heat of formation in kcal mol⁻¹. ^e μ is the dipole moment in Debyes.

Consideration of the torsional angles shows that most of the structures optimised by the different methods are essentially planar, with respect to the azobenzene moiety, even for those structures where the atoms were not constrained to lie in the z-plane. Exceptions to this generalisation are the AM1 and PM3 structures in methanol, where the acceptor ring is twisted out of the plane by 51.3° and 92.5° respectively. The nitro group lies in the plane for the constrained planar structures, and in the twisted structures, the nitro group is coplanar with the acceptor phenyl ring in the AM1 methanol optimised structure but twisted by *ca.* 15° to the acceptor phenyl ring in the case of the PM3 methanol structure. When the amino group is not constrained to lie in the plane, the hydrogen atoms of the amino group have a torsional angle of between 20.9° and 30.3° to the plane. This implies that the amino nitrogen atom is sp³ in character, which is unlikely given that in crystal structures of other donor acceptor systems containing an amino group, such as 4-nitroaniline (**4.3**), the amino group is essentially coplanar with the phenyl ring,³ indicating that the amino nitrogen has sp² character. In contrast, where there is no strong electron acceptor group, as in 1,4-phenylenediamine³ (**4.4**) the amino hydrogen atom is twisted out of the plane of the phenyl ring by 37.1° implying that the amino nitrogens are sp³ in character.



(4.3)



(4.4)

The 3-21G ab-initio structure of [VIII] is almost planar, with all torsion angles in the azobenzene moiety less than 0.5° . The hydrogen's of the amino group have a $H^{19}N^1C^2C^3$ torsion angle of 6° and are therefore have mainly sp^2 character. This hybridization indicates greater conjugation between the amino nitrogen and the azobenzene π -system and may account for the shorter C-NH₂ bond. The C⁵-N⁶, N⁷-C⁸ and C¹¹-N¹⁶ bonds are all shorter, while the N¹¹-O¹⁷ bond is longer in the 3-21G structure than in AM1 and PM3 structures. The 3-21G structure has slightly smaller C⁵-N⁶-N⁷ and N⁶-N⁷-N⁸ bond angles than in AM1 or PM3 structures. Optimisation at the 6-31G level produces a very similar geometry to the 3-21G structure with the exception of a shorter N⁶-N⁷ bond length (1.223 Å). From Table 4.3 it can be seen that many of the bond angles for the different optimization methods are similar. The bond lengths for the C-C bond in the benzene rings and internal angles of the rings are very similar and are shown to change little for each dye and will not be reported for the other structures.

Effect of dielectric constant of the solvent on geometry

The effect of solvent on the geometry of the dye is quite small with only small differences between most of the bond lengths in the solvent and gas phase optimised structures. The most significant difference are for the N¹-C² bond in constrained planar structures (1.372 in the gas phase and 1.358 in methanol) and the C¹¹-N¹⁶ bond (1.486 in the gas phase and 1.472 in methanol). The AM1 and PM3 optimizations in methanol also produce structures in which the acceptor groups are twisted out of the plane whereas gas phase optimizations give planar structures.

Optimisations at other dielectric constants produce bond lengths that are intermediate between the gas phase and methanol optimised structures. Only bond parameters for structures optimised in methanol are reported.

The molecular energies for each optimised structure, given at the bottom of Table 4.3 for dye [VIII], cannot be used to compare the stability of structures produced by the different optimisation methods, but energies of fully optimized and constrained planar structures optimised by the same method can be compared. For example, AM1 calculations predict that the freely optimised conformation of dye [VIII] is more stable by just 0.30 kcal mol⁻¹ in the gas phase than the optimised constrained structure, but in methanol the freely optimized structure is 1.76 kcal mol⁻¹ more stable. PM3 calculations give

the freely optimised structure to be 3.5 and 4.6 kcal mol⁻¹ more stable than the constrained structure in the gas phase and methanol respectively. There are also differences in the calculated dipole moments of the freely optimised and constrained structures.

Though the solvent has only a minor effect on the bond lengths, angles and torsions of the dye, it does however have a significant effect on the total heat of formation of the dye, and also on its dipole moment. For example solvent phase structures of dye [VIII] are stabilised by 20.45 (AM1) and 21.92 kcal mol⁻¹ (PM3) with respect to gas phase structures. Dipole moments are 8.4 and 8.9 Debye for the constrained AM1 gas phase and solvent phase structures respectively. The stabilisation of the molecular energies arises from the interaction of the solvent with the polar ground state of the dye. Polar solvents will stabilise the dye to a greater extent than non-polar solvents and thus the heat of formation of the dye will decrease with increasing solvent polarity. Figure 4.2 shows the effect of increasing solvent dielectric on the heat of formation of 4-(N-ethyl, N- β -hydroxyethyl)-4'-nitroazobenzene, [IX]. As the dielectric constant increases, the heat of formation of [IX] decreases. These changes in the heat of formation are most pronounced at low dielectrics while dielectrics above 32.7 produce only minor decreases the heat of formation. All of the other dyes examined exhibit similar behaviour to dye [IX].

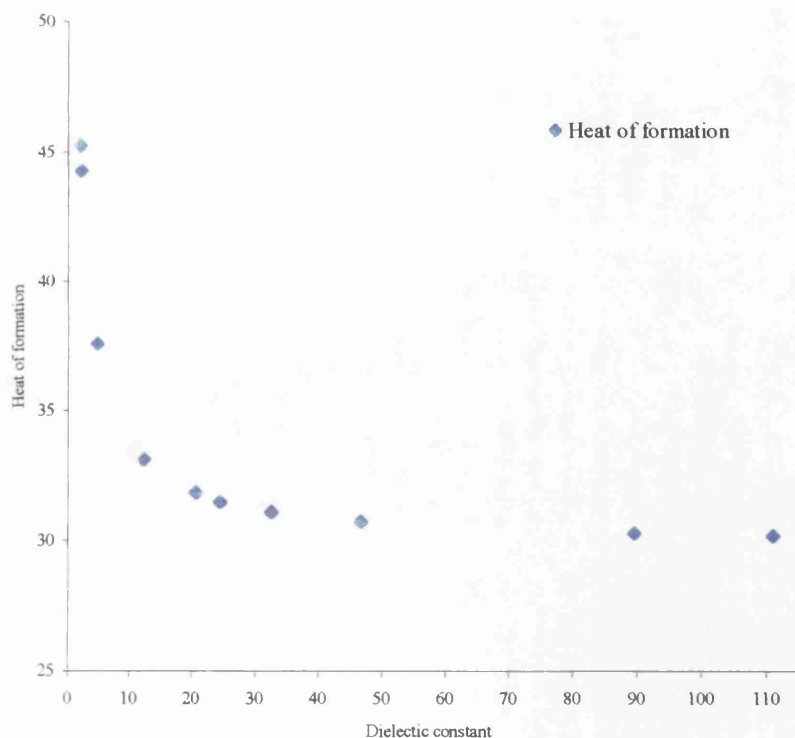


Figure 4.2 Changes in theoretically predicted heats of formation of ground state of [IX] with increasing dielectric constant.

Results of geometry optimisations

After the 4-amino-4'-nitroazobenzene [VIII], the next most structurally simple dye is 4-N,N-diethylamino-4'-nitroazobenzene [X]. The structure and atom numbering system for [X] is given in Figure 4.4. Note that this numbering system is used for all the 4-nitro substituted series of dyes and hydrogen atoms are omitted for clarity, as before. This dye differs from [VIII] only in the replacement the hydrogen atoms attached to the amino nitrogen in dye [VIII], by ethyl groups. However these ethyl groups do complicate the structure by increasing the number of structural conformations for the dye. For example, the methyl groups β to the amino nitrogen can either both be above or below the plane of the azobenzene moiety or both below the plane, or alternatively, one methyl group can be above the plane and the other below the plane (see Figure 4.3)

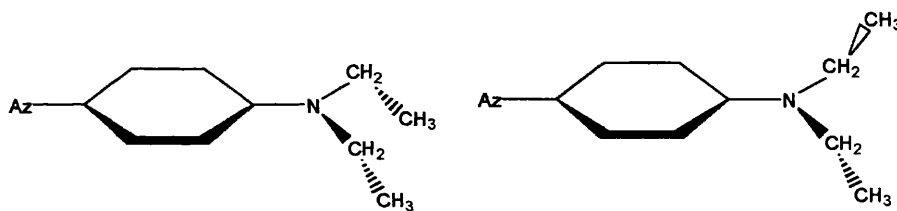


Figure 4.3 Possible conformations of the methyl group in diethyl amino azobenzene derivatives.

The conformations where the two methyl groups are above the plane is equivalent to that where the groups lie below the plane, with calculated heats of formation of $100.7 \text{ kcal mol}^{-1}$. The heat of formation in the case where one methyl group is above and the other below the plane is $100.6 \text{ kcal mol}^{-1}$. The difference between the heats of formation is very small, and suggests that both conformations are viable. The conformation with the lowest heat of formation has been used for subsequent calculations. The calculated bond lengths, bond angles and torsion angles for [X] along with the heats of formation and dipole moment of each structure are shown in Table 4.4.

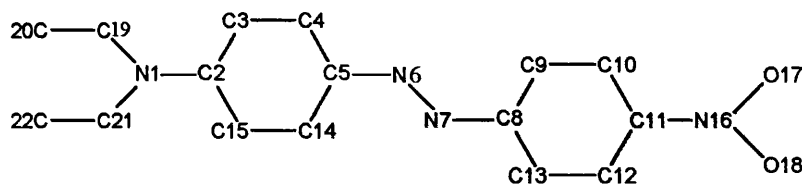


Figure 4.4 The atom numbering system for [X]. Planar structures have all of the heavy atoms of the azobenzene moiety and atoms N^1 , C^{19} and C^{20} , constrained to lie in the same plane.

Table 4.4 Calculated structural data^a, heats of formation and dipole moments for [X] optimised by AM1 method in the gas phase and solution (EPS=32.7).

| | AM1 ^b | AM1/ COSMO ^b | AM1 ^c | AM1/ COSMO ^c |
|---|------------------|----------------------------|------------------|----------------------------|
| Parameter | | (EPS=32.7) | | (EPS=32.7) |
| Bond length | | | | |
| N ¹ -C ² | 1.386 | 1.377 | 1.386 | 1.379 |
| C ⁵ -N ⁶ | 1.425 | 1.421 | 1.427 | 1.423 |
| N ⁶ -N ⁷ | 1.233 | 1.234 | 1.232 | 1.232 |
| N ⁷ -C ⁸ | 1.438 | 1.437 | 1.438 | 1.438 |
| C ¹¹ -N ¹⁶ | 1.486 | 1.475 | 1.485 | 1.475 |
| N ¹⁶ -O ¹⁷ | 1.202 | 1.207 | 1.202 | 1.207 |
| Bond Angle | | | | |
| C ⁵ N ⁶ N ⁷ | 120.27 | 120.54 | 120.27 | 120.68 |
| N ⁶ N ⁷ C ⁸ | 119.16 | 119.49 | 118.83 | 118.87 |
| Torsion Angle | | | | |
| C ¹⁹ N ¹ C ² C ³ | 0 | 0 | 14.8 | 15.9 |
| C ¹⁹ N ¹ C ² C ¹⁵ | 0 | 0 | 15.6 | 4.7 |
| C ¹⁴ C ⁵ N ⁶ N ⁷ | 0 | 0 | -4.9 | -7.9 |
| N ⁶ N ⁷ C ⁸ C ⁹ | 0 | 0 | -37.0 | 46.2 |
| C ¹⁰ C ¹¹ N ¹⁶ O ¹⁷ | 0 | 0 | -0.2 | 0.3 |
| C ⁵ N ⁶ N ⁷ C ⁸ | 0 | 0 | 179.0 | -179.2 |
| ΔH_f^d | 100.62 | 82.60 | 99.97 | 81.48 |
| μ^e | 9.62 | 12.66 | 9.58 | 12.52 |

^a Bond lengths in angstroms and bond angles and torsions in degrees. ^b Structures with heavy atoms of the azobenzene moiety and atoms N1, C19 and C21 constrained to lie in the same plane. ^c Fully optimised structures. ^d ΔH_f is the heat of formation in kcal mol⁻¹. ^e μ is the dipole moment in Debyes.

Torsion angles in Table 4.4 show that the nitrophenyl ring of AM1 freely optimised structures is twisted out of the plane by 37° in the gas phase which is almost identical to the AM1 structure of 4-dimethylamino-4'-nitroazobenzene calculated by Charlton et al.¹² In methanol, the twist of the nitrophenyl ring of [X] is 46°. The nitro group also lies in the plane, as does the amino group for the constrained structures. In the unconstrained AM1 structures however, the amino group had an approximate tetrahedral conformation also reported for 4-dimethylamino-4'-nitroazobenzene.¹²

The effect of solvent on the geometry of the dye is quite small with only small differences between most of the bond lengths in the solvent and gas phase optimised structures. The most significant differences are for the N¹-C², C¹¹-N¹⁶ and nitrogen-oxygen bonds of the nitro group. Optimisations in the other solvents also show little change from the gas phase structure and only bond parameters for structures optimised in methanol will be reported in future.

The final heats of formation for each optimised structure by the same semi-empirical optimisation method show that the fully optimised conformation of [X] is more stable than the optimised constrained structure (Table 4.4) by 0.65 kcal mol⁻¹ in the gas phase and by 1.12kcal mol⁻¹ in methanol.

The next dye calculated [IX] in the series of 4-nitro substituted aminoazobenzenes has an ethyl group and an β -hydroxyethyl group attached to the donor amino nitrogen atom. The alkyl groups of [IX] can again adopt several possible conformations. The methyl and hydroxymethyl components of the alkyl groups can either both be above the plane of the azobenzene moiety or both below the plane, or alternatively, the methyl component can be above the plane and the hydroxymethyl component below the plane. In addition, the presence of the hydroxy group, means that depending on which ethyl group contains the hydroxy group, there are two further possible structures for each of the alkyl group conformations. As for dye 20, the differences in the heat of formation of the 4-(N- β -hydroxy, N-ethyl)amino-4'-nitroazobenzene [IX] conformations is small, with the highest (AB) and lowest (AA) energy conformers separated by only 0.66 kcal mol⁻¹ (Table 4.5).

Table 4.5 The Heats of Formation (ΔH_f), for the possible conformations of [IX]. Alkyl groups above the plane of the azobenzene moiety are denoted A, and below the plane are denoted B.

| Ethyl group conformation | β -hydroxyethyl group conformation | Position of hydroxy group attachment | Heat of Formation ΔH_f / kcal mol ⁻¹ |
|--------------------------|--|--------------------------------------|---|
| A | A | HO ²³ -C ²⁰ | 55.31 |
| A | B | HO ²³ -C ²⁰ | 55.96 |
| B | B | HO ²³ -C ²² | 55.31 |
| B | A | HO ²³ -C ²² | 55.93 |

The bond lengths, bond angles and torsions for each optimisation method are given in Table 4.6. As several conformations were calculated, the geometry with the lowest heat of formation is reported.

Conformations

In the discussion which follows, where different conformations of alkyl groups are possible, inter-atomic distances, bonding angles and torsional angles, dipole moments μ_d , and heats of formation produced by each optimisation method are reported for the lowest energy conformation calculated.

Table 4.6 Calculated structural data, heats of formation and dipole moments [IX] optimised by AM1 and PM3 methods in the gas phase and solution (EPS=32.7) and by ab initio methods using the 3-21G basis sets.*

| Parameter | AM1 ^b | AM1/ COSMO ^b | AM1 ^c | AM1/ COSMO ^c | PM3 ^b | PM3/ COSMO ^b | PM3 ^c | PM3/ COSMO ^c | 3-21G |
|---|------------------|----------------------------|------------------|----------------------------|------------------|----------------------------|------------------|----------------------------|--------|
| Bond length | | | | | | | | | |
| N ¹ -C ² | 1.386 | 1.382 | 1.396 | 1.393 | 1.417 | 1.409 | 1.433 | 1.438 | 1.376 |
| C ⁵ -N ⁶ | 1.425 | 1.421 | 1.426 | 1.427 | 1.437 | 1.435 | 1.438 | 1.442 | 1.408 |
| N ⁶ -N ⁷ | 1.233 | 1.234 | 1.233 | 1.231 | 1.233 | 1.235 | 1.233 | 1.230 | 1.244 |
| N ⁷ -C ⁸ | 1.438 | 1.437 | 1.438 | 1.439 | 1.449 | 1.450 | 1.449 | 1.451 | 1.424 |
| C ¹¹ -N ¹⁶ | 1.486 | 1.475 | 1.486 | 1.475 | 1.497 | 1.471 | 1.497 | 1.470 | 1.446 |
| N ¹⁶ -O ¹⁷ | 1.202 | 1.207 | 1.202 | 1.207 | 1.216 | 1.223 | 1.215 | 1.223 | 1.245 |
| N ¹⁶ -O ¹⁸ | 1.202 | 1.206 | 1.202 | 1.207 | 1.215 | 1.223 | 1.215 | 1.223 | 1.245 |
| N ₁ -C ¹⁹ | 1.446 | 1.449 | 1.450 | 1.449 | 1.481 | 1.484 | 1.486 | 1.489 | 1.469 |
| C ¹⁹ -N ²⁰ | 1.522 | 1.522 | 1.521 | 1.520 | 1.519 | 1.518 | 1.517 | 1.517 | 1.541 |
| N ¹ -C ²¹ | 1.440 | 1.444 | 1.444 | 1.448 | 1.480 | 1.481 | 1.484 | 1.486 | 1.463 |
| C ²¹ -C ²² | 1.538 | 1.536 | 1.537 | 1.534 | 1.539 | 1.537 | 1.538 | 1.538 | 1.530 |
| C ²² -O ²³ | 1.417 | 1.416 | 1.418 | 1.416 | 1.400 | 1.405 | 1.409 | 1.406 | 1.441 |
| Bond Angle | | | | | | | | | |
| C ⁴ C ⁵ N ⁶ | 116.34 | 116.26 | 116.35 | 116.30 | 115.59 | 115.44 | 115.58 | 115.83 | 117.13 |
| C ¹⁴ C ⁵ N ⁶ | 125.80 | 125.80 | 125.76 | 125.45 | 124.58 | 124.67 | 124.56 | 123.90 | 124.58 |
| C ⁵ N ⁶ N ⁷ | 120.25 | 120.54 | 120.15 | 120.59 | 120.41 | 120.64 | 120.41 | 120.47 | 117.20 |
| N ⁶ N ⁷ C ⁸ | 119.18 | 119.49 | 119.26 | 118.87 | 119.41 | 119.45 | 119.41 | 118.94 | 115.50 |
| N ⁷ C ⁸ C ⁹ | 125.41 | 125.26 | 125.42 | 122.86 | 124.60 | 124.48 | 124.57 | 120.46 | 124.07 |
| N ⁷ C ⁸ C ¹³ | 115.68 | 115.56 | 115.64 | 117.30 | 115.29 | 115.21 | 115.30 | 118.39 | 115.95 |
| C ¹⁰ C ¹¹ N ¹⁶ | 119.71 | 119.54 | 119.71 | 119.49 | 120.12 | 120.19 | 120.11 | 120.05 | 119.17 |
| C ¹² C ¹¹ N ¹⁶ | 119.65 | 119.49 | 119.64 | 119.45 | 120.08 | 120.16 | 120.08 | 120.05 | 119.15 |
| C ¹¹ N ¹⁶ O ¹⁷ | 119.00 | 120.08 | 118.99 | 120.08 | 119.48 | 121.12 | 119.47 | 121.15 | 117.57 |
| C ¹¹ N ¹⁶ O ¹⁸ | 118.99 | 120.05 | 118.98 | 120.06 | 119.49 | 121.17 | 119.48 | 121.19 | 117.57 |
| Torsional Angle | | | | | | | | | |
| C ¹⁹ N ¹ C ² C ³ | 0 | 0 | 13.7 | -5.1 | 0 | 0 | 19.3 | 20.3 | 0.7 |
| C ¹⁹ N ¹ C ² C ¹⁵ | 0 | 0 | -14.5 | -29.5 | 0 | 0 | -17.6 | -18.6 | -0.1 |
| C ⁴ C ⁵ N ⁶ N ⁷ | 180 | 180 | 180 | 171.1 | 180 | 180 | -179.9 | -179.9 | 179.9 |
| C ¹⁴ C ⁵ N ⁶ N ⁷ | 0 | 0 | -0.2 | -10.4 | 0 | 0 | 0.4 | 0.5 | 0.1 |
| N ⁶ N ⁷ C ⁸ C ⁹ | 0 | 0 | 1.3 | 47.1 | 0 | 0 | -0.7 | -0.7 | -0.2 |
| N ⁶ N ⁷ C ⁸ C ¹³ | 180 | 180 | -178.9 | -137.7 | 180 | 180 | 179.4 | 179.3 | 179.8 |
| C ¹⁰ C ¹¹ N ¹⁶ O ¹⁷ | 0 | 0 | 0 | 0.6 | 0 | -19.1 | 0 | 0.1 | 0 |
| C ¹² C ¹¹ N ¹⁶ O ¹⁸ | 0 | 0 | 0 | 0.5 | 0 | -19.0 | 0.1 | 0 | 0 |
| C ⁵ N ⁶ N ⁷ C ⁸ | 180 | 180 | -179.9 | -179.6 | 180 | 180 | -180 | -179.9 | 180 |
| ΔH_f^d | 55.307 | 31.091 | 54.474 | 30.0259 | 28.474 | -0.483 | 30.295 | -3.109 | NA |
| μ^e | 8.688 | 8.474 | 8.196 | 9.938 | 7.455 | 9.62 | 7.25 | 8.517 | NA |

*For key, see Table 4.4.

Consideration of the torsion angles shows that all of the structures optimised by the different methods are essentially planar, with respect to the azobenzene moiety, with the exception of the methanol optimised AM1 structure. This structure has the donor and acceptor rings twisted by 10° and 47° respectively to the C⁵N⁶N⁷C⁸ azo bridge. The nitro group lies in the plane, as does the amino group for all the constrained structures and the 3-21G *ab initio* structure, with the exception of the constrained PM3 methanol optimised structure which has the nitro group twisted out of the plane by 19°. In the unconstrained AM1 methanol optimised structure, the nitro group is coplanar with the acceptor phenyl ring. In the unconstrained PM3 structures however, the amino group is twisted out of the azobenzene plane by up to 20.3°. The unconstrained structures also have the N-(C₂H₅)(C₂H₅OH) twisted out of the plane by torsion angles of between 13.7° and 29°. It can be seen from Table 4.6 that many of the bond angles for the different optimisation methods are similar. The most noticeable differences are between the C¹⁹N¹C² angle in the freely optimised PM3 structure and the other structures and the angles for the azo bridge and the C¹¹N¹⁶O¹⁷ angle of the nitro groups where the 3-21G optimised structure is most different to the other structures. The major differences between the AM1 and PM3 and the *ab initio* geometries is the length of the azo -N=N- bond. It is predicted to be longer (1.244 Å) by both the 3-21G and 4-31G* methods than the AM1 and PM3 bond length (1.230–1.235 Å). This is still shorter than the 1.271 Å -N=N- bond in the closely related crystal structure of 4-diethyl-2'-cyano-4'-nitroazobenzene.³ The alkyl groups at the amino nitrogen atom in the semi-empirical structures of [IX] are pushed slightly out of the plane of the molecule by about 20°, indicating sp³ character. The *ab initio* structures are essentially planar. The planar 3-21G and constrained semi-empirical structures have shorter N1-C2 bond lengths indicating a greater interaction between the amino nitrogen lone pair electrons and the azobenzene π-system. There is also a significant difference in the C¹¹-N¹⁶ and N¹⁶-O¹⁷ bond lengths, again suggesting a difference in the degree of interaction between the nitro group and the azobenzene π-system for the different optimisation methods. The C¹¹-N¹⁶ bond length is much shorter (1.446 Å) in the 3-21G structure than in either the AM1 (1.475-1.486) or the PM3 (1.470-1.497 Å) structures. The N¹⁶-O¹⁷ and N¹⁶-O¹⁸ bond lengths also differ significantly with 3-21G being longer (1.243 Å) than the AM1 (1.202-1.207 Å) or PM3 (1.215-1.223 Å) structures. The most significant difference therefore, occur for the N¹-C², C¹¹-N¹⁶ and nitrogen-oxygen bonds of the nitro group.

The final heats of formation for each optimised structure by the same semi-empirical optimisation method can again be compared. These energies, are given in Table 4.6 for both the AM1 and PM3 methods. From Table 4.5, the fully optimised AM1 conformation of [IX] is more stable than the

constrained structure by 0.83 kcal mol⁻¹ in the gas phase, and by 1.07 kcal mol⁻¹ in methanol. The PM3 method gives the freely optimised structures to be more stable than the constrained structures by 1.82 kcal mol⁻¹ and 2.63 kcal mol⁻¹ in the gas phase and methanol respectively.

Other dyes containing the 4'-nitro substituent

The 4-diethylamino-2-methylthio-4'-nitroazobenzene [I], 4-(N-β-cyanoethyl, N-ethyl)amino-4'-nitroazobenzene [XII], 4-diethylamino-2'chloro-4'-nitroazobenzene [XIII] and 4-diethylamino-2'cyano-4'-nitro-6'bromoazobenzene [XVII] dyes also contain the 4'-nitro substituent, and the calculated values for the inter-atomic distances, bonding angles and torsion angles for all the 4'-nitro dyes along with their dipole moments μ_d , and heats of formation for each optimisation method are summarized in Table 4.7 to Table 4.10.

Table 4.7 Summary of calculated bond lengths, angles and torsions for fully optimised AM1 structures of [I], [VIII], [IX], [X], [XII], [XIII] and [XVII] in the gas phase.

| Dye | bond lengths (Å) | | | | | | C-X | bond angles (°) | | ΔH_f (kcal mol ⁻¹) | μ (D) |
|--------|--|---|--|---|---|---|--|---|---|--|-----------|
| | N ¹ -C ² | C ⁵ -N ⁶ | N ⁶ -N ⁷ | N ⁷ -C ⁸ | C ¹¹ -N ¹⁶ | N ¹⁶ -O ¹⁷ | | C ⁵ N ⁶ N ⁷ | N ⁶ N ⁷ C ⁸ | | |
| [I] | 1.387 | 1.425 | 1.233 | 1.438 | 1.485 | 1.202 | 1.694 ^a | 120.01 | 119.99 | 100.99 | 10.46 |
| [VIII] | 1.386 | 1.427 | 1.233 | 1.438 | 1.486 | 1.202 | NA | 120.18 | 119.26 | 101.42 | 8.40 |
| [IX] | 1.396 | 1.426 | 1.233 | 1.438 | 1.486 | 1.202 | NA | 120.15 | 119.26 | 54.47 | 8.20 |
| [X] | 1.386 | 1.427 | 1.232 | 1.438 | 1.485 | 1.202 | NA | 120.27 | 118.84 | 99.97 | 9.59 |
| [XII] | 1.396 | 1.427 | 1.231 | 1.437 | 1.487 | 1.202 | 1.696 ^b | 120.28 | 118.77 | 49.71 | 8.21 |
| [XIII] | 1.400 | 1.429 | 1.231 | 1.438 | 1.486 | 1.202 | - | 120.15 | 118.91 | 131.45 | 7.55 |
| [XVII] | 1.383 | 1.414 | 1.236 | 1.431 | 1.487 | 1.201 | 1.873 ^c | 121.04 | 119.60 | 103.72 | 6.00 |
| | torsion angles (°) | | | | | | | | | | |
| | C ¹⁹ N ¹ C ² C ³ | C ²¹ N ¹ C ² C ¹⁵ | C ¹⁴ C ⁵ N ⁶ N ⁷ | C ⁴ C ⁵ N ⁶ N ⁷ | C ⁵ N ⁶ N ⁷ C ⁸ | N ⁶ N ⁷ C ⁸ C ⁹ | N ⁶ N ⁷ C ⁸ C ¹³ | C ¹⁰ C ¹¹ N ¹⁶ O ¹⁷ | C ¹² C ¹¹ N ¹⁶ O ¹⁸ | | |
| [I] | 13.2 | 18.4 | -5.0 | -175.6 | -178.9 | -34.4 | 149.6 | -0.3 | -0.3 | | |
| [VIII] | 20.9 | -20.9 | 0 | 180 | -179.2 | 51.3 | -133.8 | 0.9 | 0.8 | | |
| [IX] | 13.7 | -14.5 | -0.2 | 180 | -179.9 | 1.3 | -178.9 | 0 | 0 | | |
| [X] | 14.9 | 15.6 | -5.1 | 175.4 | 179.0 | -37.0 | 147.3 | -0.2 | -0.2 | | |
| [XII] | 14.1 | -13.4 | -2.4 | 177.9 | 178.5 | -48.9 | 136.8 | -0.1 | 0.2 | | |
| [XIII] | 7.4 | -20.8 | -4.5 | 176.0 | 179.1 | -35.7 | 148.4 | -0.2 | -0.2 | | |
| [XVII] | 14.5 | 12.9 | 6.0 | -174.5 | 179.1 | -37.6 | -3.0 | -0.1 | 0.1 | | |

^a C-X is the C⁴-S bond. ^b C-X is the C¹³-Cl bond. ^c C-X is the C¹³-Br bond

Table 4.8 Summary of calculated bond lengths, angles^a for constrained^b AM1 geometry optimisations (heavy atoms of the azobenzene moiety and atoms 19 and 20 constrained to lie in the same plane) of [I], [VIII], [IX], [X], [XII], [XIII] and [XVII] in the gas phase.

| Dye | bond lengths (Å) | | | | | | bond angles (°) | | ΔH_f (kcal mol ⁻¹) | μ (D) | |
|--------|--------------------------------|--------------------------------|--------------------------------|--------------------------------|----------------------------------|----------------------------------|--------------------|--|--|-----------|--|
| | N ¹ -C ² | C ⁵ -N ⁶ | N ⁶ -N ⁷ | N ⁷ -C ⁸ | C ¹¹ -N ¹⁶ | N ¹⁶ -O ¹⁷ | C-X | C ⁵ N ⁶ N ⁷ | | | N ⁶ N ⁷ C ⁸ |
| [I] | 1.386 | 1.423 | 1.234 | 1.437 | 1.485 | 1.202 | 1.694 ^a | 120.45 | 119.07 | 101.64 | 10.56 |
| [VIII] | 1.372 | 1.426 | 1.233 | 1.438 | 1.486 | 1.202 | - | 120.24 | 119.22 | 101.44 | 9.12 |
| [IX] | 1.386 | 1.425 | 1.233 | 1.438 | 1.486 | 1.202 | - | 120.25 | 119.49 | 55.31 | 8.69 |
| [X] | 1.386 | 1.425 | 1.233 | 1.438 | 1.486 | 1.202 | - | 120.27 | 119.16 | 100.62 | 9.62 |
| [XII] | 1.386 | 1.424 | 1.234 | 1.436 | 1.487 | 1.202 | 1.696 ^b | 120.15 | 119.16 | 50.89 | 8.69 |
| [XIII] | 1.391 | 1.427 | 1.233 | 1.438 | 1.486 | 1.202 | NA | 120.13 | 119.27 | 132.23 | |
| [XVII] | 1.382 | 1.414 | 1.239 | 1.427 | 1.487 | 1.201 | 1.421 ^c | 119.63 | 121.48 | 104.98 | 6.13 |

^a C-X is the C⁴-S bond. ^b C-X is the C¹³-Cl bond. ^c C-X is the C¹³-Br bond.

Table 4.9 Summary of calculated bond lengths, angles and torsions^a for fully solvent (EPS=32.7) optimised AM1 structures of [I], [VIII], [IX], [X], [XII], [XIII] and [XVII].

| Dye | bond lengths (Å) | | | | | | bond angles (°) | | ΔH_f (kcal mol ⁻¹) | μ (D) | |
|--------|--------------------------------|--------------------------------|--------------------------------|--------------------------------|----------------------------------|----------------------------------|--------------------|--|--|-----------|--|
| | N ¹ -C ² | C ⁵ -N ⁶ | N ⁶ -N ⁷ | N ⁷ -C ⁸ | C ¹¹ -N ¹⁶ | N ¹⁶ -O ¹⁷ | C-X | C ⁵ N ⁶ N ⁷ | | | N ⁶ N ⁷ C ⁸ |
| [I] | 1.379 | 1.426 | 1.231 | 1.439 | 1.475 | 1.207 | 1.701 ^a | 120.38 | 118.83 | 80.44 | 13.82 |
| [VIII] | 1.389 | 1.426 | 1.231 | 1.439 | 1.475 | 1.207 | - | 120.74 | 118.85 | 79.23 | 10.84 |
| [IX] | 1.393 | 1.427 | 1.231 | 1.439 | 1.475 | 1.207 | - | 120.59 | 118.87 | 30.26 | 9.94 |
| [X] | 1.379 | 1.423 | 1.232 | 1.438 | 1.475 | 1.207 | - | 120.68 | 118.87 | 81.48 | 12.52 |
| [XII] | 1.395 | 1.428 | 1.230 | 1.439 | 1.477 | 1.206 | 1.698 ^b | 120.38 | 118.79 | 25.65 | 9.33 |
| [XIII] | 1.399 | 1.427 | 1.230 | 1.439 | 1.475 | 1.207 | NA | 120.76 | 118.72 | 107.61 | 9.83 |
| [XVII] | 1.375 | 1.415 | 1.232 | 1.434 | 1.476 | 1.206 | - | 121.45 | 119.20 | 75.76 | 7.74 |

| Dye | torsion angles (°) | | | | | | | | | |
|--------|--|---|--|---|---|---|--|---|---|--|
| | C ¹⁹ N ¹ C ² C ³ | C ²¹ N ¹ C ² C ¹⁵ | C ¹⁴ C ⁵ N ⁶ N ⁷ | C ⁴ C ⁵ N ⁶ N ⁷ | C ⁵ N ⁶ N ⁷ C ⁸ | N ⁶ N ⁷ C ⁸ C ⁹ | N ⁶ N ⁷ C ⁸ C ¹³ | C ¹⁰ C ¹¹ N ¹⁶ O ¹⁷ | C ¹² C ¹¹ N ¹⁶ O ¹⁸ | |
| [I] | 7.1 | 18.3 | 18.5 | -163.9 | -179.8 | -50.7 | 134.4 | -1.0 | -0.8 | |
| [VIII] | 26.1 | -25.5 | -0.1 | -179.8 | -179.2 | 51.3 | -133.8 | 0.9 | 0.8 | |
| [IX] | -5.1 | -29.5 | -10.4 | 171.1 | -179.6 | 47.1 | -137.7 | 0.6 | 0.5 | |
| [X] | 15.9 | 4.7 | -7.9 | - | -179.2 | 46.2 | - | 0.3 | - | |
| [XII] | 2.0 | -25.8 | 20.4 | -161.5 | 179.3 | -55.6 | 130.2 | -0.1 | -0.1 | |
| [XIII] | 6.2 | -26.3 | 3.1 | -177.2 | 179.5 | -49.6 | 135.2 | -1.0 | -0.9 | |
| [XVII] | 10.7 | 12.7 | 3.9 | -176.1 | 178.6 | -70.8 | 116.5 | -1.3 | -1.0 | |

^a C-X is the C⁴-S bond. ^b C-X is the C¹³-Cl bond.

Table 4.10 Summary of calculated bond lengths and angles^a for constrained^b AM1 geometry optimisations (heavy atoms of the azobenzene moiety and atoms 19 and 20 constrained to lie in the same plane) of [I], [VIII], [IX], [X], [XII], [XIII] and [XVII] in solvent (EPS=32.7).

| Dye | bond lengths (Å) | | | | | | bond angles (°) | | ΔH_f (kcal mol ⁻¹) | μ (D) | |
|--------|--------------------------------|--------------------------------|--------------------------------|--------------------------------|----------------------------------|----------------------------------|-----------------|--|--|-----------|--|
| | N ¹ -C ² | C ⁵ -N ⁶ | N ⁶ -N ⁷ | N ⁷ -C ⁸ | C ¹¹ -N ¹⁶ | N ¹⁶ -O ¹⁷ | C-X | C ⁵ N ⁶ N ⁷ | | | N ⁶ N ⁷ C ⁸ |
| [I] | 1.376 | 1.420 | 1.235 | 1.436 | 1.475 | 1.207 | 1.701 | 120.46 | 119.46 | 81.46 | 14.25 |
| [VIII] | 1.358 | 1.419 | 1.235 | 1.436 | 1.475 | 1.207 | NA | 120.60 | 119.60 | 80.99 | 12.77 |
| [IX] | 1.382 | 1.422 | 1.234 | 1.437 | 1.475 | 1.207 | NA | 120.54 | 119.49 | 31.09 | 10.49 |
| [X] | 1.377 | 1.421 | 1.235 | 1.416 | 1.466 | 1.202 | | 120.54 | 119.50 | 82.60 | 12.66 |
| [XII] | 1.381 | 1.421 | 1.234 | 1.436 | 1.477 | 1.206 | 1.699 | 120.51 | 119.25 | 27.19 | 10.21 |
| [XIII] | 1.383 | 1.423 | 1.234 | 1.437 | 1.470 | 1.207 | NA | 120.46 | 119.55 | 109.35 | 10.46 |
| [XVII] | 1.375 | 1.415 | 1.238 | 1.429 | 1.476 | 1.206 | 1.421 | 119.67 | 121.21 | 79.75 | 7.67 |

^a C-X is the C⁴-S bond. ^bC-X is the C¹³-Cl bond.

Structure [XII] has essentially the same structure as [IX] the only difference being the β -cyano-ethyl group instead of the β -hydroxyethyl group of [IX]. The conformations possible for [IX] are also possible for [XII] so results reported are for the lowest energy conformation.

It might be expected, that the bond lengths, angles and torsion angles of [XII] would be similar to those of [IX]. However, the freely optimised gas phase structure of [XII] has the acceptor ring twisted by 48.9° compared with the essentially planar structure of [IX]. The free and constrained methanol optimised structures though are very similar with respect to their bond lengths, angles and torsions to the corresponding [IX] structures. The structure of [XIII] is also very similar to that of [IX]. The presence of a chloro substituent on the acceptor phenyl ring dye provides an interesting variation to the other dyes. In addition to the conformations possible for [IX], there are two possibilities for the position of the chloro substituent with respect to the azo nitrogen atoms in [XIII]. These two situations are displayed in Figure 4.5, where the magenta and blue coloured Cl atoms represent the two different positions possible for the chlorine atom. The conformation containing the blue chlorine atom has a heat of formation of 50.9 kcal mol⁻¹, compared to 52.1 kcal mol⁻¹ for the conformation containing the magenta chlorine, and is therefore the more stable structure. This could be due to a greater steric interaction between the magenta chlorine atom and the lone pair electrons of N⁶ (refer to Chapter 1). The bond parameters in therefore, refer to the more stable C¹³-Cl conformer.

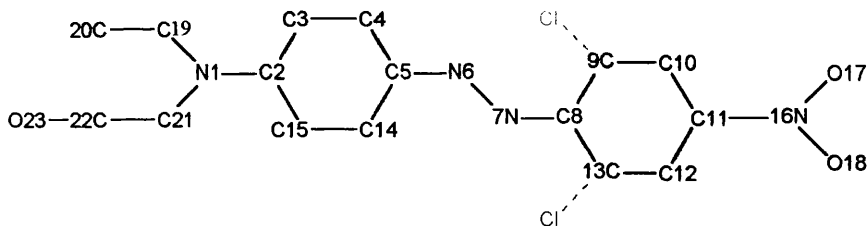


Figure 4.5 The atom numbering system for [XIII]. Planar structures have all of the heavy atoms of the azobenzene moiety and atoms N¹, C¹⁹ and C²⁰, constrained to lie in the same plane.

The optimised structures of [XIII] in the gas phase and solvent are very similar to that for [IX], except for the free gas phase AM1 structure in which the acceptor ring is twisted by 35.7°. The introduction of the additional chlorine electron acceptor substituent therefore, has only a minor effect on the geometry of the donor acceptor azo dye.

The final dye in the series of 4-nitro substituted dyes is [II] where the methanethiol group can be attached at the C⁴ or C¹⁴ position. There are several alternative structures for [II] which include, the different orientations of the N-ethyl groups (either both above or below the plane, or one ethyl group is above and one below the plane). The orientation of the ethyl groups does not greatly affect the heat of formation, but the orientation of the SCH₃ group does produce a significant difference in the heat of formation, with the conformations where the SCH₃ group, is attached at the C⁴ position having the lowest energy. Many of the bond lengths, angles and torsions are similar to those of [IX], but in the structures constrained to be planar, the N¹-C² bond length is slightly shorter.

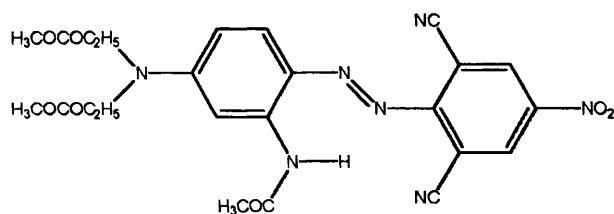
Summary of geometries of 4'-nitro substituted dyes

Full optimisations of the 4'-nitro substituted dyes, [II], [VIII], [IX], [X], [XII], [XIII] and [XVII] using the AM1 method gave non-planar geometries in the gas phase, with the exception of [IX], which was essentially planar. In the non-planar structures, the nitrophenyl ring was twisted by 37° in the 4-diethyl-4'-nitroazobenzene [X] which is very similar to the 37.3° obtained in gas phase AM1 calculations on 4-dimethyl-4'-nitroazobenzene by Charlton et al.¹² The other 4'-nitro substituted dyes were twisted by between 34° and 47°. Using the COSMO method (EPS=32.7), the nitrophenyl ring was twisted by between 47° and 55° to the phenyl azo plane. Structures optimisations with the heavy atoms constrained to lie in the same plane had heats of formation similar to the fully optimised structures, suggesting that these planar conformations are also valid. Torsion angles from crystal data

(see Table 4.1) show that most donor-acceptor type azobenzenes are essentially planar, with twisting of either phenyl ring by between 0° and 10° . The N^6-N^7 bond length was between 1.230\AA and 1.235\AA while the N^1-C^2 bond was between 1.387\AA and 1.400\AA for fully optimised gas phase structures and between 1.372\AA and 1.391\AA in constrained planar gas phase structures. These bond lengths are consistent with results of previous gas phase AM1 calculations on 4-dimethylamino-4'-nitroazobenzene¹². AM1/COSMO structures have N^1-C^2 bond lengths which are slightly shorter (1.379\AA - 1.399\AA), for fully optimised structures and significantly shorter (1.358\AA - 1.383\AA) in constrained structures, than in the gas phase. The $C^{11}-N^{16}$ bond length is around 1.486\AA for gas phase structures and 1.475\AA in methanol. The N^6-N^7 bond length in all the crystal structures examined (see Table 4.1) was longer (1.254 - 1.294\AA) than in any of the AM1 calculated structures. In all of these structures, are longer than in calculated structures. The N^1-C^2 and $C^{11}-N^{16}$ bond lengths of the crystal structures, are shorter than in calculated gas phase structures, but similar to bond lengths in methanol optimised structures at an average of 1.370 and 1.462\AA respectively.

The major difference between the AM1 and ab-initio geometries is the length of the azo N^6-N^7 bond. It is predicted to be longer (1.244) by the 3-21G method than the AM1 bond length (1.230 - 1.235), but is still shorter than the average bond length of crystal structures. However, calculations at the 4-31G* and 6-31G level produce even shorter N^6-N^7 bond (1.22\AA). The other major difference is the hybridisation of the amino group, which has sp^3 character in semi-empirical structures, as the ethyl groups are pushed slightly out of the plane of the molecule. In contrast *ab initio* and crystal structures have a planar sp^2 hybridized amino group. There may also be a slight twisting of one of the phenyl rings, usually the acceptor ring, out of the plane resulting in a non-zero $N^6N^7C^8C^9$ torsional angle.

The structure of the blue dye 2-acetamido-4-diethylamino-2',6'-dicyano-4'-nitroazobenzene (**4.5**) has been calculated by Morley using the AM1 method and also at the *ab initio* STO-3G level. The AM1 structure was distorted in a similar way to the other azobenzenes, while the STO-3G structure was essentially planar and had both the amino and nitro groups coplanar with the attached phenyl rings. The acetamido group was also planar, with the amino hydrogen intra-molecularly bonded to the azo nitrogen, with a bond length of 1.81\AA . Structure (**4.5**) is very similar to 2-acetamido-4-diethylamino-2'-cyano-4'-nitro-6'-bromoazobenzene [XVII] and the AM1 structures of these dyes are very similar. The crystal structure of [XVII] CEMSPC10³, which is essentially planar and has an N^6-N^7 azo bond length of 1.281\AA , which is very close to the 1.287\AA in the STO-3G structure of (**4.5**).



(4.5)

Unconstrained AM1 optimisations of [XI] yield structures which are almost planar for the azobenzene moiety, but some of the unconstrained PM3 structures are slightly twisted. Both the amino groups have their alkyl groups and hydrogen atoms with torsion angles of up to 24° to the plane. In unconstrained structures, the C-N(C₂H₄OH)₂ bond length is slightly longer than the donor acceptor dyes, while the C-NH₂ bond is similar in length to the C-NR₂ bonds in other dyes. In constrained optimised structures, the C-N(C₂H₄OH)₂ bond length is again slightly longer than in the donor acceptor dyes while the C-NH₂ bond is similar in length to the C-NH₂ bond in [VIII]. This implies that the NH₂ substituent is a stronger electron donor group than the N(C₂H₄OH)₂ group.

The bond angles in [XI] are similar to those of [XIV]. Freely optimised structures have both the aminoalkyl groups and the hydrogen atoms of the amino group out of the plane making torsional angles of 22° and 6° and 23.8° respectively in the gas phase. There is a difference of $1.53 \text{ kcal mol}^{-1}$ in the heat of formation of the AM1 free and constrained structures in the gas phase while in methanol, the difference is $1.95 \text{ kcal mol}^{-1}$. The difference between heats of formation between PM3 gas phase free and constrained structures is $1.22 \text{ kcal mol}^{-1}$ in the gas phase and $2.57 \text{ kcal mol}^{-1}$ in methanol. These energy differences are larger than the corresponding differences for the donor-acceptor azo dyes. For both AM1 and PM3 calculations, the freely optimized structure is lower in energy.

Dyes containing the 2'-nitro substituent

The second set of azo dyes calculated in the current work, consist of 4-(N-β-hydroxyethyl, N-ethyl)amino-2'-nitroazobenzene [IV], 4-(N-β-hydroxyethyl, N-ethyl)amino-2'-nitro-4'-chloroazobenzene [VI], 4-di(β-hydroxyethyl)amino-2'-nitro-4'-chloroazobenzene [VII], 2-chloro-4-di(β-hydroxyethyl)amino-2'-nitro-4'-chloroazobenzene [III], which contain the 2'-nitro substituent. These dyes have been optimised by AM1 and PM3 methods both in the gas phase and in solvent field COSMO calculations and the results of these calculations for each dye are now discussed.

The simplest structure considered is [IV] (Figure 4.6), which contains only the 2'-nitro substituent and an β -hydroxyethyl and ethyl groups attached to the amino donor substituent. The 2'-nitro group can either be attached to atom C¹³ as shown in Figure 4.6, or to atom C⁹. If the nitro group is attached to the C⁹ atom, then it has a greater interaction with the lone pair electrons of the azo nitrogen atom N⁶ than the structure where the nitro group is attached to C¹³. This interaction is unfavourable and the C¹³-NO₂ structure (Figure 4.6) has a lower heat of formation than the alternative C⁹-NO₂ conformation. The bonding parameters for AM1 (gas phase and methanol), PM3 (gas phase and methanol) and 3-21G (gas phase) optimised structures are given in Table 4.11, together with the final energy and dipole moment for each structure. There is a much greater variation in the bonding torsions for the [IV], than for the previous dyes. The C²-N¹R₂ and C¹³-NO₂ bonds in [IV] are slightly longer in [IV] than in the 4'-nitro substituted dyes, particularly in the freely optimised structures, while the N⁶-N⁷ bond is marginally shorter.

The most prominent differences are for the torsion angles of the nitro substituent. In the constrained structures, the 2'-nitro group is rotated out of the plane by 58°-60° for AM1 structures and 90° in PM3 structures. This contrasts with the 4'-nitro substituted dyes in which the 4'-nitro group is coplanar to the acceptor phenyl ring.

For full optimisations, the NR₂ group is twisted out of the plane by approximately 10°-13° and the donor ring has a torsion angle of 5°-10° with respect to the donor phenyl ring plane. The acceptor phenyl ring is twisted out of this plane by between 43° and 63°.

The crystal structure of 4-di-(β -ethoxyethyl)amino-2'-nitroazobenzene¹⁸ has a similar twist of the nitrophenyl ring by 44.5°. Gas phase AM1 calculations on this dye by Charlton et al.¹² produced a structure in which both the donor and acceptor phenyl rings were twisted in different directions with an overall torsion of *ca.* 50°. The nitro group was also found to be twisted.

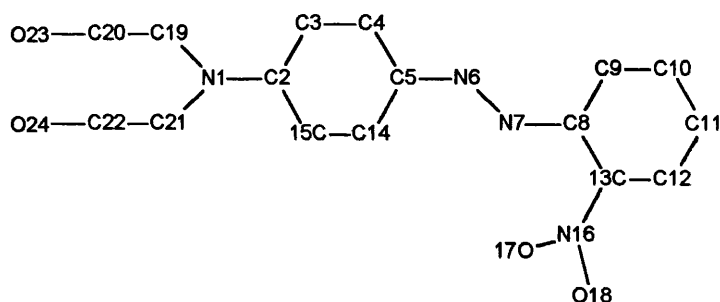


Figure 4.6 Structure and atom numbering system for [IV]. The same numbering system is used for dyes [III], [V], [VI] and [VII].

Table 4.11 Calculated structural data, heats of formation and dipole moments and geometries for [IV] optimised by AM1 and PM3 methods in the gas phase and solution (EPS=32.7) and at the 3-21G level. *

| Parameter | AM1 ^a | AM1 /COSMO ^a | AM1 ^b | AM1 /COSMO ^b | PM3 ^a | PM3 /COSMO ^a | PM3 ^b | PM3 /COSMO ^b | 3-21G |
|---|------------------|----------------------------|------------------|----------------------------|------------------|----------------------------|------------------|----------------------------|-------|
| Bond length | | | | | | | | | |
| N ¹ -C ² | 1.390 | 1.381 | 1.394 | 1.390 | 1.416 | 1.407 | 1.432 | 1.435 | 1.379 |
| C ⁵ -N ⁶ | 1.426 | 1.422 | 1.428 | 1.426 | 1.436 | 1.433 | 1.438 | 1.439 | 1.410 |
| N ⁶ -N ⁷ | 1.233 | 1.234 | 1.230 | 1.230 | 1.233 | 1.234 | 1.233 | 1.231 | 1.243 |
| N ⁷ -C ⁸ | 1.436 | 1.435 | 1.437 | 1.438 | 1.449 | 1.448 | 1.449 | 1.452 | 1.419 |
| C ¹³ -N ¹⁶ | 1.495 | 1.488 | 1.491 | 1.480 | 1.506 | 1.483 | 1.506 | 1.475 | 1.450 |
| N ¹⁶ -O ¹⁷ | 1.198 | 1.202 | 1.199 | 1.204 | 1.213 | 1.219 | 1.213 | 1.220 | 1.236 |
| N ¹⁶ -O ¹⁸ | 1.202 | 1.206 | 1.203 | 1.207 | 1.213 | 1.219 | 1.213 | 1.222 | |
| N ¹ -C ¹⁹ | 1.441 | 1.445 | 1.441 | 1.446 | 1.481 | 1.483 | 1.484 | 1.487 | |
| N ¹ -C ²⁰ | 1.445 | 1.450 | 1.447 | 1.452 | 1.483 | 1.486 | 1.486 | 1.490 | |
| Bond Angle | | | | | | | | | |
| C ¹⁹ N ¹ C ² | 121.80 | 121.94 | 121.29 | 121.00 | 121.45 | 121.45 | 118.75 | 118.11 | |
| C ²¹ N ¹ C ² | 120.71 | 120.84 | 119.95 | 119.73 | 121.09 | 121.13 | 118.06 | 117.66 | |
| N ¹ C ² C ³ | 121.75 | 121.95 | 121.97 | 121.91 | 120.73 | 120.91 | 120.62 | 120.38 | |
| N ¹ C ² C ¹⁵ | 121.31 | 121.39 | 120.93 | 121.22 | 120.48 | 120.50 | 120.37 | 120.45 | |
| C ⁴ C ⁵ N ⁶ | 116.39 | 116.30 | 116.33 | 116.39 | 115.61 | 115.63 | 115.58 | 115.57 | |
| C ¹⁴ C ⁵ N ⁶ | 125.67 | 125.80 | 125.62 | 125.50 | 124.56 | 124.56 | 124.54 | 124.27 | |
| C ⁵ N ⁶ N ⁷ | 120.27 | 120.47 | 120.20 | 120.72 | 120.45 | 120.53 | 120.41 | 120.85 | 115.9 |
| N ⁶ N ⁷ C ⁸ | 119.41 | 119.34 | 118.20 | 118.81 | 119.60 | 119.76 | 119.64 | 118.69 | 115.4 |
| N ⁷ C ⁸ C ⁹ | 125.47 | 125.67 | 122.70 | 121.62 | 124.57 | 125.16 | 124.49 | 120.35 | |
| N ⁷ C ⁸ C ¹³ | 116.92 | 117.01 | 118.98 | 119.87 | 115.77 | 115.24 | 115.89 | 119.22 | |
| C ¹⁰ C ¹¹ N ¹⁶ | 121.02 | 120.50 | 121.35 | 120.95 | 121.01 | 120.26 | 121.02 | 122.61 | |
| C ¹² C ¹¹ N ¹⁶ | 117.85 | 117.84 | 117.87 | 118.05 | 118.97 | 119.42 | 118.97 | 118.29 | |
| C ¹³ N ¹⁶ O ¹⁷ | 119.52 | 120.39 | 119.83 | 120.64 | 118.88 | 120.36 | 118.89 | 121.44 | |
| C ¹³ N ¹⁶ O ¹⁸ | 118.05 | 119.10 | 118.02 | 119.23 | 118.89 | 120.36 | 118.85 | 120.24 | |
| Torsional Angle | | | | | | | | | |
| C ¹⁹ N ¹ C ² C ³ | 0 | 0 | -1.7 | 10.2 | 0 | 0 | 18.7 | 22.2 | -1.4 |
| C ¹⁹ N ¹ C ² C ¹⁵ | 0 | 0 | 5.3 | -13.2 | 0 | 0 | -16.2 | -15.7 | -1.4 |
| C ¹⁴ C ⁵ N ⁶ N ⁷ | 0 | 0 | -49.3 | 11.5 | 0 | 0 | 1.3 | 18.4 | 5.2 |
| N ⁶ N ⁷ C ⁸ C ⁹ | 0 | 0 | -42.9 | -63.2 | 0 | 0 | 5.8 | 60.0 | -11.4 |
| C ⁸ C ¹³ N ¹⁶ O ¹⁷ | -59.6 | -60.6 | -40.8 | -38.9 | -91.4 | 90.3 | 88.6 | 41.8 | -32.5 |
| C ¹² C ¹³ N ¹⁶ O ¹⁸ | -58.1 | -59.7 | -59.7 | -37.8 | -88.8 | 90.6 | 86.1 | 41.3 | -32.5 |
| C ⁵ N ⁶ N ⁷ C ⁸ | 180 | 180 | 180 | 178.5 | 180 | 180 | 180 | -179.2 | 179.8 |
| ΔH_f (kcal mol ⁻¹) | 56.61 | 33.97 | 55.81 | 31.95 | 29.45 | 5.72 | 28.35 | 0.92 | - |
| μ (D) | 3.65 | 5.21 | 4.40 | 5.88 | 3.50 | 4.76 | 3.27 | 6.57 | - |

*For key see Table 4.4

The next dye in the series is 4-(N- β -hydroxyethyl, N-ethyl)amino-2'-nitro-4'-chloroazobenzene [VI], which is the 4'-chloro substituted derivative of [IV]. Once again, and as for all these dyes, there are two possibilities for the conformation of the ortho nitro group. It might be expected that where the ortho nitro group is attached to atom C¹³ is energetically more favourable than the alternative conformation and, this was found to be the case for all of the 2'-nitro substituted dyes. A summary of

the structural data, heats of formation and dipole moments of the semi-empirical and ab-initio optimised structures is given in Table 4.12 to Table 4.15.

Table 4.12 Summary of calculated structural data^a, heats of formation and dipole moments for fully optimised gas phase AM1 structures of [III], [IV], [V], [VI] and [VII].

| Dye | bond lengths (Å) | | | | | | | bond angles (°) | | ΔH_f | μ | |
|-------|--------------------------------|--------------------------------|--------------------------------|--------------------------------|----------------------------------|----------------------------------|---------------------|-------------------|--|--------------|--------|--|
| | N ¹ -C ² | C ⁵ -N ⁶ | N ⁶ -N ⁷ | N ⁷ -C ⁸ | C ¹³ -N ¹⁶ | N ¹⁶ -O ¹⁷ | C ¹¹ -Cl | C ⁴ -X | C ⁵ N ⁶ N ⁷ | | | N ⁶ N ⁷ C ⁸ |
| [III] | 1.389 | 1.427 | 1.231 | 1.436 | 1.493 | 1.199 | 1.701 | 1.696 | 120.01 | 118.83 | 1.33 | 4.53 |
| [IV] | 1.394 | 1.428 | 1.230 | 1.437 | 1.491 | 1.202 | - | - | 120.2 | 118.2 | 55.80 | 4.40 |
| [V] | 1.396 | 1.427 | 1.229 | 1.434 | 1.490 | 1.203 | 1.470 | - | 120.6 | 119.41 | -31.62 | 4.89 |
| [VI] | 1.390 | 1.429 | 1.231 | 1.436 | 1.492 | 1.199 | 1.702 | - | 120.34 | 118.88 | 51.70 | 4.80 |
| [VII] | 1.396 | 1.429 | 1.231 | 1.437 | 1.492 | 1.199 | 1.702 | - | 119.84 | 118.84 | 6.19 | 6.63 |

| Dye | torsion angles (°) | | | | | | | | | |
|-------|--|---|---|--|---|---|--|--|---|--|
| | C ¹⁹ N ¹ C ² C ³ | C ²¹ N ¹ C ² C ¹⁵ | C ⁴ C ⁵ N ⁶ N ⁷ | C ¹⁴ C ⁵ N ⁶ N ⁷ | C ⁵ N ⁶ N ⁷ C ⁸ | N ⁶ N ⁷ C ⁸ C ⁹ | N ⁶ N ⁷ C ⁸ C ¹³ | C ⁸ C ¹³ N ¹⁶ O ¹⁷ | C ¹² C ¹³ N ¹⁶ O ¹⁸ | |
| [III] | 10.9 | 17.3 | 11.9 | -169.9 | 179.5 | -43.2 | 143.1 | -44.6 | -42.5 | |
| [IV] | -1.7 | 4.5 | 5.3 | -49.3 | 180 | 137.6 | -42.9 | -40.8 | -42.9 | |
| [V] | 13.7 | -13.4 | 0.3 | -180 | 178.4 | 119.0 | -69.5 | -36.7 | -34.7 | |
| [VI] | 23.1 | 6.4 | 1.3 | -179.2 | 178.7 | 135.9 | -51.1 | -43.0 | -41.0 | |
| [VII] | -6.9 | -17.5 | 16.9 | -165.4 | -179.8 | -43.1 | 143.1- | 43.6 | -41.5 | |

^a Bond lengths in amstrongs and angles in degrees. ^b ΔH_f is the heat of formation in kcal mol⁻¹. ^c μ_D is the dipole moment in Debyes.

Table 4.13 Summary of calculated structural data, heats of formation and dipole moments for constrained AM1 geometry optimisations (heavy atoms of the azobenzene moiety and atoms 19 and 21 constrained to lie in the same plane) of structures [III], [IV], [V], [VI] and [VII] in the gas phase.*

| Dye | bond lengths (Å) | | | | | | | bond angles (°) | | torsion angles (°) [†] | | ΔH_f | μ | |
|-------|--------------------------------|--------------------------------|--------------------------------|--------------------------------|----------------------------------|----------------------------------|---------------------|-------------------|--|--|--|--------------|--------|---|
| | N ¹ -C ² | C ⁵ -N ⁶ | N ⁶ -N ⁷ | N ⁷ -C ⁸ | C ¹³ -N ¹⁶ | N ¹⁶ -O ¹⁷ | C ¹¹ -Cl | C ⁴ -X | C ⁵ N ⁶ N ⁷ | N ⁶ N ⁷ C ⁸ | C ⁸ C ¹³ N ¹⁶ O ¹⁷ | | | C ¹² C ¹³ N ¹⁶ O ¹⁸ |
| [III] | 1.388 | 1.425 | 1.233 | 1.435 | 1.497 | 1.198 | 1.701 | 1.695 | 119.92 | 119.28 | -60.1 | -58.8 | 2.17 | 4.20 |
| [IV] | 1.390 | 1.426 | 1.233 | 1.436 | 1.495 | 1.198 | - | - | 120.27 | 119.41 | -58.5 | -60.0 | 56.61 | 3.65 |
| [V] | 1.386 | 1.422 | 1.234 | 1.435 | 1.496 | 1.198 | 1.471 | - | 120.24 | 119.23 | -60.8 | -59.5 | -30.05 | 4.03 |
| [VI] | 1.389 | 1.424 | 1.233 | 1.435 | 1.497 | 1.198 | 1.471 | - | 120.05 | 119.88 | -61.1 | -59.8 | 52.79 | 4.94 |
| [VII] | 1.387 | 1.425 | 1.233 | 1.436 | 1.495 | 1.198 | 1.702 | - | 119.88 | 119.32 | -59.3 | -57.8 | 7.26 | 5.86 |

*For key see Table 4.12. [†] Note that all other torsion angles are 0° or 180°

Table 4.14 Summary of calculated structural data^a, heats of formation and dipole moments for fully optimised AM1 structures of [III], [IV], [V], [VI] and [VII] in solvent (EPS=32.7).*

| Dye | bond lengths (Å) | | | | | | bond angles (°) | | ΔH_f | μ | | |
|-------|--------------------------------|--------------------------------|--------------------------------|--------------------------------|----------------------------------|----------------------------------|---------------------|-------------------|--------------|--------|--|--|
| | N ¹ -C ² | C ⁵ -N ⁶ | N ⁶ -N ⁷ | N ⁷ -C ⁸ | C ¹³ -N ¹⁶ | N ¹⁶ -O ¹⁷ | C ¹¹ -Cl | C ⁴ -X | | | C ⁵ N ⁶ N ⁷ | N ⁶ N ⁷ C ⁸ |
| [III] | 1.381 | 1.426 | 1.229 | 1.438 | 1.480 | 1.204 | 1.703 | 1.698 | 120.24 | 119.15 | -26.75 | 7.52 |
| [IV] | 1.390 | 1.426 | 1.230 | 1.438 | 1.480 | 1.204 | - | - | 120.72 | 118.81 | 31.95 | 5.88 |
| [V] | 1.396 | 1.427 | 1.229 | 1.434 | 1.490 | 1.203 | - | - | 120.60 | 119.49 | -31.63 | 4.89 |
| [VI] | 1.384 | 1.424 | 1.229 | 1.438 | 1.480 | 1.204 | 1.698 | - | 120.88 | 119.12 | 28.25 | 5.41 |
| [VII] | 1.390 | 1.426 | 1.229 | 1.439 | 1.479 | 1.205 | 1.703 | - | 120.50 | 118.85 | -23.33 | 7.72 |

| Dye | torsion angles (°) | | | | | | | | | |
|-------|--|---|--|---|---|---|--|--|---|--|
| | C ¹⁹ N ¹ C ² C ³ | C ²¹ N ¹ C ² C ¹⁵ | C ¹⁴ C ⁵ N ⁶ N ⁷ | C ⁴ C ⁵ N ⁶ N ⁷ | C ⁵ N ⁶ N ⁷ C ⁸ | N ⁶ N ⁷ C ⁸ C ⁹ | N ⁶ N ⁷ C ⁸ C ¹³ | C ⁸ C ¹³ N ¹⁶ O ¹⁷ | C ¹² C ¹³ N ¹⁶ O ¹⁸ | |
| [III] | 6.6 | 8.9 | -22.7 | -15.7 | 177.9 | -81.7 | 177.9 | 33.0 | -31.7 | |
| [IV] | 10.2 | -13.2 | 11.5 | -169.2 | 178.5 | -63.2 | 124.6 | -38.9 | -37.8 | |
| [V] | 13.7 | -13.4 | 0.3 | -180.0 | 178.4 | -69.5 | 119.0 | -36.7 | -34.7 | |
| [VI] | -0.5 | 19.2 | -10.5 | 170.3 | 178.5 | -84.6 | 103.7 | -33.2 | -31.9 | |
| [VII] | 22.4 | 2.8 | -13.2 | 168.7 | 177.8 | -76.5 | 114.5 | -34.4 | -33.3 | |

*For key see Table 4.12

Table 4.15 Summary of calculated structural data^a, heats of formation and dipole moments calculated bond lengths for constrained AM1 geometry optimisations (heavy atoms of the azobenzene moiety and atoms 19 and 21 constrained to lie in the same plane) of structures [III], [IV], [V], [VI] and [VII] in solvent (EPS=32.7).*

| Dye | bond lengths (Å) | | | | | | bond angles (°) | | torsion angles (°) [†] | | ΔH_f | μ | | |
|-------|--------------------------------|--------------------------------|--------------------------------|--------------------------------|----------------------------------|----------------------------------|---------------------|-------------------|--|--|--------------|-------|--|---|
| | N ¹ -C ² | C ⁵ -N ⁶ | N ⁶ -N ⁷ | N ⁷ -C ⁸ | C ¹³ -N ¹⁶ | N ¹⁶ -O ¹⁷ | C ¹¹ -Cl | C ⁴ -X | C ⁵ N ⁶ N ⁷ | N ⁶ N ⁷ C ⁸ | | | C ⁸ C ¹³ N ¹⁶ O ¹⁷ | C ¹² C ¹³ N ¹⁶ O ¹⁸ |
| [III] | 1.381 | 1.422 | 1.234 | 1.435 | 1.489 | 1.201 | 1.703 | 1.697 | 120.30 | 119.21 | -58.8 | -57.7 | -24.70 | 5.73 |
| [IV] | 1.381 | 1.422 | 1.234 | 1.435 | 1.488 | 1.202 | NA | NA | 120.47 | 119.34 | -60.6 | -59.7 | 33.97 | 5.21 |
| [V] | 1.370 | 1.429 | 1.234 | 1.433 | 1.487 | 1.200 | 1.463 | NA | 120.21 | 118.39 | -60.6 | -59.3 | -55.73 | 4.03 |
| [VI] | 1.379 | 1.420 | 1.234 | 1.435 | 1.488 | 1.202 | 1.704 | NA | 120.18 | 119.35 | -60.4 | -59.5 | 30.40 | 6.69 |
| [VII] | 1.383 | 1.423 | 1.233 | 1.435 | 1.488 | 1.202 | 1.704 | NA | 120.18 | 119.35 | 59.4 | -58.3 | -21.13 | 5.73 |

*For key see Table 4.12 [†]Note that all other torsion angles are 0° or 180°

The bond lengths angles and torsions of [VI] are very similar to those of [IV]. The four dyes, [VII], [III], [III] and [VII] have similar structures, with respect to their bond lengths, angles and torsions and can be grouped together. The 2-methyl-4-(N-β-hydroxyethyl, N-ethyl)amino-2'-nitroazobenzene-4'-ethanoate [V] is discussed with these dyes as it also contains the 2'-nitro substituent.

Dyes [III] and [VII], are structurally very similar to one another. Both dyes have 2-chloro substituted donor phenyl rings as well as 2'-nitro substituted acceptor phenyl rings. In addition, both dyes have a di-(β -hydroxyethyl)amino donor group. In fact the only difference between the dyes is the 4'-chloro substituent present in [III], but absent in [VII]. Since the two groups attached to the amino nitrogen are identical, there are only the 2 possible conformations of both above (or both below) or one above and one below the azobenzene plane. The conformation with the lowest energy is chosen for each dye. The presence of the 2-chloro substituent and the 2'-nitro substituent means that there are four possible conformations: a) where the chlorine atom is attached to C⁴ and the nitro group is attached to C⁹; b) where the chlorine atom is attached to C¹⁴ and the nitro group is attached to C¹³; c) where the chlorine atom is attached to C¹⁴ and the nitro group is attached to C⁹ and d) where the chlorine atom is attached to C⁴ and the nitro group is attached to C¹³. The final combination is in fact calculated to be the most stable conformation.

Not surprisingly, the same conformation of the 2-chloro and 2'-nitro substituent in [III] produces the lowest heat of formation. The acceptor phenyl rings in the freely optimised AM1 structures are twisted by 43° and the 2'-nitro group is twisted by 42.5° and 41.5° respectively for [III] and [VII] in the gas phase and 34° and 37° in methanol. The torsion angle of the donor phenyl ring with respect to the C⁵N⁶N⁷C⁸ plane is around 12° for [III] and 16° for [VII] which is greater than that in [IV] and [VI].

The results of gas phase calculations are again consistent with previous calculations on 4-dimethyl-2'-nitroazobenzene¹² where the both phenyl rings were twisted in different directions with an overall torsion of *ca.* 50°, and the nitro group is also twisted in the fully optimised structure. In a calculations where the heavy atoms were constrained to lie in the same plane, with the exception of the nitro group¹², the nitro group was twisted further out of the plane by 52°, and the heat of formation was slightly lower than for the unconstrained structure. In the 2'-nitro substituted dyes examined in this work, the nitro groups are twisted by *ca.* 60° in constrained structures, and heats of formation are lower in energy for some dyes but higher in energy for others than the fully optimised structures. Though structure [V] is grouped with the 2'-nitro substituted dyes, it can also be compared with dye 3, as these dyes both contain an ester group substituted at the 4-position of the acceptor phenyl ring. The same combinations of the two ortho substituents as for [III] are possible in [V], with the chlorine atom in [III] being replaced by a methyl group. The bond lengths of [V] are similar to those of the other 2'-nitro dyes, as are the bond angles and torsions. In the freely optimised dye 5 structures, the

nitro group makes a torsional angle of 36.7° to the acceptor phenyl ring, but in the constrained structures, the angle is 61° to the plane.

The 4-(N-β-hydroxyethyl, N-ethyl)aminoazobenzene-4'-ethanoate [III], has the same basic structure as [V] but minus the 2-methyl and 2'-nitro substituents. The differences between [III] and [V] are clear by comparison of the torsional angles of the dyes, which show that in contrast to [V], [III] is almost planar.

Table 4.16 Summary of calculated bond lengths, angles and torsions for AM1 geometry optimisations of [III] in the gas phase and in solvent (EPS=32.7).*

| Structure | Bond lengths | | | | C-X | Bond angles | | ΔH_f^c | μ_D^d |
|------------------------|--------------------------------|--------------------------------|--------------------------------|--------------------------------|-------|------------------|------------------|----------------|-----------|
| | N ¹ -C ² | C ⁵ -N ⁶ | N ⁶ -N ⁷ | N ⁷ -C ⁸ | | NNC ^d | NNC ^a | | |
| AM1 ^b | 1.399 | 1.429 | 1.232 | 1.438 | 1.469 | 119.99 | 119.42 | -32.66 | 3.858 |
| AM1 ^c | 1.388 | 1.427 | 1.233 | 1.438 | 1.469 | 120.05 | 119.38 | -31.16 | 4.287 |
| AM1/COSMO ^d | 1.396 | 1.429 | 1.230 | 1.440 | 1.467 | 120.33 | 118.96 | -54.45 | 5.541 |
| AM1/COSMO ^e | 1.382 | 1.424 | 1.233 | 1.427 | 1.468 | 120.35 | 119.69 | -53.40 | 6.074 |

| Structure | C ¹⁹ N ⁷ C ² C ³ | C ²¹ N ¹ C ² C ¹⁵ | C ⁴ C ⁵ N ⁶ N ⁷ | C ¹⁴ C ⁵ N ⁶ N ⁷ | C ⁵ N ⁶ N ⁷ C ⁸ | N ⁶ N ⁷ C ⁸ C ⁹ | N ⁶ N ⁷ C ⁸ C ¹³ |
|------------------------|--|---|---|--|---|---|--|
| | AM1 ^b | 14.5 | -15.0 | -0.1 | -179.9 | 180 | -178.6 |
| AM1 ^c | 0 | 0 | 0 | 180 | 0 | 180 | 180 |
| AM1/COSMO ^d | -5.4 | -31.6 | -16.4 | 165.8 | 179.9 | 46.1 | -138.3 |
| AM1/COSMO ^e | 0 | 0 | 0 | 180 | 0 | 180 | 180 |

*For key see Table 4.12

As well as the donor acceptor azo dye that have been discussed so far, four donor acceptor azothiophene dyes have also been examined [XV],[XVI],[XVIII] and [XIX]. Calculations on the azothiophene dyes have followed the same format as for the azobenzene dyes, with calculations in the gas phase and in methanol on both free and constrained structures. There are two possibilities concerning the orientation of the thiophene ring with respect to the rest of the molecule and these two possible conformations are illustrated in Figure 4.7.

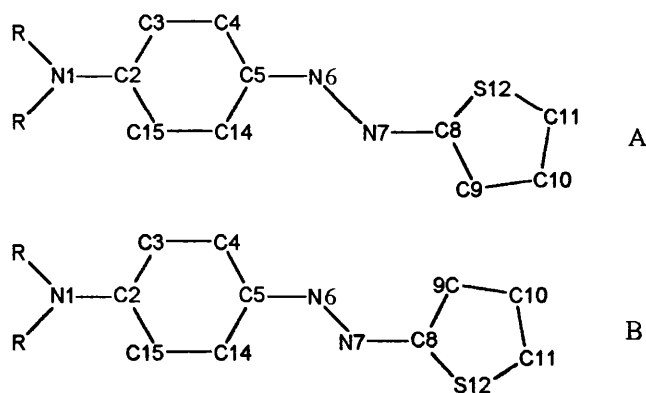


Figure 4.7 The two possible orientations for the thiophene ring in azothiophenes.

The preferred conformation will depend on the position of substituents on both the thiophene ring and the phenyl ring. Initial calculations on the dinitrothiophene dye [XV] showed that the energy for the alternative conformations of dye [XV] are $-56.13 \text{ kcal mol}^{-1}$ and $-54.93 \text{ kcal mol}^{-1}$ for structures [XV]A and [XV]B respectively. The structures and atom numbering systems and the bonding parameters for the optimised structures of each of the four azothiophenes are given below. For each dye, the conformation with the lowest heat of formation is displayed.

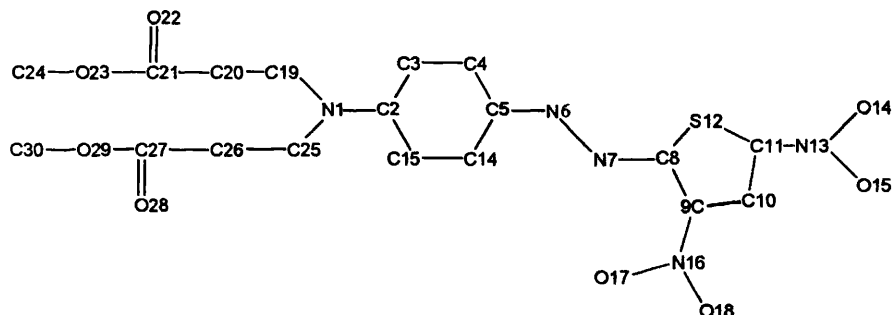


Figure 4.8 The structure and atom numbering system for [XV]. Note that the same numbering system is used for dyes [XV],[XVI],[XVIII] and [XIX].

Structure [XV] contains two electron accepting nitro substituents on the thiophene ring, as well as large ester groups attached to the donor amino nitrogen. In [XV], the C-NR₂ bond length is similar, the N=N bond length is slightly longer but both the C-NO₂ bonds are shorter than in the azobenzene dyes.

The thiophene ring is twisted by 46.7° out of the plane, whilst the 2'-nitro group has a torsional angle of 33° to the thiophene ring. The 4'-nitro group is however planar with the thiophene ring.

The most important bond lengths, angles and torsions for AM1 optimisations of dyes [XV], [XVI] and [XIX] are reported in Table 4.17 to Table 4.20. Consideration of bond lengths shows that the C-NR₂ bond is similar in length in gas phase structures and also in the freely optimised methanol structures. However methanol optimised structures where the amino group is constrained to lie in the plane have a much shorter C-NR₂ bond length. [XV], [XVI], and [XIX]

Table 4.17 Summary of calculated structural data, heats of formation and dipole moments for fully optimised gas phase AM1 structures of [XV], and [XVI] and [XIX].*

| Dye | bond lengths/ Å | | | | | | | bond angles (°) | | ΔH_f | μ | |
|-------|--------------------------------|--------------------------------|--------------------------------|--------------------------------|---------------------------------|----------------------------------|----------------------------------|----------------------------------|--|--------------|---------|--|
| | N ¹ -C ² | C ⁵ -N ⁶ | N ⁶ -N ⁷ | N ⁷ -C ⁸ | C ⁹ -N ¹⁶ | N ¹⁶ -O ¹⁷ | C ¹¹ -N ¹³ | N ¹⁶ -O ¹⁷ | C ⁵ N ⁶ N ⁷ | | | N ⁶ N ⁷ C ⁸ |
| [XV] | 1.392 | 1.421 | 1.234 | 1.414 | 1.469 | 1.200 | 1.460 | 1.200 | 120.59 | 119.12 | -51.77 | 6.77 |
| [XVI] | 1.381 | 1.402 | 1.241 | 1.410 | 1.471 | 1.200 | | | 122.39 | 118.46 | 70.69 | 7.04 |
| [XIX] | 1.397 | 1.422 | 1.232 | 1.416 | - | - | 1.458 | 1.201 | 122.27 | 119.27 | -155.61 | 7.21 |

| Dye | torsion angles (°) | | | | | | | | |
|-------|--|---|--|---|---|---|--|---|--|
| | C ¹⁹ N ¹ C ² C ³ | C ²⁵ N ¹ C ² -1 ⁵ | C ¹⁴ C ⁵ N ⁶ N ⁷ | C ⁴ C ⁵ N ⁶ N ⁷ | C ⁵ N ⁶ N ⁷ C ⁸ | N ⁶ N ⁷ C ⁸ C ⁹ | N ⁶ N ⁷ C ⁸ S ¹² | C ¹² C ¹¹ N ¹³ O ¹⁵ | C ¹⁰ C ⁹ N ¹⁶ O ¹⁸ |
| [XV] | -2.1 | 12.6 | 3.0 | -178.0 | -179.1 | 46.7 | -138.7 | 33.4 | 32.8 |
| [XVI] | 13.3 | 14.6 | -7.3 | 173.7 | 179.7 | 1.8 | -177.1 | 56.1 | 53.5 |
| [XIX] | -14.3 | 3.7 | -0.9 | 178.6 | -179.4 | 46.4 | -139.7 | 0.3 | - |

*For key see Table 4.12

Table 4.18 Summary of calculated structural data^a, heats of formation and dipole moments for constrained^b AM1 geometry optimisations (heavy atoms of the azobenzene moiety and atoms 19 and 25 constrained to lie in the same plane) of structures [XV] and [XVI] and [XIX] in the gas phase.*

| Dye | bond lengths/ Å | | | | | | | bond angles (°) | | torsion angles (°) | | ΔH_f | μ | |
|-------|--------------------------------|--------------------------------|--------------------------------|--------------------------------|---------------------------------|----------------------------------|----------------------------------|----------------------------------|--|--|---|--------------|---------|--|
| | N ¹ -C ² | C ⁵ -N ⁶ | N ⁶ -N ⁷ | N ⁷ -C ⁸ | C ⁹ -N ¹⁶ | N ¹⁶ -O ¹⁷ | C ¹¹ -N ¹³ | N ¹⁶ -O ¹⁷ | C ⁵ N ⁶ N ⁷ | N ⁶ N ⁷ C ⁸ | C ¹² C ¹¹ N ¹³ O ¹⁵ | | | C ¹⁰ C ⁹ N ¹⁶ O ¹⁸ |
| [XV] | 1.389 | 1.418 | 1.237 | 1.413 | 1.477 | 1.461 | | | 120.79 | 120.59 | 69.7 | 69.4 | -51.25 | 6.3 |
| [XVI] | 1.381 | 1.414 | 1.239 | 1.427 | 1.487 | 1.201 | 1.421 | | 122.54 | 118.38 | 58.4 | 56.0 | 71.13 | 7.2 |
| [XIX] | 1.397 | 1.418 | 1.234 | 1.414 | - | - | 1.459 | 1.201 | 122.91 | 119.36 | 0.2 | - | -155.85 | 7.0 |

*For key see Table 4.12

Table 4.19 Summary of calculated structural data, heats of formation and dipole moments for fully optimised AM1 structures of [XV] and [XVI] and [XIX] in solvent (EPS=32.7).*

| Dye | bond lengths/ Å | | | | | | | | bond angles (°) | | ΔH_f | μ |
|-------|--------------------------------|--------------------------------|--------------------------------|--------------------------------|---------------------------------|----------------------------------|----------------------------------|----------------------------------|--|--|--------------|-------|
| | N ¹ -C ² | C ⁵ -N ⁶ | N ⁶ -N ⁷ | N ⁷ -C ⁸ | C ⁹ -N ¹⁶ | N ¹⁶ -O ¹⁷ | C ¹¹ -N ¹³ | N ¹⁶ -O ¹⁷ | C ⁵ N ⁶ N ⁷ | N ⁶ N ⁷ C ⁸ | | |
| [XV] | 1.395 | 1.425 | 1.233 | 1.421 | 1.452 | 1.205 | 1.442 | 1.207 | 120.53 | 118.56 | -98.87 | 5.83 |
| [XVI] | 1.376 | 1.417 | 1.235 | 1.419 | 1.442 | 1.207 | - | - | 121.05 | 118.96 | 37.67 | 7.691 |
| [XIX] | 1.392 | 1.437 | 1.227 | 1.425 | 1.439 | 1.208 | - | - | 120.39 | 119.51 | -194.99 | 9.28 |

| Dye | torsion angles (°) | | | | | | | | | |
|-------|--|---|---|--|---|---|--|---|--|--|
| | C ¹⁹ N ¹ C ² C ³ | C ²⁵ N ¹ C ² C ¹⁵ | C ⁴ C ⁵ N ⁶ N ⁷ | C ¹⁴ C ⁵ N ⁶ N ⁷ | C ⁵ N ⁶ N ⁷ C ⁸ | N ⁶ N ⁷ C ⁸ C ⁹ | N ⁶ N ⁷ C ⁸ S ¹² | C ¹² C ¹¹ N ¹³ O ¹⁵ | C ¹⁰ C ⁹ N ¹⁶ O ¹⁸ | |
| [XV] | -14.7 | 6.8 | -13.9 | 167.8 | -178.5 | 46.2 | -137.0 | 33.0 | 33.5 | |
| [XVI] | 10.6 | 12.4 | -21.8 | 161.0 | - | 32.6 | -149.3 | -0.9 | 36.2 | |
| [XIX] | -5.4 | 3.0 | -57.4 | - | 178.9 | 59.7 | -127.8 | -0.5 | | |

*For key see Table 4.12

Table 4.20 Summary of calculated structural data^a, heats of formation and dipole moments calculated bond lengths for constrained AM1 geometry optimisations (heavy atoms of the azobenzene moiety and atoms 19 and 25 constrained to lie in the same plane) of structures [XV] and [XVI] and [XIX] in solvent (EPS=32.7).*

| Dye | bond lengths/ Å | | | | | | | | bond angles (°) | | torsion angles (°) | | ΔH_f | μ |
|-------|--------------------------------|--------------------------------|--------------------------------|--------------------------------|---------------------------------|----------------------------------|----------------------------------|----------------------------------|--|--|---|--|--------------|-------|
| | N ¹ -C ² | C ⁵ -N ⁶ | N ⁶ -N ⁷ | N ⁷ -C ⁸ | C ⁹ -N ¹⁶ | N ¹⁶ -O ¹⁷ | C ¹¹ -N ¹³ | N ¹⁶ -O ¹⁷ | C ⁵ N ⁶ N ⁷ | N ⁶ N ⁷ C ⁸ | C ¹² C ¹¹ N ¹³ O ¹⁵ | C ¹⁰ C ⁹ N ¹⁶ O ¹⁸ | | |
| [XV] | 1.387 | 1.421 | 1.235 | 1.416 | 1.466 | 1.202 | 1.442 | 1.207 | 120.6 | 119.44 | -75.2 | -75.7 | -106.63 | 8.2 |
| [XVI] | 1.375 | 1.411 | 1.237 | 1.415 | 1.464 | 1.442 | | | 121.65 | 119.24 | -0.3 | 68.8 | 39.03 | 9.3 |
| [XIX] | 1.389 | 1.411 | 1.231 | 1.414 | - | - | 1.438 | 1.208 | 124.42 | 119.32 | -0.3 | - | 188.84 | 10. |

*For key see Table 4.12

Geometry

The geometry of the azothiophene dye [XV] has been previously determined by Morley at the AM1 and PM3 levels of theory and also at the ab-initio STO-3G level.¹⁴ The STO-3G structure of [XVI] has also been previously calculated.¹⁹ Both the AM1 and PM3 methods of calculation produced a twisted structure of [XV] where the thiophene ring was approximately orthogonal to the phenylazo group. This compares to torsion angles of 46° between the thiophene ring and the phenyl azo group in

structures calculated in this work. The PM3 C-S, -N=N- and C-NO₂ bond lengths of 1.73, 1.25 and 1.49 Å respectively, were consistent with Morley's results. The STO-3G structure was essentially planar as was the STO-3G structure of [XVI].

Rotation calculations

From the AM1 calculated structures of these donor-acceptor dyes, it is clear that both planar and twisted geometries are energetically viable for some dyes, with energy differences between planar and twisted structures of around 0 to 1 kcal mol⁻¹. The visible spectra of azo dyes in solution contain broad absorption bands, suggesting the presence of several conformers. It is therefore possible that there are a number of conformations of the ground state molecules that have similar energies. The effect of modifying the torsion angle of one of the phenyl rings of the dye on the heat of formation should indicate the geometries of the more stable conformers. Starting from the optimised planar conformer of dyes [IX], [XIV], [IV] and [XV] in methanol, the donor or acceptor phenyl ring was rotated by 360° by modifying the torsion angle C14-C5-N6-N7 or N6-N7-C8-C9 in steps of 2°. The heat of formation produced after each 2° rotation can then be plotted against the angle of rotation of the phenyl ring. The effect of rotating the donor ring or the acceptor ring for [IX] is shown in Figure 4.9. The original flat structure is an energy minimum, and any rotation of the donor phenyl ring, from this minimum energy conformation, results in an increase in the heat of formation. Rotations of the donor phenyl ring by up to 30° result in ΔH_f increases of less than 1 kcal mol⁻¹, but rotations beyond 30° give a steep increase in ΔH_f , with structures where donor phenyl ring is twisted by between 90° and 280° having the highest energies of just over 60 kcal mol⁻¹.

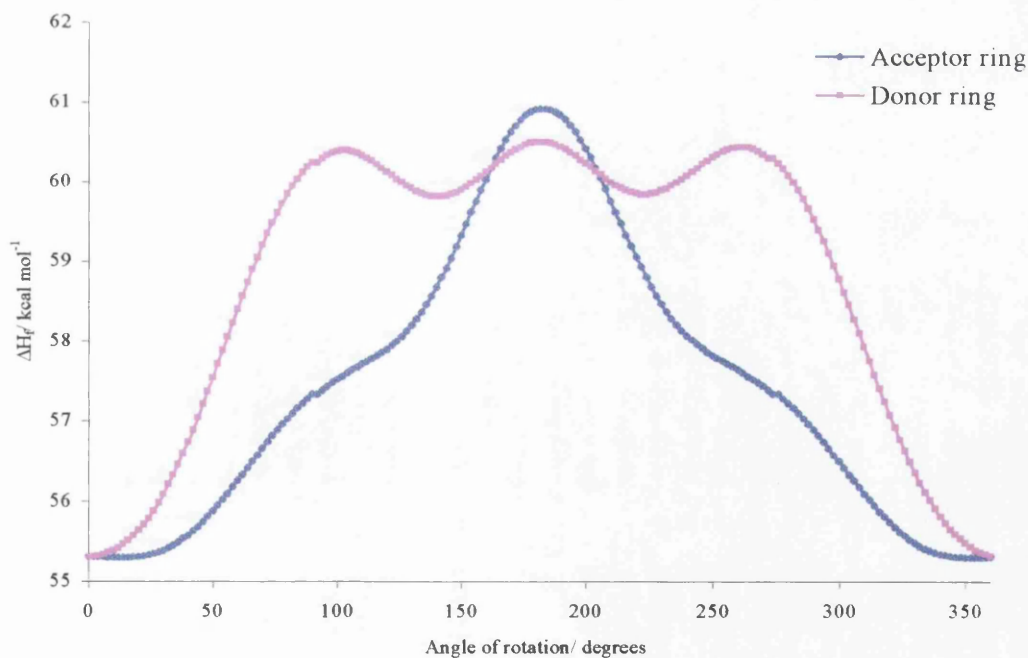


Figure 4.9 Changes in heat of formation with angle of rotation of the donor and acceptor phenyl rings of [IX] in methanol.

The changes in the heat of formation with rotation of the acceptor phenyl ring (Figure 4.9) are more gradual than for the donor phenyl ring. For rotations up to 30° in either direction, the heat of formation is essentially the same as for the minimum energy optimised structure. From 40° to 90° the energy rises approximately 2 kcal mol^{-1} , and the highest energy conformation occurs at a ring rotation of 180° . This information suggests that the planar conformation of [IX] is the most stable geometry, but rotations of the acceptor phenyl ring, of up to 30° are energetically feasible. Larger rotations and rotations of the donor phenyl ring are predicted to be unfavourable.

The variation in the heat of formation with rotation of the acceptor ring of the 4-di(β -hydroxyethyl)aminoazobenzene [XIV] which does not contain an electron withdrawing substituent, produces a similar shaped curve to that of the 4'-nitro substituted dye [IX], but the curve obtained from rotation of the donor ring is slightly different. The shapes of the curves for 4-di(β -hydroxyethyl)amino-4'-aminoazobenzene [XI] are almost identical to those of [XIV].

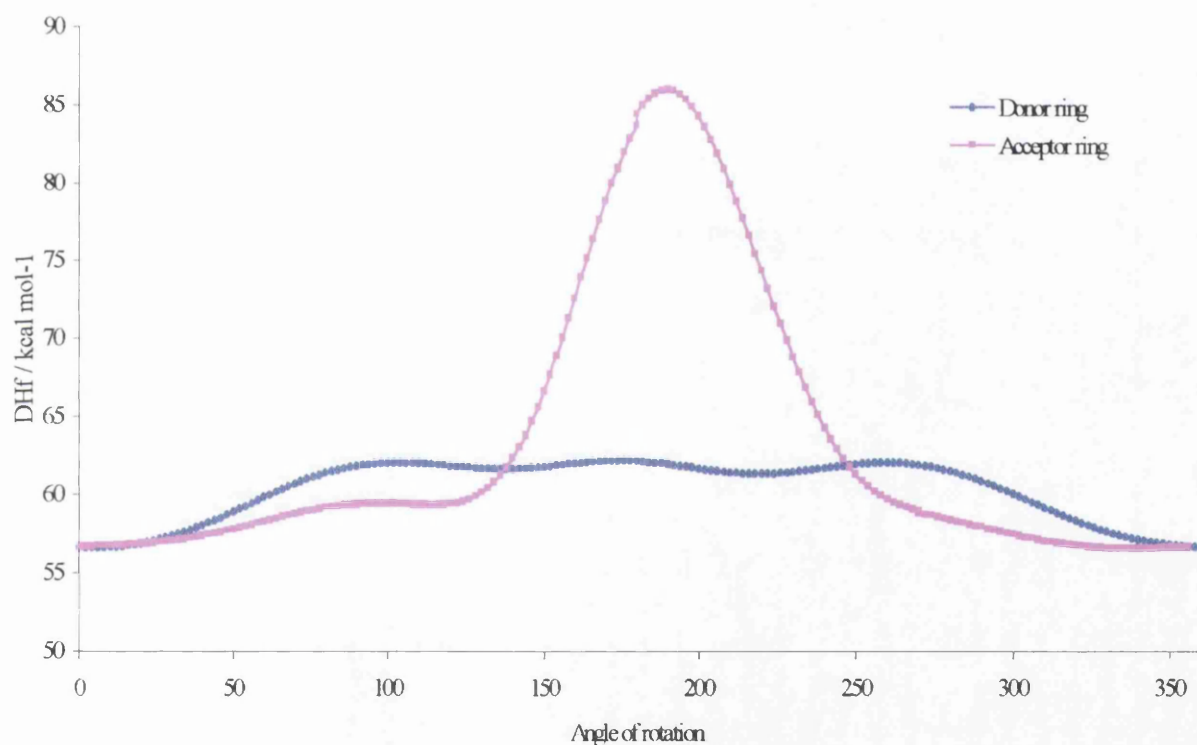


Figure 4.10 Changes in the heat of formation of [IV] in methanol with rotation of the donor or acceptor phenyl rings

The change in the heat of formation with rotation of the donor ring of [IV] (Figure 4.10) is very similar to that for [IX]. However, rotation of the acceptor ring produces a different shaped curve. Here, rotations of the ring by up to 130° in the positive direction and 100° in the negative direction

and produce an increase of less than 3 kcal mol⁻¹. Between 120 and 195°, there is a sharp increase in the heat of formation by almost 20 kcal mol⁻¹.

From 195 to 260°, the heat of formation falls to around 60 kcal mol⁻¹. This curve suggests that rotations of the acceptor ring by 120° in the positive direction and by 100° in the negative direction are energetically feasible, but rotations beyond this produce a large increase in the heat of formation and are highly unfavourable.

Rotation of the 2'-nitro group

Dyes that contain the 2'-nitro substituent, usually have the nitro group rotated by anything between 25° and 90° out of the plane. The effect of rotating the 2'-nitro group on the heat of formation of the dye can be calculated in a similar way to the rotation of the phenyl rings. The variation in the heat of formation with the rotation of the 2'-nitro group for [IV] is shown in Figure 4.11.

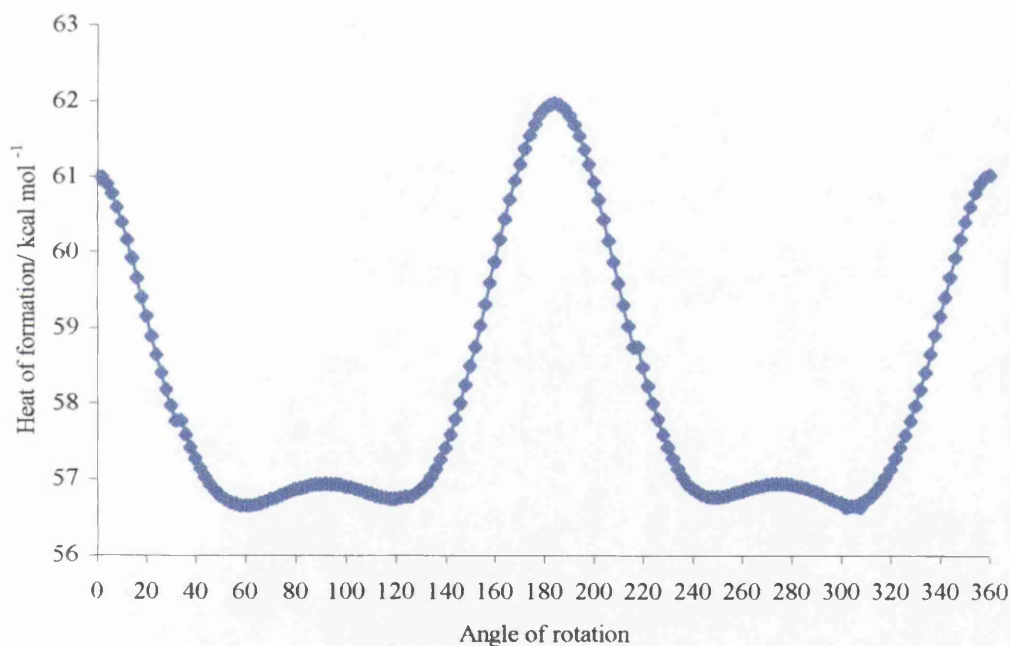


Figure 4.11 Changes in the heat of formation of [IV] on rotation of the 2'-nitro substituent.

The minimum energy is produced at rotation (torsion) angles of 301.9° (-58.1°) and 58.9° out of the plane and the most energetically unstable conformations are at 0 and 180, i.e. when the nitro group is in the plane.

Rotation of the N-alkyl amino group produces very unfavourable energy changes and the most stable structure has a planar conformation of the N-alkyl amino group, which is not surprising as the lone pair electrons of the nitrogen atom of this group interacts with the π system of the rest of the dye to a greater extent in a planar conformation.

The azothiophene [XV] has a similar curve for donor phenyl rotation to the donor acceptor azo dyes. The curve produced by rotation the acceptor thiophene ring (Figure 4.12) is however, completely different. The minimum energy conformer has an angle of rotation of 46.45° out of the plane. The heat of formation of the conformation where the thiophene ring is planer with the rest of the molecule, is 9-10 kcal mol⁻¹ higher in energy than the most stable structure.

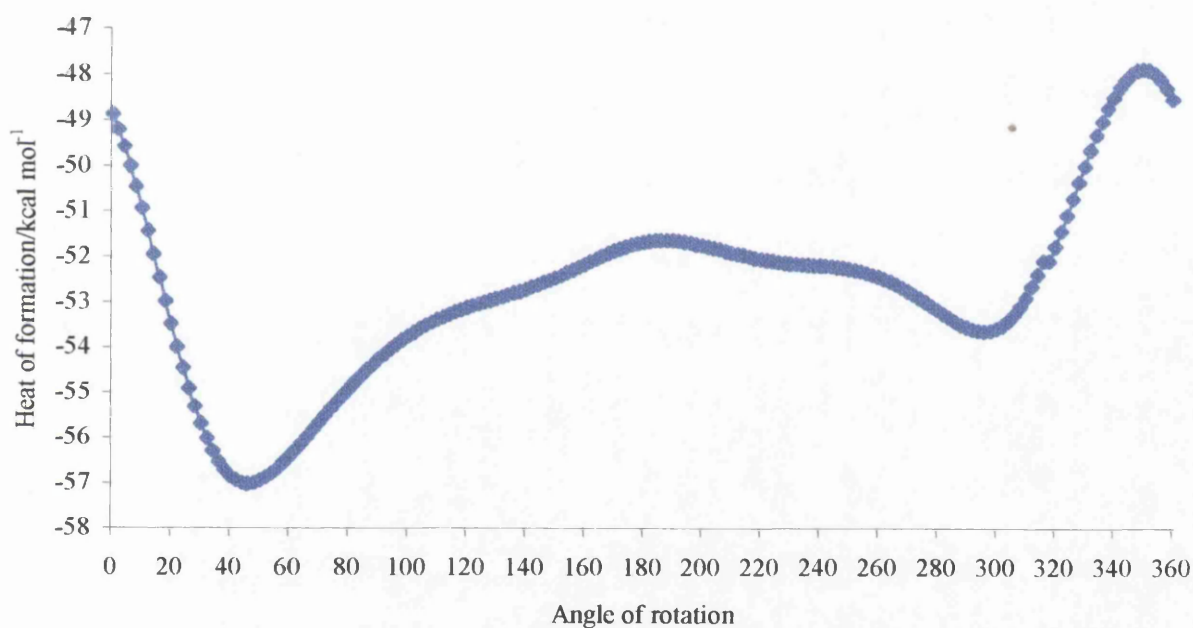


Figure 4.12 Change in heat of formation on rotation of the acceptor thiophene ring of [XV].

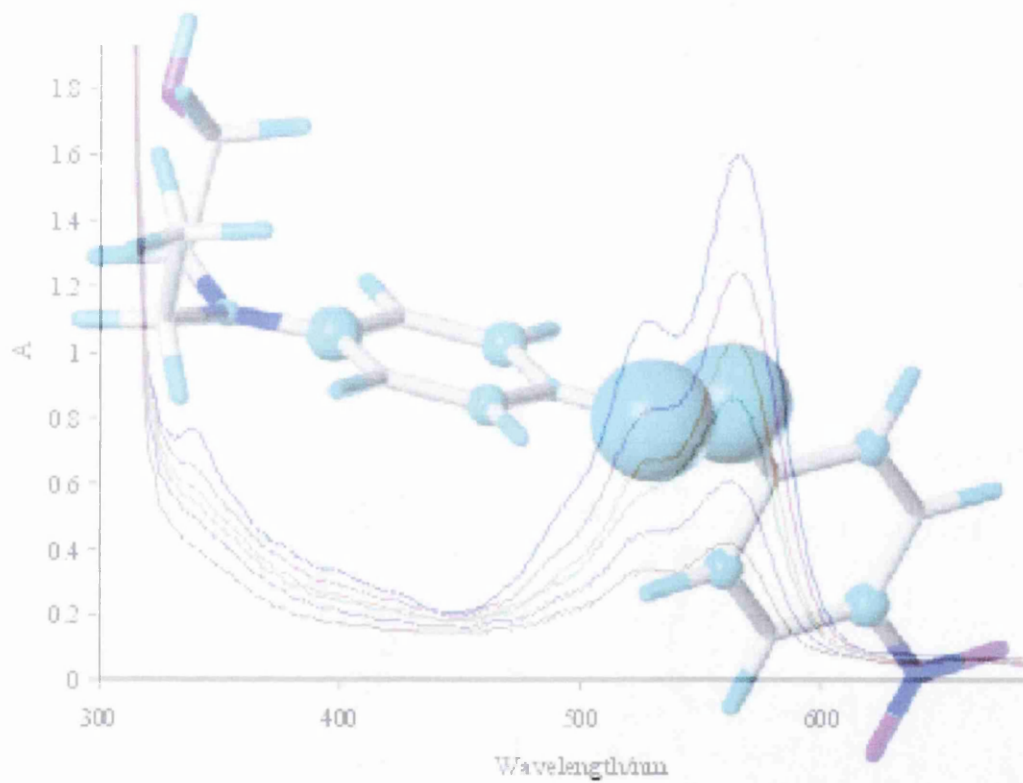
These calculations suggest that rotations of the donor phenyl ring by up to 30° and the acceptor ring by up to 60° , in donor-acceptor azobenzenes, are energetically feasible. The nitro group is twisted out of the plane in the 2'-nitro substituted dyes and conformations where the nitro group lies in the plane are energetically unfavourable. In contrast, the most favourable conformation of 4'-nitro substituted dyes has the nitro group coplanar with the rest of the molecule.

References

- ¹ Silicon Graphics on the world wide web at <http://www.sgi.com/>
- ² SYBYL molecular modelling software, Tripos Associates, St Louis, Missouri, 1989; Tripos, inc. on the world wide web at <http://www.tripos.com/> ; N. Van Openbosch, R. Cramer and F.F. Giarrusso, *J. Mol. Graphics* **3** (1985) 110.
- ³ Cambridge Structural Database, Cambridge Crystallographic Data Centre, University Chemical Laboratory, Lensfield Road, Cambridge, CB2 2EW, UK.
- ⁴ M.J.S. Dewar and E.G. Zeobisch, E.F. Healy and J.J.P. Stewart *J. Am. Chem. Soc.* **107** (1985) 3902; M.J.S. Dewar and E.G. Zeobisch, *Theochem.* **49** (1988) 1.
- ⁵ (a) J.J.P. Stewart, *J. Comput. Chem.* 1989 **10**, 209; (b) A. Holder, *J. Mol. Struct. (Theochem.)* (1997) 401, preface.
- ⁶ M.J.S. Dewar and W. Thiel, *J. Am. Chem. Soc.* **99** (1977) 4899.
- ⁷ MOPAC 93 (J.J.P. Stewart and Fujitsu Limited: Tokyo, Japan; copyright (Fujitsu Limited, 1993) obtained from QCPE, Department of Chemistry, Indiana University, Bloomington, IN 47405, USA.
- ⁸ MOPAC 93 manual, Fuhitsu Ltd.: Tokyo Japan (1993).
- ⁹ A. Klamt and G. Shuurmann, *J. Chem. Soc., Perkin Trans 2.*, (1993) 799.
- ¹⁰ A. Klamt, *J. Phys. Chem.* **100** (1996) 3349.
- ¹¹ C.J. Cramer and D. G. Truhlar, *J. Am. Chem. Soc.*, **113** (1991) 8305
- ¹² M.H. Charlton , R. Docherty, D.J. McGeein and J.O. Morley, *J. Chem. Soc. Faraday Trans.*, **89**(11) (1993) 1671 and references therein.
- ¹³ J. Del Bene and H.H. Jaffe, *J. Chem. Phys.*, **48** (1968) 1807.
- ¹⁴ J.O. Morley, M.G. Hutchings, J. Zyss and I. Ledoux, *J. Chem. Soc. Perkin Trans. 2.*, (1997) 1139
- ¹⁵ J.O. Morley, *J. Chem. Soc. Faraday Trans.*, **90** (1994) 1849.
- ¹⁶ W.J. Hehre, L. Radom, P. v. R. Schleyer and J.A. Pople, *Ab Initio Molecular Orbital Theory*, Wiley, New York, (1986).
- ¹⁷ J. A. Riddick , W. B. Bunger, *Techniques of Organic chemistry Vol.II, Organic Solvents*, 3rd ed., Wiley-Interscience, New York (1970)
- ¹⁸ S.A. McIntosh, H.S. Freeman and P. Singh, *Tex. Res. J.*, 1989, **59**, 389
- ¹⁹ J.O. Morley, *J. Chem. Soc. Faraday Trans.*, 1994, **90** (13), 1849-1852

Chapter 5

Cis-Trans Isomerisation and Electronic Transitions of Azo Dyes



Chapter 5 Cis-trans isomerisation and electronic transitions of azo dyes

In the discussion that follows, the electronic properties of azo dyes are examined. Also discussed is the cis-trans isomerisation reaction, which may have some relationship with the lightfastness properties of the dyes.

Cis and Trans isomers

Cis-trans isomerisation may be a means for the dissipation of energy from the excited states of azobenzenes¹, and it is possible that the relative ease of the dissipation of electronic energy (via isomerisation) may be related to the lightfastness of azo dyes. Azobenzene isomerises quite slowly and its cis isomer has a lifetime of milliseconds in glycerol². Donor acceptor azobenzenes isomerise much more quickly and the lifetime of their cis isomers is very short in comparison to azobenzene itself.

Azobenzene

Structures of cis and trans azobenzene calculated by Nandita and Umpathy³ at ab initio level using density functional theory (DFT) were found to be in good agreement with crystal structures of azobenzene. Crystal structures for trans azobenzene, available on the Cambridge Structural Database⁴, have both phenyl rings of the azobenzene slightly twisted out of the plane of the molecule by equal amounts. The torsion angles of each phenyl ring with respect to the $C^4N^5N^6C^7$ plane (Figure 5.1) which has a torsion angle of 0° , are reported in Table 5.1.

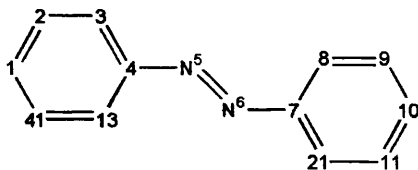


Figure 5.1 Numbering convention for azobenzene.

Table 5.1 Structural data^a for crystallographic and calculated structures of trans-azobenzene^b and cis-azobenzene^c.

| Structure | Azobenzene Structure | Bond lengths | | Bond angles | | | Bond Torsions | | |
|--------------------------|------------------------|-------------------------------|--------------------------------|--|---|--|--|---|---|
| | | C ⁴ N ⁵ | N ⁵ -N ⁶ | C ³ C ⁴ N ⁵ | C ¹³ C ⁴ N ⁵ | C ⁴ N ⁵ N ⁶ | C ¹³ C ⁴ N ⁵ N ⁶ | C ⁴ N ⁵ N ⁶ C ⁷ | N ⁵ N ⁶ C ⁷ C ⁸ |
| Trans^b | CSD^d | | | | | | | | |
| | AZOBEN01b | 1.433 | 1.243 | 115.50 | 124.10 | 113.58 | 18.2 | 0 | -18.2 |
| | AM1/PM3 ^b | | | | | | | | |
| | AM1 ^e | 1.436 | 1.231 | 115.36 | 125.33 | 119.73 | 0 | 180 | 0 |
| | AM1/COSMO ^f | 1.440 | 1.228 | 117.24 | 123.10 | 119.29 | -43.4 | 180 | 43.4 |
| | PM3 ^g | 1.447 | 1.232 | 115.31 | 124.41 | 119.89 | -0.6 | 180 | 0.6 |
| | PM3/COSMO ^h | 1.452 | 1.227 | 117.53 | 121.30 | 119.12 | -63.5 | 180 | -63.5 |
| Cis^c | CSD^d | | | | | | | | |
| | AZBENC | 1.494 | 1.170 | 114.60 | 125.62 | 122.82 | -39.2 | -27.1 | 136.8 |
| | AZBENC01 | 1.443 | 1.251 | 117.35 | 122.46 | 121.93 | -57.0 | -7.7 | 130.6 |
| | AM1/PM3 ^b | | | | | | | | |
| | AM1 ^e | 1.442 | 1.204 | 118.05 | 122.53 | 129.23 | -48.6 | -2.3 | 137.0 |
| | AM1/COSMO ^f | 1.439 | 1.206 | 118.06 | 122.28 | 129.44 | -49.4 | -2.3 | 135.6 |
| | PM3 ^g | 1.453 | 1.216 | 119.75 | 119.25 | 126.65 | 96.6 | 0 | -89.3 |
| | PM3/COSMO ^h | 1.453 | 1.219 | 120.27 | 118.42 | 126.66 | 107.0 | -0.2 | -78.1 |

^a Bond lengths in amstrongs, bond angles and torsion angles in degrees. ^d Codenames of crystal structures taken from reference 4. ^e Full AM1 optimisation in the gas phase. ^f Full AM1 optimisation in methanol. ^g Full PM3 optimisation in the gas phase. ^h Full PM3 optimisation in methanol.

Trans azobenzene

Crystal structures of trans azobenzene have both phenyl rings twisted out of the plane by between 5° and 20°. In contrast to this, gas phase optimisations of any of these crystal structures by the AM1 and PM3 methods yield completely flat and almost planar structures respectively. However, AM1 and PM3 optimisations of crystal structures in methanol gives a calculated azobenzene structure where each phenyl ring is twisted out of the plane by 43.4° Torsion angles found in the crystal structures probably result from packing forces which are not present in solution or in the gas phase. Thus some differences between calculated structures and crystal data is not surprising.

Cis-azobenzene

The crystal structure of cis azobenzene (AZBENC01)⁴, is shown along with the MOPAC AM1 and PM3 optimised structures in Figure 5.2.

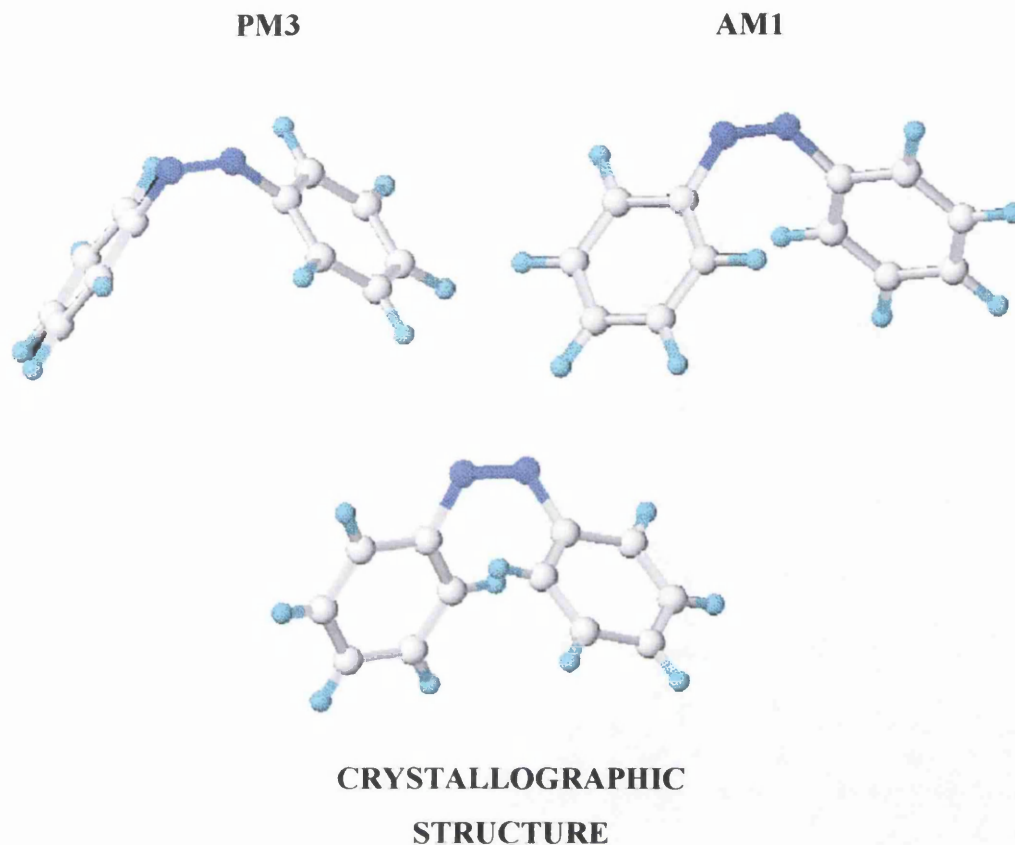


Figure 5.2 A comparison of the crystallographic structure AZBENC01 with cis azobenzene gas phase structures calculated using the PM3 and AM1 methods.

The AM1 optimised geometry is quite similar to the crystal structures for cis azobenzene except it has both phenyl rings twisted by approximately 47° compared with 39.2° in the crystal structure AZOBENC and 57° for crystal structure AZOBENC01.[†] The PM3 structure however, has both phenyl rings twisted by approximately 80° in the same direction. The structures of cis-azobenzene optimised in methanol are very similar to those optimised in the gas phase.

[†]Angles refer to the torsion angle $C^{13}C^4N^5N^6$

Cis-trans isomers of Aminoazobenzene and a donor acceptor azobenzenes

The AM1 calculated structures of 4-aminoazobenzene and the donor acceptor dye, diethylamino-4-nitroazobenzene [X], have similar bond lengths to those of cis azobenzene. However, the torsion angles of donor and donor-acceptor azobenzenes are significantly different to those of azobenzene itself (compare Figure 5.2 to Figure 5.3). In methanol and gas phase optimised structures, the donor phenyl ring is twisted out of the plane by 23-26°, whilst the acceptor ring has a much greater twist of between 78° and 90° in 4-aminoazobenzene and [X] respectively.

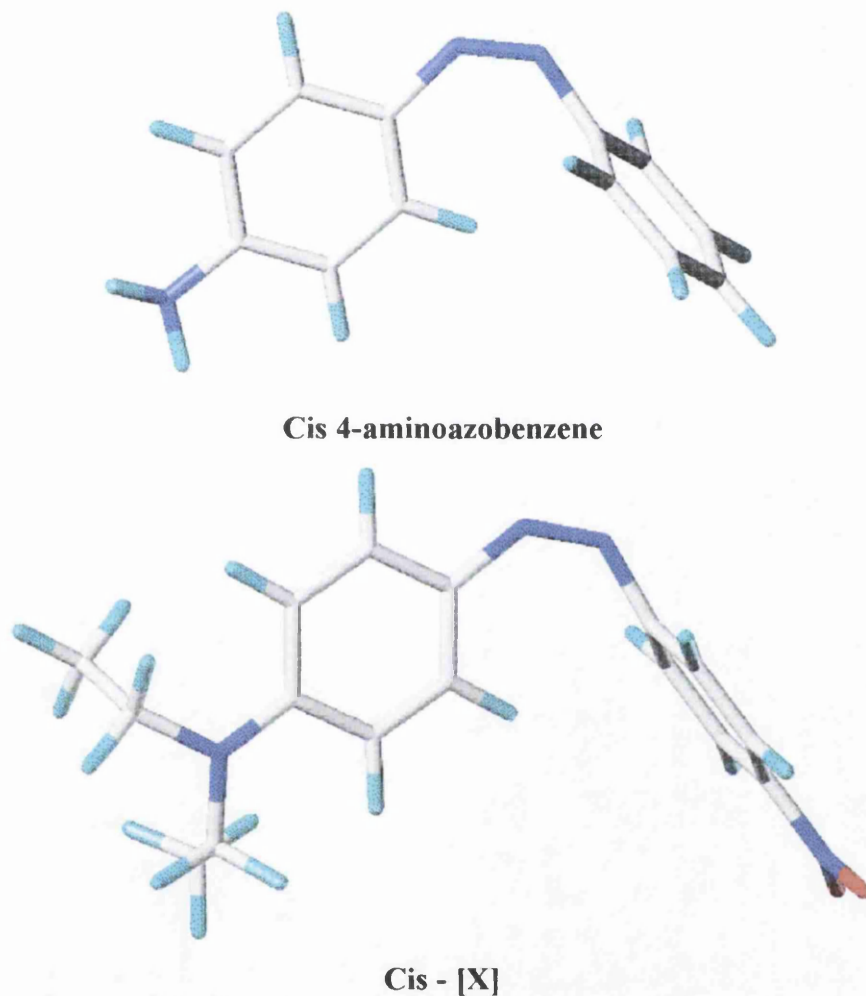


Figure 5.3 Calculated AM1 structures of the Cis isomers of 4-aminoazobenzene and 4-dimethylamino-4'-nitroazobenzene [X].

The mechanism of cis-trans isomerisation of donor-acceptor azobenzenes has been examined by Shaabani and Zahedi⁵ using the AM1 and PM3 methods. They calculated the energy barrier for the inversion and rotation of the donor and the acceptor phenyl rings of 4-dimethylamino-4'-nitroazobenzene, and also the difference in energy between cis and trans isomers of some substituted

azobenzenes. The trans isomers were found to be more stable than the cis by between 0.5 and 5 kcal mol⁻¹ by the PM3 method. However, the AM1 method predicted the cis form to be 1.6-6.3 kcal mol⁻¹ more stable than the trans isomer. Shaabani and Zahedi calculated the energies in the gas phase only. In the current work, the heats of formation, ΔH_f , of some other cis and trans azobenzenes were calculated by the AM1 and PM3 methods in the gas phase and in methanol, and the energy differences between the cis and trans isomers of each molecule are compared in Table 5.2.

Table 5.2 Heats of formation of Cis and trans isomers of azobenzene, 4-aminoazobenzene, 4-amino-4'-nitroazobenzene [VIII], 4-diethylamino-4'-nitroazobenzene [X] and 4-(N-diethyl, N- β -hydroxyethyl)amino-2'-nitroazobenzene [IV].

| Gas phase structures ^b | AM1 | | | PM3 | | |
|--|-------|--------|--------------------------|-------|-------|--------------------------|
| | Cis | Trans | $\Delta E_{(Cis-Trans)}$ | Cis | Trans | $\Delta E_{(Cis-Trans)}$ |
| Azobenzene | 95.28 | 99.89 | -4.61 | 92.79 | 90.55 | 2.24 |
| 4-aminoazobenzene | 92.82 | 97.42 | -4.60 | 90.3 | 87.9 | 2.40 |
| [VIII] | 96.43 | 101.15 | -4.72 | 81.74 | 79.45 | 2.29 |
| [X] | 96.52 | 99.97 | -3.45 | 70.92 | 66.99 | 3.93 |
| [IV] | 54.16 | 55.81 | -1.64 | 34.04 | 28.35 | 5.69 |
| <u>Methanol structures^c</u> | | | | | | |
| Azobenzene | 85.29 | 91.75 | -6.45 | 84.17 | 84.12 | 0.06 |
| 4-aminoazobenzene | 77.32 | 84 | -6.69 | 84.12 | 78.36 | 5.76 |
| [VIII] | 72.7 | 79.18 | -6.48 | 52.11 | 51.81 | 0.3 |
| [X] | 74.21 | 81.48 | -7.27 | 42.04 | 40.79 | 1.25 |
| [IV] | 26.13 | 31.95 | -5.82 | -3.16 | 0.92 | -4.08 |

^a ΔH_f is the heat of formation in kcal mol⁻¹. ^b Full optimisations in the gas phase. ^c Full optimisations in methanol. ^d

$\Delta E_{(Cis-Trans)}$ is the heat of formation of the trans isomer subtracted from the cis isomer.

The heats of formation for AM1 optimised cis-azobenzene are lower than for trans-azobenzene, both in the gas phase and in methanol. For PM3 optimised structures, the trans isomer has a lower heat of formation than the cis isomer in the gas phase, whilst in methanol, the heats of formation of both isomer are almost identical. The difference in the heat of formation of the cis and trans isomers of 4-aminoazobenzene and 4-amino-4'-nitroazobenzene are similar to that of azobenzene, for AM1 calculations in the gas phase and in solvent and for PM3 gas phase calculations. The PM3 methanol

optimised trans 4-aminoazobenzene structure is $5.76 \text{ kcal mol}^{-1}$ more stable than the cis isomer, while for 4-amino-4'-nitroazobenzene and azobenzene, the energy difference between cis and trans isomers is very small ($0.30 \text{ kcal mol}^{-1}$ for the AM1 method and $0.06 \text{ kcal mol}^{-1}$ respectively). The energy differences are quite similar for dye 20, but for dye 4, the AM1 method predicts a slightly smaller energy difference between its cis and trans isomers, whilst for the PM3 method the trans isomer is $5.7 \text{ kcal mol}^{-1}$ in the gas phase, but in methanol, the cis isomer is more stable by $4.1 \text{ kcal mol}^{-1}$. Results of these calculations in gas phase are consistent with those of Shaabini and Zahedi⁵, who reported good agreements between PM3 and experimental data, but AM1 results that were contrary to all experimental evidence. However, results of PM3 calculations in methanol do not show any apparent trend.

The small difference in the heats of formation between cis and trans isomers, indicates that fast inter-conversion between the cis and trans isomers of the donor acceptor dye may be possible. The rate of inter-conversion will also depend on the barrier height between the cis and trans isomers. The activation energy for cis-trans isomerisation in n-heptane was reported to be much lower for 4-amino-4'-nitroazobenzene than for azobenzene⁶ and Shaabini and Zahedi⁵ calculated that a donor-acceptor azobenzene had a lower energy barrier to rotation than an aminoazobenzene which, in turn had a lower energy barrier than azobenzene. If the mechanism of cis-trans isomerisation involves rotation of the acceptor phenyl ring then the lower energy barrier and similar energies of the cis and trans isomers would suggest easier inter-conversion between isomers for 4-amino-4'-nitroazobenzene than for azobenzene or 4-aminoazobenzene. It has been suggested that there is a connection between the rate of cis-trans isomerisation and lightfastness, with dyes that undergo rapid isomerisation having high lightfastness.⁷ Gas phase PM3 cis-trans energy differences were highest for [IV] which also had poor lightfastness relative to the other azo dyes. However, $\Delta E_{(\text{Cis-Trans})}$ in methanol and AM1 results in the gas phase and in methanol showed no apparent relationship with lightfastness. It may be the case that the energy barrier to rotation or inversion is the more important parameter in determining the rate of isomerisation. The effect of solvent on the rate of isomerisation of donor acceptor azobenzenes is to increase the rate in more polar solvents.⁸ In aprotic solvents, this is due to stabilisation of a dipolar transition state via a non-specific dielectric effect, and in protic solvents, the transition state is also stabilised by a specific hydrogen bonding interaction between the solvent and the nitro group of the dye. The effect of solvent on the mechanism of cis-trans isomerisation has been examined at the *ab initio* STO-3G level by Kikuchi⁹ (see introduction).

Calculated electronic spectra

Spectroscopic calculations on dyes [II]-[XIX] have been performed using the CNDOVS method.¹⁰ The calculated visible absorption band and higher energy absorptions are assessed and compared to experimental data.

The geometry of azobenzenes has a significant effect on their electronic transitions. For example the electronic absorption spectrum for trans azobenzene is quite different to that of cis azobenzene. In the essentially planar trans azobenzene, there is a weak long wavelength absorption at 444 nm, attributed to a symmetry forbidden $n-\pi^*$ transition by Griffiths¹¹. A second absorption band at 316 nm is suggested to originate from an allowed $\pi-\pi^*$ which is much more intense than the band at 444 nm. The extinction coefficient for the $n-\pi^*$ band at 444 nm is higher than would be normally expected for a symmetry forbidden transition and this is attributed by Griffiths to arise from coupling between the $n-\pi^*$ and $\pi-\pi^*$ states which are close together in energy.

In cis-azobenzene the lone pair orbitals overlap in such a way that the $n-\pi^*$ absorption is symmetry allowed, resulting in an $n-\pi^*$ absorption of much greater than in the trans isomer. Griffiths also ascribes the high intensity of the $n-\pi^*$ band in cis-azobenzene to coupling between $n-\pi^*$ and $\pi-\pi^*$ states. Hartmann also concludes from PPP-type calculations that mixing between n orbitals and π orbitals in the non planar cis-conformation of azobenzene, results in the long wavelength $n-\pi^*$ transition gaining intensity from allowed $\pi-\pi^*$ transitions.¹² The positions of the high energy transitions in cis-azobenzene are also said to be affected by the mixing of the $n-\pi^*$ and $\pi-\pi^*$ wave functions and this is the explanation given for the spectral differences mentioned above. This is an extreme example of how different geometries cause differences in absorption spectra, as cis and trans azobenzene have very different geometries. The nature of the transitions involved in the calculated electronic spectra of donor-acceptor azobenzenes,¹³ have been investigated by an analysis of molecular orbitals, similar to that performed by Akaba et al. on benzylideneanilines using the CNDO/S method.¹³

Spectroscopic calculations on azo dyes using the PPP methods have produced good agreement with experimental data.^{14,15} However, the PPP method is usually only applicable to planar structures and is therefore inappropriate for calculations on some of the non-planar structures produced by AM1 and PM3 geometry optimisations.

Single electron configuration interaction (C.I.)

Transitions energies calculated by the CNDOVS method for the visible absorption band of some donor-acceptor azobenzenes by Charlton et al. correlated well with experimental data.¹⁶ The

CNDOVS method was therefore used to perform spectroscopic calculations on planar and non-planar geometries of [II]-[XIX]. CNDOVS is a single C.I. all valence electron method parameterised for dyes and pigments and based on the CNDO/S method.¹⁷ While the default CNDOVS calculation produces the first 50 excited states from single electron transitions, it can be adjusted to give the first 200 states. The method calculates energies for transitions from the ground state to each excited state, along with the oscillator strength of each transition. In these studies, only transitions with an oscillator strength above 0.05 have been considered, as transitions with smaller oscillator strengths than this are thought to be insignificant (these transitions have a low probability of taking place). An analysis of each excited state shows which molecular orbital transitions are involved in each excited state. For example, the first excited state may consist of the HOMO → LUMO plus a contribution from the HOMO → LUMO+1 transition etc. There are usually small contributions from other orbital transitions, but in general the HOMO → LUMO transition is the largest contribution. The general expression for an excited state S_n takes the form of Equation (5-1),

$$S_n = a_1 \psi_{\text{HOMO} \rightarrow \text{LUMO}} + a_2 \psi_{\text{HOMO} \rightarrow \text{LUMO}+1} + a_3 \psi_{\text{HOMO}-1 \rightarrow \text{LUMO}} + \dots \quad \text{Equation (5-1)}$$

where a_1 - a_n are the weighting coefficients.

The origin of each electronic transition can be found by considering the molecular orbitals involved, which may have contributions from s, p_x , p_y , and p_z atomic orbitals on individual atoms in the molecule. In general, the electronic spectra for conjugated systems arise mainly from the p_z component, or π type orbital. If however, there are contributions from s, p_x , and p_y , of nitrogen atoms, then the orbital may originate from the lone pair electrons of nitrogen atoms and thus have n-type character. Electronic transitions may therefore, be π - π^* or n- π^* , but often the situation is more complicated than this, and transitions may be a mixture of n- π^* and π - π^* . Only the first three excited states in each calculation, with significant oscillator strength, have been considered as the method is not reliable for short wavelength UV absorptions. Initial calculations were carried out on the simplest donor acceptor structure considered in the present studies, 4-amino-4'-nitroazobenzene, with two values of the spectroscopic constant, at 0.65 or 0.58 as in previous studies.¹⁶ The spectroscopic constant distinguishes between the core Hamiltonians for σ and π orbitals (Equation (5-2) and Equation (5-3) respectively).

$$H^\sigma = \frac{1}{2} (\beta_A^0 + \beta_B^0) S_{ik} \quad \text{Equation (5-2)}$$

$$H^\pi = \frac{1}{2} K (\beta_A^0 + \beta_B^0) S_{ik} \quad \text{Equation (5-3)}$$

β_A^0 and β_B^0 are empirical bonding parameters on atoms A and B and S_{ik} is the overlap integral between orbitals ϕ_i on atom A and ϕ_k on atom B.

Electronic transitions of 4-amino-4'-nitroazobenzene [VIII] optimised in the gas phase

Transition energies for optimised structures of [VIII] are given in Table 5.3.

Table 5.3 Calculated transition energies and oscillator strengths of [VIII] using the CNDOVS method.

| Structure | K^a | Excited state | λ | f |
|-----------|-------|---------------|-----------|------|
| [VIII]a | 0.65 | 2 | 389.92 | 1.26 |
| | | 5 | 304.89 | 0.13 |
| | | 9 | 264.94 | 0.11 |
| [VIII]a | 0.58 | 2 | 425.3 | 1.14 |
| | | 5 | 332.1 | 0.09 |
| | | 8 | 289.5 | 0.07 |
| [VIII]b | 0.65 | 2 | 396.5 | 1.14 |
| | | 4 | 303.7 | 0.11 |
| | | 9 | 261.6 | 0.12 |
| [VIII]b | 0.58 | 2 | 433.3 | 1.02 |
| | | 5 | 331.6 | 0.07 |
| | | 9 | 289.6 | 0.16 |

^a K is the spectroscopic constant. ^b λ is the wavelength in nm. ^c f is the oscillator strength. [VIII]a is an AM1 gas phase optimised structure with heavy atoms constrained to lie in the same plane. [VIII]b is constructed from the crystal structure HOMEW^d.

The transitions of the constrained AM1 gas phase structure [VIII]b are made up predominantly of the excitations given in Equation (5-4)-Equation (5-6).

$$S_1 = \psi_2 = 0.97\phi_{45-46} \quad \text{Equation (5-4)}$$

$$S_2 = \psi_5 = -0.23\phi_{40-46} - 0.94\phi_{45-49} \quad \text{Equation (5-5)}$$

$$S_3 = \psi_9 = -0.83\phi_{43-46} - 0.45\phi_{45-47} \quad \text{Equation (5-6)}$$

The first excited state S_1 arises from a HOMO to LUMO (45-46) excitation with S_2 and S_3 made up primarily excitations from molecular orbitals 45-49 and 43-46 respectively. An analysis of the contributions to molecular orbitals from each atom showed that the HOMO and LUMO orbitals, 45 and 46, are exclusively π in character and therefore the 45-46 transition is $\pi-\pi^*$. The second and third transitions involve orbitals occupied orbitals 40, 43, 45 and unoccupied orbitals 47 and 49. All

of these molecular orbitals contain only p_z atomic orbital contributions and thus all transitions involved in states S_1 , S_2 and S_3 are π - π^* in nature.

Electronic transitions in 4-(N- β -hydroxyethyl, N-ethyl)amino-4'-nitroazobenzene [IX]

The transition energies and oscillator strengths are predicted by the CNDOVS program for the constrained planar AM1 optimised structure of [IX] as shown in Table 5.4.

Table 5.4 Calculated transition energies and oscillator strengths of [IX] using the CNDOVS method ($K=0.65$).

| State | λ/nm | f |
|-------|---------------------|------|
| 2 | 418.8 | 1.22 |
| 3 | 326.4 | 0.12 |
| 9 | 277.3 | 0.22 |
| 11 | 258.9 | 0.14 |

The states S_1 , S_2 and S_3 are primarily made up of the excitations given in Equation (5-7) to Equation (5-8).

$$S_1 = \psi_2 = 0.97\phi_{60-61} \quad \text{Equation (5-7)}$$

$$S_2 = \psi_3 = -0.97\phi_{60-64} \quad \text{Equation (5-8)}$$

$$S_3 = \psi_9 = -0.89\phi_{58-61} + 0.29\phi_{60-62} \quad \text{Equation (5-9)}$$

$$S_4 = \psi_{11} = -0.81\phi_{55-61} - 0.43\phi_{60-63} + 0.22\phi_{60-65} \quad \text{Equation (5-10)}$$

An analysis of the atomic orbital coefficients of each molecular orbital involved in the electronic transitions of this planar conformation of [IX] showed that coefficients involving p_x or p_y orbitals were close to zero and molecular orbitals were made up from p_z components. This implies that the molecular orbitals have π -type character and all the transitions are π - π^* in nature.

The results for the planar structures of 4-amino-4'-nitroazobenzene [VIII] and 4-(N- β -hydroxyethyl, N-ethyl)amino-4'-nitroazobenzene [IX] indicate that only π - π^* transitions are predicted to have significant oscillator strength, with transitions involving the molecular orbital of n-type character, having a low oscillator strength and consequently low probability of occurring. However, the CNDOVS method predicts some probability of n- π^* transitions occurring in non-planar structures.

The greater the degree of twisting of the phenyl rings out of the plane, the greater the involvement of

$n-\pi^*$ transitions. This can be explained in terms of overlap between the phenyl ring π -systems and the lone pair electrons of the azo nitrogen atoms. In a planar molecule, the lone pairs are orthogonal to the π -system, but as the molecule is twisted, the lone pairs can partially overlap with the phenyl ring π -systems. Overlap with the azo π electrons is subsequently decreased. The electronic transitions of these donor acceptor dyes involve a HOMO-LUMO transition for the first excited state and a HOMO to LUMO+4 transition for the second excited state. The groups attached to the amino nitrogen have quite a significant effect on the calculated wavelength of donor acceptor azobenzenes and replacement of the amino group in [VIII] by the aminoalkyl group, as in 4-(N- β -hydroxyethyl, N-ethyl)amino-4'-nitroazobenzene [IX] and 4-diethylamino-4'-nitroazobenzene [X] results in a bathochromic shift of around 30nm.

Introducing an additional electron donating substituent into the donor phenyl ring has the effect of shifting the transition energies of dyes to longer wavelengths, as is exemplified by the thiomethyl substituted dye, [I], which has a calculated transition energy of 450nm ($K=0.65$) compared to an experimental value of 471nm obtained in cyclohexane. The bathochromic shift produced by additional electron withdrawing substituents on the acceptor phenyl ring is also reproduced in calculated spectra.

Table 5.5 Calculated spectra ($K=0.65$) for constrained AM1 optimised and freely AM1 optimised structures of [I].

| Structure | Constrained optimised | | Free optimised | |
|--------------------|-----------------------|------|---------------------|------|
| State | λ/nm | f | λ/nm | f |
| 2 = S ₁ | 450 | 0.81 | 433 | 0.71 |
| 3 = S ₂ | 372 | 0.30 | 366 | 0.22 |
| 4 = S ₃ | 351 | 0.52 | 349 | 0.63 |
| 5 = S ₄ | 308 | 0.11 | 308 | 0.10 |

The contributions of specific electronic transitions to each state S₁, S₂ and S₃ for the planar structure ((Equation (5-11) to Equation (5-13)) showed that the visible absorption band, at 450nm, is comprised mainly of a HOMO→LUMO transition whereas the bands at 372 and 351nm involve predominantly HOMO-1→LUMO and HOMO→LUMO+1 transitions respectively.

$$S_1 = 0.96\phi_{63-64} + 0.18\phi_{62-64} - 0.12\phi_{62-65} - 0.12\phi_{63-66} - 0.11\phi_{63-65} \quad \text{Equation (5-11)}$$

$$S_2 = -0.87\phi_{62-64} - 0.32\phi_{63-65} + 0.23\phi_{62-65} - 0.17\phi_{63-64} - 0.16\phi_{63-66} \quad \text{Equation (5-12)}$$

$$S_3 = 0.83\phi_{63-65} + 0.29\phi_{63-66} - 0.33\phi_{62-64} + 0.12\phi_{63-64} \quad \text{Equation (5-13)}$$

The same electronic transitions (see Equation (5-14) to Equation (5-16)) are involved in the absorption bands at 433, 366 and 349nm of the non-planar, freely optimised structure, where the acceptor phenyl ring is twisted by *ca.* 30° to the plane of the phenylazo group

$$S_1 = -0.94\phi_{63-64} + 0.20\phi_{62-64} - 0.14\phi_{63-65} + 0.13\phi_{62-65} - 0.11\phi_{63-66} \quad \text{Equation (5-14)}$$

$$S_2 = +0.87\phi_{62-64} + 0.42\phi_{63-65} + 0.26\phi_{63-66} + 0.25\phi_{62-65} - 0.16\phi_{63-64} \quad \text{Equation (5-15)}$$

$$S_3 = 0.72\phi_{63-65} - 0.45\phi_{62-64} - 0.21\phi_{63-68} + 0.15\phi_{63-64} - 0.11\phi_{62-65} \quad \text{Equation (5-16)}$$

An analysis of the atomic orbital coefficients for molecular orbitals 62-66 showed that molecular orbitals are comprised essentially of p_z components in both structures. There is a large p_z component originating from the amino nitrogen atom and also from the sulphur atom. There is also a small contribution to orbitals 63-66 from d_z orbital coefficients of sulphur. The non-planar structure has only very small contributions to molecular orbitals from p_x and p_x orbitals, which contrasts with the large components of these orbitals in molecular orbitals of azobenzene, indicating n-type character. It must be noted however, that the CNDOVS method is not reliable for predicting $n-\pi^*$ transitions.

Azothiophene systems

The effect of replacing the acceptor phenyl ring by a heterocyclic thiophene ring has a pronounced effect on the predicted electronic transitions, with a large bathochromic shift observed relative to the azobenzene type dyes. The calculated transition energies for the visible absorption band are compared to experimental wavelengths in cyclohexane in (Table 5.6). In general the correlation between experimental data and calculated transition energies of the azo dyes examined in this work is very good (Figure 5.4), although the predicted transition energies of dyes with experimental absorption maxima in the region of 600nm is significantly underestimated. Excellent correlations have been found by Morley^{18,19} between experimental data and transition energies calculated using spectroscopic constant ($K=0.46$) for a heavily substituted azobenzene similar to [XVII] and the azothiophene dye [XV].

Table 5.6 Comparison of experimental data with calculated transition energies for the visible absorption maxima of planar AM1 structures of [I]-[XIX], listed in order of increasing λ_{max} in cyclohexane.

| Dye | λ_{max} order | $\lambda/\text{nm}^{\text{a}}$ | $\lambda/\text{nm}^{\text{b}}$ | $\lambda/\text{nm}^{\text{c}}$ |
|---------|------------------------------|--------------------------------|--------------------------------|--------------------------------|
| [VIII] | 1 | 389.9 | 425.3 | 395 |
| [XIV] | 2 | 402.1 | 410.5 | 400 |
| [XI] | 3 | 411.6 | 449.2 | 409 |
| [III] | 4 | 411.2 | 443 | 420 |
| [VII] | 5 | 414.6 | 446.3 | 423 |
| [IV] | 6 | 414.2 | 446 | 424 |
| [XII] | 7 | 410.5 | 443.6 | 434 |
| [II] | 8 | 424.9 | 456.6 | 433 |
| [VI] | 9 | 427.0 | 458.9 | 435 |
| [IX] | 10 | 418.8 | 452.0 | 447 |
| [X] | 11 | 418.2 | 451.8 | 457 |
| [V] | 12 | 430.9 | 465.0 | 461 |
| [XIII] | 13 | 430.81 | 463.0 | 471 |
| [I] | 14 | 450.3 | 482.4 | 470 |
| [XV] | 15 | 490.7 | 528.3 | 561 |
| [XVIII] | 17 | 477.7 | 514.9 | 564 |
| [XVII] | 18 | 480.3 | 518.3 | 600 |
| [XVI] | 19 | 525.6 | 568.8 | 606 |

^a Transition energies calculated using the CNDOVS method with the spectroscopic constant at 0.65.

^b Spectroscopic constant set at 0.58. ^c Experimentally determined λ_{max} values, obtained in cyclohexane.

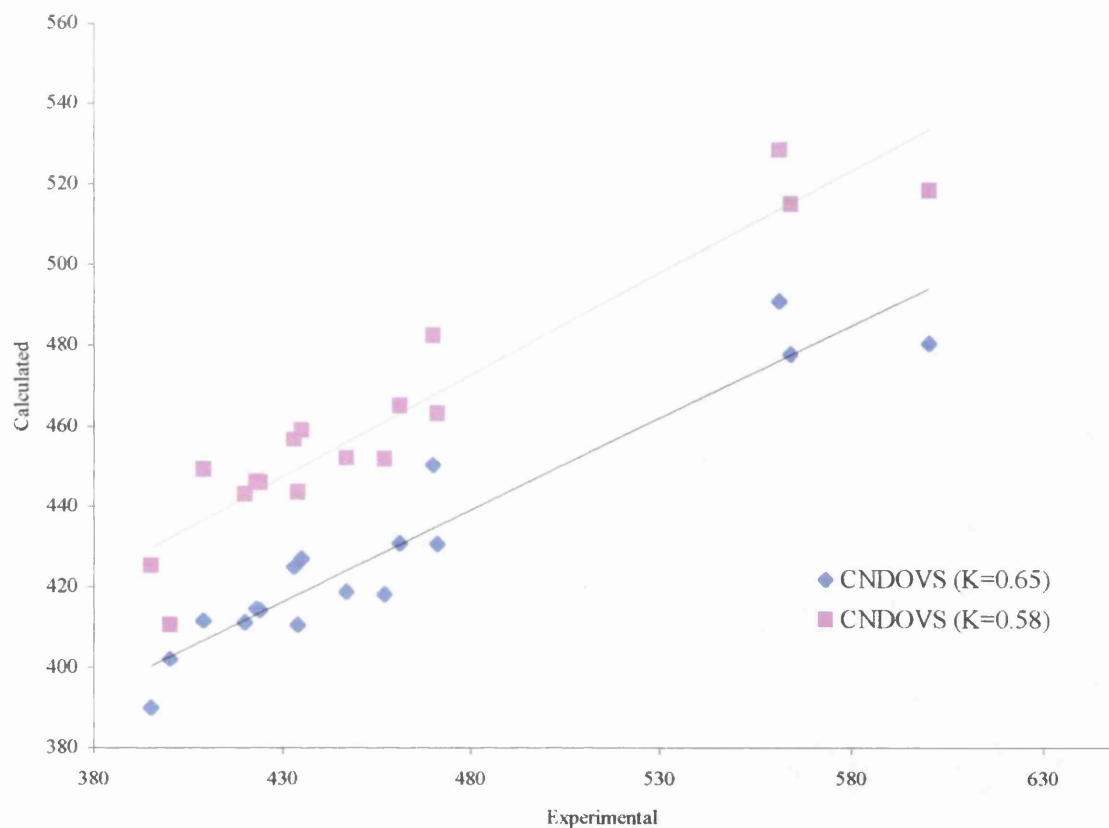


Figure 5.4 Experimental absorption energies (λ , nm) obtained in cyclohexane versus absorption energies (nm) calculated using the CNDOVS method with the spectroscopic constant set at 0.65 and 0.58.

The effect of geometry on transition energies

The calculated transition energies of planar AM1 structures have a much better correlation with experimental spectroscopic data than the twisted AM1 structures (see Table 5.7), which produce shorter wavelengths, suggesting that in solution the geometry of the dyes are likely to be planar.

As well as the degree of twisting in dye structures, the length of the azo $-N=N-$ bond is critical in the calculation of transition energies as was previously established by Charlton et al¹⁶. Crystal structures of donor acceptor type azobenzenes (see Table 4.1), have $N=N$ bond lengths in the range of 1.25 to 1.29 Å, whereas the bond length in semi-empirical structures calculated in this work and in previous work by Charlton and Morley et al., is between 1.23 and 1.24 Å¹⁶. Morley also calculated a bond length of 1.278 for 4-dimethyl-4'-nitroazobenzene at the ab initio STO-3G level, but calculations in this work using the 3-21G and 6-31G basis sets gave shorter bond lengths of 1.244 Å. Spectroscopic calculations on a planar AM1 structure of [IX] with a bond length of 1.233 Å gave a transition energy of 420.8 nm (454.1 nm; $K = 0.58$; 200 states), while a structure with a modified $N=N$ bond

length of 1.27 Å, gave a transition energy of 437nm (470nm; $K = 0.58$; 200 states) which is even closer to the experimental value of 447nm.

Table 5.7 Transition energies and oscillator strengths for planar and non-planar conformations of dyes calculated using the CNDOVS method.

| Dye | Geometry | λ/nm^a | f^c | λ/nm^b | f^c |
|--------|----------|-----------------------|-------|-----------------------|-------|
| [XI] | Planar | 416.2 | 1.39 | 449.2 | 1.23 |
| [XI] | twisted | 405.7 | 1.34 | 438.1 | 1.19 |
| [XIV] | Planar | 403.4 | 1.16 | 433.8 | 1.06 |
| [XIV] | twisted | 395.4 | 1.16 | 426.6 | 1.06 |
| [IV] | Planar | 416.0 | 1.57 | 446.0 | 1.03 |
| [IV] | twisted | 386.0 | 1.01 | - | - |
| [VIII] | Planar | 391.4 | 1.27 | 425.3 | 1.14 |
| [VIII] | Twisted | 379.7 | 1.26 | 415.0 | 1.14 |
| [IX] | Planar | 420.8 | 1.23 | 452.0 | 1.12 |
| [IX] | twisted | 409.6 | 1.21 | 442.7 | 1.11 |
| [XV] | Planar | 493.5 | 1.02 | 528.3 | 0.98 |
| [XV] | twisted | 453.8 | 0.753 | 485.6 | 0.67 |

^a Calculated using $K = 0.65$. ^b Calculated using $K = 0.58$

Multi-electron configuration interaction (C.I.)

The excited states examined so far have used the single electron C.I. CNDOVS method to give the transition energies and oscillator strengths from the ground state to each excited state. Analysis of each excited state has also revealed the molecular orbital transitions involved in each excited state and the atomic orbital contributions to each molecular orbital. The atomic orbital contributions were used to designate molecular orbitals as n-type or π -type in character.

The above information, with the exception of predicted oscillator strengths, can be generated also from AM1 C.I. calculations. The multi electron configuration interaction or MECI calculations involve both single and double excitations of electrons (single electronic excitations involve the excitation of one electron only, whereas double electronic excitations involve the simultaneous excitation of two electrons). The inclusion of these double excitations has the effect of lowering the heat of formation of the excited state. The level of stabilisation can be ascertained by restricting the calculation to include only single excitations by including the keyword CIS. If this keyword is omitted then the both single and double excitations are included by default. The energy penalty when using only single excitations is very high compared to single plus double excitations for the first excited state and for the second excited state, because only a very small number of orbitals are involved. Triplet states can also be calculated with the MECI treatment. The effects of solvent on the ground and excited states of molecules can be simulated in these calculations using the COSMO method. It is not possible to simulate these effects using CNDOVS.

The MECI treatment of 4-(N-hydroxyethyl, N-ethyl)amino-4'-nitroazobenzene [IX] predicts the energies of excited singlet and triplet states relative to the ground state, S_0 (see Table 5.8). The lowest energy excited state is a triplet (T_1). The next lowest state is a singlet (S_1) followed by two triplet states, T_2 and T_3 , which are calculated to be lower in energy than the second excited singlet state S_2 . 4-(N-hydroxyethyl, N-ethyl)amino-4'-nitroazobenzene has 120 valence electrons and therefore has 60 doubly occupied molecular orbitals. Orbital 60 is thus the HOMO with orbital 59 the HOMO-1 and orbital 58 the HOMO-2. The unoccupied molecular orbitals 61, 62 and 63 are assigned as the LUMO, LUMO+1 and LUMO+2 respectively. To examine how the level of CI may affect the results for these calculations, the results of calculations on [IX] using C.I = 4 and C.I. = 6 are compared.

Table 5.8 The first six states produced by a MECI (C.I.= 4) calculation on [IX].

| State | Spin | Relative energy (eV) | |
|-------|---------|----------------------|----------------|
| 1 | Singlet | 0 | S ₀ |
| 2 | Triplet | 2.71 | T ₁ |
| 3 | Singlet | 3.37 | S ₁ |
| 4 | Triplet | 4.11 | T ₂ |
| 5 | Triplet | 4.81 | T ₃ |
| 6 | Singlet | 4.85 | S ₂ |

The wave functions for each state, can be written in terms of the electronic transitions that contribute to each state. These transitions are represented by ψ_m , where m is the electronic configuration from each transition. The wave functions for the first five states are given in equations Equation (5-17) to Equation (5-22). The magnitude of the coefficient in front of each transition ψ_m determines the contribution of that transition state. For example, the first state S₀, is almost exclusively ψ_1 , whereas the second state T₁, has contributions from the transitions ψ_2 , ψ_7 , ψ_3 , ψ_{13} , ψ_4 and ψ_{19} . Only transitions which have coefficients larger than ± 0.1 are reported, as contributions from transitions with coefficients smaller than this are not of major significance to the state wavefunction and are too numerous to list as pointed out previously.

$$S_0 = -0.99\psi_1 \quad \text{Equation (5-17)}$$

$$T_1 = 0.55\psi_2 + 0.39\psi_3 + 0.19\psi_4 + 0.55\psi_7 + 0.39\psi_{13} + 0.19\psi_{19} \quad \text{Equation (5-18)}$$

$$S_1 = -0.61\psi_2 - 0.29\psi_3 - 0.15\psi_4 - 0.11\psi_8 + 0.61\psi_7 + 0.29\psi_{13} + 0.15\psi_{19} \quad \text{Equation (5-19)}$$

$$T_2 = -0.41\psi_3 + 0.56\psi_4 - 0.41\psi_{13} + 0.56\psi_{19} \quad \text{Equation (5-20)}$$

$$T_3 = 0.37\psi_2 - 0.38\psi_3 - 0.34\psi_4 - 0.22\psi_5 - 0.17\psi_6 + 0.37\psi_7 - 0.38\psi_{13} - 0.34\psi_{19} - 0.22\psi_{25} - 0.17\psi_{31} \quad \text{Equation (5-21)}$$

$$S_2 = -0.24\psi_2 - 0.60\psi_3 - 0.16\psi_5 - 0.13\psi_6 + 0.11\psi_{10} + 0.13\psi_8 + 0.24\psi_7 + 0.60\psi_{13} + 0.16\psi_{25} - 0.13\psi_{31} - 0.11\psi_{20} \quad \text{Equation (5-22)}$$

A C.I. = 4 level calculation involves electronic transitions between two highest molecular orbitals and the two lowest unoccupied molecular orbitals, leading to 36 possible microstates or

configurations. There are 20 singlets, 15 triplets and 1 quintet, produced by this evaluation. The electrons and orbitals involved in each transition ψ_m in Equation (5-17) to Equation (5-22) are illustrated in Table 5.9. It is obvious from Table 5.9 that the transitions ψ_2 and ψ_7 involve the excitation of electron 1 and electron 2 respectively, of the doubly occupied molecular orbital, but are otherwise identical as both involve a HOMO→LUMO transition. As such these transitions are energetically equivalent. The configurations ψ_3 and ψ_{13} are similarly equivalent as are many of the other configurations involved in each excited state wavefunction. Equivalent configurations are therefore grouped together. Note that the numbering system for electronic configurations was assigned arbitrarily by the MECI calculation and does not indicate the order of energy for configurations. The representation of the electronic configurations produced in the MOPAC output of the MECI calculation²⁰ (Table 5.9) gives no indication of the spin multiplicity. It should be pointed out therefore, that in the wavefunction of triplet states, the coefficients in front of energetically equivalent configurations have the same sign, indicating that the spins of the unpaired electrons are the same, whereas in singlet states the coefficients have opposite signs, indicating that unpaired electrons have opposite spins.

Table 5.9 Electronic configurations involved in the first six states produced by the MECI (C.I.=4) treatment of [IX] in order of energy before configuration interaction.²⁰

| M.O | Energy | 59 | 60 | 61 | 62 | Energy | 59 | 60 | 61 | 62 | |
|-------------|--------|----|----|----|----|-------------|-------|----|----|----|---|
| ψ_1 | 0 | 1 | 1 | 0 | 0 | | | | | | |
| | | 1 | 1 | 0 | 0 | | | | | | |
| ψ_2 | 4.07 | 1 | 1 | 0 | 0 | ψ_7 | 4.07 | 1 | 0 | 1 | 0 |
| | | 1 | 0 | 1 | 0 | | | 1 | 1 | 0 | 0 |
| ψ_3 | 4.54 | 1 | 1 | 0 | 0 | ψ_{13} | 4.54 | 1 | 0 | 0 | 1 |
| | | 1 | 0 | 0 | 1 | | | 1 | 1 | 0 | 0 |
| ψ_4 | 4.75 | 1 | 1 | 0 | 0 | ψ_{19} | 4.75 | 0 | 1 | 1 | 0 |
| | | 0 | 1 | 1 | 0 | | | 1 | 1 | 0 | 0 |
| ψ_5 | 6.06 | 1 | 1 | 0 | 0 | ψ_{25} | 6.06 | 0 | 1 | 0 | 1 |
| | | 0 | 1 | 0 | 1 | | | 1 | 1 | 0 | 0 |
| ψ_6 | 8.97 | 1 | 1 | 0 | 0 | ψ_{31} | 8.97 | 0 | 0 | 1 | 1 |
| | | 0 | 0 | 1 | 1 | | | 1 | 1 | 0 | 0 |
| ψ_{10} | 10.48 | 1 | 0 | 1 | 0 | ψ_{20} | 10.48 | 0 | 1 | 1 | 0 |
| | | 0 | 1 | 1 | 0 | | | 1 | 0 | 1 | 0 |
| ψ_8 | 12.99 | 1 | 0 | 1 | 0 | | | | | | |
| | | 1 | 0 | 1 | 0 | | | | | | |

The T_1 triplet state is predominantly comprised of the states ψ_2 and ψ_7 involving orbitals 60 and 61, that is a HOMO→LUMO transition. The first excited singlet state S_1 is also made up largely from a HOMO→LUMO transition, but also contains contributions from HOMO→LUMO+1 and LUMO-1→HOMO. The next state T_2 involves the HOMO→LUMO+1 and LUMO-1→HOMO transitions, while T_3 also involves the HOMO→LUMO, HOMO-1→LUMO+1 transitions and contributions from ψ_6 and ψ_{31} , which are configurations involving double excitations. The second excited singlet state, S_2 , has a large HOMO→LUMO+1 component and smaller components from both single and double excitations.

An analysis of the atomic orbital coefficients of these molecular orbitals showed that only the p_z components were significant and all other components were close to zero, indicating that all four orbitals have π character and thus all electronic transitions may be assigned as π - π^* .

The C.I.=4 calculation only involves the two highest occupied and two lowest unoccupied orbitals, and may therefore be inadequate for the determination of the second excited state, as this state may involve contributions from transitions involving other orbitals. Increasing the level of CI to C.I. = 6 to include the HOMO-2 and LUMO+2 orbitals increases the number of microstates calculated to 400, and should give a more reliable prediction of this state. The results for the C.I. = 6 calculation on the AM1 optimised structure of [IX] are now examined. The first six states and their energies relative to the ground state are given in Table 5.10.

Table 5.10 The first six states produced by a MECI (C.I. = 6) calculation on [IX].

| State | Spin | Relative energy (eV) | |
|-------|---------|----------------------|-------|
| 1 | Singlet | 0 | S_0 |
| 2 | Triplet | 2.67 | T_1 |
| 3 | Singlet | 3.32 | S_1 |
| 4 | Triplet | 3.94 | T_2 |
| 5 | Triplet | 4.35 | T_3 |
| 6 | Singlet | 4.60 | T_4 |
| 7 | Singlet | 4.72 | S_2 |

The C.I. = 6 calculation produces the following wavefunction for each excited state:

$$S_0 = -0.99\psi_1 \quad \text{Equation (5-23)}$$

$$T_1 = \begin{matrix} -0.55\psi_2 & -0.37\psi_3 & -0.21\psi_5 \\ -0.55\psi_{21} & -0.37\psi_{13} & -0.21\psi_{81} \end{matrix} \quad \text{Equation (5-24)}$$

$$S_1 = \begin{matrix} +0.61\psi_2 & +0.27\psi_3 & +0.16\psi_5 & +0.11\psi_{22} \\ -0.61\psi_{21} & -0.27\psi_{41} & -0.16\psi_{81} & \end{matrix} \quad \text{Equation (5-25)}$$

$$T_2 = \begin{matrix} -0.43\psi_3 & +0.51\psi_5 & -0.19\psi_{11} \\ -0.41\psi_{43} & +0.51\psi_{81} & -0.19\psi_{201} \end{matrix} \quad \text{Equation (5-26)}$$

$$T_3 = \begin{matrix} 0.19\psi_5 & -0.17\psi_6 & -0.49\psi_{11} & -0.42\psi_{12} \\ +0.19\psi_{81} & -0.17\psi_{101} & -0.49\psi_{201} & -0.42\psi_{221} \end{matrix} \quad \text{Equation (5-27)}$$

$$T_4 = \begin{matrix} -0.47\psi_4 & -0.48\psi_7 & +0.19\psi_{13} \\ -0.47\psi_{61} & -0.48\psi_{121} & +0.19\psi_{241} \end{matrix} \quad \text{Equation (5-28)}$$

$$S_2 = \begin{matrix} +0.20\psi_2 & -0.59\psi_3 & -0.15\psi_6 & +0.13\psi_8 & +0.11\psi_{12} & -0.13\psi_{25} \\ -0.20\psi_{21} & -0.59\psi_{41} & +0.15\psi_{101} & -0.13\psi_{141} & -0.11\psi_{221} & +0.13\psi_{82} \end{matrix} \quad \text{Equation (5-29)}$$

The electronic configurations contributing to each state are displayed in Table 5.11.

Table 5.11 Electronic configurations involved in the first seven states produced by the MECI (C.I.=6) treatment of [IX] in order of energy before configuration interaction.²⁰

| M.O Energy (eV) | 58 | 59 | 60 | 61 | 62 | 63 | M.O Energy (eV) | 58 | 59 | 60 | 61 | 62 | 63 | |
|-----------------|-------|----|----|----|----|----|-----------------|-------|----|----|----|----|----|---|
| ψ_1 | 0.00 | 1 | 1 | 1 | 0 | 0 | | | | | | | | |
| | | 1 | 1 | 1 | 0 | 0 | | | | | | | | |
| ψ_2 | 4.07 | 1 | 1 | 1 | 0 | 0 | ψ_{21} | 4.07 | 1 | 1 | 0 | 1 | 0 | 0 |
| | | 1 | 1 | 0 | 1 | 0 | | | 1 | 1 | 1 | 0 | 0 | 0 |
| ψ_3 | 4.54 | 1 | 1 | 1 | 0 | 0 | ψ_{41} | 4.54 | 1 | 1 | 0 | 0 | 1 | 0 |
| | | 1 | 1 | 0 | 0 | 1 | | | 1 | 1 | 1 | 0 | 0 | 0 |
| ψ_5 | 4.75 | 1 | 1 | 1 | 0 | 0 | ψ_{81} | 4.75 | 1 | 0 | 1 | 1 | 0 | 0 |
| | | 1 | 0 | 1 | 1 | 0 | | | 1 | 1 | 1 | 0 | 0 | 0 |
| ψ_{11} | 5.66 | 1 | 1 | 1 | 0 | 0 | ψ_{201} | 5.66 | 0 | 1 | 1 | 1 | 0 | 0 |
| | | 0 | 1 | 1 | 1 | 0 | | | 1 | 1 | 1 | 0 | 0 | 0 |
| ψ_{12} | 6.02 | 1 | 1 | 1 | 0 | 0 | ψ_{221} | 6.02 | 0 | 1 | 1 | 0 | 1 | 0 |
| | | 0 | 1 | 1 | 0 | 1 | | | 1 | 1 | 1 | 0 | 0 | 0 |
| ψ_6 | 6.06 | 1 | 1 | 1 | 0 | 0 | ψ_{101} | 6.06 | 1 | 0 | 1 | 0 | 1 | 0 |
| | | 1 | 0 | 1 | 0 | 1 | | | 1 | 1 | 1 | 0 | 0 | 0 |
| ψ_7 | 6.07 | 1 | 1 | 1 | 0 | 0 | ψ_{121} | 6.07 | 1 | 0 | 1 | 0 | 0 | 1 |
| | | 1 | 0 | 1 | 0 | 1 | | | 1 | 1 | 1 | 0 | 0 | 0 |
| ψ_4 | 6.07 | 1 | 1 | 1 | 0 | 0 | ψ_{61} | 6.07 | 1 | 1 | 0 | 0 | 0 | 1 |
| | | 1 | 1 | 0 | 0 | 1 | | | 1 | 1 | 1 | 0 | 0 | 0 |
| ψ_{13} | 7.69 | 1 | 1 | 1 | 0 | 0 | ψ_{241} | 7.69 | 0 | 1 | 1 | 0 | 0 | 1 |
| | | 0 | 1 | 1 | 0 | 1 | | | 1 | 1 | 1 | 0 | 0 | 0 |
| ψ_8 | 8.97 | 1 | 1 | 1 | 0 | 0 | ψ_{141} | 8.97 | 1 | 1 | 1 | 0 | 0 | 0 |
| | | 1 | 0 | 0 | 1 | 1 | | | 1 | 0 | 0 | 1 | 1 | 0 |
| ψ_{25} | 10.48 | 1 | 1 | 0 | 1 | 0 | ψ_{82} | 10.48 | 1 | 0 | 1 | 1 | 0 | 0 |
| | | 1 | 0 | 1 | 1 | 0 | | | 1 | 1 | 0 | 1 | 0 | 0 |
| ψ_{22} | 12.99 | 1 | 1 | 0 | 1 | 0 | | | | | | | | |
| | | 1 | 1 | 0 | 1 | 0 | | | | | | | | |

As in the C.I.= 4 treatment of [IX], the lowest energy excited state was a triplet, followed by the first excited singlet S_1 . However, the C.I.=6 calculation predicted that the next three states were triplets T_2 , T_3 and T_4 , all of which were lower in energy than the second singlet S_2 . The T_1 and S_1 states were predominantly comprised of HOMO-LUMO and HOMO \rightarrow LUMO+1 transitions, as before. The T_2 state arose mainly from a HOMO \rightarrow LUMO+1 and HOMO-1 \rightarrow LUMO, T_3 is composed of HOMO-2 \rightarrow LUMO and HOMO-2 \rightarrow LUMO+1, and T_4 has contributions from HOMO \rightarrow LUMO+2 and HOMO-1 \rightarrow LUMO+2 transitions. The S_2 state is primarily composed of a HOMO \rightarrow LUMO+1 transition. There are obviously several differences in both the order of the excited states and the transitions involved in these states using different levels of C.I.

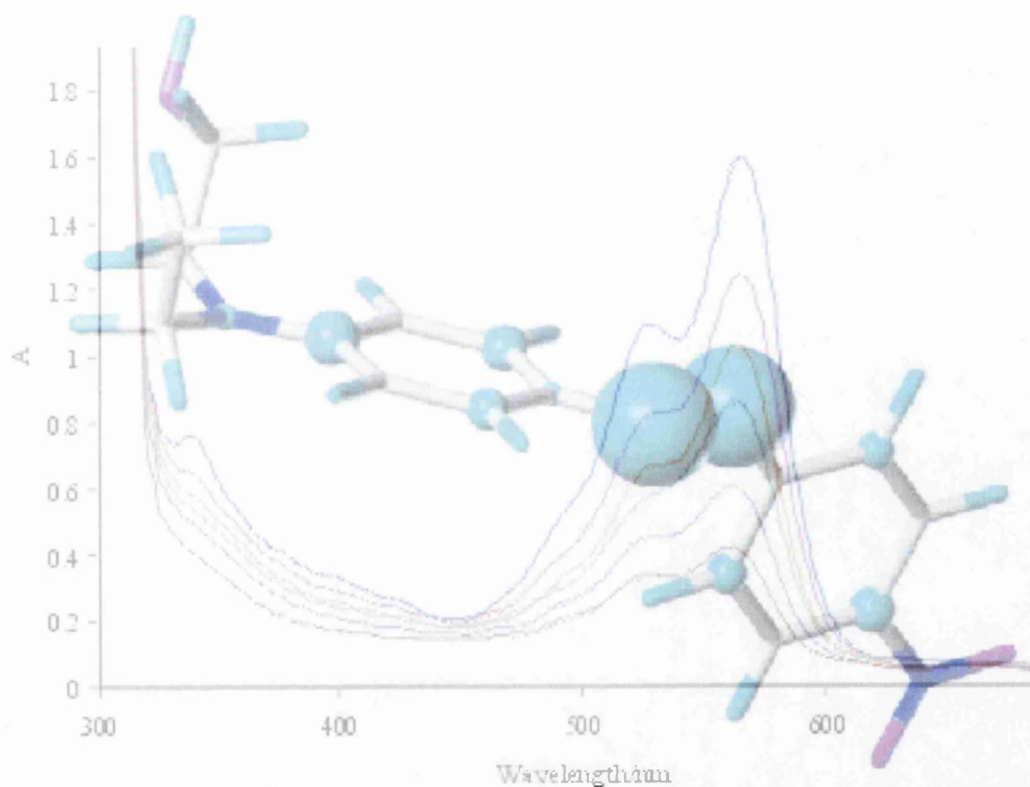
An analysis of the atomic orbital coefficients of the individual atoms involved in molecular orbitals 58-63, showed that as before, only the p_z component was significant, implying that all the transitions involved in these states were π - π^* in nature.

References

- ¹ H. Rau, E. Luddecke, *J. Am. Chem. Soc.*, **104** (1982) 1616.
- ² H. Gorner; H. Gruen and D. Schulte-Frohllnde, *J. Phys. Chem.*, **84** (1980) 3031.
- ³ B. Nandita and S. Umpathy, *J. Phys. Chem. A.*, **101** (1997) 5555.
- ⁴ Cambridge Structural Database, Cambridge Crystallographic Data Centre, University Chemical Laboratory, Lensfield Road, Cambridge, CB2 2EW, UK.
- ⁵ A. Shaabani, M. Zahedi, *Journal of Molecular structure (Theochem)*., **506** (2000) 257.
- ⁶ K. Matczyszyn, W. Bartkowiak, J. Leszczynski. *Journal of Molecular structure.*, **565-566** (2001) 53.
- ⁷ E.A. Kramer, *CHIMIA.*, **40** (1986) 160 and references therein.
- ⁸ S. Kirk, T. Flemming Mattox and D.G. Whitten, *J. Org. Chem.* **48** (1983) 2808.
- ⁹ O. Kikuchi , M. Azuki, Y Inadomi, K. Morihashi, *J. Molecular Structure (Theochem)*., **468** (1999) 95.
- ¹⁰ J. Del Bene and H.H. Jaffe, *J. Chem. Phys.*, **48** (1968) 1807
- ¹¹ J. Griffiths, *Color and Constitution of Organic Molecules*, Academic Press (1976) 180, and references therein.
- ¹² J. Fabian , H. Hartmann; *Light Absorption of Organic Colourants*: Publ. Springer-Verlag (1980) Chapter 7 and references therein.
- ¹³ R. Akaba, K. Tokumaru and T. Kobayachi, *Bull. Chem. Soc. Japan.*, **53**, (1980)1993.
- ¹⁴ M. Miracec, W. Shcmidt, S. Aurora, S. Timbe, *Rev. Roum. Chem.*
- ¹⁵ K. Wojciechowski; *Dyes and Pigments*, **33**, No.2 (1997) 149.
- ¹⁶ M.H. Charlton , R. Docherty, D.J. McGeein and J.O. Morley, *J. Chem. Soc. Faraday Trans.*, **89** (11) (1993) 1671 and references therein.
- ¹⁷ J. Del Bene and H.H. Jaffe, *J. Chem. Phys.*, **48** (1968) 1807.
- ¹⁸ J.O. Morley, *J. Mol. Struct. (Theochem)*., **362** (1996) 235.
- ¹⁹ J.O. Morley, M.G. Hutchings, J. Zyss and I. Ledoux, *J. Chem. Soc. Perkin Trans. 2.*, (1997) 1139.
- ²⁰ MOPAC 93 manual, Fuhitsu Ltd.: Tokyo Japan (1993).

Chapter 6

Calculated Dipole Moments, Transition Energies and Electronic State Properties of Azo Dyes



Chapter 6 Calculated dipole moments, transition energies and excited state properties of donor-acceptor azo dyes

The visible absorption maximum of a dye structure can be calculated, using the AM1 method in the MOPAC package, from the energy difference between its ground and first excited singlet state. As was previously mentioned, the geometry of the dye has a large effect on its electronic properties and thus both the wavelength and the dipole moment will change significantly with changes in the geometry. The length of the azo bond, the torsion angles of the phenyl rings, and the hybridisation of the amino group are all critical, with in general, a shift to longer wavelength for more planar dye structures. Slight torsional twisting of the phenyl rings causes a slight hypsochromic shift of λ_{\max} . For example, the fully AM1 optimised structure of 4-(N- β -hydroxyethyl, N-ethyl)amino-4'-nitroazobenzene [IX], which has its acceptor phenyl ring twisted out of the plane by 43° degrees has a calculated transition energy in methanol of 487nm, compared to 507nm, for a planar structure where the heavy atoms were constrained to lie in the same plane. The difference in the heats of formation between the twisted and planar ground state structures is quite small, with the freely optimised structure around 1kcal mol⁻¹ lower in energy than the planar structure. However, the planar constrained structure has a lower energy for the first excited state than the twisted structure, which results in a longer wavelength. These results are similar to those observed for transition energies of twisted and planar structures calculated using the CNDOVS method. Crystal structures of azobenzenes available on the Cambridge Structural Database¹ are essentially planar and the transition energies, calculated using a MECI treatment on planar structures, are much closer to experimental values for the visible absorption maximum obtained in solution than transition energies calculated on twisted structure. This evidence suggests that in solution, the azo dyes are likely to adopt a planar conformation. Transition energies calculated for structures where the amino group is constrained to be completely planar are bathochromically shifted with respect to structures where the amino group is sp³ hybridised. Transition energies for dyes [I]-[XIX] in the gas phase, calculated using MECI (C.I.=4), (Table 6.1) occur at much shorter wavelengths, and show a poor correlation with experimental data obtained in cyclohexane.

The calculated dipole moments for ground state AM1 structures show considerable variation with different substituents (Table 6.1). The dipole moments of the dyes are far higher than for all of the other dyes examined in this work. Dipole moments of 4'-nitro substituted dyes are similar to the value of 9.42 D calculated for the AM1 structure of 4-dimethylamino-4'-nitroazobenzene, optimised in the gas phase by Charlton et al, which overestimated the experimental value of 8.1 D in dioxane.²

Table 6.1 Transition wavelengths and ground state dipole moments of [I]-[XIX].

| Dye | μ | $\lambda_{\text{AMI}}/\text{nm}^{\text{a}}$ | $\lambda_{\text{CH}}/\text{nm}^{\text{b}}$ | Dye | μ | $\lambda_{\text{AMI}}/\text{nm}^{\text{a}}$ | $\lambda_{\text{CH}}/\text{nm}^{\text{b}}$ |
|--------|-------|---|--|---------|-------|---|--|
| [I] | 10.46 | 409.5 | 470 | [XI] | 2.17 | 363.3 | 409 |
| [II] | 4.53 | 376.4 | 433 | [XII] | 8.21 | 379.6 | 434 |
| [III] | 3.86 | 354.7 | 420 | [XIII] | 7.55 | 374.2 | 471 |
| [IV] | 4.40 | 390.1 | 424 | [XIV] | 3.03 | 365.4 | 400 |
| [V] | 4.89 | 407.9 | 461 | [XV]1 | 8.53 | 436.9 | 561 |
| [VI] | 4.80 | 380.7 | 435 | [XVI] | 7.04 | 474.6 | 606 |
| [VII] | 6.63 | 390.4 | 423 | [XVII]1 | | 449.8 | 600 |
| [VIII] | 8.40 | 384.7 | 395 | [XVIII] | | | 564 |
| [IX] | 8.20 | 378.4 | 447 | [XIX] | | | 561 |
| [X] | 9.59 | 379.6 | 457 | | | | |

^a λ is the AM1/MECI calculated transition energy ^b λ_{CH} is the experimental visible absorption maximum obtained in cyclohexane.

The effect of solvent on the long wavelength absorption of the dyes

The inclusion of a solvent parameter in the calculation has a major effect on the predicted wavelength of the dyes. The calculated λ_{max} values for some of the dyes in different solvent fields are shown in Figure 6.1 and can be compared with the corresponding experimental wavelengths (Figure 6.2).

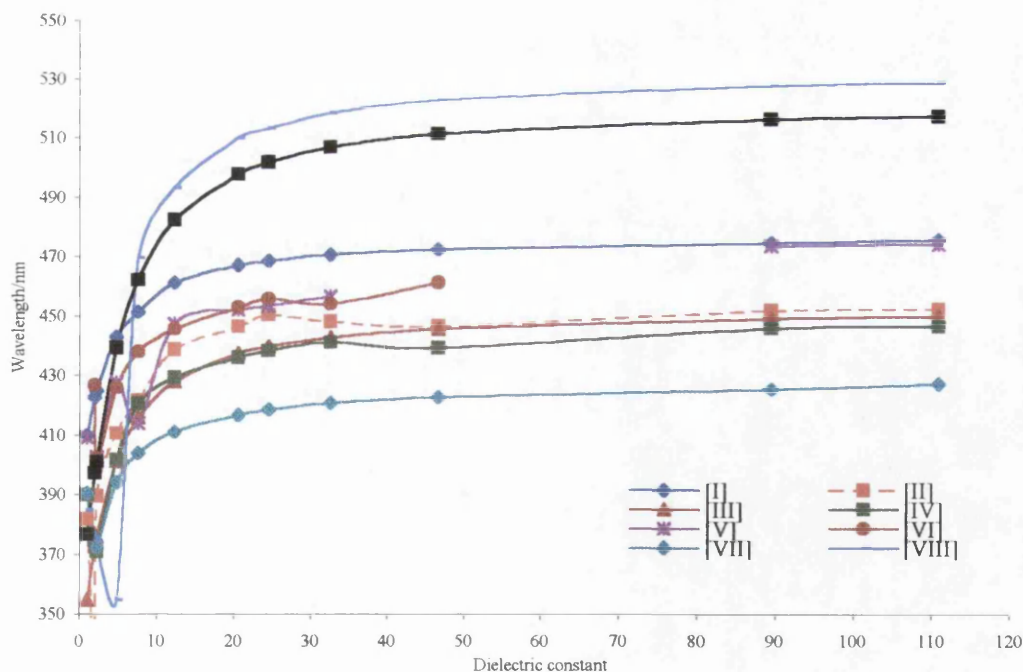


Figure 6.1 Visible absorption maxima, calculated using the AM1/COSMO C.I. method, for [I] -[IX] at different dielectric constants.

The calculated wavelengths of the dyes form a relatively smooth curve, with a large bathochromic shifts on increasing the dielectric constant through the range 2 to 24.6. Further increases in the dielectric constant produce a more gradual bathochromic shift. In contrast, the actual effect of solvents with increasing dielectric constants on the wavelengths of the dyes results in a much more erratic curve. The reason for this irregular curve is due to a dielectric effect and a separate hydrogen bonding interaction of protic solvents with the dyes (see Chapter 2). In initial theoretical calculations only the dielectric effect was explored.

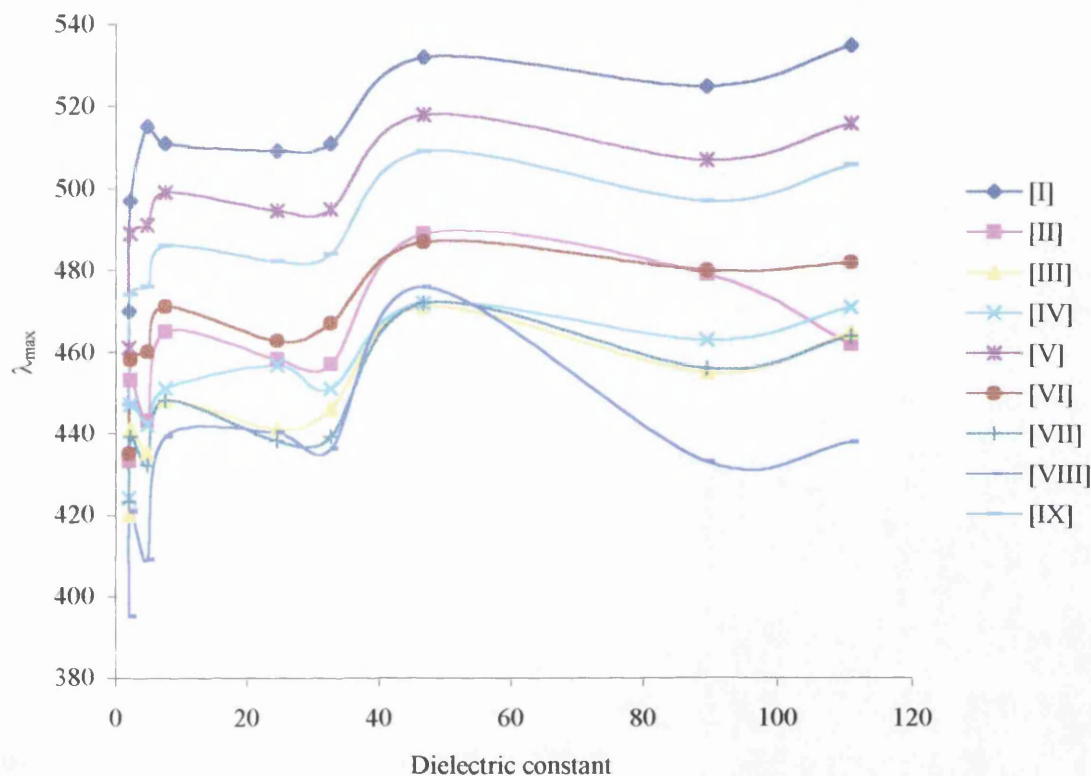


Figure 6.2 Experimental visible absorption maxima of [I] -[IX] obtained in solvents of different dielectric constant.

From inspection of the experimental data (Figure 6.2), these azo dyes are positively solvatochromic, meaning that they undergo a bathochromic shift of the long wavelength absorption band in solvents of increasing polarity. The reason for this bathochromic shift is the differential stabilisation of the excited state over the ground state of the molecule, by polar solvent. For the azo dyes, the electronic excitation of the molecule on absorption of light involves a movement of charge in the molecule creating an excited state which is more polar in character than the ground state of the molecule. As a

result, this polar excited state will be stabilised to a greater extent by polar solvents than non-polar solvents. The ground state is also slightly polar and will therefore be stabilised by polar solvent, but not to the same extent as the excited state. This explanation is illustrated by considering the change in heats of formation in of [IX] for the ground state and the excited state respectively, with increasing dielectric constant, shown in Figure 6.3.

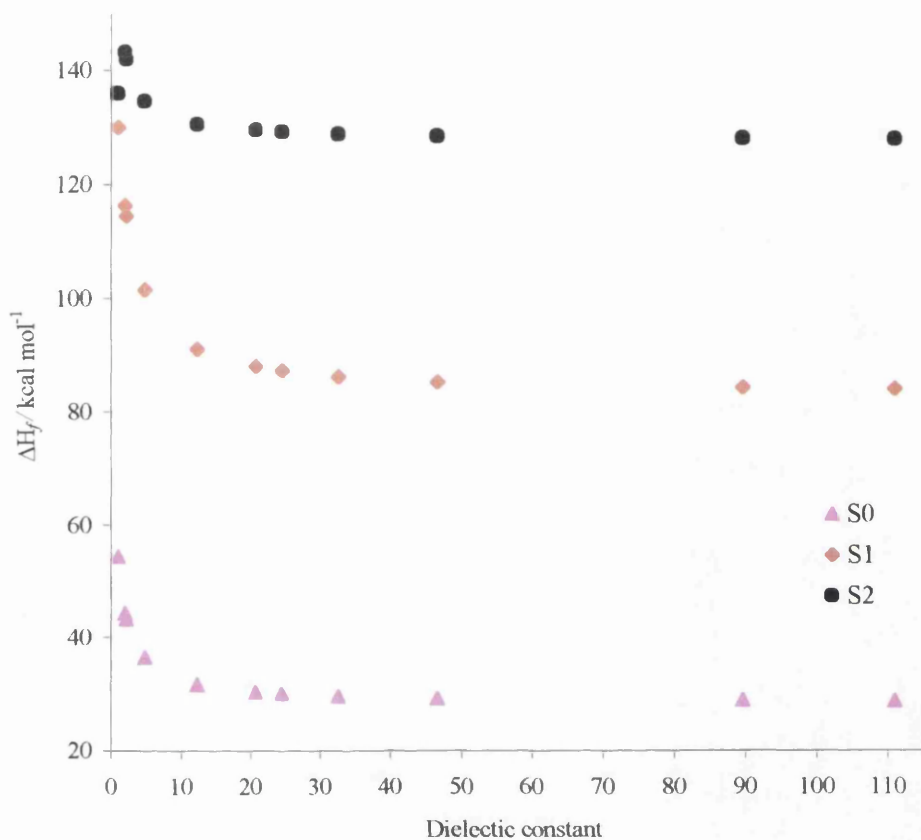


Figure 6.3 Changes in the calculated heats of formation (ΔH_f) of the ground state S_0 (see Figure 4.2), first excited singlet S_1 and second excited singlet S_2 of [IX] with increasing dielectric constant.

The ground state (discussed previously in Chapter 4) and first excited state heats of formation are increasingly stabilised in more polar solvent. The greatest increase in stability is seen at low dielectrics, after which, the increase in stability is relatively small. For the second excited singlet state, the stabilisation in more polar solvents is much less pronounced.

The correlation between experimental data and calculated transition energies is much better in solvents of high dielectric constant than in the gas phase, and the correlation between experimental and theoretical wavelengths in methanol is quite good (Figure 6.4).

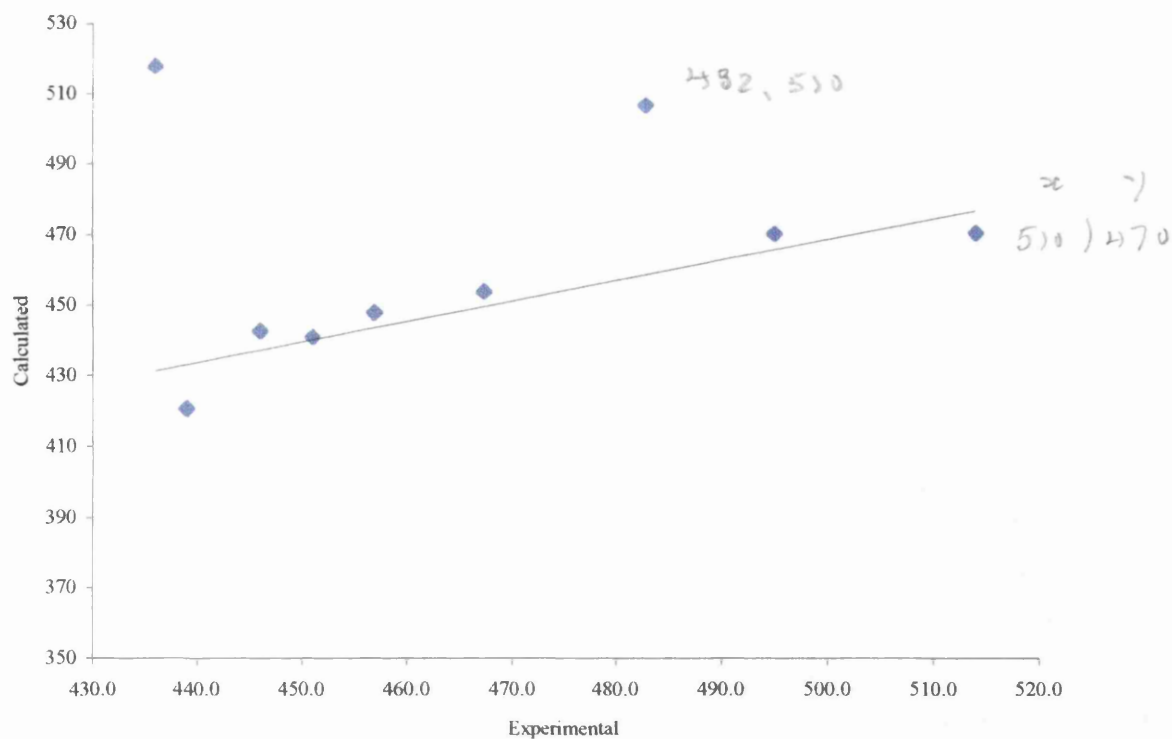


Figure 6.4 Experimental absorption energies versus calculated absorption energies for visible absorption maxima of [I] -[IX] in methanol. Absorption energies were calculated using the AM1/COSMO method at C.I.= 4.

Initial calculations using C.I. = 4, on a set of nine dyes, gave good correlations with experimental absorption maxima obtained in methanol with the exception of [VIII] and [IX] (see Table 6.2). Calculations on the full set of 19 dyes at C.I. levels 4 (Figure 6.5), 6 and 8 (Figure 6.6) gave good correlation for some dyes, but others had poor agreement with experimental data. Some of the effects of substituents were reproduced quite well. For example, dyes containing the nitro group at the 2' position were correctly predicted at shorter wavelengths than dyes containing the 4'-nitro group.

As it was explained in the introduction (Chapter 1, Section 1.2), the 2' and 4' positions on the acceptor ring produce similar electronic effects when the substituent groups are small, for example the cyano group produces a wavelength of 466 nm when it is at the 4' position and 462 nm when at the 2' position. The larger nitro group however, produces a much greater difference in the wavelength of the dye when at the 2' and 4' positions respectively. This is exemplified by comparing the absorption maxima of [IV] and [IX] in methanol. [IX] which has the nitro group at the 4' position has λ_{\max} at 482 nm while [IV], which has the same structure except the nitro group is at the 2'-position has λ_{\max} at 440 nm. The 2'-nitro group is of course twisted and cannot exert the same

electron withdrawing effect as the planar 4'-nitro group. The CN substituent on the other hand is linear and can exert its full effect at the 2' and 4' positions.

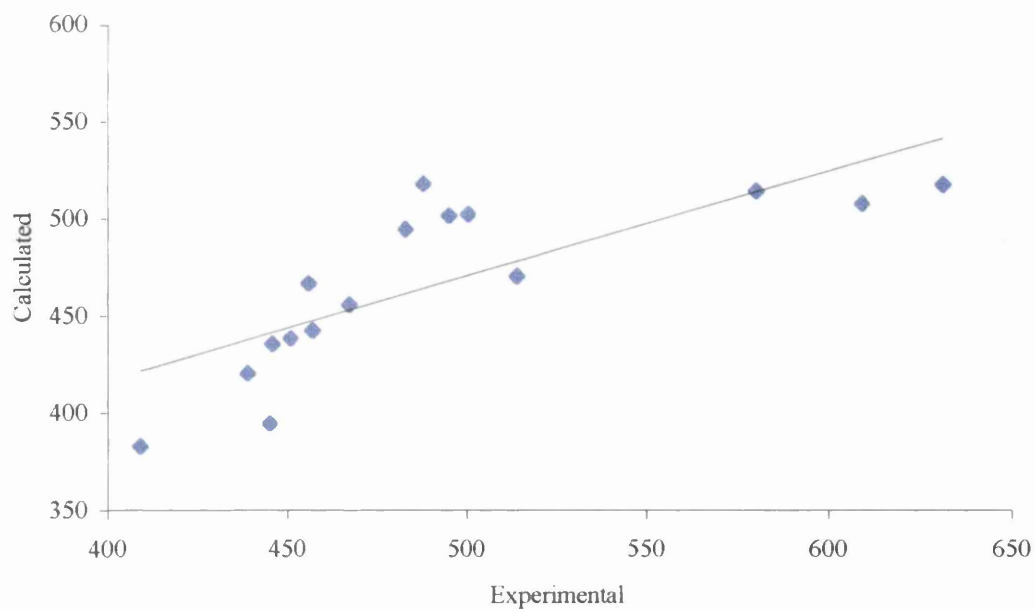


Figure 6.5 Experimental absorption energies (λ , nm) versus calculated absorption energies (nm) of the visible absorption maxima of [I] -[XIX] in methanol at C.I. levels 4.

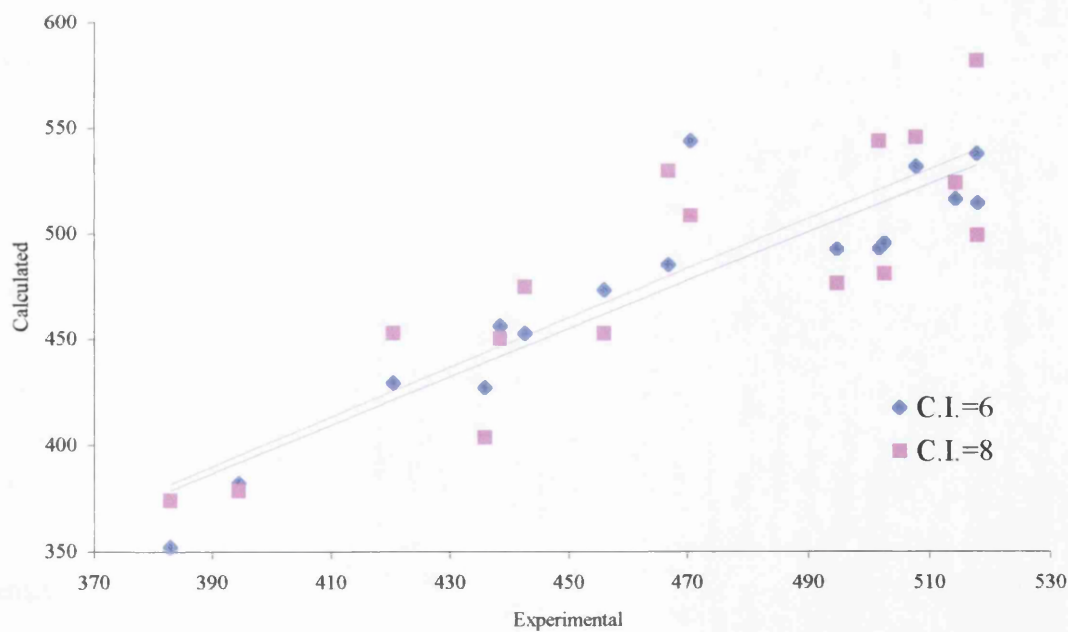


Figure 6.6 Experimental absorption energies (λ , nm) versus calculated absorption energies (nm) of the visible absorption maxima of [I] -[XIX] in methanol at C.I. levels 6 and 8.

Investigations into the predicted transition energies of 4-amino-4'-nitroazobenzene [VIII] and 4-(N- β -hydroxyethyl, N-ethyl)amino-4'-nitroazobenzene [IX]

The two notable deviations of the calculated wavelengths from the experimental curve in Figure 6.4 were found for [VIII] and [IX], with the predicted transition energies in methanol, too low. These dyes have been examined in greater depth to try and ascertain factors which may influence the predicted wavelength.

The Franck-Condon transition energies were calculated for several geometries including structures where all the heavy atoms and the amino group were constrained to lie in the same plane, and freely optimised structures, which have the nitrophenyl ring twisted by ca 37° to the plane of the phenylazo group; the results of these calculations are summarised in Table 6.2.

Table 6.2 Wavelengths of constrained and freely optimised structures of [VIII] and [IX] in methanol calculated using C.I. = 4 , 6 and 8.

| Dye | Structure | ΔE_{ci4} | ΔE_{ci6} | ΔE_{ci8} | λ_{ci4} | λ_{ci6} | λ_{ci8} | λ_{max}^d |
|--------|------------------------------------|------------------|------------------|------------------|-----------------|-----------------|-----------------|-------------------|
| [VIII] | Constrained optimised ^a | 55.10 | 54.65 | 58.05 | 518.8 | 523.1 | 492.4 | 439 |
| [VIII] | Constrained optimised ^b | 60.15 | 59.74 | 65.05 | 475.3 | 478.6 | 439.5 | |
| [VIII] | Freely optimised ^c | 60.86 | 60.75 | 67.47 | 469.7 | 470.6 | 423.7 | |
| [IX] | Constrained optimised ^a | 56.36 | 56.61 | 58.77 | 507.3 | 505.0 | 486.5 | 482 |
| [IX] | Freely optimised ^c | 58.67 | 58.65 | 64.68 | 487.7 | 487.4 | 441.9 | |

^a Heavy atoms and the amino group constrained to lie in the same plane. ^b Heavy atoms group constrained to lie in the same plane apart from the amino group. ^c Twisted structures have the nitro-phenyl ring twisted by ca. 37° to the amino-phenylazo group. ^d λ_{max} is the experimental visible absorption maximum in methanol.

Transition energies of [VIII] and [IX] are much too low at C.I. levels 4 and 6, but values at C.I.=8, were close to experimental data. In fact several of the 4'-nitro dyes had calculated transition energies that had much longer wavelengths than experimental values.

Hydrogen bonding effects of the solvent

It has been reported that the dielectric solvent field used to simulate solvent effects in AM1/COSMO (EPS=32.7) calculations is insufficient to predict the behaviour of dyes which have the capacity for hydrogen bonding in protic solvents.^{3,4} However, attempts to model the hydrogen bonding interactions between the methanol molecule and the azo dyes [VIII] and [IX], were not particularly successful.

Hydrogen bonding interactions were simulated at the amino and nitro groups by applying MOPAC charges to the dye and methanol solvent molecules and then, using the DOCKING option in Sybyl⁵, manoeuvring the solvent molecule in a steric and electrostatic force field system to find the most energetically favourable position. As the solvent molecule is positioned near the dye, a combination of potential and steric energies gives a total energy for the position of the solvent. The more negative this energy is, the more energetically favourable is the position of the solvent in relation to the dye. The whole system of dye and solvent molecules can then be optimised in methanol using the AM1/COSMO method.

Transition energies of [VIII] and [IX] with specific hydrogen bonding interactions produced even longer wavelengths than in the absence of docked solvent molecules at C.I. levels 4 and 6, but values at C.I.=8, were similar. This probably results from unrealistic interactions between the methanol molecules and the hydrogen atoms of the aromatic rings and an overestimation of the stabilisation of the nitro group, which was also seen in the dielectric field model, but is exaggerated using this approach.

An indication of the effect of solvation on the electronic properties of the dye is given by the ground and excited state dipole moments of [VIII] and [IX] (Table 6.3) calculated in the dielectric field of the solvent only. The ground state dipole moments of [VIII] and [IX] do not change that much between gas phase and methanol (EPS=32.7). However, there is a very large increase in the dipole moments of the excited state for the dielectric field solvent model.

Table 6.3 Calculated dipole moments^a for the ground state and Frank-Condon first excited states of [VIII] and [IX].

| Dye | AM1/gas phase | | AM1/COSMO (EPS = 32.7) | |
|--------|---------------|------------|------------------------|------------|
| | μ_G | μ_{EX} | μ_G | μ_{EX} |
| [VIII] | 9.42 | 13.39 | 13.13 | 35.37 |
| [IX] | 9.00 | 14.10 | 10.99 | 34.96 |

^a μ_G is the ground state and μ_{EX} the excited state dipole moments in Debyes.

Significant changes were also seen for charge distributions in the ground and excited states of 4-amino-4'-nitroazobenzene [VIII] in methanol (see Figure 6.7). Charge distributions are displayed by red and blue spheres, indicating areas of positive and negative charge respectively. Note that different levels of C.I may produce different charge distributions, though C.I. = 4 and C.I. = 6 charge distributions were found to be similar. Charge distribution plots shown refer to C.I. = 6 calculations unless otherwise stated. In the COSMO dielectric field model of the ground state, there is a large negative charge on the amino nitrogen and a small negative charge on the nitrogen atom attached to the nitro-phenyl ring, whereas in the Franck-Condon first excited state, the charge on the amino nitrogen is much smaller and there is a small negative charge on the azo nitrogen attached to the amino-phenyl ring. There is a clear movement of charge from the donor amino phenyl group to the acceptor nitrophenyl group. In the Frank-Condon second excited state, charge has moved from the azo nitrogen atoms onto both the donor and acceptor aromatic rings.

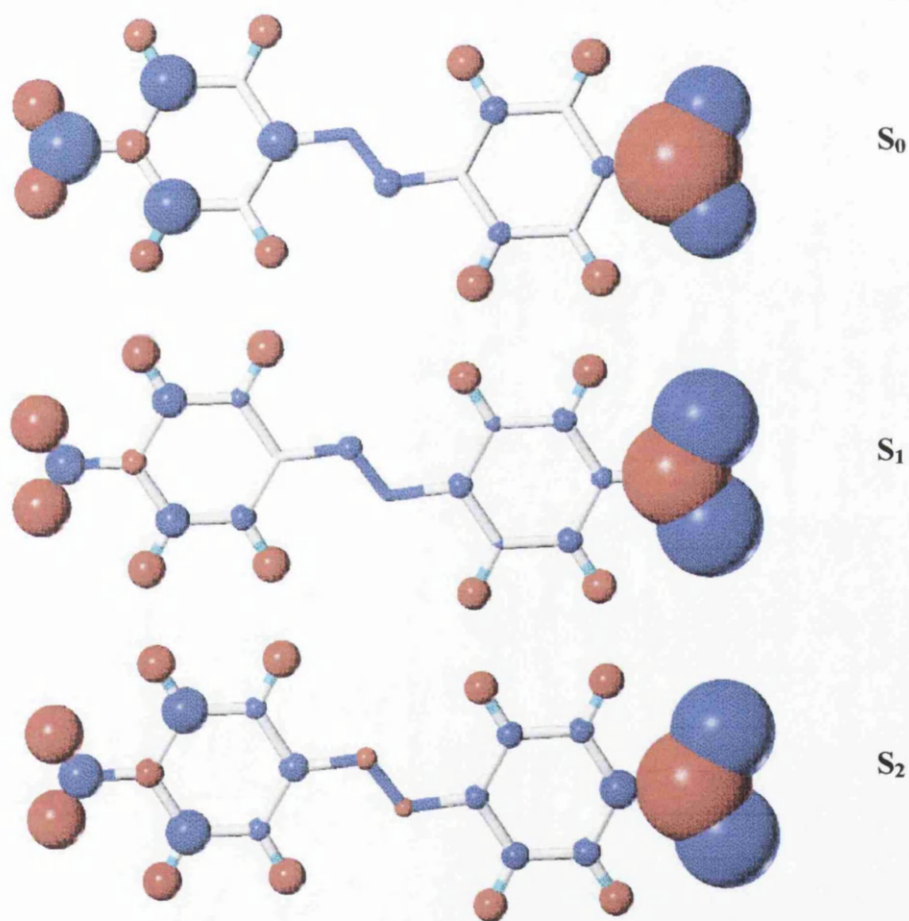


Figure 6.7 Charge distribution plots for the ground state (S_0), first excited state (S_1) and second excited state (S_2) of [VIII] optimised in methanol. Charges are represented by red spheres (positive) and blue spheres (negative), with the diameter of the sphere proportional to the magnitude of charge on each atom.

Effect of dye structure on charge distribution

The position and nature of different substituents on the dye greatly affect the charge distribution in the molecule. The charge distributions in gas phase and in methanol of 4-(N- β -hydroxyethyl, N-ethyl)amino-4'-nitroazobenzene **[IX]** and 4-(N- β -hydroxyethyl, N-ethyl)amino-2'-nitroazobenzene **[IV]** were very similar to those of the corresponding structures of **[VIII]** for the ground state (Figure 6.8). In the Frank-Condon first excited state of **[IX]** though, there is a change in the charge distribution, with a smaller negative charge on the amino nitrogen and greater negative charge on the azo nitrogen atoms than in **[VIII]**. In contrast to the 4'-nitro substituted dyes **[VIII]** and **[IX]**, the azo nitrogen atoms in first excited state of structure **[IV]** had a small positive charge, illustrating the marked effect on the electronic properties of the 2'-nitro group (see Figure 6.8).

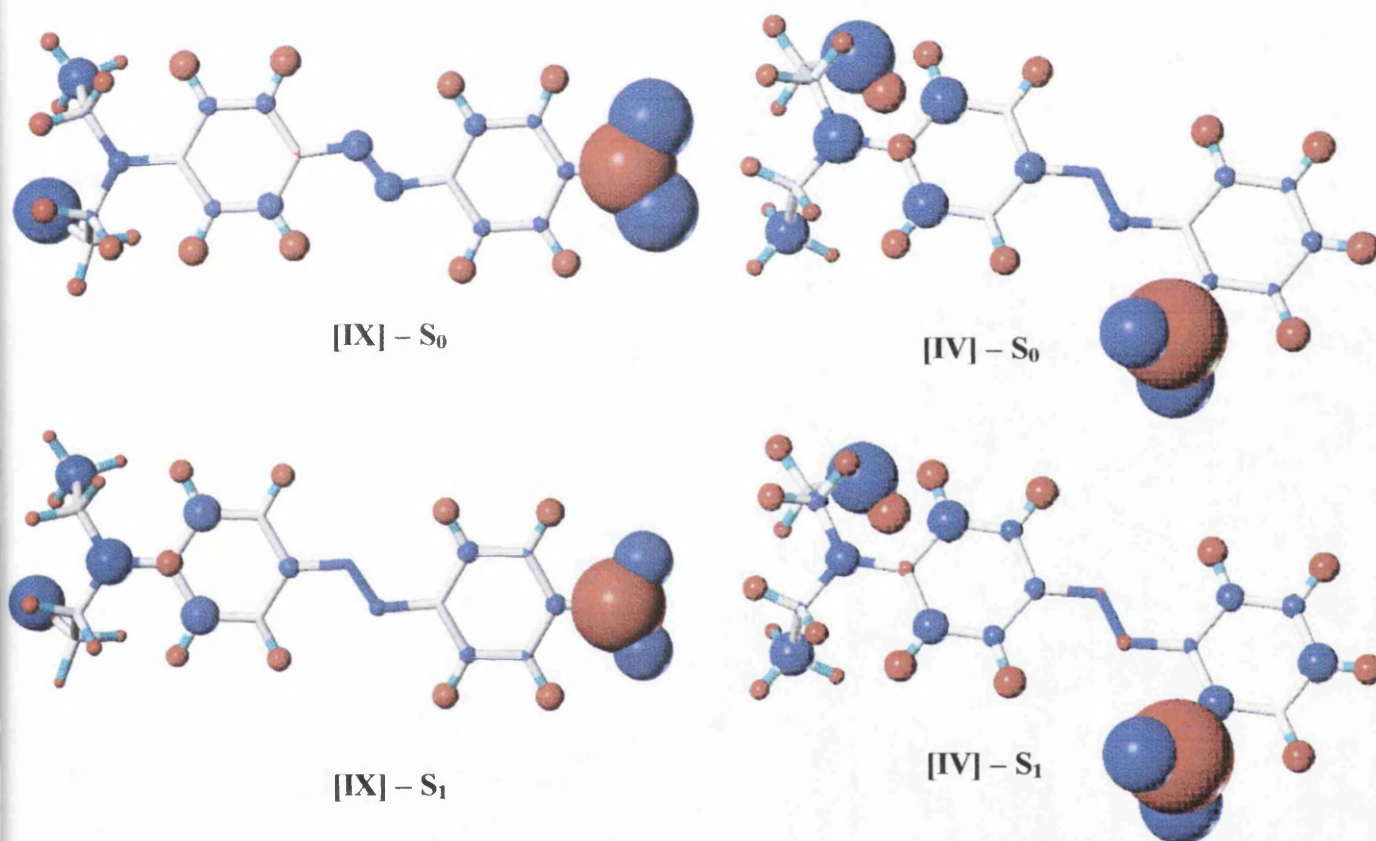


Figure 6.8 Charge distribution plots for the ground state (S_0) and the Frank-Condon first excited state (S_1) of structures **[IX]** and **[IV]** at C.I. = 6 in methanol.

The solvation model clearly affects the charges and dipole moments of the Franck-Condon S_1 state, with charge moving from the amino nitrogen atom in the ground state on to the azo nitrogen atoms in the excited state. The first excited state is much more polar than the ground state in both cases and polar solvents therefore give greater stabilization of the excited state relative to the ground state. This results in decreased transition energies leading to a bathochromic shifts of absorption bands.

However, the solvent models seem to overestimate this stabilisation, and the predicted bathochromic shifts are far too large for structures [VIII] and [IX].

Prediction of the Franck-Condon second excited state

Photo-degradation of azo dyes takes place with UV irradiation below 350nm and this work has shown that irradiation of the second absorption band is primarily responsible for the permanent photo fading of the dye (see Chapter 1)⁶ in line with Albini's inference that some higher lying state is involved in photo-degradation reactions⁷. It is important therefore, to consider the second excited state in the attempt to find some method for the prediction of the lightfastness of these dyes.

The energy required for the transition from the ground state of the dye to its second excited state can be calculated also in MOPAC by configuration interaction (CI) calculations. As in the calculation of the wavelength of the first excited state of the dye, a CI calculation on the ground state must be performed. Since electronic excitation to the second excited state is again a Franck-Condon type transition, with no rearrangement of the geometry in the time of the transition, the ground state structure is also used for the calculation of the second excited state. The second excited singlet state is calculated using the keyword ROOT = 3.

Gas phase predictions of transition energies to the second excited singlet S₂

Figure 6.9 shows the correlation between the MOPAC/AM1 and CNDOVS predicted wavelengths and experimental wavelengths of the dyes in cyclohexane for the second excited state. The CNDOVS method does not accommodate any parameters for the inclusion of solvent effects and therefore is compared to gas phase AM1 calculations and experimental values in cyclohexane, which is the closest approximation to experimental gas phase values available. Both the CNDOVS and AM1 values are quite erratic and are predicted at much longer wavelengths than the experimental values for the second absorption band. However, the third predicted CNDOVS absorption energy is predicted to have similar wavelengths to the second experimental absorption band. Note that this third excited state often has slightly higher oscillator strength than the second excited state.

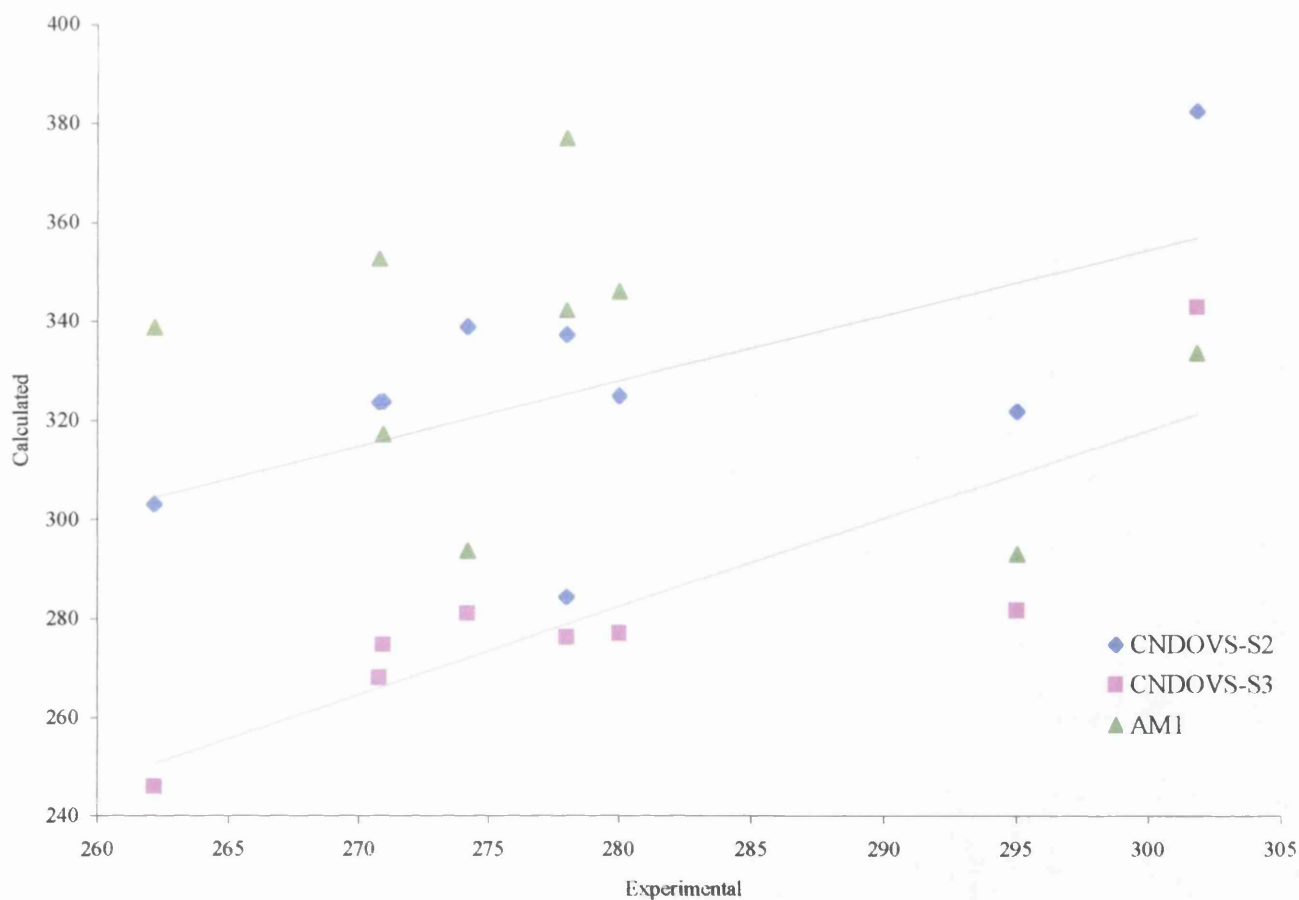


Figure 6.9 Experimental absorption energies (λ , nm) of the second absorption band of [I]-[IX] obtained in cyclohexane, versus absorption energies (nm) calculated using the AM1 (C.I.=4) and CNDOS methods. The AM1/MECI absorption energies were for the second excited singlet state relative to the ground state, while absorption energies for the second and third excited singlet states predicted by the CNDOS method are also compared.

Predictions of transition energies to the second excited singlet S_2 in methanol

The absorption energies of the second absorption band of dyes [I]-[IX] calculated by the AM1/COSMO method in methanol are much closer to experimental values than gas phase predictions (see Figure 6.10).

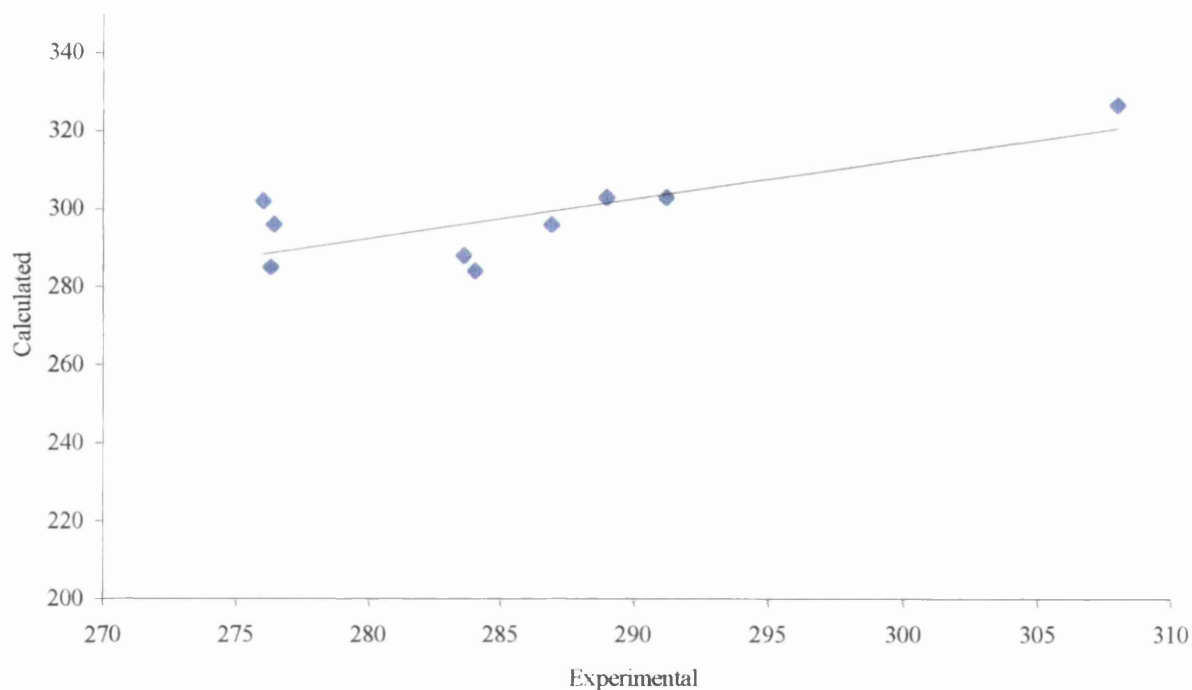


Figure 6.10 Experimental absorption energies (λ , nm) of the second absorption band of [II]-[IX] obtained in methanol, versus absorption energies (nm) calculated using the AM1/COSMO (EPS=32.7) method at C.I.=4.

CNDOVS calculations on 4-amino-4'-nitroazobenzene give the predominant excitations in S_2 as the HOMO \rightarrow LUMO+3 and in S_3 as a mixture of HOMO-2 \rightarrow LUMO and HOMO \rightarrow LUMO+1, which are all π - π^* transitions. If these CNDOVS calculations are correct and the second excited state involves transitions from the HOMO-2, then the C.I. = 4 calculations used for the MOPAC prediction of the 2nd excited state may be inadequate. The C.I.= 4 calculations only take into account the two highest occupied and two lowest unoccupied molecular orbitals and calculates 36 possible states from excitations involving electrons in these orbitals.

The suggestion is therefore, that more orbitals are required for the accurate prediction of the second excited state. This means that to consider the second excited state fully requires a higher level of CI calculation. Unfortunately, the MOPAC package available was limited to a maximum of C.I. = 6/8. Using a greater level of C.I. increased the number of possible electronic transitions that can be calculated. The effect of increasing the level of CI from 4 to 6 to 8, on the second excited state, is to shift the transition energies from 288 to 354 to 358nm respectively.

Solvent effects on the second excited state

The effect of solvent on wavelength of the second absorption band of the dyes examined was much smaller than the shifts encountered for the first absorption band. The experimental shifts of the second absorption band in moving from cyclohexane to methanol were between 5 and 15nm compared to a shift of around 60nm for the first band.

The reason for this may be attributed to the orbital origins of the second excited state. The first excited state involves a charge transfer transition from the HOMO-LUMO, where there is a movement of electron density from the donor end of the molecule to the acceptor end, which can be clearly identified in Figure 6.7. The excited state that results from this transition is more polar than the ground state and is thus stabilised by polar solvent. This stabilisation produces a bathochromic shift of the long wavelength absorption band when moving from non-polar to polar solvents.

Figure 6.7 shows negative charges on both the donor and acceptor phenyl rings of [VIII] in the Frank-Condon second excited state, and small positive charges on the azo nitrogen atoms. There is not such a obvious movement of charge from the donor to the acceptor end of the molecule in this state and thus the second excited may be less polar than the first excited state and may consequently be stabilised to a lesser degree by polar solvents. This would result in a smaller bathochromic shift for the second absorption band compared to the first absorption band.

Excited state geometry optimisations

The excited state species thought most likely to be involved in the permanent photo-degradation of the azo dyes is a high lying triplet.⁷ This high lying triplet is reached by intersystem crossing from the singlet state energetically above it, which has been proved to be the second excited singlet (Chapter 2), reached by a Frank-Condon type transition. This excitation process and the possible transitions that occur following this are illustrated in Figure 6.11.

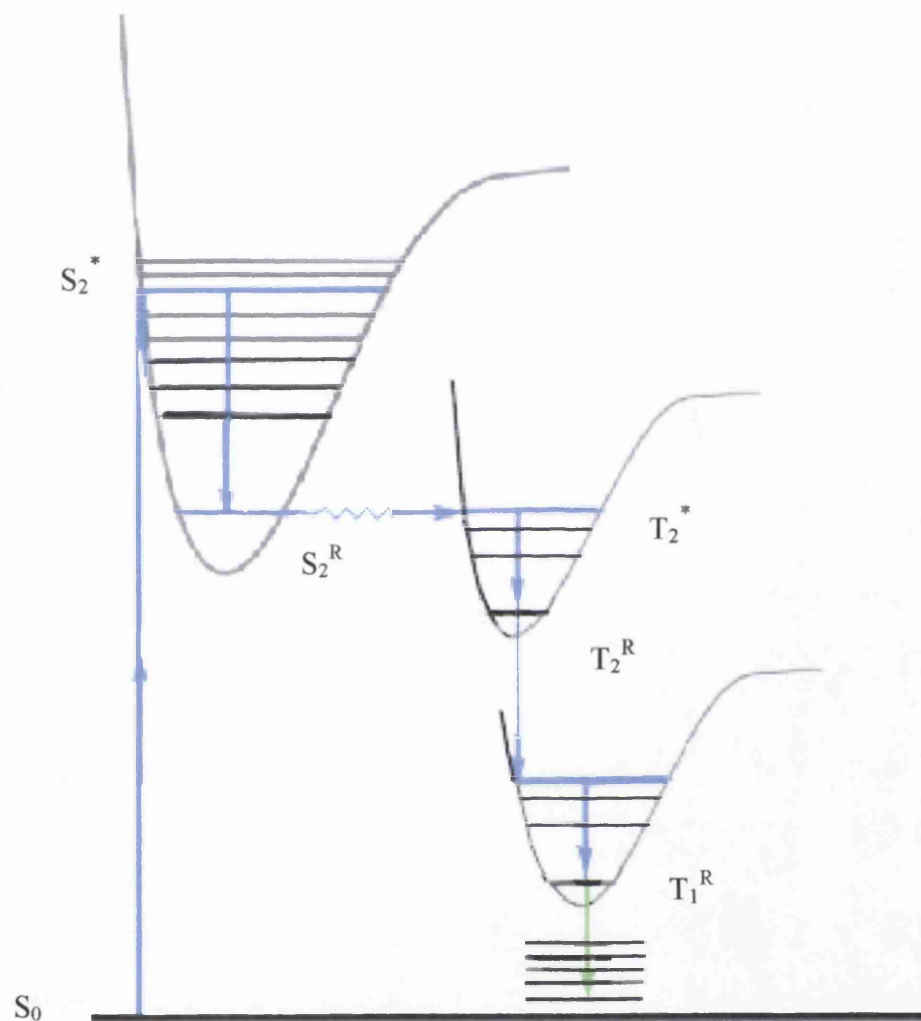


Figure 6.11 Possible relaxation processes following excitation to the second excited state singlet state. The definition of the term for each state is given in Figure 6.12.

- S_0 is the ground state.
- S_1^* is the first excited singlet state after a Franck-Condon transition, and has same geometry as the ground state.
- S_1^R is the relaxed geometry of the first excited singlet.
- S_2^* is the second excited singlet state formed after a Franck-Condon transition and has same geometry as the ground.
- S_2^R is the relaxed geometry of the second excited singlet.
- T_1^* is the energy of the first excited triplet state at the S_1^R geometry.
- T_1^R is the relaxed geometry of the first excited triplet.
- T_2^* is the energy of the first excited triplet state at the S_2^R geometry.
- T_2^R is the relaxed geometry of the second excited triplet.

Figure 6.12 Definition of terms for ground and excited state species.

The Frank-Condon transition results in an excited state species, S_2^* which has the geometry of the ground state but an excited electronic configuration. As a result this species is likely to be highly unstable and will vibrationally relax very quickly to a more stable geometry, S_2^R . The S_2^* state, though highly unstable, is unlikely to exist long enough to undergo any reactions and the relaxed single S_2^R is also probably too short lived to react. Following vibrational relaxation, the S_2^R state may decay by internal conversion to the first excited singlet state and subsequently to the ground state, S_0 , or alternatively internal conversion directly to the ground state may occur. There is also a small probability of intersystem crossing to an excited triplet state T_2^* . Intersystem crossing is most likely to occur when the vibrational level of the singlet coincides with the vibrational level of the triplet state. This may occur at a point when the geometry of the singlet has relaxed and is the same as the geometry of the triplet state⁸. Following intersystem crossing, the triplet can vibrationally relax into the lowest vibrational state of the triplet T_2^R , where it is trapped until it either relaxes to a lower triplet state or it can undergo intersystem crossing to an energetically lower singlet state (see Figure 6.11).

The triplet state T_2^* may be unstable and this state may be involved in photo-degradation processes, depending on whether it persists long enough to react. It is more likely that the relaxed triplet T_2^R is the reactive species as it should have a lifetime long enough to undergo a reaction. The experimental quenching of the photo-degradation reaction by oxygen also suggests that the reactive

species is a triplet. In addition, high lying triplets are said to have some probability of abstracting hydrogen from the solvent.⁷

Relative energies of excited states

The rate of photo-fading for each dye, may depend on one or more processes following excitation to S_2^* , including the lifetimes of the S_2^* and S_2^R states, the rate of intersystem crossing from S_2^R to T_2^* and the lifetimes of the T_2^* and T_2^R states. The energy differences between either S_2^* and T_2^* , S_2^* and T_2^R , S_2^R and T_2^* or S_2^R and T_2^R may determine the rate of intersystem crossing.

The energies of the S_2^* , S_2^R , T_2^* and T_2^R states have been calculated to explore possible mechanisms for photofading. The energy of S_2^* was calculated from a single point, second excited state, MECI calculation on the ground state structure, while the structure and energy of S_2^R was obtained from a full geometry optimisation of this state. A single point triplet calculation at the S_2^R geometry gave T_2^* and a further full geometry optimisation gave the relaxed structure, T_2^R . The energy gap between T_2^R and T_1 may also have some bearing on the lifetime of T_2^R , as it may determine rate of decay of T_2^R to T_1 . The energy differences between these states are reported and a correlation with experimental data has been attempted. The effect of the size of the configuration interaction was also explored using 4 to 8 frontier orbitals to ascertain whether the simple CI used would be adequate for this study.

A detailed analysis of the results of calculations performed on three dyes; 4-amino-4'-nitroazobenzene [VIII] (the simplest example donor-acceptor azobenzene), 4-(N- β -hydroxyethyl, N ethyl)amino-4'-nitroazobenzene [IX], (an N-alkyl substituted dye containing the 4'-nitro group) and 4-(N- β -hydroxyethyl, N ethyl)amino-2'-nitroazobenzene, [IV] (an example of a 2-nitro substituted dye), is reported in the following discussion.

The heats of formation of the excited singlet states of [VIII] are given in Table 6-4 with triplet state energies given in Table 6-5. Energies for structures in the gas phase and in methanol are compared for C.I. levels 4, 6 and 8.

Table 6-4 Calculated heats of formation, ΔH_f^a , of excited singlet states structures of [VIII] optimised in the gas phase^b and in methanol^c by the AM1 method at different levels of C.I.

| CI level | S ₀ | S ₁ [*] | S ₁ ^R | S ₂ [*] | S ₂ ^R |
|------------------------------|----------------|-----------------------------|-----------------------------|-----------------------------|-----------------------------|
| Gas Phase^b | | | | | |
| 4 | 100.26 | 174.57 | 144.34 | 184.69 | 162.96 |
| 6 | 99.99 | 170.27 | 143.43 | 177.29 | 162.92 |
| 8 | 91.92 | 166.66 | 135.91 | 171.93 | 156.42 |
| Methanol^c | | | | | |
| 4 | 79.98 | 135.08 | 123.79 | 176.41 | 142.07 |
| 6 | 79.92 | 134.57 | 120.63 | 157.54 | 142.02 |
| 8 | 73.10 | 131.16 | 112.39 | 152.73 | 135.78 |

^a ΔH_f is the heat of formation in kcal mol⁻¹.

Table 6-5 Calculated heats of formation, ΔH_f^a , of excited triplet states structures of [VIII] optimised in the gas phase^b and in methanol^c by the AM1 method at different levels of C.I.

| C.I level | T ₁ [*] | T ₁ ^R | T ₂ [*] | T ₂ ^R |
|--------------------|-----------------------------|-----------------------------|-----------------------------|-----------------------------|
| (Gas Phase) | | | | |
| c.i.=4 | 136.77 | 133.62 | 212.52 | 156.24 |
| c.i.=6 | 135.81 | 133.62 | 212.45 | 153.16 |
| c.i.=8 | 127.63 | 125.19 | 186.89 | 147.42 |
| (Methanol) | | | | |
| c.i.=4 | 117.37 | 110.65 | 190.95 | 140.74 |
| c.i.=6 | 114.21 | 107.84 | 190.93 | 137.30 |
| c.i.=8 | 105.08 | 107.80 | 186.89 | 132.49 |

^a ΔH_f is the heat of formation in kcal mol⁻¹.

The energy of each excited state relative to the ground state in the gas phase (Table 6-5) and in methanol (Table 6-6) showed significant differences between energies calculated at different levels of C.I. Differences of up to 18 kcal mol⁻¹ were seen for the same state calculated at different levels of C.I. However, the energies of some states differ by under 1 kcal mol⁻¹ (see Figure 6.13 and Figure 6.14).

Treatment of the second excited using C.I. = 4 is limited to transitions between 4 frontier orbitals. Higher levels of C.I. take in to account an increased number of transitions, which provides a more refined description of the second excited state. Therefore, only calculations using C.I.= 6 or 8 are discussed further.

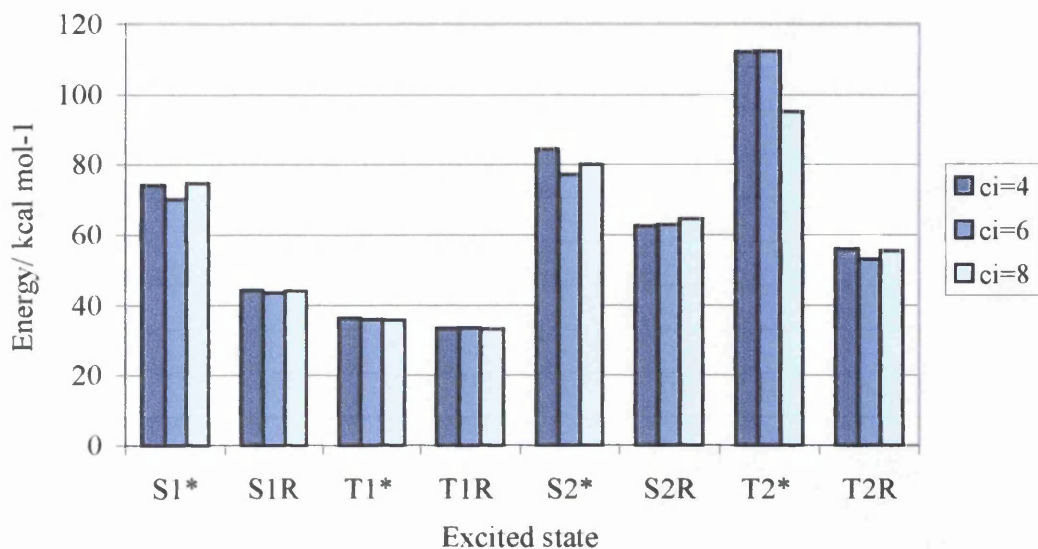


Figure 6.13 Jablonski type diagram for heats of formation (kcal mol⁻¹) of gas phase excited states of [VIII] in the gas phase relative to the ground state.

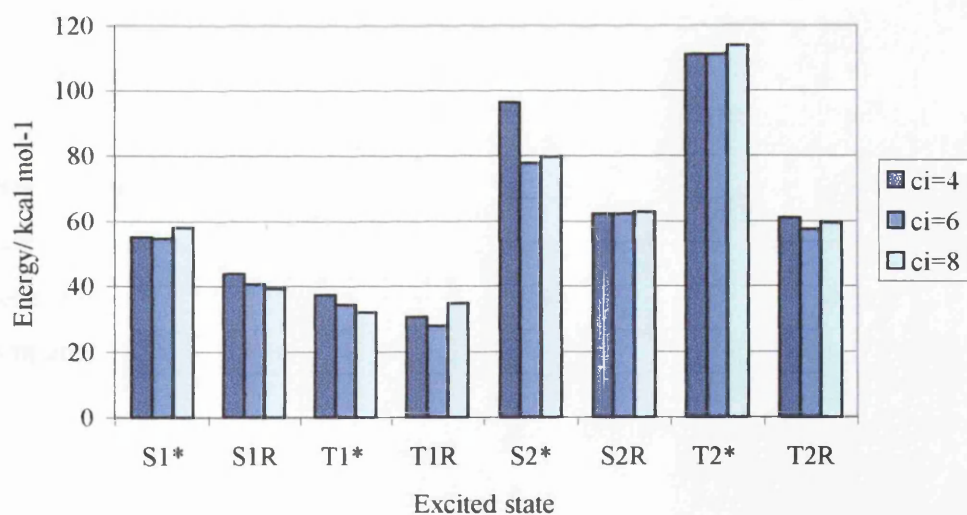


Figure 6.14 Jablonski type diagram for heats of formation (kcal mol⁻¹) of excited states of [VIII] in the methanol relative to the ground state.

The energies of S_2^* , S_2^R , T_2^* , T_2^R , T_1^* and S_2^R relative to the ground state, given in Table 6-6, showed no correlation with experimentally determined half-lives of the dyes in methanol under degassed or oxygenated conditions.

Table 6-6 Comparison between calculated heats of formation ΔH_f , relative to the ground state, for the excited states of [I]-[XVIII] using C.I. level 6, and half-lives^a.

| Structure | S_2^* | S_2^R | T_2^* | T_2^R | T_1^* | T_1^R | $\tau_{1/2}$ |
|-----------|---------|---------|---------|---------|---------|---------|--------------|
| [VI] | 75.74 | 60.30 | 94.95 | 59.84 | 41.91 | 31.56 | 0.65 |
| [VII] | 76.30 | 61.50 | 95.56 | 58.42 | 39.89 | 31.80 | 0.86 |
| [IV] | 76.44 | 63.08 | 106.76 | 59.31 | 38.03 | 29.12 | 0.87 |
| [VIII] | 77.62 | 62.10 | 111.01 | 57.38 | 34.29 | 27.92 | 1.06 |
| [IX] | 82.70 | 61.81 | 95.96 | 57.46 | 32.38 | 35.96 | 1.12 |
| [XIV] | 87.57 | 68.70 | 101.47 | 68.64 | 52.00 | 49.10 | 1.38 |
| [V] | 74.36 | 64.49 | 109.14 | 68.25 | 38.29 | 34.38 | 1.44 |
| [X] | 80.22 | 62.34 | 109.91 | 80.22 | 35.52 | 28.52 | 1.48 |
| [III] | 82.80 | 64.34 | 96.28 | 68.59 | 31.84 | 32.16 | 1.8 |
| [XI] | 81.06 | 60.72 | 88.70 | 62.85 | 30.04 | 30.07 | 1.96 |

^a $\tau_{1/2}$ is the half-life in methanol under anaerobic conditions.

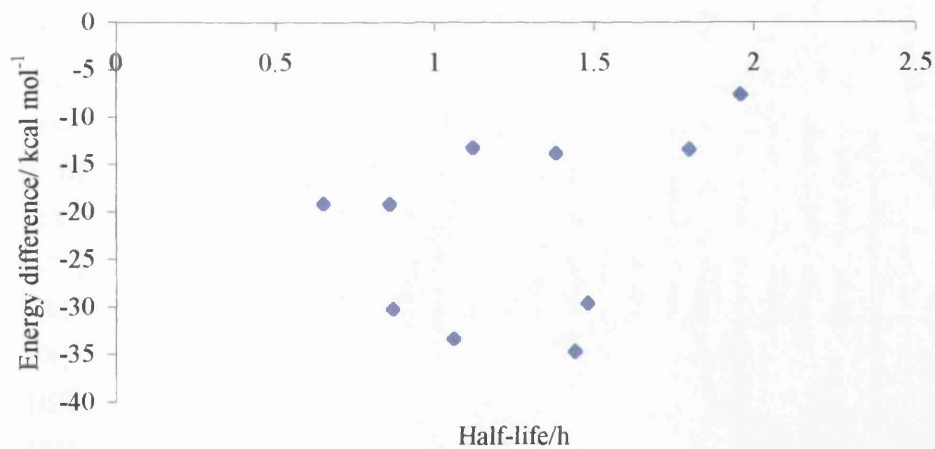
The lifetimes of excited states and rates of intersystem crossing may be dependent on their relative energies. In general, the closer the singlet and triplet states are in energy, the greater the probability of intersystem crossing occurring.⁸ It is more likely therefore, that there will be a correlation between the experimental data and the energy gaps between excited states participating in the photo reaction. The rate of intersystem crossing from S_2 to T_2 may be related to the energy gaps between these states. Energy gaps between all possible S_2 and T_2 states involved in intersystem crossing are compared to the half-lives of dyes in Table 6-7.

Table 6-7 Comparison of energy gaps between all possible S_2 and T_2 states, and half-lives.

| Dye | $S_2^* - S_2^R$ | $S_2^* - T_2^*$ | $S_2^* - T_2^R$ | $S_2^R - T_2^*$ | $S_2^R - T_2^R$ | $T_2^R - T_1^*$ | $T_2^R - T_1^R$ | Order | ${}^b\tau_{1/2}$ | ${}^c\tau_{1/2}$ |
|--------|-----------------|-----------------|-----------------|-----------------|-----------------|-----------------|-----------------|-------|------------------|------------------|
| [VI] | 15.45 | -19.21 | 15.91 | -34.66 | 0.46 | 17.93 | 28.28 | 1 | 0.65 | 4.77 |
| [VII] | 14.80 | -19.26 | 17.89 | -34.06 | 3.09 | 18.52 | 26.61 | 2 | 0.86 | 3.84 |
| [IV] | 13.36 | -30.32 | 17.13 | -43.68 | 3.77 | 21.28 | 30.19 | 3 | 0.87 | 3.52 |
| [VIII] | 15.51 | -33.39 | 20.24 | -48.90 | 4.73 | 23.08 | 29.46 | 4 | 1.06 | 10.52 |
| [IX] | 20.89 | -13.25 | 25.25 | -34.15 | 4.35 | 25.08 | 21.50 | 5 | 1.12 | 12.71 |
| [XIV] | 18.87 | -13.90 | 18.93 | -32.77 | 0.06 | 16.64 | 19.54 | 6 | 1.38 | 8.33 |
| [V] | 9.87 | -34.78 | 6.11 | -44.65 | -3.76 | 29.96 | 33.87 | 7 | 1.44 | 4.77 |
| [X] | 17.87 | -29.69 | 0.00 | -47.57 | -17.87 | 44.69 | 51.70 | 8 | 1.48 | |
| [III] | 18.46 | -13.48 | 14.21 | -31.94 | -4.25 | 36.75 | 36.43 | 9 | 1.8 | 12.42 |
| [XI] | 20.33 | -7.64 | 18.20 | -27.97 | -2.13 | 32.81 | 32.79 | 10 | 1.96 | 15.46 |

^aEnergy gaps in kcal mol⁻¹. ^b $\tau_{1/2}$ and ^c $\tau_{1/2}$ are half-lives in hours of dyes in methanol, irradiated under anaerobic and oxygenated conditions respectively and listed in order of increasing ^b $\tau_{1/2}$.

Attempts were made to correlate the above energy differences and half-lives of dyes under anaerobic conditions by plotting $S_2 - T_2$ energy gaps against the half-lives of dyes (Figure 6.15 and Figure 6.16). These plots showed that there was no apparent correlation between half-lives and calculated energy differences. In fact none of the energy differences in Table 6-7 showed any recognizable trend. Similarly, plots of energy gaps against the half-lives of dyes in oxygenated solution showed no apparent trend.

**Figure 6.15** Energy difference $S_2^* - T_2^*$ versus half of dyes

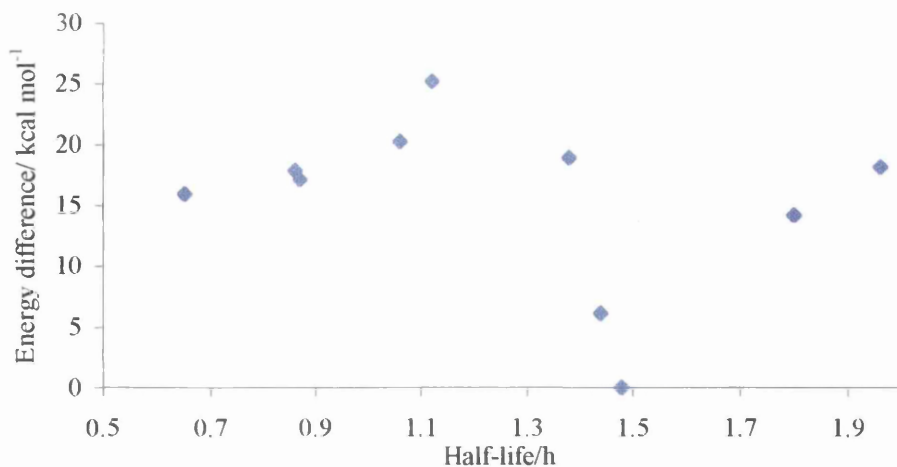


Figure 6.16 The energy difference $S_2^*-T_2^R$ versus half-life of dyes

If T_2 is the reactive species then the lifetime of this state may be critical, as a longer lifetime increases the chance it reacting. Decay of T_2 to T_1 is suggested to be the overwhelming process⁹, and the rate of this decay may be related to the energy gap between these states. Energy differences for dyes are compared to their half-lives in Table 6-8, but a plot of $T_2^R-T_1^R$ against the half-lives of dyes (Figure 6.17) again showed no apparent trend.

Table 6-8 Comparison of energy gaps $T_2^R-T_1^*$ and $T_2^R-T_1^R$ states, and half-lives.

| Dye | Order | $T_2^R-T_1^*$ | $T_2^R-T_1^R$ | ^b $\tau_{1/2}$ | ^c $\tau_{1/2}$ |
|--------|-------|---------------|---------------|---------------------------|---------------------------|
| [VI] | 1 | 17.93 | 28.28 | 0.65 | 4.77 |
| [VII] | 2 | 18.52 | 26.61 | 0.86 | 3.84 |
| [IV] | 3 | 21.28 | 30.19 | 0.87 | 3.52 |
| [VIII] | 4 | 23.08 | 29.46 | 1.06 | 10.52 |
| [IX] | 5 | 25.08 | 21.50 | 1.12 | 12.71 |
| [XIV] | 6 | 16.64 | 19.54 | 1.38 | 8.33 |
| [V] | 7 | 29.96 | 33.87 | 1.44 | 4.77 |
| [X] | 8 | 44.69 | 51.70 | 1.48 | - |
| [III] | 9 | 36.75 | 36.43 | 1.8 | 12.42 |
| [XI] | 10 | 32.81 | 32.79 | 1.96 | 15.46 |

^aEnergy gaps in kcal mol⁻¹. ^b $\tau_{1/2}$ and ^c $\tau_{1/2}$ are half-lives in hours of dyes in methanol, irradiated under anaerobic and oxygenated conditions respectively and listed in order of increasing ^b $\tau_{1/2}$.

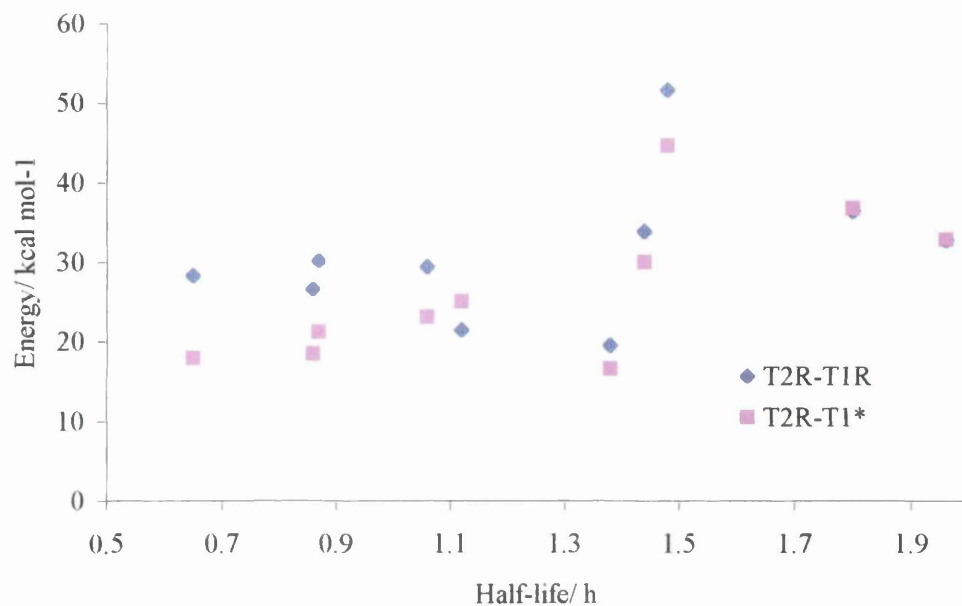


Figure 6.17 The energy differences $T_2^R-T_1^*$ and $T_2^R-T_1^R$ versus half-life of dyes.

It is of course possible, that not all the dyes photo-degrade by the same mechanisms. It is also possible that the high lying triplet species involved in photo-degradation is not the second triplet T_2 , but some higher triplet state T_n , which may also be lower in energy than S_2^* .

Excited state structures and properties

As well as the relative energies of excited states, the lightfastness of a dye may also be dependent on the geometry and electronic properties of its excited states. The geometry of the excited state structure may be important to the reactivity of the species, for example, a twisted species may be more likely to react than a planar structure. Alternatively, if the S_2 and T_2 states have similar geometry, there may be an increased probability of intersystem crossing between the singlet and triplet states. If the reactive species in the photo-degradation reaction is a triplet, an increased probability of intersystem crossing to this triplet state, will result in an increased probability of photo-degradation.

The distribution of the unpaired electrons in the reactive triplet may also be critical, as the site of reactivity is likely to be located in the vicinity of these unpaired spins. For example, if the unpaired spins are centred on the azo nitrogen, then the dye may react at this site. Alternatively, if the spins are distributed throughout the molecule, then molecule may be relatively unreactive. The distributions of

the unpaired electrons in each dye have therefore been assessed from the previous calculations (described above).

The first excited states

Experimental evidence has proved conclusively that photo-degradation of the azo dyes examined in this work, proceeds via some high lying state reached by irradiation of the second absorption band in the region of 280 to 310nm. Although the first excited singlet and triplet states are said to undergo only photo-isomerisation,⁷ the properties of these states have been assessed for the purpose of comparison with the second excited singlet and triplet states. Even though the majority of photo-degradation reactions were conducted in methanol, it is interesting to note the changes in geometry that occur when the dielectric field effect is included in the calculations to imitate the effect of the solvent. Structures optimised in the gas phase are therefore compared to structures optimised in methanol.

The calculated structures for S_1^R , S_2^R , $T_{1(S1)}$ (first triplet state at the geometry of the optimised S_1^R state), $T_{2(S2)}$ (second triplet state at the geometry of the optimised S_2^R state), T_2^R , and T_1^R in the gas phase and in methanol have been analysed. The same convention for labelling atoms, bond angles and torsion angles (Figure 6.18) is used for all the excited state structures reported. Calculated structural data for the first excited singlet and triplet states is compared to data for ground state structures in Table 6-9.

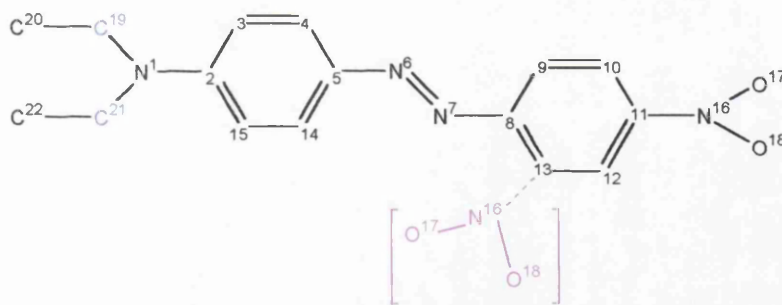


Figure 6.18 Labeling convention for azo dyes structures. Note that in structure [VIII] the alkyl groups attached to N^1 are replaced by hydrogen atoms and that structures [VIII] and [IX] both contain the nitro group attached at C^{11} only, while in structure [IV] the nitro is attached only at C^{13} .

The first excited singlet state

The structure of first excited singlet S_1 (Figure 6.19) like the ground state structure of [VIII], is essentially planar in the gas phase and in methanol. The bond lengths of the S_1 structures however, differ significantly from ground state structures, as they have longer C-NR₂ bonds and shorter N=N- bonds (refer to Table 6-9). The bond angles of the S_1 states are also much larger than in S_0 .

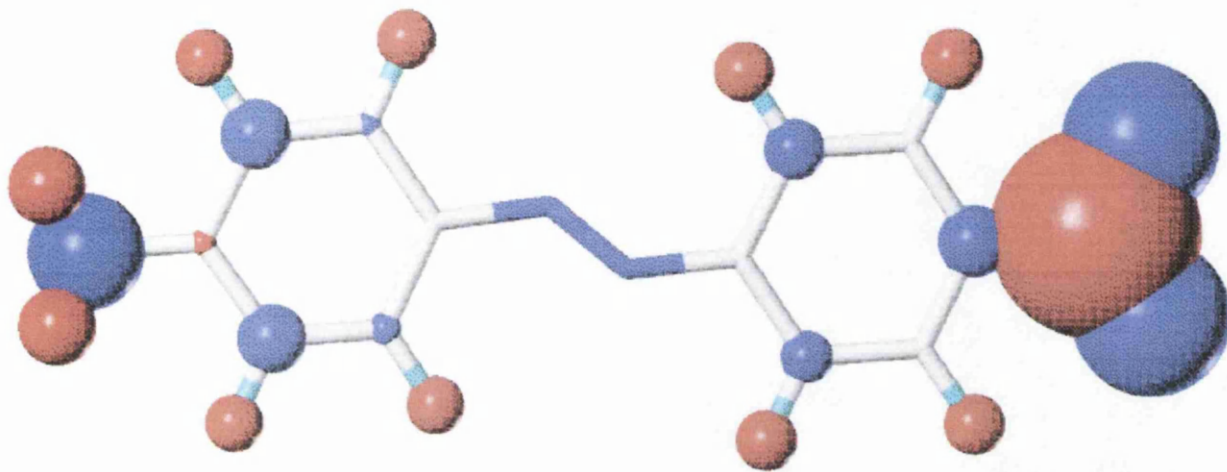


Figure 6.19 Structure and charges of the relaxed S_1^R excited singlet state of [VIII] in methanol. (Red spheres represent positive charge and blue spheres negative charge, with the diameter of the sphere proportional to the magnitude of the charge on each atom.)

The structure of first excited singlet S_1^R of [IX] (Figure 6.20) is also essentially planar in the gas phase and in methanol. The bond lengths, of the S_1^R gas phase structure are again significantly different from the ground state S_0 , with the excited singlet structures having longer N¹-C² bonds and shorter N⁶-N⁷ bonds (refer to Table 6-9). The bond angles of the S_1^R states are also much larger than in S_0 .

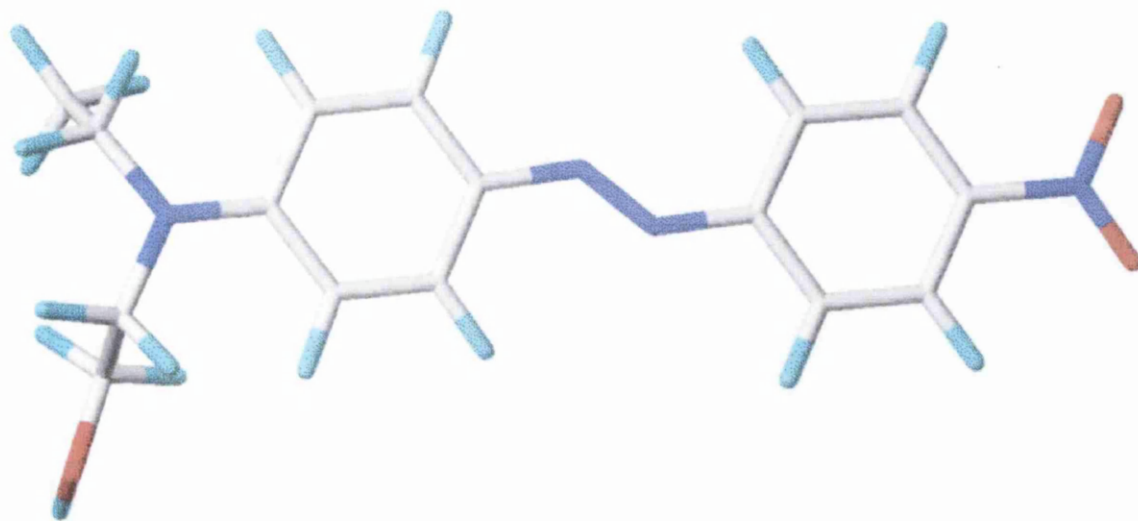


Figure 6.20 Structure of the relaxed first excited singlet S_1^R of [IX] in the gas phase.

Even the structure of the 4-(N- β -hydroxyethyl, N-ethyl)amino-2'-nitroazobenzene [IV] is planar (Figure 6.21) and has similar bond lengths and bond angles to the S_1 structures of the two other dyes.

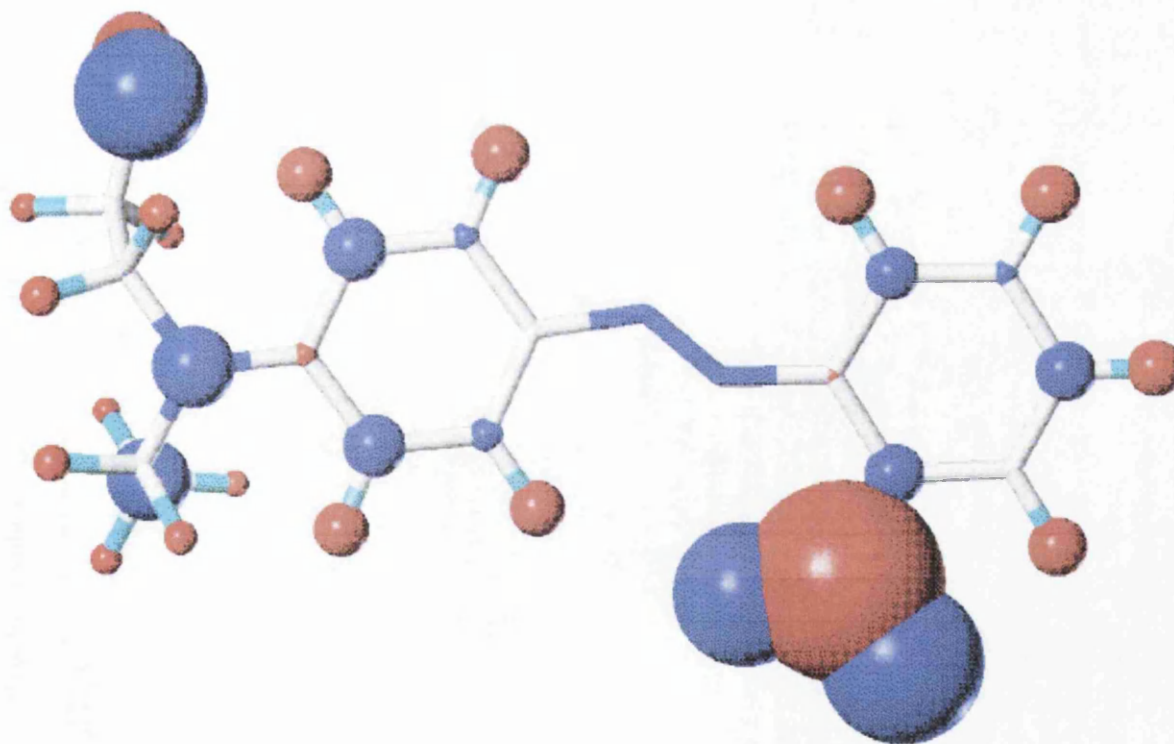


Figure 6.21: Structure and charges of the relaxed S_1^R excited singlet state of [IV] in methanol.

Table 6-9 Calculated structural data of AM1 relaxed structures of the first excited singlet and triplet states of [VIII], [IX] and [IV] in the gas phase (G) and in methanol (M). Structural data for ground states is included for comparison.

| Structure | bond lengths (Å) | | | bond angles (°) | | | torsion angles (°) | | | | | | |
|---------------------------------|--------------------------------|--------------------------------|--------------------------------|--------------------------------|--------------------------------|---|--|--|---|--|---|---|---|
| | N ¹ -C ² | C ² -N ⁶ | N ⁶ -N ⁷ | N ⁷ -C ⁸ | N ⁷ -C ⁸ | C ¹ -N ⁶ -O ¹⁷ | C ¹ -N ⁶ -N ⁷ | H ¹⁹ N ¹ C ² C ³ | H ²¹ N ¹ C ² C ¹⁵ | C ¹⁴ C ⁵ N ⁶ N ⁷ | N ⁶ N ⁷ C ⁸ C ⁹ | C ⁵ N ⁶ N ⁷ C ⁸ | C ¹⁰ C ¹¹ N ¹⁶ O ¹⁷ |
| [VIII] | | | | | | | | | | | | | |
| S ₀ (G) | 1.372 | 1.426 | 1.233 | 1.438 | 1.486 | 1.202 | 120.24 | 119.22 | 0 | 0 | 0 | 0 | 0 |
| S ₀ (M) | 1.358 | 1.419 | 1.235 | 1.436 | 1.475 | 1.207 | 120.60 | 119.35 | 0 | 0 | 0 | 0 | 0 |
| S ₁ ^R (G) | 1.391 | 1.389 | 1.221 | 1.372 | 1.478 | 1.204 | 133.00 | 133.95 | -23.3 | 23.2 | 0.2 | 0.3 | 179.7 |
| S ₁ ^R (M) | 1.388 | 1.397 | 1.211 | 1.366 | 1.455 | 1.209 | 133.57 | 134.96 | -23.2 | -24.5 | -0.1 | 0.2 | 179.8 |
| T ₁ ^R (G) | 1.394 | 1.428 | 1.222 | 1.393 | 1.487 | 1.202 | 131.03 | 132.68 | -23.8 | 23.6 | 112.7 | 11.7 | -106.8 |
| T ₁ ^R (M) | 1.392 | 1.410 | 1.242 | 1.394 | 1.425 | 1.221 | 121.51 | 121.31 | -0.1 | 0.2 | 94.5 | 0.1 | 180 |
| [IX] | | | | | | | | | | | | | |
| S ₀ (G) | 1.386 | 1.425 | 1.233 | 1.438 | 1.486 | 1.202 | 120.25 | 119.49 | 0 | 0 | 0 | 0 | 0 |
| S ₀ (M) | 1.382 | 1.422 | 1.234 | 1.437 | 1.475 | 1.207 | 120.54 | 119.49 | 0 | 0 | 0 | 0 | 0 |
| S ₁ ^R (G) | 1.401 | 1.388 | 1.221 | 1.372 | 1.478 | 1.204 | 132.98 | 133.97 | 15.5 | 14.5 | -0.2 | -0.4 | -179.6 |
| S ₁ ^R (M) | 1.400 | 1.398 | 1.210 | 1.365 | 1.455 | 1.209 | 133.70 | 135.46 | -32.4 | -1.1 | -0.0 | -0.3 | -179.8 |
| T ₁ ^R (G) | 1.390 | 1.351 | 1.259 | 1.392 | 1.486 | 1.202 | 131.94 | 125.74 | 10.2 | -13.8 | 11.6 | 10.9 | -101.5 |
| T ₁ ^R (M) | 1.355 | 1.398 | 1.244 | 1.390 | 1.430 | 1.219 | 123.54 | 121.35 | -5.9 | 2.7 | 94.9 | -0.2 | 179.8 |
| [IV] | | | | | | | | | | | | | |
| S ₀ (G) | 1.390 | 1.426 | 1.233 | 1.435 | 1.497 | 1.198 | 120.27 | 119.41 | 0 | 0 | 0 | 0 | -60.1 |
| S ₀ (M) | 1.381 | 1.422 | 1.234 | 1.435 | 1.488 | 1.202 | 120.47 | 119.34 | 0 | 0 | 0 | 0 | -60.6 |
| S ₁ ^R (G) | 1.406 | 1.397 | 1.217 | 1.363 | 1.476 | 1.204 | 130.44 | 137.08 | 7.0 | -28.0 | 1.1 | 0 | 179.9 |
| S ₁ ^R (M) | 1.401 | 1.402 | 1.218 | 1.357 | 1.456 | 1.203 | 131.18 | 138.71 | 7.9 | -28.5 | 0.6 | 0.1 | 179.9 |
| T ₁ ^R (G) | 1.400 | 1.400 | 1.358 | 1.240 | 1.430 | 1.201 | 137.67 | 125.58 | -23.8 | 8.1 | 6.6 | -68.9 | -110.9 |
| T ₁ ^R (M) | 1.376 | 1.340 | 1.261 | 1.432 | 1.480 | 1.202 | 134.85 | 122.73 | -2.7 | -16.1 | -8.7 | -110.2 | 108.4 |

The charges on S_1^R in the gas phase and in methanol are very similar, but they differ from the ground state, as the azo nitrogen atoms are essentially neutral, whereas in the ground state, they have a small negative charge.

Optimised structures of the relaxed first triplet state (T_1^R)

The relaxed first excited triplet state of [VIII] in the gas phase (Figure 6.22) is a slightly bent structure. The effect of solvent on the geometry of the excited triplet structures is quite dramatic with calculated structural data for the relaxed first triplet state T_1^R , in the gas phase (Figure 6.23) and in methanol quite different, with respect to torsion angles. In the optimised gas phase structure of the first triplet state of [VIII] (Figure 6.24) the donor phenyl ring is twisted by 67° to the azo bridge, which itself has a torsion angle of 73° . The nitrophenyl ring is twisted by 11° with respect to the phenyl azo bridge. However, in the structure of T_1^R in methanol, the azo group and the nitrophenyl ring are coplanar and are twisted by 95° to the plane of the donor phenyl ring (Figure 6.25).

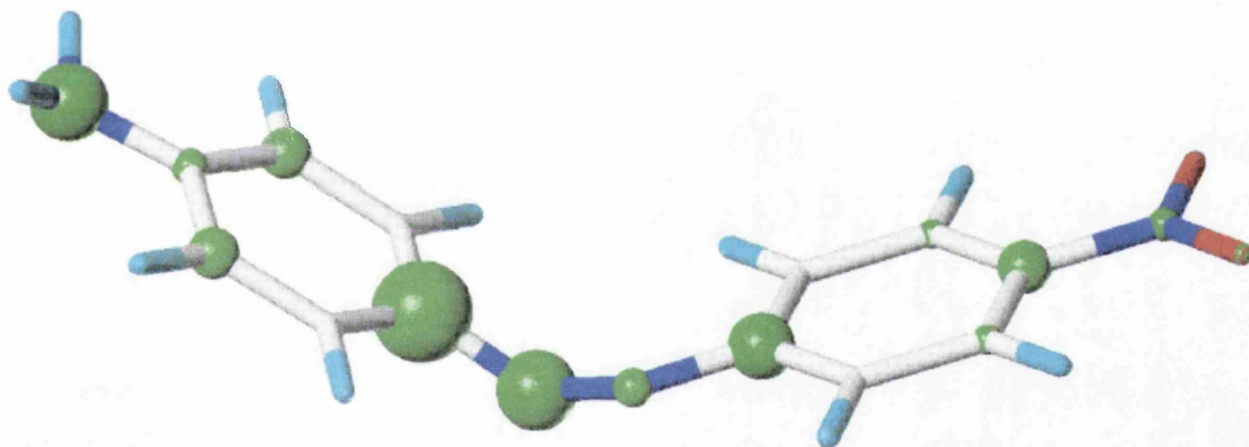


Figure 6.22 Structure and spin densities of the first triplet state T_1^R of [VIII] in the gas phase. Spin densities (see text) are represented by green spheres, with the diameter of the sphere proportional to the magnitude of the spin density.

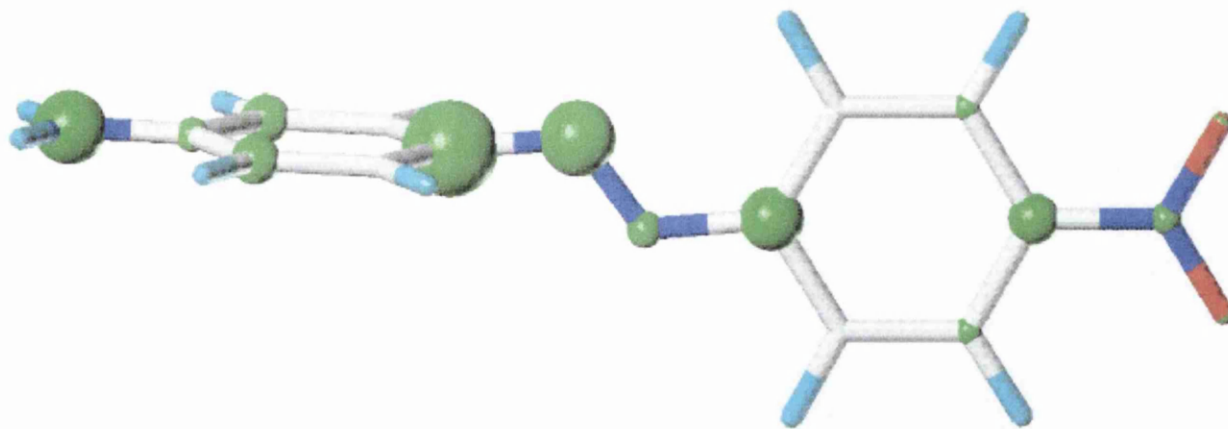


Figure 6.23 Structure of the first triplet T_1^R of **[VIII]** optimised in methanol. Spin densities (see text) are represented by green spheres, with the diameter of the sphere proportional to the magnitude of the spin density.

Spin densities

Triplet states have two electrons with unpaired spins. The probability of finding one of these unpaired electrons at each atom in the molecule, is given by the spin density. Spin densities may be localised predominantly on a few atoms or spread over several atoms in the molecule. The sum of the spin density functions for the whole molecule will equal the number of unpaired electrons i.e. 2. Spin densities are calculated using the keywords **TRIPLET** and **ESR** in addition to the keywords used for other C.I calculations. In this work spin densities have been represented as green spheres on each atom in the molecule, with the size of each sphere reflecting the magnitude on each atom.

The spin densities of the optimised triplet state T_1^R in the gas phase (see Figure 6.22) are spread throughout the molecule with the majority of the spin centred on the donor amino nitrogen, the C⁵ carbon and the donor azo nitrogen atom, with much smaller proportions at carbon atoms 2, 4 and 6 in both the donor and acceptor phenyl rings (Figure 6.24). In methanol, the spin densities at the azo nitrogen atoms are have a very similar arrangement (Figure 6.23).

The first triplet state of **[IX]** (Figure 6.24) is quite different from that of **[VIII]** in the gas phase, with respect to torsion angles. The spin densities of these structures are also noticeably different with most of the spin density localised on the azo nitrogen atoms of **[IX]**, compared to the more diffuse arrangement in the T_1^R structure of **[VIII]**.

The effect of solvent on the geometry of the excited triplet structure of **[IX]** is quite dramatic as the structure of the first triplet state of **[IX]** in methanol (Figure 6.25) had the nitrophenyl ring twisted by 90° to the plane of the phenyl azo group, similar to the geometry of the T_1^R state of **[VIII]** in methanol.

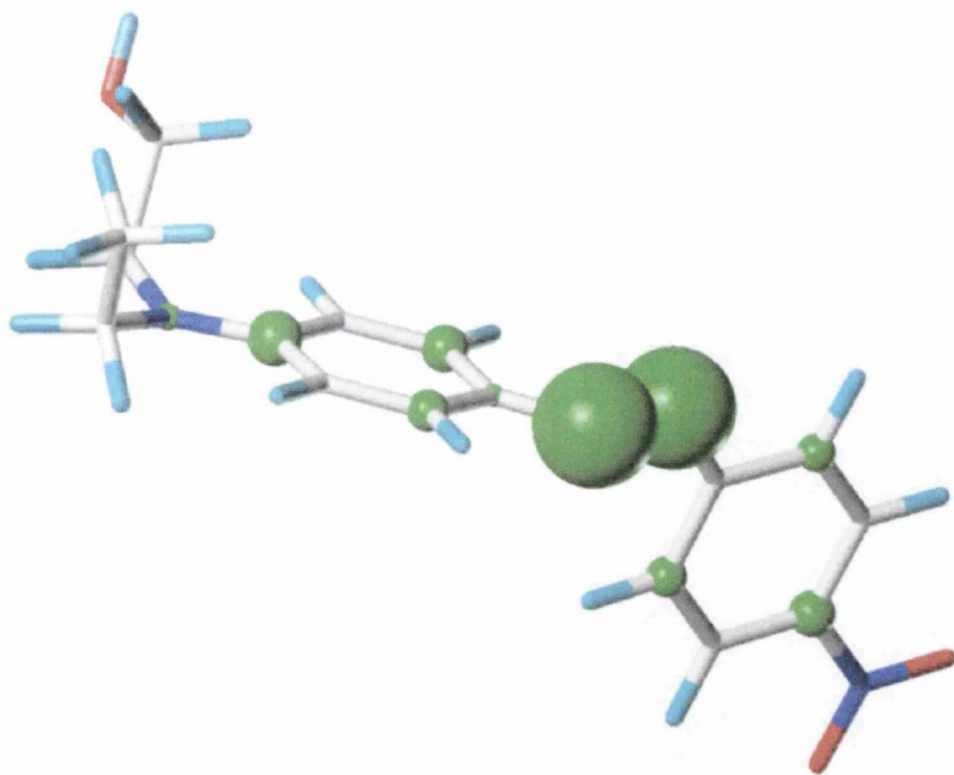


Figure 6.24 Structure of the first triplet state T_1^R of **[IX]** in the gas phase. Green spheres represent spin densities.

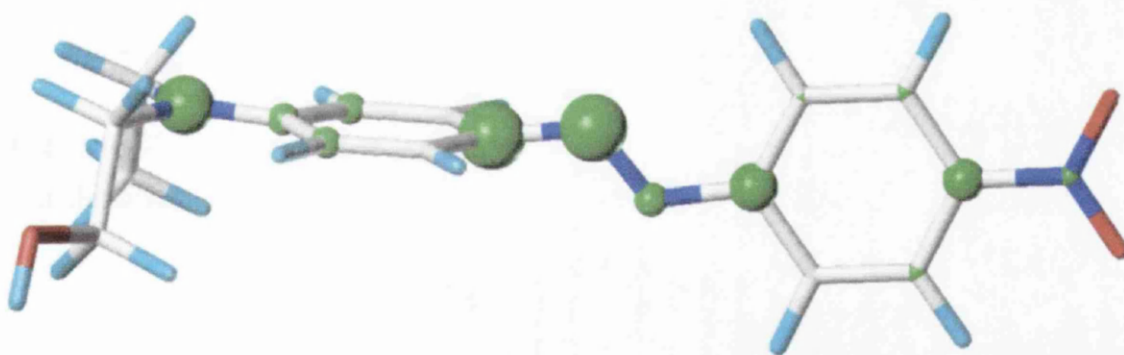


Figure 6.25 Structure of the first triplet T_1^R of **[IX]** optimized in methanol. Green spheres represent spin densities.

As mentioned in the paragraph above, the spin densities of the optimised triplet state T_1^R in the gas phase are centered principally on the azo nitrogen atoms, with much smaller proportions at atoms C^2 , C^4 and C^6 in the donor phenyl ring and C^8 and C^{11} in the acceptor phenyl ring (Figure 6.24). In methanol, the spin densities at the azo nitrogen atoms are greatly reduced (Figure 6.25) and there was also an increase in the spin densities at the donor amino nitrogen and at atom C^2 of the donor phenyl ring and at C^8 and C^{11} of the acceptor phenyl ring. The position of the spin densities in this state is similar to that seen for the T_1^R state of [VII] in methanol.

The first excited triplet state of [IV] in the gas phase Figure 6.26 has a slightly bent structure with a similar structure in methanol. The spin densities of the optimised triplet state T_1^R are predominantly localised at the azo nitrogen atoms in both the gas phase and in methanol. (Figure 6.27). This distribution of spin densities is different from that in [VIII] and [IX].

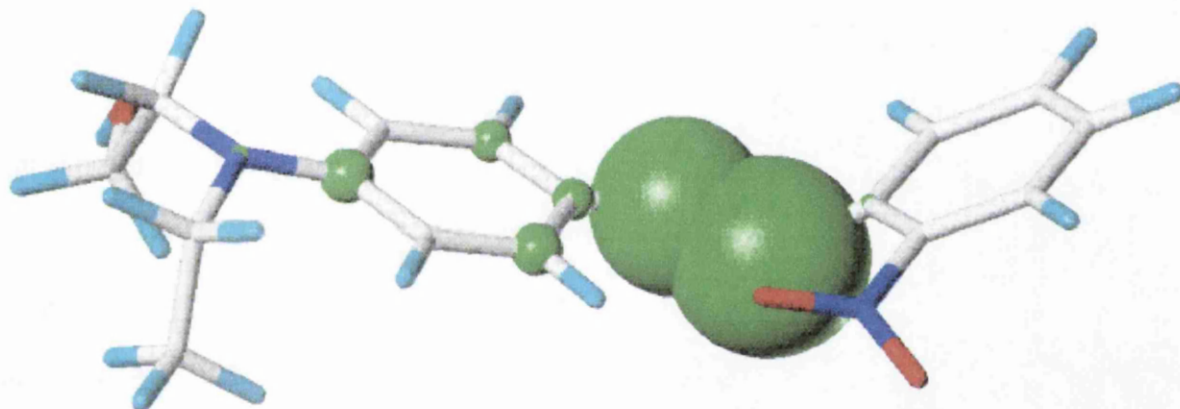


Figure 6.26 Structure of the first triplet state T_1^R of [IV] in the gas phase. Green spheres represent spin densities.

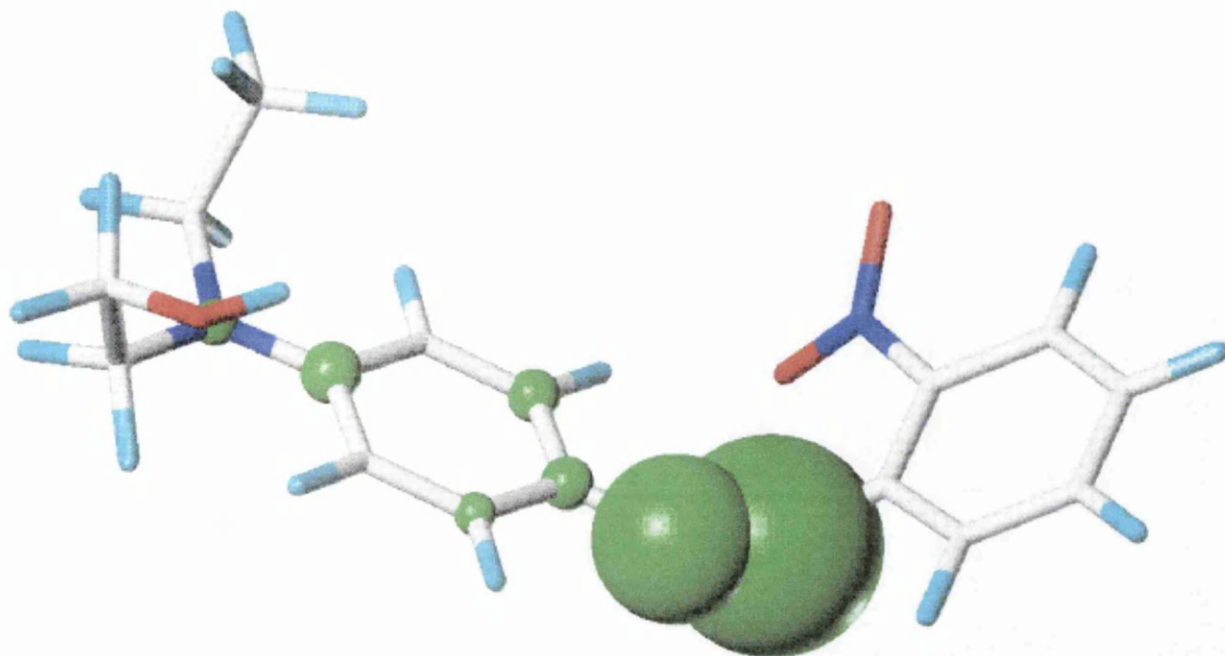


Figure 6.27 Structure of the first triplet T_1^R of [IV] optimised in methanol. Green spheres represent spin densities.

Electron spin resonance studies by Remi et al.¹⁰ on azo dyed cellulosic systems after exposure to light showed stable free radicals at one of the carbon atoms in the chromophore.

Second excited singlet and triplet states

The relaxed second excited singlet state (S_2^R)

In contrast to either the S_0 or S_1^R states, the second excited singlet state S_2^R has a non planar geometry and has both phenyl rings of the molecule twisted out of the plane as well as the azo bridge being twisted in both the gas phase and in methanol. The azo bond lengths in the S_2^R structures are much shorter than in the ground state. There seems to be little difference between the geometry of S_2^R in the gas phase (Figure 6.28) and in methanol (Figure 6.29) though the charges on the azo nitrogen atoms are slightly different and the nitrogen of the nitro group has a slightly greater positive charge in methanol than in the gas phase.

Table 6-10 Calculated structural data of AM1 relaxed excited state structures of [VIII], [IX] and [IV] in the gas phase (G) and in methanol (M).

| Structure | bond lengths (Å) | | | bond angles (°) | | | torsion angles (°) | | | | | | | |
|---------------------------------|--------------------------------|--------------------------------|--------------------------------|--------------------------------|----------------------------------|----------------------------------|--|--|--|---|--|---|---|---|
| | bond | lengths | (Å) | bond | angles | (°) | torsion | angles | (°) | | | | | |
| [VIII] | N ¹ -C ² | C ⁵ -N ⁶ | N ⁶ -N ⁷ | N ⁷ -C ⁸ | C ¹¹ -N ¹⁶ | N ¹⁶ -O ¹⁷ | C ³ N ⁶ N ⁷ | N ⁶ N ⁷ C ⁸ | H ¹⁵ N ¹ C ² C ³ | H ²¹ N ¹ C ² C ¹⁵ | C ¹⁴ C ³ N ⁶ N ⁷ | N ⁶ N ⁷ C ⁸ C ⁹ | C ³ N ⁶ N ⁷ C ⁸ | C ¹⁰ C ¹¹ N ¹⁶ O ¹⁷ |
| S ₂ ^R (G) | 1.397 | 1.428 | 1.206 | 1.433 | 1.489 | 1.201 | 132.18 | 132.73 | 24.7 | -24.6 | -56.8 | -27.5 | -103.9 | -0.1 |
| S ₂ ^R (M) | 1.397 | 1.431 | 1.212 | 1.432 | 1.483 | 1.202 | 130.80 | 131.22 | 25.5 | -25.4 | -61.9 | -44.8 | -103.1 | 0.2 |
| F ₂ ^R (G) | 1.381 | 1.333 | 1.221 | 1.372 | 1.476 | 1.205 | 128.93 | 131.94 | -22.0 | 22.1 | -2.2 | 11.1 | -179.0 | -0.6 |
| F ₂ ^R (M) | 1.342 | 1.381 | 1.249 | 1.384 | 1.433 | 1.227 | 130.08 | 130.76 | 0.7 | 0.3 | -20.6 | -21.2 | -20.3 | 1.4 |
| [IX] | N ¹ -C ² | C ⁵ -N ⁶ | N ⁶ -N ⁷ | N ⁷ -C ⁸ | C ¹¹ -N ¹⁶ | N ¹⁶ -O ¹⁷ | C ³ N ⁶ N ⁷ | N ⁶ N ⁷ C ⁸ | C ¹³ N ¹ C ² C ³ | C ²¹ N ¹ C ² C ¹⁵ | C ¹⁴ C ³ N ⁶ N ⁷ | N ⁶ N ⁷ C ⁸ C ⁹ | C ³ N ⁶ N ⁷ C ⁸ | C ¹⁰ C ¹¹ N ¹⁶ O ¹⁷ |
| S ₂ ^R (G) | 1.408 | 1.427 | 1.207 | 1.433 | 1.490 | 1.201 | 132.19 | 132.68 | 27.2 | -7.4 | -59.2 | -25.2 | -104.0 | 0.3 |
| S ₂ ^R (M) | 1.416 | 1.426 | 1.203 | 1.420 | 1.480 | 1.203 | 134.2 | 135.17 | -5.6 | 35.5 | -54.2 | -49.1 | -98.3 | 0.3 |
| F ₂ ^R (G) | 1.392 | 1.325 | 1.243 | 1.393 | 1.477 | 1.207 | 134.83 | 126.54 | 0.4 | -30.5 | 3.0 | -13.9 | 175.9 | -0.1 |
| F ₂ ^R (M) | 1.371 | 1.345 | 1.221 | 1.372 | 1.431 | 1.220 | 139.07 | 130.29 | 4.1 | -13.8 | 4.3 | -9.6 | 168.2 | -0.2 |
| [IV] | N ¹ -C ² | C ⁵ -N ⁶ | N ⁶ -N ⁷ | N ⁷ -C ⁸ | C ¹¹ -N ¹⁶ | N ¹⁶ -O ¹⁷ | C ³ N ⁶ N ⁷ | N ⁶ N ⁷ C ⁸ | C ¹³ N ¹ C ² C ³ | C ²¹ N ¹ C ² C ¹⁵ | C ¹⁴ C ³ N ⁶ N ⁷ | N ⁶ N ⁷ C ⁸ C ⁹ | C ³ N ⁶ N ⁷ C ⁸ | C ⁸ C ¹³ N ¹⁶ O ¹⁷ |
| S ₂ ^R (G) | 1.412 | 1.427 | 1.205 | 1.430 | 1.493 | 1.198 | 132.63 | 132.73 | 6.2 | -31.9 | 58.4 | 22.8 | 104.1 | -52.2 |
| S ₂ ^R (M) | 1.415 | 1.428 | 1.207 | 1.432 | 1.488 | 1.199 | 132.78 | 132.62 | 7.7 | -35.5 | -58.5 | 24.7 | 105.4 | -44.5 |
| F ₂ ^R (G) | 1.391 | 1.341 | 1.239 | 1.372 | 1.479 | 1.203 | 126.15 | 136.55 | 9.1 | -22.7 | 6.0 | -4.8 | -172.3 | -29.3 |
| F ₂ ^R (M) | 1.365 | 1.373 | 1.211 | 1.357 | 1.425 | 1.222 | 128.86 | 141.97 | -6.7 | -14.0 | -5.1 | -0.8 | -175.4 | 0.1 |

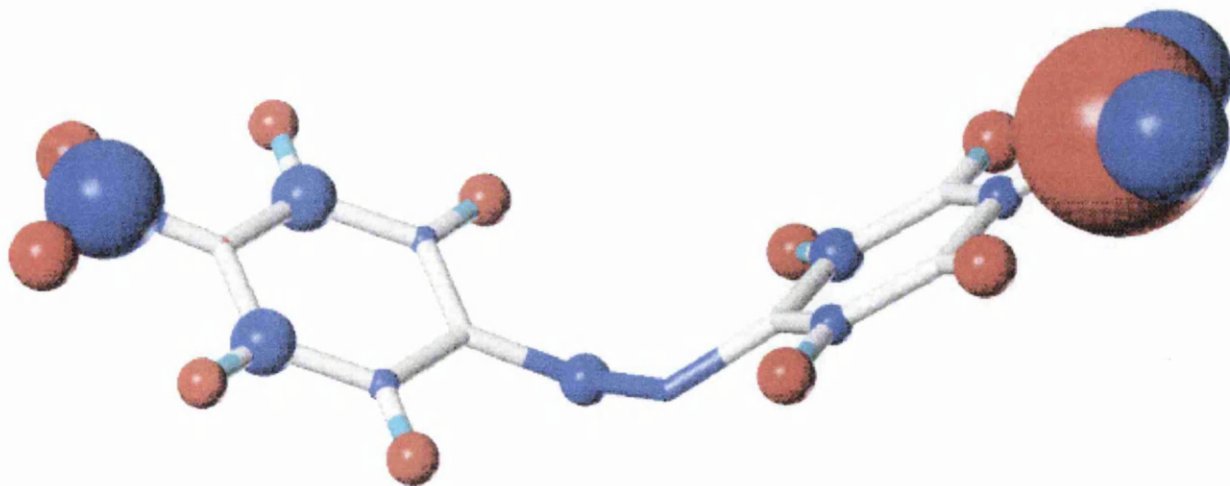


Figure 6.28 Structure and charges of the relaxed S_2^R excited singlet state of [VIII] in the gas phase. (Red spheres represent positive charge and blue spheres negative charge, with the diameter of the sphere proportional to the magnitude of the charge on each atom.)

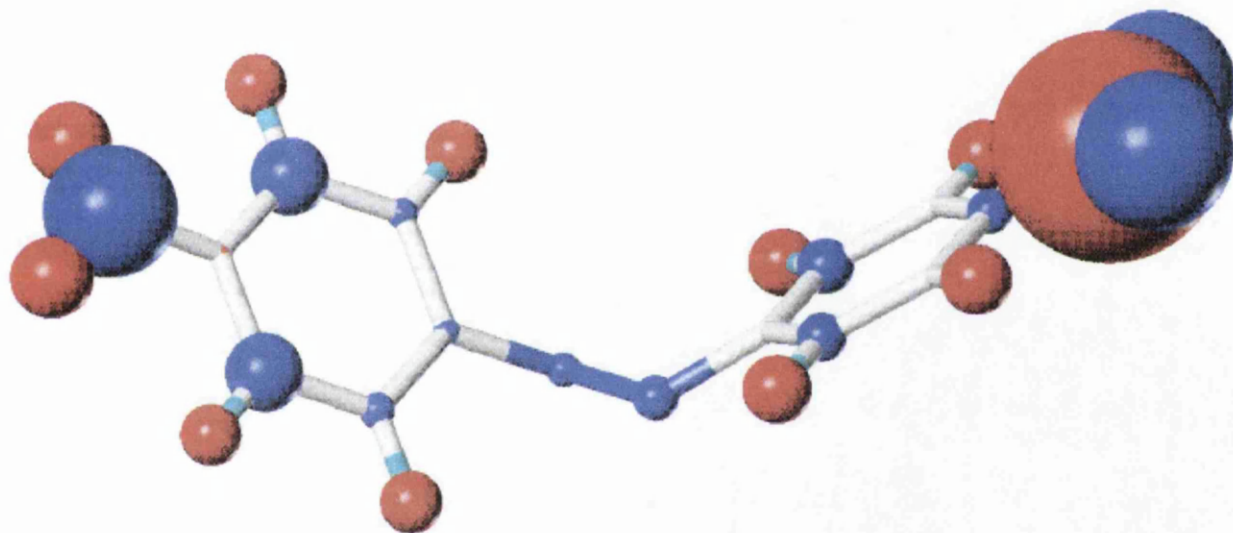


Figure 6.29 Structure and charges of the relaxed S_2^R excited singlet state of [VIII] in methanol.

As for [VIII] the second excited singlet state S_2^R of [IX] (Figure 6.30) has a non planar geometry and has both phenyl rings of the molecule twisted out of the plane as well as the azo bridge being twisted in both the gas phase and in methanol. The azo bond lengths is again much shorter than in ground state structures and other bond lengths and bond angles are very similar to those of the S_2 structure of [VIII]. The torsion angles were also very similar between the S_2^R states of both dyes in the gas phase and in methanol.

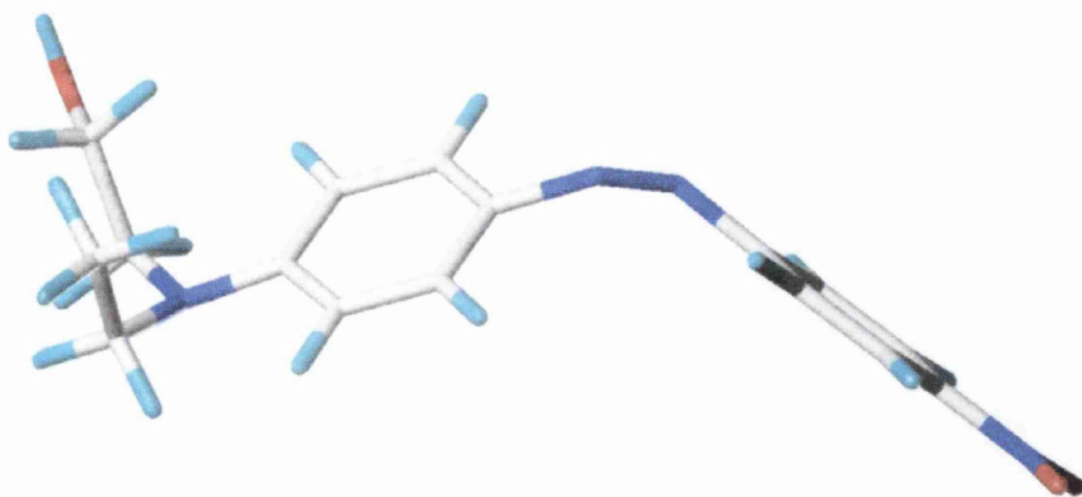


Figure 6.30 The second excited singlet state, S_2^R structure of [IX] in methanol.

The structure of the S_2^R state of [IV] in methanol (Figure 6.30) is similar to that of the gas phase S_2^R structure and both structures had similar bond lengths, bond angles and torsion angles to the S_2^R states of dyes [VIII] and [IX]. The charge distribution in the S_2^R of [IV] in the gas phase and in methanol are very similar.

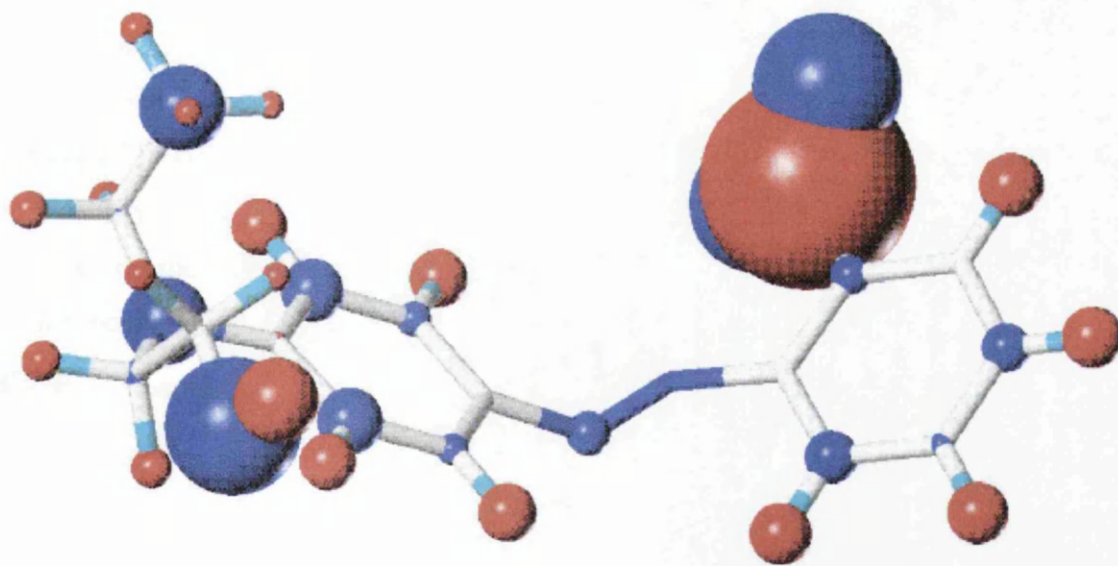


Figure 6.31 Structure and charges of the relaxed S_2^R excited singlet state of [IV] in the gas phase.

The relaxed second excited triplet state (T_2^R)

The relaxed second excited triplet state of **[VIII]** has an almost planar structure (Figure 6.34) in the gas phase, with the donor ring twisted slightly to the nitrophenylazo plane. The spin densities are localised almost entirely at the azo nitrogen atoms with the density slightly greater at acceptor azo nitrogen. There is also some spin density at carbon atom C^2 and low values at some other carbon atoms and at the amino nitrogen atom.

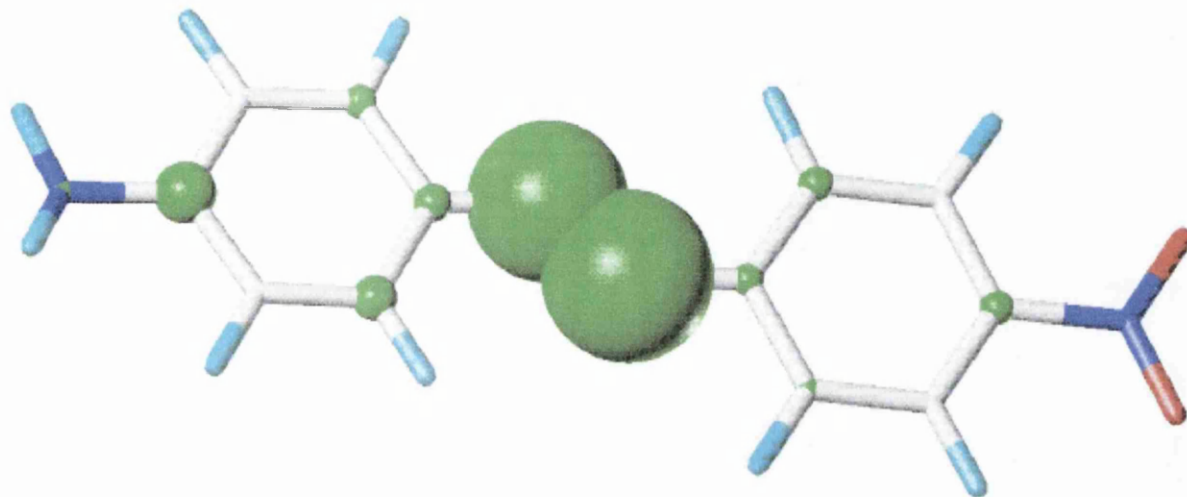


Figure 6.32 Structure and spin densities for the second excited triplet state T_2^R of **[VIII]** in the gas phase.

In contrast to the essentially planar gas phase structure, the relaxed second triplet T_2^R (Figure 6.33) is highly twisted in methanol, with a cis arrangement of the phenyl rings about the azo bond. The spin density of **[VIII]** is affected significantly by the solvent and there is a major difference between the spin density distributions in the second triplet in the gas phase and in methanol, with spin density not localised on the azo nitrogen atoms, as in the gas phase structures of T_2^R , but distributed over several atoms including the amino nitrogen, carbon atoms C^2 and C^5 , the acceptor azo nitrogen and the nitro group.

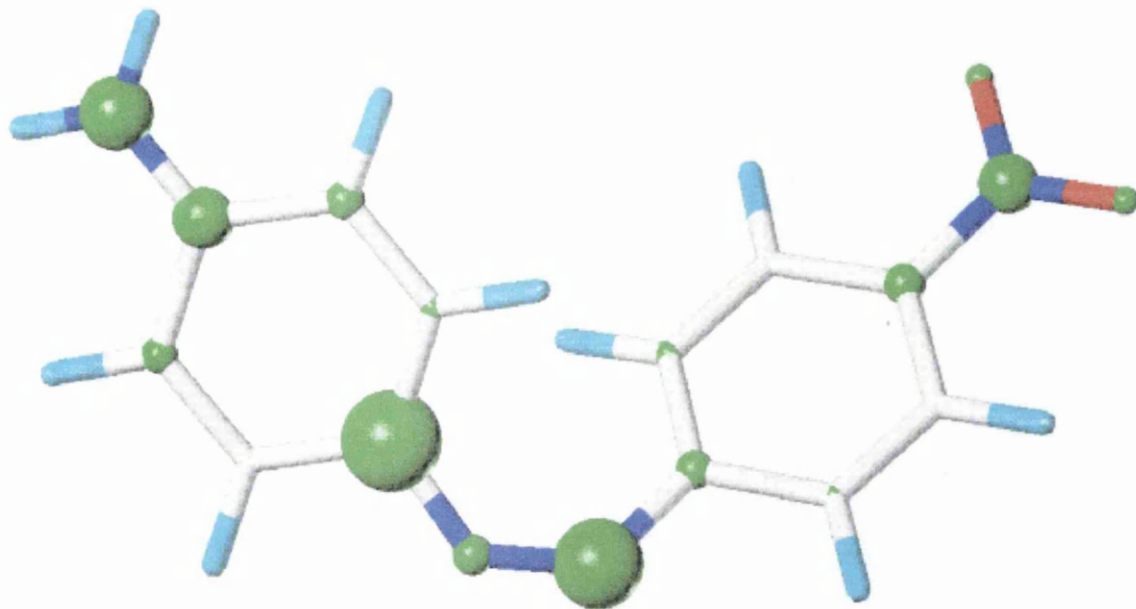


Figure 6.33 Structure and spin densities for the second excited triplet state T_2^R of [VIII] in methanol.

The second excited triplet state of [IX] has an almost flat structure (Figure 6.34) in the gas phase, with the donor ring twisted slightly to the nitrophenylazo plane. The spin densities are localised almost entirely at the azo nitrogen atoms with the density about 1.5 times greater at donor azo nitrogen. There is also some spin density at carbon atom C^2 and low values at some other carbon atoms and at the amino nitrogen atom.

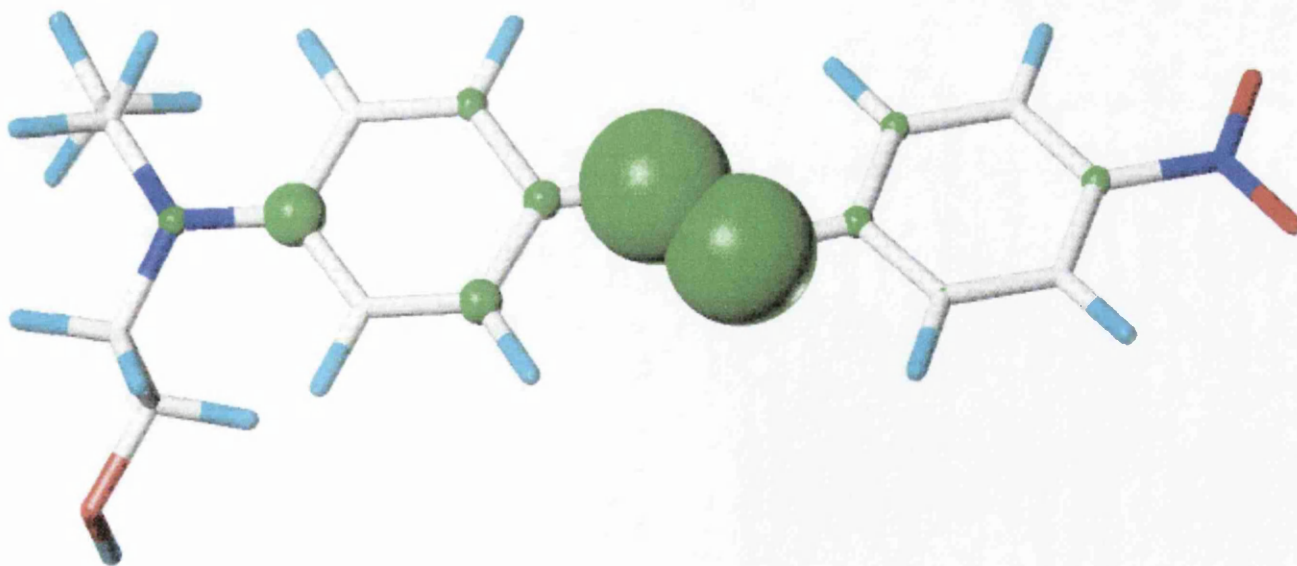


Figure 6.34 Structure and spin densities for the second excited triplet state T_2^R of [IX] in the gas phase.

The spin density is affected significantly by the solvent and there is also a noticeable difference between the spin densities of the T_2^R in the gas phase and also in methanol. Much of the spin density of [IX] in methanol is localised on the azo nitrogens, as in the gas phase structures of T_2^R . However, the magnitude of spin density at the second azo nitrogen was considerably smaller than in the gas phase while atom C^8 had a larger spin density.

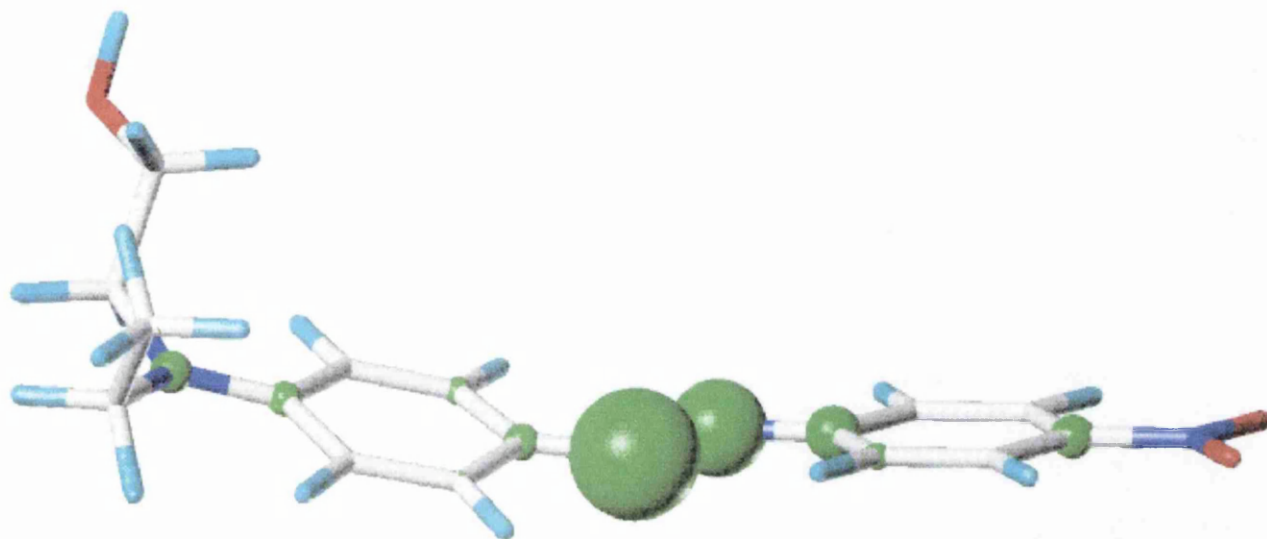


Figure 6.35 Structure and spin densities for the second excited triplet state T_2^R of [IX] in methanol.

The second excited triplet state of [IV] has slightly bent structure (Figure 6.34) in the gas phase, with the donor ring twisted slightly to the nitrophenylazo plane. The spin densities are localised mainly at the azo nitrogen atoms, with the density slightly greater at acceptor azo nitrogen, and at the amino nitrogen atom. The geometry of T_2^R in methanol is slightly more twisted than in the gas phase.

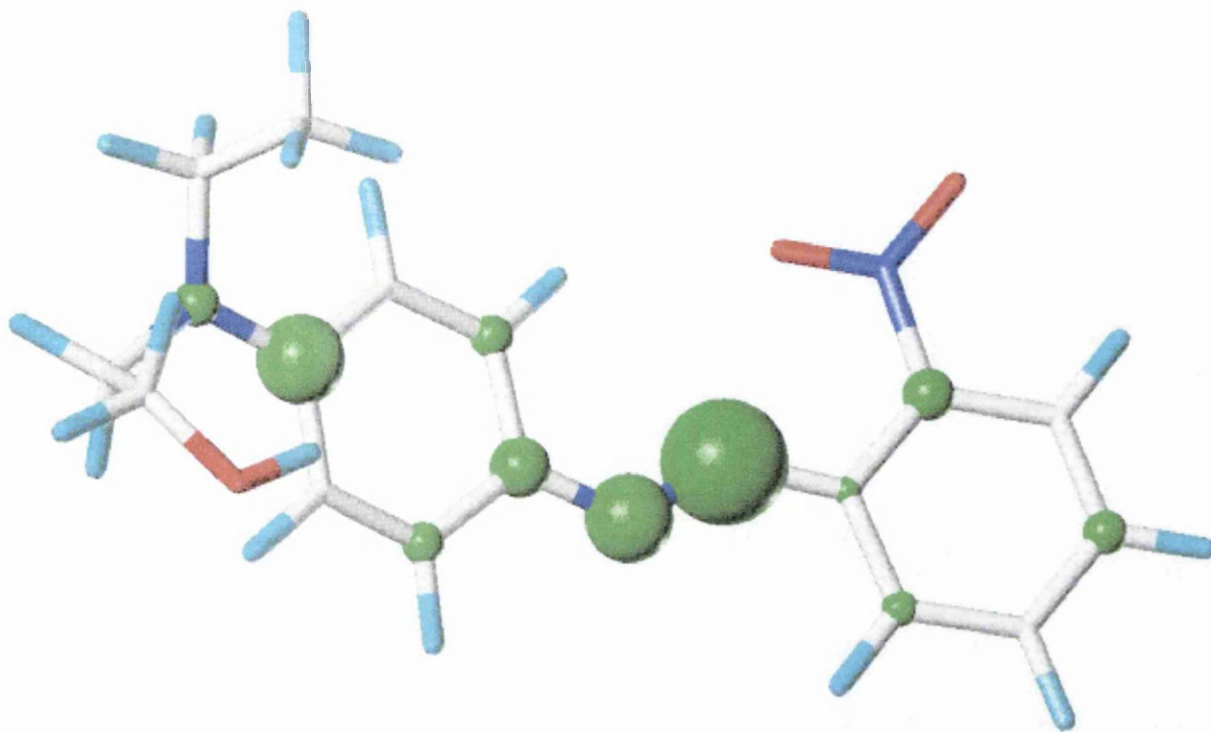


Figure 6.36 Structure and spin densities for the second excited triplet state T_2^R of [IV] in the gas phase.

The geometry of the relaxed T_2^R state in methanol (Figure 6.37) was practically planar and was very similar to the gas phase structure. However, in methanol the distribution of spin density is largely centred on the azo nitrogen atoms, with a small amount of spin density located at the nitro group. The spin density on carbon atom C^1 much less significant than in the gas phase structure.

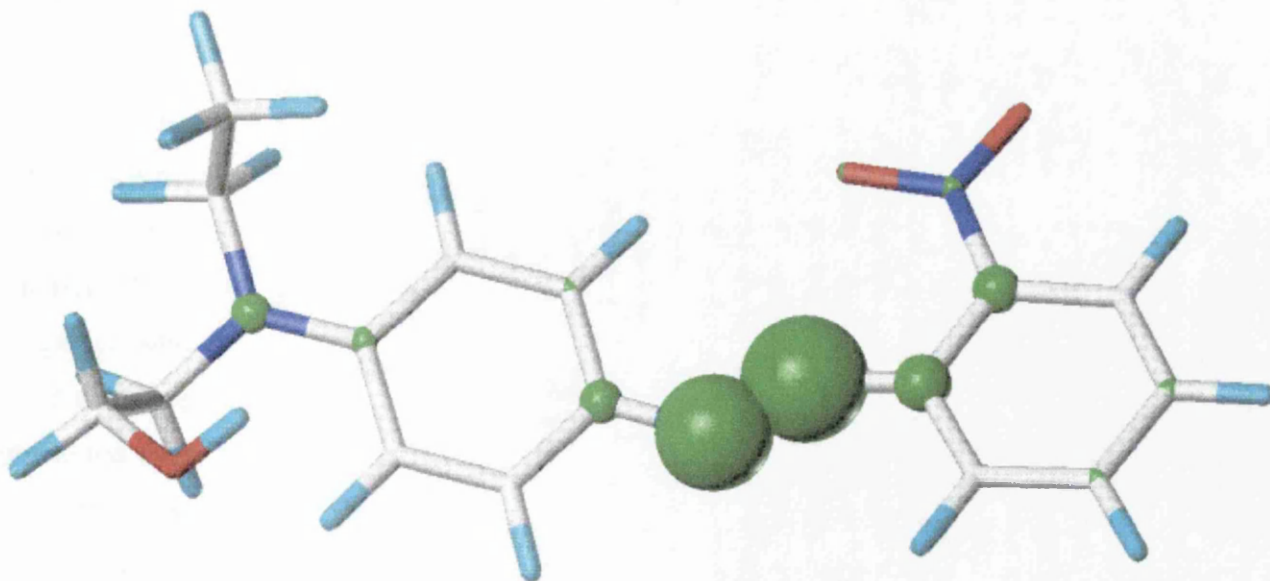


Figure 6.37: Structure and spin densities for the second excited triplet state T_2 of [IV] in methanol.

The positions of the spin density in the molecule may be significant in predicting the reactive site of the molecule and the spin densities for atoms N¹, C², C⁵, N⁶, N⁷, and the nitro group are compared for each dye in Table 6-11.

Table 6-11 Spin densities distribution in dyes.^a

| Dye | N ¹ | C ² | C ⁵ | N ⁶ | N ⁷ | C ⁸ | C ¹¹ | N ¹⁶ | O ¹⁶ | O ¹⁷ | $\tau_{1/2}$ | $\tau_{1/2}^{\circ}$ |
|--------|----------------|----------------|----------------|----------------|----------------|----------------|-----------------|-----------------|-----------------|-----------------|--------------|----------------------|
| [IV] | 0.12 | - | 0.16 | 0.36 | 0.34 | 0.13 | - | - | - | - | 0.87 | 3.52 |
| [V] | 0.15 | - | 0.16 | 0.53 | 0.33 | 0.12 | - | - | - | - | 1.44 | 4.77 |
| [VI] | 0.12 | - | 0.13 | 0.33 | 0.36 | 0.17 | - | - | - | - | 0.65 | 4.77 |
| [VII] | 0.18 | 0.14 | 0.24 | 0.44 | 0.36 | 0.11 | - | - | - | - | 0.86 | 3.84 |
| [VIII] | 0.11 | - | 0.10 | 0.23 | 0.10 | 0.25 | - | 0.15 | 0.07 | 0.07 | 1.06 | 10.52 |
| [IX] | 0.16 | 0.18 | 0.07 | 0.23 | 0.14 | 0.10 | 0.10 | 0.13 | 0.07 | 0.07 | 1.12 | 12.71 |
| [XI] | 0.16 | 0.19 | 0.19 | 0.16 | 0.15 | 0.19 | 0.18 | 0.15 | - | - | 1.96 | 15.46 |
| [XIV] | 0.13 | - | - | 0.38 | 0.42 | - | - | - | - | - | 1.38 | 8.33 |
| [XV] | 0.16 | 0.10 | 0.20 | 0.42 | 0.28 | 0.11 | - | - | - | - | 0.7 | 1.82 |

^a Spin densities are greater than 0.05 are reported. $\tau_{1/2}$ is the half-life in methanol under anaerobic conditions and $\tau_{1/2}^{\circ}$ is the half-life in oxygenated methanol.

The spin densities at the azo nitrogen atoms of the 2'-nitro substituted azo dyes, [IV]-[VII] are much larger than for [VIII] and [XI]; two dyes which have higher lightfastness than the 2'-nitro substituted dyes. The 2'-nitro dyes also have significant spin densities located at the carbon atoms attached to the azo group. Note also the greater spin density on the nitro group of [VIII] compared to the other dyes, which have almost no spin density at this group. The location of the spin density in the relaxed T₂^R state does seem to have some correlation with the rates of photo-degradation, and also the site of reactivity. For example, dyes containing the 2'-nitro group, which almost certainly cleave at the azo bridge (possibly at one of the carbon nitrogen bonds) and have relatively poor lightfastness, have major components of the spin density located at atoms C⁵, N⁶, N⁷ and C⁸. In contrast, the 4'-nitro substituted dyes, which have higher lightfastness, have lower spin densities at atoms C⁵, N⁶, N⁷ and C⁸. These dyes seemed to undergo reduction of the nitro group and not cleavage at the azo bridge, and the component of spin density at the nitro group of these dyes was much higher than in the other dyes.

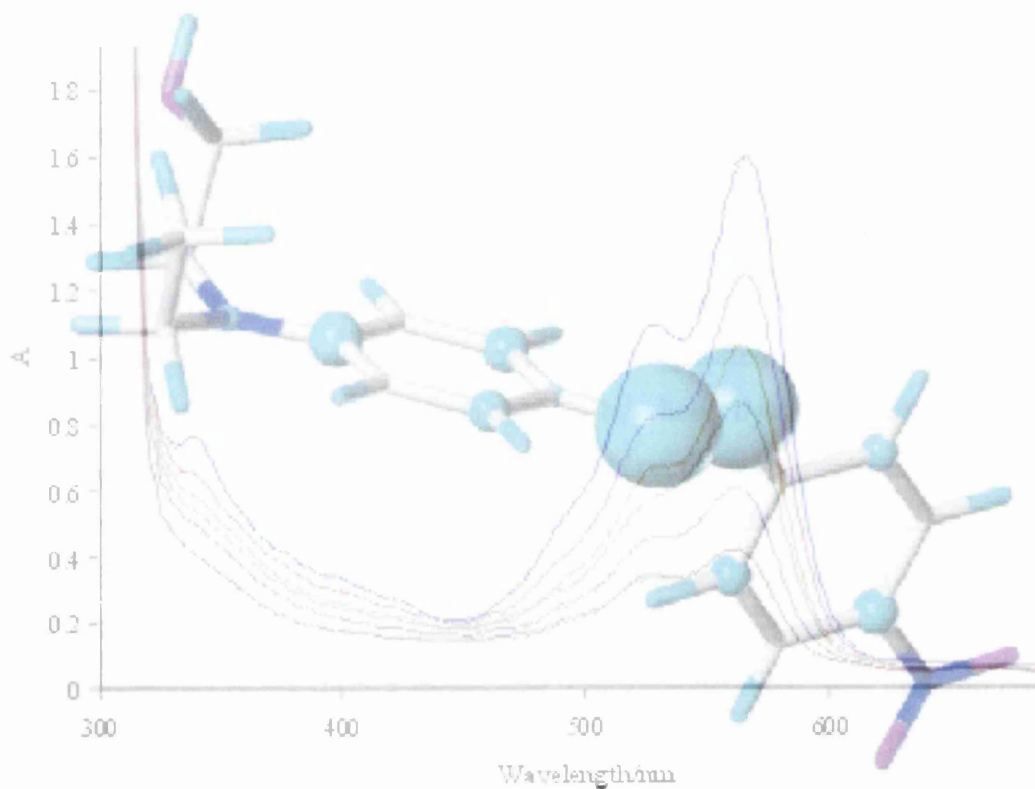
It is concluded that neither the energy levels between the various excited states considered nor the location of the spin density in the second excited triplet state have a clear correlation with the observed rates of photo-degradation. Further calculations are required to explain the energies and electronic properties of the excited states. These more detailed studies however, fell outside the remit originally proposed by Zeneca for this project and will be addressed in a future study.

References

- ¹ Cambridge Structural Database, Cambridge Crystallographic Data Centre, University Chemical Laboratory, Lensfield Road, Cambridge, CB2 2EW, UK.
- ² M.H. Charlton, R. Docherty, D.J. McGeein and J.O. Morley, *J. Chem. Soc. Faraday Trans.*, **89**(11) (1993) 1671-1675 and references therein.
- ³ J.O. Morley, R.M. Morley, R. Docherty and M.H. Charlton, *J. Am. Chem. Soc.*, **119** (1997) 10192.
- ⁴ C. Reichardt, *Solvents and solvent effects in organic chemistry*, Verlag Chemie, New York (1988).
- ⁵ SYBYL molecular modelling software, Tripos Associates, St Louis, Missouri, 1989; Tripos, inc. on the world wide web at <http://www.tripos.com/>; N. Van Openbosch, R. Cramer and F.F. Giarrusso, *J. Mol. Graphics* **3** (1985) 110.
- ⁶ J. Griffiths and C. Hawkins, *J. Chem. Soc., Chem. Commun.* 1972, 463; *J. Chem. Soc. Perkin Trans. 2.*, (1977) 747.
- ⁷ A. Albini, E. Fasani and S. Pietra, *J. Chem. Soc. Perkin Trans. 2* (1984) 1689 and references therein.
- ⁸ P.W. Atkins, *Physical Chemistry*, 5th edition, Oxford University Press (1994).
- ⁹ A. Albini, E. Fasani and S. Pietra, *J. Chem. Soc. Perkin Trans. 2.*, (1983) 1021.
- ¹⁰ E. Remi, O. Horvath, A. Vig, A. Rockenbauer, L. Horecz, P. Aranyosi and I. Rusznak, *Radiat. Phys. Chem.* **48** No. 3 (1996) 461.

Chapter 7

Conclusions



Conclusions

The photo-degradation of series of donor acceptor azo dyes have been investigated. It has been confirmed that irradiation of the second absorption band is responsible for permanent photo-degradation. Under anaerobic conditions, the 2'-nitro substituted azobenzene and azothiophene dyes are the least lightfast, with half-lives of under one hour, whilst 4'-nitro substituted dyes had half-lives of between 1 and 1.5 hours. However, the time for complete loss of colour takes up to six hours in the case of 4-diethylamino-4'-nitroazobenzene.

Photo-degradation is retarded in the presence of oxygen by between 4 and 16 times relative to fading under anaerobic conditions. The photo reaction of 4'-nitro dyes is initially quenched by oxygen, but proceeds at a slow rate thereafter. In contrast, the 2'-nitro substituted dyes fade at a slow but constant rate. The heavily substituted azobenzene and azothiophene dyes also have relatively poor lightfastness under anaerobic and oxygenated conditions. This may be due to increased rates of singlet oxygen sensitisation by these dyes. The order of reaction under anaerobic and under oxygenated conditions depends on the substituents of the dye and only some dyes fade with zero order kinetics. Rates of fading are an order of magnitude faster in propan-2-ol but slower in t-butanol suggesting that the rate of photo-degradation of the dyes is related to the ease of hydrogen abstraction from the solvent.

Analysis of UV/vis spectra shows that 2'-nitro substituted dyes undergo complete loss of intensity of the visible absorption peak and a corresponding increase in the absorption in the UV region of the spectrum when irradiated under anaerobic conditions, indicating cleavage at the azo bridge and subsequent formation of mono-phenyl derivatives. In contrast, under oxygenated conditions, there is a gradual loss of intensity at the visible absorption maximum, but no notable newly formed peaks are detected in the UV region suggesting that cleavage at the azo bridge is less significant.

Chromatography of the photo-degradation products formed under oxygenated conditions shows around 8 peaks and over 12 peaks under anaerobic conditions, which have been assigned as photo-products. Some peaks with similar retention times were detected under both sets of conditions but other peaks were exclusive to anaerobic or oxygenated fading. Most of these peaks eluted before the dye itself and products are therefore likely to be smaller in size or more polar than the original dye. Mass spectrometry of the photo-product solutions gave mass/charge ratios for some of the products detected by HPLC. From fragmentation patterns and accurate mass spectra, it has been concluded that under anaerobic conditions one of the main products of 4-(N- β -hydroxyethyl, N-ethyl)amino-4-nitroazobenzene was the reduced form of this dye, 4-(N-

β -hydroxyethyl, N-ethyl)amino-4-aminoazobenzene. This conclusion was supported by UV/vis spectra. Fragmentation patterns of photo-products also suggested dealkylation reactions at the alkyl amino group. The expected anilines were not detected by mass spectrometry, and UV/Vis spectra of suspected nitro aniline products were different to those of photo-products. However, the retention times of a solution of photo-degraded nitroaniline were similar to those of peaks detected in a photofaded solution of 4-(N- β -hydroxyethyl, N-ethyl)amino-2'-nitro-4'-chloroazobenzene. This suggests that either the anilines may be formed initially and consequently degraded themselves or the photo-degradation products of the dye are not the anilines, but some derivative of the anilines.

Theoretical geometry optimisations using the semi-empirical AM1 and PM3 methods and at ab initio level using the 3-21G, 4-31G and 6-31G* basis sets produce reasonable structures when compared with crystal data. The azo bond length is predicted to be shorter in semi-empirical structures than ab initio ones, but all methods underestimate the length of this bond, with respect to crystal data. Ab initio structures are essentially planar, but AM1 and PM3 structures have the acceptor phenyl ring twisted by approximately 35°. The nitro group of 2'-nitro dyes is twisted by between 30° and 90° depending on the planarity of the phenyl rings. Heats of formation for structures that were constrained to be planar are around 1 kcal less stable than freely optimised twisted structures. Conformational analysis predicts that the acceptor ring can be rotated by up to 60° degrees and the donor ring rotated by around 30° before there is a significant increase in the heat of formation. Rotation of the nitro group out of the plane is energetically favourable in 2'-nitro substituted dyes, but not in 4'-nitro substituted dyes.

Heats of formation of cis and trans isomers of azo dyes calculated using the AM1 and PM3 methods does not produce any apparent trend between the energy difference between the cis and trans isomers and the rate of fading of dyes. The rate of cis-trans isomerisation may depend more critically on the energy barrier between cis and trans isomers than the difference in energy between them.

Calculated transition energies of the visible absorption maximum by the CNDOVS method for twisted structures occur at shorter wavelengths than the experimental absorption maxima obtained in hexane, but planar structures produce good agreements with experimental data. Adjustment of the spectroscopic constant from 0.65 to 0.58 produces even better correlations. Transition energies of the second absorption band are predicted to be at longer wavelengths than experimental results. Analyses of excited states showed that the visible absorption arises from a HOMO-LUMO transition and is mainly π - π^* in character, and higher energy absorptions of

planar structures of donor-acceptor dyes were also π - π^* in nature. In contrast non-planar structures show some contributions from n - π^* transitions for these higher energy bands.

A configuration interaction (C.I.) treatment of gas phase AM1 structures shows poor correlations with experiment, but improvements are produced by the AM1/COSMO dielectric field solvent model. However, transition energies of 4-nitro dyes in methanol are predicted to be at longer wavelengths than those experimentally observed.

Increasing the level of C.I. from 4 to 8, had little overall effect on the transition energies of visible absorption maxima.

The second excited state resulting from a Frank-Condon transition has also been calculated using the C.I. treatment. Calculations at C.I. level 4 gave transition energies in the region of 300nm, which is close to the wavelength of the second absorption band experimentally. However, higher levels of C.I. led to the prediction of longer wavelength transition energies.

The relaxed first and second excited singlet and triplet states have also been calculated in the gas phase and in methanol. The first singlet state is essentially planar in both phases, while the first triplet adopts a twisted structure, where the acceptor nitro-phenylazo group is orthogonal to the donor amino-phenyl ring. The relaxed second excited singlet state is slightly bent in the gas phase and had similar geometries in methanol. The relaxed second excited triplet has a similar bond and torsion angles to the relaxed second excited singlet, but the $-N=N-$ bond lengths are longer in the triplet state structures. Attempts at correlating the energies of relaxed states, Frank-Condon states and the ground states of dyes with half-lives in methanol under anaerobic and oxygenated conditions were unsuccessful and no recognizable trends were produced. The distribution of the two unpaired electrons in the triplet states of each dye molecule has been calculated, and there appears to be some correlation between the magnitude of spin density located at the azo bridge $C-N=N-C$ and rates of photofading. Dyes that have relatively low lightfastness had a greater component of spin density located at these atoms. A tentative relationship between sites of reactivity and spin density is also proposed, as the dyes which have relatively low lightfastness are thought to undergo photo-cleavage at the azo bridge, while 4'-nitro substituted dyes react at the nitro group, which has a greater component of spin density at the nitro group than for the 2-nitro substituted dyes.

It may be the case, that some other transition state, or a higher triplet state is responsible for the photo-degradation process. It must also be noted that even predictions of the first excited state produced erroneous results for several dyes and it is possible that the level of theory explored may be inadequate for calculating these type of excited states.